UNIVERSITY OF SOUTHAMPTON

FACULTY OF NATURAL AND ENVIRONMENTAL SCIENCES

Chemistry

Transmembrane Anion Transport: Investigating Mechanism and Selectivity

by

Harriet Jane Clarke

Thesis for the degree of Doctor of Philosophy

November 2017

UNIVERSITY OF SOUTHAMPTON

ABSTRACT

FACULTY OF NATURAL AND ENVIRONMENTAL SCIENCES

Chemistry

Thesis for the degree of Doctor of Philosophy

TRANSMEMBRANE ANION TRANSPORT: INVESTIGATING MECHANISM AND SELECTIVITY

By Harriet Jane Clarke

In the last decade, the development of synthetic anion transporters has attracted much attention. A variety of small molecules have been established to facilitate the transport of biologically relevant anions such as chloride, bicarbonate and sulfate across lipid bilayers. This interest has been piqued due to their potential as therapeutics for 'channelopathies' such as cystic fibrosis and in some cases their anion transport has been linked to anti-cancer activity in cells.

This thesis explores a new series of chloride transporters which possessed high binding affinity for oxo-anions such as phosphate and bicarbonate. They were found to transport via an antiport mechanism, with a preference for Cl^-/NO_3^- over Cl^-/HCO_3^-. The series also exhibited some self-association characteristics, which appeared detrimental to their transport activity.

The transmembrane transport of fluoride was also investigated using a series of strapped calix[4]pyrroles. The fluoride transport was monitored directly using ion selective electrode and NMR techniques. The length of the strap was found to modulate the fluoride over chloride selectivity, showing fluoride selectivity for the shortest strapped calix[4]pyrroles.

Furthermore the fundamental transport mechanism of these calix[4]pyrroles was elucidated as electrogenic by extending the series and employing cationophore coupling techniques. The smallest strapped receptor showed unprecedented Cl^- selectivity even in the presence of fatty acid. Additional studies showed the rest of the series' halide and nitrate selectivity follows an anti-Hofmeister bias.

TABLE OF CONTENTS

TABLE OF FIGURES

Acknowledgements

The biggest thanks must go to my supervisor Prof. Phil Gale for all the help and support over the past three years and for believing in me when I was a project student by giving me the opportunity to do a PhD. Special thanks must go to Dr. Jon Kitchen for stepping in as my supervisor when Phil left for sunnier shores!

I would like to thank Prof. Stefan Kubik and Fabian Sommer for performing ITC measurements. Thank you to Ms. Julie Herniman and Dr. Neil Wells for High resolution mass spectrometry measurements and NMR help. I am indebted to Dr. Mark Light for his patience and invaluable help when teaching me the magic that is X-ray crystallography, you really are a crystal genius!

I am very grateful to the EPSRC for funding my PhD project, and thanks must also go to the RSC for a travel grant that allowed me to attend an international conference giving me the opportunity to present my work.

Words cannot describe how grateful I am for the Gale group family for helping keep me sane throughout the ups and downs of research. Issy, Cally and Lou for encouraging me to do this PhD in the first place and for welcoming me to the Gale group with lots of food and wine! Thank you to Wim for being my guiding light when I knew nothing in the 1st year and for keeping me supplied with tea. Jenny, Xin, Nat and Ethan your knowledge knows no bounds and the ideas and help have been invaluable. Mike, the last six months in Southampton have been tough and I honestly don't think I would be even near finished without your support and friendship. Furthermore, your ability to eat all the cake that I stress bake astounds me. Stu, Laura and Annie, my fellow PhDs, you cheer me up even when the chemistry doesn't work and there are no other people I would rather share the vesicles room nest with.

Finally, a huge thank you must go to my family and friends, especially Charlie and Sarah for having me to stay whilst I wrote the dreaded thesis, without all the love and support I would have descended into insanity long ago!

Abbreviations

ATP	Adenosine triphosphate
CF	Cystic fibrosis
CFTR	Cystic fibrosis transmembrane conductance regulator
CHOL	Cholesterol
CLC	Chloride channel
DCM	Dichloromethane
DNA	Deoxyribonucleic acid
DMPE	1,2-ditetradecanoyl-*sn*-glycero-3-phosphoethanolamine
DMSO	Dimethylsulfoxide
EC_{50}	Effective concentration for 50 % response
FRT	Fischer rat thyroid
GUV	Giant unilamellar vesicle
HPTS	8-Hydroxypyrene-1,3,6-trisulfonic acid
HRMS	High resolution mass spectrometry
IC_{50}	Half maximal Inhibitory Concentration
ISE	Ion selective electrode
ITC	Isothermal titration calorimetry
logP	Octanol/water partition coefficient
LUV	Large unilamellar vesicle
MTT	MTT (3-(4,5-Dimethylthiazol-2-yl)-2,5-Diphenyltetrazolium Bromide)
NBD	Nucleotide binding domain
NMDG	N-Methyl-D-glucamine
NMR	Nuclear magnetic resonance
POPC	1-Palmitoyl-2-oleoyl-sn-glycero-3-phosphocholine
POPE	1-Palmitoyl-2-oleoyl-sn-glycero-3-phospho-ethanolamine
POPG	1-Palmitoyl-2-oleoylphosphatidylglycerol
QSAR	Quantitative structure activity relationship
SAR	Structure activity relationship
TBA	Tetrabutylammonium
TEA	Tetraethylammonium
THF	Tetrahydrofuran
TMD	Transmembrane domain
UV-Vis	Ultraviolet-Visible spectroscopy
YFP	Yellow fluorescent protein

Chapter 1: Introduction

1.1 Anions in the biological environment

Anions such as chloride, bicarbonate and phosphate are abundant in nature. They play a significant role in many important physiological processes. The spatial distribution of these anions in biological environments is not equal and the balance of anion gradients is essential for maintaining life. For example, they can act as energy sources to drive metabolic processes.[1] In a cell the phospholipid membrane acts as a barrier to the cell's contents.[2,3] Small, neutral or lipophilic molecules, such as water or carbon dioxide, can pass through the semi-permeable plasma membrane unaided. However, large hydrophilic or charged molecules rely on the action of membrane proteins. The function of these membrane proteins is vital for maintenance of cellular pH,[4] osmotic balance[5] and cell signalling,[6] amongst other important functions.[2]

Membrane proteins can transport ions via three different mechanisms, a channel, relay or mobile carrier mechanism as seen in Figure 1.1. In nature a membrane protein channel is usually voltage gated and they tend to have low selectivity, whereas a mobile carrier and relay proteins show higher selectivity as their transport is usually monomeric and not gated.[2]

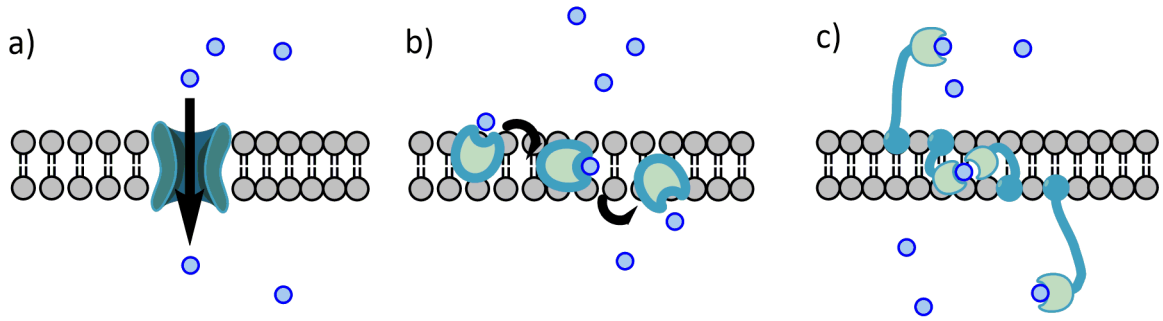

Figure 1.1 Schematic representation of a) an ion channel transport mechanism, where the protein forms a membrane spanning pore through which the ion can diffuse. b) A mobile carrier transport mechanism, where the protein forms a complex with the ion and the complex diffuses across the membrane. c) A relay transport mechanism, where the protein is anchored to one side of the bilayer. It then forms a complex with the ion and passes the ion to a protein anchored on the other side of the bilayer.

Additionally, membrane proteins have three possible methods to facilitate passive ion transport across lipid bilayers, shown in Figure 1.2. Uniport is the transport of one ion down a concentration gradient across a bilayer, this process is usually voltage gated as the process results in a net charge

across the membrane. Antiport is the exchange of two ions of the same charge across the membrane down each ion's respective concentration gradient, resulting in a net neutral charge. Finally, symport is the transport of two ions with different charges across the membrane in the same direction, also resulting in a net neutral charge. Antiport and symport may be referred to as co-transport as they require the movement of two ions during the process.

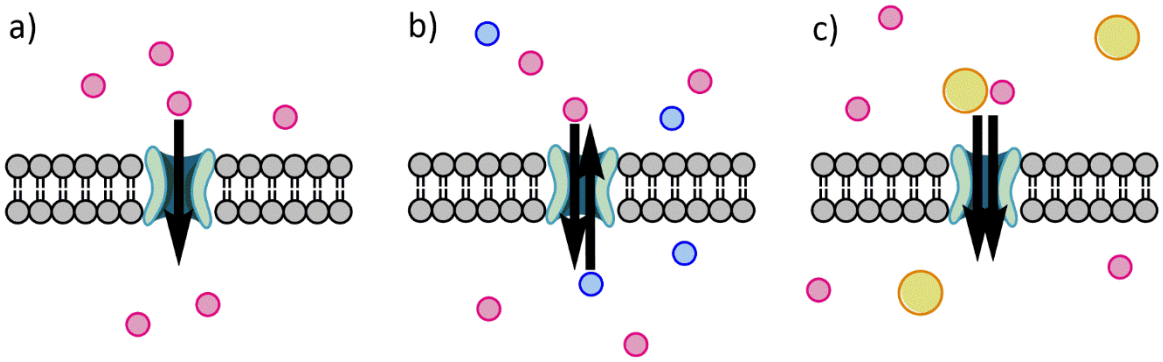

Figure 1.2 Three possible transport processes. In the schematic, the protein is represented by the turquoise ion channel. a) Uniport: transport of A^- (red) in one direction across the bilayer, b) antiport: transport of A^- (red) and A_2^- (blue) in opposing directions and c) symport: transport of C^+ (yellow) and A^- (red) in the same direction.

Mutations in the genes which code for ion channels or proteins can cause degenerative diseases. In 1989 one of the possible causes of Cystic Fibrosis (CF) was linked to an ion channel deficiency.[7] The Cystic fibrosis transmembrane conductance regulator (CFTR) is an ATP-gated channel depicted in Figure 1.3, which regulates the transport of anions such as HCO_3^- but more notably Cl^-. It is a member of the ABC transporter family and is made up of five functional domains,[8,9] two transmembrane domains (TMDs) that form the channel,[10] two nucleotide binding domains (NBDs)[11,12] and a regulatory domain. It is found in epithelial cells of the lungs, intestine, reproductive tracts, sweat glands and pancreatic ducts. A number of mutations, predominantly in NBD1,[11,12] can result in the recessive degenerative disease CF.[13] CF sufferers develop reduced levels of anion (mostly Cl^-) transport resulting in a reduced level of water movement. This lack of water movement leads to thick dehydrated mucous secretions which cause infections and inflammation particularly in the lungs.[14] As of yet, there is no cure for CF and in the UK median life expectancy is about 41 years.[15]

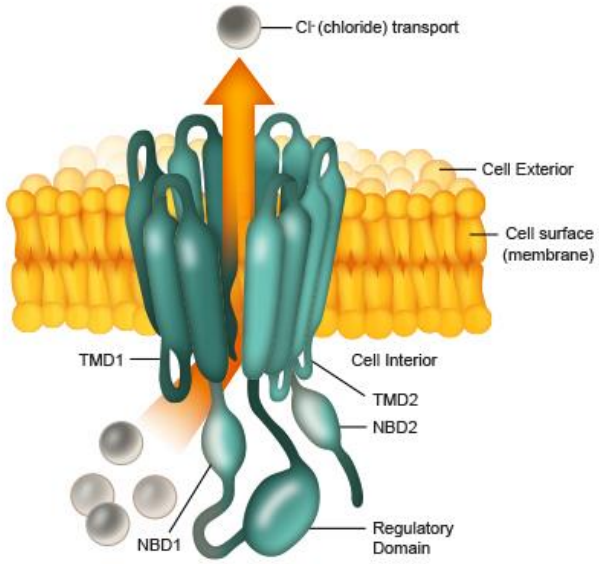

Figure 1.3 Depiction of the Cystic fibrosis transmembrane conductance regulator (CFTR). TMD= Transmembrane domain and NBD= Nucleotide binding domain. © Copyright 2017 Fishawack Facilitate Ltd.[12]

Other chloride specific channel proteins such as voltage-gated chloride channels known as CLCs, play a vital physiological role and mutations for specific CLCs cause a variety of diseases. Hereditary mutations on CLC-5 cause hypercalciuria which can lead to kidney stones due to a build-up of excess salts in the urine. [13] Bartter Syndrome is an autosomal recessive disorder due to transmutations on CLC K_b, it causes severe salt wasting which leads to accumulation of Cl^- intracellularly, followed by depletion of extracellular volume. This causes low blood pressure, hypokalaemia and alkalosis.[13]

Anion channels specific for Cl^-/HCO_3^-antiport are essential for intracellular pH (pH_i) regulation in osteoclasts within healthy bones. Malfunction of these channels can give rise to metabolic bone diseases such as osteoporosis.[16] Other important HCO_3^- channels include NBCs (Na^+/HCO_3^- co-transporters)[17] and CBEs (HCO_3^-/Cl^- exchangers) which help maintain pH_i in cardiac cells, preventing common heart defects. [18]

One ion long to be thought a spectator anion with no precise function was SO_4^{2-} but in the last 30 years it has been found to be the major source of sulfur in humans as it is the most abundant anion in human plasma.[19] The diastrophic dysplasia sulfate transporter (DTDST) is the most essential sulfate transporter in the body, and genetic mutation of this channel causes insufficient sulfation of cartilage which can lead to dwarfism and spinal deformities.[20]

The link between faulty anion channels and specific genetic diseases, most notably CF, was the initial driving force for the development of synthetic anion channels and carriers in anticipation for their use as potential therapeutics. Early studies focused on how ion transport was facilitated within the biological environment. Several naturally occurring ionophores were discovered and their transport abilities were probed with the hope of uncovering characteristics required for successful anion transport.

1.2 Naturally occurring ion transporters

A range of naturally occurring ionophores have been discovered over the years, predominantly cationophores, one of the most notable of these is the antibiotic valinomycin. Valinomycin is a depsipeptide with alternating α-hydroxy acids and α-amino acids, its structure can be seen in Figure 1.4.

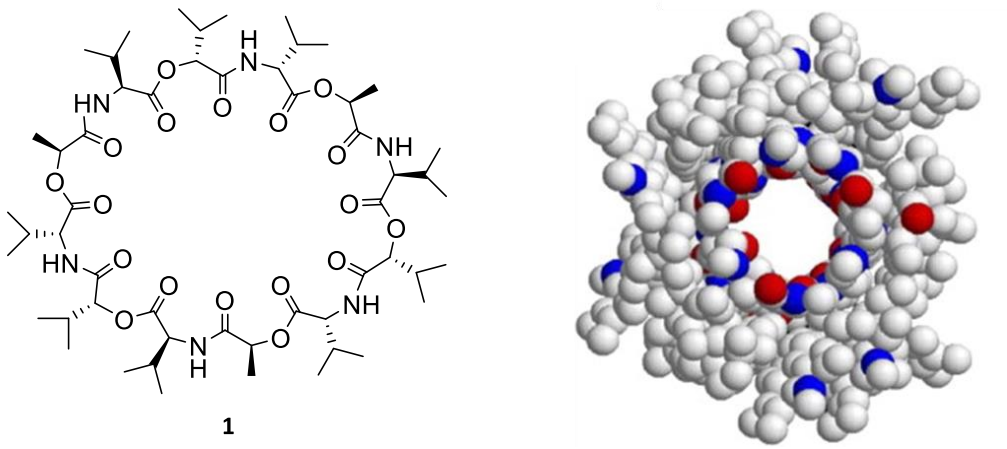

1

Figure 1.4 **Left-** The structure of naturally occurring cationophore, valinomycin, **1**. **Right-** A top down view of the space filled structure of the naturally occurring ion channel gramicidin.[21] Copyright © 2007 Elsevier B.V. All rights reserved.

Valinomycin **1** was found to increase the potassium permeability of biological membranes, specifically mitochondrial and erythrocyte, in an early study in 1967 by Pressman *et al.*[22] The depsipeptide was found to possess a high selectivity for potassium over the other alkali group 1 metals with a stability constant 10^2 times higher than for sodium.[23,24] Solid state structures show the oxygens form an octahedral cage around the potassium, mimicking the hydration shell formed around potassium in aqueous media.[24,25] It has been widely used in transport studies to provide a source of complementary cation transport and to modulate membrane conductance.[26,27]

Another naturally occurring cationophore is the linear pentadecapeptide antibiotic gramicidin which was isolated by Dubos from the soil bacterium *Bacillus brevis.*[28] It possesses an interesting alternating chiral structure of *L*- and *D*- amino acids which allows it to adopt different conformations depending on its environment.[29] Figure 1.4 shows its single stranded helical dimer form, which is predominantly known as its channel form. This is able to span bilayer membranes with the carboxy functions exposed to the membrane interface, and the amino functions inside the lipid bilayer tail region.[21]

Gramicidin acts as cation selective pore, with conductance's of ≈ 10^7 ions per second,[30] and is frequently used in membrane channel studies.[31–33]

During the following decades, discoveries of naturally occurring anion receptors and transporters were substantially less common than that of cationophores. One family that has been thoroughly studied is the prodigiosins (Figure 1.5). First isolated from *Serratia* and *Streptomyces* in the 1930s[34] prodigiosins possess a tripyrrolic structure and drew research attention due to their promising anticancer, antimalarial and immunosuppressive activity.[35–38]

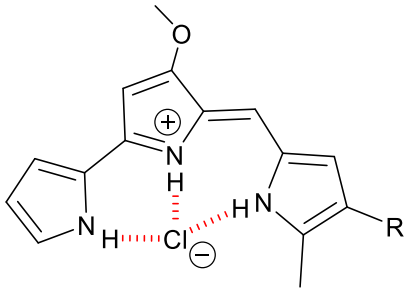

2

Figure 1.5 General structure of the prodigiosins in the lipophilic complex formed with the addition of HCl.

The immunosuppressive activity of the prodigiosins was first observed in culture broths of microorganisms being screened for immunomodulating substances.[39] Early studies showed undecylprodigiosin (R= $C_{11}H_{23}$) could inhibit the proliferation of T and B cells. These studies were ceased quite early on however, due to undecylprodigiosin's excessive toxicity displayed in mice.[40] These high levels of toxicity for the majority of compounds within the prodigiosin family have hampered efforts to develop them as anticancer therapeutics. [36] The mechanism for the biological activity of prodigiosins is still highly disputed, some studies have shown they can facilitate oxidative damage to the DNA. [36,41–44] Furstner *et al.* suggest prodigiosins exhibit an intercalative binding mode within the DNA predominantly at the AT binding site. [44] Additionally, Williamson *et al.* demonstrate bacterial prodigiosins and synthetic derivatives can act as proapoptotic agents against several cell lines with multiple cellular targets.[43]

The anionophoric activity of prodigiosin has also been investigated as a possible mechanism for cytotoxicity. [45–47] Prodigiosin **2** (R= C_5H_{11}) can facilitate the symport of H^+/Cl^- through liposomal membranes which deacidifies the lysosome.[45] Following these liposomal co-transport results, Gale, Davis and co-workers studied prodigiosin, synthetic analogues and other mimics in vesicle based assays.[46,47] They found interesting additional antiport properties observing extremely efficient Cl^-/NO_3^- and Cl^-/HCO_3^- antiport across vesicle membranes. They also proposed that the assay

conditions direct the mechanism of transport utilised by the prodigiosins in a study of antiport vs symport.

Another class of naturally occurring anion transporters closely related to the prodigiosin family are marine alkaloids known as tambjamines (**3**). They bear a 4-methoxy-2,2-bipyrrolleamine, and were isolated from S*igillina Signifera*. Research has also found promising anticancer and antimicrobial properties.[48–50] Their total synthesis was first reported by Pinkerton *et al.,*[51] and natural derivatives are still being discovered. Despite their promising biological activity, the tambjamine's anionophoric nature was not fully investigated until much later.

In 2012, Quesada and co-workers found that unlike the prodigiosins their predominant transport mechanism was Cl^-/NO_3^- or Cl^-/HCO_3^- exchange as opposed to H^+/Cl^- symport, as previously assumed, most likely due to the fact they remain protonated at physiological pH with a pKa ≈ 10.[52]

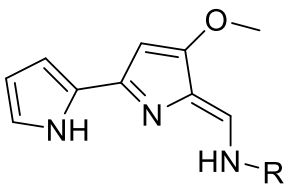

3

Figure 1.6 General structure of the tambjamine alkaloids.

Since 2012, in depth studies of the tambjamine's optimum lipophilicity, quantitative structure activity relationship (QSAR) and cell studies have been performed and will be discussed later.[48–50,53,54] During cell studies the transporters were found to induce pH_i acidification and hyperpolarisation of cellular membranes in lung cancer cell lines and were found to be particularly effective against cancer stem cells.[49] This ability has been linked to the anionophoric activity and studies into this link are ongoing. Unfortunately, one major issue that the tambjamines share with prodigiosins is their prominent level of toxicity not only to cancer cells but also healthy cells, so improving their selectivity for cancer cells without removing their cytotoxicity will be key in their development for use as anticancer agents.[48]

1.3 Anion binding

In order to transport an anion across a lipid membrane the anion must first be bound by the potential transporter. This interaction must be some form of non-covalent interaction that is thermodynamically favourable to allow for release of the anion once transport is complete. Over the last half century anion receptor chemistry has developed rapidly. Supramolecular chemists have built up a catalogue of effective anion binding scaffolds for various applications including anion recognition, sensing and extraction. The next section focuses on the development of these anion receptors which then lead to their use as anion transporters.

1.3.1 Early anion binding

The first examples of anion binding by synthetic scaffolds were published in the late 1960s. The first example from Shriver and Biallas utilised a Lewis acid, base binding approach. Boron based Lewis acid **4** was used to chelate a methoxide anion, with the methoxide anion acting as the electron pair donor.[55]

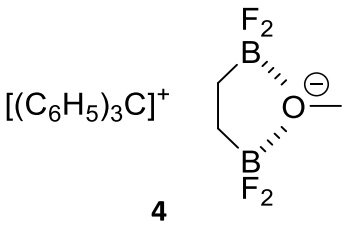

4

Figure 1.7 Structure of the Lewis acid chelate methoxy complex synthesised by Shriver and Biallas.

Only a year later Park and Simmons synthesised a series of macrocyclic ammonium based receptors which, when protonated at low pH, employed electrostatic interactions and hydrogen bonds to bind halide anions.[56] Even at this early stage the importance of size selectivity was apparent. The smaller macrocycles, **5** and **6**, displayed no measurable binding event. The larger macrocycle **7** (n=3) allowed for Cl^- and limited Br^- binding with binding constants of 4 and 1 M^{-1} in 50 % TFA respectively, only **8** exhibited I^- binding.

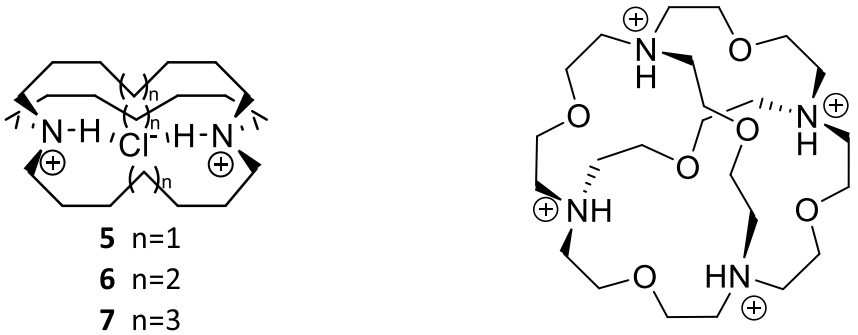

Figure 1.8 Structures of Park and Simmons macrocyclic ammonium ions **5–8** and an example of Graf and Lehn's cryptates **9**.

Following these early anion binding projects, the development of anion receptors was slow, in 1976 Graf and Lehn published seminal work on macro-tricyclic ligands, known as cryptates, that could form stable halide selective complexes.[57] The complexes were formed via a tetra-protonated, tetrahedral array of N^+– H···X^- hydrogen bonds. Again, the size and shape of the cavity was key to the binding characteristics. Compound **9** was found to be optimal receptor size for the spherical halide anions. No complexation was observed with polyatomic anions such as NO_3^-, CF_3COO^- and ClO_4^- or the large diffuse I^-. At the time, this was the most stable chloride complex using the combination of electrostatics and hydrogen bonds to get a stability constant of log K_s= > 4.0 in water at pH 1.5.[57] Schmidtchen followed this work with a size complementary study of ammonium based macrotricyclic structures (Figure 1.9) that relied predominantly on electrostatic attraction with no need for protonation of the nitrogen atoms.[58] Anions have a range of shapes and sizes, and the spherical halides are very popular targets for anion binding, but there is a large size disparity through the series F^- < Cl^- < Br^- < I^-. Schmidtchen expanded the cavity from n= 6 (Br^- selective, **10**) to n= 8 which allowed for the binding of I^- by **11**, its cavity radius of 3.8 Å was then large enough to incorporate the 2.28 Å ionic radius of I^-.

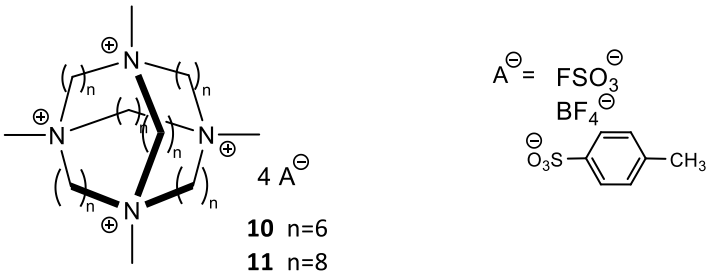

Figure 1.9 Structure of Schmidtchen's macrotricyclic ammonium receptors **10** and **11**.

The major drawback to the combination approach of electrostatics and hydrogen bonding to complex anions is that the binding mode is affected by the pH conditions in the study. Protonation

is essential for hydrogen bonding; hence receptors rely on an external factor for the anion binding event to occur, thus alternative approaches were explored.

The first example of a neutral hydrogen bonding receptor was developed by Pascal and co-workers.[59] A study of the sulfate-binding protein in *Salmonella typhimurium* led to the discovery that the sulfate is only bound by hydrogen bonds, mostly from the amide NH's within the polypeptide backbone deep within the protein which shields the binding site from solvent.[60] Taking inspiration from this natural phenomenon Pascal synthesised neutral amide containing macrocycle **12**,[59] with roughly inward pointing NHs able to bind and encapsulate the anion. Although only preliminary, ^{1}H and ^{19}F NMR studies suggested an association of fluoride with macrocycle **12**.

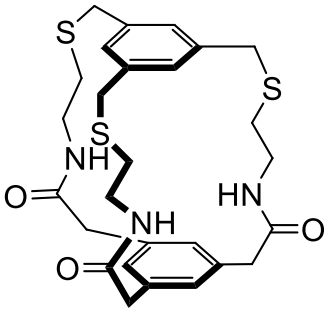

12

Figure 1.10 Structure of Pascal and co-worker's (1, 3, 5)cyclophane.

Over the last couple of decades many neutral hydrogen bonding anion receptors have been developed. The versatility of the hydrogen bond is one reason it is such a common approach, they can be tuned by addition of electron donating or withdrawing substituents. Due to the directional nature of the hydrogen bond, receptors can be designed to favour the shape of the desired target. The preferred approach has involved the use of NH as the hydrogen bond donor; ureas, amides, thioamides, thioureas, sulfonamides, squaramides and guanidiniums have all been used successfully as anion receptors and recognition agents. All types of binding moieties will not be covered here but more details can be found in a variety of anion complexation reviews.[61–71]

The first instance of anion binding using a urea functionality came from Wilcox and co-workers.[72] Figure 1.11 shows the proposed binding mode for the mono-(*m*-nitroaryl)urea host **13** with a tosylate ion. UV-Vis spectrophotometry was used to calculate the binding constants for a range of oxo-anions and they all exhibited strong binding with K values in the range of 10^{3}–10^{4} M^{-1} in chloroform. The incorporation of the electron withdrawing *m*-nitro group increased the binding affinity, presumed to be due to increased acidity of the urea NHs.

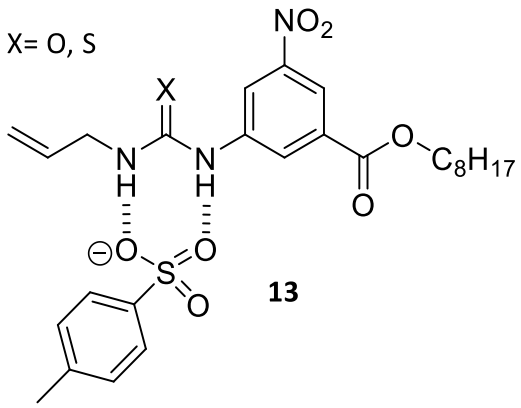

Figure 1.11 The proposed binding mode of the urea motif with a tosylate ion.

Taking inspiration again from nature Kubik and co-workers synthesised a mimic of a peptide subunit dubbed a 'molecular oyster' **14** (Figure 1.12).[73] It was found to selectively encapsulate and complex sulfate using amide NHs; much like a pearl in an oyster shell. The stability constant for sulfate binding in a water: methanol (1:1) solution was 3.5 x 10^5 M^{-1}. Once again size selectivity appeared to be the driving force for the trend observed in the compound's complex stability. Larger anions (I^-, SO_4^{2-}) formed more stable complexes over smaller halides (Cl^-, Br^-). As a follow up study, dynamic combinatorial chemistry was performed to optimise the length of the linking group to improve selectivities for specific anions.[74]

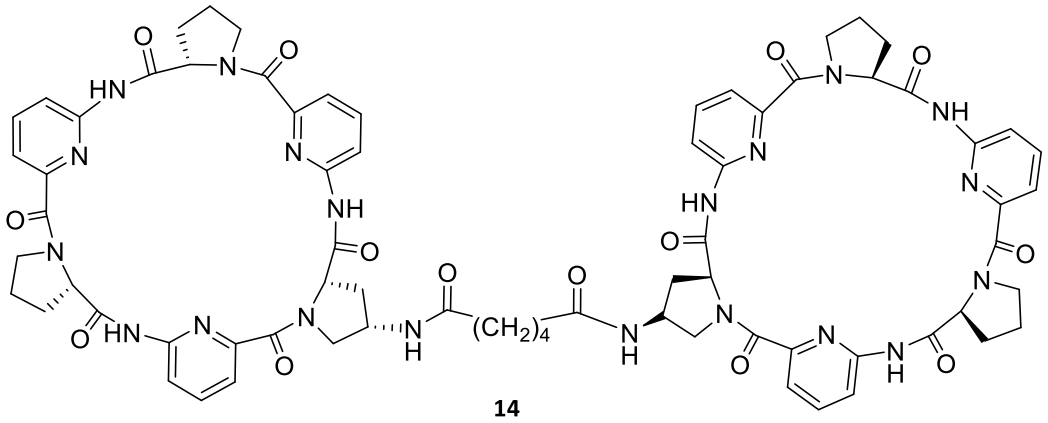

Figure 1.12 Structure of Kubik and co-workers 'molecular oyster'.

Another popular NH based receptor motif is the squaramide. Its hydrogen bonding pattern, featuring two convergent NH hydrogen donors, is like that of urea. One early example from Prohens *et al.*[75] demonstrated the binding of a tris-squaramide receptor **15** with tricarboxylate anions such as cyclohexentricarboxylate and trimesoate, the latter gave a K_a of 3.9 x 10^3 M^{-1} in DMSO. They proposed a binding mode from 2D ROESY experiments with each individual squaramide unit binding each carboxylic acid motif, essentially forming a partial cage around the anion (Figure 1.13).

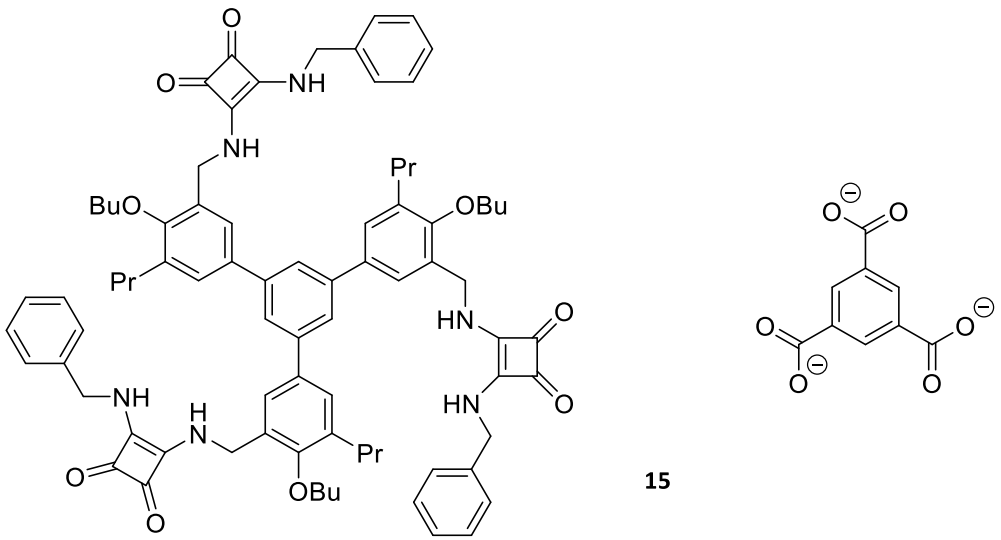

15

Figure 1.13 Structure of the tris-squaramide for binding to trimesoate (right).

Many of these NH binding motifs ((thio)ureas, (thio)amides, squaramides) have an interesting duality whereby they possess good hydrogen bond donors but also hydrogen bond acceptors. In the case of squaramides, this property is useful when attempting to design ditopic receptors.[76] It can however, cause self-assembly and aggregation in solution which competes with the binding event. To overcome this effect, other NH binding motifs were developed, such as heterocyclic NH receptors, using pyrrole, indole, carbazole and indolocarbazole.

The calixpyrroles, utilised throughout this thesis, were first synthesised in 1886 by Baeyer.[77] They are colourless macrocycles made from the condensation of four pyrrole rings linked through the *meso* positions by carbon atoms (Figure 1.14). They were previously called porphyrinogens as they were common porphyrin precursors, and since their renaming in 1996 by Sessler *et al.*[78,79] they have been well established in the anion receptor field.

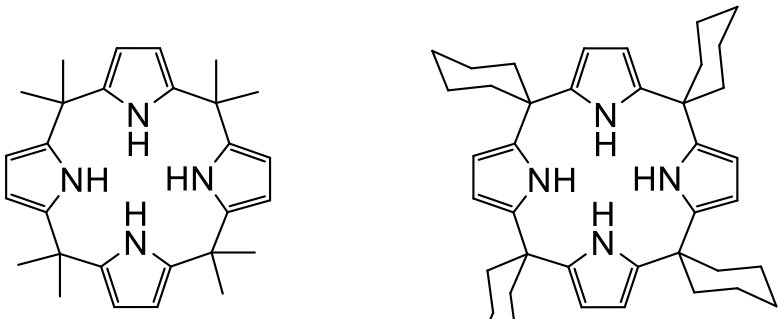

16 17

Figure 1.14 Structures of *meso*-methylsubstituted calix[4]pyrrole **16** and tetraspirocyclohexylcalix[4]pyrrole **17**.

Single crystal X-ray analysis of both **16** and **17** showed they adopt a 1,3-alternate conformation in the solid state, i.e. adjacent pyrrole molecules have opposing orientations.[78,79] However, when the chloride and fluoride complexes of these structures were elucidated it was clear they formed a cone-like configuration with all the pyrrole molecules orientated in one direction forming four NH hydrogen bonds to the anion. From the shorter hydrogen bond distances 2.790(2) Å compared to 3.264(7)–3.331(7) Å) for fluoride and chloride respectively it was surmised that the fluoride anion was bound more tightly in the solid state.[78] This preference was paralleled in the solution phase anion binding results, with a strong selectivity for the fluoride anionic guest with a stability constant of 17 170 M^{-1} compared to 350 M^{-1} with chloride in dichloromethane for receptor **16**.

Although NH has been the most prevalent hydrogen bond donor used in anion receptors, other hydrogen bond donors have been used on their own or in addition to NH. Few research groups have studied hydroxy binding which is interesting considering its prevalence in nature as a hydrogen bond donor and acceptor. Smith and co-workers performed a high throughput assay[80] screening some simple bisamides and phenols for chloride affinity and catechol **18** was identified as a potentially useful chloride receptor. Following this a more in-depth anion binding study was performed for the compounds shown in Figure 1.15.[81] **18** showed strong binding and selectivities for chloride with a binding affinity of 1570 M^{-1} for chloride compared to 55 M^{-1} for bromide in acetonitrile; it also outperformed **19** which had a chloride affinity of 110 M^{-1}. This was attributed to the more effective positions of the OH groups around the ring for catechol **18**. They also demonstrate nitro-catechol **20** has higher halide binding affinity (Cl^- 3800 M^{-1}), as a consequence of the electron withdrawing nitro-group, an effect that has been noted previously.[81]

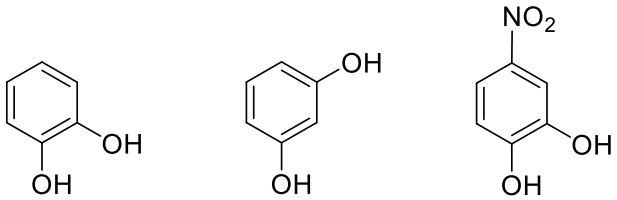

Figure 1.15 Structures of the phenolic compounds, from left to right, catechol, resorcinol and nitrocatechol.

Further examples of hydroxyl-containing receptors include those reported by Kondo *et al.*[82,83] shown in Figure 1.16. Receptor **21** was found to have promising Cl^-, $H_2PO_4^-$ and AcO^- binding ability in acetonitrile, with the confirmation that the OH groups are involved in the binding event.[82] Receptor **22** was the first silanediol based anion receptor and was found to function as a strong anion receptor specifically for acetate and chloride with association constants of 5570 M^{-1} and 144 M^{-1} in chloroform

respectively. More recently it has been developed with anthryl and pyrenyl groups appended to improve its ratiometric response.[84]

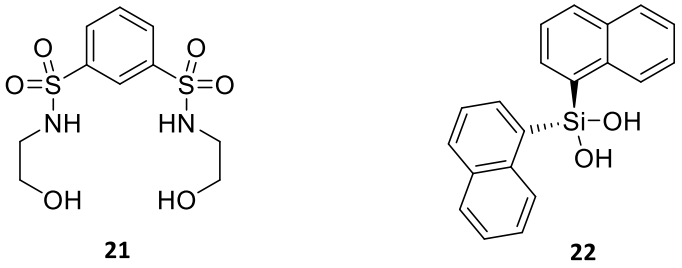

Figure 1.16 Structures of hydroxyl containing anion receptors **21** and **22** from Kondo *et al.*

The use of CH hydrogen bond donors has been slightly less prevalent than NH donor's due to their less acidic nature resulting in weaker binding energies. However, use of multiple weakly binding hydrophobic CH moieties can be valuable when attempting to bind hydrophobic anions.

Existing macrocyclic structure **23** in Figure 1.17 was used to bind HF_2^- a commonly overlooked anion for binding, despite its prevalence in acidic fluoride solutions. Ramabhadran *et al.*[85] used computer aided design and solution studies to model **23**'s binding with HF_2^- using Cl^- binding as calibration, HF_2^- was found to bind in a tilted conformation with a binding affinity 25 x less than Cl^- in chloroform solution. Computer aided design was then utilised to reshape and elongate the triazolophane **23** to design receptor **24**. Adding electron withdrawing groups and intramolecular hydrogen bonds allowed for the accommodation of HF_2^- in a non-tilted conformation. The binding affinity was found to be equivalent to Cl^- in chloroform with a K_a- 6.2 x10^5 M^{-1}.[85]

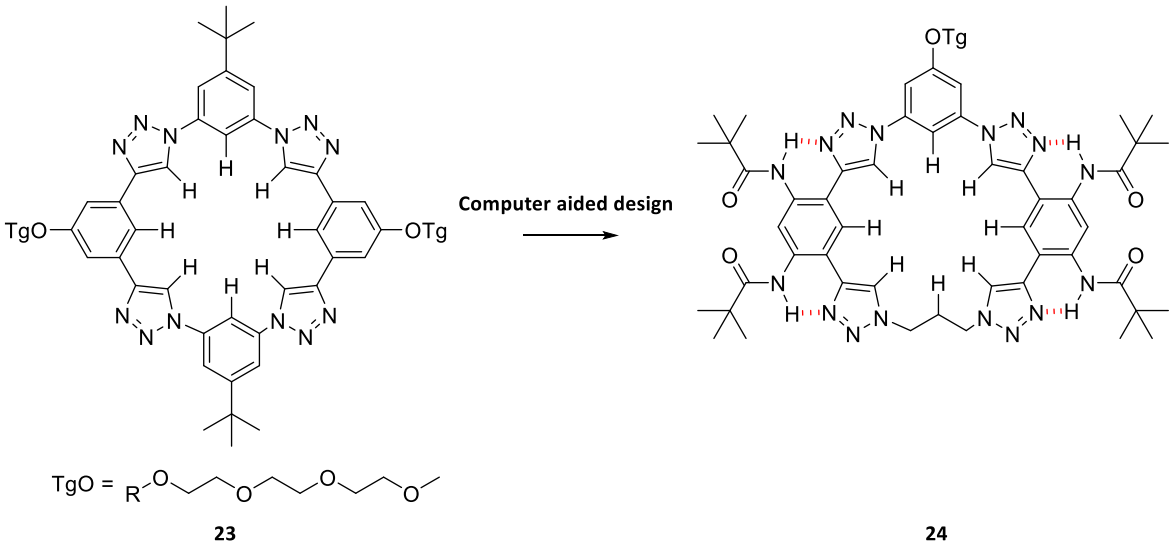

Figure 1.17 Original and modified triazolophane, created by computer aided design.

Halogen bonds are another anion binding approach frequently utilised in this field.[68,69] According to IUPAC a halogen bond "occurs when there is evidence of a net attractive interaction between an electrophilic region associated with a halogen atom in a molecular entity and a nucleophilic region in another, or the same, molecular entity."[86] Usually the halogens are thought of as electron rich, however, the distribution of the electron density is anisotropic especially when involved in the formation of one covalent bond.[87] An electropositive crown is formed opposite the covalent bond which known as a σ-hole, and can act as a halogen bond donor to anions. The stronger the electron withdrawing groups covalently linked to the halogen atom, the more exaggerated the σ-hole, for interaction with an anion, becomes. This effect is more apparent for heavy, polarisable atoms like iodine and hence these halogens form the strongest halogen bonds.[87,88]

Halogen bonding in anion recognition was demonstrated by Metrangolo and co-workers.[89] They found the tripodal receptor **25** could bind NaI selectively, due to the presence of anionic and cationic binding sites. The binding of receptor **25** was much more effective than for receptor **26** which does not form traditional halogen bonds, with binding constants of 2.6 x 10^5 and 1.3 x 10^4 M^{-1} in chloroform respectively. Drawing inspiration from the positive results seen for I^- binding using the iodoperfluorobenzoate groups Taylor and co-workers designed a urea based receptor which could alter the anion selectivity seen previously in the literature.[90] The addition of a urea enabled the anion to potentially participate in both hydrogen bonding and halogen bonding and therefore increasing its overall anion affinity. Figure 1.18 shows the proposed binding mode of the urea based receptor **27**, with near linear halogen bond formation as suggested by computational modelling. The authors propose the improved association constants with chloride (2.4 x 10^3 M^{-1} in MeCN-d_3) are due to the four bonding interactions more efficiently surrounding the spherical anion.[90]

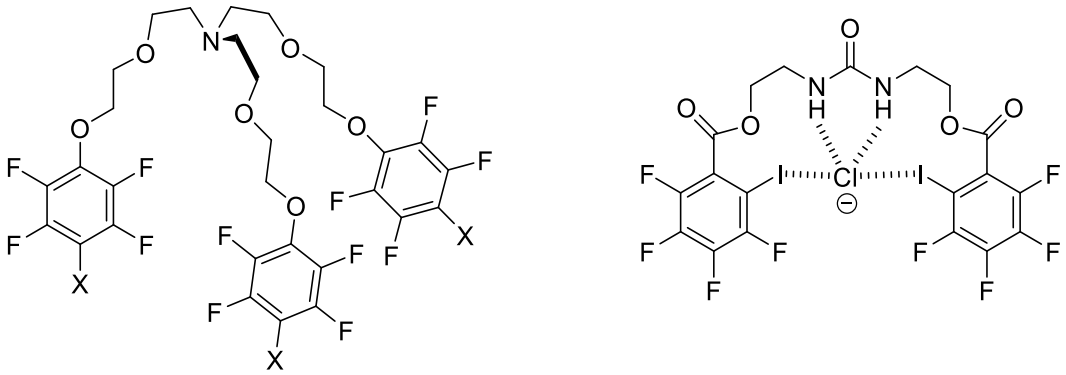

25 X=I
26 X=F

27

Figure 1.18 **Left-** Structure of the tripodal receptor used for halogen bonding by Metrangolo and co-workers. **Right-** Urea based halogen bonding receptor utilised by Taylor and co-workers.

Other forms of interactions, van de Waals forces, hydrophobic interactions, solvophobic interactions, aromatic interactions such as π-π stacking and anion- π interactions are utilised in the anion recognition field. However, they tend to be used in combination with other approaches due to their weaker nature.

Further considerations for anion binding, investigated by a collaboration of Sessler, Schmidtchen and Gale, are the solvent effects on the association constants.[91] The investigation was initiated after disparities in solution phase anion binding data for calix[4]pyrrole **16** were noted. The binding of **16** with TBA chloride salts in a range of solvents spanning different polarities and dielectric constants was probed. Binding constants were measured in acetonitrile, dimethylsulfoxide, nitromethane, 1, 2-dichloroethane and dichloromethane by both isothermal calorimetry and NMR titration techniques. The binding constants were found to be very dependent on the solvent used, with a K_a range of $4.3 \times 10^2 - 2.5 \times 10^5$ M^{-1} observed for the different solvents. Dichloromethane showed the weakest binding and acetonitrile the strongest. Interestingly the differences in binding affinity for the solvents did not correlate with any of the solvent's properties (permittivity, polarizability, dielectric constant, donor or acceptor strength of the solvent). It was noted that in general weaker anion association was observed in more polar solvents, most likely due to the competition with water. However, as solvents became less polar, counter ion effects were more apparent which also reduced the anion binding affinity. The authors recommended anion binding should be performed in the same solvents with the same counter ion to allow for comparative data, and that binding characterisation in a range of different solvents and using different counter ions is essential in the development of new anion receptors.[91]

1.3.2 Advanced anion binding and applications

Many research groups have utilised colourimetric sensors for the development of naked eye anion recognition receptors. One of the first examples of this was by Nishizawa *et al.* who utilised a donor-acceptor chromophore where a thiourea binding motif is appended to a *p*-nitrophenol group (Figure 1.19).[92] In this case hydrogen bonding to the anion stabilised the excited state of the chromophore **28**, accompanied by a charge transfer from the thiourea donor nitrogen to the electron-withdrawing nitro- group. This stabilisation induced a bathochromic shift in the absorption spectrum and a naked eye colour change from colourless to yellow.[92] Selectivity however, was not particularly apparent with this receptor.

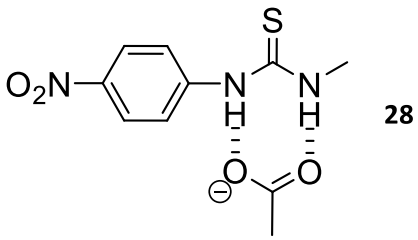

Figure 1.19 Structure of the binding mode with acetate of the nitrophenyl thiourea **28**.

Due to the increasing interest in naked eye anion recognition, with particular uses for anion detection purposes in nature and industry, Sessler and co-workers embarked on a study of simple commercially available colorimetric amines.[93] The project entailed observing changes in the absorption spectra of a range of compounds, including the two diaminoanthraquinones depicted in Figure 1.20, upon addition of F^-, Cl^-, Br^-, I^-, $H_2PO_4^-$ and HSO_4^- in DCM. Vivid colour changes were observed with several of the compounds and specific anions. 1, 2-Diaminoanthraquinone **29** exhibited a change from the compound alone (yellow) to purple with F^-, to red with Cl^- and to orange with Br^-. Differentiation of the halides was a remarkable result for a compound already available commercially. 1,8-Diaminoanthraquinone **30** also gave colour changes but 1,4- and 1,5-, diaminoanthraquinone showed no significant changes. The authors proposed that less basic anions e.g. halides (excluding F^-) do not interact significantly with single NH groups, and suggested that the 1, 2- and the 1, 8-positions are close enough that both NH sites can be involved in the binding event.[93]

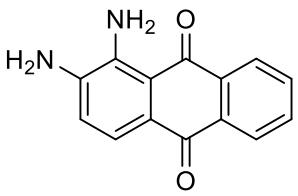

29

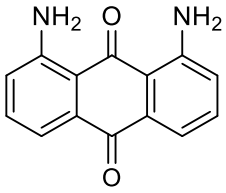

30

Figure 1.20 Structures of 1,2-diaminoanthraquinone and 1, 8-diaminoanthraquinone.

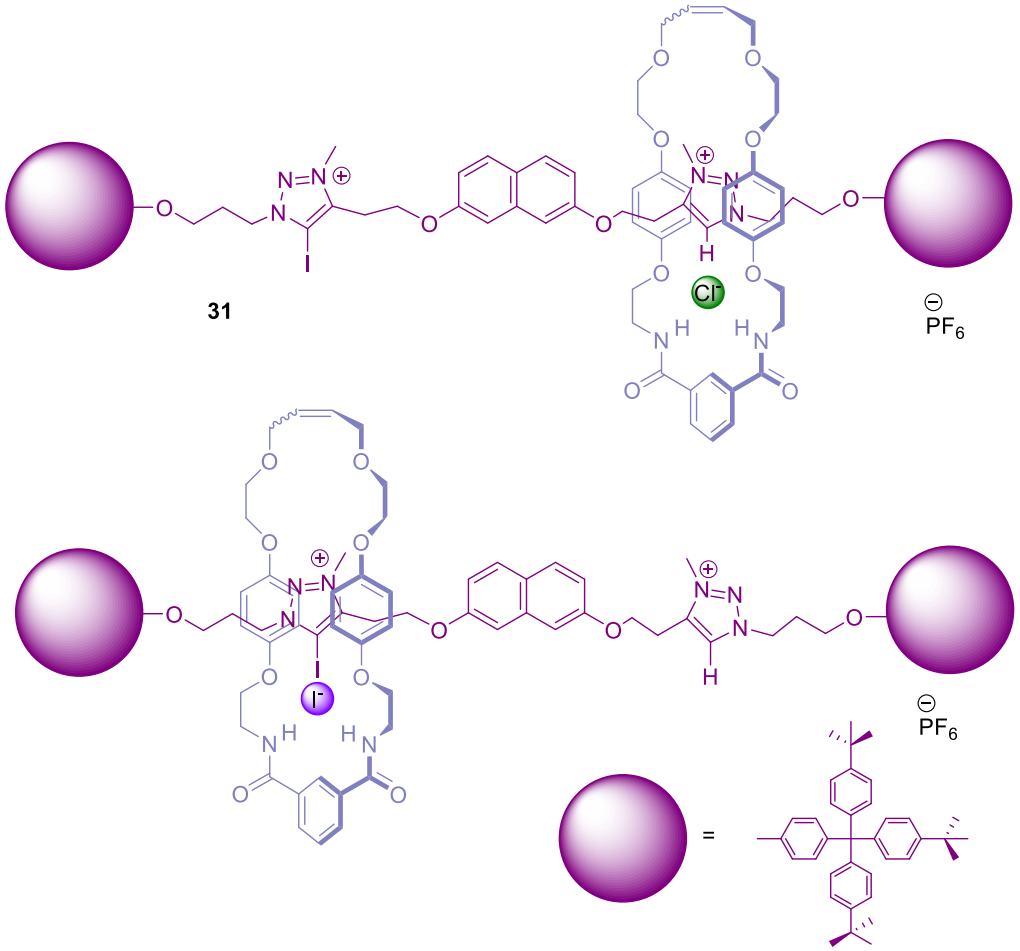

Figure 1.21 Beer and co-workers' two station rotaxane, top- with Cl^- bottom-with I^-.

In addition to anion recognition, the complexation of anions can be used in the assembly of mechanically interlocked molecules and templating. Beer and co-workers reported using halogen and hydrogen bonding anion recognition to control molecular motion within a two station rotaxane **31** (Figure 1.21).[94] One anion recognition site contained an iodotriazolium halogen bonding station and the other utilised a protic triazolium for hydrogen bonding. The isophthalamide containing macrocycle preferred to reside at the prototriazolium site in the absence of anions and in the presence of Cl^- anions with the formation of CH---Cl^- and NH---Cl^- hydrogen bonds. Addition of I^- caused a conformational change, with the macrocycle shuttling to the iodotriazolium station to allow for CI---I^- halogen bond formation in addition to NH---I^- hydrogen bonds.

Using light as an external trigger, Feringa and co-workers designed a bis-urea based receptor **32** that upon irradiation could interconvert between three isomers with different phosphate complexation properties.[95] Figure 1.22 displays the three accessible isomers, the *cis* isomers were found to have a much higher binding affinity for $H_2PO_4^{2-}$ than the *trans* isomer, proposed to be due to the co-operative binding of four hydrogen bonds as opposed to only two in the *trans* isomer. The authors observed a higher binding affinity for the stable *cis* isomer than for the unstable form, attributed to

the difference in torsion angles around the central double bond found from computational models, resulting in a more open binding site for the unstable *cis* form. ^{31}P NMR was used to demonstrate the ability to control the levels of phosphate bound by switching between isomers.

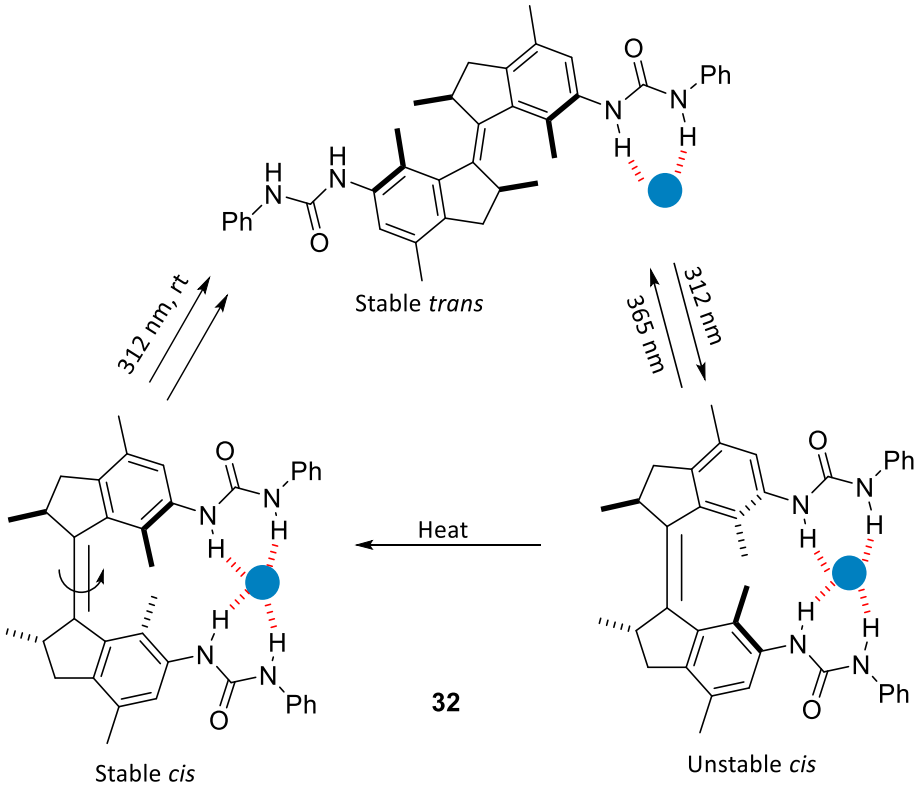

Figure 1.22 Proposed isomerisation behaviour and anion binding modes of bis-urea designed by Feringa *et al.*[95]

1.4 From anion binding to anion transport- the development of synthetic anion transporters

Initiated by the success of selective chloride binding using small synthetic receptors, supramolecular chemists began to design receptors with the ability to transport anions across lipid membranes as potential therapeutics for channelopathies, such as CF. The following section discusses the development of these transporters and methods used to test the transport within the laboratory and in cell based assays.

1.4.1 Overview of transport assays used in past and present literature

The majority of anion transport studies reported have used synthetic lipid vesicle assays.[96] These assays are a simple and versatile method allowing for a diverse range of internal and external solutions to be utilised, meaning a range of anion transport processes can be investigated. Measurement of the actual transport is simple but varied, especially for chloride transport. Ion selective electrode techniques,[97] halide selective fluorescence probe lucigenin[98] and pH sensitive probe 8-hydroxypyrene-1,3,6-trisulfonic acid (HPTS)[33] have all been successfully used to monitor anion transport and will be discussed briefly in the following section.

Unilamellar vesicles

Generally, large unilamellar vesicles (LUVs) are used in laboratory transport assays, they are synthesised from pure phospholipid and are one of the simplest models of a lipid bilayer. When testing new synthetic anion transporters, their use is beneficial over the use of cells due to the lack of membrane proteins, so any transport observed is solely attributed to the synthetic anion transporter. Details of vesicle preparation can be found in the experimental details and follow well reported methods from the literature.[96,99] These simple cell models allow for the control of the composition of internal and external solutions, be it salt composition, concentration or pH which allows for boundless experimental possibilities.

Ion selective electrodes

Ion selective electrodes (ISEs) can be used to monitor the concentration of anions in the external solution, the electrode is 'blind' to the anions encapsulated inside the vesicles. Anion transport (commonly chloride) facilitated by a synthetic receptor from the internal to the external solution is usually driven by the anion concentration gradient, this dissipation in gradient is measured by the ion selective electrode. The electrode potential can be converted into equivalent anion concentration, normally calculated using an electrode calibration curve built with NaX solutions of

known concentration. At the end of a transport experiment the vesicles can be lysed with detergent giving a value for '100 %' anion efflux.

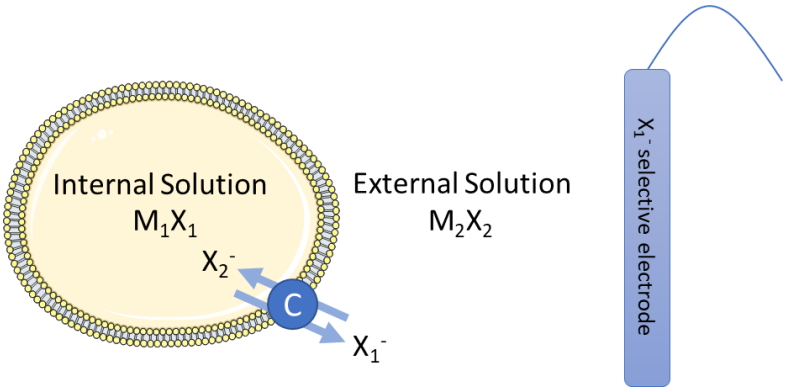

Figure 1.23 A schematic of a lipid vesicle assay used to measure anion efflux by ion selective electrode. C= anion transporter, X_1 = internal anion to be measured, X_2= external anion, M_1 and M_2 = Metal cations. In this case the transporter can dissipate the anion concentration gradients via an antiport mechanism.

Common fluorescence assays

Two common fluorescent probes utilised in transmembrane transport assays are HPTS and lucigenin (Figure 1.24). HPTS is a membrane impermeable fluorescent probe sensitive to changes in pH,[100] it can be encapsulated inside a vesicle and can monitor intravesicular pH by measuring the ratio of its acid form (λ_{ex} = 403 nm, λ_{em} = 510 nm) and its basic form (λ_{ex} = 460 nm, λ_{em} = 510 nm). Matile and co-workers have utilised this probe extensively to measure anion transport indirectly.[26,33,101] A transmembrane pH gradient is applied to the vesicles encapsulated with a metal salt (MX) and HPTS. Addition of the anion transporter can facilitate the dissipation of the pH gradient by A^-/OH^- antiport, H^+/A^- symport, M^+/H^+ antiport or M^+/OH^- symport.

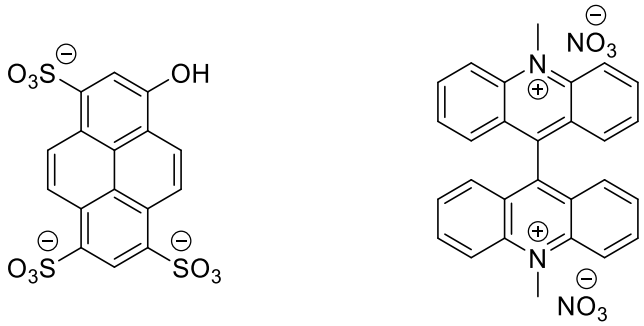

Figure 1.24 The structures of pH sensitive probe HPTS and halide sensitive probe lucigenin (λ_{ex} = 368 nm and λ_{em} = 505 nm).

Lucigenin is a membrane impermeable fluorescent probe selectively sensitive to halides,[102] its fluorescence is quenched by their presence. It can be encapsulated inside a vesicle and can be used to measure chloride influx or efflux,[98] giving either quenching or enhancing fluorescence effect. This probe is used throughout the literature and is particularly useful when an anion transporters lipophilicity prevents delivery to the membrane and pre-incorporation within the vesicle is necessary. A pulse of chloride can instead be added to the vesicle suspension to initiate the transport, which is not possible with and ISE set up.

Quantification of anion transport

There are a number of ways anion transport has been quantified, one of the most common ways is using Hill analysis.[103] First proposed by A. V. Hill in 1913, the Hill equation was used to model the cooperative oxygen-iron interactions involved in haemoglobin within blood. Since then the equation has been widely applied to pharmacological modelling[104] and Equation 1.1 is the adapted version used to calculate the effective concentration of transporter required to facilitate 50 % anion efflux (EC_{50}).

$$y = \frac{V_{max} \times x^n}{k^n + x^n}$$

Equation 1.1 The adapted Hill equation used to calculate EC_{50} values. y is the anion efflux at a time point, k is the EC_{50}, V_{max} is the maximum anion efflux possible and n is the Hill coefficient, reported to represent the average stoichiometry of host to guest involved in the transport.[104–106]

Dose response studies must be performed for Hill analysis, but the method can be applied to a variety of different assays including the fluorescence and ISE methods discussed above (using fluorescence response and anion efflux percentages). Calculation of EC_{50} values allows for direct comparison of transport efficiencies of a range of different receptors.

Other methods to quantify transport data include calculating transport half-life values from initial transport rates and reporting transport rates with respect to receptor to lipid ratio. This approach is commonly used for lipophilic transporters that are be pre-incorporated into the vesicles as the approximate concentration of receptor localised within the bilayer is known.[107,108]

1.4.2 Development of anion transporters

The first breakthrough in the field of anion transport came from Gokel and co-workers who designed and prepared the first synthetic voltage gated chloride membrane transporter **33**.[109] During the

design process the authors noted that proline was found in many naturally occurring anion channels. This led them to develop a transporter with an amino acid sequence that centred around a proline residue (Figure 1.25) flanked with glycine residues. The authors proposed it would insert into lipid membranes, due to its design as a mimic for a phospholipid monomer, in its size, polarity and functional group position. Voltage clamp methods using a planar lipid membrane supported the formation of a stable anion selective, membrane spanning pore.

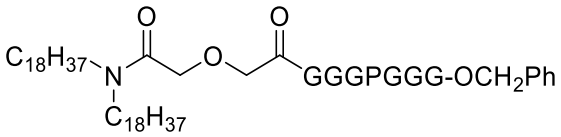

33

Figure 1.25 The first membrane anchored peptide channel, selective for Cl^-.

Following this seminal work chloride transport facilitated by a small synthetic transporter was reported by Davis, Sheppard, Smith and co-workers, utilising steroidal based receptors the 'cholapods' depicted in Figure 1.26. Derived from cholic acid they displayed high binding affinity for chloride (>10^7 M^{-1}) tested using an extraction method from a water saturated chloroform solution. They were found to function as chloride transporters by NMR, electrochemical and fluorescence methods.[110]

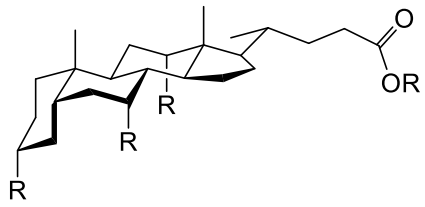

Figure 1.26 The general structure of the cholapods reported by Davis, Sheppard, Smith and co-workers.

Matile and co-workers then demonstrated a novel method for the transport of chloride, synthesising oligo(*p*-phenylene)-N,N-naphthalenediimides (O-NDIs, Figure 1.27).[31] These O-NDIs **34** were found to function as anion π-slides within egg yolk phosphatidylcholine large unilamellar vesicles (EYPC-LUVs). The vesicles were loaded with pH sensitive probe HPTS, and transport was initiated by addition of a pH gradient. Dissipation of this pH gradient was attributed to two potential transport mechanisms, O-NDI facilitated H^+/M^+ symport or OH^-/A^- exchange. Replacement of the extravesicular NaCl with KCl, RbCl and CsCl had no significant effect on the transport affinity of the O-NDIs, hence the transport was attributed to OH^-/A^- exchange. They employed anomalous mole fraction effects (AMFE) to uncover the ion hopping mechanism, facilitated by the O-NDIs. The chloride transport efficiency in the presence of a mixture of anions (Cl^-/I^-) diminished compared with a solution of pure

Cl^-, suggesting the single occupancy of one binding site by the stronger binding chloride (as compared to I^-), is not sufficient for transport. The pure Cl^- solution allowed for continuous multi-Cl^- hopping along the π-acidic NDI sites. The presence of multiple π binding sites was supported by DFT calculations.

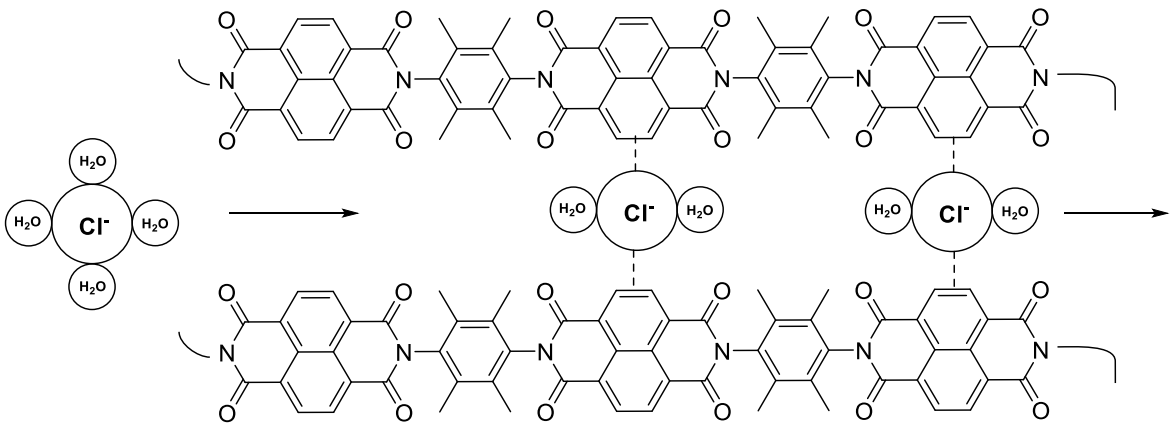

Figure 1.27 Anion- π slides for multi chloride transmembrane hopping.

Matile and other researchers in the field have produced many elegant examples of membrane spanning, pore forming anion transporters that have been reviewed in detail.[26,64,101,111] However, the research in this thesis concentrates on small mobile membrane carriers that bind anions utilising hydrogen-bonding interactions so this will be the focus for the following section.

Davis, Gale, Quesada and co-workers developed conformationally controlled isophthalamide receptors (Figure 1.28),[112] as small synthetic anion carriers. Addition of a hydroxy moiety *ortho*- to the amide in **35** allowed for intramolecular hydrogen bonding from the carbonyl to the proton of the hydroxyl group. This changed the conformation from *syn-anti* (**35**) to a stabilised *syn-syn* (**36**) making the cleft more favourable for hydrogen bonding via the two NH groups due to the element of preorganisation. **37** was made as a control, the authors presumed it would form intramolecular hydrogen bonds from the NH groups to the OMe, stabilising the *anti-anti* conformation; this was supported by the ^{1}H NMR spectra. As expected the preorganisation of the binding site in **36** resulted in stronger binding to Cl^-, Br^- and I^- than **35**. **37** showed no binding presumably due to the NH intramolecular hydrogen bond formation. Transmembrane Cl^- transport was investigated using the halide sensitive fluorescent dye lucigenin encapsulated in EYPC LUVs, and only **36** demonstrated significant transport activity. The transport was also shown to be pH modulated, with the activity ceasing at pH 9.1, seemingly due to deprotonation of the phenol (pKa≈8) and the breakdown of the preorganisation of the binding site.[112]

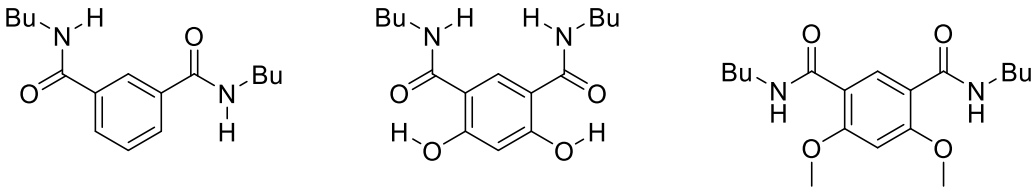

35
syn-anti

36
syn-syn

37
anti-anti

Figure 1.28 Isophthalamides **35–37** for conformational control in their predominant conformations.

Davis and co-workers continued their development of the cholapods, with early structure activity relationship (SAR) studies indicating some correlation between binding strength and transport activity, however, it was still clear that many other factors were involved.[107] This study found **38** (Figure 1.29) to be the most efficient of the cholapods, with a transport half-life of 26 s at a transporter to lipid ratio of 1:25000. This was attributed to the 3α-acetoxy group improving transport and the electron withdrawing NO_2 substituents increasing the acidity of the thioureas and hence giving strong chloride binding. The series was extended to include macrocyclic cholaphanes, which provide a similar array of hydrogen bond donors but a greater degree of anion encapsulation by the additional strap, which is thought to help shield the anion from competing solvent interactions. **39** and **40** were found to improve chloride transport rates by 18x and 4x respectively compared to non-cyclic analogous cholapods. Interestingly the cholaphanes did not significantly increase the chloride binding affinity, confirming that binding affinity is not the sole factor influencing transport rates.[113]

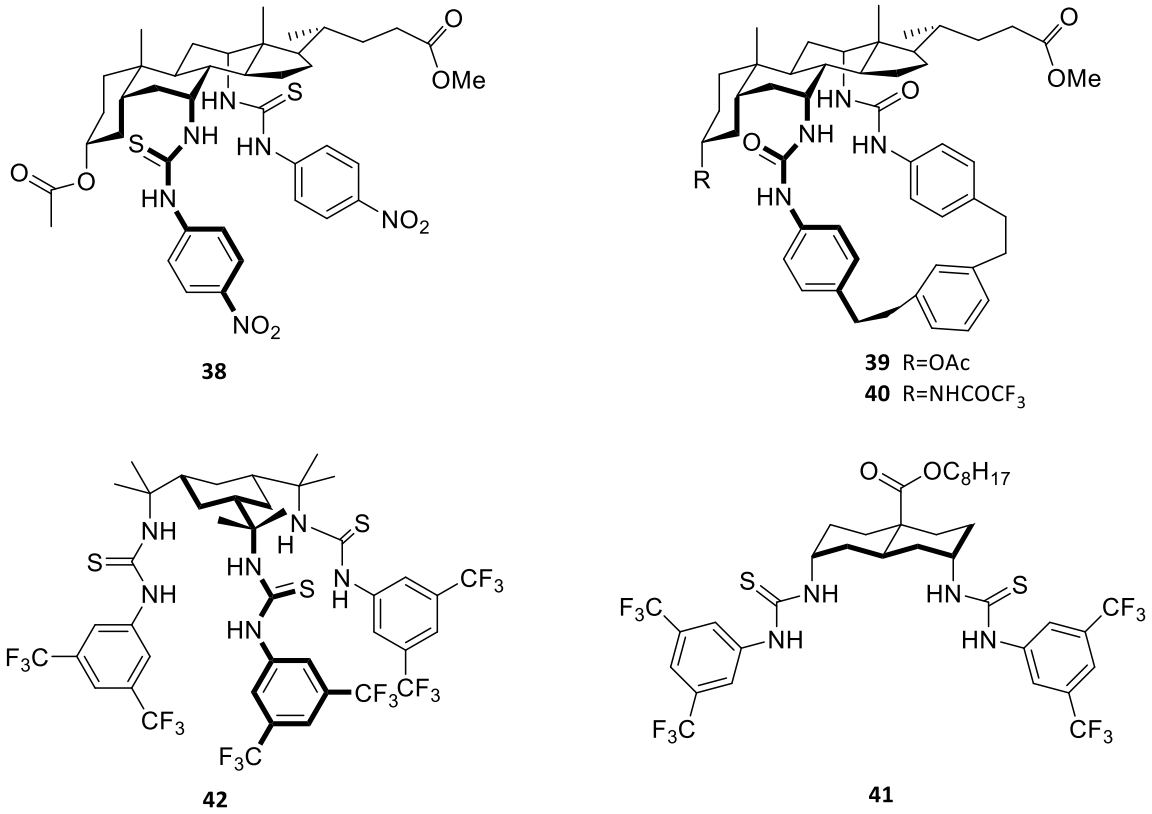

Figure 1.29 Structures of small lipophilic structures developed by the Davis group, **38** is a cholapod, **39** and **40** are cholaphanes, **41** a transdecalin and **42** a cyclohexane.

One drawback of the cholapod scaffold is their extreme lipophilicity (logP≈ 8) which despite lending them high affinity for the bilayer might potentially affect their deliverability in future therapeutic applications. Previous studies had all involved pre-incorporation into the vesicular membrane, as opposed to addition to the aqueous media and then localisation into the membrane. Their high molecular weights also made them less 'drug-like' than other scaffolds.

Davis and co-workers soon started to focus on smaller molecule receptors, that follow Lipinski's rule of five.[114] This states that a compound is more likely to be absorbed by the body and be membrane permeable if its molecular weight is less than 500, its logP is less than five, the number of hydrogen bond donors is less than five and the number of hydrogen bond acceptors is less than ten. This also makes a compound likely to be more deliverable through aqueous media compared to large, highly lipophilic compounds.

In 2011, the Davis group reported the development of diureido trans decalins such as **41** (Figure 1.29) as anion carriers.[115] These scaffolds possessed lower molecular weight, with more compact structures and were more 'drug-like' and less lipophilic than the related cholapods, but they are still

very effective chloride receptors ($K_a > 10^6\ M^{-1}$) and transporters. It was found that appending electron deficient aromatic groups, such as phenyl-bis CF_3 improved transport rates, most likely due to electron withdrawing effects and their lipophilic nature. A further study in 2014 showed **41** could transport Cl^- at a rate of 850 Cl^-/s for a single transporter molecule. This efficiency is comparable to the CFTR protein on a weight by weight basis, which was a remarkable finding. [108]

Additionally, in 2014, the Davis group reported that using simple cyclohexane scaffolds in receptors such as **42** halved the number of synthesis steps required previously for the decalins and cholapods.[116] These accessible structures were found to be extremely active transporters and include the most active transporter reported by the Davis group to date, which showed significant transport even at receptor concentrations as low as 1: 500 000 with respect to lipid. The new structure maintained the 1,5-diaxial arrangement of hydrogen bond donors, but had an additional binding group and the simplified tri-substituted cyclohexane scaffold allowed for some additional flexibility compared to the decalins and cholapods. The authors found the activity of **42** hard to rationalise, due to its similarity in size and lipophilicity to a phenyl-bis CF_3 substituted cholapod. The transport ability of **42** was three times greater, but its anion binding affinity was ten times less, thus they surmised that the difference in flexibility may change the kinetics (the on-off rates) for binding, which are likely to be critical for transport rate compared to the actual strength of binding.[117]

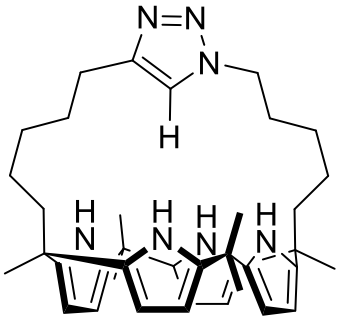

43

Figure 1.30 Triazole strapped calix[4]pyrrole.

Gale and co-workers have developed a range of small molecule transporters utilising NH binding groups including ureas,[118] thioureas,[119] squaramides,[120] indoles[121] and pyrroles[46]. Following the success of calix[4]pyrroles as anion receptors, their transport mechanisms were investigated in 2008.[97] During a collaborative study by Gale, Quesada and Sessler the *meso*-octamethylcalix[4]pyrrole **16** was found to transport CsCl across a vesicle membrane measured with a chloride selective electrode. CsCl was encapsulated inside the vesicle and transport was explored with external solutions containing $NaNO_3$ and Na_2SO_4. A positive response for transport with the

latter supports a M^+/Cl^- symport mechanism, as transport ability is maintained despite the change to highly charged, hydrophilic external anion[122] SO_4^{2-} (which is unlikely to be transported). This symport mechanism was confirmed by changing the internal solution to NaCl, KCl and RbCl, and observing no chloride efflux in the presence of these different cations. The authors proposed that this is most likely due to reduced size complementarity for different cations with the underside of the cone-like pyrrole ring observed when an anion binds.[78,79] Chloride transport was attributed to a caesium selective calixpyrrole-bound ion pair with caesium binding to the underside of the pyrrole ring pre-organising and stabilising the chloride binding to the top of the cone-like form of pyrrole NHs .[97]

Interestingly the addition of a triazole strap (**43**) from opposing *meso*- carbons on the calixpyrrole (Figure 1.30) maintained the CsCl selective transport, but additional Cl^-/NO_3^- exchange was observed within an ISE assay regardless of the presence of caesium. This was attributed to the supplementary hydrogen bond interaction from the triazole CH stabilising the binding of the anion without the need for the ion pair complex formation.[123]

Other work from Gale and co-workers, in early 2010, focused on a series of tripodal tris-(thio)ureas based on tris(2-aminoethyl)amine (tren) which were found to function as Cl^-/NO_3^- antiporters and more significantly as Cl^-/HCO_3^- antiporters.[124] HCO_3^- transport had only been observed on two previous occasions due to the hydrophilic nature of the bicarbonate anion.[125,126] The thioureas **44** and **45** were the most effective transporters in this series, presumably due to their increased lipophilicity, which is a common trend observed with many of these small simple (thio)urea based carriers. An NMR assay was used to measure the HCO_3^- transport directly. Carbon-13 labelled HCO_3^- was loaded inside vesicles, the internal ^{13}C NMR signal was found to be 161 ppm and the external was found at 160 ppm. Addition of transporters **44** and **45** promoted $H^{13}CO_3^-$ efflux, leading to observation of only the external signal at 160 ppm. This was confirmed by addition of membrane impermeable paramagnetic Mn^{2+} which caused the signal to broaden into the baseline confirming the intravesicular $H^{13}CO_3$ had all been exchanged into the extravesicular solution.

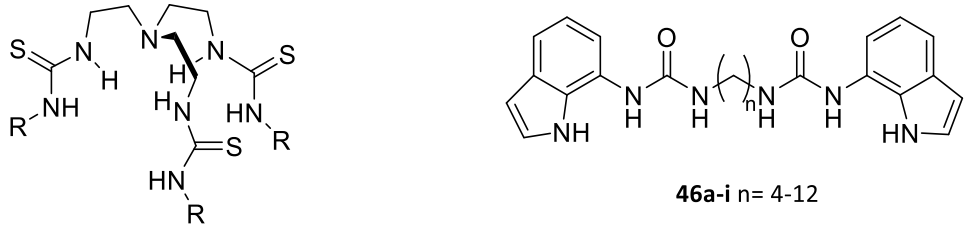

44 R= *n*-Bu
45 R= Ph

46a-i n= 4-12

Figure 1.31 **Left-** tren based thioureas for HCO_3^- transport. **Right-** tuneable bis-indoleureas.

Succeeding this positive result for simple urea based transporters, several other anion transporter scaffolds were utilised for Cl^-/NO_3 and Cl^-/HCO_3^- antiport by Gale and co-workers. Tuneable bis-indole ureas such as **46** were used in a structure activity relationship (SAR) study focused on the variation of alkyl chain length and its effect on the Cl^-/NO_3^- antiport ability.[127] Complementary molecular dynamics simulations found that increasing flexibility of the scaffold reduced the likelihood of multiple binding site co-operation, however the flexibility of the transporter was found to be not necessarily detrimental to the binding affinity. An optimum chain length was found for **46e** (n=9), with longer chained transporters taking longer to internalise into the membrane to allow for them to function.

Studies into the effect of fluorination of anion transporters have been of note, due to fluorinated compounds showing high metabolic stability and less toxicity than their un-fluorinated analogues.[128] In addition to these useful medicinal properties, aromatic fluorination results in increased lipophilicity and hydrogen bond acidity making fluorinated anion transporters an interesting proposition. Busschaert *et al.* utilised SAR techniques to investigate the effect of increasing fluorination on the tren-based urea scaffold.[129] Fluorination was found to increase anion transport abilities compared to un-fluorinated analogues, the authors demonstrated this is most likely due to the increased lipophilic effects as opposed to the increase anion binding affinity using ^{1}H NMR titrations and solid-state analysis. From the same group, Karagiannidis *et al.* also found highly fluorinated structures are amongst the most effective chloride transmembrane transporters. With *ortho*-phenyldiamine bis-urea **48** in Figure 1.32 possessing more effective Cl^-/HCO_3^- antiport activity than the natural product prodigiosin.[118]

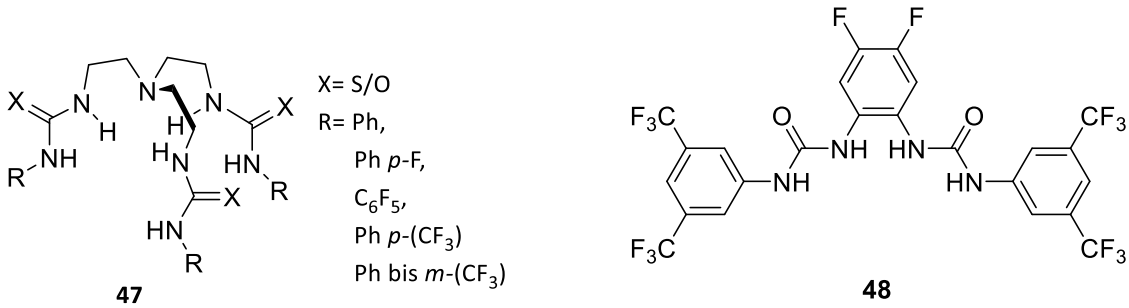

Figure 1.32 **Left-** Fluorinated tren-based thioureas from SAR study and SO_4^{2-} transport. **Right-** structure of the *ortho*-phenyldiamine bisurea.

Following the success of using the urea motif as a hydrogen bond donor, a systematic study was performed with simple analogous ureas, thioureas and squaramides by Busschaert *et.al.*[120] Squaramides had been utilised in anion receptor chemistry notably by Fabbrizzi and co-workers,[130] due to their similar hydrogen bonding array and electronic properties to ureas. More recently

squaramides are believed to be stable to nucleophilic attack and hence they are being utilised in medicinal chemistry research for their reduced toxicity,[131] making them good potential candidates for drugs or anion transporter therapeutics. The squaramide transporters all outperformed their urea and thiourea counterparts, with **49** giving a Cl^-/NO_3^- EC_{50} of 0.01 mol% with respect to lipid concentration. The authors attributed this effect to their greater chloride affinity than their (thio)urea counterparts, with more encapsulating convergent hydrogen bond donors. Deliverability is a key consideration within the field of anion transport, and the ability to improve the transport without significantly increasing the lipophilicity is highly desirable, so this initial squaramide study was promising.

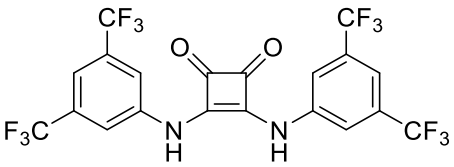

49

Figure 1.33 Structure of most efficient simple squaramide transporter.

Due to the biological relevance of Cl^- and HCO_3^- anion transport studies have generally focused on these two anions. More recently, however, the transport of other anions has been reported. Artificial transmembrane transport of the strongly hydrated sulfate anion was not reported until 2014.[132] Sulfate is abundant in human blood plasma and is a key sulfur source for most organisms,[19] and due to sulfate's large, charge diffuse and hydrophilic nature[122] it is a difficult anion to target for transport. Jolliffe, Gale and co-workers however, have reported that a series of tripodal thioureas (Figure 1.32) based on a tren scaffold and a cyclopeptide scaffold (Figure 1.34) are able to transport sulfate within vesicle assays.[132] Previous ^1H NMR binding studies of the tren based compounds **47** showed a strong affinity for sulfate in DMSO.[129] The cyclopeptide scaffold was used due to its high sulfate binding affinity,[133–135] and its cage like structure was thought to be able to form multiple hydrogen bonds to the anion to shield it from the external environment, vital for transporting something so hydrophilic across a lipid bilayer. The authors demonstrated a direct measurement of sulfate transport across the membrane utilising a novel ^{33}S NMR assay and receptor **50** showed selectivity for SO_4^{2-} over Cl^- and NO_3^-. It was more effective than the tren-based transporters, which the authors attributed to the characteristics mentioned earlier.

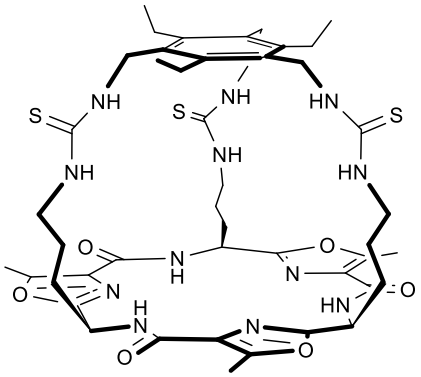

50

Figure 1.34 Tripodal cyclic peptide structure, shown to transport SO_4^{2-}.

The Gale group have reported several examples of the transport of different carboxylate anions.[136,137] It has been noted that the failure of transport of the neurotransmitter glutamate is one of the causes of neurodegenerative diseases such as Huntingdon's and Alzheimer's,[138] making carboxylate structures desirable candidates for transport. Moore *et al.* utilised a series of bis-ureas (Figure 1.35) to demonstrate the transport of fumarate and maleate.[136] The transport selectivity of receptor **51** was found to be pH controllable, due to the different pKa_1 and pKa_2 of fumarate and maleate (3.02, 4.38 and 1.92, 6.23 respectively). At pH 7.2 the only significant transport observed was Cl^-/maleate antiport, presumably due to its predominantly mono-anionic form as opposed to fumarate which would be in the di-anionic form, making it harder to transport. When the pH was lowered to 4 both maleate and fumarate transport was observed. Following this interesting pH control result, Haynes *et al.* attempted to transport lactate and pyruvate selectively.[137] This was achieved by conformational control, receptor **52** was found to be selective for lactate over pyruvate attributed to the additional hydrogen bonding interaction (Figure 1.35) from the carbonyl to the lactate hydroxyl group, stabilising the binding site and further shielding the polar hydroxyl group from the bilayer.

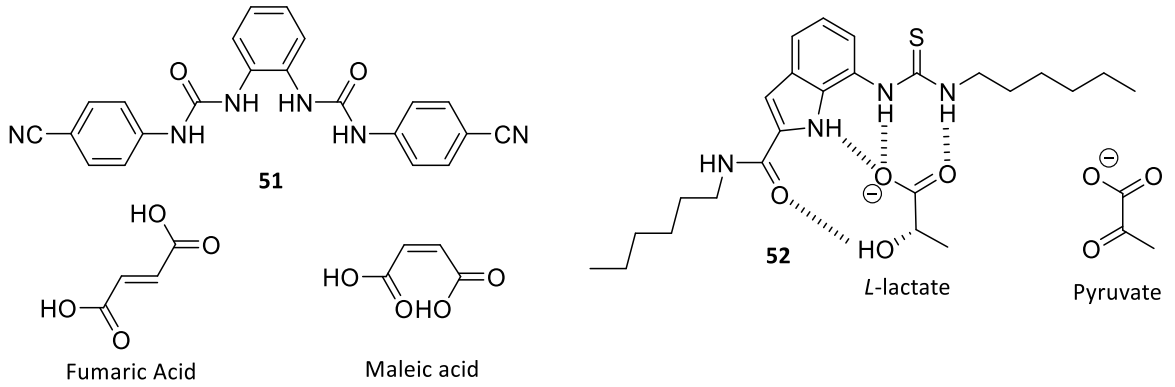

Figure 1.35 **Left-** Structure of one of the bis-ureas **51** utilised for transporting fumarate and maleate, acidic structures shown. **Right-** Proposed binding mode of the amido-indole thiourea **52** structure with *L*-lactate, showcasing the additional hydrogen bonding stabilisation from the hydroxy group, pyruvate structure shown for comparison.

Use of a dual host approach has enabled the transport of glycine across a lipid bilayer. Wu *et al.* used squaramide **49** in combination with the aromatic aldehyde **53** which can bind zwitterionic glycine through a non-covalent interaction (hydrogen bonding from the squaramide to the carboxylate function of glycine), and the formation of one dynamic covalent bond (imine/enamine formation between the aldehyde and amino function on glycine). This dynamic three component complex (Figure 1.36) can diffuse across the membrane where the process is reversed, and the glycine is released. The authors also developed a novel and easy fluorescence assay to measure this amino acid transport which consists of encapsulating a Cu^{2+}-calcein complex (Figure 1.36) within the vesicles. The fluorescence emission of calcein is quenched by Cu^{2+} binding, but is recovered when amino acids compete for the binding of Cu^{2+}. [139]

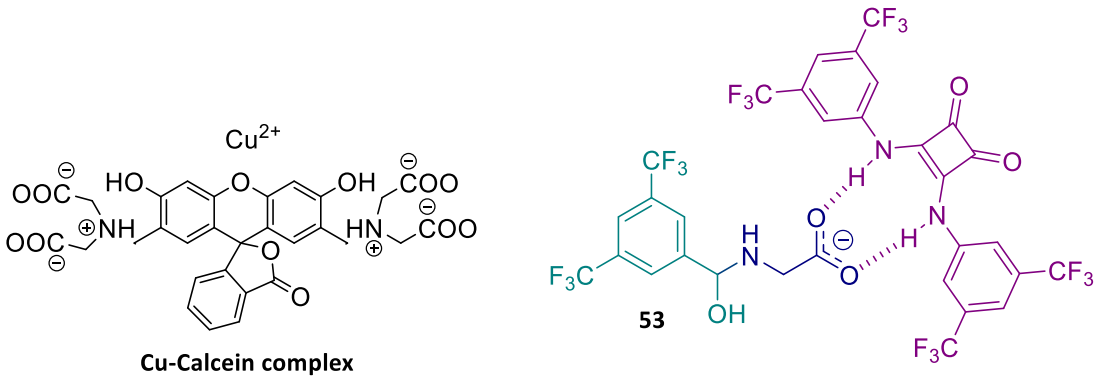

Figure 1.36 Structure of Cu^{2+}-Calcein fluorophore and the dual binding mode for glycine with a hydrogen bonding interaction to the squaramide and dynamic covalent bond formation with an aromatic aldehyde **53**.

In a breakthrough study in 2012, Gokel and co-workers exploited simple isophthalanilides and dipicolinanilides for transporting DNA plasmids into *E.Coli* cells.[140] They found the transport of **54** to be about 2-fold more effective than the DMSO and H_2O controls, **54** was also found to transport larger plasmids of greater than 20 kilobases by ten-fold than that of the controls. The series transport ability diminished in the order of the substituents *sigma* parameter (Hammett coefficient), with **54** being the most effective DNA transformation facilitator with the least electron withdrawing substituents. The authors proposed the binding mode (Figure 1.37) involved the DNA phosphate residues binding into the pocket formed by the tris-arenes, in a 1:1 stoichiometry essentially enveloping the plasmid in a "hydrophobic coat" and diffusing across the membrane.[140]

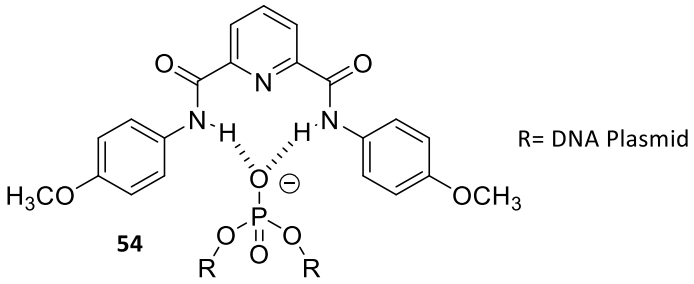

Figure 1.37 Schematic of the proposed binding mode of the phosphate group from within the DNA plasmid by one of the tris-arenes.

An interesting study from Jeong and co-workers demonstrated selective K^+/Cl^- transmembrane symport. By appending an aza-crown ether to a cyano-urea based Cl^-/NO_3^- antiporter the formation of a contact ion pair complex with KCl was achieved.[141] Figure 1.38 depicts the two transporters, the smaller aza-crown **55** showed moderate sodium chloride selectivity and the larger aza-crown **56** demonstrated unprecedented potassium chloride selectivity. The contact ion pair formation was confirmed via single crystal X-ray crystallography, and symport was established using both K^+ and Cl^- selective electrodes.[141]

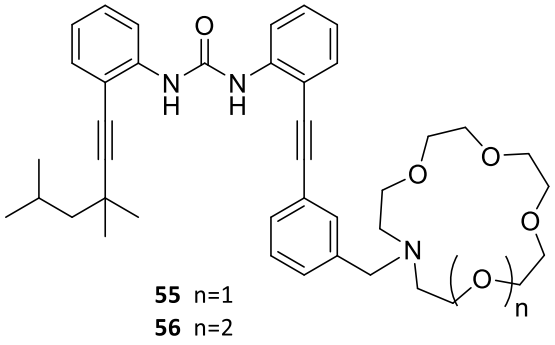

Figure 1.38 Structure of aza-crown ether cyanourea based metal chloride transporters.

In the past five years, focus has turned towards the fundamentals of anion transport, as previous studies have shown there are many competing factors involved in the transport process, the need to ascertain what makes the best transporter is essential. For example, what mechanism is required, be it uniport, antiport or symport for the desired therapeutic effect and the characteristics the transporter must possess to employ this desired mechanism.

To try to answer some of these questions two Quantitative Structure Activity Relationship (QSAR) analyses have been employed.[142] These studies had the aim of elucidating molecular parameters key for efficient transport which could then be used to predict transport properties in the future. The studies involved the building of a database of molecular parameters such as constitutional descriptors, topological descriptors, charge indices, geometrical descriptors and general molecular properties for a series of compounds all from the same class of transporter. The series of compounds had varied substituents and the descriptors for each compound were compared with its transport ability. Computational modelling could then be used to make a model from these values to help predict future proposed anion transporters efficiency.

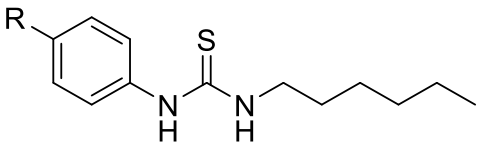

57

Figure 1.39 General structure of the 1-hexyl-3-phenyl thioureas used in the QSAR study. R= Br, CF_3, Cl, CN, $COCF_3$, COMe, COOMe, F, H, I, NO_2, O(CO)Me, OCF_3, OEt, OMe, SMe, SO_2Me, Me, Et, Pr, Bu, Pent.

The study from Busschaert *et al.*[143] used 22 1-hexyl-3-phenyl thioureas **57** with a variety of *para*-substituents (Figure 1.39). Four compounds were removed from the model to use as a test of its prediction power. The Hammett coefficient alone was found to have a strong correlation to the anion binding affinity of the series, due to *p*- substituent effects on the pKa and subsequently the hydrogen donor ability of the thiourea NH's. It was also shown that there was not aromatic CH participation in binding. Overall the model demonstrated the transport affinity was dominated by lipophilicity (logP), with smaller contributions from anion binding (σ_p) and the SPAN parameter (a measure of molecular size). The model accurately predicted the transport ability of the four compounds which were removed from the series prior to modelling. This type of modelling, however, is still limited to similar transporters of the same class, i.e. phenyl thioureas.[143]

Following this promising study from the Gale group, Knight *et al.* also undertook an ambitious QSAR study with a series of 43 tambjamine structures based on Figure 1.6 to see if similar parameters were

important for the transport.[54] Remarkably, even with such different binding motifs, the tambjamine study also showed logP was the most important parameter correlating with transport efficiency. It was found within each tambjamine structural subgroup (e.g. aromatic, halide, alkyl etc), that logP vs log(1/EC_{50}) showed a parabolic dependence, giving an optimal logP for each small group of tambjamines.[54] This supports previous optimum lipophilicity findings within the Quesada group.[53]

With the importance of lipophilicity being consistent throughout the anion transport literature of the past decade a more in-depth study of the balance of lipophilicity was performed in a collaboration from Davis, Gale and co-workers.[144]

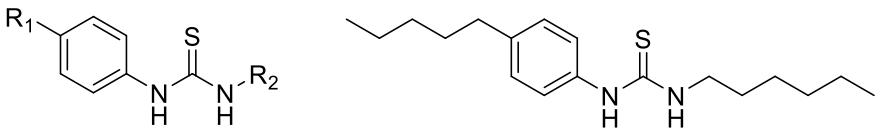

58

Figure 1.40 **Left-** Basic structure of the thioureas used in the lipophilic balance study. R_1 and R_2 were H or alkyl and together = C_{total} = 11. **Right-** Most effective transporter **58** within this lipophilic balance study.

A series of N-arylthioureas were synthesised in the general form in Figure 1.40 where R_1 and R_2 were H or alkyl. The lipophilicity of this system varied according to the total number of aliphatic carbons in R_1 and R_2 (C_{total}), but the anion binding strength was similar across the series. C_{total} was kept constant, making the series of equal binding affinity and lipophilicity, but varying in the binding site position relative to the length of the molecule. The anion transport activity was evaluated using a lucigenin assay for Cl^- transport and this demonstrated that the most effective compound was **58**. Compound **58** had a centrally located anion binding site as opposed to an unequal distribution of lipophilicity on either site of the binding site. This result showed that the balance of lipophilicity plays a significant role in the determining transport efficacy. It was suggested that an even distribution of lipophilicity and a central binding site helps promote transition between the apolar and polar regions of the bilayer. It was also surmised that compound **58** had a reduced activation energy for the transport compared with a compound with uneven distribution of lipophilicity as compound **58** is less stable and less likely to mimic a surfactant (polar head group and lipophilic tail) when it partitions into the lipophilic membrane (Figure 1.41).

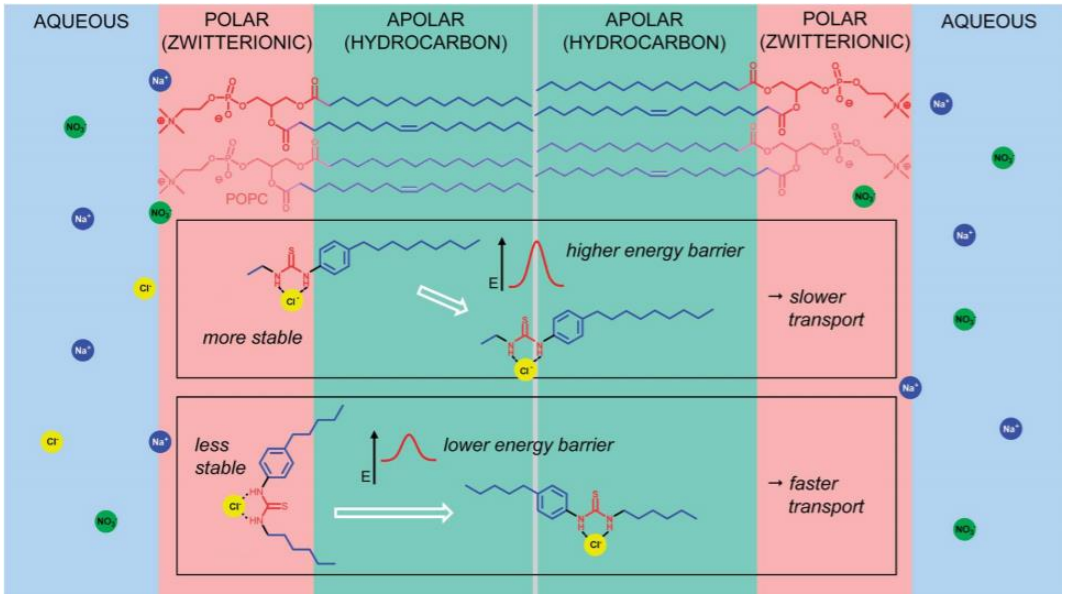

Figure 1.41 Rationale of the effect of lipophilic balance on transport ability by Valkenier *et al.*[144] Reproduced with permission from The Royal Society of Chemistry.

With increasing evidence for lipophilicity being one of the key parameters for the ability of an anion transporter, Spooner and Gale decided to investigate how anionophores behaved in different lipid environments, using phospholipids POPC, POPG, POPE and DPPC (Figure 1.43).[145] Given the need to develop actual therapeutic candidates for use *in vivo,* assessing membrane constitution and its effect on anionophoric ability was vital.

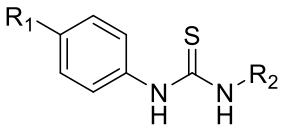

Figure 1.42 General structure of the thioureas used in the study by Spooner and Gale. R_1 and R_2 were differing alkyl chains ranging from H to Octyl.

Figure 1.42 depicts the general structure of the thioureas synthesised for this study with a range of alkyl substituents to span a logP of 2–9. Measurement of the series' transport activity using a standard Cl^-/NO_3^- antiport ISE assay, initially with pure POPC vesicles identified the optimum logP range was 5–6. The same assay was repeated using vesicles composed of POPG and POPE:POPC (3:1) (POPE does not form vesicles alone at room temperature due to a higher phase transition temperature). POPG exhibited slow transport across the range, but POPE containing vesicles showed a faster transport rate which was attributed to relief of the elastic potential energy introduced by the non-bilayer forming POPE constituent. Use of DPPC vesicles at higher temperature (due to high phase transition temperature) showed no significant changes in the rate of transport, suggesting diffusion through the tail region is not rate-limiting. Interestingly, although the rate of transport

changed across the different lipid environments the best transporter remained the same; suggesting the optimum logP is not a property of the lipid membrane but of the class of transporter itself. However, the author stressed it is still important to evaluate the potential lipid environment when designing transporters as they significantly changed the transport efficiency.[145]

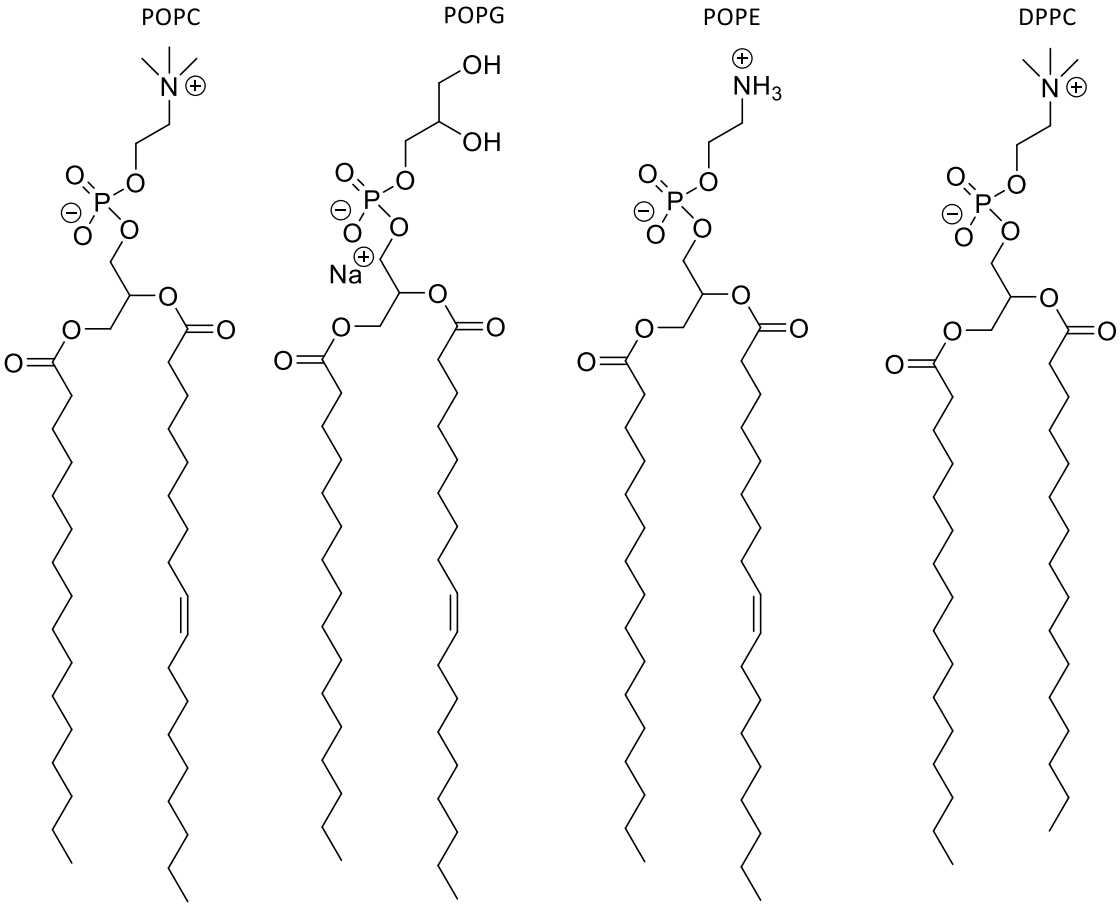

Figure 1.43 Structures of phospholipids utilised in the study by Spooner *et al.* POPC= 1-palmitoyl-2-oleoyl-*sn-glycero*-3- phosphocholine, POPG= 1-palmitoyl-2-oleoyl-*sn-glycero*-3-phosphoglycerol, POPE= 1-palmitoyl-2-oleoyl-*sn-glycero*-3-phosphoethanolamine and DPPC= dipalmitoyl-*sn-glycero*-3-phosphocholine.

With the driving force of anion transporter design always returning to their potential use as therapeutics, it is unsurprising that a number of *in vitro* studies testing anionophores within cells have been published.

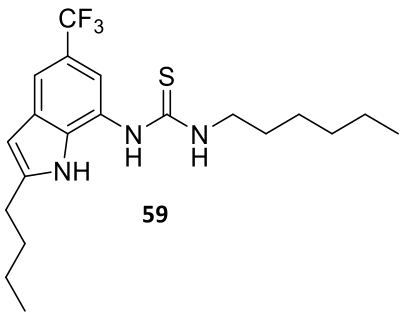

59

Figure 1.44 Structure of the most effective indole-thiourea **59**.

In 2012, Gale and co-workers developed small drug-like indole ureas (Figure 1.44) that exhibited efficient transport within vesicle based assays.[121] They found the introduction of CF_3 groups improved lipophilicity and the overall transport efficiency. Receptor **59** was found to act as an effective anti-cancer agent in GLC4 small-cell lung carcinoma, and in A375 melanoma cells was found to cause apoptosis via acidification of the cell cytoplasm.

Turning the focus to potential CF therapeutics, Li *et al.* undertook a large scale *in vitro* study with the cholapods, trans decalins and cyclohexane receptors, found to be highly efficient lipophilic transporters by Davis and co-workers.[146] They reported a new fluorescence based assay, utilising halide sensitive yellow fluorescent protein-fisher rat thyroid (YFP-FRT) cells. FRT cells are particularly useful in this case due to their lack of epithelial ion channels, and are relatively impermeable to anions. This means the positive response observed can be attributed to the synthetic anionophores.

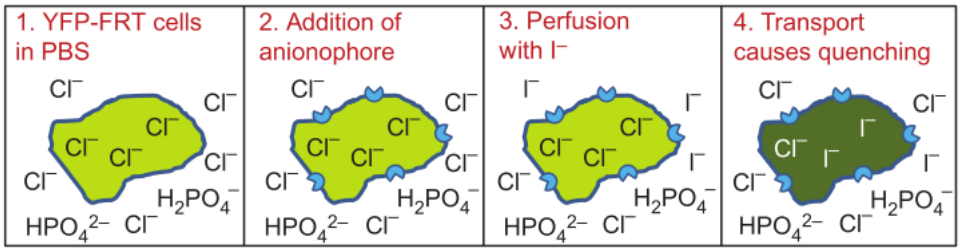

Figure 1.45 Schematic of the YFP-FRT fluorescence based assay used by Li *et al.*[146] © 2015, Rights Managed by Nature Publishing Group.

As seen in Figure 1.45 the cells were incubated with the transporter for 10 min. If necessary for solubilisation, POPC lipid was added to aid deliverability to the cell membrane. The cells were washed with phosphate buffer (PBS) and the fluorescence was monitored using a fluorescence microscope. NaI solution was added externally allowing the compounds to effect Cl^-/I^- exchange across the cell membrane, the influx of I^- quenches the fluorescence of YFP. This response was found to be reversible by washing the cells again with PBS and observing the fluorescence recovery, due to the removal of I^- from inside the cell. The most effective transporter **42** showed significant anion

transport ability, which was still observed after 2 hours of repeated cycles of PBS and NaI confirming the receptor does not leach from the membrane. Additional XTT cytotoxicity studies in three different cell lines showed **42** exhibited little toxicity towards epithelial cells (the cell type most effected in CF) and its transport was unaffected by protein serums which would be present *in vivo*.[146]

In recent work by Shin and co-workers,[147] two strapped calixpyrroles **60** and **61** (Figure 1.46) were found to facilitate Cl^- transport in liposomes utilising a dual host approach with monensin facilitated Na^+ transport coupling to the receptor Cl^- transport. The authors proceeded to try and replicate this process in cells. MTT cell viability assays across a range of cell lines showed **60** and **61** decreased viable cell concentrations in a dose dependent manner, with IC_{50} values of 10–15 μM. Subsequently, they monitored the intracellular ion concentrations using YFP-FRT cells, the YFP fluorescence was quenched by synthetic chloride transport coupled to Na^+ influx through naturally occurring Na^+ channels within the cells to maintain ion balance across the membrane. To support this observation the authors used A549 and HeLa cells with a sodium sensitive probe (SBFI-AM), to confirm this Na^+ influx. Flow cytometry was also used with HeLa and A549 cells treated with fluorescein-annexin V and propidium iodide (PI), and the results suggested positive binding and PI uptake which is indicative of apoptosis.

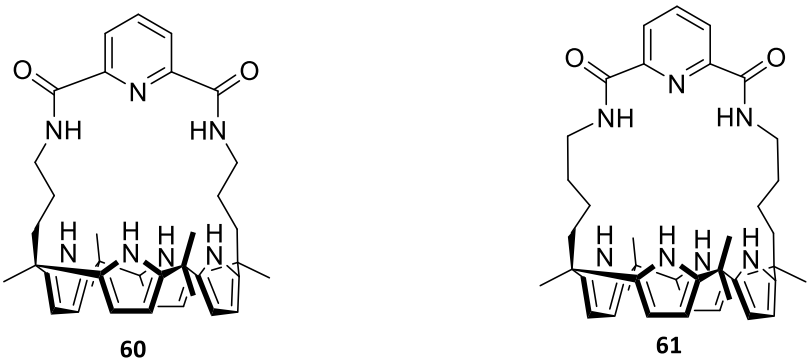

Figure 1.46 Structures of the di-amide strapped calix[4]pyrroles.

The membrane potential probe (JC-1) was then used to confirm the dissipation of the membrane potential which is an additional hallmark of apoptosis. Interestingly, the authors confirmed the apoptotic effects were directly related to the disruption of the natural equilibria of NaCl, as cells cultured in cell media with Cl^- or Na^+ free buffer showed no significant apoptotic effects. Remarkably, additional studies also demonstrated **60** and **61** could facilitate the generation of reactive oxygen species, cause the release of cytochrome C and trigger apoptosis via a caspase pathway.[147]

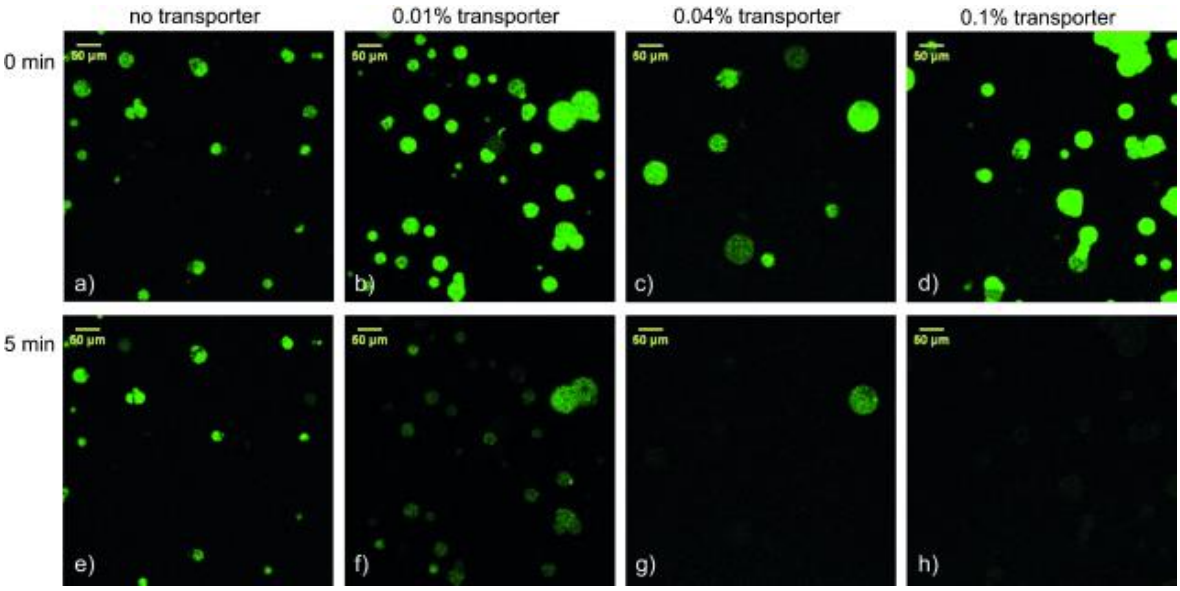

Figure 1.47 Fluorescence microscopy images of lucigenin-containing GUVs, with varying amounts of transporter **42** before and 5 min after addition of NaCl. [148] © 2015 The Authors. Published by Wiley-VCH Verlag GmbH &Co. KGaA.

To gain visual insight into the mode of anionophoric activity, two innovative approaches have been developed by Davis and co-workers and Gale and co-workers. Firstly, Valkenier *et al.*[148] used giant unilamellar vesicles (GUVs) grown on a cross-linked dextran-(polyethyleneglycol) hydrogel substrate containing encapsulated lucigenin as cell-sized models, to enable visualisation of the lucigenin quenching by chloride transport using a confocal microscope. They tested transdecalin transporter **42** from Figure 1.29 within this assay and it exhibited lucigenin dose dependent decay over five minutes, as can be seen in Figure 1.47. This correlated to previous fluorescent results from LUVs, but came with a higher level of certainty owing to the actual visualisation of the effect. Additionally, Rhodamine-B labelled lipid was also added to a GUV suspension to investigate the formation of multilamellar vesicles, which are characterised by a higher intensity of rhodamine B fluorescence around one vesicle and a slower quenching of lucigenin fluorescence.[148]

The alternative approach used by Berry *et al.* was the development of a series of naphthalimide appended (thio)urea transporters **62–64**, to attempt to visualise the anionophores within cells and investigate where they localise.[149] Initially the thioureas **a** (Figure 1.48) were found to be the most efficient transporters within vesicle based assays, whilst the ureas **b** showed no significant activity. MTT cell viability assays were performed for both MCF-7 breast cancer cells and A549 lung cancer cells and **63** and **64** were found to be toxic for both. However, they were more effective against the A549 cells, with the most lipophilic compounds **64a** and **64b** showing the lowest IC_{50} values of 7.7 and 7.6 µM respectively. The compounds were then incubated within A549 cells over a 24-hr period and their fluorescence was monitored using a fluorescence microscope. Interestingly the least

lipophilic and non-toxic transporters **62a** and **62b** were found to localise into spherical organelles after one hour, whereas the more lipophilic and toxic transporters were found distributed homogenously across the cell cytoplasm, locating nowhere specifically. [149]

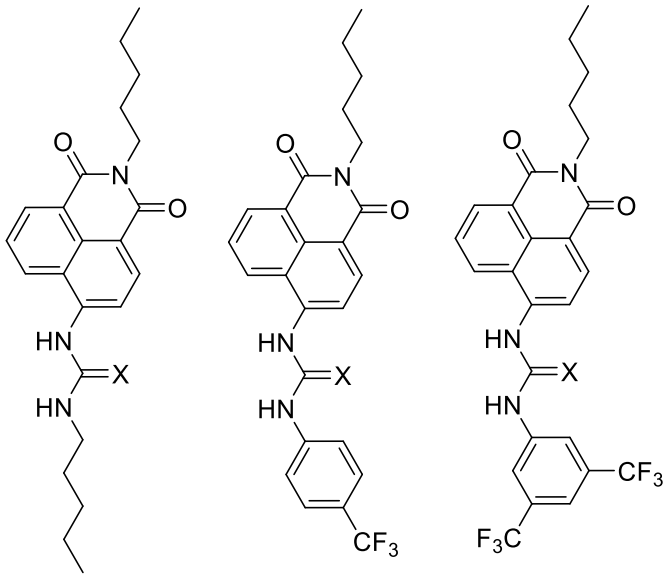

62a X= S
62b X= O

63a X= S
63b X= O

64a X= S
64b X= O

Figure 1.48 Structures of the fluorescent naphthalimide (thio)urea transporters.

Jeong and co-workers demonstrated an unprecedented level of chloride transport control within both laboratory vesicles and YFP-FRT cells, by utilising a series of photo-responsive diazobenzene bis-urea structures.[150] Figure 1.49 depicts the most efficient *meta* receptors **65a** and **65b** tested. The chloride binding affinity was assessed for the *trans* isomers via ^{1}H NMR titrations in DMSO:$CDCl_3$ 1:9. Irradiation with UV light gave the corresponding *cis* isomers which were found to possess stronger binding affinity for chloride by roughly one order of magnitude, which was anticipated by the authors due to the four convergent NH hydrogen bond donors to allow for binding in a chelate manner which the *trans* isomers cannot. In lipid vesicles, the *cis* isomers showed moderate transport rates, with **65a** and **65b** giving EC_{50} values of 0.38 and 0.15 mol% respectively. Conversely, the *trans* isomers showed little to no transport; the authors attributed this to the difference in binding affinity but also the change in structure affecting partitioning and shuttling rates. They also confirmed that chloride transport could be switched on *in situ* via irradiation of the vesicular solution for 20 s. Following these impressive results, *in vitro* cell studies were performed. **65a** and **65b** facilitated reduction of YFP fluorescence in FRT cells compared to controls used, with only the *cis-meta* linked analogues shown in Figure 1.49 showing activity, despite the analogous *para* linked receptors performing well in the vesicle transport studies.[150]

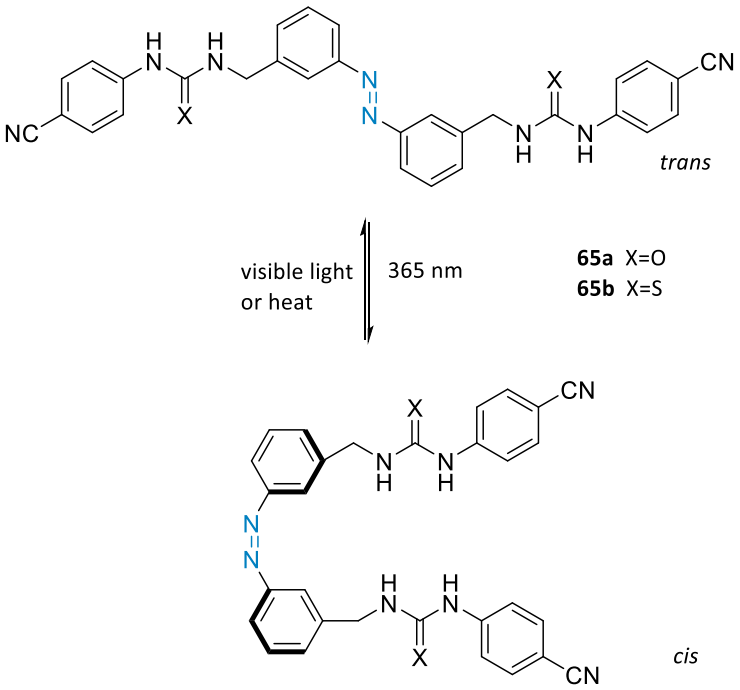

Figure 1.49 Molecular structures of the *meta* linked *cis* and *trans* isomers used in the study by Jeong and co-workers.

1.5 Considerations when designing anion transporters

The field of anion transport is growing. New scaffolds for binding and innovative approaches to monitor and assess transport are being developed each year. The optimum parameters for what makes a successful anion transporter are quickly being clarified, but there is still a way to go if genuine anionophoric therapeutics are to be established outside of *in vivo* applications. It appears that a fine balance of the following properties is key for this development.

From the review of the literature, it is clear the lipophilicity of a receptor plays an intrinsic role in its ability to partition into the hydrophobic tail region of the phospholipid membrane. If a receptor is too lipophilic however, delivery through aqueous media can be hampered. The optimum lipophilicity and the perfect lipophilic balance of a transporter changes with transporter class so it is important to assess this characteristic fully for each new scaffold developed. Binding interactions between the receptor and anion must be sufficient and stable to counteract the energy penalty of desolvation of the anion within aqueous media, binding however must be reversible and kinetically fast to allow for continuous shuttling of anions across the membrane. Increased binding affinity has been achieved in a number of ways with additional hydrogen bond donors or increasing the acidity of existing donors via addition of electron withdrawing substituents.

Solvophobicity of the anion and the receptor must be considered for anion binding and transport. Especially as the process of anion transport involves the desolvation and binding of an anion within an aqueous environment, and the transporting of the anion across the lipophilic membrane to release it within another aqueous environment. It makes sense that an anion's solvophobic effects should be considered. The Hofmeister series,[151–153] traditionally known for classification of ions based on their ability to 'salt out' or precipitate proteins, has also been linked to solvation effects of the ions.[152] Figure 1.50 shows the original Hofmeister series, with sulfate, phosphate and fluoride having a better 'salting out' ability and with it a higher hydration energy, hence their difficultly to bind and transport.

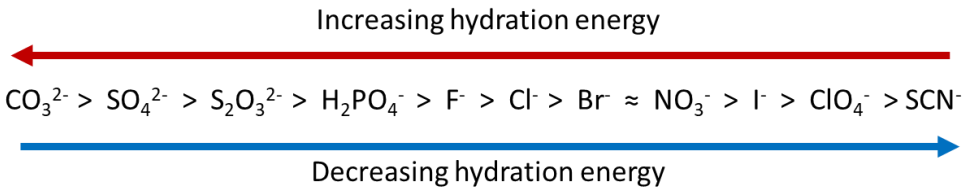

Figure 1.50 The Hofmeister series.

Selectivity, size and shape complementarity of the receptor for the anion transport target is also important. Selectivity is key for their use in the biological environment, it is essential to prevent

unwanted side processes occurring, which may reduce the receptors overall effectiveness. The design of the receptor for a particular shape or sized anion is becoming increasingly viable with the ever-developing field of computational modelling saving precious synthetic efforts. It is also becoming increasingly obvious that the fundamental transport mechanism is key to a transporter's overall effects in live cells be it H^+/A^- symport, A_1^-/A_2^- antiport or M^+/A^- cotransport.[147] In a recent study by Wu *et al* transporters were classified into two categories electrogenic and electroneutral,[154] the former describes a process which changes the net charge across a membrane and the latter does not. Thus, it is vital to fully understand the transport mechanism, before development for a specific therapeutic application begins. This latter point is one on the main focuses for the body of this work and will be discussed in detail later.

Finally, in addition to the balancing act of the aforementioned characteristics of a potential anionophoric therapeutic, ADMET requirements must be fulfilled.[155] These include the absorption, distribution, metabolism, excretion and toxicity properties of a compound. In an ideal world, a compound that is easily absorbed into the blood, distributed quickly to its target, easily metabolised into non-toxic by-products which are easily excreted and has potent anionophoric activity would be a perfect candidate for *in vivo* applications. Generally following Lipinski's rules[114] will help fulfil these requirements, but it is still important to keep in mind when designing a transporter.

1.6 Aims of this thesis

This introduction chapter has discussed some key developments in the fields of anion binding and transport from their beginnings to more recent times, and as mentioned in the previous section the optimum parameters for what makes a good transporter are rapidly being clarified. The aims of this thesis are to continue the development of new chloride transporting scaffolds whilst also broadening the field of anion transport targets as essential biological functions come to light. Using the new knowledge gained from structure activity relationship analysis and the ever-strengthening link between transport mechanism and action in cells from the literature is essential for successful development of anion transporters with actual therapeutic promise.

In the process of addressing this challenge, three pathways were followed, leading to the three chapters within this thesis. Binding and transport studies were evaluated by titration techniques and vesicle based assays discussed earlier. Chapter 2 examines a new binding motif for chloride and its anion binding and transport properties. Chapter 3 scrutinises a previously used calix[4]pyrrole scaffold for a new anion transport target, and due to the recent development of new mechanism elucidating assays chapter 4 evaluates the halide transport mechanism and selectivity of an extended series of these legacy receptors.

Chapter 2: Binding and transport study of a series of dibenzamide based receptors

Parts of the work in this chapter has been published as Harriet J. Clarke, Wim Van Rossom, Peter N. Horton, Mark E. Light and Philip A. Gale (2015). "Anion transport and binding properties of NN' –(phenylmethylene)dibenzamide based receptors" *Supramolecular Chemistry* **28**: 10-17.

2.1 Introduction

Ureas and thioureas have previously been found to form stable complexes with a range of anions and have been used successfully as transmembrane chloride transporters.[156,157] A 2011 study by Andrews *et al.* compared the chloride transport ability of a simple series of (thio)ureas and (thio)amides **66–71** (Figure 2.1). The urea based receptors were found to function more efficiently than the analogous amide structures,[119] presumably due to their increased number of hydrogen bond donors (NHs) and their ability to bind the anion via two convergent hydrogen bonds. Previous studies have also shown isophthalamides and squaramides can facilitate chloride transport,[125] once again utilising the convergent hydrogen bonding motif.

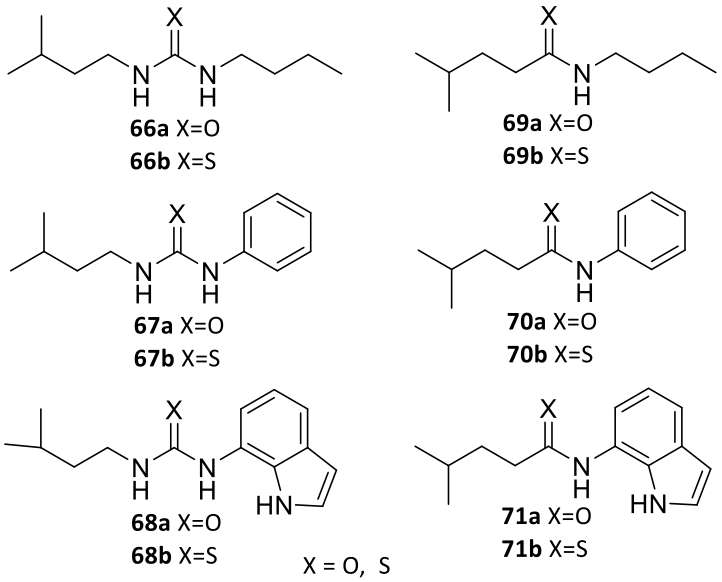

Figure 2.1 The structures of a simple series of (thio)urea and (thio)amides utilised for a comparative transmembrane study by Andrews *et al.*

Encouraged by the effectiveness of these motifs in anion receptor, transporter and self-assembly chemistry a series of N, N′- (phenylmethylene)dibenzamide based receptors were synthesised (Figure 2.2) and their binding and transport affinity was studied. Biological studies into the function

of cannabinoid receptors (CB_1 and CB_2), present throughout the body, which are known to modulate appetite, memory and pain sensation, found functionalised bis-benzamide structures were able to bind in the cannabinoid receptor pocket via hydrogen bonding, acting as inverse agonists.[158] These favourable binding properties made this bis-benzamide motif an interesting possibility for anion binding and transport.

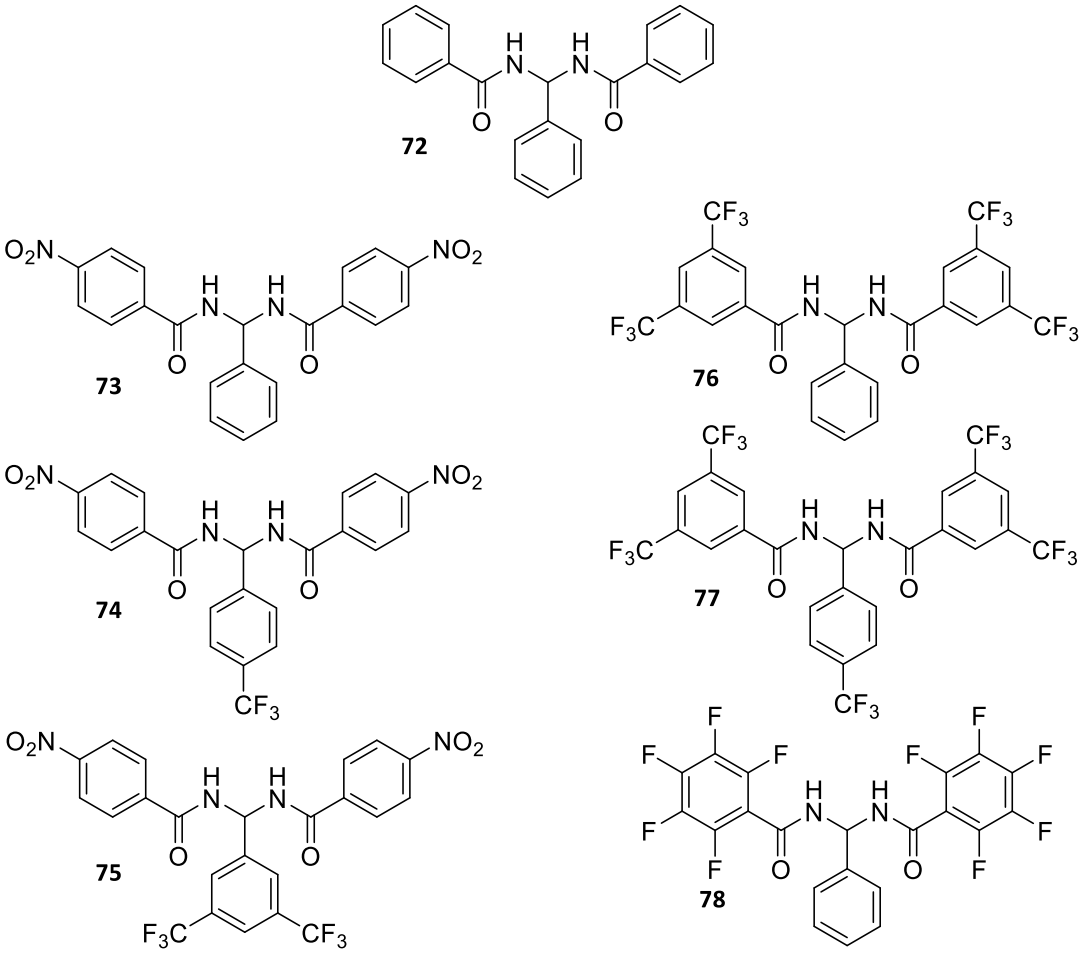

Figure 2.2 Structures of the benzamide series **72–78**.

The bisamide based receptors **72–78**, like ureas, possess a near parallel array of hydrogen bond donors. Nitro and trifluoromethyl substituents were used due to their electron withdrawing properties. These are known to increase the acidity of the hydrogen bond donors present in the structure, which in turn was expected to increase the overall anion binding affinity of the receptors.[159] Trifluoromethyl substituents have also previously been used to enhance the lipophilicity of anion receptors,[120,129] making them more effective transmembrane anion transporters. Generally fluorinated compounds are also found to be less toxic and have a high metabolic stability,[128,129,160] which is important when designing potential therapeutics.

2.2 Synthesis

The series was synthesised from commercially available compounds, following a procedure adapted from the literature.[158] Generally, the appropriate benzamide (2 equiv) and benzaldehyde (1 equiv) in DMF or toluene were stirred overnight at 50 °C under nitrogen with TMSCl or $ZnCl_2$ used as a catalyst. Addition of a few drops of water when cool gave a white precipitate which was collected and purified by trituration in diethyl ether. Full details and characterisation can be found in the experimental details and appendix A.

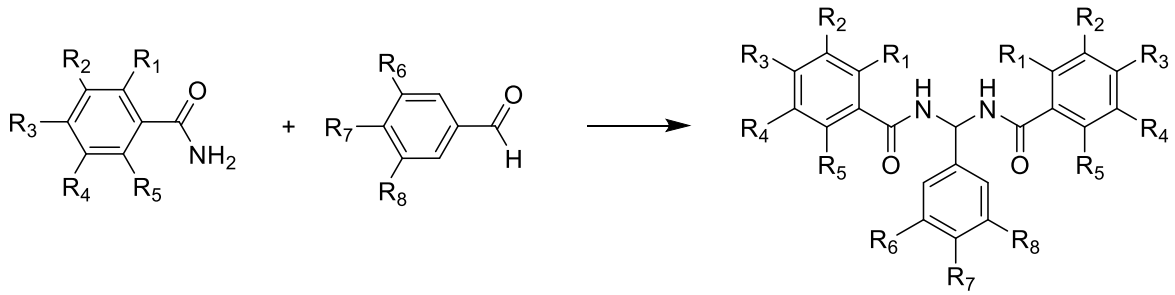

72- 31 % **75-** 81 % **78-** 20 %
73- 44 % **76-** 66 %
74- 42 % **77-** 8 %

Scheme 1 General synthesis of the benzamide receptor series. Full details and characterisation can be found in the experimental details and appendix A.

Seven compounds were synthesised via Scheme 1, with differing substituents R_1-R_8 can be seen in Figure 2.2 and gave a range of electron withdrawing effects and lipophilicities (Table 2.1).

Table 2.1 LogP values calculated using VCC labs.[161]

Receptor	logP (VCC Labs)
72	2.71
73	3.02
74	3.52
75	3.81
76	5.1
77	5.44
78	4.32

2.3 Binding studies

Proton NMR binding studies were carried out in two different solvent systems for **72–78** to determine their affinity for a range of anions. Binding constants were obtained for complexation with chloride, bicarbonate and dihydrogen phosphate in DMSO-d_6:H_2O (99.5:0.5, v/v) and a less competitive solvent system acetonitrile-d_3:DMSO-d_6 :H_2O (59.75:39.75:0.5, v/v) by fitting the chemical shift of the amide NH to a 1:1 binding isotherms using WinEQNMR2.[162] Titrations were performed with nitrate as the guest anion but showed no association.

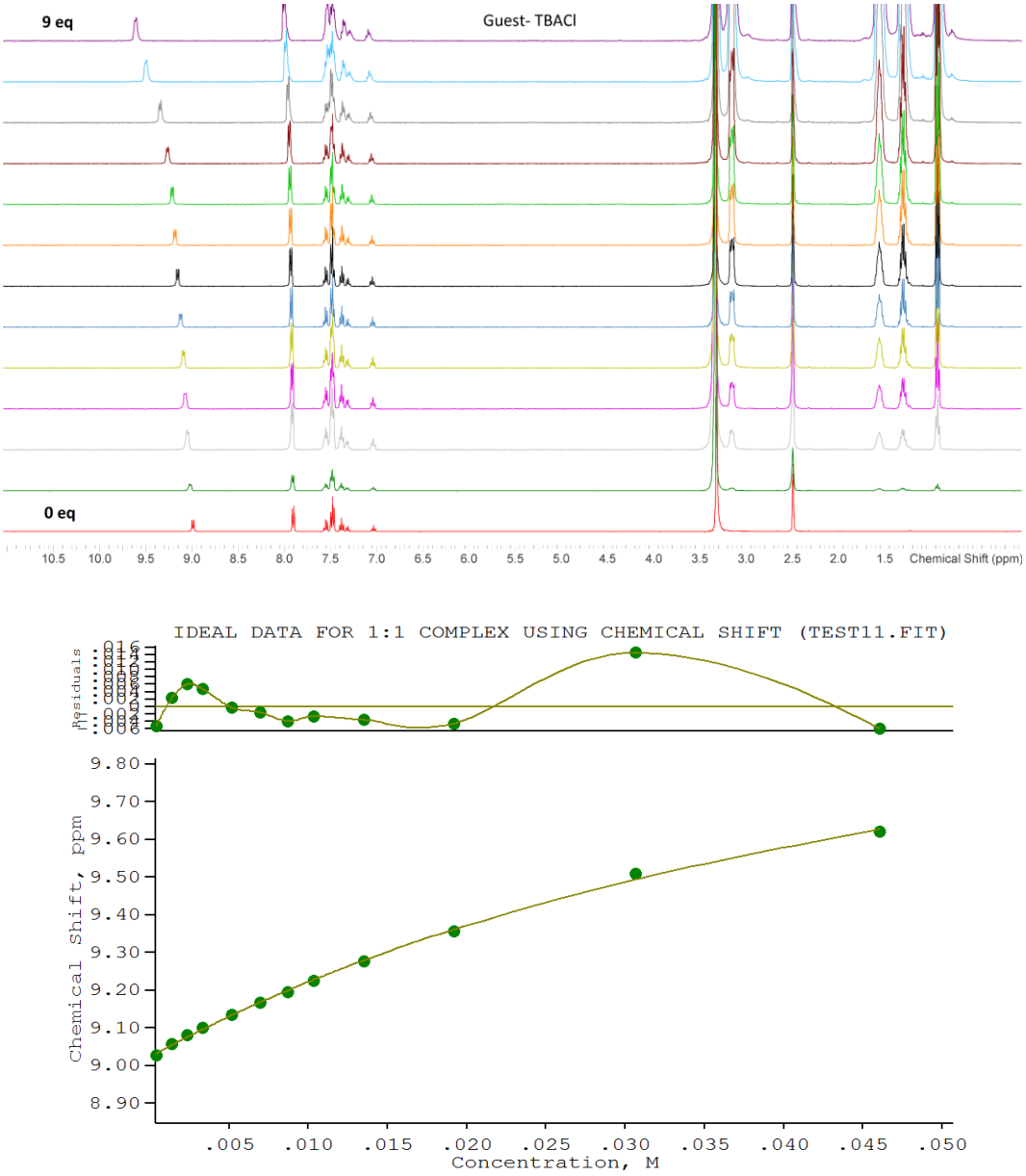

Figure 2.3 Stack plot (top) and binding curve (bottom) for ^{1}H NMR titration for receptor **72** with TBA Cl in DMSO-d_6:H_2O (99.5:0.5, v/v).

An example of a stack plot and binding curve for the receptors can be seen in Figure 2.3 and the general trend in binding constants for the benzamide receptors can be found in Table 2.2 which

indicates the chloride affinity is quite low compared to bicarbonate and dihydrogen phosphate, suggesting the compounds have a stronger affinity towards oxo-anionic species. The receptors largely show strong affinity for dihydrogen phosphate with receptor **74** giving a constant of 8290 M^{-1}, most likely attributed to the more favourable binding mode in which presumably two parallel hydrogen bonds form to the oxo-anion, Figure 2.4. The errors associated with these binding constants reflect the poor data collected, the reason for this poor data is discussed later in the chapter.

Table 2.2 Apparent binding constants (M^{-1}) in **A** DMSO-d_6:H_2O (99.5:0.5, v/v) and **B** acetonitrile-d_3:DMSO-d_6 :H_2O (59.75:39.75:0.5, v/v), calculated using WinEQNMR2 errors in the range of ± 1-20 %.[162]

	Receptor													
	72		73		74		75		76		77		78	
Anion	**A**	**B**	**A**	**B**	**A**	**B**	**A**	**B**	**A**	**B**	**A**	**B**	**A**	**B**
Cl^-	19	46	19	47	17	67	18	54	11	27	10	49	<10	<10
HCO_3^- [a,b]	275	550	771	1680	745	-[c]	796	-[c]	266	314	307	-[c]	-[c]	-[c]
$H_2PO_4^-$	370	296	2270	1630	8290	3410	1350	4030	673	530	1320	4370	-[c]	-[c]

Notes: Guests were added as tetrabutylammonium salts, unless stated otherwise. All data was fitted to a 1:1 receptor:anion isotherm within WinEQNMR2. [a]Peak broadening upon addition of the anionic guest. [b]Guest was added as a tetraethylammonium salt. [c]No association constant could be calculated due to the broadening and subsequent disappearance of the NH signal upon addition of the anionic guest.

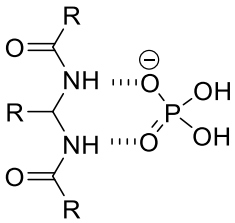

Figure 2.4 The presumed hydrogen bonding motif between the receptor and dihydrogen phosphate.

Since the publication of the work discussed in this chapter, our research group has started utilising a new more efficient and easier to use method for the calculation of anion binding constants. For consistency throughout this thesis the anion binding data for the bis-benzamides was also subjected to this new method utilising global fitting analysis.[163,164] The results can been found in Table 2.3, they show very similar general trends confirming a preference for oxo-anions. Most binding constants were very close to the original values, but in general gave lower errors in the fitting which can be found in Appendix B. There were only a few marked differences, with receptor **74** giving a constant in DMSO double that found previously for titration with $H_2PO_4^-$, most likely due to the additional global fitting analysis and alternative regression methods. The other major difference in the calculated results is the result for receptor **78** which shows a large binding constant in DMSO (107 M^{-1}) where previously a constant could not be calculated. Although this constant also comes with a

large error ≈ 36 %, hence, this result was deemed unreliable as previously a constant of < 10 M^{-1} was calculated.

Table 2.3 Apparent binding constants (M^{-1}) in **A** DMSO-d_6:H_2O (99.5:0.5, v/v) and **B** acetonitrile-d_3:DMSO-d_6 :H_2O (59.75:39.75:0.5, v/v) calculated using Bindfit errors in the range of ± 0.1 – 15 %.[163]

	Receptor													
	72		73		74		75		76		77		78	
Anion	**A**	**B**	**A**	**B**	**A**	**B**	**A**	**B**	**A**	**B**	**A**	**B**	**A**	**B**
Cl^-	27	51	19	57	24	76	25	66	33	26	13	52	107	11
HCO_3^- [a,b]	261	564	815	1808	755	-[c]	617	-[c]	276	277	290	-[c]	-[c]	-[c]
$H_2PO_4^-$	344	300	2414	1694	16090	3241	1302	3402	821	484	1017	4778	-[c]	-[c]

Notes: Guests were added as tetrabutylammonium salts, unless stated otherwise. All data was fitted to a 1:1 receptor:anion isotherm within bindfit. [a]Peak broadening upon addition of the anionic guest. [b]Guest was added as a tetraethylammonium salt. [c]No association constant could be calculated due to the broadening and subsequent disappearance of the NH signal upon addition of the anionic guest.

2.4 Transport studies

2.4.1 Chloride/nitrate antiport assay

The anion transport abilities of the bis-benzamide receptors was investigated using several phospholipid vesicle-based assays. In general, large unilamellar 1-palmitoyl-2-oleyl-*sn*-glycero-3-phosphocholine (POPC) vesicles (LUVs, 200 nm) were prepared with the chosen internal salt solution (usually NaCl) buffered to pH 7.2 with sodium phosphate salts, and were suspended in the chosen external solution also buffered to pH 7.2 with sodium phosphate salts; to obtain a final lipid concentration of 1 mM. The receptor was added as a DMSO solution and the resulting chloride efflux was measured using a chloride selective electrode. At 300 s, the vesicles were lysed with 50 µL polyoxyethylene (8) lauryl ether detergent to give a value for 100 % chloride efflux to allow for calibration of the other results.

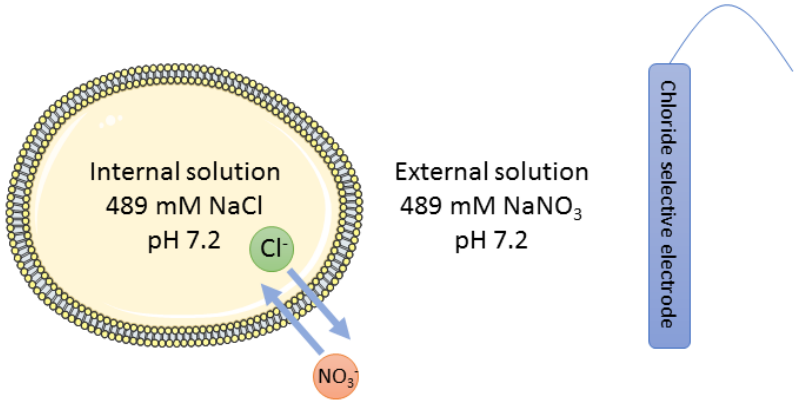

Figure 2.5 Overview for Cl^-/NO_3^- antiport assay. Conditions- Internal: NaCl 489 mM buffered to pH 7.2 with sodium phosphate salts 5 mM. External: $NaNO_3$ 489 mM buffered to pH 7.2 with sodium phosphate salts 5 mM.

Initially, the receptor's ability to facilitate Cl^-/NO_3^- antiport was studied using the assay conditions described in Figure 2.5. All the receptors were tested at 2 mol% with respect to lipid in a DMSO solution and the results can be seen in Figure 2.6. Receptor **75** displays the most effective chloride transport over the course of the experiment reaching > 80 % chloride efflux after 300 s. Increasing fluorination of the central phenyl ring for **73**–**75** showed progressively more efficient transport, this supports previous studies attributing the improved transport to increased lipophilicity of the receptor and with that a greater ability to partition into the membrane.[124,129] Unusually receptors **76** and **77** despite being highly fluorinated, do not show the best transport abilities and the reason for this is discussed later. Receptors **72** and **78** show no chloride efflux in these assay conditions.

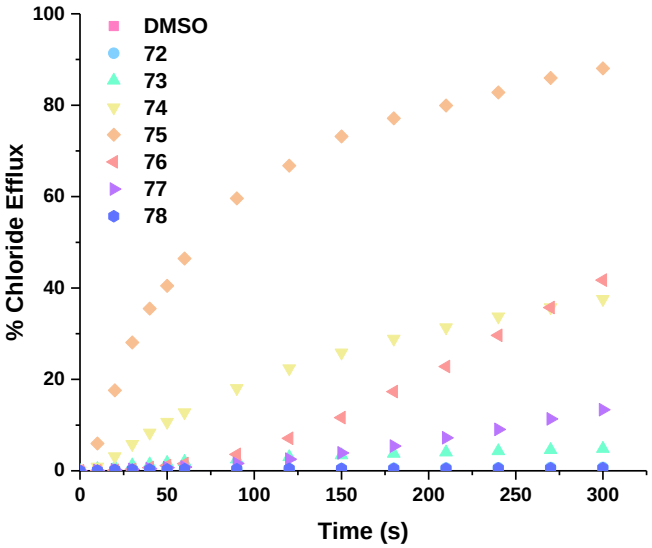

Figure 2.6 Chloride efflux facilitated by **72–78** at 2 mol% loading (w.r.t lipid) from POPC vesicles described in Figure 2.5. The receptor was added at t= 0 s and the vesicles were lysed at t= 300 s, each point is an average of 3 repeats.

2.4.2 Chloride symport assays (MCl or HCl co-transport)

In the assay depicted in Figure 2.5 two possible transport mechanisms could be taking place, an antiport mechanism (Cl^-/NO_3^- exchange) or a symport mechanism (Na^+/Cl^- co-transport). To rule out a metal co-transport mechanism the previous POPC assay was repeated using different internal salts. KCl and CsCl (489 mM) were encapsulated inside the vesicles and the chloride efflux was once again monitored using a chloride selective electrode. This resulted in no significant change outside of experimental error in chloride efflux at 2 mol% loading of the receptors that can be seen in Figure 2.7, so a metal cotransport mechanism was ruled out.

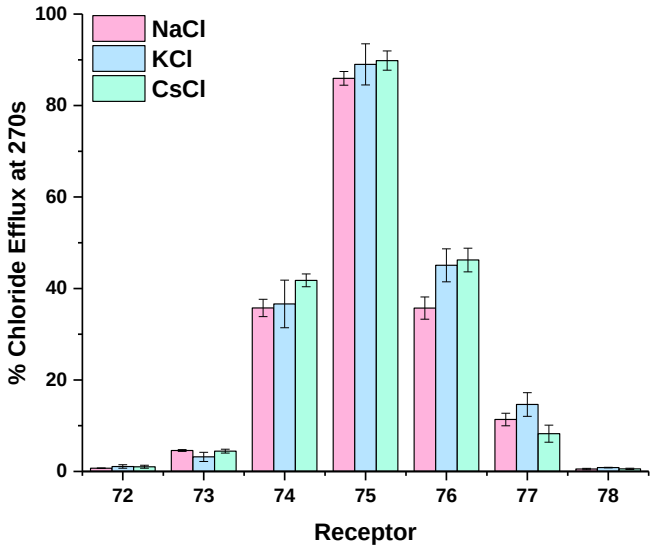

Figure 2.7 Chloride efflux facilitated by **72**–**78** (2 mol%) at 270 s from POPC vesicles (internal soln: NaCl, KCl and CsCl 489 mM, external soln $NaNO_3$ 489 mM). Each bar represents 3 repeats with the receptor added at t= 0s and the vesicles lysed at t= 300 s.

Another possible symport mechanism could be H^+/Cl^- co-transport. To investigate this mechanism the assay was performed with the external salt changed to Na_2SO_4. Sulfate was used as it is hydrophilic and has a higher charge than NO_3^- so there is a larger dehydration penalty[122] involved in transporting it. In the absence of a very encapsulating receptor SO_4^{2-} transport is unlikely so it can be used as the external anion. If no chloride efflux is observed we can deduce the mechanism is not H^+/Cl^- symport. As hypothesised, with external sulfate no distinguishable chloride efflux was observed over 300 s, and the plot can be found in Appendix C, confirming the most likely mechanism for the bis-benzamide receptors is an antiport process. Subsequently, a Cl^-/HCO_3^- antiport process was investigated.

2.4.3 Chloride/bicarbonate antiport assay

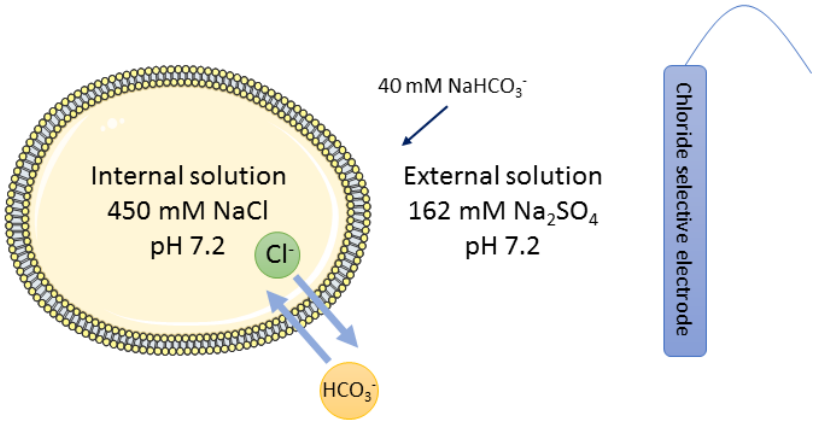

Figure 2.8 Overview for Cl^-/HCO_3^- antiport assay. Conditions- Internal: NaCl 450 mM buffered to pH 7.2 with sodium phosphate salts 20 mM. External: Na_2SO_4 162 mM buffered to pH 7.2 with sodium phosphate salts 20 mM. Pulse: $NaHCO_3$ 40 mM.

The assay conditions were changed slightly, keeping the external salt as Na_2SO_4 (162 mM), but with a higher concentration (20 mM) of sodium phosphate buffer the assay in Figure 2.8 was set up. The receptor was added as a 2 mol% DMSO solution at t= 0 s. After t= 120 s a pulse of $NaHCO_3$ was added so that the external bicarbonate concentration was 40 mM and the chloride efflux was monitored until t= 420 s when the vesicles were lysed to give 100 % chloride efflux. The previously mentioned described assay showed no transport with sulfate present, so any transport observed is most likely due to Cl^-/HCO_3^- antiport.

Figure 2.9 shows the Cl^-/HCO_3^- antiport ability of **72–78**. Again **72** and **78** exhibit no chloride efflux, but all receptors show less chloride efflux across the assay timescale than in the Cl^-/NO_3^- assay leading to the deduction that the bis-benzamides are better Cl^-/NO_3^- than Cl^-/HCO_3^- antiporters. Although the chloride efflux was lower (~30 % after 400 s) receptor **75** once again showed the most effective transport.

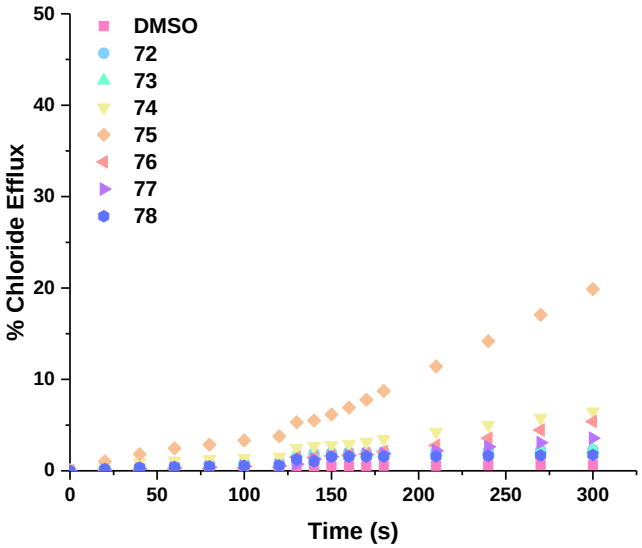

Figure 2.9 Chloride efflux facilitated by **72–78** at 2 mol% loading (w.r.t lipid) from POPC vesicles described in Figure 2.8. The receptor was added at t= 0 s and a $NaHCO_3$ 40 mM pulse was added at t= 120 s, the vesicles were lysed at t= 300 s, and each point is an average of 3 repeats.

2.4.4 Hill analysis

Quantification of these transport results was attempted by performing the Cl^-/NO_3^- assay in dose response tests and then using Hill analysis.[103] Receptors **72** and **78** were excluded due to inactivity in the previous assays (no measurable chloride efflux at 2 mol%). Hill analysis enables calculation of EC_{50} values (the effective concentration of receptor needed to facilitate 50 % chloride efflux) and Hill coefficients both of which can be found in Table 2.4.

Table 2.4 EC_{50} and Hill coefficient (*n*) values for receptors **73–77**.

Receptor	EC_{50}	*n*
73	-[a]	-[a]
74	5.4 ± 0.7	0.78
75	0.37 ± 0.02	1.07
76	-[b]	-[b]
77	3.8 ± 0.1[c]	2.5[c]

Notes: To an extent all receptors tested displayed signs of self-aggregation at high concentration, consistency of runs was hard to achieve, therefore Hill analysis may be unreliable.[a] Unable to fit to the Hill equation due to poor transport activity.[b] Possible self-aggregation of receptor, could not produce consistent results for Hill analysis.[c] Treat Hill analysis with caution due to poor fit and unusual behaviour in testing.

Over the course of the dose response tests it was clear receptor **75** was quantitatively the best transporter with the lowest EC_{50} value of 0.37. However, some unusual behaviour was observed from

all the receptors to varying extents. When adding the receptor in DMSO solutions the more concentrated the stock solution the less consistent the runs, and in some cases the chloride efflux diminished at high loadings. This behaviour has been noted before with squaramide receptors and was attributed to self-aggregation or precipitation.[120] This effect was most apparent for receptors **76** and **77** and the Hill analysis seemed particularly unreliable, it was also noted that these receptors possessed a different kinetic transport profile. Figure 2.6 shows that transport for **76** and **77** takes longer to commence, giving a more sigmoidal shape to the kinetic profile, receptor **77** also gives a more sigmoidal shape in the Hill plot. A sigmoidal shape for transport profiles has been reported previously by Haynes *et al.*[165] and this was attributed to the receptors lying outside the optimum lipophilicity range proposed by Saggiomo *et al.*[53] Receptors **76** and **77** possess logP values of 5.1 and 5.44 respectively (Table 2.1 calculated using VCC labs[161]) which do lie above the range proposed (logP ~ 4),[53] although, more recent literature has shown that the optimum lipophilicity is a property of transporter class[54,143,145] and it may not be comparable. However, the optimum logP for the bis-benzamides based on **75** being the most efficient transporter should lie between 3.52 and 5.1 (**74** and **76** lipophilicities) although a more detailed study would be needed to confirm this. Possessing a logP above this would rationalise the slow initial transport rate for the highly fluorinated receptors, as the crucial delivery through the aqueous external media to the membrane is hindered. However, the least lipophilic compounds (**72** and **73**) are unlikely to partition well into the membrane and hence no transport is observed.

Another rationale to the unusual behaviour of these receptors could be due to self-aggregation or precipitation. Unlike the squaramides, the benzamides were quite soluble in DMSO and no visible precipitation was observed during the testing, so this seemed unlikely to be causing the strange behaviour although it couldn't be ruled out completely. Self-aggregation did seem like a plausible cause as it has been noted as being counterproductive to transport previously[166,167] and the bisamide structure may have the ability to form intermolecular hydrogen bonds.

Some of the receptor's Hill analysis determined a Hill coefficient which can be found in Table 2.4. Hill coefficients can be used to give an indication of the stoichiometry of the transport process,[105] generally the Hill coefficients are low $n < 3$ and for receptors **74** and **75** ≈ 1, so it is unlikely that the receptors assemble into membrane spanning pores. However, receptor **77** has a Hill Coefficient of 2.5 which indicates more than one receptor may be in contact with the anion during the transport process forming a cluster or aggregate. For example, Matile *et.al.* have reported a capsule system of transport where more than one receptor encapsulates the anion and allows for transport across the lipid membrane. [105,168] Due to the unusual behaviour during dose response tests and a Hill coefficient

of $n > 1$ the transport stoichiometry was investigated further using POPC vesicles doped with cholesterol (7:3).

2.4.5 Mechanistic studies

The assay was performed as before with Cl^-/NO_3^- conditions but with the differing membrane composition (30 % cholesterol) for receptors **73–77**. Addition of cholesterol into the membrane is thought to order the bilayer and reduce fluidity.[169,170] Therefore, cholesterol doping has been used previously to ascertain a mobile carrier mechanism; with a carrier's dependence on diffusion through the membrane, an increased bilayer viscosity would most likely slow down the transport rate.

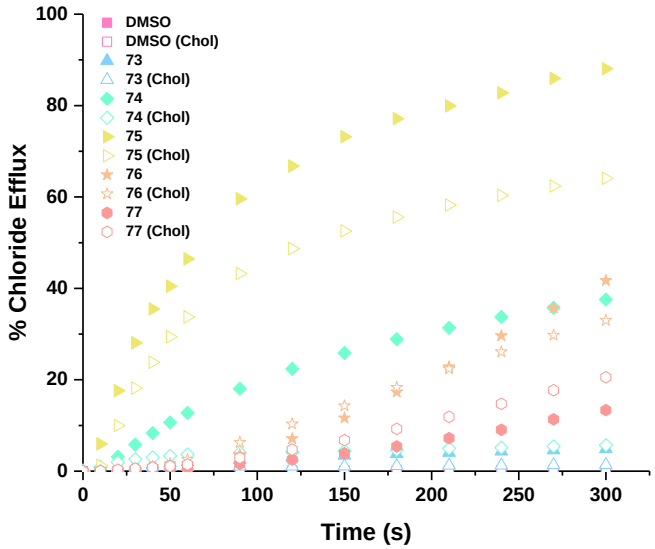

Figure 2.10 Chloride efflux facilitated by **73**-**77** at 2 mol% loading (w.r.t lipid) from POPC:Chol (7:3) vesicles compared to pure POPC vesicles. The receptor was added at t= 0 s and the vesicles were lysed at t= 300 s, each point is an average of 3 repeats.

As expected receptors **73–75** exhibit a decrease in transport activity with the addition of cholesterol. However, Figure 2.10 shows an increase in transport activity for receptor **77** and a very slight change for receptor **76**. This may be indicative of a non-mobile carrier mechanism. However, the results of U-tube tests which can be seen in Figure 2.11, deemed channel formation unlikely. The test was set up within a glass tube in the shape of a U (Figure 2.11), and each respective receptor was dissolved in nitrobenzene which was added to the tubes as the organic phase. Either side of this organic phase an aqueous solution of NaCl and $NaNO_3$ was added as the source and receiver phases. Over the course of eight days the chloride concentration of the receiver phase was monitored with a chloride selective electrode. The increase of chloride concentration for all receptors, to varying extents, in

the receiver phase supports a mobile carrier mechanism as the length of the organic phase makes channel formation highly improbable.

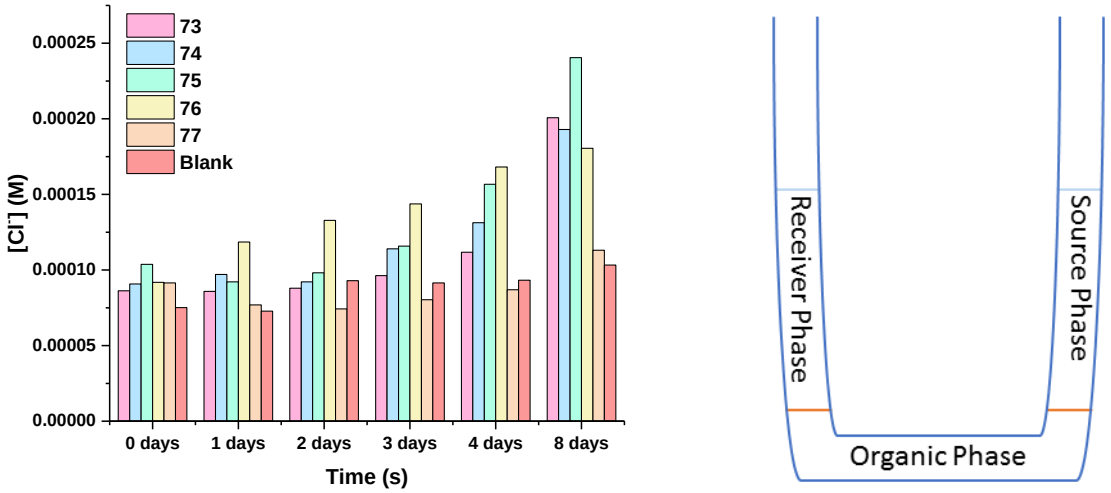

Figure 2.11 **Left-**The change in the concentration (M) of chloride anions in the receiver phase of a U-tube facilitated by receptors **73–77**. **Right-** Overview of U-tube set up: Source phase- Aqueous NaCl, Organic phase- Nitrobenzene receptor solution, Receiver phase- Aqueous $NaNO_3$. Tiny amounts of receptor precipitation were observed over the 8 days, most noticeably with receptor **74**.

The differing responses in the cholesterol assay must be due to some other effect, although this is still unclear, Haynes *et al.* reported a similar increase in activity for receptors containing highly lipophilic substituents such as trifluoromethyl.[165] It was proposed that addition of cholesterol into the bilayer affects the receptors ability to partition within the membrane and thus the differing lipophilic nature of the receptors would contribute to this process. What is clear is there are many factors involved in the receptors delivery and partitioning into the membrane that a cholesterol study alone cannot solve.[145]

2.5 NMR dilution studies

Further study of the unusual concentration dependence was necessary to try to ascertain if self-aggregation was the key to this behaviour. Self-aggregates typically exhibit higher logP values and lower solubility than their monomeric counterparts,[171] so this would explain why receptors **76** and **77** display more aggregate characteristics. One method frequently used in cases like this is a dilution study. Initially, a dilution study using UV-Vis characterisation was attempted, but unfortunately the bis-benzamide receptors did not absorb at a measurable point on the spectrum so NMR dilution studies were conducted instead.

Typical NMR spectra of aggregators can display changes in the number and nature of the signals present which is indicative of multiple aggregate species in solution. Specifically, changes in shape of the resonance peaks, typically broadening, may indicate a change in the size and tumbling rate of the species in solution. Furthermore, slight changes in chemical shifts (δ ppm) may be detected, resulting from local environmental changes in the magnetic field around the molecule when aggregates form.[172] Proton NMR spectra were obtained for receptors **72**–**78** at a range of concentrations (1–100 mM). Inserts from the spectra of receptor **76** can be seen in Figure 2.12 and full spectra can be found in Appenidx C.

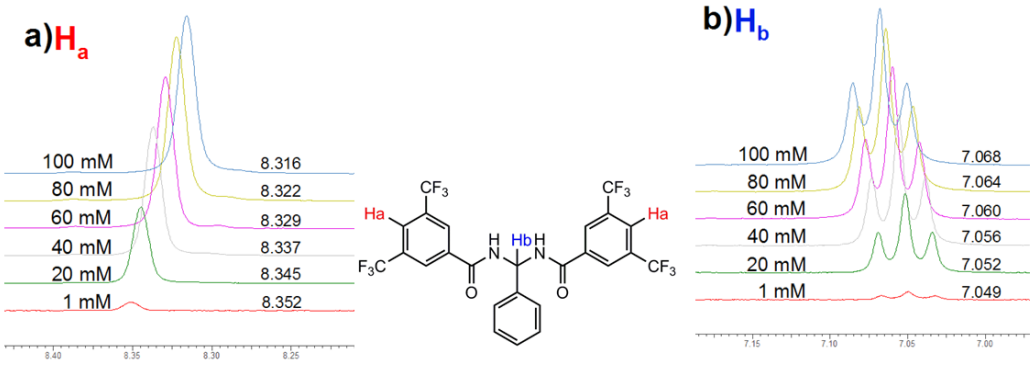

Figure 2.12 Stack plots of changing concentrations (1–100 mM) for receptor **76** in DMSO-d_6, a) Small upfield shift of proton H_a and b) Small downfield shift of proton H_b.

Most of the receptors showed small but noticeable shifts for proton H_b and NH protons which can be found in Appendix C. Receptor **76** was the only receptor to show changes to other protons (H_a). Interestingly receptor **75** displayed the least noticeable shifts which supports the fact it showed the least concentration dependence during vesicle studies and was the most efficient chloride transporter. These NMR studies help to support the rationale that self-association of some of these bis-benzamide receptors causes the unusual behaviour observed when testing the transport,

although nothing could be confirmed for definite. It does mean however that the binding constants calculated in 2.3 should be regarded as apparent values only.

2.6 Crystallography

Receptors **73** and **77** were both isolated as crystalline solids by slow evaporation at room temperature of DMSO and acetonitrile solutions of **73** and **77** respectively with an excess of TBA Cl (5 equiv). Interestingly no chloride complex crystals were isolated which may indicate their preference for intermolecular hydrogen bonds over chloride complexation. The structures of the crystals were elucidated by single crystal X-ray diffraction and details can be found in the experimental details and Appendix A.

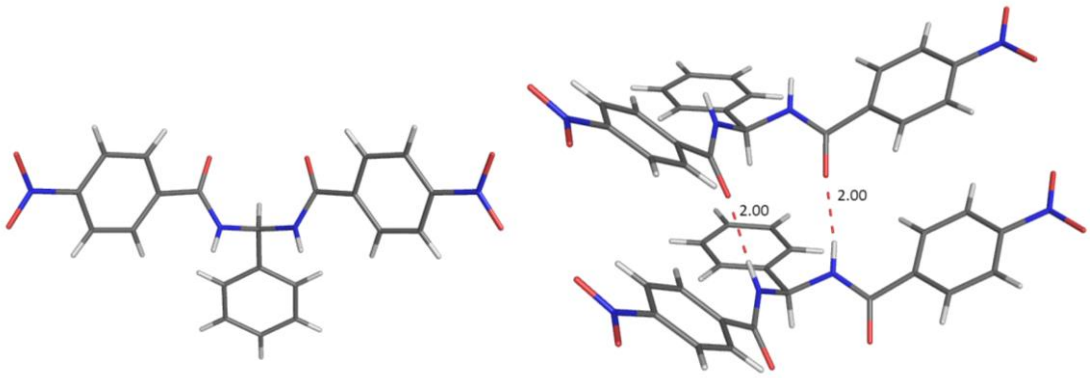

Figure 2.13 **Left-** Uncomplexed receptor **73**. **Right-** Self-aggregate through hydrogen bonding to adjacent receptor molecule. Hydrogen bond length in red- 2.00 Å.

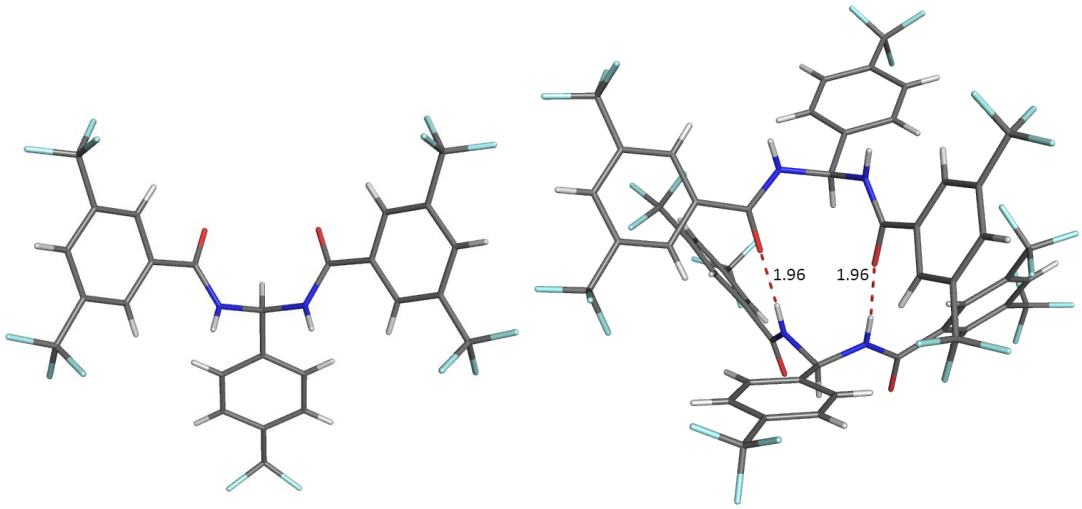

Figure 2.14 **Left-** Uncomplexed receptor **77**. **Right-** Self-aggregate through hydrogen bonding to adjacent receptor molecule. Hydrogen bond length in red- 1.96 Å.

Figure 2.13 and Figure 2.14 demonstrate that in the solid state the receptors adopt a conformation in which the hydrogen bond donors are near parallel. Receptor **77** forms an interlocked dimer, compared to receptor **73**, which forms a dimer in which the monomers are orientated in the same direction. Both receptors form continuous hydrogen bonded arrays in the solid state via two NH···O (1.96–2.00 Å) interactions between the amide groups on adjacent receptors.

2.7 Conclusions

A series of *N, N'* –(phenylmethylene)dibenzamide based receptors were synthesised and fully characterised, and were found to function primarily as Cl^-/NO_3^- antiporters but also to a small extent as Cl^-/HCO_3^- antiporters. They are most likely to function via a mobile carrier mechanism although evidence of self-aggregation in solution and interesting behaviour in a cholesterol doped assay was observed which complicated unambiguous determination of the transport mechanism.

Self-aggregation was supported by NMR dilution studies and was most apparent in fluorinated receptor **76** and least apparent in the most efficient chloride antiporter receptor **75**. It was proposed that the self-association properties of this motif may effectively increase the logP and in turn this could both enhance or diminish the transport properties of the compounds depending on where they lie on the optimum lipophilicity scale. It is becoming increasingly evident that substituent effects and lipophilicity are important parameters which can directly affect the binding, partitioning and transport abilities.

Although the transport abilities of this series are moderate, one can envisage this hydrogen-bonding motif being used alongside, or instead of, urea in a variety of self-assembled structures due to the formation of two near linear hydrogen-bonding interactions.

Chapter 3: Transmembrane fluoride transport

Parts of the work in this chapter has been published as Harriet J. Clarke, Ethan N. W. Howe, Xin Wu, Fabian Sommer, Masafumi Yano, Mark E. Light, Stefan Kubik, and Philip A. Gale (2016). "Transmembrane fluoride transport: Direct measurement and selectivity studies" *Journal of the American Chemical Society* 138: 16515–16522, and is reproduced with permission from the American Chemical Society. http://pubs.acs.org/doi/abs/10.1021%2Fjacs.6b10694.

3.1 Introduction

As discussed in the introduction to this thesis, in the past decade the development of synthetic anion transporters has attracted much attention. A wide variety of small molecules have been developed to facilitate the transmembrane transport of biologically relevant anions such as chloride,[2,33,62,64,101,108,156,157] bicarbonate,[119,124,126,173] and sulfate.[132] The driving force for this research is to synthesise therapeutics for the treatment of diseases which involve faulty ion channels.[13]

Previously overlooked as a biologically relevant anion focus has turned to fluoride in the past few years. Fluoride has been used as an additive in water and oral hygiene products[174] and is found at levels of 10 –100 μM[175] in the aqueous environment. Exposure to elevated levels of fluoride (above 1.5 mgL^{-1})[176,177] can be detrimental to health and can lead to fluorosis, affecting teeth and bones.[178] Due to this its use in water treatment is controversial. To the best of my knowledge, no small synthetic molecule has been shown to facilitate fluoride transmembrane transport or measured directly. Fluoride is small, hard and basic and has a higher hydration penalty[179] than chloride and bicarbonate, making fluoride complexation in aqueous solutions challenging.

In organic environments, deprotonation of anion receptors by fluoride,[180–186] driven by the formation of bifluoride, is a competing process to complexation. This deprotonation event can be accompanied by a vivid colour change, useful for anion recognition but not for transport. The use of Lewis acidic metal centres by Gabbaï and co-workers in fluoride sensors has allowed for fluoride detection in water below the maximum contaminant level (4 ppm) set by the Environment Protection Agency.[187–189] Additionally, some Lewis acid compounds have been found to act as fluoride anionophores across artificial PVX-DOS membranes in the field of ion-selective electrodes,[190] and fluoride sensing using boronic acid derivatives has been a successful strategy by Shinkai, James, and others.[191–193]

In early work from Sessler and co-workers, fluoride transport through a liquid membrane system was facilitated by a protonated sapphyrin within a U-tube.[194] The transmembrane exchange of fluoride enabled by the protein capnophorin in red blood cells has also been investigated utilising ^{19}F NMR techniques.[195] In other interesting and more relevant work Matile[196] and Berezin[197] have shown promising indirect results for fluoride as a potential target for lipid bilayer transport and provide strong precedent that fluoride transmembrane transport is achievable.

Over the past five years, seminal work by Miller and co-workers has revealed the existence of two naturally occurring, phylogenetically unrelated families of fluoride exporter anion channels. The first is CLC^F a H^+/F^- co-transporter found solely in bacterial unicellular organisms[175,198–200] and the second is a small membrane channel uniporters known as 'Fluc' proteins which are widespread amongst unicellular and eukaryotic organisms.[201–203] These channels appear to possess high selectivity for fluoride over chloride, it has been proposed the reason for this is due to the narrow bore of the permeation pathway found in a crystal structure of a Fluc channel from *Bordetella pertussis*.[203] The crystal structure also revealed an interesting double-barrelled channel architecture.[203,204]

Unicellular organisms display pH dependant hypersensitivity to elevated fluoride levels which can be built up as a consequence of the weak acid accumulation effect.[205] The weak acid accumulation effect as depicted in Figure 3.1 is caused by the permeable nature of HF and its weak acidic pKa of 3.4. HF can cross the cell membrane from the acidic external environment down its pH gradient to the neutral interior of the membrane where it dissociates forming H^+ and F^-. This process causes a build-up of fluoride in the cell cytoplasm, and at certain levels it can inhibit growth enzymes and cease cell development. The fluoride channels mentioned above can expel this cytoplasmic fluoride to bring the concentration back down below growth enzyme inhibitory levels.

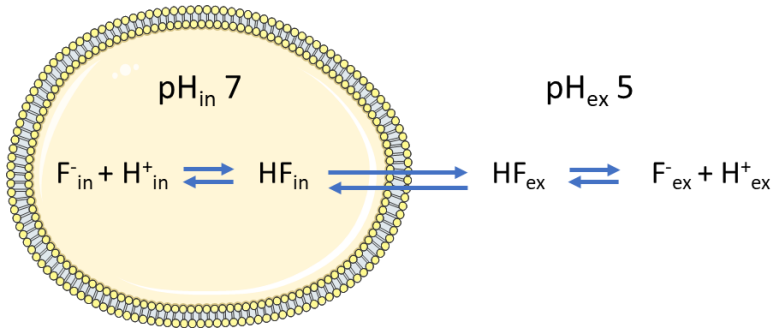

Figure 3.1 Schematic of the weak acid accumulation effect.[205]

This chapter focuses on an investigation into whether it is possible to facilitate the transmembrane transport of fluoride using small molecule anion transporters and to determine whether the transport was selective for fluoride over chloride utilising vesicle based assays and direct measurement with a fluoride selective electrode.

In order to avoid deprotonation of the receptor by fluoride due to its highly basic nature, the acidity of the receptor must be considered. Ureas, thioureas and squaramide based receptors recently utilised within the Gale group for transmembrane chloride transport were too acidic, and would likely be deprotonated by fluoride. A less acidic anion receptor was required for this investigation, such as the calixpyrrole motif. Previous anion binding studies have found the parent calix[4]pyrrole **16** (Figure 3.2) binds fluoride strongly without deprotonation.[78,79] In transport studies **16** has been found to facilitate CsCl symport[97] and the strapped calix[4]pyrroles **79**–**81** have shown moderate Cl^-/NO_3^- and Cl^-/HCO_3^- antiport abilities.[206] These characteristics made the calix[4]pyrroles good candidates for potential transmembrane fluoride transport, Figure 3.2 shows the receptors utilised in this study.

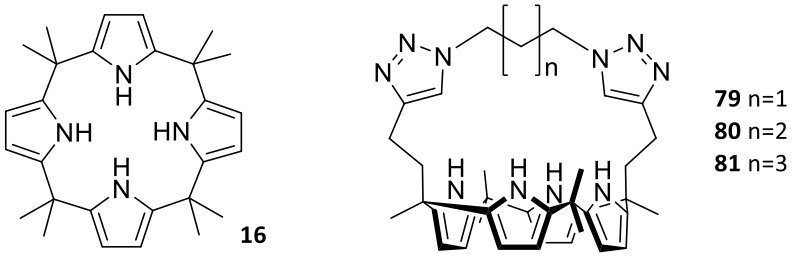

Figure 3.2 Structures of the parent calix[4]pyrrole and the three strapped calix[4]pyrroles used in this study.

Another consideration was the set-up of the fluoride transport assay, due to the membrane permeability of HF, the pH of the vesicle solution had to be controlled. The pKa of HF is 3.4 so keeping the intra and extra vesicular solutions at pH 7.2 would hopefully prevent too much background HF permeation. The HPTS base pulse assay traditionally used throughout the literature to study the transport of a variety of anions,[33] was initially attempted. However, without the addition of a transporter rapid HF permeation was observed which fully dissipated the pH gradient within 100 s, the plot can be found in Appendix C. An alternative assay would need to be used and this will be discussed later.

3.2 Synthesis

The strapped calix[4]pyrroles **79–81** were synthesised following the literature procedure used by Yano *et.al.*[206] and the outline of steps (a)–(c) can be found in Scheme 2 with more details and characterisation in the experimental details and Appendix A.

Steps (ai) and (aii) involved a copper catalysed alkyne-azide click reaction to afford the ditriazole-diketone products, (ai) utilised sodium azide to prepare bis-azides from dibromoalkanes *in situ* due to their highly explosive nature. Subsequent coupling with 5-hexyn-2-one, synthesised according to the literature,[207] produced the ditriazole-diketone product. These ditriazole-diketones were dissolved in fresh pyrrole with catalytic amounts of tri-fluoroacetic acid (TFA) (step (b)) to afford the pyrrole functionalised ditriazole which was purified via column chromatography. Lastly, step (c) shows acid catalysed condensation with acetone which resulted in the cyclisation and formation of the final strapped calix[4]pyrroles **79–81**. All final compounds were fully characterised and further details can be found in the experimental details and Appendix A.

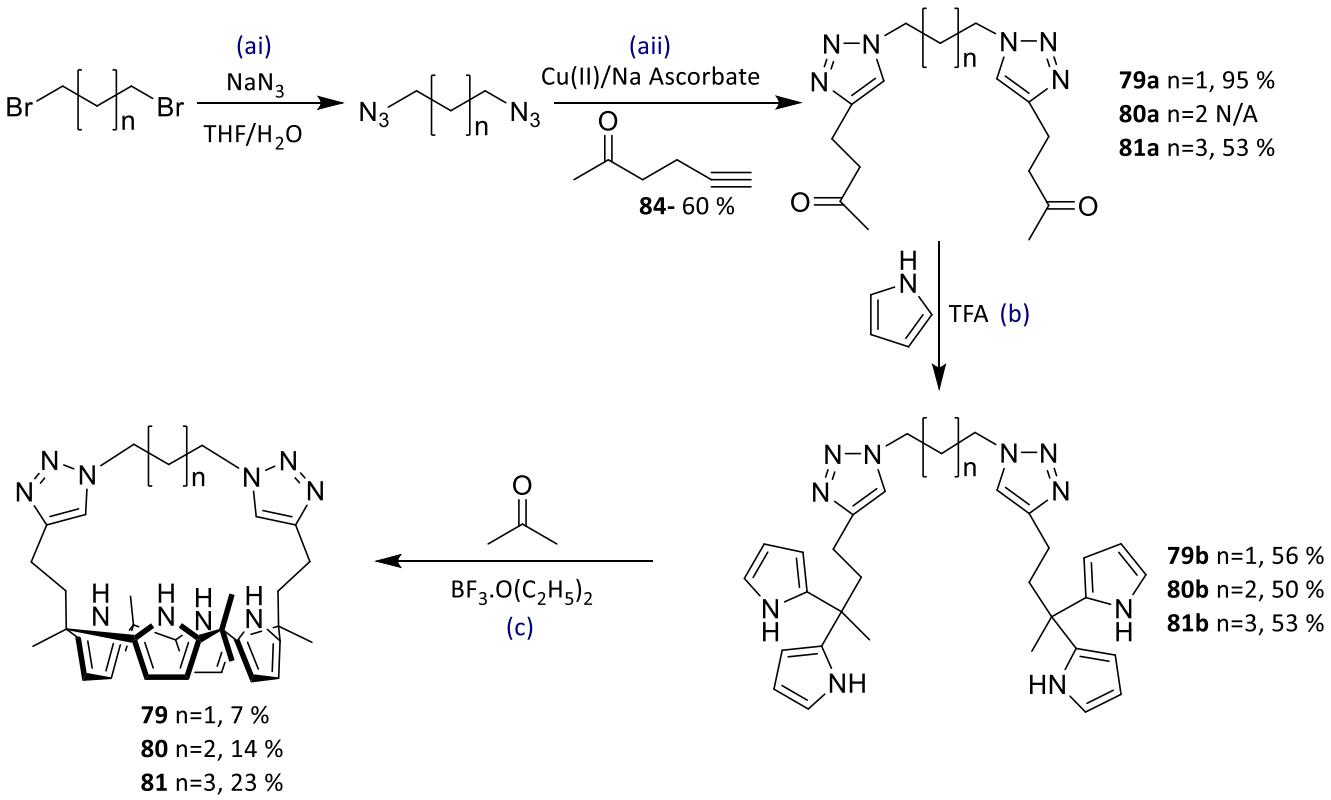

Scheme 2 Synthesis of the strapped calix{4]pyrroles **79–81**.

3.3 Binding studies

The fluoride binding affinity of the calix[4]pyrroles **16, 79–81** was evaluated using ^{1}H NMR titration methods and isothermal titration calorimetry (ITC). Previous binding studies conducted with this series showed slow exchange on the NMR time scale for titrations with tetrabutylammonium chloride (TBACl).[206]

3.3.1 NMR Titrations

Proton NMR titration studies were conducted in DMSO-d_6:H_2O (99.5:0.5, v/v) with tetrabutylammonium fluoride and acetate (TBAF and TBAOAc). As previously observed for TBACl, titration with TBAF resulted in slow exchange of the fluoride complex and the free calix[4]pyrrole on the NMR timescale.

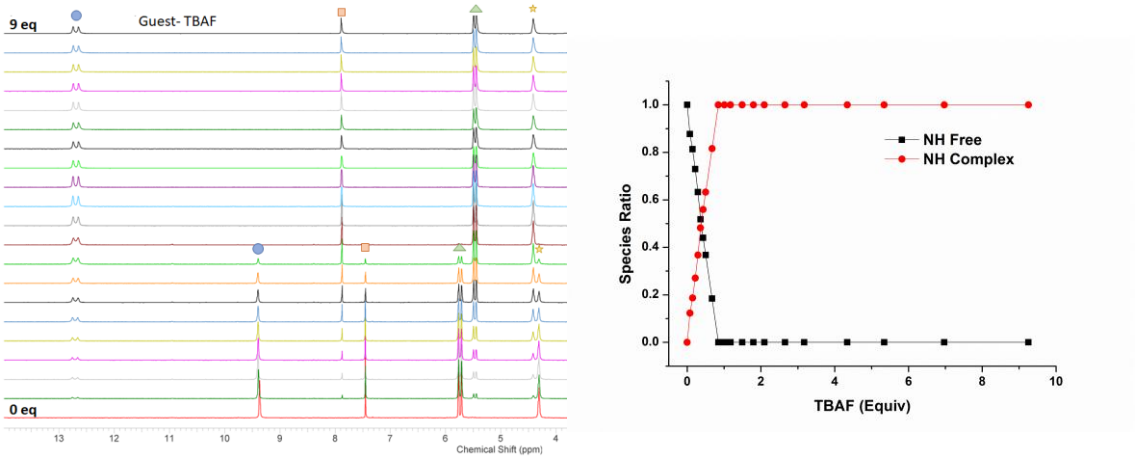

Figure 3.3 Stack plot for receptor **80** ^{1}H NMR titration with TBAF in DMSO-d_6:H_2O (99.5:0.5, v/v). Blue circle follows the pyrrole NH signal, orange square follows the triazole CH signal, green triangle follows the pyrrole CH signal and the yellow star follows an alkyl CH_2 (left). Species ratio plotted for the evolution of the complex versus the free receptor (right).

All the receptors showed a similar binding event, stack plots and species ratio plots can be found in Appendix B. For an example Figure 3.3 displays the spectra stack plot and species ratio of receptor **80** and shows a downfield shift of the pyrrole NH and the triazole CH resonance. A coupling of the NH resonance to the ^{19}F nucleus of the fluoride anion is also observed which is usually indicative of a strong hydrogen bonding event. Slow exchange was also observed upon addition of TBAOAc with compounds **79–81**, and a stability constant of 6060 M^{-1} was derived from global fitting analysis using Bindfit,[163,164] for receptor **16** in DMSO-d_6:H_2O (99.5:0.5, v/v). An interesting splitting effect for the pyrrole NH signal was observed for the titration of **79** with TBAOAc, suggesting two environments,

which was attributed to the OAc^- not binding symmetrically within the cavity of the smallest strapped receptor. These spectra can be found in Appendix B.

Due to the slow exchanging nature of these NMR experiments determination of a quantitative association constant was difficult. It is well known that trying to determine an association constant directly from the relative ratios of the free host and complexed host is limited, due in part to obtaining accurate integration values from the NMR experiments.[164] It is also likely that the calix[4]pyrroles have a $K_a > 10^5$ M^{-1} (this was seen for chloride binding previously) which is the practical limit for NMR titration determination. Another method for association constant determination was required.

3.3.2 Isothermal titration calorimetry

Quantification of the binding affinity was performed by F. Sommer using ITC, which is a powerful technique that can measure the enthalpy (H) increase on addition of a guest to a host within an isothermal calorimeter.[164] The instrument measures the heat formed and absorbed during the titration allowing for calculation of an association constant, the free energy changes (ΔG), the molar enthalpy changes (ΔH) and the entropy (ΔS).

ITC was performed in acetonitrile using tetraethylammonium salts allowing for comparison with previously published results for this series of receptors. The results summarised in Table 3.1 show the receptors demonstrate exothermic complexation with the addition of both salts with slightly unfavourable entropic contributions apart from **16** and **81** with TEAF. The series binds very strongly to fluoride, with K_a values of $\geq 10^6$ M^{-1} with no indication of deprotonation, supporting their suitability for fluoride transport. The binding is about ten-fold better than with TEACl compared with the literature which reports a K_a range of 10^5–10^6 M^{-1}.[206] Acetate binding was slightly weaker than fluoride binding, with a K_a range of 10^5–10^6 M^{-1}. As expected, acetate binding was stronger for **16**, **80** and **81** compared to **79**, and along with the unusual splitting observed within NMR titration, was attributed to the shorter strap restricting the binding cavity. The relevance of acetate binding will be discussed in more detail later in this chapter and the next. ITC binding isotherms can be found in Appendix B.

Table 3.1 Overview of the association constants and thermodynamic state functions for the 1:1 complexation of tetraetylammonium salts with **16**, **79**–**81** as measured in acetonitrile by ITC at 303 K.

Receptor	K_a (M^{-1})	ΔG (kJmol^{-1})	ΔH (kJmol^{-1})	$T\Delta S$ (kJmol^{-1})
		Fluoride		
16	3.5×10^6	-38.0	-30.1	7.9
79	1.3×10^6	-35.5	-44.5	-9.0
80	1.1×10^7	-40.8	-44.6	-3.8
81	1.9×10^7	-42.2	-34.5	7.7
		Acetate		
16	5.2×10^5	-33.2	-45.3	-12.1
79	1.3×10^5	-29.7	-41.4	-11.7
80	1.7×10^6	-36.3	-42.7	-7.3
81	1.2×10^6	-35.4	-42.7	-7.3

3.4 Solid state analysis

Receptor **79** was isolated as a crystalline solid in a complex with both TBAF and TBACl, by slow diffusion of petroleum spirits into a chloroform solution of **79** with TBAF (5 equiv) and slow evaporation of a methanol solution of **79** and TBACl (in excess) respectively. The solid-state structures of **79** complexed with fluoride and chloride can be seen in Figure 3.4 (a) and (b). They show the anion bound within the strapped cavity of the calix[4]pyrrole receptor, with shorter N···F distances of 2.747(3)–2.787(3) Å observed compared to N···Cl distances 3.247(2)–3.271(2) Å. An additional long-range stabilising effect was observed from the triazole CH for the fluoride complex. Hence the fluoride appears to be more strongly bound, at least in the solid state.

Figure 3.4 (c) depicts the solid-state structure **80**·CsF isolated as a crystalline solid by slow diffusion of an ethanol solution of caesium fluoride into a dichloromethane solution of **80**. This structure is similar to the caesium chloride complex of the parent macrocycle **16**,[208] with N···F distances of 2.775(3)–2.828(4) Å and the caesium atom sitting in the calixpyrrole's cone shaped cavity formed by the four pyrrole rings.

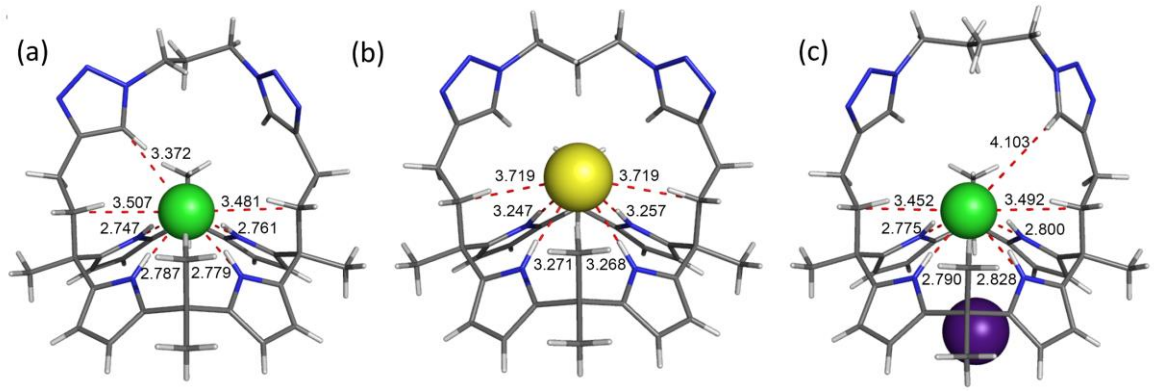

Figure 3.4 (a) Single crystal X-ray structure of **79**·TBAF complex (TBA excluded for clarity). (b) Single crystal X-ray structure of **79**·TBACl complex (TBA excluded for clarity). (c) Single crystal X-ray structure of **80**·CsF complex (ethanol excluded for clarity). N···F, N···Cl, C···F, and C···Cl distances are displayed as red dashed lines, with measurements. Full crystallographic data can be found in the experimental details and Appendix A.

3.5 Transport studies

3.5.1 Valinomycin coupled fluoride assay

The fluoride transport activity of receptors **16**, **79–81** was probed using a vesicle-based ISE assay which was adapted from the literature.[200] Figure 3.5 displays large unilamellar vesicles (LUVs, 200 nm) composed of POPC loaded with KF (300 mM) and suspended in potassium gluconate (KGlc, 300 mM). All solutions were buffered to pH 7.2 with HEPES buffer (10 mM). Transport was initiated by addition of valinomycin (Vln, 0.1 mol%), followed by the receptor at t = 30 s, fluoride efflux was then measured using a fluoride selective electrode.

The use of potassium gluconate as the external salt is due to its hydrophilicity and large polar structure, making its transport negligible. The driving force for the assay is the large fluoride gradient. Despite this gradient, in the absence of valinomycin and an anion transporter the background fluoride efflux is minimal, suggesting little HF permeation. Valinomycin facilitated potassium transport enables the calix[4]pyrrole's fluoride transport, by dissipating the membrane potential that would build up if the transporter worked alone.[154,198]

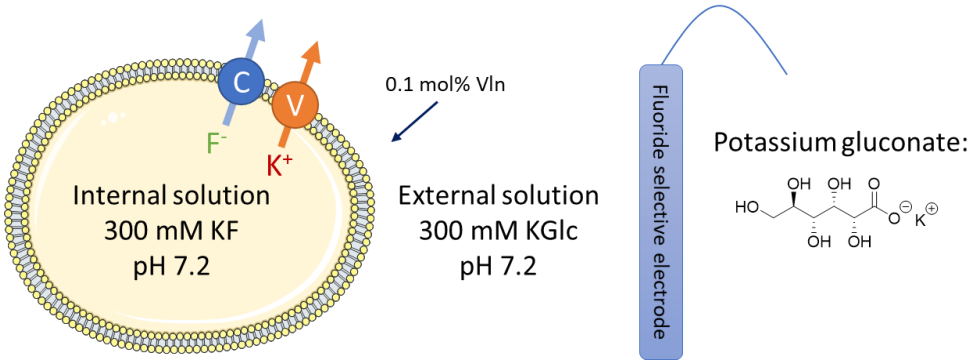

Figure 3.5 Overview of the valinomycin coupled KF transport assay. Conditions- Internal: KF 300 mM buffered to pH 7.2 with HEPES buffer 10 mM. External: KGlc 300 mM buffered to pH 7.2 with HEPES buffer. Pulse: 0.1 mol% valinomycin.

The results for this assay are shown in Figure 3.6. Receptors **79–81** all functioned as fluoride transporters at 2 mol% (w.r.t. lipid). Compound **80** was the most effective transporter under these conditions showing > 80 % fluoride efflux after 300 s, but all three receptors showed effective transport of > 70 %. As expected the parent calix[4]pyrrole **16** was ineffective in this assay and showed no transport.

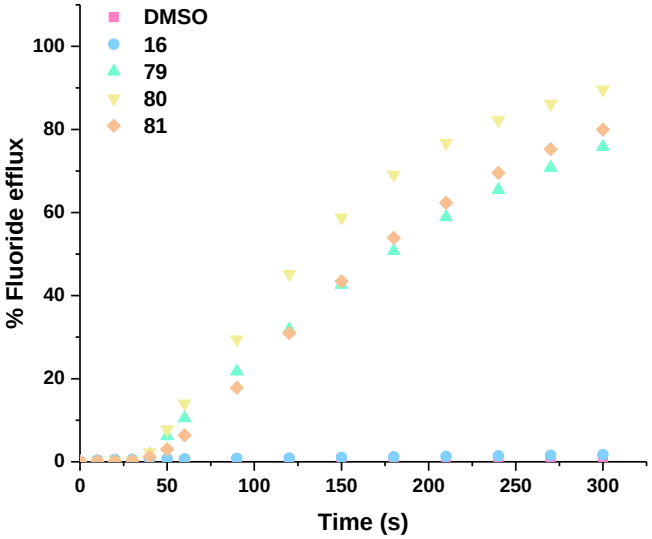

Figure 3.6 Fluoride efflux facilitated by **16, 79–81** at 2 mol% loading (w.r.t. lipid) from POPC vesicles described in Figure 3.5. The transport was initiated by the addition of a DMSO solution of Vln (0.1 mol%) at t= 0 s and then the receptor at t= 30 s. The vesicles were lysed at 300 s, each point is an average of 3 repeats.

3.5.2 Metal fluoride co-transport assay

Following this encouraging result, the assay was repeated with different internal salt solutions (MF 300 mM, M= Na, K, Rb and Cs) in the absence of valinomycin. To ascertain the series' ability to facilitate group 1 metal fluoride symport (co-transport). As mentioned previously the parent calix[4]pyrrole has a high affinity for caesium halides. The small halides bind and organise the pyrrole rings into a cone conformation, providing an electron rich cup for the large charge diffuse Cs^+ cation to bind within.[97,209] The caesium then in turn stabilises the binding of the anion. Early transmembrane transport research confirms the parent calix[4]pyrrole can selectively co-transport CsCl across lipid bilayers (Internal: CsCl 488 mM, External: Na_2SO_4 162mM).[97] Further to this, addition of a strap can enhance the binding of chloride within the cavity providing encapsulation for the anion binding sites. This additional encapsulation enables chloride uniport and hence the strapped calix[4]pyrroles can facilitate exchange processes such as Cl^-/NO_3^- antiport.[123,206]

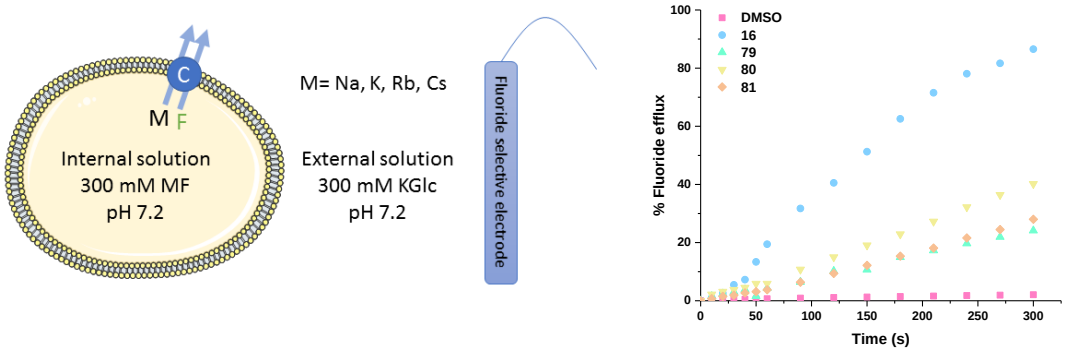

Figure 3.7 **Left-** Overview of the MF co-transport assay. Conditions- Internal: MF 300 mM buffered to pH 7.2 with HEPES buffer 10 mM (M= Na, K, Rb, Cs). External: KGlc 300 mM buffered to pH 7.2 with HEPES buffer. Right- Fluoride efflux facilitated by **16, 79–81** at 2 mol% loading (w.r.t. lipid). The transport was initiated by the addition of a DMSO solution of the receptor at t= 30 s. The vesicles were lysed at 300 s, each point is an average of 3 repeats.

Under the conditions of the assay all receptors function as CsF co-transporters, with the parent macrocycle **16** outperforming the strapped receptors. Negligible transport was observed with NaF, KF and RbF and these results can be found in Appendix C.

3.5.3 Fluoride over chloride selectivity

The majority of previously published anion transport studies have primarily involved chloride as the target anion and in the biological environment chloride is more abundant than fluoride. With fluoride's smaller ionic radius and higher dehydration penalty (ΔG_h= -465 kJmol^{-1} compared to -340 kJmol^{-1} for chloride)[122] making it a difficult anion to select for. As detailed earlier Miller and co-workers have elucidated a crystal structure of a fluoride specific Fluc channel from *Bordetella pertussis*, they surmise that the fluoride over chloride selectivity is due to the narrow bore of the permeation pathway making it size selective for fluoride.[203] The fluoride over chloride selectivity of **79–81** was investigated, with the hypothesis that the differing length straps would impact the anion selectivity observed.

To establish this selectivity, a series of dose response studies were performed utilising the valinomycin coupled assay used formerly. For the fluoride dose response studies, the assay conditions described in Figure 3.5 were used and for the chloride dose response studies the same assay was used but the POPC vesicles were loaded with KCl (300 mM) and the chloride efflux was measured using a chloride selective electrode. The fluoride and chloride efflux were measured for at least six different concentrations again over a period of 300 s. The chloride or fluoride efflux at

270 s for each concentration were then plotted to form a curve shown in Figure 3.8, which also shows plots of the kinetic profile of the dose response testing. Hill analysis,[103] was performed to give EC_{50} values, the effective concentration of receptor needed to achieve 50 % anion efflux. This allowed for a quantitative comparison between the fluoride and chloride transport activity of the series.

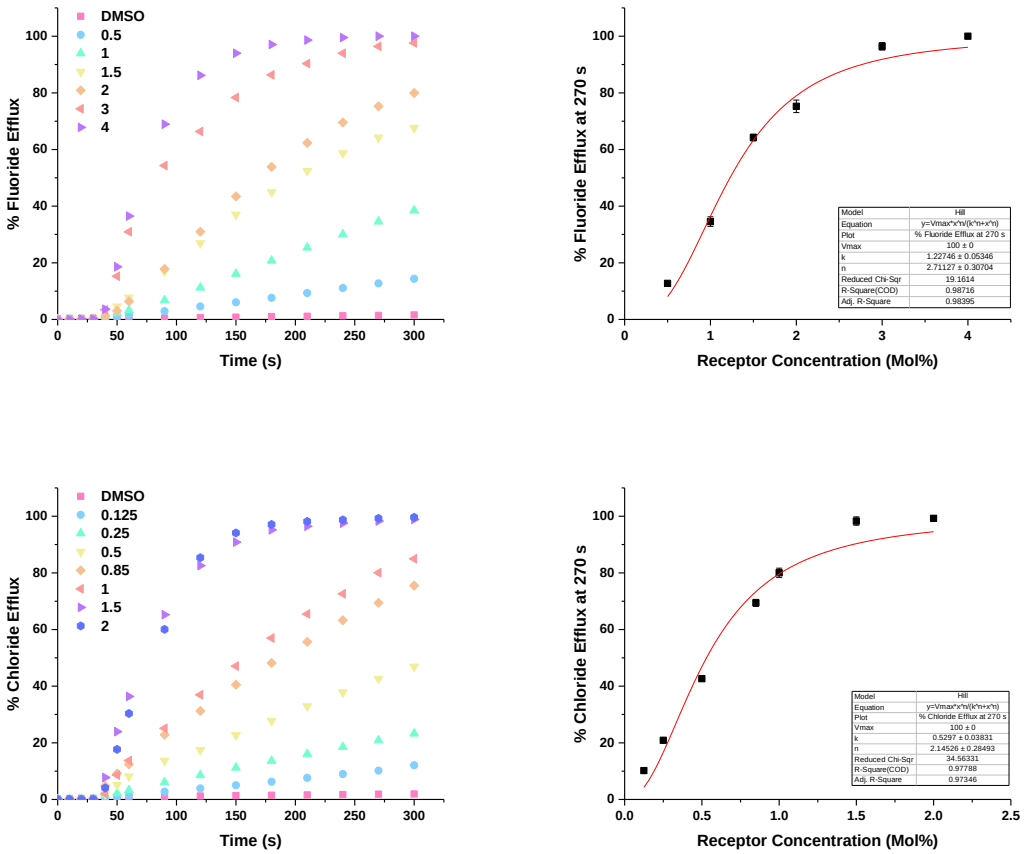

Figure 3.8 All results for receptor **81**. **Left-** Kinetic profile plot. **Right-** Hill plot. Fluoride dose response (top) EC_{50}- 0.9 ± 0.04 mol% and chloride dose response (bottom) EC_{50} - 1.6 ± 0.1 mol%.

The fluoride selectivity factor (S_F) was then calculated by dividing the EC_{50} Cl^-/EC_{50} F^- and the results are shown in Table 3.2. The shorter strapped calix[4]pyrroles **79** and **80** show a preference for fluoride over chloride anion transport compared to **81** which shows marginal chloride selectivity. This selectivity has been attributed to the size of the straps, the larger strap is able to encapsulate the larger chloride anion. All Hill analysis plots can be found in Appendix C.

Table 3.2 Transport activity from the fluoride and chloride ISE assays with fluoride selectivity factors (S_F), from Hill analysis.

Receptor	EC_{50}, mol%[a]		S_F[b]
	F^-	Cl^-	
16	-[c]	-[c]	-[c]
79	1.3 ± 0.06	2.4 ± 0.14	1.8
80	0.9 ± 0.03	1.6 ± 0.10	1.8
81	1.2 ± 0.05	0.5 ± 0.03	0.4

Notes: [a]EC_{50} at 270 s of receptor with respect to lipid. [b]Fluoride selectivity determined from EC_{50} for chloride transport divided by EC_{50} for fluoride selectivity. $S_F > 1$ indicates fluoride selectivity. [c]No transport ability in this assay; no Hill analysis results or selectivity factors calculated.

3.5.4 Osmotic response assay

Due to the membrane permeable nature of HF it is important to rule out the possibility that the receptors are transporting H^+ or OH^- and the positive fluoride response observed is a consequence of this undesirable transport process.

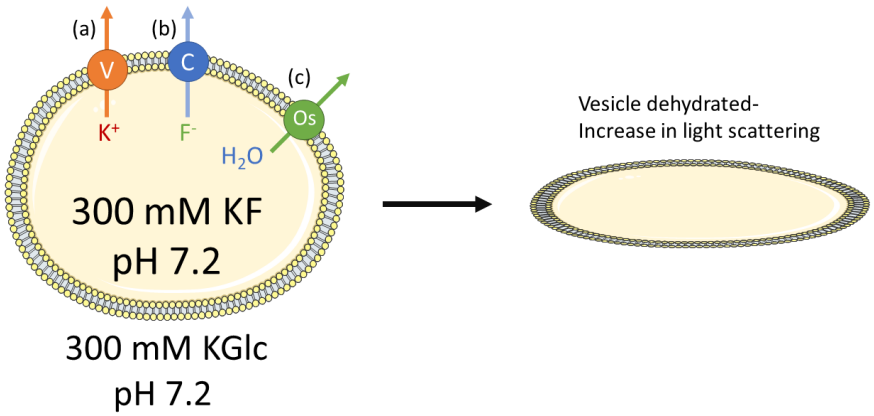

Figure 3.9 Overview of the KF osmotic response assay. Conditions- Internal: KF 300 mM buffered to pH 7.2 with HEPES buffer 10 mM. External: KGlc 300 mM buffered to pH 7.2 with HEPES buffer. Pulse: 0.1 mol% valinomycin. V= valinomycin, C= calix[4]pyrrole transporter and Os= osmosis.

An osmotic response assay was designed to help rule out this H^+/OH^- transport. Figure 3.9 displays large unilamellar vesicles (LUVs, 400 nm) composed of POPC loaded with KF (300 mM) and suspended in KGlc (300 mM). All solutions were buffered to pH 7.2 with HEPES buffer (10 mM). As before, transport was initiated by addition of valinomycin (0.1 mol%) and the transporter (4 mol%) (Figure 3.9 (a) and (b)). Transport of KF initiates the formation of an osmotic gradient, water then leaves the vesicle via osmosis (Figure 3.9 (c)) and this process causes vesicle shrinkage. The vesicle dehydration causes an increase of 90° light scattering which can be monitored using a fluorimeter at λ= 600 nm.

Receptors **79–81** showed an increase in light scattering and therefore a positive response for Vln-coupled KF efflux as seen in Figure 3.10. To rule out H^+ and OH^- transport, which as previously mentioned could cause background HF permeation, a control osmotic assay utilising the acetate ion was performed.

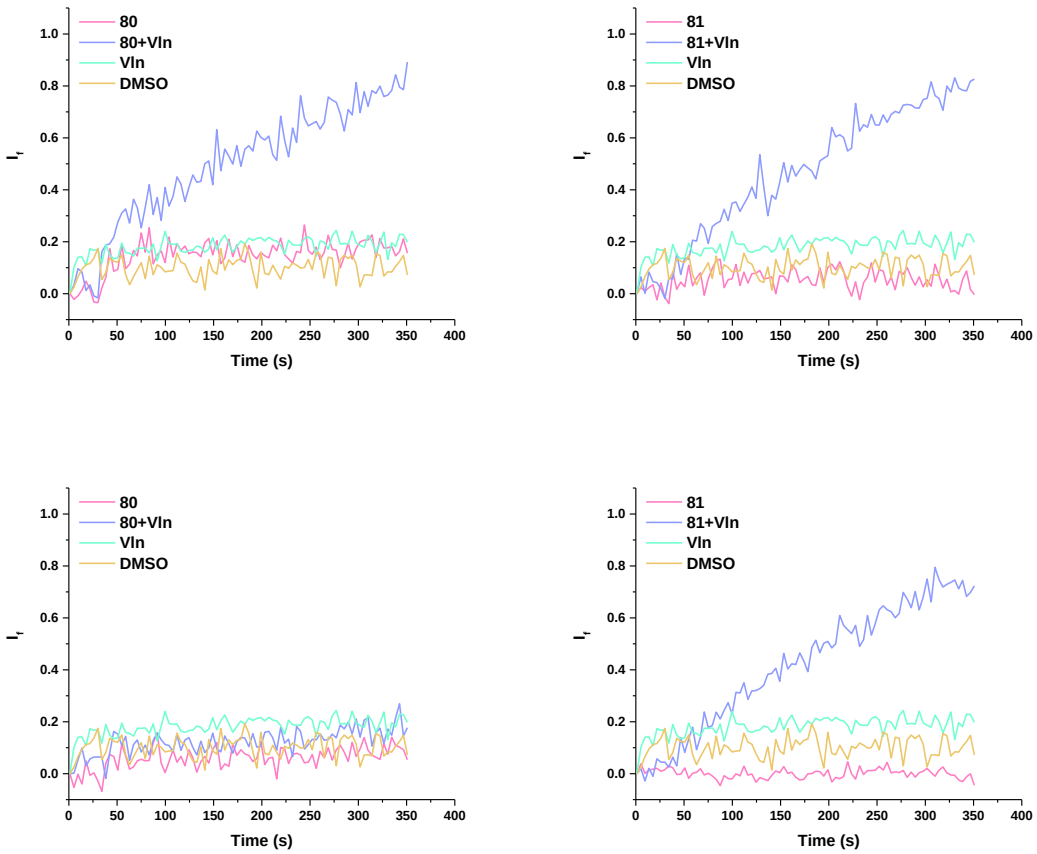

Figure 3.10 Overview of the osmotic assay results for **80** and **81** at 2 mol% loading (w.r.t. lipid) from POPC vesicles described in Figure 3.9. The transport was initiated by the addition of a DMSO solution of Vln (0.1 mol%) and the receptor, at t= 500 s CCCP (5 mol%) was added to give maximum vesicle dehydration after t=600 s. Each plot is an average of 3 repeats. **Top-** light scattering caused by the efflux of fluoride and consequent dehydration of the vesicle via osmosis. **Bottom**- light scattering caused by the efflux of acetate (or acetic acid) and consequent dehydration of the vesicle via osmosis.

The acetate ion alone is membrane impermeable (unless transported); however protonation of acetate as a consequence of H^+ or OH^- transport potentially facilitated by the cali[4]pyrrole strapped receptors, forming membrane permeable acetic acid may give a positive response to this assay. The osmotic assay was repeated but this time potassium acetate was encapsulated. Figure 3.10 shows the results for **80** and **81**, no permeabilization of acetate was seen for **16, 79** and **80**, which is

evidence in support of the absence of H^+ and OH^- transport. Conversely, **81** shows a positive result for the acetate control assay, which was attributed to the larger strapped cavity allowing for acetate binding and transport, and not H^+ or OH^- transport. This deduction is supported with the stronger binding observed for acetate in the ITC study and further studies in Chapter 4:.

3.6 ^{19}F NMR assay

As an alternative direct measurement of fluoride transport a simple fluoride NMR assay was designed. Due to the natural 100 % abundance of the fluoride-19 isotope no isotopic labelling was required as seen in previous NMR assays used within the group.[125,132] Initially the intravesicular and extravesicular ^{19}F NMR signals were observed (Figure 3.11), unfortunately there was not a significant difference in signals, so alone this could not be used as a test for fluoride transport.

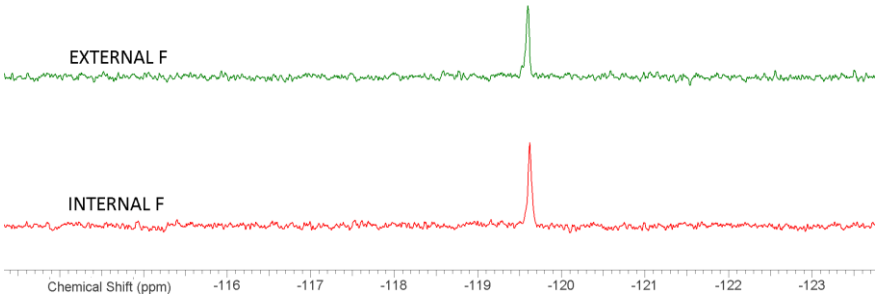

Figure 3.11 The ^{19}F NMR spectra of intravesicular KF and extravesicular KF.

As utilised in the previous NMR assays within the group,[125,132] paramagnetic Mn^{2+} was employed. As Mn^{2+} cannot cross the lipid bilayer only external fluoride in contact with Mn^{2+} will give broadened or reduced signals. The vesicle set up was the same as for the KF ISE assay although larger POPC LUVs (500 nm) were used to give an enhanced signal in the NMR spectrum. They were loaded with KF (300 mM) and suspended in potassium gluconate (KGlc, 300 mM). All solutions were buffered to pH 7.2 with HEPES buffer (10 mM). 1 mL test solutions were set up with a lipid concentration of 1 mM in the NMR tube. Mn^{2+} was added to the external solution (1 mol%).

This NMR assay differs to previous NMR assays for HCO_3^- and SO_4^{2-} due to its fluoride uniport nature; previous assays have relied on Cl^- exchange with the desired anion, but this vesicle set up helps to rule out artificially weak transport results due to the chloride transport being rate limiting.[210] A ^{19}F NMR spectra was obtained pre-transporter addition, valinomycin (0.1 mol%) and the transporter (2 mol%) were added again as DMSO solutions, the NMR tube was inverted and left to stand for 30 min. A second ^{19}F NMR spectra was run and the vesicles were lysed and left to stand for another 30 min, a final ^{19}F NMR spectra was taken. The results for **80** can be seen in Figure 3.12 before transporter and valinomycin addition, the spectra show a single peak signifying internal fluoride (black spectrum). Following the addition of a transporter the fluoride signal has been broadened into the baseline, due to the interaction with external Mn^{2+} signifying fluoride transport out of the vesicle. Transport was observed for **79–81**, but no significant signal change was observed with **16** or the DMSO blank and all the spectra can be found in Appendix C. After the vesicles were lysed the signal remains broadened, or the signal is broadened in the case of **16** and the DMSO blank.

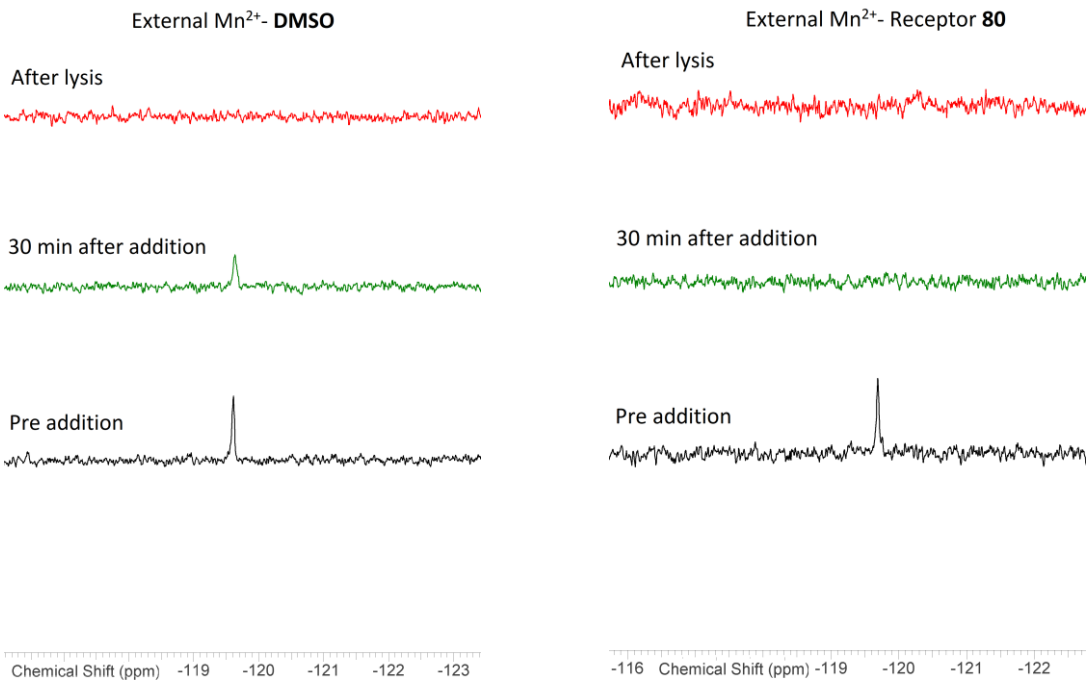

Figure 3.12 ^{19}F NMR experiments to detect fluoride transport with external Mn^{2+} a 'switch off' method. **Left-** DMSO added as a control. **Right-** Receptor **80** and Vln added as a 2 mol% and 0.1 mol% DMSO solution respectively.

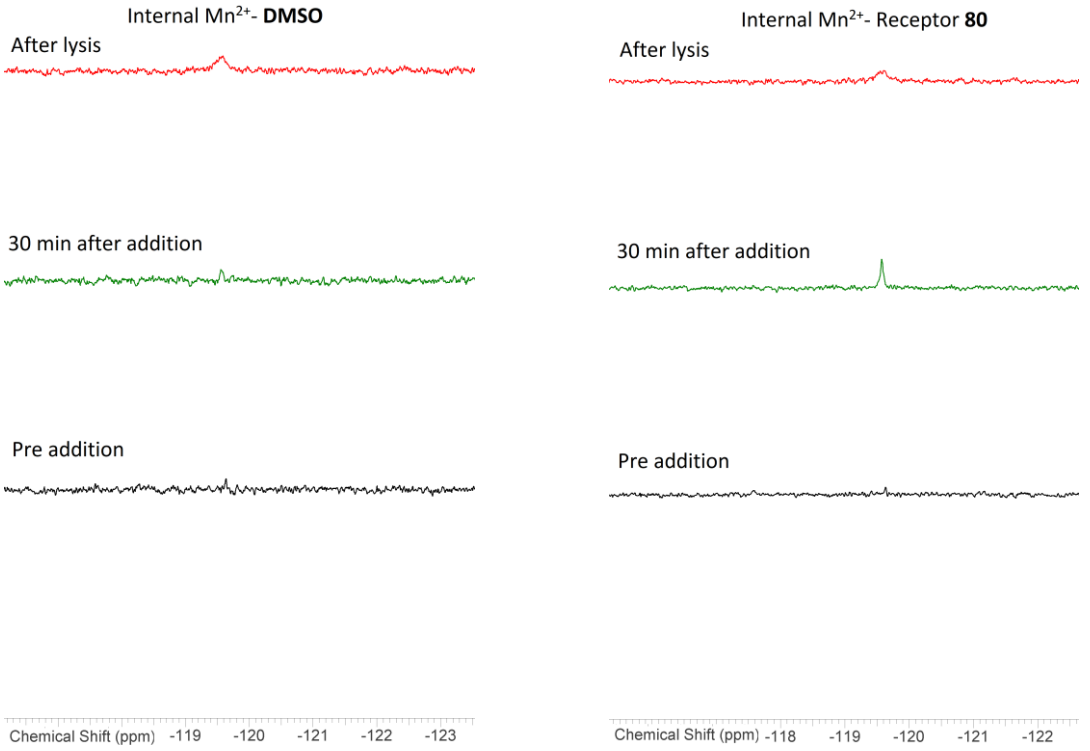

Figure 3.13 ^{19}F NMR experiments to detect fluoride transport with internal Mn^{2+} a 'switch on' method. **Left-** DMSO added as a control. **Right-** Receptor **80** and Vln added as a 2 mol% and 0.1 mol% DMSO solution respectively.

To confirm this transport with a 'switch on' method Mn^{2+} was incorporated inside the vesicle, this way round there is no ^{19}F NMR signal prior to addition of Vln and the transporter. The subsequent transport should lead to the appearance of a ^{19}F signal. The results for receptor **80** can be seen in Figure 3.13. A small signal for the ^{19}F was observed pre-addition of transporter, which could be due to the poor solubility of the Mn^{2+}, leaving it unable to quench the signal fully. Increasing the concentration of Mn^{2+} in the internal solution did not solve this issue and caused visible precipitation. Another possible cause could be low level background leakage of fluoride which would not have been detected in the previous test due to its 'switch off' nature. It is clear however, that following incubation with the transporter the intensity of the ^{19}F NMR signal has increased significantly more than the blank which did not increase over this time, supporting the proposed transport.

It may be noted that after vesicle lysis the ^{19}F NMR signal is not fully quenched and this has been attributed to the poor solubility of the Mn^{2+} previously mentioned. Upon lysis, there is not enough Mn^{2+} left in solution to quench the fluoride signals which due to the change in volume are now more dispersed. It is clear this assay needs optimisation, but it does help to support **79–81**'s ability to function as fluoride transporters.

3.7 Conclusions

This chapter has shown the first example of a direct measurement of small synthetic molecule facilitated, transmembrane fluoride transport using a fluoride ion-selective electrode. The parent calix[4]pyrrole **16** and strapped calix[4]pyrroles **79**–**81** have been used for this investigation with their valinomycin coupled fluoride transport activity and metal fluoride co-transport activity probed. As previously seen in the literature they possess an affinity for caesium when involved in metal fluoride co-transport which was attributed to the anion binding process organising the pyrroles into the electron rich cup for the Cs^+ to sit in.

The shorter strapped receptors **79** and **80** show moderate selectivity for fluoride over chloride in the Vln coupled dose response assays and although this selectivity is moderate, with nothing to compare it with at present it is a good starting point in these selectivity studies.

A new ^{19}F NMR assay has been designed and utilised to support the fluoride transport studies. With both a switch on and off method attempted using the paramagnetic agent $MnSO_4$. Ideally more time for studies in this area would improve this assay.

Chapter 4: Chloride versus H^+/OH^- selectivity with additional halide studies

Parts of the work in this chapter has been published as Harriet J. Clarke, Ethan N. W. Howe, Xin Wu, Fabian Sommer, Masafumi Yano, Mark E. Light, Stefan Kubik, and Philip A. Gale (2016). "Transmembrane fluoride transport: Direct measurement and selectivity studies" *Journal of the American Chemical Society* **138**: 16515–16522 and is reproduced with permission from the American Chemical Society. http://pubs.acs.org/doi/abs/10.1021%2Fjacs.6b10694.

4.1 Introduction

After the success of utilising the strapped calix[4]pyrroles **79–81** for transport studies in Chapter 3:, the series of these transporters was extended to examine their chloride over H^+/OH^- transport selectivity. The transport mechanism of an anion transporter is a crucial factor that needs to be fully understood before any potential applications can be trialled.

Transmembrane pH gradients are vital for healthy cell maintenance.[4] It is important when assessing an ionophore for use as a potential therapeutic to ascertain whether it can facilitate H^+ or OH^- transport alongside its desired ionophoric activity as this may interfere with its intended purpose. The ability to disrupt transmembrane pH gradients may be a useful characteristic when designing an anticancer agent. As discussed earlier, prodigiosins can function as H^+/Cl^- symporters which has been linked to their ability to deacidify lysosomes within cancer cells, causing apoptosis.[45,211] However, this cytotoxic process is not desirable when trying to design replacements for defective channels as potential therapeutics for diseases such as Bartter syndrome or CF.[13] Essentially research is moving to uncover a potential anionophore that can act as a 'valinomycin for chloride',[212] and display pure chloride uniport in a selective and highly active manner.

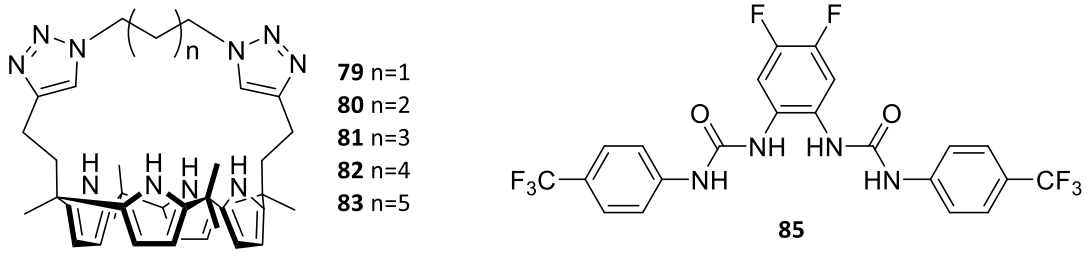

Figure 4.1 Structures of the strapped calix[4]pyrroles **79–83** and a bis-urea **85** utilised in the chloride selectivity study.

In a recent breakthrough study by Wu *et al.*,[154] assays were designed to assess the ability of ionophores to transport H^+ or OH^- coupled with Cl^- transport and quantify the selectivity of Cl^- transport over H^+/OH^-. The study clarified two different transport mechanisms, electrogenic and electroneutral transport. Electrogenic is a term used, in this case, to describe an ionophore that's transport action results in a change in net charge across a membrane. Alternatively, electroneutral transport does not cause a build-up of charge by additional transport of H^+ or OH^-, this however results in a disruption of the pH gradient which as mentioned previously can cause toxicity in a biological environment. It classified anionophores into these categories using a cationophore coupled assay involving the use of valinomycin and monensin, exploiting their cationophoric mechanisms to characterise the anionophoric mechanism. The selectivity of anionophores positively correlated with the degree of Cl^- encapsulation and is influenced by the acidity of the hydrogen bonding receptors.

The strapped calix[4]pyrrole's NH hydrogen bond donors are less acidic than (thio)ureas and squaramides and are highly encapsulating so it was envisaged they would be more selective for Cl^- over H^+/OH^-. The mechanism and Cl^- over H^+/OH^- selectivity of the extended series of strapped calix[4]pyrroles was examined in this chapter and compared with the highly active non-encapsulating bis-urea **85** (Figure 4.1). Assays were performed primarily using the cationophores valinomycin (Vln) and monensin (Mon) (Figure 4.2) to see if they functioned via an electrogenic or an electroneutral mechanism or if they acted in a non-selective manner and could facilitate both processes. Subsequently, their Cl^- over H^+/OH^- selectivity was quantified using an NMDG HPTS assay. Furthermore, the maintenance of their selectivity was probed in the presence of fatty acids which are found in the cell membrane and therefore must be considered when designing an anion transporter.

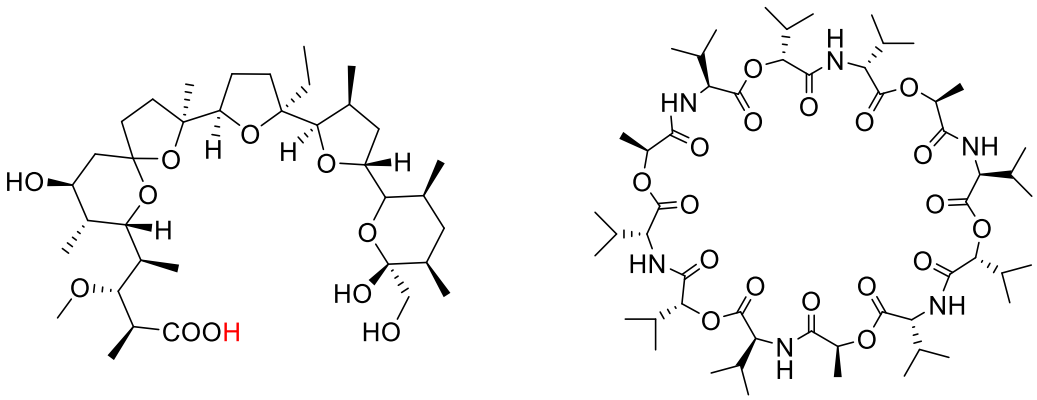

Monensin (Mon) **Valinomycin (Vln)**

Figure 4.2 Structures of cationophores monensin and valinomycin.

As an additional study, the overall halide selectivity of the strapped calix[4]pyrroles **79–83** was investigated, with their size discriminating strap length potentially useful for specific halide transport purposes which could be highly desirable. The transport of environmentally scarce iodide, is a vital process for healthy function of the thyroid gland usually mediated by a Na^+/I^- symporter (NIS), with the iodide transport process being the rate limiting step of the biosynthesis of thyroid hormones.[213,214] The essential role of the NIS role within the thyroid was confirmed using gene cloning and mutation studies in patients with dyshormonogenetic goiters a rare genetic disorder which is caused by problems with the production and distribution of thyroid hormone.[215] Hence, the ability to selectively transport iodide over environmentally abundant chloride could be an interesting concept for potential anionophoric therapeutics. Although in practise, the actual measurement and detection of bromide and iodide transport proved difficult.

.

4.2 Synthesis

Extending the calix[4]pyrrole series involved the synthesis of a six methylene and an eight methylene strapped calix[4]pyrrole **82** and **83**. Similar to the synthetic strategy from Chapter 3:, **82** and **83** were synthesised following the literature procedure outlined by Yano *et al.*[206] and full characterisation of all steps can be found in the experimental details and Appendix A. Compounds **82** and **83** were synthesised in yields of 35 and 21 % respectively and some details of the workup were slightly adapted for these larger strapped calixpyrroles.

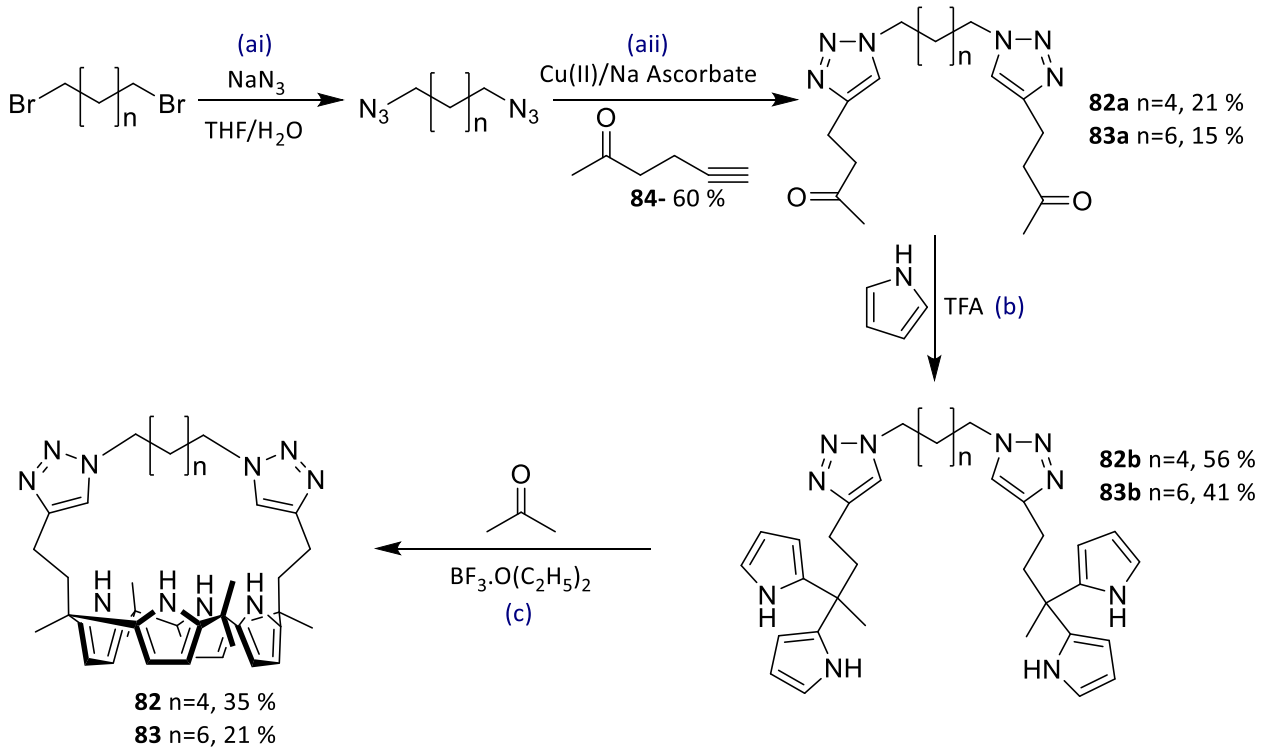

Scheme 3 Synthesis of the extended strapped calix[4]pyrroles **82** and **83**.

4.3 Binding Studies

Proton NMR titration studies were conducted in DMSO-d_6:H_2O (99.5:0.5, v/v) with tetrabutyl-ammonium acetate, fluoride, chloride, bromide, iodide (TBAOAc, TBAF, TBACl, TBABr and TBAI) for **79–83** if not previously performed. Formerly observed slow exchange on the NMR timescale was detected for most receptors **79–83** with TBAOAc, TBAF, TBACl and TBABr. Receptor **79** showed less slow exchange character, but broadening of the signals prevented quantification of the binding. Weak interaction was observed for titrations with TBAI and binding constants were only calculated for **82** and **83** using global fitting analysis with Bindfit,[163,164] resulting in a K_a of 11 M^{-1} for both receptors. As expected, the larger more charge diffuse iodide anion interacts weakly with the hydrogen-bond donors. All the receptors showed similar binding trends, stack plots and species ratio plots can be found in Appendix B. For illustration, an example of the NMR spectra stack plot and binding curves of receptor **82** with TBABr and TBAI are shown in Figure 4.3.

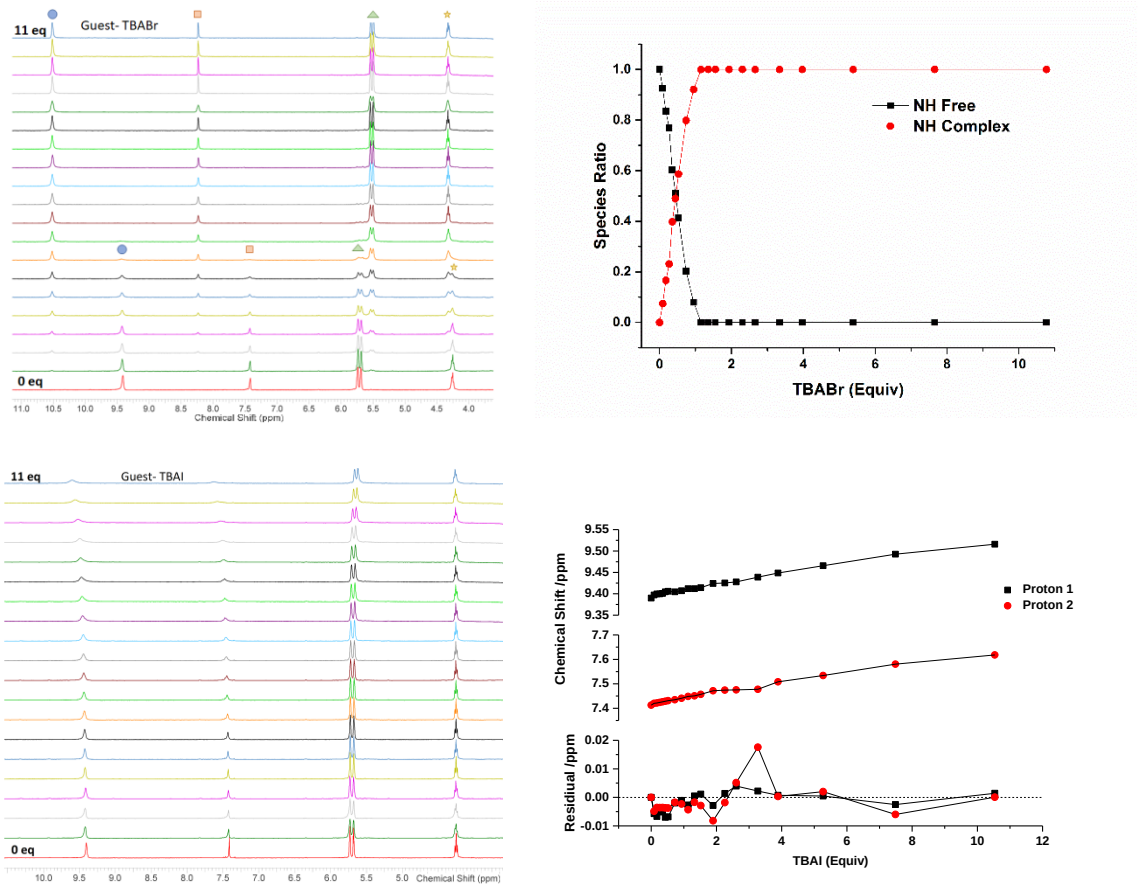

Figure 4.3 Stack plots for receptor **82** ^{1}H NMR titration with TBABr (top) and TBAI (bottom) in DMSO-d_6:H_2O (99.5:0.5, v/v). Blue circle follows the pyrrole NH signal, orange square follows the triazole CH signal, green triangle follows the pyrrole CHs signal and the yellow star follows an alkyl CH_2. Species ratio (top) and bindfit output (bottom).

4.4 Solid state analysis

Receptors **82** and **83** were isolated as crystalline solids as complexes with TBACl by slow diffusion of petroleum spirits into a DCM solution of **82** with TBACl (5 equiv) and slow evaporation from a DMSO solution of **83** and TBACl (in excess) respectively.

The solid state structures of these complexes can be seen in Figure 4.4 and show the anion bound within the strapped cavity of the calix[4]pyrrole receptor. Receptor **82** and **83** shows N···Cl interactions that range from 3.305–3.332 Å and 3.269–3.380 Å respectively. Receptor **82** displays one triazole C···Cl long range hydrogen bond (3.710 Å), while both triazoles of **83** display potential long range C···Cl hydrogen bonds although these have lengths of > 4 Å so are weak. Both receptors also show long range C···Cl hydrogen bonds from the axial methylene groups from the strap with distances of 3.340–3.930 Å.

Both solid state structures showed some disordering within the structure; details of the disordered atoms and full crystallographic information can found in Appendix A. As the strap length increased disorder within crystal structures was expected as it increases the flexibility within the strap, it is well known that long alkyl chains such as TBA often cause disorder within solid state structures.

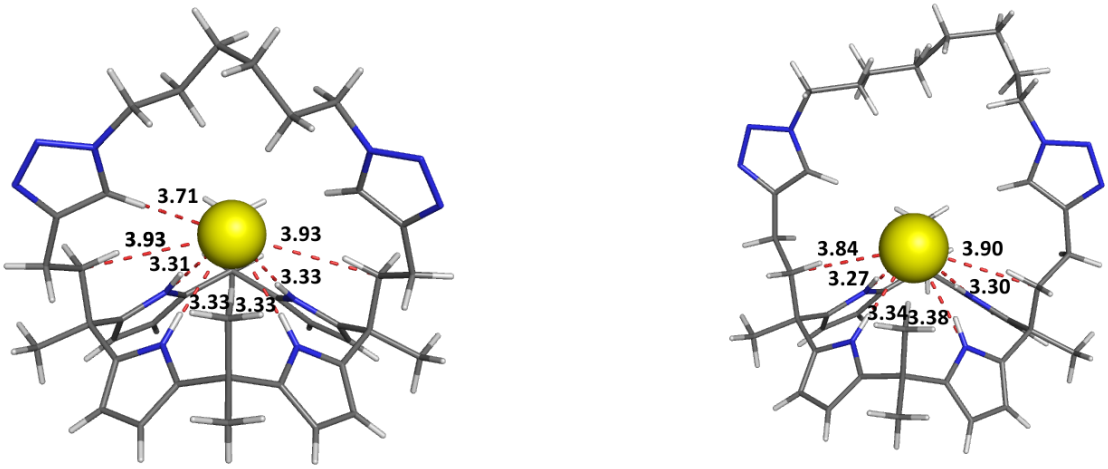

Figure 4.4 **Left-** Single crystal X-ray structure of **82**·TBACl complex (the minor orientation of the disordered atoms and TBA are excluded for clarity). **Right-** Single crystal X-ray structure of **83**·TBACl complex (the minor orientation of the disordered atoms, TBA and DMSO are excluded for clarity). N···Cl and C···Cl distances are displayed as red dashed lines, with measurements in Å. Full crystallographic data can be found in Appendix A.

4.5 Transport studies

4.5.1 Valinomycin and monensin coupled assay

From the previous chapter it is known that the strapped calix[4]pyrroles **79–81** can couple to valinomycin. Valinomycin is an electrogenic transporter, where the transport of K^+ leads to a change of net charge across the membrane. In the case of the potassium-anion (KX) transport assay (Figure 3.5) there is a net transfer of charge across the membrane by valinomycin-enabled potassium transport (Figure 4.5), thus dissipating the membrane potential[216] that is produced by the receptor's anion transport process, to give the overall KX efflux. If a transporter can couple to valinomycin it can therefore function as an electrogenic chloride transporter as seen in Figure 4.6.

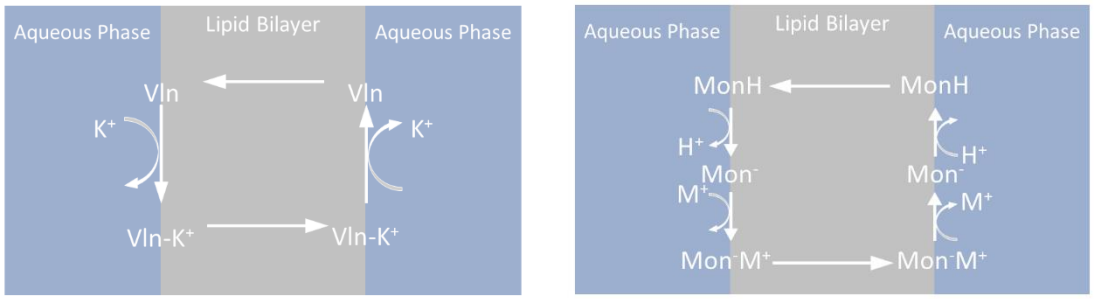

Figure 4.5 **Left-** Transmembrane electrogenic potassium transport facilitated by valinomycin (Vln) **Right-** Transmembrane electroneutral M^+/H^+ antiport facilitated by monensin (Mon).

Monensin is a cationophore with a fundamentally different transport mechanism to valinomycin. It has a carboxylic group which can be deprotonated (Figure 4.2) and therefore can function via an electroneutral mechanism. This means it can transport without a change in the net charge across the membrane. It facilitates M^+/H^+ exchange (Figure 4.5), coupling to an electroneutral transporter which can either enable H^+/Cl^- symport or Cl^-/OH^- antiport and therefore dissipate the pH gradient which could build up if the transporter acted alone. Wu *et al.* provided evidence that prodigiosin cannot function as an electrogenic transporter and hence transports with an electroneutral mechanism (Figure 4.6), allowing for coupling to monensin. They also show simple urea receptors can couple to both valinomycin and monensin suggesting their ability to facilitate non-specific electroneutral and electrogenic transport.[154]

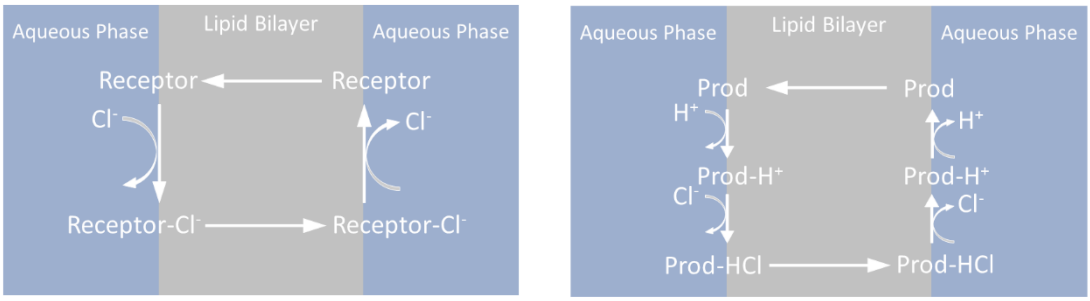

Figure 4.6 **Left-** Transmembrane electrogenic chloride transport facilitated by a receptor. **Right-** Transmembrane H^+/Cl^- transport facilitated by the electroneutral transporter prodigiosin (Prod).

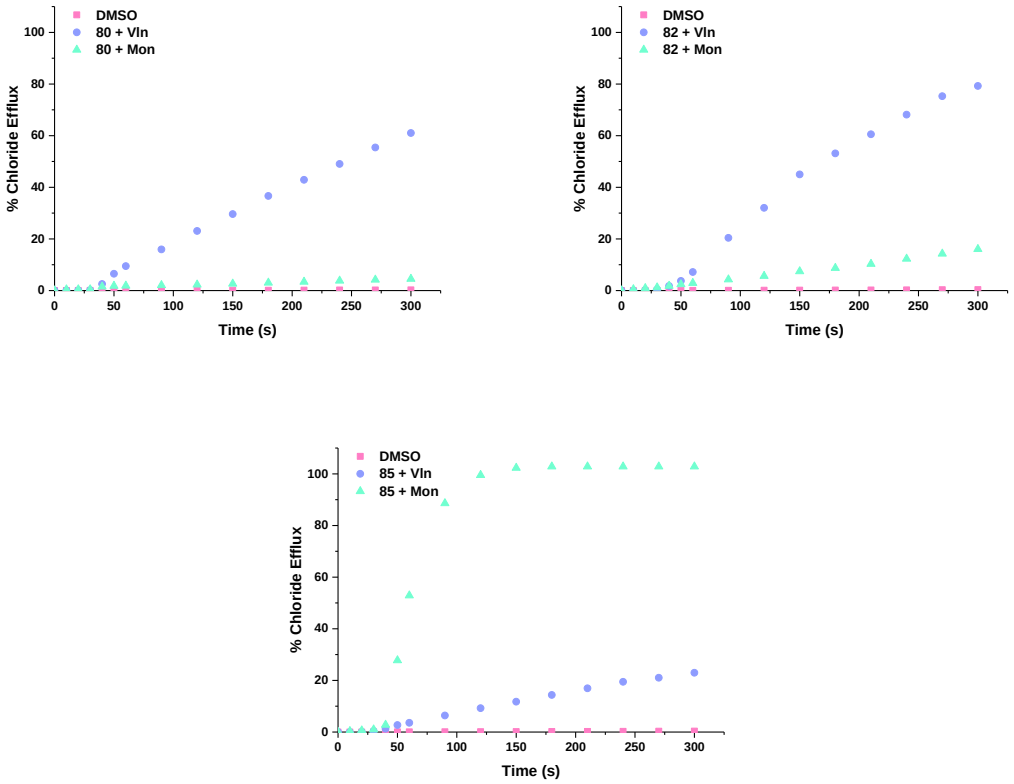

Figure 4.7 Coupling to valinomycin and monensin for **80**, **82** and **85**. Chloride efflux facilitated at 2 mol% loading (0.02 mol% **85)** (w.r.t. lipid) from POPC vesicles. The transport was initiated by the addition of a DMSO solution of Vln (0.1 mol%) or Mon (0.1 mol%) at t= 0 s and then the receptor at t= 30 s. The vesicles were lysed at 300 s, each point is an average of 3 repeats. Full results of this assay can be found in Appendix C.

Receptors **79-83** and **85** were tested within the KX assay used in Chapter 3: with the addition of valinomycin and monensin (0.1 mol%) monitored using a chloride ISE. Overall strapped calix[4]pyrroles **79–83** show exclusive coupling to valinomycin, although, a minor amount of additional coupling to monensin was observed for the two larger strapped receptors. This supports

the hypothesis that these receptors function with an electrogenic transport mechanism, as compared to **85**, which couples predominantly to monensin suggesting a primarily electroneutral mechanism.

4.5.2 NMDG selectivity assay

Quantification of the Cl^- over H^+/OH^- selectivity of the receptors **79–83** and **85** was performed using a modified NMDG-Cl HPTS assay, [33,154] which involved the use of gramicidin D (Gra or G) a naturally occurring proton channel, and oleic acid (OA), a naturally occurring monounsaturated omega-9 fatty acid (Figure 4.11).

Figure 4.8 shows large unilamellar vesicles (LUVs, 200 nm) composed of POPC loaded with 8-hydroxypyrene-1, 3, 6-trisulfonic acid (HPTS, a pH-sensitive dye, 1 mM) and *N*-methyl-*D*-glucamine chloride (NMDG-Cl, 100 mM) and suspended in NMDG-Cl (100 mM). All solutions were buffered to pH 7.0 with HEPES buffer (10 mM). Transport was initiated by the addition of the transporter and a base pulse (NMDG, 5 mM) at t= 0 s. The base pulse generates a pH gradient across the bilayer, the dissipation of this gradient was monitored by following the HPTS fluorescence ratio (Base form, λ_{ex}= 460 nm, λ_{em}= 510 nm divided by the acidic form, λ_{ex}= 403 nm, λ_{em}= 510 nm).

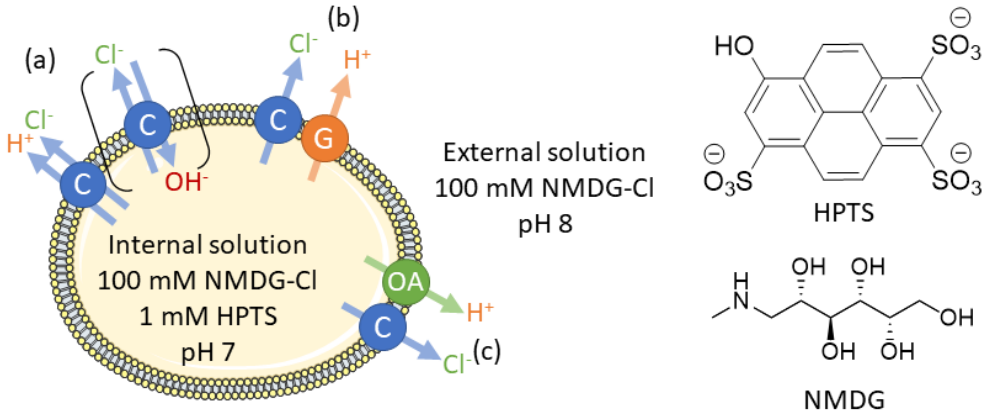

Figure 4.8 Overview of NMDG-Cl HPTS assay. Conditions- Internal: NMDG-Cl 100 mM and HPTS 1 mM buffered to pH 7 with HEPES buffer 10 mM. External: NMDG-Cl 100 mM buffered to pH 7 with HEPES buffer 10 mM, pulse: NMDG to bring external pH to 8. The transport was initiated by addition of a DMSO solution of the transporter. (a) The transporter was added alone and the electroneutral (H^+/Cl^- symport or Cl^-/OH^- antiport) transport was monitored by following the pH gradient dissipation. (b) Gramicidin (G) was added which facilitates H^+ transport, this will allow electrogenic Cl^- transporters to function within the assay, the transport was monitored by following the pH gradient dissipation. (c) Oleic acid (OA) was added to evaluate the receptor's ability to uphold selectivity in the presence of fatty acids.

This assay measures the receptor's electroneutral H^+/Cl^- symport (Cl^-/OH^- antiport) ability. If the receptor functions as a selective electrogenic Cl^- transporter as found for the strapped calix[4]pyrroles, it is proposed the H^+/OH^- transport will be the rate limiting factor for transport in Figure 4.8(a). Addition of the proton channel Gra (Figure 4.8(b)) should accelerate the H^+ transport, removing the rate limiting effect.

Quantification of the transport in both cases (with and without the proton channel) permits a selectivity factor (S_G) for Cl^- over H^+/OH^- transport to be calculated. Addition of oleic acid evaluates the transporter's preference for chloride over its ability to contribute to the fatty acid transmembrane proton shuttling. Receptors have been found to accelerate the flip-flop of the fatty acid in the lipid bilayer membrane.[217] As described in Figure 4.9(a) the neutral oleic acid molecules within the membrane undergo a flip-flop across the membrane from the interior (pH 7) to the exterior (pH 8). Protons are deposited by deprotonation of the carboxylic group (pK_a 5.0[218] in bulk water, apparent pK_a 7.6[219] in EYPC vesicles) causing a decrease in the transmembrane pH gradient. An anion receptor can then bind to the deprotonated carboxylate head group, masking the anionic charge from the bilayer, and translocate the headgroup back to the interior to complete the cycle, resulting in enhanced dissipation of the pH gradient.[217,220,221]

Figure 4.9(b) shows the effect described above within the NMDG assay, with overall H^+/Cl^- symport being observed. Experimentally, this process can artificially accelerate the pH gradient dissipation. Hence, the Cl^- over H^+/OH^- selectivity will decrease with the presence of fatty acids within the membrane if the receptor can bind to the carboxylate head group. Since the presence of free (unesterified) fatty acid is ubiquitous in cellular membranes (~1 %),[222] this is important and undesirable in our ongoing effort in the development of Cl^- over H^+/OH^- selective anionophores for potential therapeutics for channelopathies.[154,217]

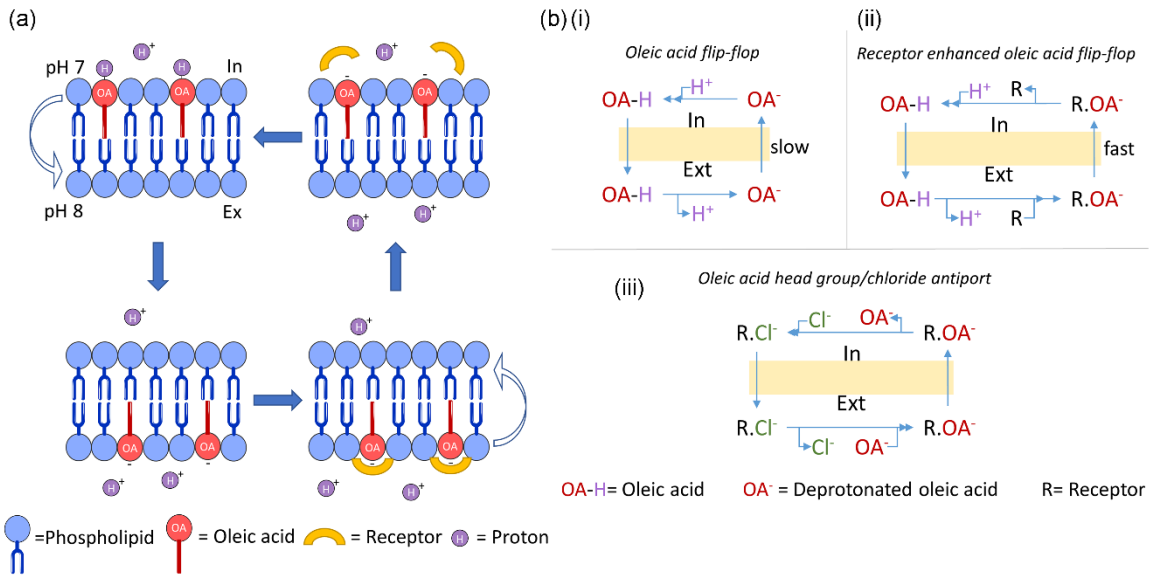

Figure 4.9 Proposed mechanism of fatty acid movement and proton shuttling across lipid bilayers, enhanced by anion receptors and subsequently increasing the HPTS fluorescence response in the NMDG-Cl assay, contributing to the pH gradient dissipation. (a) A receptor capable of complexation of the deprotonated headgroup of a fatty acid can enhance the proton shuttling by masking the charged headgroup to accelerate the movement of the charged fatty acid back across the membrane to complete the cycle. (b)-(i) Schematic to show the natural function of the oleic acid flip-flop with the slow rate determining step. (ii) Schematic to show how a receptor can complex the deprotonated carboxylate head group to accelerate the rate determining step by masking the anionic charge on the headgroup. (iii) Schematic to show this process in relation to the NMDG assay, causing formal Cl^-/OA^- antiport and overall H^+/Cl^- symport facilitated by a receptor and oleic acid, thus artificially increasing the pH dissipation rate.

Dose response experiments and Hill analysis were performed using the NMDG assay described in Figure 4.8 in the absence and presence of Gra and oleic acid to give EC_{50} values. The ratio of these EC_{50} values was used to quantify the chloride selectivity, giving selectivity factors S_G and $S_{OA/G}$ presented in Table 4.1.

Receptors **79**–**83** show good selectivity for Cl^- over H^+/OH^- along the series, with S_G values of 18.2–10.3. As hypothesised receptor **85** the non-encapsulating acidic bis-urea showed very little selectivity with an S_G value of 1.4, and the smallest strapped calix[4]pyrrole **79** with the three methylene chain possessing the highest selectivity for chloride, these results support the previous findings that a higher degree of anion encapsulation enforces a higher degree of anion desolvation and hence better selectivity for chloride.

Table 4.1 Summary of Cl^- over H^+/OH^- selectivity for **79**-**83** and **85**.

Receptor	EC_{50} (mol%)	$EC_{50}Gra^a$ (mol%)	$S_G{}^b$	$EC_{50}OA^c$ (mol%)	$F_{OA}{}^d$	$S_{OA/G}{}^e$	$S_{OA/G}$-$S_G{}^f$
79	10.9 ± 0.3	0.6 ± 0.03	18.2	11.2 ± 0.2	1.0	18.7	0.5
80	4.1 ± 0.1	0.4 ± 0.02	10.3	3.6 ± 0.04	1.1	9.0	-1.3
81	2.7 ± 0.04	0.2 ± 0.01	13.5	1.6 ± 0.09	1.7	8.0	-5.5
82	1.5 ± 0.1	0.1 ± 0.004	15.0	0.4 ± 0.02	3.8	4.0	-11.0
83	1.1 ± 0.04	0.1 ± 0.007	11.0	0.5 ± 0.03	2.2	5.0	-6.0
85	$1.3 \pm 0.08 \times 10^{-4}$	$9.3 \pm 0.5 \times 10^{-5}$	1.4	$2.0 \pm 0.06 \times 10^{-4}$	0.65	2.1	0.7

Notes: [a] EC_{50} in the presence of gramicidin D; this value shows the total H^+/Cl^- symport (Cl^-/OH^- antiport) activity possible, with no rate-limiting H^+/OH^- transport. The Gra concentration has been optimised at 0.1 mol% to prevent this having a limiting effect. [b] Cl^- over H^+/OH^- selectivity factor S_G is calculated by dividing EC_{50} in the absence of Gra by the EC_{50} Gra. $S_G > 1$ indicates Cl^- selectivity. [c] EC_{50} in the presence of oleic acid (2 mol%); this value shows the effect of fatty acids on the selectivity. [d] Factor of overall H^+/Cl^- symport enhancement in the presence of OA, calculated by dividing the EC_{50} in the absence of OA by EC_{50} OA. $F_{OA} > 1$ suggests the that the receptor can assist the flip flop of OA^-, enhancing the pH dissipation. [e] Cl^- over H^+/OH^- selectivity value in the presence of oleic acid, calculated by dividing the EC_{50} OA by the EC_{50} Gra. $S_{OA/G} > 1$ indicates Cl^- selectivity. [f] If $S_{OA/G}$-$S_G \approx 0$, there is no selectivity loss in the presence of OA.

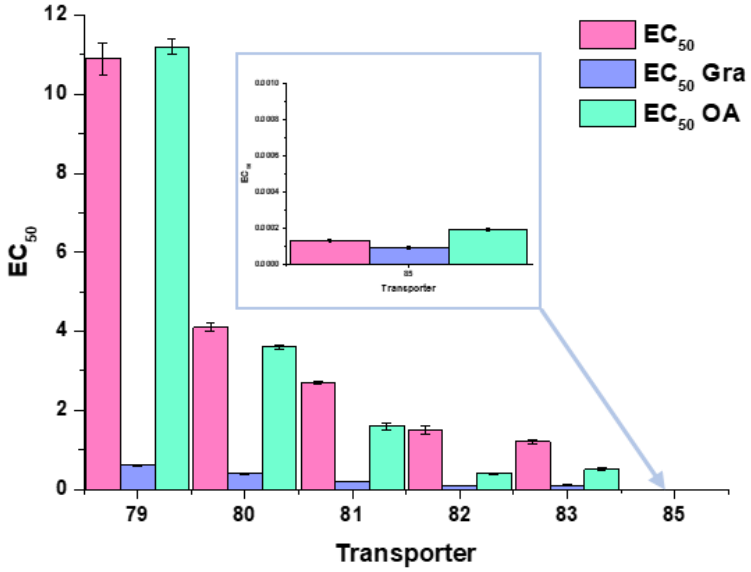

Figure 4.10 Bar chart of EC_{50} results for dose response studies with **79**–**83, 85** from POPC vesicles described in Figure 4.8. The H^+/Cl^- symport was measured by monitoring the HPTS fluorescence ratio after the addition of a 5 mM NMDG pulse (with an additional pulse of Gra (0.1 mol%) or OA (2 mol%) as appropriate). The Hill equation was used to fit the dose-response curves for **79**–**83, 85** alone, with Gra and with OA. Kinetic profiles and Hill plots can be found in Appendix C.

Figure 4.10 shows the EC_{50} values in a bar chart to help visualise this selectivity. In the presence of oleic acid, the effect of artificially enhanced H^+/Cl^- symport presumably due to the additional assisted fatty acid flip-flop process outlined in Figure 4.9 is negligible in receptors **79** and **80**. However, there is a definitive increase as you go from the three-methylene to the eight-methylene strap, with F_{OA} values of 1.1–3.8. This result correlates to the findings in the osmotic assay and ITC study in Chapter 3: that **81** is likely to bind and transport acetate, as it is more inclined to bind the oxoanionic carboxylate head group of oleic acid (Figure 4.11) to enhance its proton shuttle effect and therefore accelerate the dissipation of the pH gradient. This resulted in a loss of Cl^- over H^+/OH^- selectivity ($S_{OA/G}$) for **81**–**83** of -5.5 – -11.0, there is a small loss for **80**, but the selectivity of the shortest strapped receptor **79** was not compromised in the presence of oleic acid.

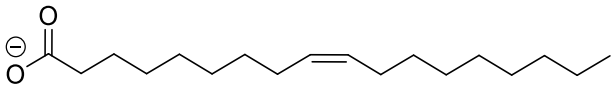

Figure 4.11 Monounsaturated omega-9 fatty acid, oleic acid OA (deprotonated).

These results reiterate the advantageous effect of encapsulation and imposed steric hindrance in the design of synthetic anion transporters for overall Cl^- over H^+/OH^- selectivity and the continued hunt for a valinomycin like transporter for anions specifically chloride.

4.5.3 Osmotic response assay

To support the hypothesis that the larger strapped calix[4]pyrroles **81–83** can facilitate fatty acid flip-flop due to complexation with the carboxylate group, acetate (OAc) transport was evaluated using the osmotic assay, similar to the one discussed in Chapter 3:. Unlike oleic acid which intercalates within the lipid bilayer membrane; the transport of acetate can be unambiguously determined by the osmotic assay, and the degree of acetate transport correlates with the ability to enhance fatty acid flip-flop. The osmotic assay will only respond to an overall KOAc transport in the presence of valinomycin. In addition, the electrogenic transport of chloride for all the strapped calix[4]pyrroles will be validated again using the osmotic assay in a similar manner.

Figure 4.12 displays large unilamellar vesicles (LUVs, 400 nm) composed of POPC were loaded with KX (300 mM) (X=Cl or OAc) and suspended in KGlc (300 mM). All solutions were buffered to pH 7.2 with HEPES buffer (10 mM). Like before transport was initiated by a90ddition of Vln (0.1 mol%) and the transporter (4 mol%) (Figure 4.12(a) and (b)), transport of KX starts the formation of an osmotic gradient, water then leaves the vesicle via osmosis (Figure 4.12(c)) and this process causes vesicle shrinkage. The vesicle dehydration causes an increase of 90° light scattering which can be monitored using a fluorimeter at λ= 600 nm.

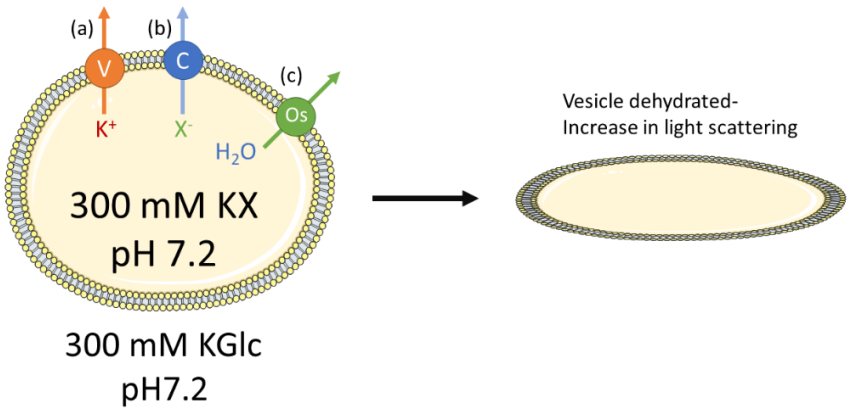

Figure 4.12 Overview of the KX osmotic response assay. Conditions- Internal: KX 300 mM (X= Cl or OAc) buffered to pH 7.2 with HEPES buffer 10 mM. External: KGlc 300 mM buffered to pH 7.2 with HEPES buffer. Pulse: 0.1 mol% valinomycin. V= valinomycin, C=calix[4]pyrrole transporter and Os= osmosis.

Full results from this osmotic assay described in Figure 4.12 can be found in Appendix C. The assay confirms that all the strapped calix[4]pyrroles **79–83** can facilitate KCl symport in the presence of valinomycin, resulting in osmotic shrinkage, the results for **79** and **82** are shown in Figure 4.13. Only **81–83** display a positive response for acetate transport, supporting the hypothesis that the size of the strap modulates the binding and transport of acetate, hence correlating with the ability to enhance fatty acid flip-flop as shown from the NMDG HPTS assay discussed earlier.

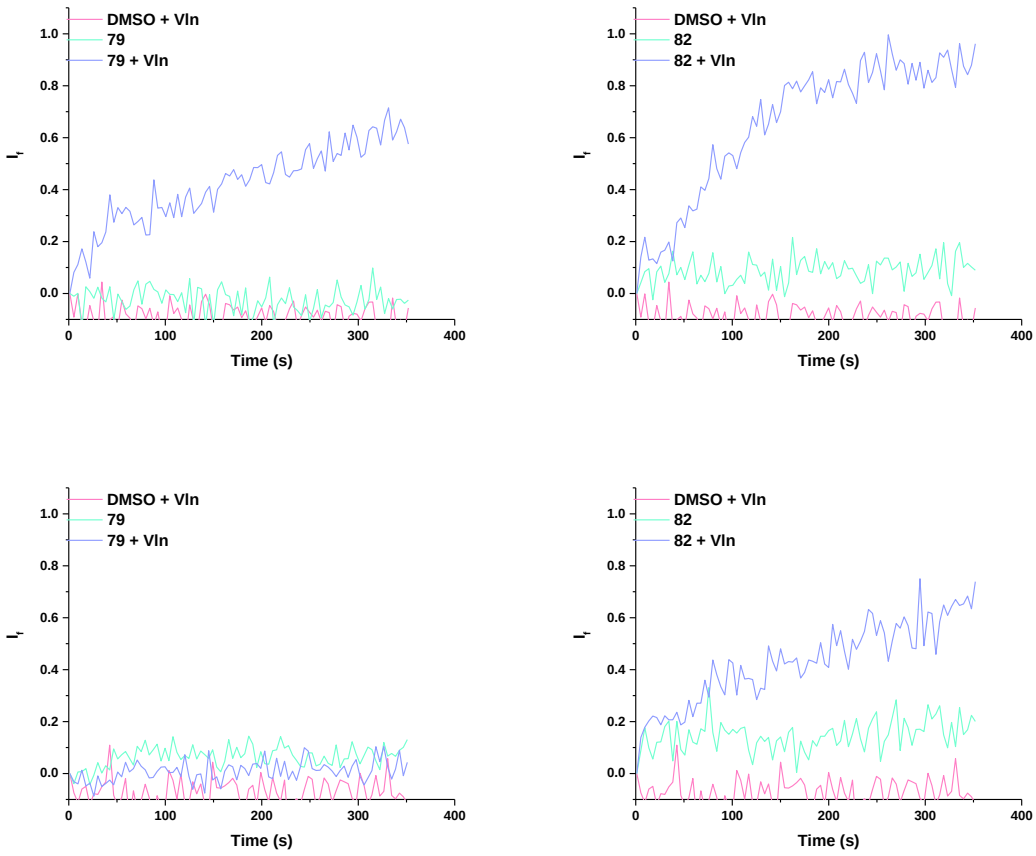

Figure 4.13 Overview of the osmotic assay results for **79** and **82** at 2 mol% loading (w.r.t. lipid) from POPC vesicles described in Figure 4.12. The transport was initiated by the addition of a DMSO solution of Vln (0.1 mol%) and the receptor, at t= 500 s CCCP (5 mol%) or penta-fluoropropylthiourea (8 mol%) was added to give maximum vesicle dehydration after t=600 s. Each plot is an average of 3 repeats. **Top-** light scattering caused by the efflux of chloride and consequent dehydration of the vesicle via osmosis. **Bottom-** light scattering caused by the efflux of acetate and consequent dehydration of the vesicle via osmosis.

4.5.4 KX HPTS assay

As an additional study the transport selectivity of chloride, bromide, iodide and nitrate for the strapped calix[4]pyrroles was investigated. However, this proved to be problematic as previously used methods for measuring the anion transport were not feasible. The NMDG HPTS assay, normally set up by titrating the corresponding acid into a solution of NMDG to reach the required pH, when performed with HI, I_2 was formed by the decomposition of HI. I_2 has been found to transport I^- itself

via halogen bonding.[168,223] The transport of I^- by the large excess of I_2 out performs the transport by the calix[4]pyrroles, hence making this assay unfeasible.

An adapted HPTS assay originally utilised by Matile *et al.*[33] was performed using potassium salts and a potassium hydroxide base pulse. With an internal solution of KX 100 mM and HPTS 1 mM buffered to pH 7 with HEPES buffer 10 mM. The external solution was KX 100 mM buffered to pH 7 with HEPES buffer 10 mM, X= Cl, Br, I and NO_3. This assay was adapted for the measurement of the H^+/X^- symport or X^-/OH^- antiport (both electroneutral) processes facilitated by the anion transporters alone as well as coupled with the addition of carbonyl cyanide *m*-chlorophenyl hydrazine (CCCP) as the protonophore. Gramicidin could not be used in this case as it can facilitate the transport of cations K^+ and Na^+.[30,224] This assay was attempted for Cl^-, Br^- and I^- and additionally with NO_3^-. Unfortunately, with the addition of CCCP with KBr and KI vesicles, ≈ 80 % pH dissipation is observed with no transporter added, possibly due to CCCP back transport (following proton transport) coupling to background Br^- or I^- leakage due to their more permeable nature than Cl^- and NO_3^-.[225]

Nonetheless, the electroneutral transport EC_{50} values of the KCl, KBr, KI and KNO_3 mediated by the transporters alone are displayed in Table 4.2 which follow the Hofmeister trend, with the general transport trend being $I^- > NO_3^- \approx Br^- > Cl^-$ for most cases. This makes sense, as previously mentioned the Hofmeister series has been linked to the dehydration penalty, with Cl^- and Br^- more strongly hydrated, there is a larger energy cost to bind and encapsulate them. This Hofmeister effect is corroborated by the intrinsic halide anion membrane permeability, which shows I^- to be the most permeable, four times that of bromide which is six times more permeable that chloride.[225] However, **79** demonstrated the ability to overcome the general trend with a transport ability of $Cl^- > NO_3^- \approx Br^- > I^-$, due to the small encapsulated binding site being selective for Cl^-. It should be noted that the transport of H^+/OH^- by this receptor is very poor, resulting in difficulties in obtaining good data for Hill analysis in some cases (shown in Appendix C). Nonetheless, this study has shown size-dependent selectivity and the overcoming of the general Hofmeister trend in anion transport.

Table 4.2 EC_{50} results from KX HPTS assay (X=Cl, Br, I and NO_3^-).

	EC_{50} (mol%)			
Receptor	**Cl^-**	**Br^-**	**I^-**	**NO_3^-**
79	10.4 ± 0.8	19.6 ± 0.3	34.5 ± 1.5	14.7 ± 0.5
80	5.9 ± 0.7	5.9 ± 0.4	2.5 ± 0.2	6.1 ± 0.3
81	4.5 ± 0.5	3.7 ± 0.7	0.5 ± 0.09	4.6 ± 0.1
82	3.8 ± 0.6	2.9 ± 0.1	0.5 ± 0.1	0.8 ± 0.08
83	0.9 ± 0.1	2.6 ± 0.2	0.8 ± 0.07	1.1 ± 0.07

4.5.5 CsX osmotic response assay

Following the problems with studying the full halide selectivity using the HPTS assay, an alternative method was proposed, an osmotic response assay was utilised to ascertain the CsX symport affinity. As discussed earlier in this thesis the calix[4]pyrrole structure can accommodate a Cs^+ ion on the underside cone of the four pyrrole ring, this can occur simultaneously with the binding of the anion via hydrogen bonding from the four pyrrole NHs. In Chapter 3: the strapped calixpyrroles were shown to facilitate CsF symport in addition to fluoride and chloride uniport, and previous studies have shown the parent calix[4]pyrrole can only transport Cl^- in the presence of a Cs^+.[226]

The osmotic assay was set up with large unilamellar vesicles (LUVs, 400 nm) composed of POPC, which were loaded with CsX (300 mM) (X=F, Cl, Br or I) and suspended in KGlc (300 mM). All solutions were buffered to pH 7.2 with HEPES buffer (10 mM). Unlike previously, only the transporter was added to initiate transport, as no cationophore is necessary. As shown in Figure 4.14 **79** displays the poorest transport across the caesium salts, and as expected its symport ability diminishes as the anion gets larger and more diffuse. Receptor **80** showed the best transport across all the anions, with the three largest strapped receptors **81–83** showing similar responses across the anion series, which suggests increasing the length of the strap past a certain point is not beneficial if you require specific selectivity. Interestingly Figure 4.15 shows an unusual kinetic profile for receptor **83**, purple line, also seen in the KCl osmotic response performed earlier. It displays a more sigmoidal kinetic profile which is attributed to its higher lipophilicity (logP- 6.45) than the other transporters. This higher level of lipophilicity can impede delivery through the aqueous media before partitioning into the membrane and hence the initial transport rate is slower compared to shorter strapped receptors. The logP values for the series span from 5.64–6.45 with the expected order increasing lipophilicity with the increase in strap length. These differences in lipophilicity will play a role in the transport effectiveness, as discussed throughout this thesis, transport is a complex process with many factors contributing to efficacy.

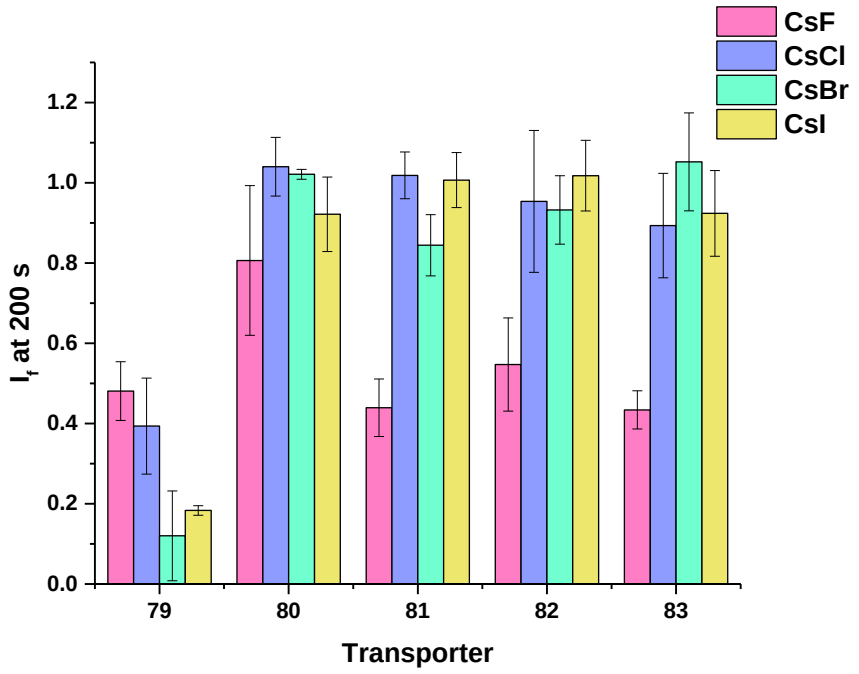

Figure 4.14 A bar chart showing the I_f at 200 s for 79–83 at 4 mol% loading (w.r.t. lipid) in the CsX osmotic assay. Internal: CsX 300 mM (X= F, Cl, Br or I) buffered to pH 7.2 with HEPES buffer 10 mM. External: KGlc 300 mM buffered to pH 7.2 with HEPES buffer.

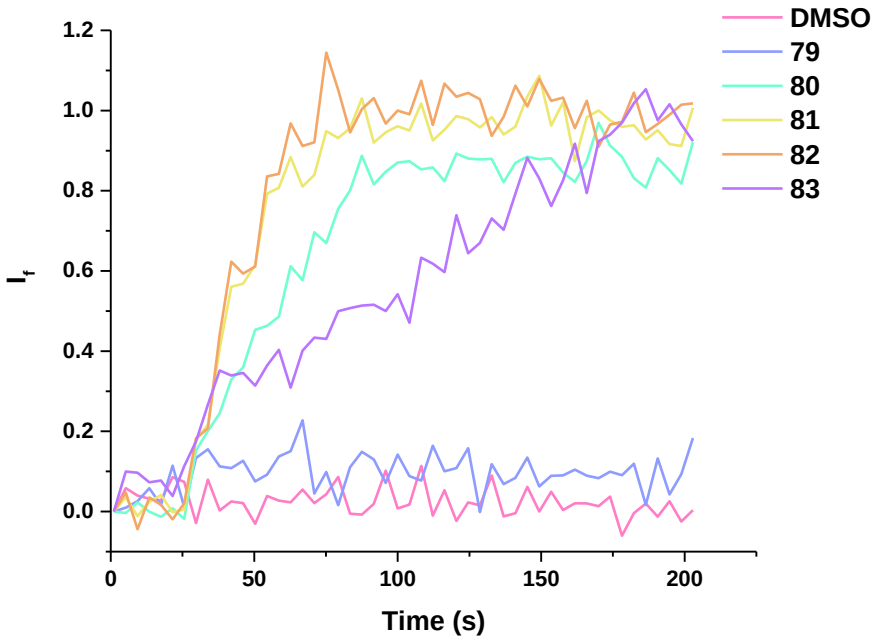

Figure 4.15 Kinetic profile from the caesium salt osmotic response assay, for CsI with receptors 79–83 at 4 mol% loading (w.r.t. lipid) from POPC vesicles described above. The transport was initiated by the addition of a DMSO solution of the receptor at t= 30 s, each plot is an average of 2 repeats.

4.6 Conclusions

Extension of the series of strapped calix[4]pyrroles, isolating two novel receptors and their chloride complexes was achieved. The chloride over proton or hydroxide selectivity of the full series was investigated and quantified, finding all the receptors highly selective for Cl^- > H^+/OH^-, supporting previous findings that encapsulation is the key to selectivity.[154] As strap length increases, Cl^- selectivity diminishes and H^+/OH^- transport improves. This is supported by the minor increase in coupling to monensin for receptor **82** and **83**, i.e. the nature of the transport mechanism evolves from electrogenic and becomes slightly electroneutral.

In addition to elucidating the transport mechanism, the transport selectivity was also investigated in the presence of naturally occurring oleic acid. This confirmed that the presence of fatty acid can interfere with the transport mechanism and can artificially enhance the H^+ transport and therefore highlights the importance of considering a receptor's fatty acid headgroup affinity when designing a transporter for physiological purposes. Remarkably, the shortest strapped calixpyrrole, whilst maybe not the most effective transporter, demonstrated the best Cl^- > H^+/OH^- selectivity but also maintained this selectivity in the presence of fatty acids. To date, receptor **79** remains the only Cl^- selective anion transporter immune to the presence of free fatty acid.

Two other assays were also utilised to try and quantify the halide selectivity of the series, employing fluoride, chloride, bromide and iodide salts within the tests. Despite the restrictions to obtain full quantification of the electrogenic transport of all the halides, results were obtained for the limiting electroneutral transport and the caesium salt symport processes. These assays confirmed that the size of the strap is vital to the nature of the anion bound and transported. Essentially **79** could not facilitate CsBr or CsI symport and showed increasingly high EC_{50} values for the electroneutral transport (H^+/X^- or OH^-/X^-) down the halide series. On the other hand, the other transporters showed anti-Hofmeister bias with a trend of Cl^- < Br^- ≈ NO_3^- < I^-. The caesium affinity of the calix[4]pyrroles and halide selectivity is being investigated further within the lab. Further studies could include titration experiments to investigate and confirm how the larger strapped calix[4]pyrroles interact with phospholipid head groups. Ideally future work would focus on an effective method to measure Br^- and I^- transport, to achieve this, additional effort to elucidate the membrane permeability characteristics of these two anions compared to chloride and how these affect the viability of our testing methods is necessary.

Chapter 5: Experimental details

5.1 General remarks

Chemicals were purchased from commercial suppliers and were used without further purification unless stated otherwise. POPC was purchased from Corden Pharma or Avanti Lipids.

Melting point analyses were carried out using a Barnstead Electrothermal IA9100 melting machine.

NMR spectra (^{1}H NMR, ^{13}C {^{1}H} NMR and ^{19}F NMR) were collected on a Bruker AVII400 spectrometer, NMR titrations were also performed on the same instrument. Chemical shifts (δ) were reported in ppm and calibrated using the residual solvent peak for DMSO-d_6, acetonitrile-d_3 or chloroform-*d*. Spin multiplicities were abbreviated as follows: s= singlet, d= doublet, t= triplet, q= quartet, m= multiplet, br= broad and app= apparent.

HRMS samples were analysed using a MaXis (Bruker Daltonics, Bremen, Germany) mass spectrometer equipped with a Time of Flight analyser. Samples were introduced to the mass spectrometer via a Dionex Ultimate 3000 autosampler and uHPLC pump. Gradient 20 % acetonitrile (0.2 % formic acid) to 100 % acetonitrile (0.2 % formic acid) over five min at 0.6 mL min. Column, Acquity UPLC BEH C18 (waters) 1.7 micron 50 x 2.1 mm. High resolution mass spectra were recorded using positive/negative ion electrospray ionisation.

ITC measurements were performed on a fully computer operated Microcal VP-ITC instrument.

X-ray crystallography diffraction data was collected on various diffractometers, detailed in the crystallography section, and the crystallographic data has been deposited at the Cambridge Crystallographic Database Centre (CCDC). Images were produced using PyMOL Molecular Graphics System Version 0.99 Schrödinger, LLC and CrystalMaker®: a crystal and molecular structures program for Mac and Windows. CrystalMaker Software Ltd, Oxford, England (www.crystalmaker.com).

Ion selective electrode assay were performed using Accumet chloride or fluoride selective electrodes and fluorescence assays were carried out using a Varian Cary Eclipse Fluorescence Spectrometer.

5.2 Synthesis

5.2.1 N,N'–(phenylmethylene)dibenzamide 72

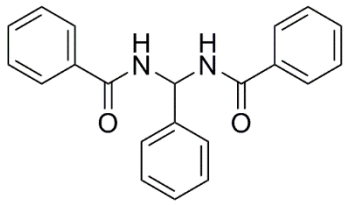

Benzamide (476 mg, 3.9 mmol) and benzaldehyde (203 µL, 2 mmol) were dissolved in dry DMF (8 mL). TMSCl (507 µL, 4 mmol) was added and the reaction was stirred at 50 °C overnight under an inert atm. A white precipitate was formed with the addition of a few drops of water and was purified by trituration with diethyl ether for 30 min. The product was isolated using vacuum filtration and washed with diethyl ether.

Yield 31%; m.p. 218.0–220.0°C.

^{1}H NMR (400 MHz, DMSO-d_6) δ ppm 9.03 (d, *J*=7.82 Hz, 2 H), 7.91 – 7.93 (m, 4 H), 7.54 – 7.58 (m, 2 H), 7.47 – 7.51(m, 6 H), 7.39 (t, *J*=7.40 Hz, 2 H), 7.30 – 7.34 (m, 1 H), 7.05 (t, *J*=7.80 Hz, 1 H). ^{13}C NMR (101 MHz, DMSO-d_6) δ ppm 166.0 (CO), 140.8 (ArC), 134.3 (ArC), 132.0 (ArCH), 128.8 (ArCH), 128.8 (ArCH), 128.1 (ArCH), 128.0 (ArCH), 127.0 (ArCH), 59.2 (CH).

LR-MS ESI$^+$ - (*m/z*)*:* 353 [M+Na$^+$]. HR-MS ESI$^+$ - (*m/z*)*:* Calc. $C_{21}H_{18}N_2NaO_2$ 353.1260 [M+Na$^+$]. Meas. 353.1255 [M+Na$^+$].

5.2.2 N,N'–(phenylmethylene)bis(4-nitrobenzamide) 73

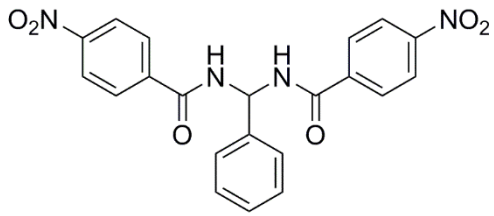

4- nitrobenzamide (662 mg, 3.9 mmol) and benzaldehyde (203 µL, 2 mmol) were dissolved in dry DMF (8 mL). TMSCl (507 µL, 4 mmol) was added and the reaction was stirred at 50 °C overnight under an inert atm. A white precipitate was formed with the addition of a few drops of water and was purified by trituration with diethyl ether for 30 min. The product was isolated using vacuum filtration and washed with diethyl ether.

Yield 44%; m.p. 253.1–254.4 °C.

^{1}H NMR (400 MHz, DMSO-d_6) δ ppm 9.53 (d, *J*=7.20 Hz, 2 H), 8.33 (d, *J*=8.68 Hz, 4 H), 8.16 (d, *J*=8.68 Hz, 4 H), 7.52 (d, *J*=7.36 Hz, 2 H), 7.42 (t, *J*=7.34 Hz, 2 H), 7.34–7.37 (m, 1 H), 7.00 (t, *J*=7.28 Hz, 1 H). ^{13}C NMR (101 MHz, DMSO-d_6) δ ppm 164.8 (CO), 149.7 (ArC), 140.0 (ArC), 139.6 (ArC), 129.7 (ArCH), 128.8 (ArCH), 128.4 (ArCH), 127.3 (ArCH), 123.9 (ArCH), 59.9 (CH).

LR-MS ESI^{+}- (*m/z*): 421 [M+H^{+}]. HR-MS ESI^{+}-(*m/z*)*:* Calc. $C_{21}H_{16}N_4NaO_6$ 443.0962 [M+Na^{+}]. Meas. 443.0969 [M+Na^{+}].

5.2.3 N,N'–((4-(trifluoromethyl)phenyl)methylene)bis(4-nitrobenzamide) 74

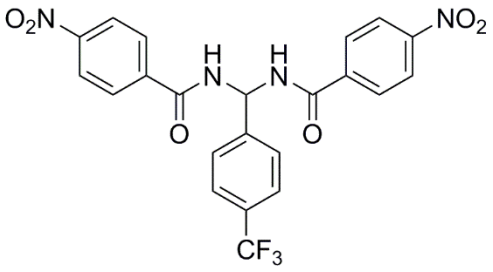

4-nitrobenzamide (340 mg, 2 mmol) and 4 (trifluoromethyl)benzaldehyde (85 µL, 0.5 mmol) were dissolved in dry DMF (8 mL). TMSCl (200 µL, 1 mmol) was added and the reaction was stirred at 50 °C overnight under an inert atm. A white precipitate was formed with the addition of a few drops of water and was purified by trituration with diethyl ether for 30 min. The product was isolated using vacuum filtration and washed with diethyl ether.

Yield 42%; m.p. 280.0–281.9 °C.

^{1}H NMR (400 MHz, DMSO-d_6) δ ppm 9.60 (d, *J*=7.08 Hz, 2 H), 8.35 (d, *J*=8.80 Hz, 4 H), 8.17 (d, *J*=8.80 Hz, 4 H), 7.74–7.80 (m, 4 H), 7.04 (t, J=7.04 Hz, 1 H). ^{13}C NMR (101 MHz, DMSO-d_6) δ ppm) 164.5 (CO), 149.3 (ArC), 143.6 (ArC), 139.3 (ArC), 129.2 (ArCH), 128.6 (q, CF3), 127.7 (ArCH), 125.2 (ArC), 123.4 (ArCH), 122.8 (ArCH), 59.2 (CH). ^{19}F NMR (400 MHz, DMSO-d_6) δ ppm -61.1 (s, 3F, CF_3).

LR-MS ESI^{+}- (m/z): 489 [M+H^{+}]. HR-MS ESI^{+}-(m/z): Calc. $C_{22}H_{15}F_3N_4NaO_6$ 511.0836 [M+Na^{+}]. Meas. 511.0845 [M+Na^{+}].

5.2.4 N,N'–((3, 5-bis(trifluoromethyl)phenyl)methylene)bis(4-nitrobenzamide) 75

Synthesised by Dr. Wim Van Rossom

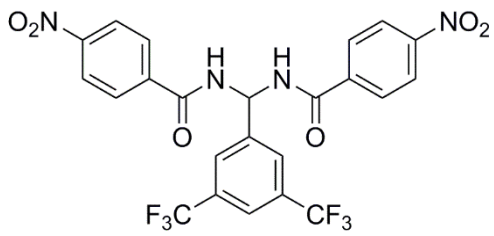

4-nitrobenzamide (1.008 g, 6 mmol), 3,5-bis (trifluoromethyl)benzaldehyde (500 µL, 3 mmol) were dissolved in dry DMF (10 mL). TMSCl (770 µL, 6 mmol) was added and the reaction was stirred at 50 °C overnight under an inert atm. A white precipitate was formed with the addition of a few drops of water and was purified by trituration with diethyl ether for 30 min. The product was isolated using vacuum filtration and washed with diethyl ether.

Yield 81 %; m.p. 283.2–285.1 °C.

^{1}H NMR (400 MHz, DMSO-d_6) δ ppm 9.68 (br d, *J*=6.84 Hz, 2 H), 8.35 (br d, *J*=8.56 Hz, 4 H), 8.25 (s, 2 H), 8.15 (app br d, *J*=8.40 Hz, 5 H), 7.09 (br t, J=6.66 Hz, 1 H). ^{13}C NMR (101 MHz, DMSO-d_6) δ ppm 164.7 (CO), 149.3 (ArC), 142.3 (ArC), 139.2 (ArC), 130.3 (q, CF_3), 129.2 (ArCH), 128.2 (app br d ArC), 124.7 (ArCH), 123.5 (ArCH), 121.9 (ArCH), 59.2 (CH). ^{19}F NMR (400 MHz, DMSO-d_6) δ ppm -61.3 (s, 6F, CF_3).

LR-MS ESI$^-$- (m/z): 555[M-H$^+$]. HR-MS ESI$^+$- (m/z): Calc. $C_{23}H_{14}F_6N_4NaO_6$ 579.0710 [M+Na+]. Meas. 579.0715 [M+Na$^+$].

5.2.5 N,N'–(phenylmethylene)bis(3, 5-bis(trifluoromethyl)benzamide) 76

Synthesised by Dr. Wim Van Rossom.

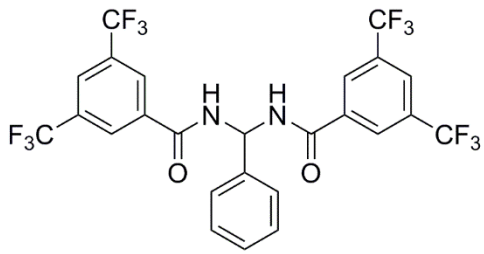

3,5-bis(trifluoromethyl)benzamide (600 mg, 2.3 mmol), benzaldehyde (138 µL, 1.2 mmol)) were dissolved in dry DMF (10 mL). TMSCl (269 µL, 2.3 mmol) was added and the reaction mixture was stirred at 50 °C overnight under an inert atm. A white precipitate was formed with the addition of a

few drops of water and was purified by trituration with diethyl ether for 30 min followed by a recrystallization from ethyl acetate. The product was isolated using vacuum filtration.

Yield 66 %; m.p. 257.1–259 °C.

^{1}H NMR (400 MHz, DMSO-d_6) δ ppm 9.72 (d, *J*=7.09 Hz, 2 H), 8.60 (s, 4 H), 8.35 (s, 2 H), 7.56 (d, *J*=7.36 Hz, 2 H), 7.44 (t, *J*=7.30 Hz, 2H) 7.36 – 7.40 (m, 1 H), 7.05 (t, *J*=6.96 Hz, 1 H). ^{13}C NMR (101 MHz, DMSO-d_6) δ ppm 162.9 (CO), 138.4 (ArC), 135.6 (ArC), 130.2 (q, CF_3), 128.4 (app br d, ArC), 128.2 (ArCH), 127.9 (ArCH), 126.8 (ArCH), 124.2 (ArCH), 121.5 (ArCH), 59.6 (CH). ^{19}F NMR (400 MHz, DMSO-d_6) δ ppm -61.3 (s, 12F, CF_3).

LR-MS ESI$^+$- (m/z): 602 [M+H$^+$]. HR-MS ESI$^+$-(m/z): Calc. $C_{25}H_{15}F_{12}N_2O_2$ 603.0936 [M+H$^+$]. Meas. 603.927 [M+H$^+$]. Diff. (ppm)

5.2.6 N,N'–((4-(trifluoromethyl)phenyl)methylene)bis(3,5-bis(trifluoromethyl)benzamide) 77

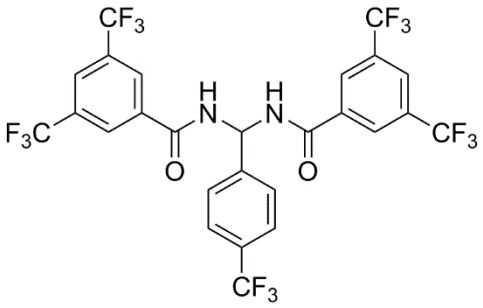

3,5-bis(trifluoromethyl)benzamide (1.03 mg, 4 mmol), 4- (trifluoromethyl) benzaldehyde (272 µL, 2 mmol) were dissolved in dry DMF (8 mL). TMSCl (507 µL, 4 mmol) was added and the reaction mixture was stirred at 50 °C overnight under an inert atm. A white precipitate was formed with the addition of a few drops of water and was purified by trituration with diethyl ether for 30 min. The product was isolated using vacuum filtration and washed with diethyl ether.

Yield 8 %; m.p. 269.0–270.0 °C.

^{1}H NMR (400 MHz, DMSO-d_6) δ ppm 9.82 (d, *J*=6.96 Hz, 2 H), 8.60 (s, 4 H), 8.33 (s, 2 H), 7.79 (app br s, 4 H), 7.10 (t, *J*=6.86 Hz, 1 H). ^{13}C NMR (101 MHz, DMSO-d_6) δ ppm 163.2 (CO), 143.2 (ArC), 135.7 (ArC), 130.5 (q, CF_3), 128.7 (q, CF_3), 128.5 (app br s, ArC) 127.9 (ArCH), 127.2 (ArC), 125.3 (app br d, ArC), 124.4 (ArCH), 121.7 (ArCH), 118.9 (ArCH), 59.5 (CH). ^{19}F NMR (400 MHz, DMSO-d_6) δ ppm -61.1 (m, 3F, CF_3), -61.3 (m, 12F, CF_3).

LR-MS ESI$^-$- (m/z): 669 [M-H$^+$]. HR-MS ESI$^+$-(m/z): Calc. $C_{26}H_{14}N_2O_2F_{15}$ 671.0810 [M+H$^+$]. Meas. 671.0806 [M+H$^+$].

5.2.7 N,N'–(phenylmethylene)bis(2, 3, 4, 5, 6-pentafluorobenzamide) 78

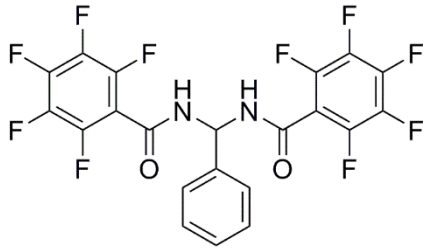

2,3,4,5,6-Pentafluorobenzamide (842 mg, 4 mmol) and benzaldehyde (203 µL, 2 mmol) were dissolved in dry toluene (5 mL). $ZnCl_2$ (~5 mg) was added as a catalyst and the reaction mixture was stirred at reflux for 24 hours under an inert atm. A white precipitate was formed over time and the product was isolated using hot vacuum filtration and washed with diethyl ether.

Yield 20 %; m.p. 253.0–256.0 °C.

^{1}H NMR (400 MHz, DMSO-d_6) δ ppm 9.95 (d, *J*=7.84 Hz, 2 H), 7.47 - 7.48 (m, 4 H), 7.38 – 7.42 (m, 1 H), 6.91 (t, *J*=7.88 Hz, 1 H). ^{13}C NMR (101 MHz, DMSO-d_6) δ ppm 156.2 (CO), 144.4 (ArC), 142.0 (ArC), 138.1 (ArC) 137.7 (ArC), 128.7 (ArCH), 128.4 (ArCH), 126.2 (ArCH), 112.0 (ArC), 58.1 (CH). ^{19}F NMR (400 MHz, DMSO-d_6) δ ppm -141.9 (dd, *J*=24.28 Hz, *J*=8.67 Hz, 4F), -152.9 (br t, *J*=22.54 Hz, 2F), -161.6 (td, *J*=22.54 Hz, 6.94 Hz, 4F).

LR-MS ESI$^-$- (m/z): 553 [M+Na$^+$]. HR-MS ESI$^+$-(m/z): Calc $C_{21}H_9O_2N_2F_{10}$ 511.0499 [M+H$^+$]. Meas 511.0511 [M+H$^+$], Calc. $C_{21}H_8O_2N_2NaF_{10}$ 533.0318 [M+Na$^+$]. Meas. 533.0330 [M+Na$^+$].

5.2.8 5-Hexyn-2-one 84

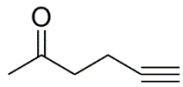

Procedure adapted from the literature,[206,207] 2, 4- Pentadione (14.3 g, 140 mmol), potassium carbonate (21.8 g, 150 mmol) were dissolved in ethanol (70 mL) and propargyl chloride (9.9 mL, 135 mmol) was added dropwise to the reaction mixture. The reaction was stirred at reflux for 24 hours. The reaction was cooled to rt. and water (150 mL) was added to the solution, followed by extraction with diethyl ether (3 x 100 mL). The organic layer was washed with water (150 mL) followed by brine (150 mL), it was then dried over magnesium sulfate. The solvent was removed under vacuum to yield

the crude product as a yellow liquid. The product was purified to give a clear liquid using vacuum distillation.

Yield 60 %

^{1}H NMR (400 MHz, DMSO-d_6) δ ppm 2.74 (t, *J*=2.69 Hz, 1H), 2.67 (t, *J*=7.21 Hz, 2H), 2.32 (td, *J*=7.18 Hz, 2.63 Hz, 2H), 2.12 (s, 3H). ^{13}C NMR (101 MHz, DMSO-d_6) δ ppm 206.4 (CO), 83.7 (C), 71.0 (CH_2), 41.4 (CH), 29.5 (CH_2), 12.3 (CH_3).

5.2.9 1, 3-Bis (4' –(3-oxobutyl)-1*H*- [1', 2', 3'] triazole) propane 79a

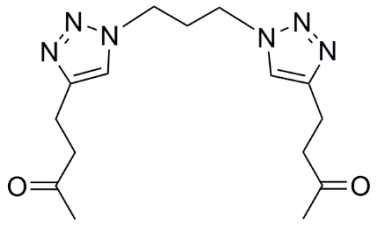

Procedure from the literature,[206] sodium azide (3 g, 46 mmol) was dissolved in water (10 mL), THF (30 mL) was added followed by 1, 3- dibromopropane (0.85 mL, 8.4 mmol). The reaction mixture was stirred at reflux under at inert atm overnight. The reaction mixture was cooled to rt. and **84** (2 g, 21 mmol in THF (2 mL)) was added followed by copper (II) sulfate pentahydrate (400 mg, 10 mol%) and sodium ascorbate (600 mg, 18 mol%) in water (4 mL). The reaction mixture was stirred at reflux under an inert atm. overnight. The reaction was cooled to rt and water (150 mL) was added followed by extraction with chloroform (3 x 100 mL). The organic layer was washed with water (100 mL) followed by sodium bicarbonate solution (5 % in 100 mL) and then brine (100 mL), it was then dried over magnesium sulfate. The solvent was removed under vacuum to yield the crude product which was purified via recrystallization from ethanol to give an off white powder.

Yield 95 %

^{1}H NMR (400 MHz, DMSO-d_6) δ ppm 7.82 (s, 2H), 4.30 (t, *J*=6.97 Hz, 4H), 2.8 (br s, 8H) 2.33 (quin, *J*=7.00 Hz, 2H), 2.11 (s, 6H).

5.2.10 1, 3-Bis (4' –(3, 3-di(pyrrol-2-yl)-1*H*-[1', 2', 3']triazole) propane 79b

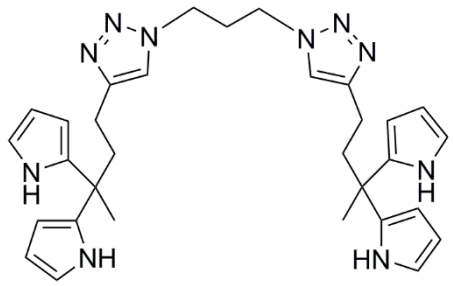

Procedure from the literature,[206] 79a (703 mg, 2.2 mmol) was dissolved in pyrrole (10 mL) followed by TFA (14 drops) the reactions mixture was stirred at 75 °C under an inert atm. for 1 hour. The reaction mixture was cooled to rt. and sodium hydroxide (0.1 M, 100 mL) was added followed by extraction with dichloromethane (100 mL). The organic layer was washed with water (100 mL) and then brine (100 mL) and was dried over magnesium sulfate. The solvent was removed under vacuum to yield the crude product which was purified using flash column chromatography (Fraction 2, eluent- ethyl acetate).

Yield 56 %

^{1}H NMR (400 MHz, DMSO-d_6) δ ppm 10.32 (br s, 4 H), 7.82 (s, 2 H), 6.57 – 6.59 (m, 4 H), 5.86 – 5.88 (m, 4 H), 5.76 – 5.77 (m, 4 H), 4.30 (t, *J*=6.97 Hz, 4 H), 2.25 – 2.41 (m, 10 H), 1.59 (s, 6 H).

5.2.11 C3 spacer bridged-calixpyrrole 79

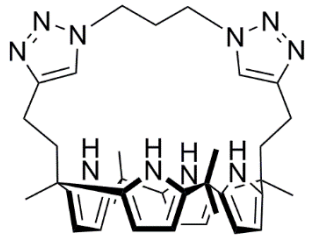

Procedure from the literature,[206] 79b (600 mg, 1.08 mmol) was dissolved in reagent grade acetone (350 mL), boron trifluoride diethyl etherate (0.15 mL, 1.22 mmol) was added dropwise. The reaction mixture was stirred at rt. under an inert atm. for 3 hours. Sodium carbonate (0.1 M, 50 mL) was added followed by extraction with dichloromethane (2 x 100 mL) the organic layer was washed with water (100 mL) and dried over magnesium sulfate. The solvent was removed under vacuum to yield the crude product which was purified using flash column chromatography (Fraction 1, eluent- ethyl acetate).

Yield- 7 %, m. p. 264 °C dec.

^{1}H NMR (400 MHz, DMSO-d_6) δ ppm 8.92 (br s, 4 H), 7.52 (s, 2 H), 5.76 – 5.78 (m, 4 H), 5.72 – 5.73 (m, 4 H), 4.36 (t, *J*=6.79 Hz, 4 H), 2.26 – 2.29 (m, 6 H), 2.14 – 2.17 (m, 4 H), 1.54 (s, 6 H), 1.50 (s, 12 H). ^{13}C NMR (101 MHz, chloroform-*d*) δ ppm 148.8 (ArC), 137.8 (ArC), 136.4 (ArC), 121.2 (ArCH), 104.7 (ArCH), 104.3 (ArCH), 47.9 (CH_2), 42.4 (CH_2), 40.2 (C), 35.9 (C), 30.0 (CH_3), 29.9 (CH_3), 29.8 (CH_3), 29.8 (CH_2), 21.7 (CH_2).

LR-MS ESI$^+$ - (*m/z*)*:* 631.7090 [M+H$^+$]. HR-MS ESI$^+$ - (*m/z*)*:* Calc. $C_{37}H_{47}N_{10}$. 631.3980 [M+H$^+$]. Meas. 631.3987 [M+H$^+$]. Calc. $C_{37}H_{46}N_{10}Na$ 653.3799 [M+Na$^+$]. Meas. 653.3807 [M+Na$^+$].

5.2.12 1, 3-Bis (4' –(3-oxobutyl)-1*H*- [1', 2', 3'] triazole) butane 80a

Previously synthesised within the lab by Masafumi Yano.[206]

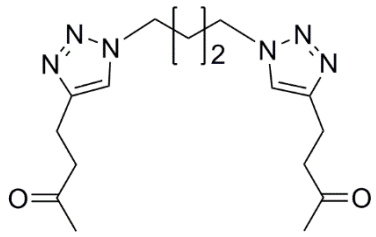

5.2.13 1, 3-Bis (4' –(3, 3-di(pyrrol-2-yl)-1*H*-[1', 2', 3']triazole) butane 80b

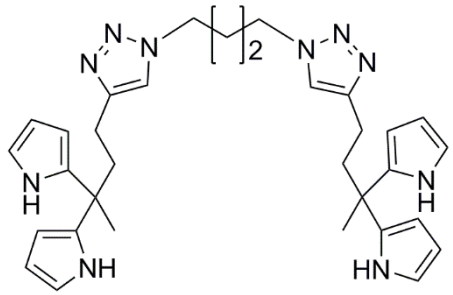

Procedure from the literature,[206] **80a** (758 mg, 2.3 mmol) was dissolved in pyrrole (10 mL) followed by TFA (15 drops) the reactions mixture was stirred at 75 °C under an inert atm. for 1 hour. The reaction mixture was cooled to rt. and sodium hydroxide (0.1 M, 100 mL) was added followed by extraction with dichloromethane (100 mL). The organic layer was washed with water (100 mL) and then brine (100 mL) and was dried over magnesium sulfate. The solvent was removed under vacuum to yield the crude product which was purified using flash column chromatography (Fraction 2, eluent-ethyl acetate).

Yield 50 %

^{1}H NMR (400 MHz, chloroform-*d*) δ ppm 7.98 (br s, 4 H), 7.11 (s, 2 H), 6.63 – 6.64 (m, 4 H), 6.09 – 6.14 (m, 8 H), 4.29 (br t, *J*= 5.50, 4 H), 2.58 – 2.63 (m, 4 H), 2.35 – 2.39 (m, 4 H), 1.88 (br quin, *J*=3.05 Hz, 4 H), 1.67 (s, 6 H).

5.2.14 C4 spacer bridged-calixpyrrole 80

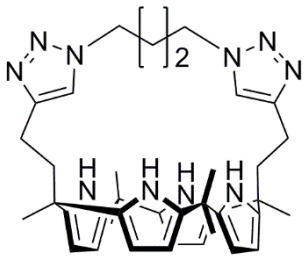

Procedure from the literature,[206] **80b** (650mg, 1.15 mmol) was dissolved in reagent grade acetone (300 mL), boron trifluoride diethyl etherate (0.15 mL, 1.22 mmol) was added dropwise. The reaction mixture was stirred at rt. under an inert atm. for 3 hours. Sodium carbonate (0.1 M, 50 mL) was added followed by extraction with dichloromethane (2 x 100 mL) the organic layer was washed with water (100 mL) and dried over magnesium sulfate. The solvent was removed under vacuum to yield the crude product which was purified using flash column chromatography (Fraction 1, eluent- ethyl acetate).

Yield 14 %, m. p. 247.0 °C dec.

^{1}H NMR (400 MHz, DMSO-d_6) δ ppm 9.39 (br s, 4 H), 7.46 (s, 2 H), 5.76 – 5.81 (m, 4 H), 5.71 – 5.72 (m, 4 H), 4.32 (br s, 4 H), 2.23 – 2.27 (m, 4 H), 2.16 – 2.20 (m, 4 H), 1.76 (br s, 4 H), 1.58 (s, 6 H), 1.48 (s, 12 H). ^{13}C NMR (101 MHz, chloroform-*d*) 149.1 (ArC), 138.0 (ArC), 136.6 (ArC), 121.0 (ArCH), 104.5 (ArCH), 103.8 (ArCH), 49.4 (CH_2), 42.0 (CH_2), 39.8 (C) 35.8 (C), 31.8 (CH_3), 30.2 (CH_3), 29.9 (CH_3), 26.7 (CH_2), 21.5 (CH_2).

LR-MS ESI$^+$ - (*m/z*)*:* 645.6825 [M+H$^+$]. HR-MS ESI$^+$ - (*m/z*)*:* Calc. $C_{38}H_{49}N_{10}$. 645.4136 [M+H$^+$]. Meas. 645.4125 [M+H$^+$]. Calc. $C_{38}H_{48}N_{10}Na$ 667.3956 [M+Na$^+$]. Meas. 667.3941 [M+Na$^+$].

5.2.15 1, 3-Bis (4' –(3-oxobutyl)-1*H*- [1', 2', 3'] triazole) pentane 81a

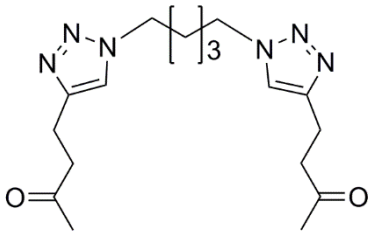

Procedure from the literature,[206] sodium azide (2.99 g, 46 mmol) was dissolved in water (10 mL), THF (30 mL) was added followed by 1, 5- dibromopentane (1.15 mL, 8.3 mmol). The reaction mixture was stirred at reflux under at inert atm. overnight. The reaction mixture was cooled to rt. and **84** (2 g, 21 mmol in THF (2 mL)) was added followed by copper (II) sulfate pentahydrate (400 mg, 10 mol%) and

sodium ascorbate (600 mg, 18 mol%) in water (4.5 mL). The reaction mixture was stirred at reflux under an inert atm. overnight. The reaction was cooled to rt. and water (150 mL) was added followed by extraction with chloroform (3 x 100 mL). The organic layer was washed with water (100 mL) followed by sodium bicarbonate solution (5 % in 100 mL) and then brine (100 mL), it was then dried over magnesium sulfate. The solvent was removed under vacuum to yield the crude product which was purified via recrystallization from ethanol to give off white powder.

Yield 53 %

^{1}H NMR (400 MHz, chloroform-*d*) δ ppm 7.29 (s, 2H), 4.27 (t, *J*=7.03 Hz, 4H), 2.86–2.98 (m, 8H), 2.16 (s, 6H), 1.91 (quin, *J*= 7.40 Hz, 4H), 1.28–1.33 (m, 2H).

5.2.16 1, 3-Bis (4' –(3, 3-di(pyrrol-2-yl)-1*H*-[1', 2', 3']triazole) pentane 81b

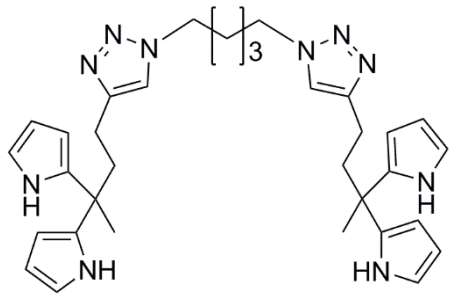

Procedure from the literature,[206] **81a** (758 mg, 2.3 mmol) was dissolved in pyrrole (10 mL) followed by TFA (15 drops) the reactions mixture was stirred at 75 °C under an inert atm. for 1 hour. The reaction mixture was cooled to rt. and sodium hydroxide (0.1 M, 100 mL) was added followed by extraction with dichloromethane (100 mL). The organic layer was washed with water (100 mL) and then brine (100 mL) and was dried over magnesium sulfate. The solvent was removed under vacuum to yield the crude product which was purified using flash column chromatography (Fraction 2, eluent-ethyl acetate).

Yield 38 %

^{1}H NMR (400 MHz, chloroform-*d*) δ ppm 8.35 (br s, 4 H), 7.09 (s, 2 H), 6.61 – 6.64 (m, 4 H), 6.11 – 6.13 (m, 4 H), 6.06 – 6.08 (m, 4 H), 4.28 (t, *J*=6.48 Hz, 4 H), 2.54 – 2.58 (m, 4 H), 2.32 – 2.37 (m, 4 H), 1.90 (br quin, *J*=7.09 Hz, 4 H), 1.65 (s, 6 H), 1.13 – 1.21 (m, 2 H).

5.2.17 C5 spacer bridged-calixpyrrole 81

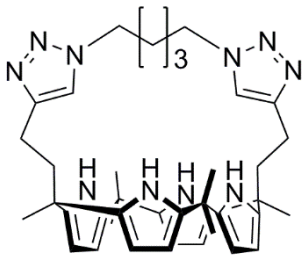

Procedure from the literature,[206] **81b** (578 mg, 1 mmol) was dissolved in reagent grade acetone (300 mL), boron trifluoride diethyl etherate (0.15 mL, 1.22 mmol) was added dropwise. The reaction mixture was stirred at rt. under an inert atm. for 3 hours. Sodium carbonate (0.1 M, 50 mL) was added followed by extraction with dichloromethane (2 x 100 mL) the organic layer was washed with water (100 mL) and dried over magnesium sulfate. The solvent was removed under vacuum to yield the crude product which was purified using flash column chromatography (Fraction 1, eluent- ethyl acetate).

Yield 23 %, m. p. 230.0 °C dec.

^{1}H NMR (400 MHz, DMSO-d_6) δ ppm 9.26 (br s, 4 H), 7.51 (s, 2 H), 5.71 – 5.72 (m, 4 H), 5.67 – 5.69 (m, 4 H), 4.27 (br t, *J*=5.93 Hz, 4 H), 2.26 – 2.30 (m, 4 H), 2.19 – 2.23 (m, 4 H), 1.80 (br quin, *J*= 6.76 4 H), 1.58 (s, 6 H), 1.50 (br d, *J*=4.52 Hz, 12 H), 1.25 (br quin, *J*= 7.76, 2 H). ^{13}C NMR (101 MHz, chloroform-*d*) δ ppm 148.4 (ArC), 137.9 (ArC), 136.5 (ArC), 120.6 (ArCH), 104.2 (ArCH), 103.7 (ArCH), 49.3 (CH_2), 41.7 (CH_2), 39.5 (C), 35.9 (C), 30.6 (CH_3), 29.5 (CH_3), 29. 4 (CH_3), 28.2 (CH_2), 22.4 (CH_2), 21.8 (CH_2).

LR-MS ESI$^+$ - (*m/z*)*:* 659.7235 [M+H$^+$]. HR-MS ESI$^+$ - (*m/z*)*:* Calc. $C_{39}H_{51}N_{10}$. 659.4293 [M+H$^+$]. Meas. 659.4288 [M+H$^+$]. Calc. $C_{39}H_{50}N_{10}Na$ 681.4112 [M+Na$^+$]. Meas. 681.4103 [M+Na$^+$].

5.2.18 1, 3-Bis (4' –(3-oxobutyl)-1*H*- [1', 2', 3'] triazole) hexane 82a

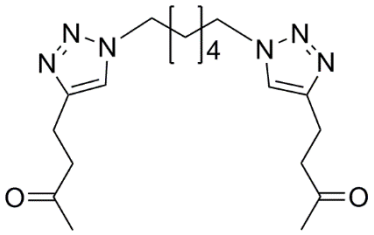

Procedure adapted from the literature,[206] sodium azide (2.96 g, 46 mmol) was dissolved in water (10 mL), THF (30 mL) was added followed by 1, 6- dibromohexane (1.3 mL, 8.3 mmol). The reaction mixture was stirred at reflux under at inert atm. overnight. The reaction mixture was cooled to rt.

and **84** (2 g, 21 mmol in THF (2 mL)) was added followed by copper (II) sulfate.pentahydrate (400 mg, 10 mol%) and sodium ascorbate (602 mg, 18 mol%) in water (4.5 mL). The reaction mixture was stirred at reflux under an inert atm. overnight. The reaction was cooled to rt. and water (150 mL) was added followed by extraction with chloroform (3 x 100 mL). The organic layer was washed with water (100 mL) followed by sodium bicarbonate solution (5 % in 100 mL) and then brine (100 mL), it was then dried over magnesium sulfate. The solvent was removed under vacuum to yield the crude product which was purified via recrystallization from ethanol to give off white powder.

Yield 21 % m.p. 121.0–124.0 °C

^{1}H NMR (400 MHz, chloroform-*d*) δ ppm 7.30 (s, 2 H), 4.28 (t, *J*=7.09 Hz, 4 H), 2.96 – 3.00 (m, 4 H), 2.88 – 2.92 (m, 4 H), 1.87 (br quin, *J*=6.88 Hz, 4 H), 1.61 (s, 6 H), 1.32 – 1.35 (m, 4 H). ^{13}C NMR (101 MHz, chloroform-*d*) δ ppm 207.8 (CO), 146.7 (ArC), 121.3 (ArCH), 49.9 (CH_2), 42.6 (CH_2), 30.0 (CH_3), 29.4 (CH_2) 25.8 (CH_2), 19.6 (CH_2).

LR-MS ESI$^+$ - (*m/z*)*:* 361.4497 [M+H$^+$]. HR-MS ESI$^+$ - (*m/z*)*:* Calc. $C_{18}H_{29}N_6O_2$ 361.2347 [M+H$^+$]. Meas. 361.2342 [M+H$^+$]. Calc. $C_{18}H_{28}N_6NaO_2$. 383.2166 [M+Na$^+$]. Meas. 383.2162 [M+Na$^+$].

5.2.19 1, 3-Bis (4' –(3, 3-di(pyrrol-2-yl)-1*H*-[1', 2', 3']triazole) hexane 82b

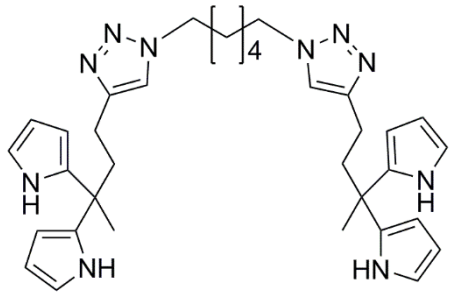

Procedure adapted from the literature,[206] **82a** (400 mg, 1 mmol) was dissolved in pyrrole (10 mL) followed by TFA (10 drops) the reactions mixture was stirred at 75 °C under an inert atm. for 1 hour. The reaction mixture was cooled to rt. and sodium hydroxide (0.1 M, 100 mL) was added followed by extraction with dichloromethane (100 mL). The organic layer was washed with water (100 mL) and then brine (100 mL) and was dried over magnesium sulfate. The solvent was removed under vacuum to yield the crude product which was purified using flash column chromatography (Fraction 2, eluent- ethyl acetate).

Yield 56 %

^{1}H NMR (400 MHz, DMSO-d_6) δ ppm 10.31 (br s, 4 H), 7.78 (s, 2 H), 6.57 – 6.60 (m, 4 H), 5.86 – 5.88 (m, 4 H), 5.75 – 5.77 (m, 4 H), 4.24 (t, *J*=7.08 Hz, 4 H), 2.35 – 2.40 (m, 4 H), 2.23 – 2.28 (m, 4 H), 1.73

–1.77 (m, 4 H), 1.59 (s, 6 H), 1.21 – 1.25 (m, 4 H). ^{13}C NMR (101 MHz, DMSO-d_6) δ ppm 147.0 (ArC), 137.9 (ArC), 121.3 (ArCH), 116.6 (ArCH), 106.3 (ArCH), 103.9 (ArCH), 49.0 (CH_2), 40.4 (CH_2), 38.5 (C), 29.4 (CH_2), 25.2 (CH_2), 25.0 (CH_3), 20.9 (CH_2).

LR-MS ESI$^+$ - (*m/z*)*:* 593.6025 [M+H$^+$]. HR-MS ESI$^+$ - (*m/z*)*:* Calc. $C_{34}H_{44}N_{10}Na$. 615.3643 [M+Na$^+$]. Meas. 615.3639 [M+Na$^+$].

5.2.20 C6 spacer bridged-calixpyrrole 82

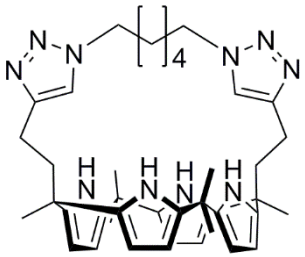

Procedure adapted from the literature,[206] **82b** (300 mg, 0.5 mmol) was dissolved in reagent grade acetone (350 mL), boron trifluoride diethyl etherate (0.15 mL, 1.22 mmol) was added dropwise. The reaction mixture was stirred at rt. under an inert atm. for 3 hours. Sodium carbonate (0.1 M, 50 mL) was added followed by extraction with dichloromethane (2 x 100 mL) the organic layer was washed with water (100 mL) and dried over magnesium sulfate. The solvent was removed under vacuum to yield the crude product which was purified using flash column chromatography (Fraction 1, eluent-ethyl acetate).

Yield- 35 %, m. p. 220.0 °C dec.

^{1}H NMR (400 MHz, DMSO-d_6) δ ppm 9.41 (br s, 4 H), 7.42 (s, 2 H), 5.72 – 5.75 (m, 4 H), 5.67 – 5.70 (m, 4 H), 4.26 (t, *J*=6.66 Hz, 4 H), 2.21 (br s, 8 H), 1.63 – 1.68 (m, 4 H), 1.60 (br s, 6 H), 1.51 (br s, 6 H), 1.48 (br s, 6 H), 1.18 – 1.23 (m, 4 H). ^{13}C NMR (101 MHz, chloroform-*d*) δ ppm 148.5 (ArC), 138.2 (ArC), 136.6 (ArC), 120.1 (ArCH), 103.4 (ArCH), 103.5 (ArCH), 49.4 (CH_2), 41.2 (CH_2), 39.6 (C), 35.8 (C), 31.7 (CH_3), 30.2 (CH_3), 29.8 (CH_3), 28.5 (CH_2), 24.2 (CH_2) 21.7 (CH_2).

LR-MS ESI$^+$ - (*m/z*)*:* 673.7308 [M+H$^+$]. HR-MS ESI$^+$ - (*m/z*)*:* Calc. $C_{40}H_{53}N_{10}$. 673.4449 [M+H$^+$]. Meas. 673.4436 [M+H$^+$]. Calc. $C_{40}H_{52}N_{10}Na$ 695.4269 [M+Na$^+$]. Meas. 695.4257 [M+Na$^+$]. Calc. $C_{40}H_{52}N_{10}K$ 711.4008 [M+K$^+$]. Meas. 711.3995 [M+K$^+$].

5.2.21 1, 3-Bis (4' –(3-oxobutyl)-1*H*- [1', 2', 3'] triazole) octane 83a

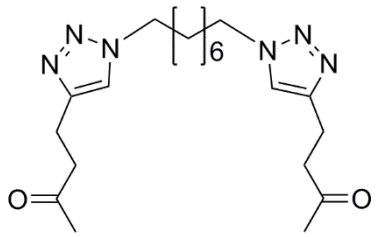

Procedure adapted from the literature,[206] sodium azide (2.97 g, 46 mmol) was dissolved in water (10 mL), THF (30 mL) was added followed by 1, 8- dibromooctane (1.5 mL, 8.3 mmol). The reaction mixture was stirred at reflux under at inert atm. overnight. The reaction mixture was cooled to rt. and **84** (2 g, 21 mmol in THF (2 mL)) was added followed by copper (II) sulfate.pentahydrate (396 mg, 10 mol%) and sodium ascorbate (600 mg, 18 mol%) in water (4.5 mL). The reaction mixture was stirred at reflux under an inert atm. overnight. The reaction was cooled to rt. and water (150 mL) was added followed by extraction with chloroform (3 x 100 mL). The organic layer was washed with water (100 mL) followed by sodium bicarbonate solution (5 % in 100 mL) and then brine (100 mL), it was then dried over magnesium sulfate. The solvent was removed under vacuum to yield the crude product which was purified via recrystallization from ethanol to give off white powder.

Yield- 15 % m. p. 124.1–127.0 °C

^{1}H NMR (400 MHz, DMSO-d_6) δ ppm 7.79 (s, 2 H), 4.26 (t, *J*=7.04 Hz, 4 H), 2.79 (br s, 8 H), 2.10 (s, 6 H), 1.75 (quin, J=7.06 Hz, 4 H), 1.14 – 1.27 (m, 8 H). ^{13}C NMR (101 MHz, DMSO-d_6) δ ppm 207.4 (CO), 145.8 (ArC), 121.7 (ArCH), 49.1 (CH_2), 41.9 (CH_2), 29.7 (CH_3), 29.6 (CH_2), 28.1 (CH_2), 25.7 (CH_2), 19.3 (CH_2).

LR-MS ESI$^+$ - (*m/z*)*:* 389.3977 [M+H$^+$]. HR-MS ESI$^+$ - (*m/z*)*:* Calc. $C_{20}H_{33}N_6O_2$ 389.2660 [M+H$^+$]. Meas. 389.2668 [M+H$^+$]. Calc. $C_{20}H_{32}N_6NaO_2$ 411.2479 [M+Na$^+$]. Meas. 411.2488 [M+Na$^+$].

5.2.22 1, 3-Bis (4' –(3, 3-di(pyrrol-2-yl)-1*H*-[1', 2', 3']triazole) octane 83b

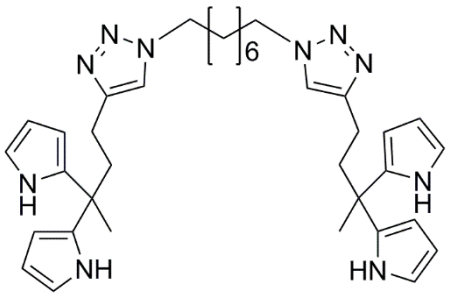

Procedure adapted from the literature,[206] **83a** (464 mg, 1.19 mmol) was dissolved in pyrrole (10 mL) followed by TFA (15 drops) the reactions mixture was stirred at 75 °C under an inert atm. for 1 hour. The reaction mixture was cooled to rt. and sodium hydroxide (0.1 M, 100 mL) was added followed by extraction with dichloromethane (100 mL). The organic layer was washed with water (100 mL) and then brine (100 mL) and was dried over magnesium sulfate. The solvent was removed under vacuum to yield the crude product which was purified using flash column chromatography (Fraction 2, eluent- ethyl acetate).

Yield- 41 %

^{1}H NMR (400 MHz, DMSO-d_6) δ ppm 10.31 (br s, 4 H), 7.77 (s, 2 H), 6.57 – 6.60 (m, 4 H), 5.86 – 5.88 (m, 4 H), 5.75 – 5.78 (m, 4 H), 4.24 (t, *J*=7.10 Hz, 4 H), 2.35 – 2.40 (m, 4 H), 2.23 – 2.28 (m, 4 H), 1.75 (quin, J=7.09 Hz, 4 H), 1.59 (s, 6 H), 1.20 – 1.28 (m, 8 H). ^{13}C NMR (101 MHz, DMSO-d_6) δ ppm 147.0 (ArC), 137.9 (ArC), 121.3 (ArCH), 116.6 (ArCH), 106.3 (ArCH), 103.9 (ArCH), 49.1 (CH_2), 40.5 (CH_2), 38.5 (C), 29.6 (CH_2), 28.2 (CH_2), 25.7 (CH_2), 25.0 (CH_3), 20.9 (CH_2).

LR-MS ESI$^+$ - (*m/z*): 621.6845 [M+H$^+$]. HR-MS ESI$^+$ - (*m/z*): Calc. $C_{36}H_{49}N_{10}$. 621.4136 [M+H$^+$]. Meas. 621.4151 [M+H$^+$]. Calc. $C_{36}H_{48}N_{10}Na$ 643.3956 [M+Na$^+$]. Meas. 643.3969 [M+Na$^+$].

5.2.23 C8 spacer bridged-calixpyrrole 83

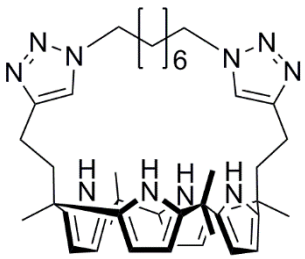

Procedure adapted from the literature,[206] **83b** (298 mg, 0.48 mmol) was dissolved in reagent grade acetone (350 mL), boron trifluoride diethyl etherate (0.15 mL, 1.22 mmol) was added dropwise. The reaction mixture was stirred at rt. under an inert atm. for 3 hours. Sodium carbonate (0.1 M, 50 mL)

was added followed by extraction with dichloromethane (2 x 100 mL) the organic layer was washed with water (100 mL) and dried over magnesium sulfate. The solvent was removed under vacuum to yield the crude product which was purified using flash column chromatography (Fraction 1, eluent-ethyl acetate).

Yield- 21 %, m. p. 188.0 °C dec.

^{1}H NMR (400 MHz, DMSO-d_6) δ ppm 9.40 (br s, 4 H), 7.49 (s, 2 H), 5.71 – 5.74 (m, 4 H), 5.68 – 5.71 (m, 4 H), 4.24 (t, *J*=6.28 Hz, 4 H), 2.27 – 2.33 (m, 4 H), 2.20 – 2.26 (m, 4 H), 1.62 – 1.71 (m, 4 H), 1.59 (br s, 6 H), 1.51 (br s, 6 H), 1.45 (br s, 6 H), 1.07 – 1.17 (m, 8 H). ^{13}C NMR (101 MHz, DMSO-d_6) δ ppm 147.7 (ArC), 138.5 (ArC), 137.0 (ArC), 121.0 (ArCH), 103.3 (ArCH), 101.8 (ArCH), 49.2 (CH_2), 40.5 (CH_2), 38.5 (C), 34.4 (C), 30.5 (CH_3), 30.4 (CH_2), 28.9 (CH_2), 27.5 (CH_3), 26.1 (CH_2), 23.9 (CH_3), 20.1 (CH_2).

LR-MS ESI$^+$ - (*m/z*)*:* 701.7790 [M+H$^+$]. HR-MS ESI$^+$ - (*m/z*)*:* Calc. $C_{42}H_{57}N_{10}$. 701.4762 [M+H$^+$]. Meas. 701.4770 [M+H$^+$]. Calc. $C_{42}H_{56}N_{10}Na$ 723.4582 [M+Na$^+$]. Meas. 723.4587 [M+Na$^+$]. Calc. $C_{42}H_{56}N_{10}K$ 739.4321 [M+K$^+$]. Meas. 739.4332 [M+K$^+$].

5.3 X-Ray Crystallography

Slow layer diffusion and slow evaporation from a variety of solvents, detailed below, of compounds **73**, **77**, **79**, **80**, **82** and **83** resulted in crystals suitable for single crystal X-ray analysis. The crystals were mounted on a MiTeGen MicroMesh support, and the diffraction data was collected on various diffractometers, detailed below and the crystallographic data for publication has been deposited at the Cambridge Crystallographic Database Centre (CCDC). Images were generally produced using PyMOL Molecular Graphics System Version 0.99 Schrödinger, LLC[227] and CrystalMaker®: a crystal and molecular structure program for Mac and Windows/ CrystalMaker Software Ltd, Oxford, England.

The X-ray crystal data for **73** was collected by Dr. P. Horton of the NCS and was collected at 100 K using an Oxford Cryostream low temperature device, with a Rigaku AFC12 goniometer equipped with an enhanced sensitivity (HG) Saturn724+ detector mounted at the window of an FT-E+ SuperBright molybdenum rotating anode generator with Very High Flux Varimax optics (70 µm focus) using CrystalClear-SM Expert 3.1 b27 (Rigaku 2013) software. Data reduction and cell refinement were performed also using CrystalClear-SM Expert 3.1 b27 (Rigaku 2013) software. The structure was solved using SUPERFLIP and the structure refinement using a full matrix least-squares method using SHELXL[228] to result in the final *R* value, all performed with OLEX^2 (Version 1.2).[229]

The X-ray crystal data for **77** was collected by Dr. M. Light of the NCS and was collected at 100 K using an Oxford Cryostream low temperature device, with a Rigaku AFC12 goniometer equipped with an enhanced sensitivity (HG) Saturn724+ detector mounted at the window of an FT-E+ SuperBright molybdenum rotating anode generator with High Flux Varimax optics (70 µm focus) using CrystalClear-SM Expert 3.1 b27 (Rigaku 2013) software. Data reduction and cell refinement were performed using CrysAlisPro, Agilent Technologies, Version 1.171.37.35. and solved using direct methods executed in SHELXT[230] and refined using a full matrix least-squares method using SHELXL[228] to result in the final *R* value, all performed with OLEX^2 (Version 1.2)[229].

The X-ray crystal data for **79** and **79** (TBA Cl complex) were collected by Dr. M. Light at 120 K, using a Bruker Nonius APEXII or KappaCCD Roper area detector diffractometer mounted at the window of a rotating Mo anode (λ(Mo-Kα) = 0.71073 Å operating at 50 kV, 85 mA. The incident beam on the APEXII side was focused using 10 cm confocal mirrors, and a graphite monochromator was employed on the KappaCCD side. The crystal-to detector distance was 30 mm or 45 mm. ϕ and ω scans were carried out to fill the asymmetric unit using 2° frames. Unit cell determination, data collection and processing were carried out using the programs DirAx,[231] COLLECT[232] and DENZO[233] and a multi-scan absorption correction was applied using SADABS.[234] The structures were solved via direct methods and refined by full matrix least squares on F.[235]

The X-ray crystal data for **79** (TBAF complex) and **80** (CsF complex) was collected by H. Clarke at 100 K using an Oxford Cryostream low temperature device, with a Rigaku AFC12 goniometer using an enhanced sensitivity (HG) Saturn724+ detector mounted at the window of a FR-E+ SuperBright molybdenum (MoKα, λ=0.71075 Å) rotating anode generator with Very High Flux Varimax optics (70 µm focus), using CrystalClear-SM Expert 3.1 b27 (Rigaku 2013) software. Data reduction and cell refinement were performed using CrysAlisPro (Version 1.171.37.31, Agilent Technologies). All Structures were solved using direct methods executed in SHELXT[230] and refined using a full matrix least-squares method using SHELXL[228] to result in the final *R* value, all performed with OLEX^2 (Version 1.2)[229].

The X-ray crystal data for **82** (TBA Cl complex) and **83** (TBA Cl complex) was collected by H. Clarke at 100 K using an Oxford Cryostream low temperature device, with a Rigaku AFC12 goniometer using an enhanced sensitivity (HG) Saturn724+ detector mounted at the window of a FR-E+ SuperBright molybdenum (MoKα, λ=0.71075 Å) rotating anode generator with Very High Flux Varimax optics (70 µm focus). Data collection, reduction and cell refinement were performed using CrysAlisPro (Version 1.171.37.31, Agilent Technologies). All Structures were solved using direct methods executed in SHELXT[230] and refined using a full matrix least-squares method using SHELXL[228] to result in the final *R* value, all performed with OLEX^2 (Version 1.2)[229].

5.4 NMR titrations

To investigate the binding process of the anion receptors in this thesis, NMR titrations were performed. TBA and TEA salts were acquired from Sigma-Aldrich and were dried overnight under high vacuum before use.

A solution of the receptor (the host) to be studied (0.005–0.01 M) was made up in the relevant deuterated solvent either DMSO-d_6:H_2O (99.5:0.5, v/v) or acetonitrile-d_3:DMSO-d_6 :H_2O (59.75:39.75:0.5, v/v). Following this a solution of the tetra-alkylammonium salt (the guest) was made to 0.1 M with the previous host solution, this keeps the host concentration consistent throughout the experiment.

To a screw cap NMR tube, 500 µL of the host solution was added and a ^{1}H NMR spectra was performed at rt. Aliquots (ranging from 2–200 µL) of the guest solution were then added to the NMR tube and the tube was inverted to ensure thorough mixing. Subsequent NMR spectra were collected following each aliquot addition. Initial aliquots were low (2–5 µL) to prevent missing the binding event, ~ 20 spectra were obtained over the course of one titration which generally covered 0–10 equivalents of guest to host.

For the N, N' - (phenyl methylene)dibenzamide receptors the NH chemical shifts were recorded and plotted against the anionic guest equivalents and this data was then fitted to a 1:1 binding model using WINEQNMR2[162] to give a binding constant, K_a and additionally NH chemical shift data were fitted to a 1:1 model using BindFit v 0.5.[163]

For the strapped calixpyrroles that didn't show slow exchange on the NMR timescale the NH chemical shift data were fitted to a 1:1 model using BindFit v 0.5.[163]

5.5 Isothermal titration calorimetry

Performed by Fabian Sommer under the supervision of Prof. Stefan Kubik. The host compounds were made up to 2–2.5 mM stock solutions in acetonitrile. These solutions were titrated in 2–8 µL aliquots into the tetraalkylammonium salt solutions (0.15 –0.25 mM) contained in the insulated cell (1.4584 mL) of a fully computer operated Microcal VP-ITC instrument. The heat output was recorded and corrected by blind titrations using just acetonitrile. Data evaluation was conducted using Origin 7 software in combination with the binding models provided by Microcal. Occasionally when necessary, a fixed constant was added or subtracted from the entire data set to improve the fit.

5.6 Vesicle-based assays

5.6.1 Vesicle preparation

Unilamellar vesicles were prepared according to literature methods.[96,110,236] A lipid film of POPC was formed under reduced pressure from a chloroform solution in an RBF of known mass. The film was dried under high vacuum for 4–6 hrs and the mass of the lipid was noted. The lipid film was rehydrated with the chosen internal solution (1 mL solution per 1 mL lipid solution) and vortexed for 5 mins. The lipid suspension was subjected to 9 freeze thaw cycles using liquid nitrogen and warm water and was then left to age at room temp for 30 min. Extrusion through a 200 nm (unless otherwise specified) polycarbonate membrane was performed 25 times to form monodisperse vesicles. Any unencapsulated internal salts were removed using dialysis in the chosen external solution or by passing through a sephadex size exclusion column with the external solution as the eluent.

5.6.2 Cl^-/NO_3^- antiport

Vesicles were prepared as stated in 5.6.1 with NaCl 489 mM buffered to pH 7.2 with 5 mM sodium phosphate salts as the internal solution and suspended in $NaNO_3$ 489 mM buffered to pH 7.2 with 5 mM sodium phosphate salts as the external solution. Test solutions were made in 5 mL vials at a lipid concentration of 1 mM. In general, a 10 µL DMSO solution of the receptor was added to initiate the transport at t = 0 s and the chloride efflux was monitored using a chloride selective electrode. After t = 300 s the vesicles were lysed using polyoxyethylene (8) lauryl ether and after t = 420 s a final chloride efflux reading was taken as 100 % for calibration purposes.

5.6.3 Cl^-/HCO_3^- antiport

Vesicles were prepared as stated in 5.6.1 with NaCl 450 mM buffered to pH 7.2 with 20 mM sodium phosphate salts as the internal solution and suspended in Na_2SO_4 162 mM buffered to pH 7.2 with 20 mM sodium phosphate salts as the external solution. Test solutions were made in 5 mL vials at a lipid concentration of 1 mM. In general, a 10 µL DMSO solution of the receptor was added to initiate the transport at t = 0 s and the chloride efflux was monitored using a chloride selective electrode. At t = 120 s, a $NaHCO_3$ solution was added to give an external $NaHCO_3$ concentration of 40 mM. After t = 420 s, the vesicles were lysed using polyoxyethylene (8) lauryl ether and after t = 540 s a final chloride efflux reading was taken as 100 % for calibration purposes.

5.6.4 Cl^-/SO_4^{2-} antiport

Vesicles were prepared as stated in 5.6.1 with NaCl 450 mM buffered to pH 7.2 with 20 mM sodium phosphate salts as the internal solution and suspended in Na_2SO_4 162 mM buffered to pH 7.2 with 20 mM sodium phosphate salts as the external solution. Test solutions were made in 5 mL vials at a lipid concentration of 1 mM. In general, a 10 µL DMSO solution of the receptor was added to initiate the transport at t = 0 s and the chloride efflux was monitored using a chloride selective electrode. After t = 300 s the vesicles were lysed using polyoxyethylene (8) lauryl ether and after t = 420 s a final chloride efflux reading was taken as 100 % for calibration purposes.

5.6.5 M^+/Cl^- cotransport assay (M = Na, K or Cs)

Vesicles were prepared as stated in 5.6.1 with MCl 489 mM buffered to pH 7.2 using 5 mM sodium phosphate salts as the internal solution and suspended in $NaNO_3$ 489 mM buffered to pH 7.2 using 5 mM sodium phosphate salts as the external solution. Test solutions were made in 5 mL vials at a lipid concentration of 1 mM. In general, a 10 µL DMSO solution of the receptor was added to initiate the transport at t = 0 s and the chloride efflux was monitored using a chloride selective electrode. After t = 300 s the vesicles were lysed using polyoxyethylene (8) lauryl ether and after t = 420 s a final chloride efflux reading was taken as 100 % for calibration purposes.

5.6.6 Cholesterol assay

Vesicles were prepared as stated in 5.6.1 but with a POPC : Cholesterol ratio of 7 : 3 following this Cl^-/NO_3^- antiport assay conditions repeated.

5.6.7 U-Tube assay

An organic phase of nitrobenzene containing the receptor was stirred in a glass U- tube between two aqueous phases (source and receiver) at room temperature for eight days. The receiver phase was monitored daily using a chloride selective electrode to measure the chloride concentration. A control with no receptor was used to ascertain background diffusion levels with the TBA counterion.

Source phase- 489 mM NaCl buffered to pH 7.2 with 5 mM sodium phosphate salts, 10 mL.

Receiver phase- 489 mM $NaNO_3$ buffered to pH 7.2 with 5 mM sodium phosphate salts, 10 mL.

Organic phase- 1 mM receptor with 2 mM TBA hexafluorophosphate (to provide counter ions and aid solubility) in nitrobenzene, 20 mL.

5.6.8 M^+/F^- cotransport assay (M= Na, K, Cs or Rb)

Vesicles were prepared as stated in 5.6.1 with MF 300 mM buffered to pH 7.2 using 10 mM HEPES as the internal solution and suspended in KGlc 300 mM buffered to pH 7.2 using 10 mM HEPES as the external solution. Test solutions were made in 5 mL vials at a lipid concentration of 1 mM. In general, a 10 µL DMSO solution of the receptor was added to initiate the transport at t = 0 s and the chloride efflux was monitored using a chloride selective electrode. After t = 300 s the vesicles were lysed using Triton X-100 detergent and after t = 420 s a final chloride efflux reading was taken as 100 % for calibration purposes.

5.6.9 Vln and Mon coupled assay

Vesicles were prepared as stated in 5.6.1 with KX 300 mM buffered to pH 7.2 with 10 mM HEPES, X = Cl^- or F^-, as the internal solution and suspended in KGlc 300 mM buffered to pH 7.2 with 10 mM HEPES as the external solution. Test solutions were made in 5 mL vials at a lipid concentration of 1 mM. In general, a 5 µL DMSO solution of Vln or Mon (0.1 mol%) was added at t = 0 s and at t = 30 s a 10 µL DMSO solution of the receptor was added to initiate the transport and the anion efflux was monitored using a chloride or fluoride selective electrode. After t = 300 s the vesicles were lysed using Triton X-100 detergent and after t = 420 s a final anion efflux reading was taken as 100 % for calibration purposes.

5.6.10 NMDG HPTS assay

Vesicles were prepared as stated in 5.6.1 with NMDG-Cl 100 mM buffered to pH 7 with 10 mM HEPES and 1 mM HPTS as the internal solution and suspended in NMDG-Cl 100 mM Buffered to pH 7 with 10 mM HEPES as the external solution. Test solutions were made to 2.2 mL or 2.5 mL in cuvettes at a lipid concentration of 0.1 mM. In general, a 5 µL DMSO of the receptor was added followed by a base pulse (NMDG 5 mM) at t = 0 s to initiate the experiment. The fluorescence ratio of HPTS acidic and basic form (λ_{ex} = 403 nm and 460 nm respectively) were measured using a fluorimeter. After t = 200 s the vesicles were lysed with Triton X-100 detergent to fully dissipate the pH gradient for calibration purposes. If the experiment involves the addition of gramicidin D (0.1 mol%) or oleic acid (2 mol%) these are added prior to the addition of the receptor.

5.6.11 Osmotic response assay

Vesicles were prepared as stated in 5.6.1 using 400 nm membranes with KX 300 mM buffered to pH 7.2 with 10 mM HEPES, X=F, Cl or OAc, as the internal solution and suspended in KGlc 300 mM

buffered to pH 7.2 with 10 mM HEPES as the external solution. Test solutions were made to 2.2 mL or 2.5 mL in cuvettes at a lipid concentration of 0.4 mM. In general, a 5 µL DMSO solution of Vln was added followed by a 5 µL DMSO of the receptor at t = 0 s to initiate the experiment and the light scattering at 600 nm was monitored with a fluorimeter. At t = 500 s CCCP (5 mol%) or pentafluoropropyl thiourea tren (8 mol%) was added and Vln (0.1 mol%) (if not added previously) were added to calibrate 100 % KX efflux.

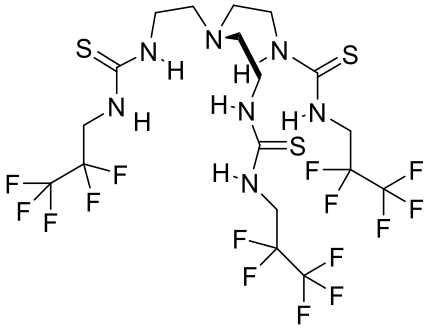

Figure 5.1 Structure of pentafluoropropyl thiourea tren compound used to calibrate the chloride osmotic assay.

5.6.12 KX HPTS assay

Vesicles were prepared as stated in 5.6.1 with KX 100 mM buffered to pH 7 with 10 mM HEPES, X= Cl, Br, I, NO_3, and 1 mM HPTS as the internal solution and suspended in KX 100 mM Buffered to pH 7 with 10 mM HEPES, X= Cl, Br, I, NO_3, as the external solution. Test solutions were made to 2.5 mL in cuvettes at a lipid concentration of 0.1 mM. In general, a 5 µL DMSO of the receptor was added followed by a base pulse (NMDG 5 mM) at t = 0 s to initiate the experiment. The fluorescence ratio of HPTS acidic and basic form (λ_{ex} = 403 nm and 460 nm respectively) were measured using a fluorimeter. After t = 200 s the vesicles were lysed with Triton X-100 detergent to fully dissipate the pH gradient for calibration purposes. If the experiment involves the addition of CCCP, this was added prior to addition of the transporter.

5.6.13 Electrode calibration and conversion of raw data

Calibration of the Accumet chloride and fluoride ion selective electrode were performed prior to the testing. The electrode was placed into a series of NaCl or NaF solutions each stirred for five min and the electrode potential (mV) was recorded. These potential values were plotted against the NaX concentration (M) and the plot was fitted to Equation 5.1 , a simplified version of the Nernst equation.

$$y = (P_1 log_{10} x) + P_2$$

Equation 5.1 Simplified Nernst equation used to calibrate electrode data.

The parameters P_1 and P_2 were calculated and from these calibration parameters the raw potential data recorded from the ISE assays was converted into concentrations. Using Equation 5.1 and solving for x gave the anion concentration at any time point in the assay, subtracting the initial anion concentration from this value gave the total anion concentration released from the vesicle at any one point of time. Using the value for 100 % anion efflux (t = 420/540 s) the percentage anion efflux was calculated for all time points throughout the course of the experiment.

5.6.14 Hill analysis

Dose response experiments were performed to enable Hill analysis and the generation of an EC_{50} value, which is the effective concentration needed for 50 % anion efflux. Ideally, at least six receptor concentrations were tested within the given assay to provide varying percentage efflux at 270 s. The data was fitted to the Hill equation[103]

$$y = V_{max} \frac{x^n}{k^n + x^n}$$

Equation 5.2 The Hill equation.[103]

Where x is the receptor concentration (mol%), y is the anion efflux (%) at 270 s, V_{max} is the maximum anion efflux possible (usually fixed to 100 %), n is the Hill coefficient and k is the receptor concentration required to facilitate 50 % efflux (or $\frac{V_{max}}{2}$) which is referred to as the EC_{50}.

5.6.15 Conversion of HPTS ratio data

The fluorimeter measures the ratio between the acidic and basic form of HPTS which are excited at different wavelengths (λ_{ex} = 403 nm and 460 nm respectively) but emit at the same wavelength (λ_{em} = 510 nm). The fractional fluorescence intensity (I_f) is calculated using the following:

$$I_f = \frac{R_t - R_0}{R_d - R_0}$$

Equation 5.3 Used to convert raw data from the HPTS assay.

Where R_t is the fluorescence ratio at a given time point, R_0 is the fluorescence ratio at t = 0 s and R_d is the fluorescence ratio after the addition of detergent and full dissipation of the pH gradient.

5.6.16 NMDG-HPTS Hill analysis

As above dose response experiments were performed to enable Hill analysis and the generation of an EC_{50} value, which in this case is the effective concentration needed for a 0.5 fractional intensity. Ideally, at least six receptor concentrations were tested within the given assay to provide varying percentage efflux at 200 s. The data was fitted to an adapted Hill equation[103]

$$y = y_0 + (y_{max} - y_0)\frac{x^n}{k^n + x^n}$$

Equation 5.4 Adapted Hill equation used in the NMDG HPTS assay.

Where x is the receptor concentration (mol%), y is I_f at 200 s, y_0 is the I_f at 200 s for the DMSO run, y_{max} is the maximum I_f value, n is the Hill coefficient and k is the receptor concentration required to facilitate 0.5 I_f which is referred to as the EC_{50}.

5.6.17 Conversion of osmotic response data

The fraction light scattering intensity (I_f) was calculated using the following equation:

$$I_f = \frac{I_t - I_0}{I_c - I_0}$$

Equation 5.5 Used to convert raw data from the osmotic assay.

Where I_t is the light scattering intensity at a given time point, I_0 is the light scattering intensity at t = 0 s and I_c is the light scattering intensity after the addition of CCCP (and Vln or the pentafluoropropyl thiourea tren if not added previously).

5.6.18 Fluoride transport NMR assay

5.6.18.1 $MnSO_4$ internal

Vesicles were prepared as stated in 5.6.1 using 500 nm membranes with KF 150 mM buffered to pH 7.2 with 10 mM HEPES and $MnSO_4$ (3 mol%) as the internal solution and suspended in KGlc 150 mM buffered to pH 7.2 with 10 mM HEPES as the external solution. Test solutions were made to 1 mL in an NMR tube to a concentration of 1 mM lipid in external solution. A ^{19}F NMR spectra was obtained, after this a 5 µL DMSO solution of Vln (0.1 mol%) and a 10 µL DMSO solution of receptor was added. The solution was left to stand for 30 min (inverted every 5 min), then another ^{19}F NMR spectra was obtained. The vesicles were lysed using Triton X-100 detergent and a final ^{19}F NMR spectra was collected.

5.6.18.2 $MnSO_4$ external

Vesicles were prepared as stated in 5.6.1 using 500 nm membranes with KF 300 mM buffered to pH 7.2 with 10 mM HEPES as the internal solution and suspended in KGlc 300 mM buffered to pH 7.2 with 10 mM HEPES and $MnSO_4$ (1 mol%) as the external solution. Test solutions were made to 1 mL in an NMR tube to a concentration of 1 mM lipid in external solution. A ^{19}F NMR spectra was obtained, after this a 5 µL DMSO solution of Vln (0.1 mol%) and a 10 µL DMSO solution of receptor was added. The solution was left to stand for 30 min (inverted every 5 min), then another ^{19}F NMR spectra was obtained. The vesicles were lysed using Triton X-100 detergent and a final ^{19}F NMR spectra was collected.

References

(1) Davis, A. P.; Sheppard, D. N.; Smith, B. D. *Chem. Soc. Rev.* **2007**, *36* (2), 348–357.

(2) Davis, J. T.; Okunola, O.; Quesada, R. *Chem. Soc. Rev.* **2010**, *39* (10), 3843–3862.

(3) Lodish, H.; Berk, A.; Zipursky, S. L.; Matsudaira, P.; Baltimore, D.; Darnell, J. *Molecular Biology*, 4th ed.; W. H. Freeman: New York, 2000.

(4) Shrode, L. D.; Tapper, H.; Grinstein, S. *J. Bioenerg. Biomembr.* **1997**, *29* (4), 393–399.

(5) Strange, K.; Emma, F.; Jackson, P. S. *Am. J. Physiol. - Cell Physiol.* **1996**, *270* (3), 711–730.

(6) Shoshan-Barmatz, V.; Israelson, A.; Brdiczka, D.; Sheu, S. *Curr. Pharm. Des.* **2006**, *12* (18), 2249–2270.

(7) Dworakowska, B.; Dołowy, K. *Acta Biochim. Pol.* **2000**, *47* (3), 685–703.

(8) Rowe, S. M.; Miller, B. S.; Sorscher, E. J. *N. Engl. J. Med.* **2005**, *352*, 1992–2001.

(9) Patrick, A. E.; Thomas, P. J. *Front. Pharmacol.* **2012**, *3*, 1–11.

(10) Riordan, J. R. *Annu. Rev. Physiol.* **2005**, *67* (1), 701–718.

(11) Vergani, P.; Lockless, S. W.; Nairn, A. C.; Gadsby, D. C. *Nature* **2005**, *433* (7028), 876–880.

(12) De Boeck, K. CFTR Info www.cftr.info/about-cf/genetics-and-cell-biology-of-cftr/cftr-structur-and-regulation/ (accessed Jul 25, 2017).

(13) Ashcroft, F, M. *Ion Channels and Disease Channelopathies.*; Academic Press: San Diego, 2000.

(14) Gadsby, D. C.; Vergani, P.; Csanády, L. *Nature* **2006**, *440* (7083), 477–483.

(15) Cystic Fibrosis Trust https://www.cysticfibrosis.org.uk/ (accessed Sep 20, 2017).

(16) Rousselle, A. V.; Heymann, D. *Bone* **2002**, *30* (4), 533–540.

(17) Bok, D.; Galbraith, G.; Lopez, I.; Woodruff, M.; Nusinowitz, S.; BeltrandelRio, H.; Huang, W.; Zhao, S.; Geske, R.; Montgomery, C.; Van Sligtenhorst, I.; Friddle, C.; Platt, K.; Sparks, M. J.; Pushkin, A.; Abuladze, N.; Ishiyama, A.; Dukkipati, R.; Liu, W.; Kurtz, I. *Nat. Genet.* **2003**, *34* (3), 313–319.

(18) Vaughan-Jones, R. D.; Spitzer, K. W.; Swietach, P. *J. Mol. Cell. Cardiol.* **2009**, *46* (3), 318–331.

(19) Markovich, D. *Physiol. Rev.* **2001**, *81* (4), 1499–1533.

(20) Superti-Furga, A.; Rossi, A.; Steinmann, B.; Gitzelmann, R. *Am. J. Med. Genet.* 1996, *63* (1), 144–147.

(21) Kelkar, D. A.; Chattopadhyay, A. *Biochim. Biophys. Acta - Biomembr.* 2007, *1768* (9), 2011–2025.

(22) Pressman, B. C.; Harris, E. J.; Jagger, W. S.; Johnson, J. H. *Proc. Natl. Acad. Sci. U. S. A.* 1967, *58* (5), 1949–1956.

(23) Ehala, S.; Kašička, V.; Makrlík, E. *Electrophoresis* 2008, *29* (3), 652–657.

(24) Lauger, P. *Science (80-.).* 1972, *178*, 24–30.

(25) Shemyakin, M. M.; Ovchinnikov, Y. A.; Ivanov, V. T.; Antonov, V. K.; Vinogradova, E. I.; Shkrob, A. M.; Malenkov, G. G.; Evstratov, A. V.; Laine, I. A.; Melnik, E. I.; Ryabova, I. D. *J. Membr. Biol.* 1969, *1*, 402–430.

(26) Matile, S.; Sakai, N. *Anal. Methods Supramol. Chem.* 2007, 391–418.

(27) Gokel, G. W.; Mukhopadhyay, A. *Chem. Soc. Rev.* 2001, *30* (5), 274–286.

(28) Dubos, R. J. *J. Exp. Med.* 1939, *70*, 1–10.

(29) Sarges, R.; Witkop, B. *J. Am. Chem. Soc.* 1965, *87* (9), 2011–2020.

(30) Hladky, S. B.; Haydon, D. A. *BBA - Biomembr.* 1972, *274* (2), 294–312.

(31) Gorteau, V.; Bollot, G.; Mareda, J.; Perez-Velasco, A.; Matile, S. *J. Am. Chem. Soc.* 2006, *128* (46), 14788–14789.

(32) Gorteau, V.; Julliard, M. D.; Matile, S. *J. Memb. Sci.* 2008, *321*, 37–42.

(33) Dawson, R. E.; Hennig, A.; Weimann, D. P.; Emery, D.; Ravikumar, V.; Montenegro, J.; Takeuchi, T.; Gabutti, S.; Mayor, M.; Mareda, J.; Schalley, C. A.; Matile, S. *Nat. Chem.* 2010, *2* (7), 533–538.

(34) Wrede, F.; Rothhaas, A. *Physiol. Chem.* 1934, *226*, 95.

(35) Castro, A. *Nature* 1967, *213*, 903–904.

(36) Manderville, R. A. *Curr. Med. Chem. Anticancer. Agents* 2001, *1* (2), 195–218.

(37) Han, S. B.; Kim, H. M.; Kim, Y. H.; Lee, C. W.; Jang, E. S.; Son, K. H.; Kim, S. U.; Kim, Y. K. *Int. J. Immunopharmacol.* 1998, *20* (1–3), 1–13.

(38) Montaner, B.; Pérez-Tomás, R. *Life Sci.* 2001, *68* (17), 2025–2036.

(39) Nakamura, A.; Nagai, K.; Suzuki, S.; Ando, K.; Tamura, G. *J. Antibiot. (Tokyo).* 1986, *39*, 1148–1154.

(40) Songia, S.; Mortellaro, A.; Taverna, S.; Fornasiero, C.; Scheiber, E. A.; Erba, E.; Colotta, F.; Mantovani, A.; Isetta, A. M.; Golay, J. *J. Immunol.* 1997, *158*, 3987–3995.

(41) Melvin, M. S.; Tomlinson, J. T.; Saluta, G. R.; Kucera, G. L.; Lindquist, N.; Manderville, R. A. *J. Am. Chem. Soc.* 2000, *122* (26), 6333–6334.

(42) Melvin, M. S.; Ferguson, D. C.; Lindquist, N.; Manderville, R. A. *J. Org. Chem.* 1999, *64* (18), 6861–6869.

(43) Williamson, N. R.; Fineran, P. C.; Gristwood, T.; Chawrai, S. R.; Leeper, F. J.; Salmond, G. P. C. *Future Microbiol.* 2007, *2* (6), 605–618.

(44) Fürstner, A.; Grabowski, E. J. *Chembiochem* 2001, *2* (9), 706–709.

(45) Ohkuma, S.; Sato, T.; Okamoto, M.; Matsuya, H.; Arai, K.; Kataoka, T.; Nagai, K.; Wasserman, H. H. *Biochem. J.* 1998, *334*, 731–741.

(46) Gale, P. A.; Light, M. E.; McNally, B.; Navakhun, K.; Sliwinski, K. E.; Smith, B. D. *Chem. Commun.* 2005, No. 30, 3773–3775.

(47) Seganish, J. L.; Davis, J. T. *Chem. Commun.* 2005, No. 46, 5781–5783.

(48) Hernando, E.; Soto-Cerrato, V.; Cortés-Arroyo, S.; Pérez-Tomás, R.; Quesada, R. *Org. Biomol. Chem.* 2014, *12* (11), 1771–1778.

(49) Soto-Cerrato, V.; Manuel-Manresa, P.; Hernando, E.; Calabuig-Fariñas, S.; Martínez-Romero, A.; Fernández-Dueñas, V.; Sahlholm, K.; Knöpfel, T.; García-Valverde, M.; Rodilla, A. M.; Jantus-Lewintre, E.; Farràs, R.; Ciruela, F.; Pérez-Tomás, R.; Quesada, R. *J. Am. Chem. Soc.* 2015, *137* (50), 15892–15898.

(50) Rodilla, A. M.; Korrodi-Gregório, L.; Hernando, E.; Manuel-Manresa, P.; Quesada, R.; Pérez-Tomás, R.; Soto-Cerrato, V. *Biochem. Pharmacol.* 2017, *126*, 23–33.

(51) Pinkerton, D. M.; Banwell, M. G.; Willis, A. C. *Org. Lett.* 2007, *9* (24), 5127–5130.

(52) Hernández, P. I.; Moreno, D.; Javier, A. A.; Torroba, T.; Pérez-Tomás, R.; Quesada, R. *Chem. Commun.* 2012, *48* (10), 1556–1558.

(53) Saggiomo, V.; Otto, S.; Marques, I.; Félix, V.; Torroba, T.; Quesada, R. *Chem. Commun.* **2012**, *48* (43), 5274–5276.

(54) Knight, N. J.; Hernando, E.; Haynes, C. J. E.; Busschaert, N.; Clarke, H. J.; Takimoto, K.; García-Valverde, M.; Frey, J. G.; Quesada, R.; Gale, P. A. *Chem. Sci.* **2016**, *7* (2), 1600–1608.

(55) Shriver, D. F.; Biallas, M. J. *J. Am. Chem. Soc.* **1967**, *89* (5), 1078–1081.

(56) Park, C. H.; Simmons, H. E. *J. Am. Chem. Soc.* **1968**, *90* (9), 2431–2432.

(57) Graf, E.; Lehn, J. M. *J. Am. Chem. Soc.* **1976**, *98* (20), 6403–6405.

(58) Schmidtchen, F. P. *Angew. Chemie Int. Ed. English* **1977**, *16* (10), 720–721.

(59) Pascal, R. A.; Spergel, J.; Van Engen, D. *Tetrahedron Lett.* **1986**, *27* (35), 4099–4102.

(60) Pflugrath, J. W.; Quiocho, F. A. *Nature* **1985**, *314*, 257–260.

(61) Gale, P. A. *Chem. Commun.* **2011**, *47* (1), 82–86.

(62) Gale, P. A.; Howe, E. N. W.; Wu, X. *Chem* **2016**, *1* (3), 351–422.

(63) Wenzel, M.; Hiscock, J. R.; Gale, P. A. *Crit. Rev.* **2012**, 480–520.

(64) Busschaert, N.; Caltagirone, C.; Van Rossom, W.; Gale, P. A. *Chem. Rev.* **2015**, *115* (15), 8038–8155.

(65) Gale, P. A. *Chem. Soc. Rev.* **2001**, *213*, 79–128.

(66) Gale, P. A. *Chem. Soc. Rev.* **2010**, *39* (10), 3546–3771.

(67) Gale, P. A.; Caltagirone, C. *Chem. Soc. Rev.* **2009**, *38* (10), 520–563.

(68) Cavallo, G.; Metrangolo, P.; Pilati, T.; Resnati, G.; Sansotera, M.; Terraneo, G. *Chem. Soc. Rev.* **2010**, *39* (10), 3772–3783.

(69) Metrangolo, P.; Meyer, F.; Pilati, T.; Resnati, G.; Terraneo, G. *Angew. Chemie - Int. Ed.* **2008**, *47* (33), 6114–6127.

(70) Kim, S. K.; Sessler, J. L. *Chem. Soc. Rev.* **2010**, *39* (10), 3784–3809.

(71) Sessler, J. L.; Camiolo, S.; Gale, P. A. *Coord. Chem. Rev.* **2003**, *240*, 17–55.

(72) Smith, P. J.; Reddington, M. V; Wilcox, C. S. *Tetrahedron Lett.* **1992**, *33* (41), 6085–6088.

(73) Kubik, S.; Kirchner, R.; Nolting, D.; Seidel, J. *J. Am. Chem. Soc.* 2002, *124* (43), 12752–12760.

(74) Otto, S.; Kubik, S. *J. Am. Chem. Soc.* 2003, *125* (26), 7804–7805.

(75) Prohens, R.; Tomàs, S.; Morey, J.; Deyà, P. M.; Ballester, P.; Costa, A. *Tetrahedron Lett.* 1998, *39* (9), 1063–1066.

(76) Quiñonero, D.; Prohens, R.; Garau, C.; Frontera, A.; Ballester, P.; Costa, A.; Deyà, P. M. *Chem. Phys. Lett.* 2002, *351*, 115–120.

(77) Baeyer, A. *Berichte der Dtsch. Chem. Gesellschaft* 1886, *19* (2), 2184–2185.

(78) Gale, P. A.; Sessler, J. L.; Kral, V.; Lynch, V. *J. Am. Chem. Soc.* 1996, *118* (16), 5140–5141.

(79) Gale, P. A.; Sessler, J. L. *Chem. Commun.* 1998, No. 0, 1–8.

(80) Smith, D. K. *Org. Biomol. Chem.* 2003, *1* (22), 3874–3877.

(81) Winstanley, K. J.; Sayer, A. M.; Smith, D. K. *Org. Biomol. Chem.* 2006, *4* (9), 1760–1767.

(82) Kondo, S. I.; Suzuki, T.; Yano, Y. *Tetrahedron Lett.* 2002, *43* (39), 7059–7061.

(83) Kondo, S. I.; Harada, T.; Tanaka, R.; Unno, M. *Org. Lett.* 2006, *8* (20), 4621–4624.

(84) Kondo, S. I.; Bie, Y.; Yamamura, M. *Org. Lett.* 2013, *15* (3), 520–523.

(85) Ramabhadran, R. O.; Liu, Y.; Hua, Y.; Ciardi, M.; Flood, A. H.; Raghavachari, K. *J. Am. Chem. Soc.* 2014, *136* (13), 5078–5089.

(86) Metrangolo, P.; Resnati, G. *IUCrJ* 2014, *1* (1), 5–7.

(87) Cavallo, G.; Metrangolo, P.; Milani, R.; Pilati, T.; Priimagi, A.; Resnati, G.; Terraneo, G. *Chem. Rev.* 2016, *116* (4), 2478–2601.

(88) Shing Ho, P. *Halogen Bonding I: Impact on Materials Chemistry and Life Sciences*; Metrangolo, P., Resnati, G., Eds.; Springer Switzerland, 2015.

(89) Mele, A.; Metrangolo, P.; Neukirch, H.; Pilati, T.; Resnati, G. *J. Am. Chem. Soc.* 2005, *127* (43), 14972–14973.

(90) Chudzinski, M. G.; McClary, C. a.; Taylor, M. S. *J. Am. Chem. Soc.* 2011, *133*, 10559–10567.

(91) Sessler, J. L.; Gross, D. E.; Cho, W. S.; Lynch, V. M.; Schmidtchen, F. P.; Bates, G. W.; Light, M. E.; Gale, P. A. *J. Am. Chem. Soc.* 2006, *128*, 12281–12288.

(92) Nishizawa, S.; Kato, R.; Hayashita, T.; Teramae, N. *Anal. Sci.* 1998, *14* (3), 595–597.

(93) Miyaji, H.; Sessler, J. L. *Angew. Chemie - Int. Ed.* 2001, *40* (1), 154–157.

(94) Caballero, A.; Swan, L.; Zapata, F.; Beer, P. D. *Angew. Chemie - Int. Ed.* 2014, *53* (44), 11854–11858.

(95) Wezenberg, S. J.; Vlatković, M.; Kistemaker, J. C. M.; Feringa, B. L. *J. Am. Chem. Soc.* 2014, *136* (48), 16784–16787.

(96) Macdonald, R. C.; Macdonald, R. I.; Menco, B. P. M.; Takeshita, K.; Subbarao, N. K.; Hu, L. *Biochim. Biophys. Acta.* 1991, *1061*, 297–303.

(97) Tong, C. C.; Quesada, R.; Sessler, J. L.; Gale, P. A. *Chem. Commun.* 2008, 6321–6323.

(98) McNally, B. A.; Koulov, A. V; Smith, B. D.; Joos, J.-B.; Davis, A. P. *Chem. Commun.* 2005, 1087–1089.

(99) Koulov, A. V; Mahoney, J. M.; Smith, B. D. *Org. Biomol. Chem.* 2003, *1* (574), 27–29.

(100) Clement, N. R.; Gould, J. M. *Biochemistry* 1981, *20* (6), 1534–1538.

(101) Matile, S.; Vargas Jentzsch, A.; Montenegro, J.; Fin, A. *Chem. Soc. Rev.* 2011, *40* (5), 2453–2474.

(102) Biwersi, J.; Tulk, B.; Verkman, A. S. *Analytical biochemistry*. 1994, pp 139–143.

(103) Hill, A. V. *Biochem. J.* 1913, *7* (1), 471–480.

(104) Goutelle, S.; Maurin, M.; Rougier, F.; Barbaut, X.; Bourguignon, L.; Ducher, M.; Maire, P. *Fundam. Clin. Pharmacol.* 2008, *22* (6), 633–648.

(105) Bhosale, S.; Matile, S. *Chirality* 2006, *18* (10), 849–856.

(106) Weiss, J. N. *FASEB J.* 1997, *11* (11), 835–841.

(107) McNally, B. A.; Koulov, A. V.; Lambert, T. N.; Smith, B. D.; Joos, J. B.; Sisson, A. L.; Clare, J. P.; Sgarlata, V.; Judd, L. W.; Magro, G.; Davis, A. P. *Chem. - A Eur. J.* 2008, *14*, 9599–9606.

(108) Valkenier, H.; Judd, L. W.; Li, H.; Hussain, S.; Sheppard, D. N.; Davis, A. P. *J. Am. Chem. Soc.* 2014, *136* (35), 12507–12512.

(109) Schlesinger, P. H.; Ferdani, R.; Liu, J.; Pajewska, J.; Pajewski, R.; Saito, M.; Shabany, H.; Gokel, G. W. *J. Am. Chem. Soc.* 2002, *124* (9), 1848–1849.

(110) Koulov, A. V.; Lambert, T. N.; Shukla, R.; Jain, M.; Boon, J. M.; Smith, B. D.; Li, H.; Sheppard, D. N.; Joos, J.-B. B.; Clare, J. P.; Davis, A. P. *Angew. Chem. Int. Ed. Engl.* **2003**, *42* (40), 4931–4933.

(111) Sakai, N.; Matile, S. *Langmuir* **2013**, *29* (29), 9031–9040.

(112) Santacroce, P. V.; Davis, J. T.; Light, M. E.; Gale, P. A.; Iglesias-Sánchez, J. C.; Prados, P.; Quesada, R. *J. Am. Chem. Soc.* **2007**, *129* (7), 1886–1887.

(113) Judd, L. W.; Davis, A. P. *Chem. Commun.* **2010**, *46*, 2227–2229.

(114) Lipinski, C. A.; Lombardo, F.; Dominy, B. W.; Feeney, P. J. *Adv. Drug Deliv. Rev.* **1997**, *23*, 3–25.

(115) Hussain, S.; Brotherhood, P. R.; Judd, L. W.; Davis, A. P. *J. Am. Chem. Soc.* **2011**, *133*, 1614–1617.

(116) Cooper, J. A.; Street, S. T. G.; Davis, A. P. *Angew. Chemie - Int. Ed.* **2014**, *53* (22), 5609–5613.

(117) Cooper, J. a.; Street, S. T. G.; Davis, A. P. *Angew. Chemie - Int. Ed.* **2014**, *53*, 5609–5613.

(118) Karagiannidis, L. E.; Haynes, C. J. E.; Holder, K. J.; Kirby, I. L.; Moore, S. J.; Wells, J.; Gale, P. A. *Chem. Commun.* **2014**, *50*, 12050–12053.

(119) Andrews, N. J.; Haynes, C. J. E.; Light, M. E.; Moore, S. J.; Tong, C. C.; Davis, J. T.; Harrell Jr., W. A.; Gale, P. A. *Chem. Sci.* **2011**, *2* (2), 256–260.

(120) Busschaert, N.; Kirby, I. L.; Young, S.; Coles, S. J.; Horton, P. N.; Light, M. E.; Gale, P. A. *Angew. Chem. Int. Ed. Engl.* **2012**, *51* (18), 4426–4430.

(121) Moore, S. J.; Wenzel, M.; Light, M. E.; Morley, R.; Bradberry, S. J.; Gómez-Iglesias, P.; Soto-Cerrato, V.; Pérez-Tomás, R.; Gale, P. A.; Pérez Tomás, R.; Wenzel, M.; Light, M. E.; Morley, R.; Bradberry, S. J.; Soto Cerrato, V.; Gomez Iglesias, P. *Chem. Sci.* **2012**, *3* (8), 2501–2509.

(122) Marcus, Y. *J. Chem. Soc. Faraday Trans.* **1991**, *87* (18), 2995–2999.

(123) Fisher, M. G.; Gale, P. A.; Hiscock, J. R.; Hursthouse, M. B.; Light, M. E.; Schmidtchen, F. P.; Tong, C. C. *Chem. Commun.* **2009**, 3017–3019.

(124) Busschaert, N.; Gale, P. A.; Haynes, C. J. E.; Light, M. E.; Moore, S. J.; Tong, C. C.; Davis, T.; Harrell, W. A. *Chem. Comm.* **2010**, *1*, 6252–6254.

(125) Davis, J. T.; Gale, P. A.; Okunola, O. A.; Prados, P.; Iglesias-Sánchez, J. C.; Torroba, T.; Quesada, R. *Nat. Chem.* **2009**, *1* (2), 138–144.

(126) Gale, P. A.; Tong, C. C.; Haynes, C. J. E.; Adeosun, O.; Gross, D. E.; Karnas, E.; Sedenberg, E. M.; Quesada, R.; Sessler, J. L. *J. Am. Chem. Soc.* 2010, No. 3, 3240–3241.

(127) Haynes, C. J. E.; Moore, S. J.; Hiscock, J. R.; Marques, I.; Costa, P. J.; Félix, V.; Gale, P. A. *Chem. Sci.* 2012, 1436–1444.

(128) Hagmann, W. K. *J. Med. Chem* 2008, *51* (15), 4359–4369.

(129) Busschaert, N.; Wenzel, M.; Light, M. E.; Iglesias-Hernández, P.; Pérez-Tomás, R.; Gale, P. A. *J. Am. Chem. Soc.* 2011, *133*, 14136–14148.

(130) Amendola, V.; Bergamaschi, G.; Boiocchi, M.; Fabbrizzi, L.; Milani, M. *Chem. - A Eur. J.* 2010, *16* (14), 4368–4380.

(131) Ian Storer, R.; Aciro, C.; Jones, L. H. *Chem. Soc. Rev.* 2011, *40* (5), 2330.

(132) Busschaert, N.; Karagiannidis, L. E.; Wenzel, M.; Haynes, C. J. E.; Wells, N. J.; Young, P. G.; Makuc, D.; Plavec, J.; Jolliffe, K. A.; Gale, P. A. *Chem. Sci.* 2014, *5* (3), 1118–1127.

(133) Young, P. G.; Clegg, J. K.; Bhadbhade, M.; Jolliffe, K. A. *Chem. Commun.* 2011, *47* (1), 463–465.

(134) Young, P. G.; Jolliffe, K. A. *Org. Biomol. Chem.* 2012, *10* (13), 2664–2672.

(135) Young, P.; Clegg, J.; Jolliffe, K. *Supramol. Chem.* 2012, *24* (2), 77–87.

(136) Moore, S.; Haynes, C.; González, J.; Sutton, J.; Brooks, S. J.; Light, M. E.; Herniman, J.; Langley, J.; Marques, I.; Felix, V.; Pérez Tomás, R.; Soto Cerrato, V.; Gale, P. A. *Chem. Sci.* 2013, *4*, 103–117.

(137) Haynes, C. J. E.; Berry, S. N.; Garric, J.; Herniman, J.; Hiscock, J. R.; Kirby, I. L.; Light, M. E.; Perkes, G.; Gale, P. A. *Chem. Commun.* 2013, *49* (3), 246–248.

(138) Masliah, E.; Alford, M.; Deteresa, R.; Mallory, M.; Hansen, L. *Ann. Neurol.* 1996, *1* (40), 759–766.

(139) Wu, X.; Busschaert, N.; Wells, N. J.; Jiang, Y.-B. B.; Gale, P. A. *J. Am. Chem. Soc.* 2015, *137* (4), 1476–1484.

(140) Atkins, J. L.; Patel, M. B.; Daschbach, M. M.; Meisel, J. W.; Gokel, G. W. *J. Am. Chem. Soc.* 2012, *134*, 13546–13549.

(141) Lee, J. H.; Lee, J. H.; Choi, Y. R.; Kang, P.; Choi, M. G.; Jeong, K. S. *J. Org. Chem.* 2014, *79*, 6403–6409.

(142) Hansch, C.; Leo, A.; Hoekman, D.; Heller, S. R. *Exploring QSAR*; American Chemical Society: Washington, DC, 1995.

(143) Busschaert, N.; Bradberry, S. J.; Wenzel, M.; Haynes, C. J. E.; Hiscock, J. R.; Kirby, I. L.; Karagiannidis, L. E.; Moore, S. J.; Wells, N. J.; Herniman, J.; Langley, G. J.; Horton, P. N.; Light, M. E.; Marques, I.; Costa, P. J.; Félix, V.; Frey, J. G.; Gale, P. A. *Chem. Sci.* 2013, *4* (8), 3036–3045.

(144) Valkenier, H.; Haynes, C. J. E.; Herniman, J.; Gale, P. A.; Davis, A. P. *Chem. Sci.* 2014, *5* (3), 1128.

(145) Spooner, M. J.; Gale, P. A. *Chem. Commun.* 2015, *51*, 4883–4886.

(146) Li, H.; Valkenier, H.; Judd, L. W.; Brotherhood, P. R.; Hussain, S.; Cooper, J. A.; Jurček, O.; Sparkes, H. A.; Sheppard, D. N.; Davis, A. P. *Nat. Chem.* 2015, *8* (1), 24–32.

(147) Ko, S.-K.; Kim, S. K.; Share, A.; Lynch, V. M.; Park, J.; Namkung, W.; Van Rossom, W.; Busschaert, N.; Gale, P. A.; Sessler, J. L.; Shin, I. *Nat. Chem.* 2014, *6* (10), 885–892.

(148) Valkenier, H.; Mora, N. L.; Kros, A.; Davis, A. P. *Angew. Chem. Int. Ed. Engl.* 2014, No. 53, 1–6.

(149) Berry, S. N.; Soto-Cerrato, V.; Howe, E. N. W.; Clarke, H. J.; Mistry, I.; Tavassoli, A.; Chang, Y.-T.; Pérez-Tomás, R.; Gale, P. A. *Chem. Sci.* 2016, *7* (8), 5069–5077.

(150) Choi, Y. R.; Kim, G. C.; Jeon, H.-G.; Park, J.; Namkung, W.; Jeong, K.-S. *Chem. Commun.* 2014, *50* (97), 15305–15308.

(151) Hofmeister, F. *Arch. Exp. Pathol. Pharmacol.* 1888, *24*, 247–260.

(152) Kunz, W.; Lo Nostro, P.; Ninham, B. W. *Curr. Opin. Colloid Interface Sci.* 2004, *9* (1–2), 1–18.

(153) Lo Nostro, P.; Ninham, B. W. *Chem. Rev.* 2012, *112* (4), 2286–2322.

(154) Wu, X.; Judd, L. W.; Howe, E. N. W.; Jiang, Y.-B.; Davis, A. P.; Gale, P. A. *Chem* 2016, *1*, 127.

(155) Hodgson, J. *Nat. Biotechnol.* 2001, *19*, 722–726.

(156) Busschaert, N.; Gale, P. A. *Angew. Chem. Int. Ed. Engl.* 2013, *52* (5), 1374–1382.

(157) Gale, P. A.; Pérez-Tomás, R.; Quesada, R. *Acc. Chem. Res.* 2013, *46* (12), 2801–2813.

(158) Yang, P.; Myint, K.; Tong, Q.; Feng, R.; Cao, H.; Gao, Y.; Gertsch, J.; Teramachi, J.; Kurihara, N.; Roodman, G. D. *J. Med. Chem.* 2012, *55*, 9973–9987.

(159) Sessler, J. L.; Gale, P. A.; Cho, W. S. *Anion Receptor Chemistry*; Stoddart, J. F., Ed.; RSC: Cambridge, 2006.

(160) Purser, S.; Moore, P. R.; Swallow, S.; Gouverneur, V. *Chem. Soc. Rev.* 2008, *37* (2), 320–330.

(161) VCClabs http://www.vcclab.org (accessed Dec 18, 2014).

(162) Hynes, M. J. *J. Chem. Soc. Dalt. Trans.* 1993, No. 2, 311–312.

(163) Bindfit www.supramolecular.org (accessed Jun 20, 2016).

(164) Thordarson, P. *Chem. Soc. Rev.* 2011, *40* (3), 1305–1323.

(165) Haynes, C. J. E.; Busschaert, N.; Kirby, I. L.; Herniman, J.; Light, M. E.; Wells, N. J.; Marques, I.; Félix, V.; Gale, P. A. *Org. Biomol. Chem.* 2014, *12* (1), 62–72.

(166) Elliott, E. K.; Daschbach, M. M.; Gokel, G. W. *Chem. - A Eur. J.* 2008, *14*, 5871–5879.

(167) Daschbach, M. M.; Negin, S.; You, L.; Walsh, M.; Gokel, G. W. *Chem. - A Eur. J.* 2012, *18*, 7608–7623.

(168) Jentzsch, A. V.; Emery, D.; Mareda, J.; Nayak, S. K.; Metrangolo, P.; Resnati, G.; Sakai, N.; Matile, S. *Nat. Commun.* 2012, *3* (May), 905.

(169) Holthuis, J. C. M.; van Meer, G.; Huitema, K. *Mol. Membr. Biol.* 2003, *20* (September), 231–241.

(170) Róg, T.; Pasenkiewicz-gierula, M.; Vattulainen, I.; Karttunen, M. *Biochim. Biophys. Acta - Biomembr.* 2009, *1788* (1), 97–121.

(171) Seidler, J.; McGovern, S. L.; Doman, T. N.; Shoichet, B. K. *J. Med. Chem.* 2003, *46*, 4477–4486.

(172) LaPlante, S. R.; Carson, R.; Gillard, J.; Aubry, N.; Coulombe, R.; Bordeleau, S.; Bonneau, P.; Little, M.; O'Meara, J.; Beaulieu, P. L. *J. Med. Chem.* 2013, *56* (12), 5142–5150.

(173) Davis, J. T.; Gale, P. a; Okunola, O. A.; Prados, P.; Iglesias-Sánchez, J. C.; Torroba, T.; Quesada, R. *Nat. Chem.* 2009, *1* (2), 138–144.

(174) Hamilton, I. R. *J. Dent. Res.* 1990, *69*, 660–663.

(175) Stockbridge, R. B.; Lim, H.-H.; Otten, R.; Williams, C.; Shane, T.; Weinberg, Z.; Miller, C. *Proc. Natl. Acad. Sci.* 2012, *109* (38), 15289–15294.

(176) Cao, S. R.; Li, Y. F. In *Proceedings of the XIX Conference of the International Society for Fluoride*

Research; Kyoto, 1992; p 38.

(177) World Health Organisation. In *Guidelines for drinking-water quality*; IWA Publishing: London, 2006; pp 1–9.

(178) Liteplo, R.; Gomes, R.; Howe, P.; Malcolm, H. Fluorides- Environmental Health Criteria 227 http://www.inchem.org/documents/ehc/ehc/ehc227.htm (accessed Sep 7, 2016).

(179) Cametti, M.; Rissanen, K. *Chem. Commun.* 2009, No. 20, 2809–2829.

(180) Camiolo, S.; Gale, P. A.; Hursthouse, M. B.; Light, M. E.; Shi, A. J. *Chem. Commun.* 2002, *3* (7), 758–759.

(181) Gale, P. A.; Navakhun, K.; Camiolo, S.; Light, M. E.; Hursthouse, M. B. *J. Am. Chem. Soc.* 2002, *124* (38), 11228–11229.

(182) Camiolo, S.; Gale, P. A.; Hursthouse, M. B.; Light, M. E. *Org. Biomol. Chem.* 2003, *1* (4), 741–744.

(183) Gunnlaugsson, T.; Kruger, P. E.; Jensen, P.; Pfeffer, F. M.; Tocci (née Hussey), G. M. *Tetrahedron Lett.* 2003, *44* (49), 8909–8913.

(184) Esteban-Gómez, D.; Fabbrizzi, L.; Licchelli, M. *J. Org. Chem.* 2005, *70*, 5717–5720.

(185) Evans, L. S.; Gale, P. A.; Light, M. E.; Quesada, R. *Chem. Commun.* 2006, No. 9, 965–967.

(186) Pandurangan, K.; Kitchen, J. A.; Gunnlaugsson, T. *Tetrahedron Lett.* 2013, *54* (22), 2770–2775.

(187) Chiu, C. W.; Gabbaï, F. P. *J. Am. Chem. Soc.* 2006, *128* (44), 14248–14249.

(188) Lee, M. H.; Agou, T.; Kobayashi, J.; Kawashima, T.; Gabbaï, F. P. *Chem. Commun.* 2007, No. 11, 1133–1135.

(189) Kim, Y.; Gabbai, F. P. *J. Am. Chem. Soc.* 2009, *131* (9), 3363–3369.

(190) Perdikaki, K.; Tsagkatakis, I.; Chaniotakis, N. A.; Altmann, R.; Jurkschat, K.; Reeske, G. *Anal. Chim. Acta* 2002, *467* (1–2), 197–204.

(191) Yamamoto, H.; Ori, A.; Ueda, K.; Dusemund, C.; Shinkai, S. *Chem. Commun.* 1996, 407–408.

(192) Dusemund, C.; Sandanayake, S.; Shinkai, S. *J. Chem. Soc., Chem. Commun.* 1995, 333–334.

(193) Cooper, C. R.; Spencer, N.; James, T. D. *Chem. Commun.* 1998, No. 13, 1365–1366.

(194) Sessler, J. L.; Ford, D. A.; Cyr, M. J.; Furuta, H. *J. Chem. Soc., Chem. Commun.* 1991, 1733–1735.

(195) Chapman, B. E.; Kuchel, P. W. *Eur. Biophys. J.* 1990, *19* (1), 41–45.

(196) Gorteau, V.; Bollot, G.; Mareda, J.; Matile, S. *Org. Biomol. Chem.* 2007, *5* (18), 3000–3012.

(197) Berezin, S. K. *J. Membr. Biol.* 2014, *247* (8), 651–665.

(198) Baker, J. L.; Sudarsan, N.; Weinberg, Z.; Roth, A.; Stockbridge, R. B.; Breaker, R. R. *Science* 2012, *335* (6065), 233–235.

(199) Lim, H.-H.; Stockbridge, R. B.; Miller, C. *Nat. Chem. Biol.* 2013, *9* (11), 721–725.

(200) Brammer, A. E.; Stockbridge, R. B.; Miller, C. *J. Gen. Physiol.* 2014, *144* (2), 129–136.

(201) Stockbridge, R. B.; Robertson, J. L.; Kolmakova-Partensky, L.; Miller, C. *Elife* 2013, *2*, e01084.

(202) Stockbridge, R. B.; Koide, A.; Miller, C.; Koide, S. *Nat. Commun.* 2014, *5*, 5120–5125.

(203) Stockbridge, R. B.; Kolmakova-Partensky, L.; Shane, T.; Koide, A.; Koide, S.; Miller, C.; Newstead, S. *Nature* 2015, *525* (7570), 548–551.

(204) Turman, D. L.; Nathanson, J. T.; Stockbridge, R. B.; Street, T. O.; Miller, C. *Proc. Natl. Acad. Sci.* 2015, *112* (18), 5697–5701.

(205) Ji, C.; Stockbridge, R. B.; Miller, C. *J. Gen. Physiol.* 2014, *144* (3), 257–261.

(206) Yano, M.; Tong, C. C.; Light, M. E.; Schmidtchen, F. P.; Gale, P. A. *Org. Biomol. Chem.* 2010, *8*, 4356–4363.

(207) Görl, C.; Alt, H. G. *J. Organomet. Chem.* 2007, *692* (26), 5727–5753.

(208) Custelcean, R.; Delmau, L. H.; Moyer, B. A.; Sessler, J. L.; Cho, W. S.; Gross, D.; Bates, G. W.; Brooks, S. J.; Light, M. E.; Gale, P. A. *Angew. Chemie - Int. Ed.* 2005, *44* (17), 2537–2542.

(209) Gale, P. A. *Acc. Chem. Res.* 2011, *44* (3), 216–226.

(210) Yang, Y.; Wu, X.; Busschaert, N.; Furuta, H.; Gale, P. A. *Chem. Commun.* 2017, *53*, 9230–9233.

(211) Montaner, B.; Pérez-Tomás, R. *Curr. Cancer Drug Targets* 2003, *3* (1), 57–65.

(212) Valkenier, H.; Davis, A. P. *Acc. Chem. Res.* 2013, *46*, 2898–2909.

(213) Carrasco, N. *Biochim. Biophys. Acta - Rev. Biomembr.* 1993, *1154* (1), 65–82.

(214) Carvalho, D. P.; Ferreira, A. C. F. *Arq. Bras. Endocrinol. Metabol.* 2007, *51* (5), 672–682.

(215) Dohán, O.; De La Vieja, A.; Paroder, V.; Riedel, C.; Artani, M.; Reed, M.; Ginter, C. S.; Carrasco, N. *Endocr. Rev.* 2003, *24* (1), 48–77.

(216) Pressman, B. C. *Annu. Rev. Biochem.* 1976, *45*, 501–530.

(217) Wu, X.; Gale, P. A. *J. Am. Chem. Soc.* 2016, *138*, 16508–16514.

(218) Riddick, J. A.; Bunger, W. B.; Sakano, T. K. *Organic Solvents: Physical properties and methods of purification*, 4th Editio.; Wiley Interscience: New York, 1986.

(219) Hamilton, J. A.; Cistola, D. P. *Proc. Natl. Acad. Sci. U. S. A.* 1986, *83* (1), 82–86.

(220) Brunaldi, K.; Miranda, M. A.; Abdulkader, F.; Curi, R.; Procopio, J. *J. Lipid Res.* 2005, *46*, 245–251.

(221) Kamp, F.; Hamilton, J. A. *Proc. Natl. Acad. Sci.* 1992, *89* (23), 11367–11370.

(222) Luckey, M. *Membrane Structural Biology with Biochemical and Biophysical Foundations*, 2nd Editio.; Cambridge University Press: Cambridge, 2014.

(223) Klotz, K. H.; Benz, R. *Biophys. J.* 1993, *65* (6), 2661–2672.

(224) Finkelstein, A.; Andersen, O. S. *J. Membr. Biol.* 1981, *59* (3), 155–171.

(225) Paula, S.; Volkov, A. G.; Deamer, D. W. *Biophys. J.* 1998, *74* (1), 319–327.

(226) Tong, C. C.; Quesada, R.; Sessler, L.; Gale, P. A. 2008, 6321–6323.

(227) Schrodinger,LLC.

(228) Sheldrick, G. M. *Acta Crystallogr. Sect. A* 2008, *64*, 112–122.

(229) Dolomanov, O. V.; Bourhis, L. J.; Gildea, R. J.; Howard, J. A. K.; Puschmann, H. J. *J. Appl. Crystallogr.* 2009, *42*, 339–341.

(230) Sheldrick, G. M. *Acta Crystallogr. Sect. A* 2015, *71*, 3–8.

(231) Duisenberg, A. J. M. *J. Appl. Crystallogr.* 1992, *25*, 92–96.

(232) Nonius, B. V. 1998.

(233) Otiwinowski, Z.; Minor, W. In *Macromolecular Crystallography*; Carter, C. W., Sweet, R. M., Eds.; Academic Press, 1997; pp 307–326.

(234) Krause, L.; Herbst-Irmer, R.; Sheldrick, G. M.; Stalke, D. *J. Appl. Crystallogr.* 2015, *48*, 3–10.

(235) Sheldrick, G. M. Gottingen 1998.

(236) Smith, B. D.; Lambert, T. N. *Chem. Commun.* 2003, 2261–2268.

Appendices

Appendix A Characterisation

A.1 NMR Spectra

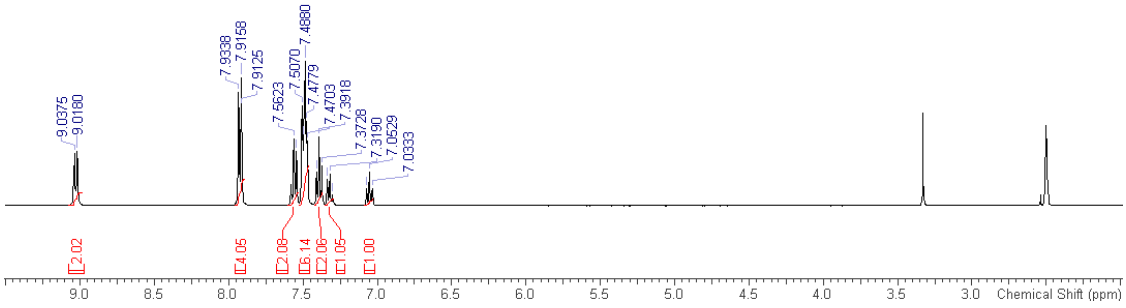

A1. 1 ^{1}H NMR spectra (400 MHz, DMSO-d_6) for receptor **72**.

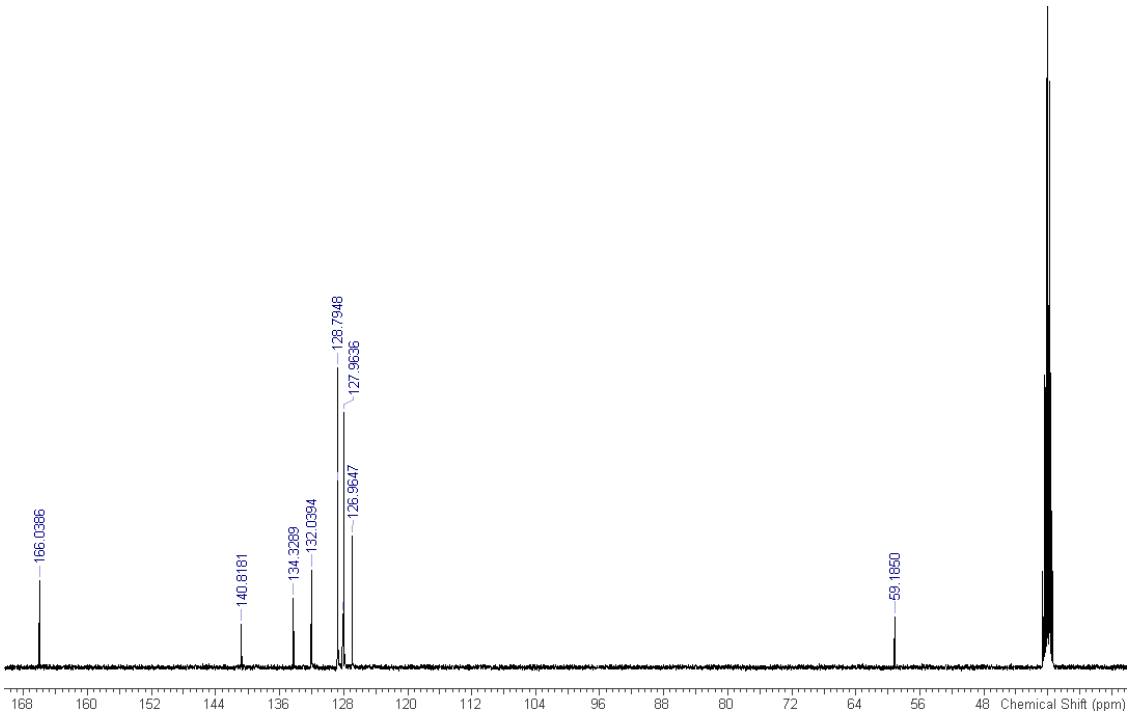

A1. 2 ^{13}C NMR spectra (101 MHz, DMSO-d_6) for receptor **72**.

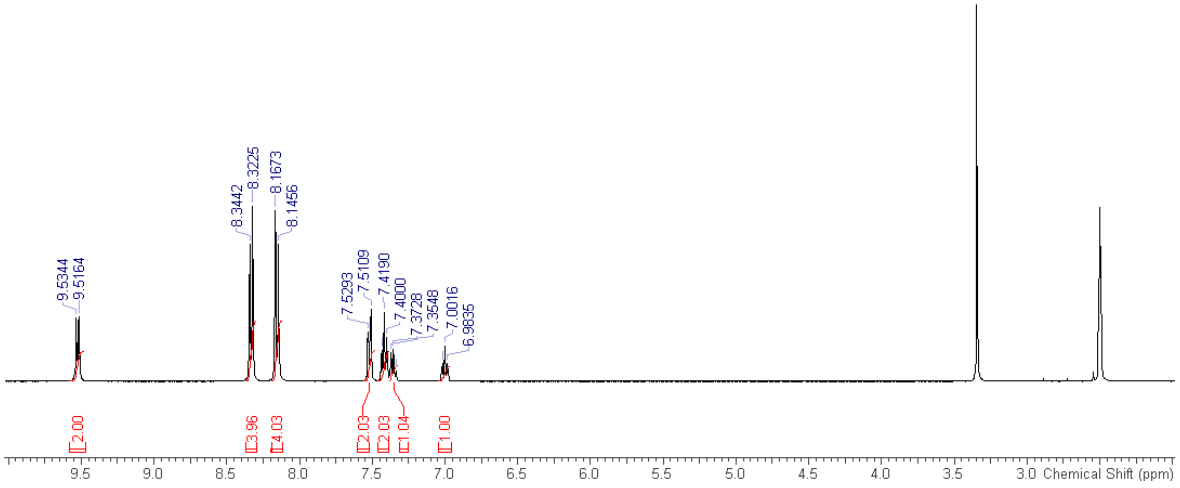

A1. 3 ^{1}H NMR spectra (400 MHz, DMSO-d_6) for receptor **73**.

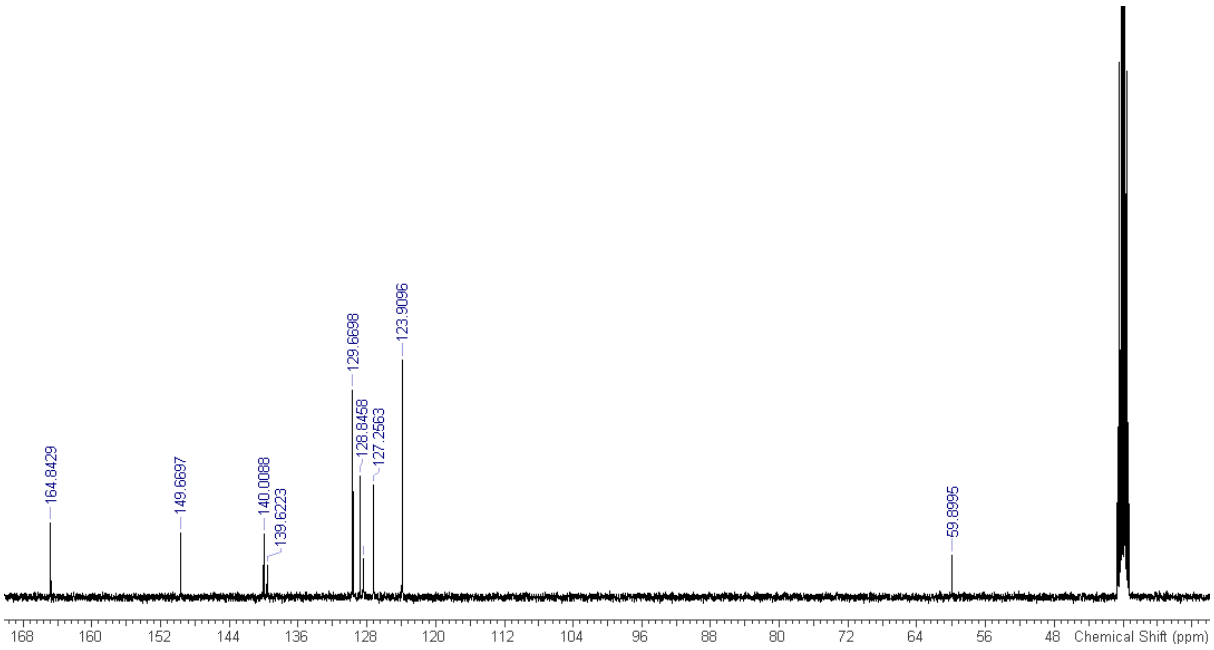

A1. 4 ^{13}C NMR spectra (101 MHz, DMSO-d_6) for receptor **73**.

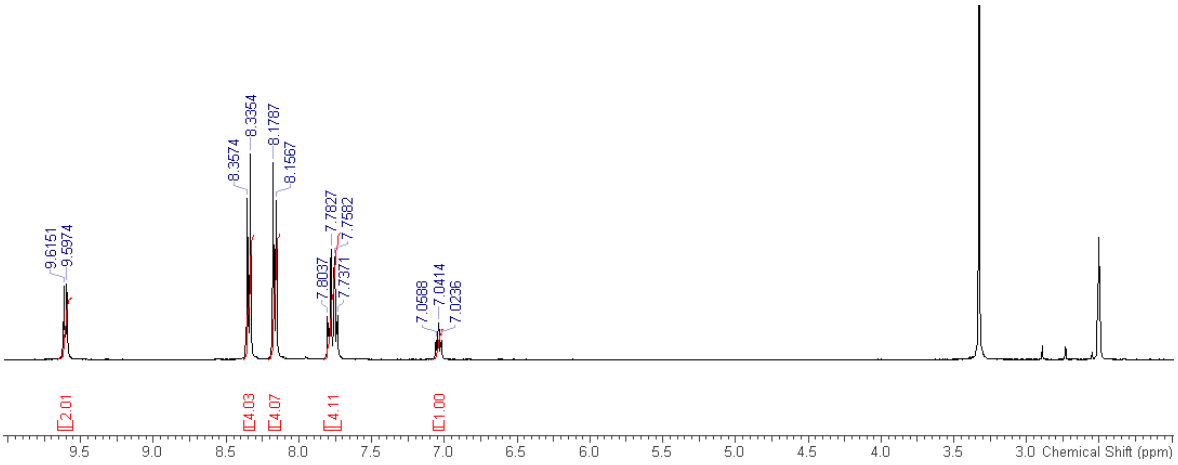

A1. 5 ^{1}H NMR spectra (400 MHz, DMSO-d_6) for receptor **74**.

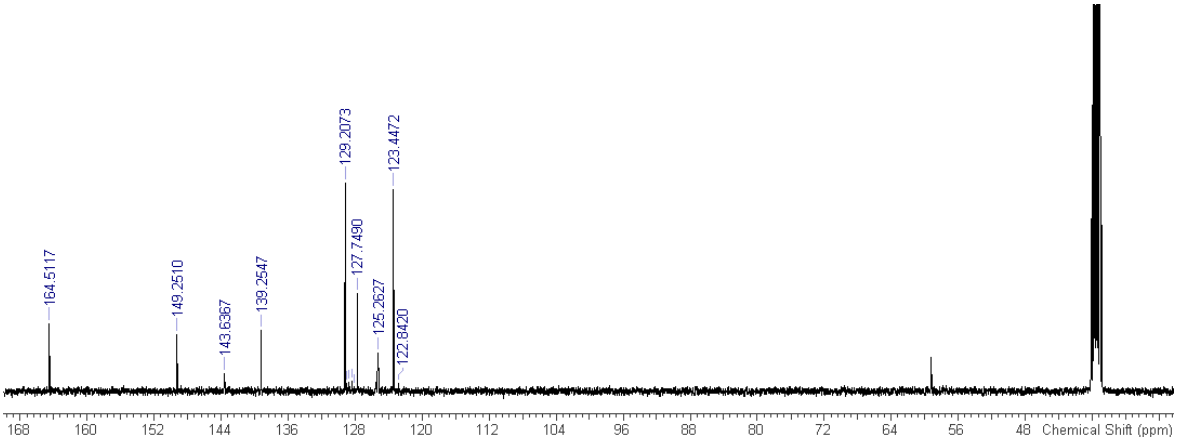

A1. 6 ^{13}C NMR spectra (101 MHz, DMSO-d_6) for receptor **74**.

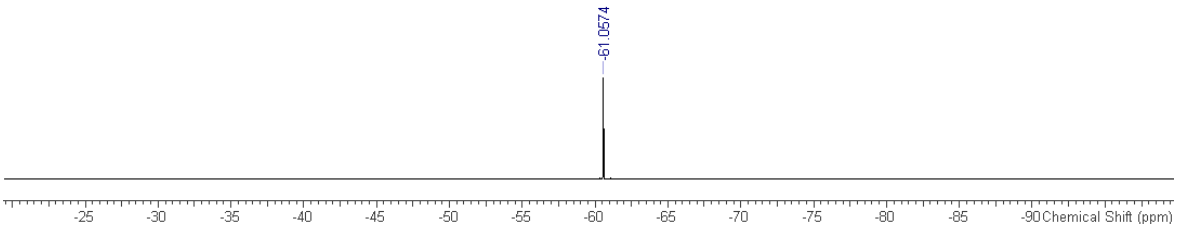

A1. 7 ^{19}F NMR spectra (376 MHz, DMSO-d_6) for receptor **74**.

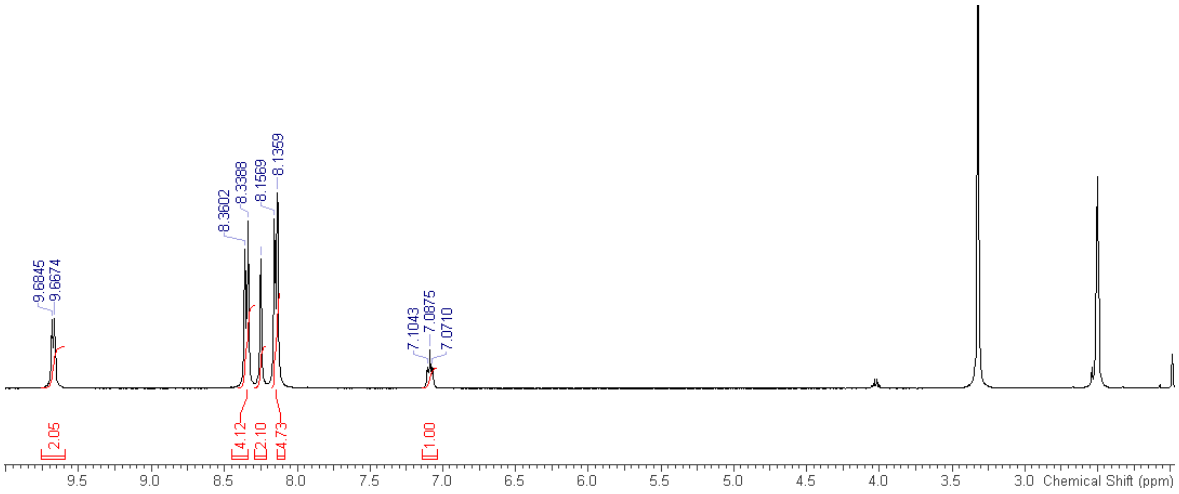

A1. 8 ^{1}H NMR spectra (400 MHz, DMSO-d_6) for receptor **75**.

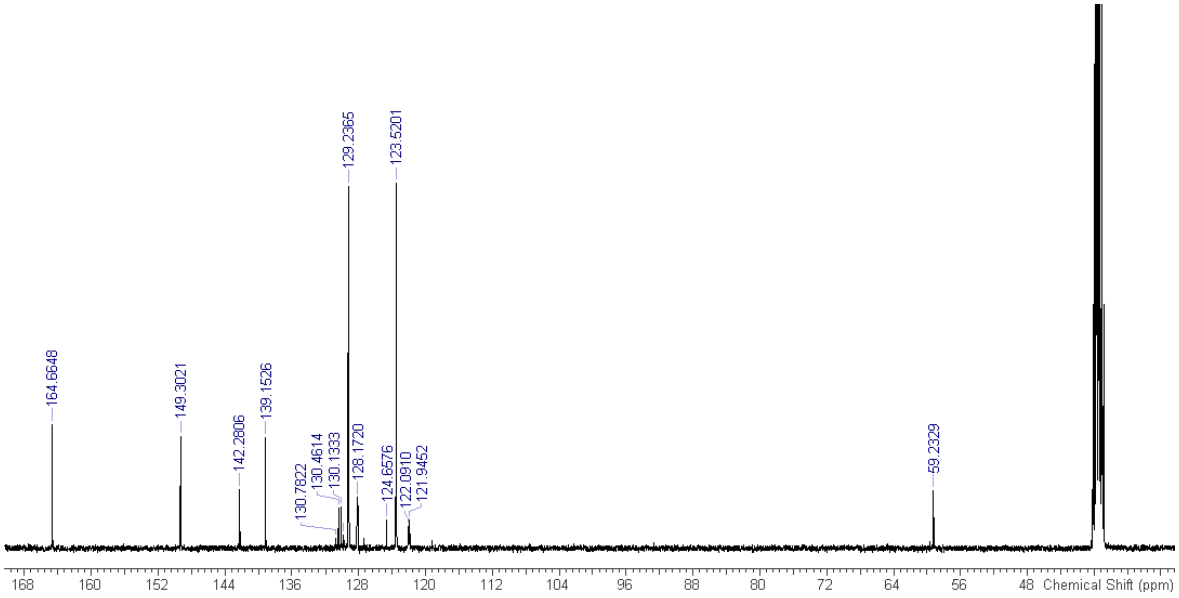

A1. 9 ^{13}C NMR spectra (101 MHz, DMSO-d_6) for receptor **75**.

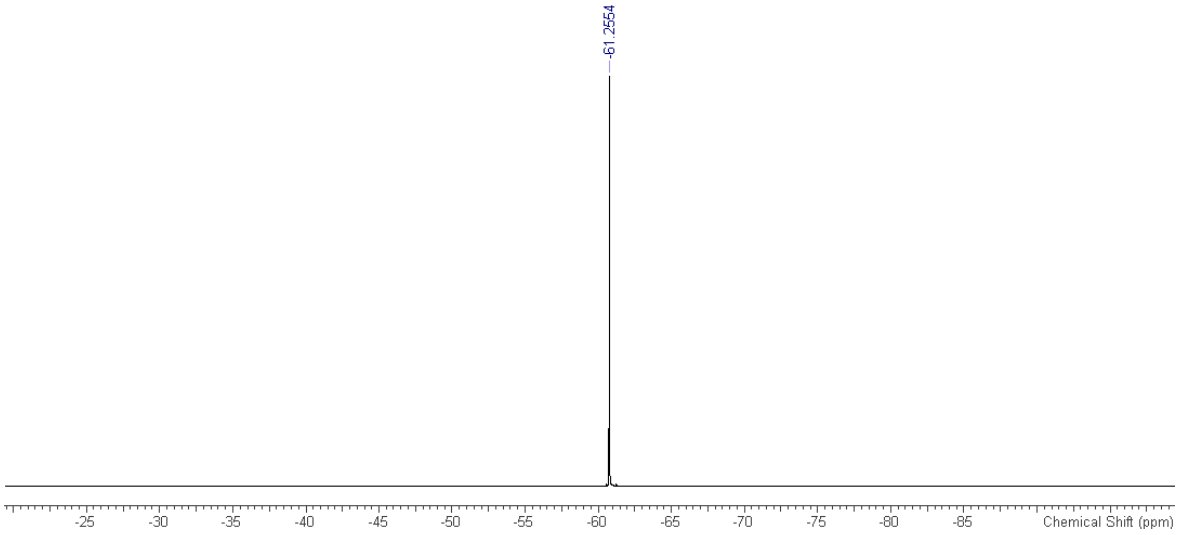

A1. 10 ^{19}F NMR spectra (376 MHz, DMSO-d_6) for receptor **75**.

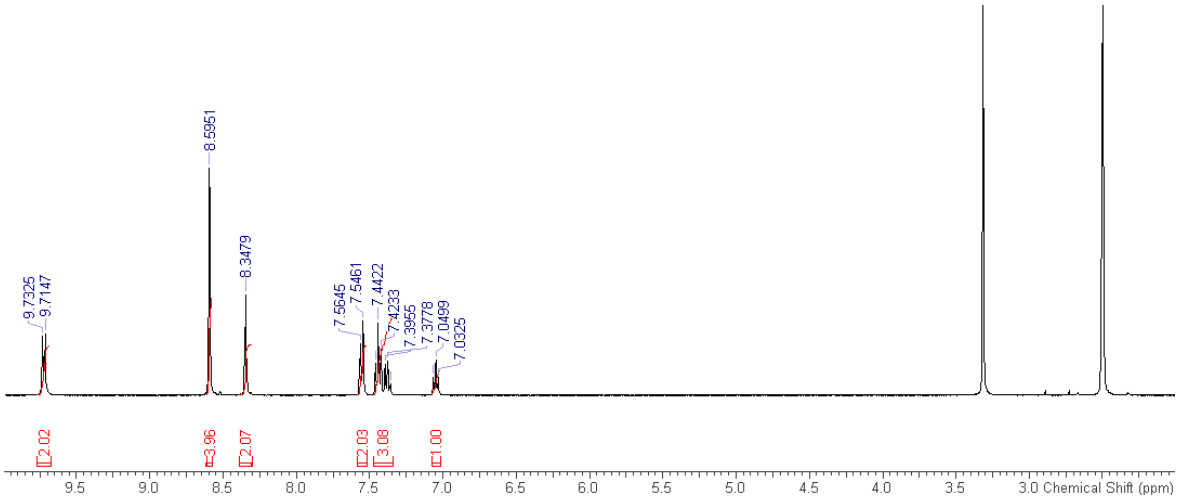

A1. 11 ^{1}H NMR spectra (400 MHz, DMSO-d_6) for receptor **76**.

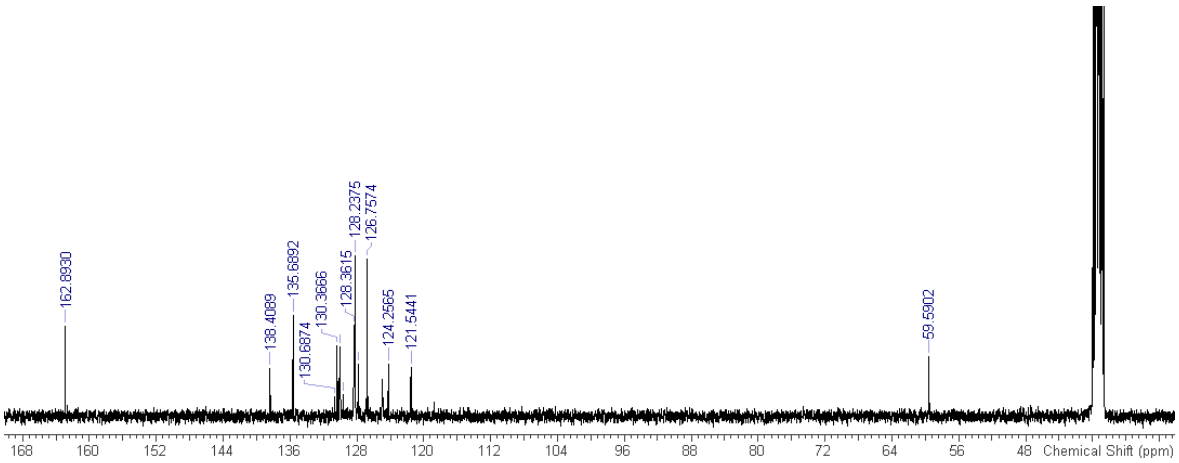

A1. 12 ^{13}C NMR spectra (101 MHz, DMSO-d_6) for receptor **76**.

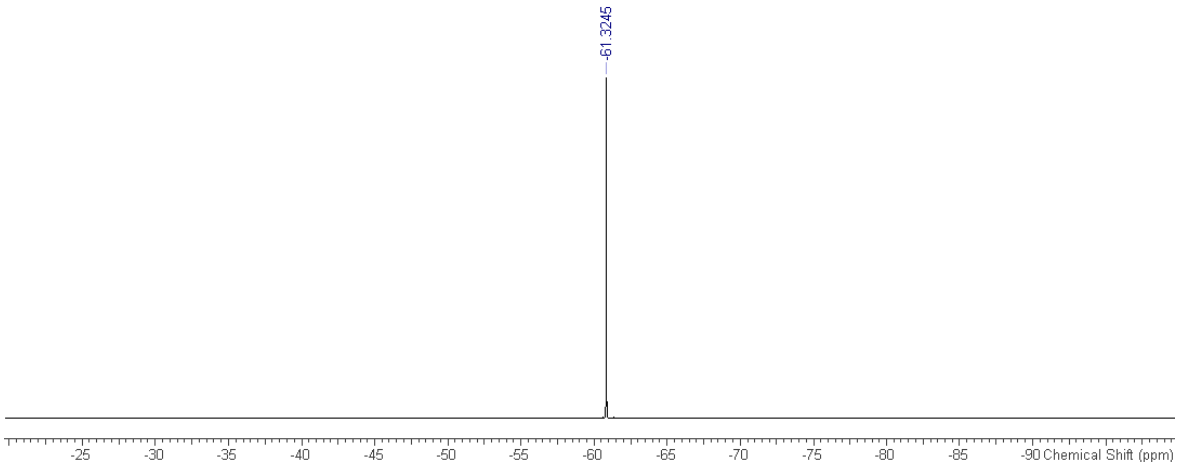

A1. 13 ^{19}F NMR spectra (376 MHz, DMSO-d_6) for receptor **76**.

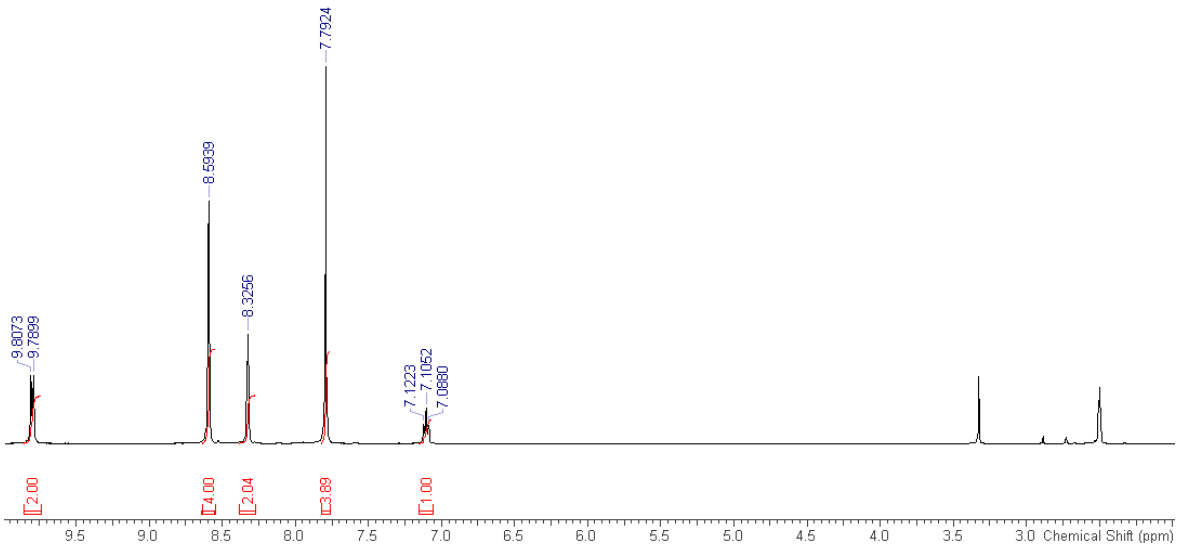

A1. 14 ^{1}H NMR spectra (400 MHz, DMSO-d_6) for receptor **77**.

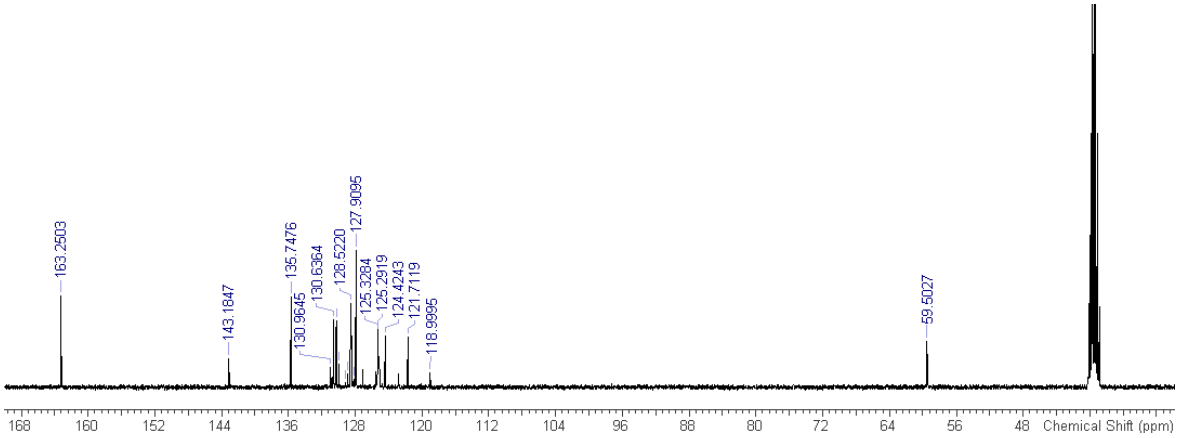

A1. 15 ^{13}C NMR spectra (101 MHz, DMSO-d_6) for receptor **77**.

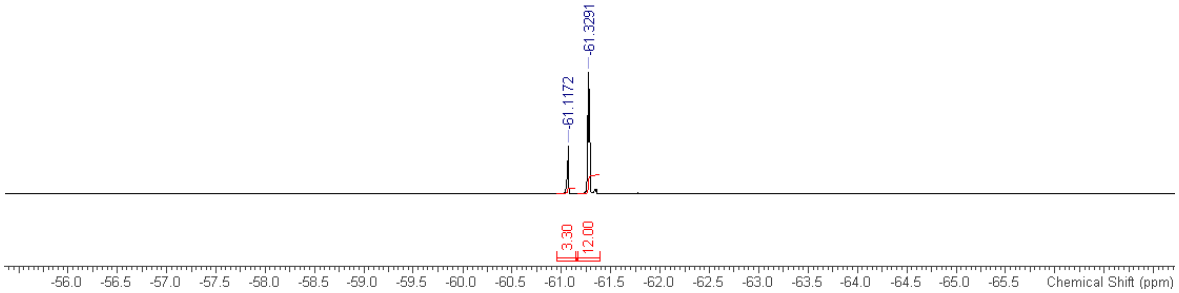

A1. 16 ^{19}F NMR spectra (376 MHz, DMSO-d_6) for receptor **77**.

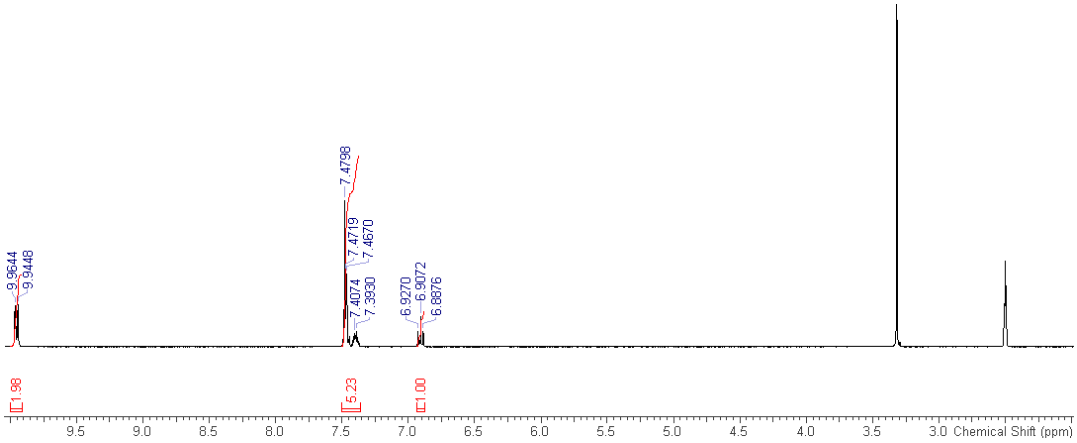

A1. 17 ^{1}H NMR spectra (400 MHz, DMSO-d_6) for receptor **78**.

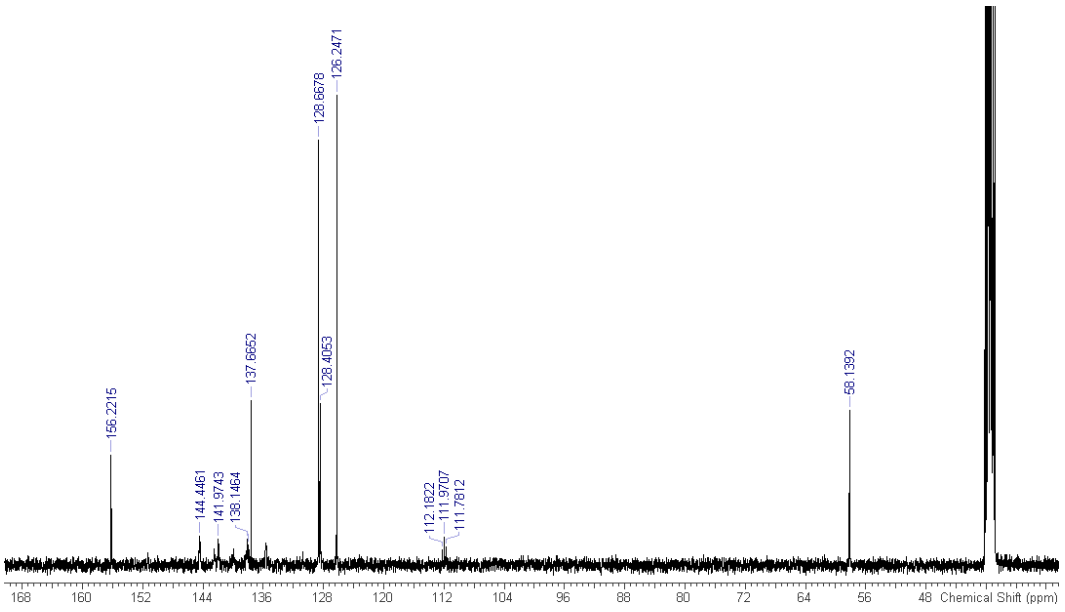

A1. 18 ^{13}C NMR spectra (101 MHz, DMSO-d_6) for receptor **78**.

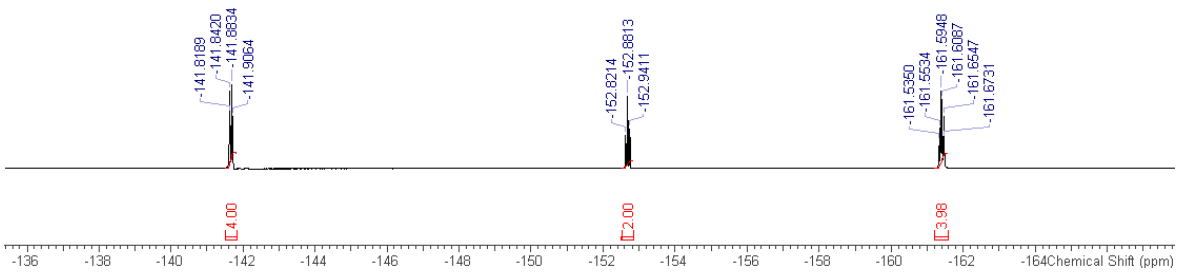

A1. 19 ^{19}F NMR spectra (376 MHz, DMSO-d_6) for receptor **78**.

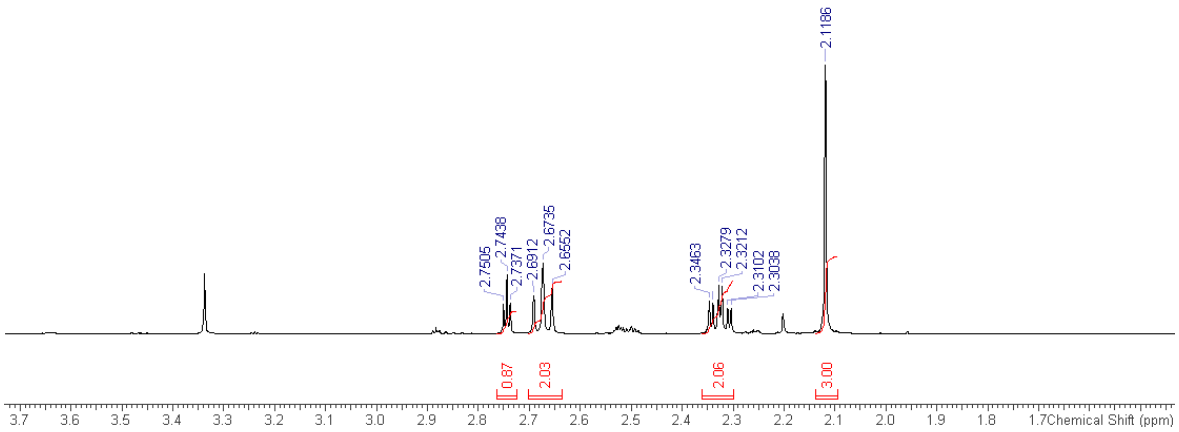

A1. 20 ^{1}H NMR spectra (400 MHz. DMSO-d_6) for compound **84**.

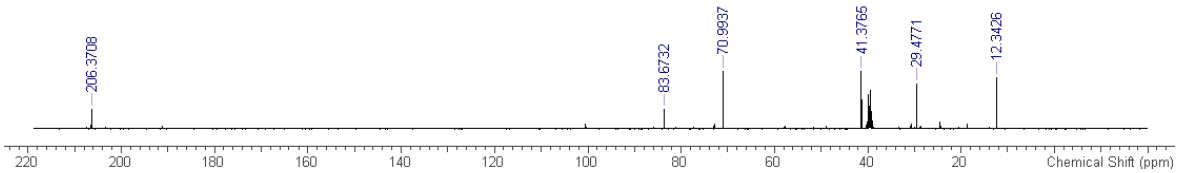

A1. 21 ^{13}C NMR spectra (101 MHz, DMSO-d_6) for compound **84**.

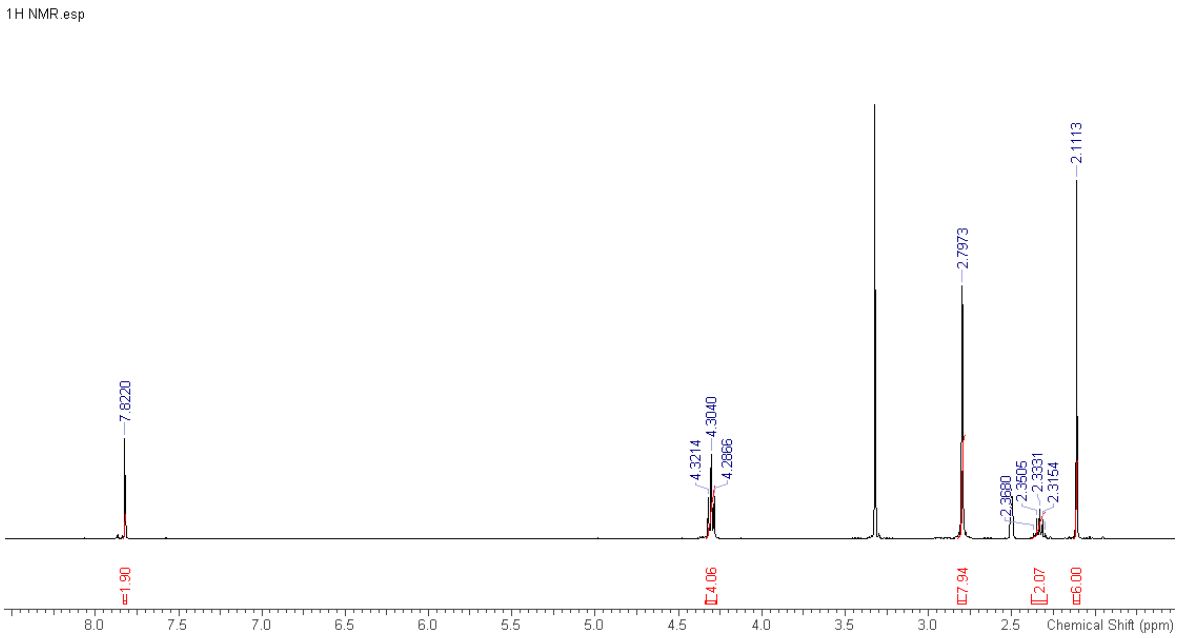

A1. 22 ^{1}H NMR spectra (400 MHz, DMSO-d_6) for compound **79a**.

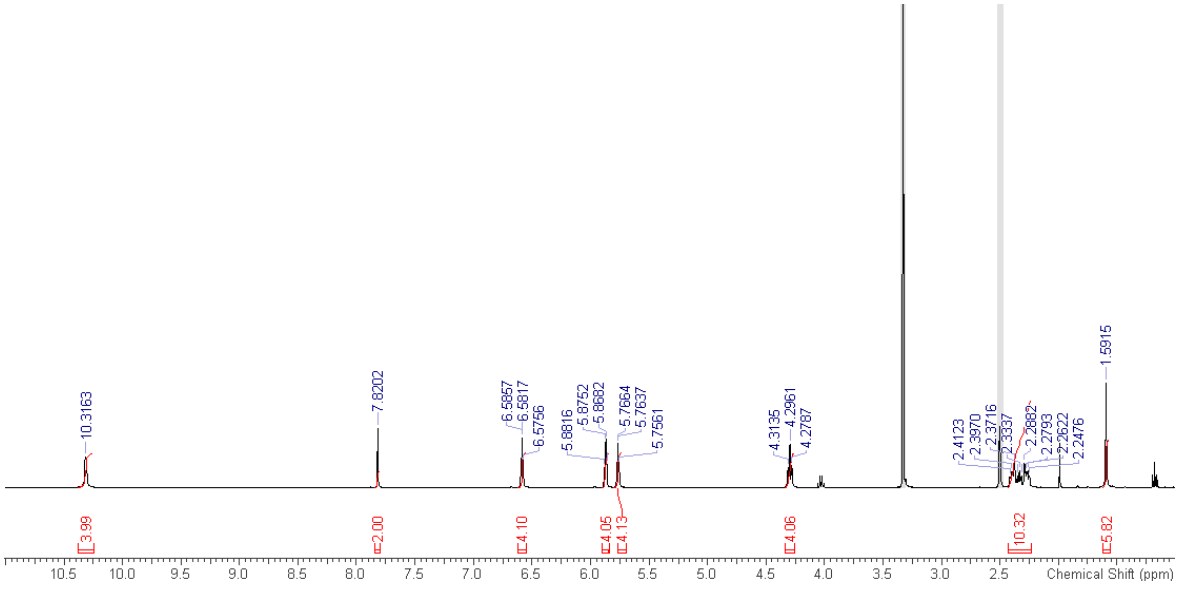

A1. 23 ^{1}H NMR spectra (400 MHz, DMSO-d_6) for compound **79b**.

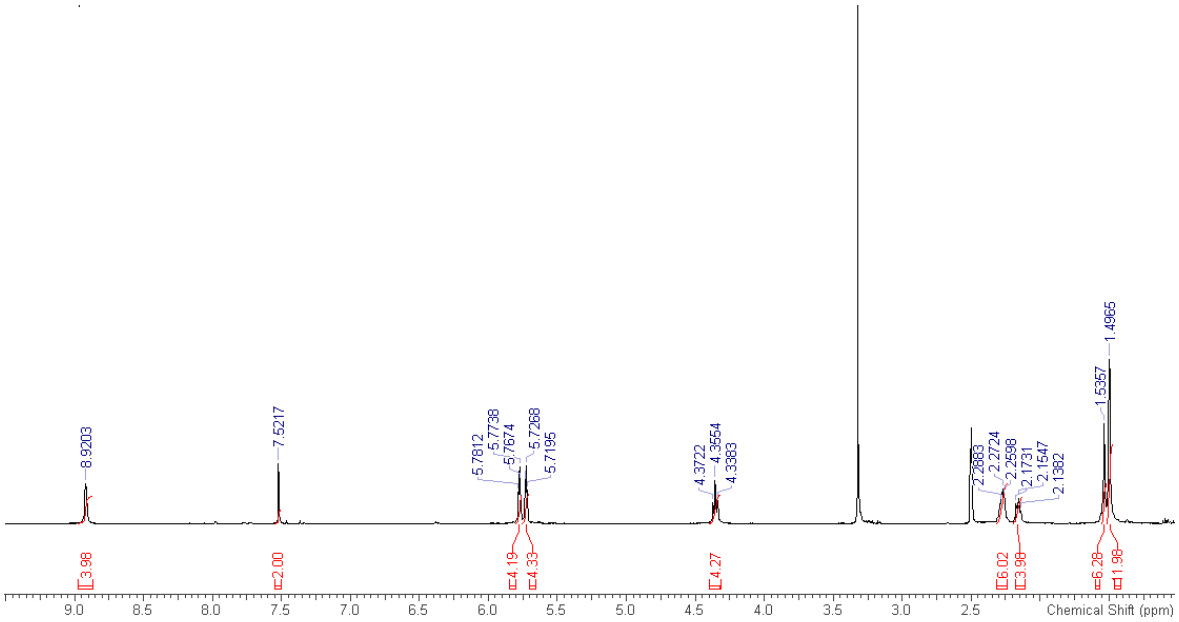

A1. 24 ^{1}H NMR spectra (400 MHz, DMSO-d_6) for receptor **79**.

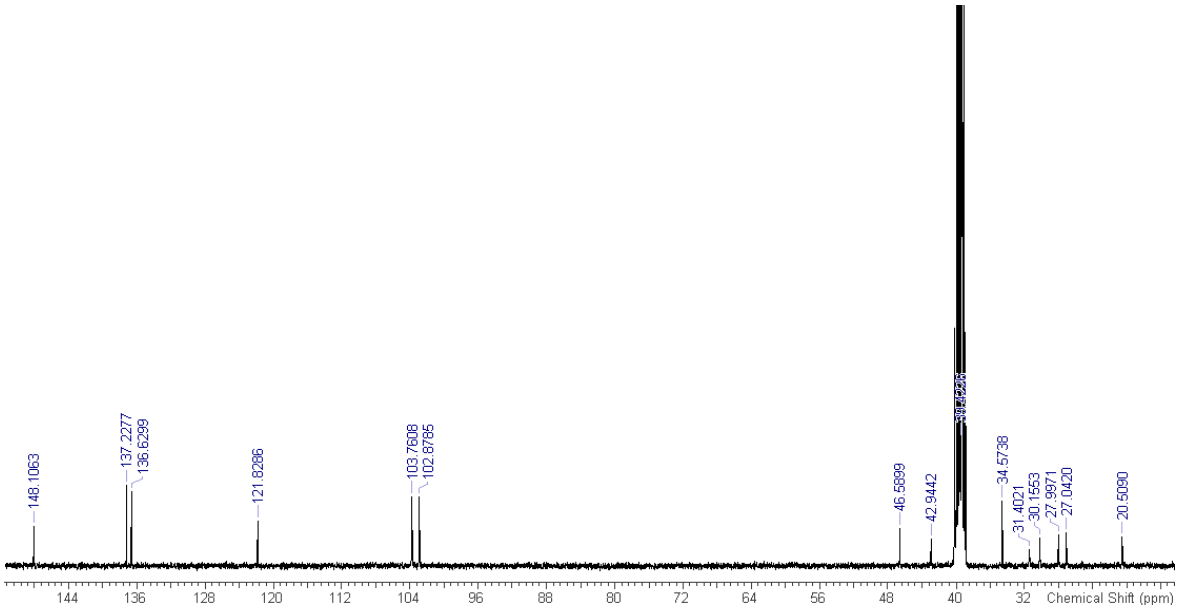

A1. 25 ^{13}C NMR spectra (101 MHz, chloroform-*d*) for receptor **79**.

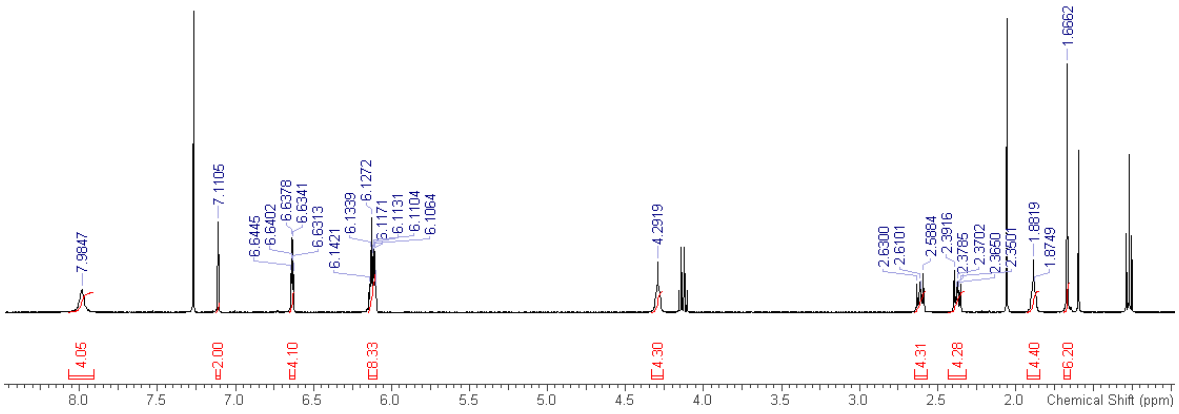

A1. 26 ^{1}H NMR spectra (400 MHz, chloroform-*d*) for compound **80b**.

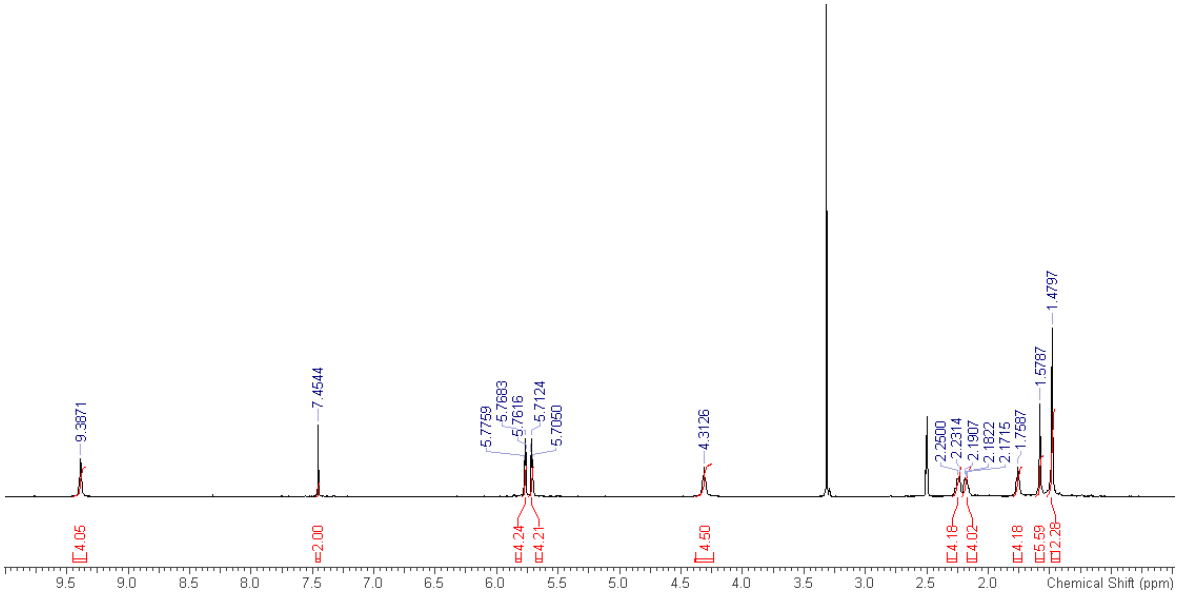

A1. 27 ^{1}H NMR spectra (400 MHz, DMSO-d_6) for receptor **80**.

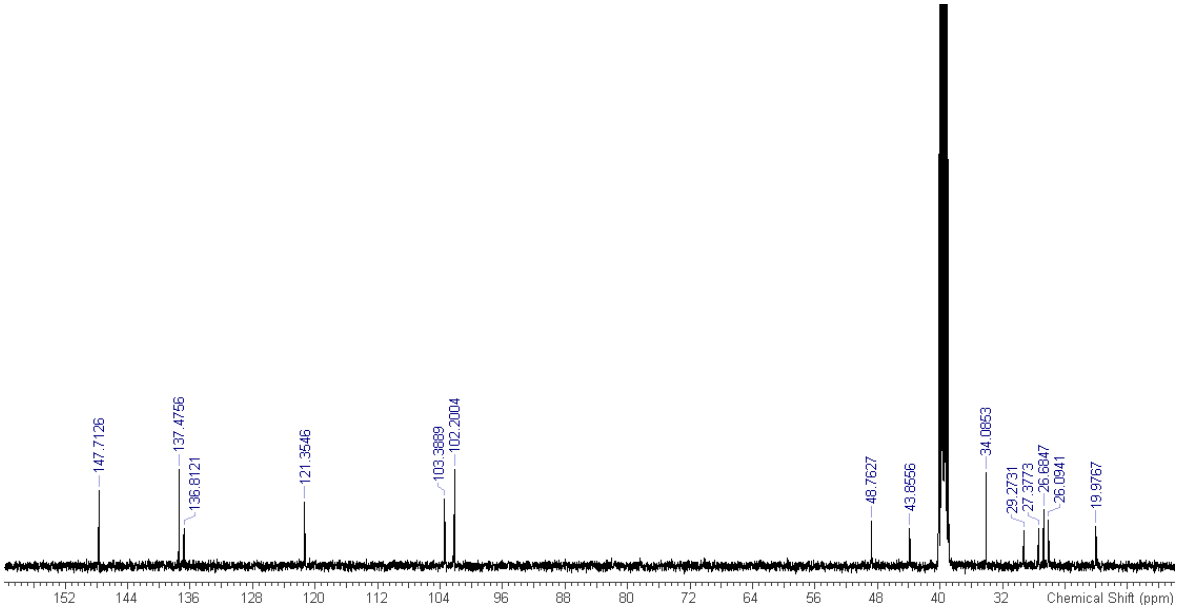

A1. 28 ^{13}C NMR spectra (101 MHz, DMSO-d_6) for receptor **80**.

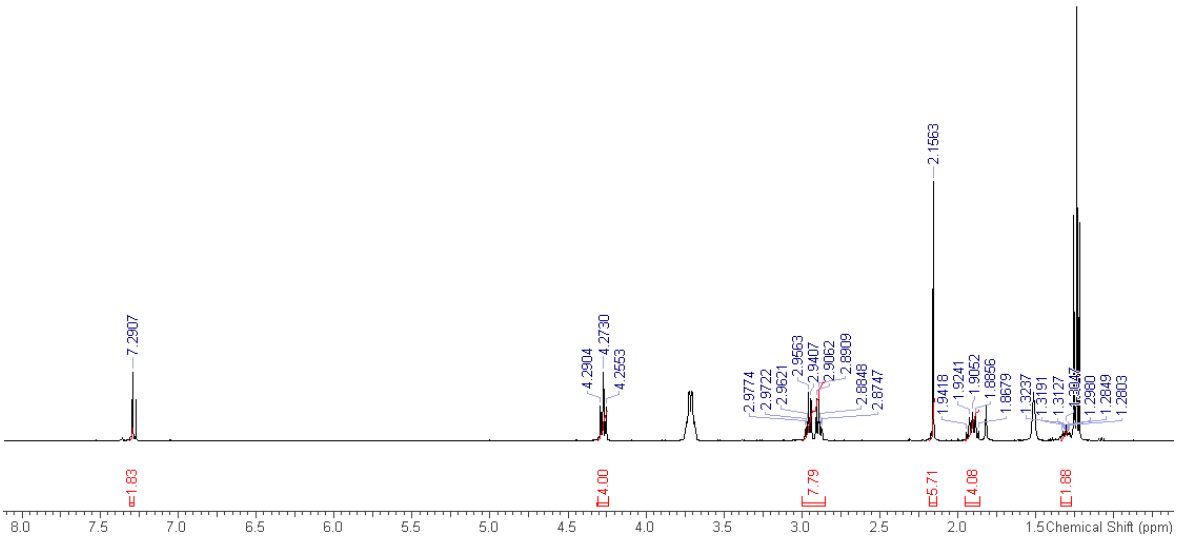

A1. 29 ^{1}H NMR spectra (400 MHz, chloroform-*d*) for compound **81a**.

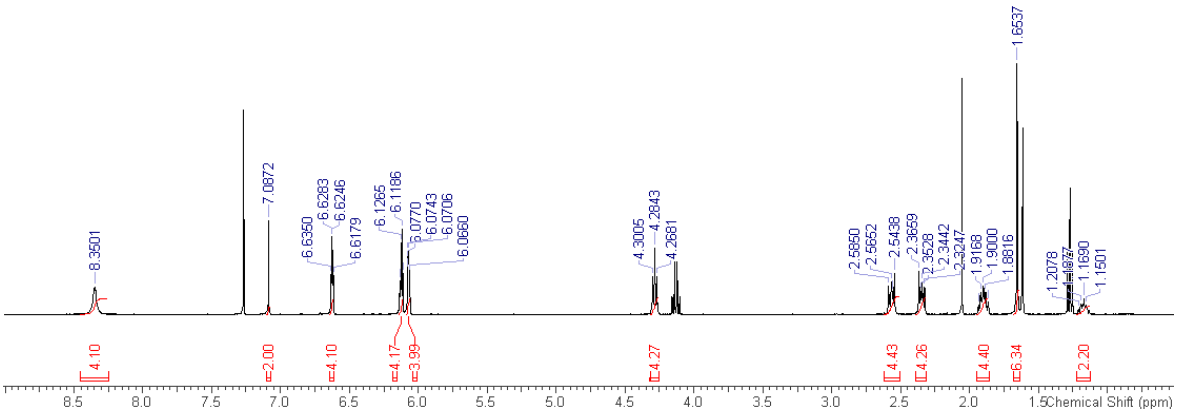

A1. 30 ^{1}H NMR spectra (400 MHz, chloroform-*d*) for compound **81b**.

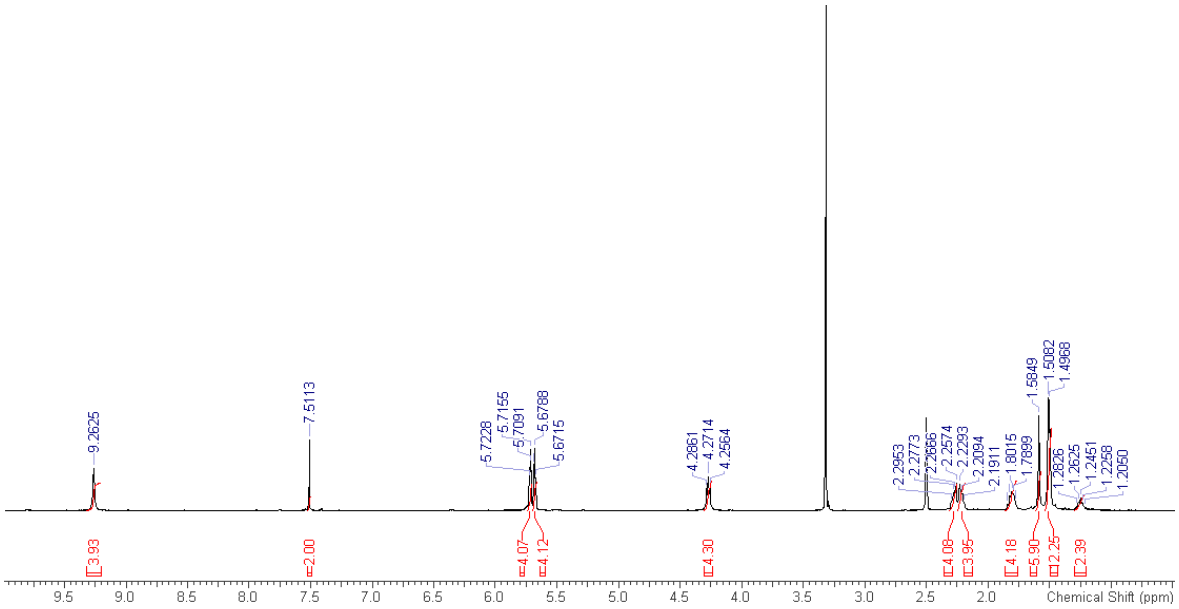

A1. 31 ^{1}H NMR spectra (400 MHz, DMSO-d_6) for receptor **81**.

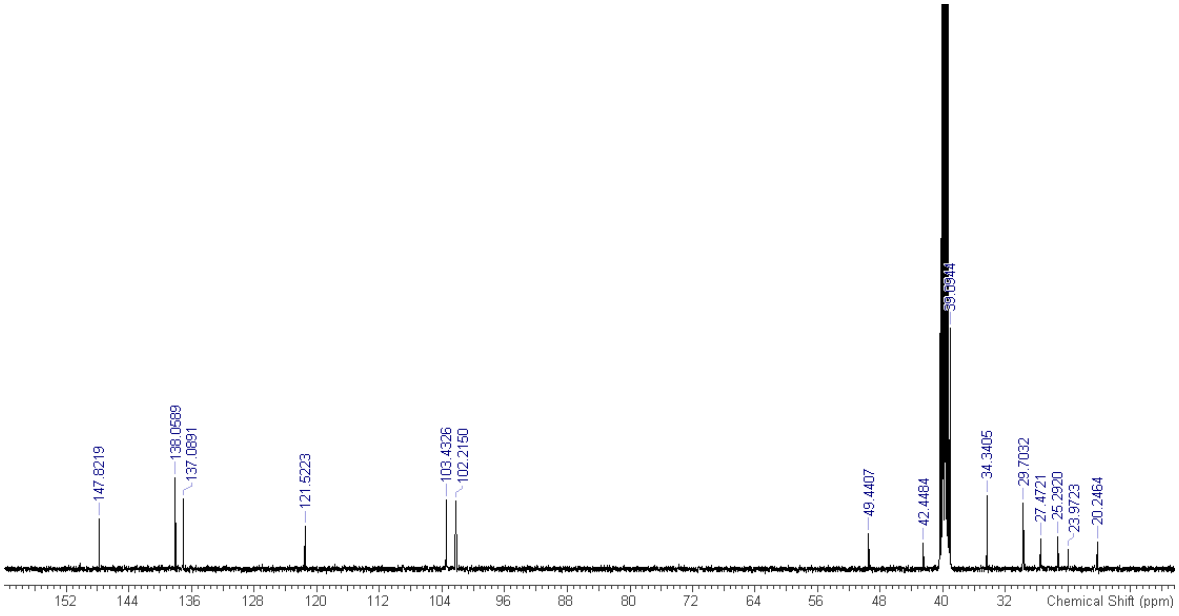

A1. 32 ^{13}C NMR spectra (101 MHz, DMSO-d_6) for receptor **81**.

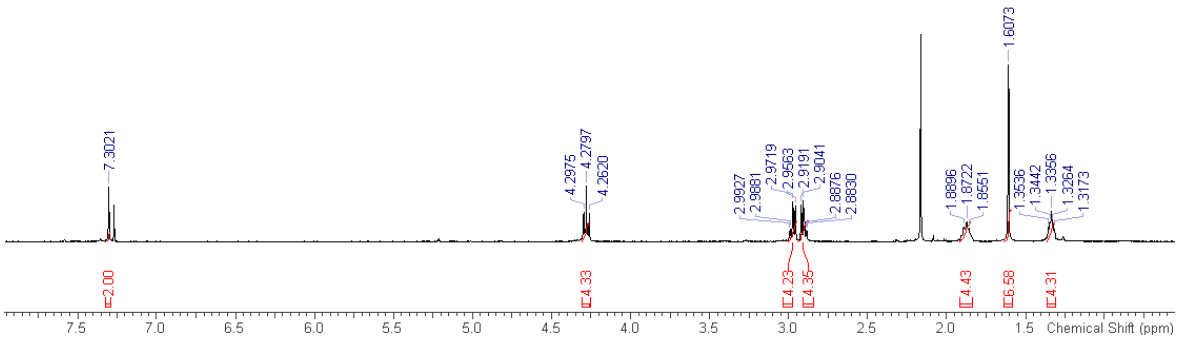

A1. 33 ^{1}H NMR spectra (400 MHz, chloroform-*d*) for compound **82a**.

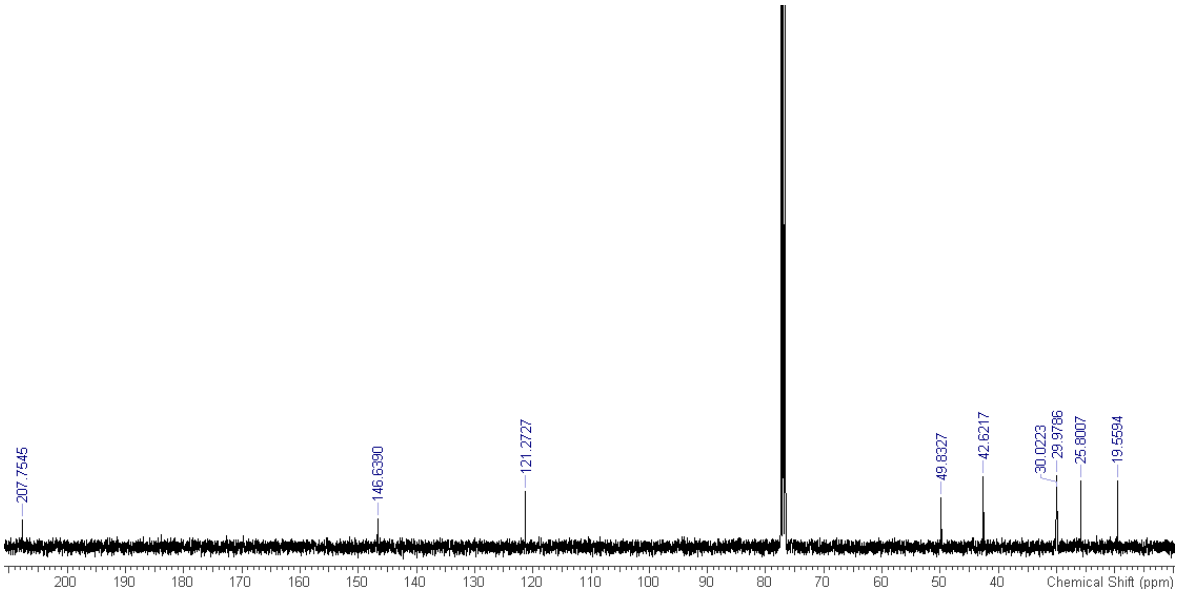

A1. 34 ^{13}C NMR spectra (101 MHz, chloroform-*d*) for compound **82a**.

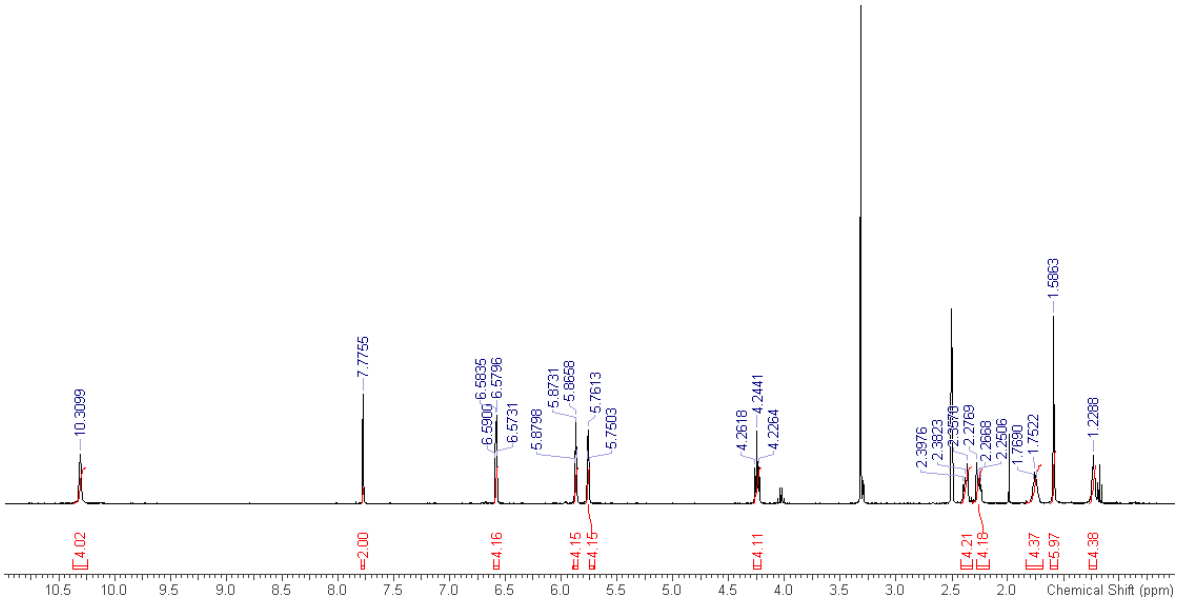

A1. 35 ^{1}H NMR spectra (400 MHz, DMSO-d_6) for compound **82b**.

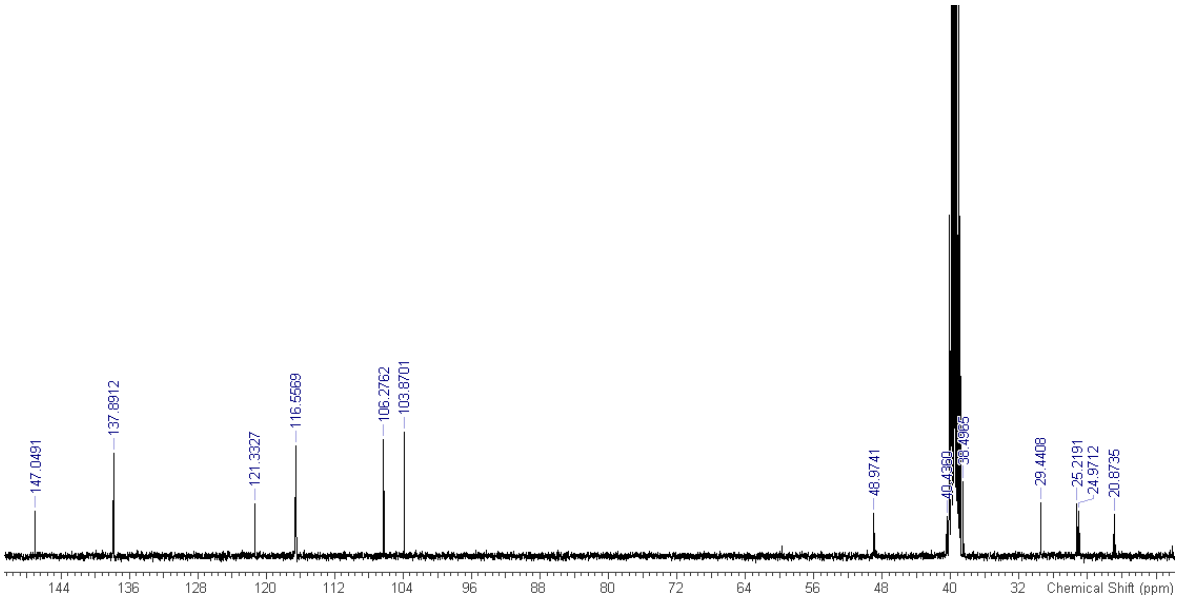

A1. 36 ^{13}C NMR spectra (101 MHz, DMSO-d_6) for compound **82b**.

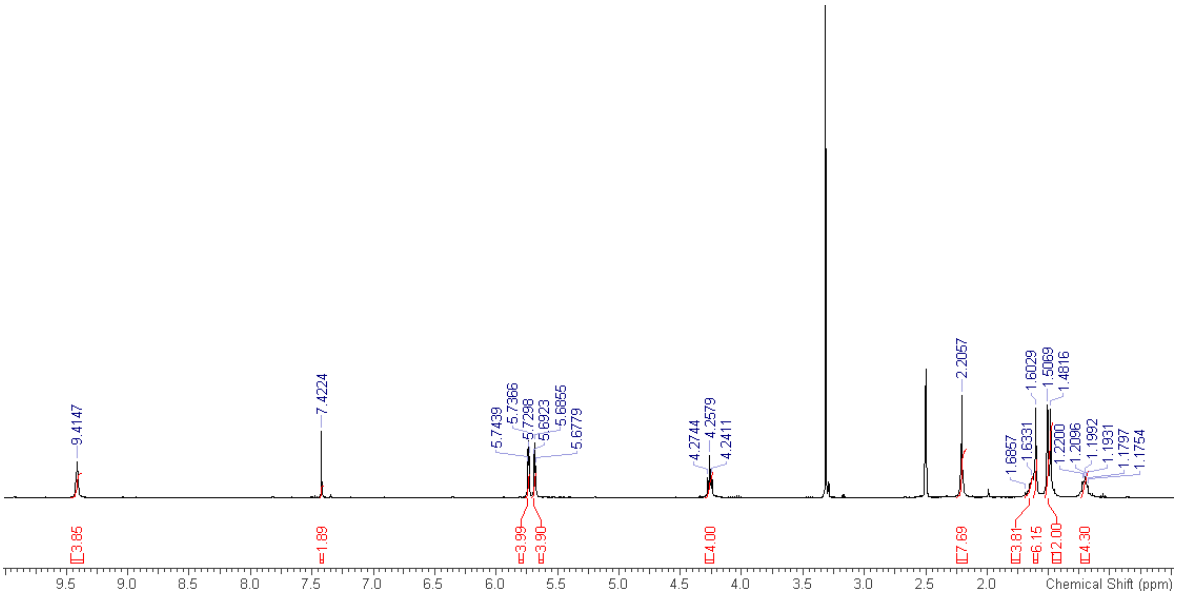

A1. 37 ^{1}H NMR spectra (400 MHz, DMSO-d_6) for receptor **82**.

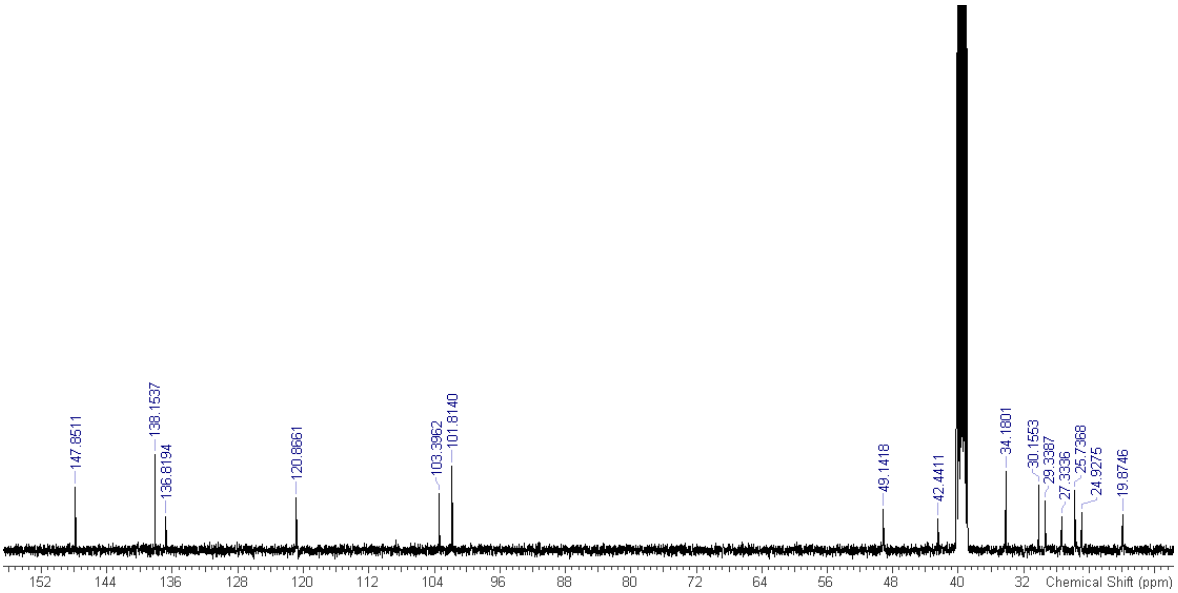

A1. 38 ^{13}C NMR spectra (101 MHz, chloroform-*d*) for receptor **82**.

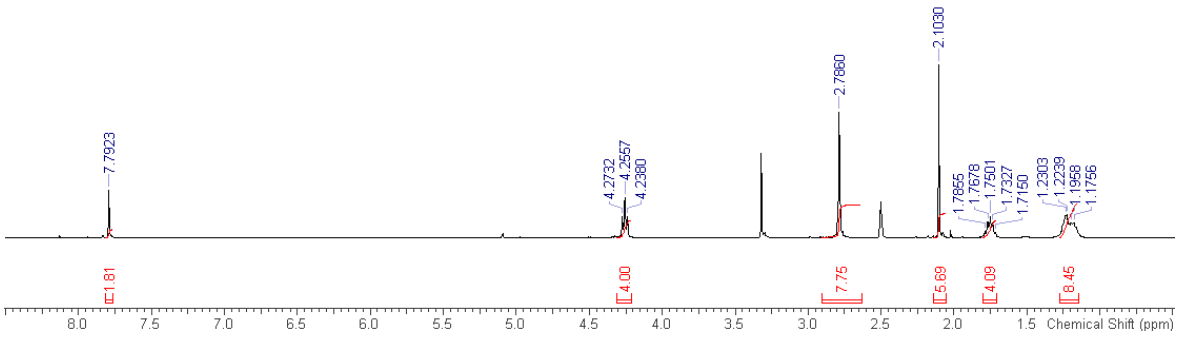

A1. 39 ^{1}H NMR spectra (400 MHz, DMSO-d_6) for compound **83a**.

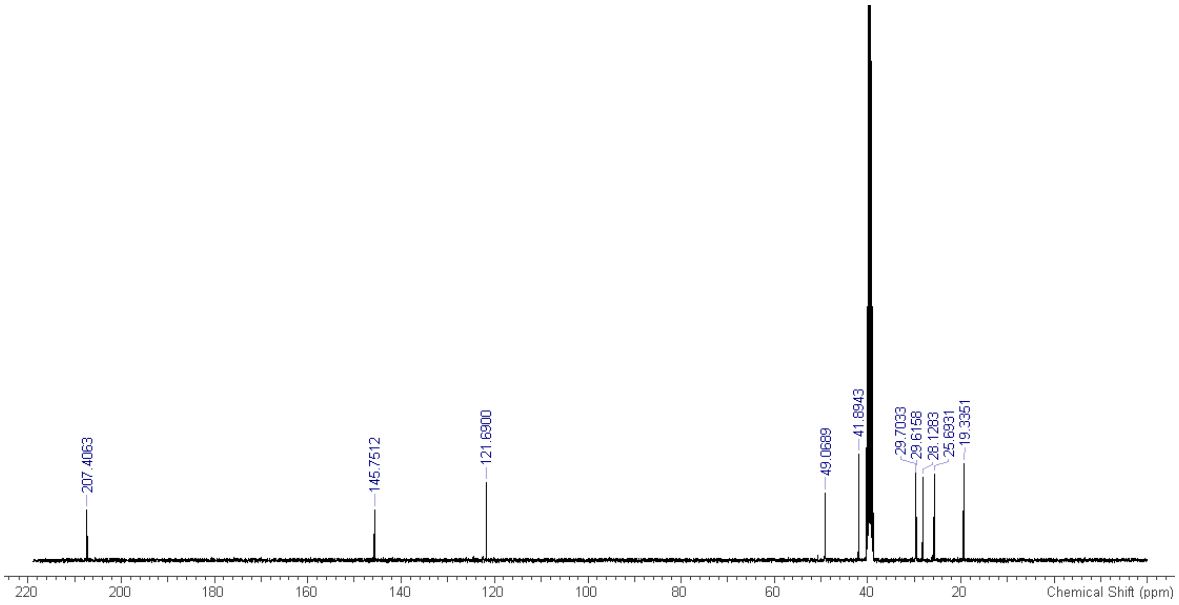

A1. 40 ^{13}C NMR spectra (101 MHz, DMSO-d_6) for compound **83a**.

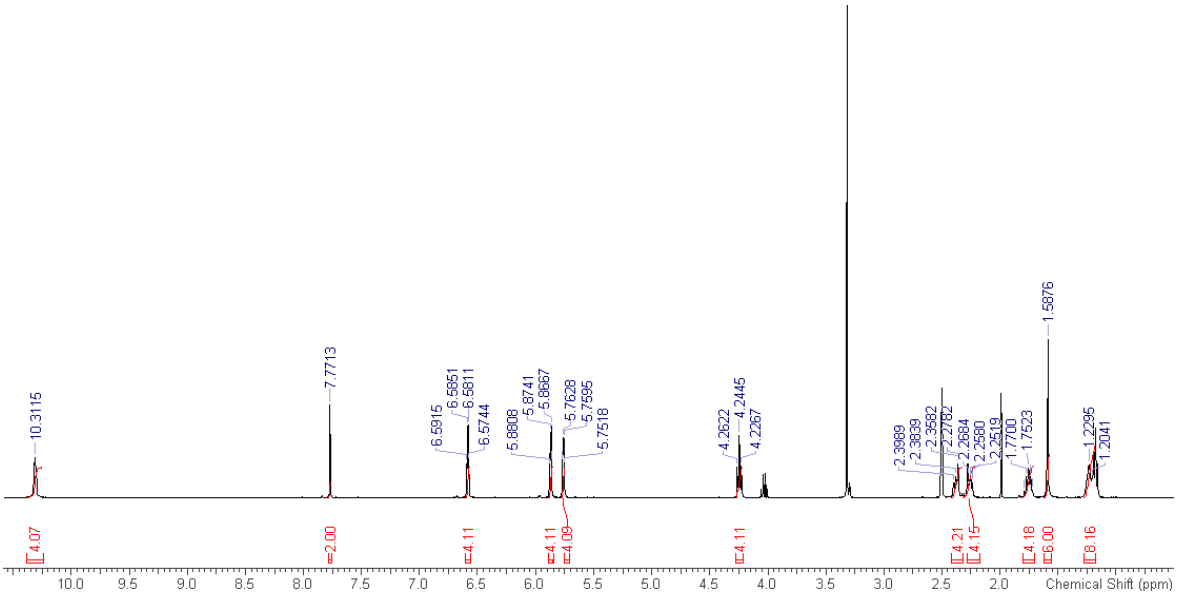

A1. 41 ^{1}H NMR spectra (400 MHz, DMSO-d_6) for compound **83b**.

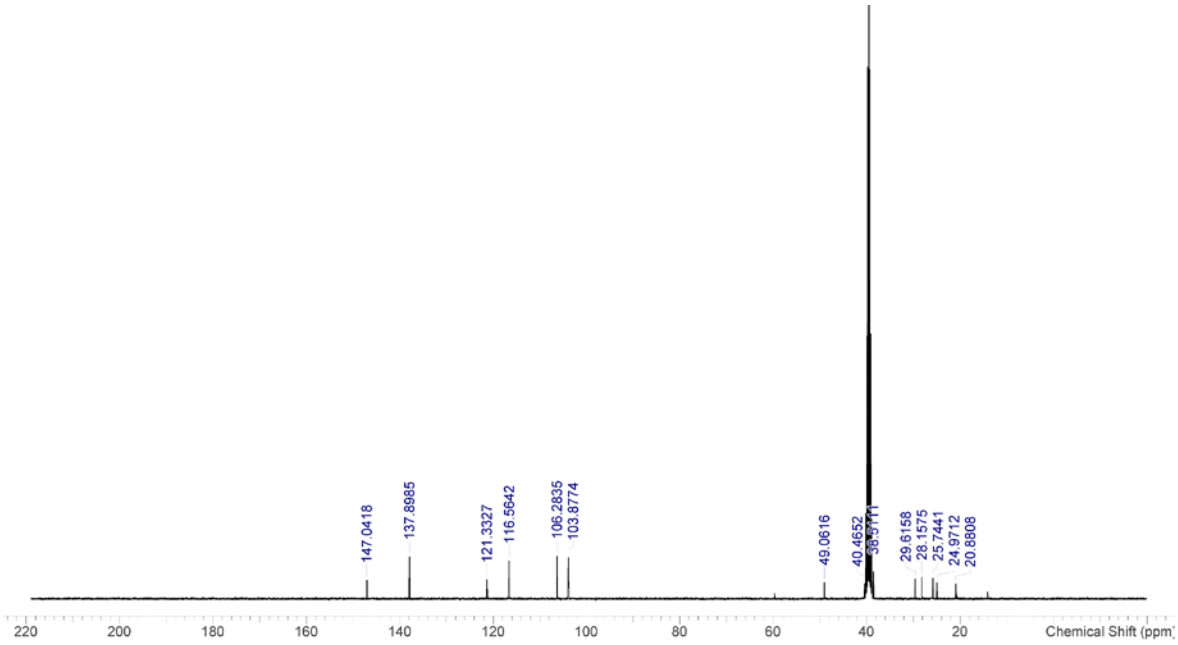

A1. 42 ^{13}C NMR spectra (101 MHz, DMSO-d_6) for compound **83b**.

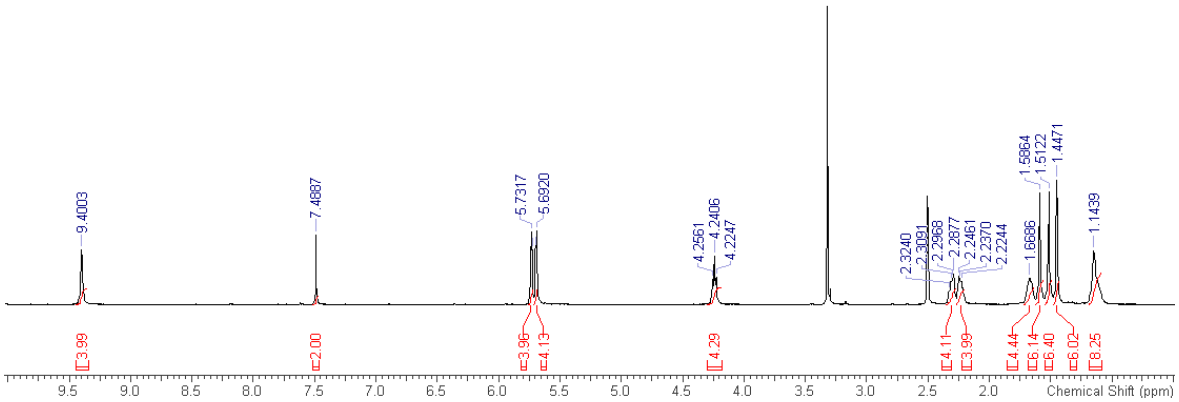

A1. 43 ^{1}H NMR spectra (400 MHz, DMSO-d_6) for receptor **83**.

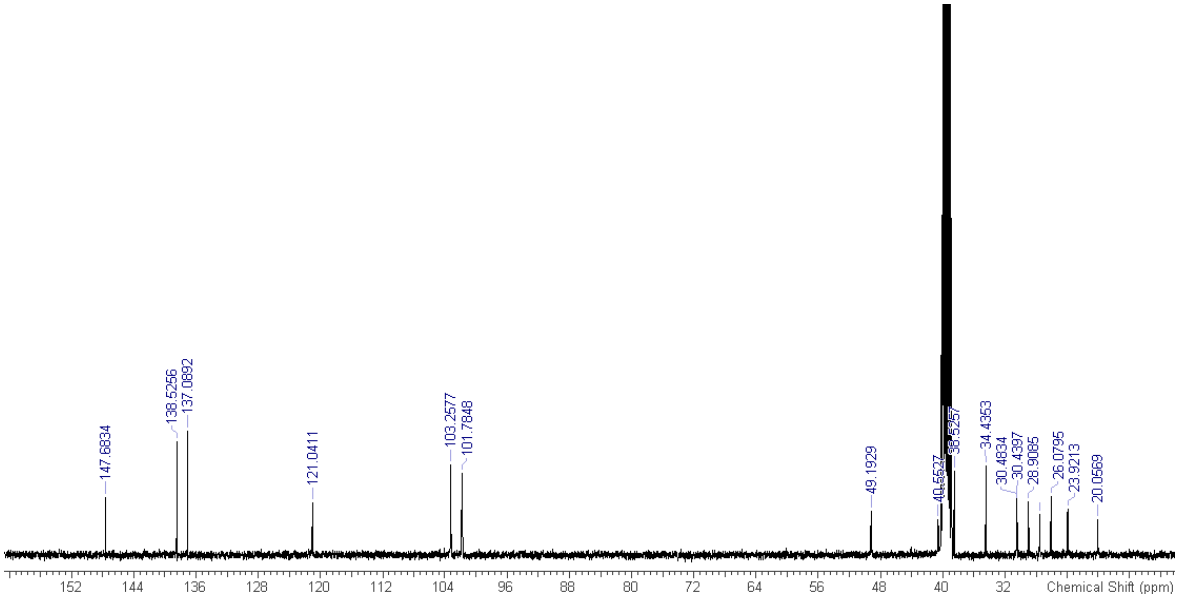

A1. 44 ^{13}C NMR spectra (101 MHz, DMSO-d_6) for receptor **83**.

A.2 HRMS

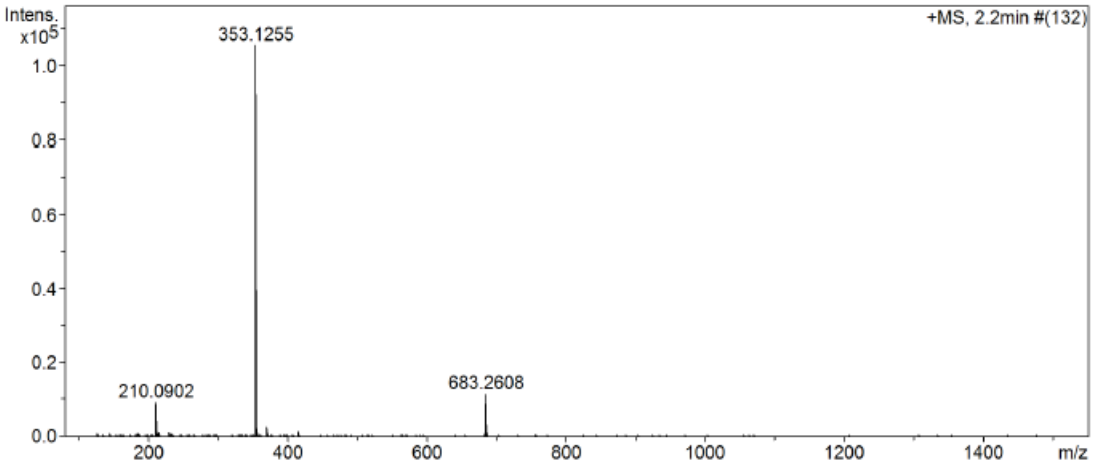

Meas. m/z	Formula	m/z	err [ppm]	err [mDa]	# Sigma	mSigma	rdb	e⁻ Conf	N-Rule
353.1255	C 19 H 13 N 8	353.1258	0.8	0.3	1	14.6	17.5	even	ok
	C 21 H 18 N 2 Na O 2	353.1260	1.6	0.6	2	14.6	13.5	even	ok

A2. 1 HRMS in MeCN for receptor **72**.

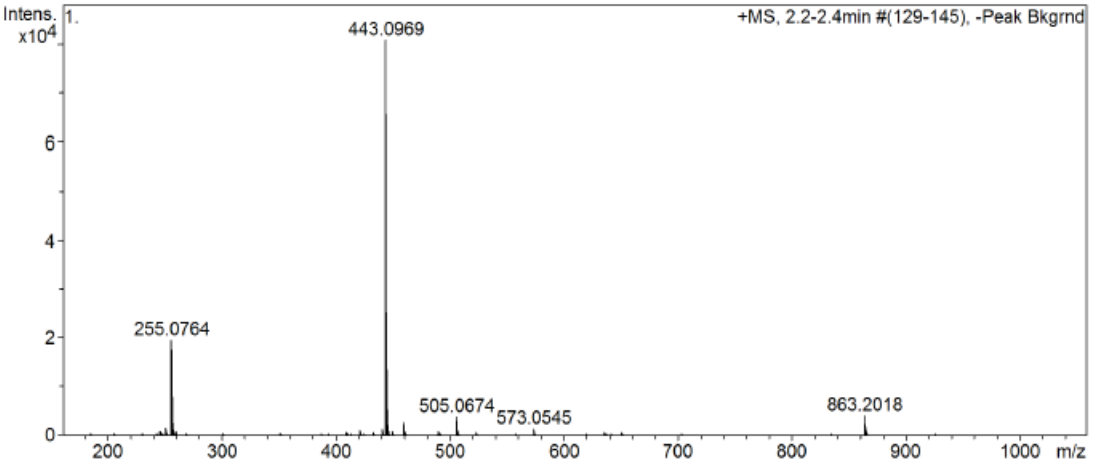

Meas. m/z	Formula	m/z	err [ppm]	err [mDa]	# Sigma	mSigma	rdb	e⁻ Conf	N-Rule
443.0969	C 22 H 19 O 10	443.0973	0.8	0.4	1	19.4	13.5	even	ok
	C 21 H 16 N 4 Na O 6	443.0962	-1.6	-0.7	2	21.1	15.5	even	ok
	C 22 H 12 N 8 Na O 2	443.0975	1.4	0.6	3	35.6	20.5	even	ok
	C 20 H 7 N 14	443.0973	0.8	0.4	4	35.8	24.5	even	ok

A2. 2 HRMS in MeCN for receptor **73**.

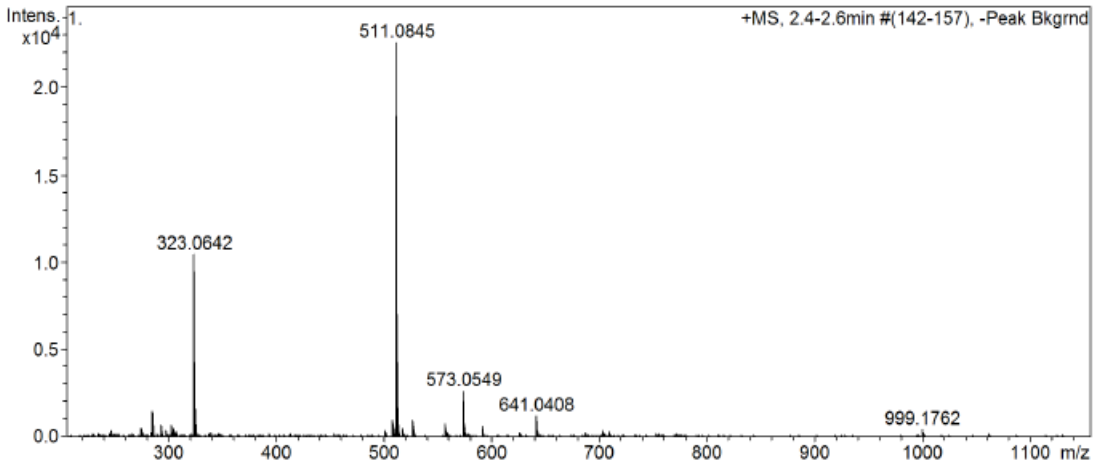

Meas. m/z	Formula	m/z	err [ppm]	err [mDa]	# Sigma	mSigma	rdb	e¯ Conf	N-Rule
511.0845	C 17 H 13 F N 10 Na O 7	511.0845	0.0	0.0	1	6.1	15.5	even	ok
	C 15 H 8 F N 16 O 5	511.0842	-0.5	-0.3	2	6.7	19.5	even	ok
	C 23 H 18 F 3 O 10	511.0847	0.3	0.2	3	12.5	13.5	even	ok
	C 22 H 15 F 3 N 4 Na O 6	511.0836	-1.8	-0.9	4	12.7	15.5	even	ok
	C 21 H 15 N 6 O 10	511.0844	-0.1	-0.1	5	12.7	17.5	even	ok
	C 23 H 20 Na O 12	511.0847	0.4	0.2	6	14.0	13.5	even	ok
	C 17 H 20 F N 2 O 15	511.0842	-0.5	-0.3	7	18.0	8.5	even	ok
	C 26 H 17 F 2 O 9	511.0835	-1.9	-1.0	8	26.6	17.5	even	ok
	C 23 H 11 F 3 N 8 Na O 2	511.0849	0.9	0.4	9	27.2	20.5	even	ok
	C 21 H 6 F 3 N 14	511.0846	0.3	0.2	10	27.5	24.5	even	ok
	C 21 H 8 N 14 Na O 2	511.0847	0.4	0.2	11	27.5	24.5	even	ok
	C 19 H 3 N 20	511.0844	-0.2	-0.1	12	27.8	28.5	even	ok
	C 27 H 13 F 2 N 4 O 5	511.0849	0.7	0.4	13	38.8	22.5	even	ok
	C 26 H 10 F 2 N 8 Na O	511.0838	-1.4	-0.7	14	46.1	24.5	even	ok
	C 30 H 12 F N 4 O 4	511.0837	-1.5	-0.8	15	55.5	26.5	even	ok
	C 31 H 8 F N 8	511.0850	1.1	0.6	16	68.1	31.5	even	ok
	C 33 H 13 F N 2 Na O 2	511.0853	1.6	0.8	17	68.2	27.5	even	ok
	C 36 H 12 N 2 Na O	511.0842	-0.6	-0.3	18	85.0	31.5	even	ok

A2. 3 HRMS in MeCN for receptor **74**.

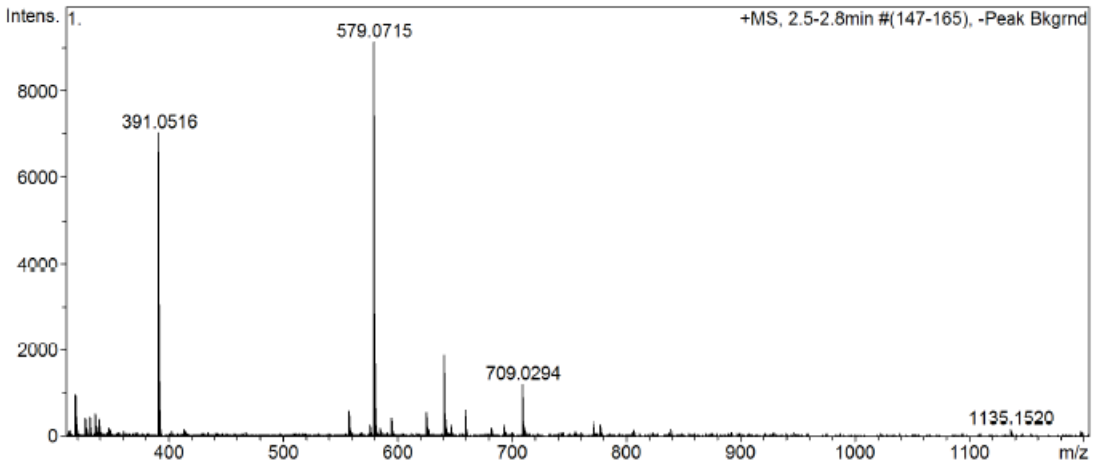

Meas. m/z	Formula	m/z	err [ppm]	err [mDa]	# Sigma	mSigma	rdb	e¯ Conf	N-Rule
391.0516	C 15 H 4 N 12 Na O	391.0523	1.7	0.7	1	7.0	19.5	even	ok
	C 14 H 8 N 8 Na O 5	391.0510	-1.7	-0.7	2	8.3	14.5	even	ok
	C 14 H 6 F 3 N 8 O 3	391.0509	-1.8	-0.7	3	8.3	14.5	even	ok
	C 16 H 11 F 3 N 2 Na O 5	391.0512	-1.1	-0.4	4	8.6	10.5	even	ok
	C 15 H 11 N 4 O 9	391.0521	1.1	0.4	5	11.9	12.5	even	ok
	C 12 H 13 F 2 N 4 O 7 Si	391.0516	-0.1	-0.0	6	21.0	8.5	even	ok
	C 20 H 6 F 2 N 6 Na	391.0514	-0.6	-0.2	7	25.1	19.5	even	ok
	C 19 H 11 F 4 N 2 O S	391.0523	1.6	0.6	8	26.3	13.5	even	ok
	C 17 H 8 F N 8 O S	391.0520	1.0	0.4	9	26.4	17.5	even	ok
	C 13 H 12 F 4 N 2 Na O 6	391.0524	1.9	0.7	10	27.3	6.5	even	ok
	C 13 H 13 F 2 N 4 O 6 S	391.0518	0.5	0.2	11	28.5	8.5	even	ok
	C 19 H 13 F N 2 Na O 3 S	391.0523	1.7	0.7	12	29.1	13.5	even	ok
	C 18 H 11 F 4 N 2 O 2 Si	391.0520	1.0	0.4	13	36.4	13.5	even	ok
	C 16 H 8 F N 8 O 2 Si	391.0518	0.4	0.2	14	36.6	17.5	even	ok
	C 18 H 13 F N 2 Na O 4 Si	391.0521	1.1	0.4	15	37.7	13.5	even	ok
	C 22 H 10 F 3 N 2 S	391.0511	-1.3	-0.5	16	39.5	17.5	even	ok
	C 20 H 7 N 8 S	391.0509	-1.9	-0.8	17	39.7	21.5	even	ok
	C 22 H 12 N 2 Na O 2 S	391.0512	-1.2	-0.5	18	41.0	17.5	even	ok
	C 24 H 8 F N 2 O 3	391.0513	-0.8	-0.3	19	42.5	21.5	even	ok
	C 15 H 12 N 8 Na S 2	391.0519	0.5	0.2	20	44.8	13.5	even	ok
	C 17 H 15 F 3 N 2 Na S 2	391.0521	1.2	0.5	21	44.9	9.5	even	ok
	C 16 H 15 F 3 N 2 Na O S Si	391.0519	0.6	0.2	22	47.1	9.5	even	ok
	C 14 H 12 N 8 Na O S Si	391.0516	-0.0	-0.0	23	47.2	13.5	even	ok
	C 14 H 19 O 9 S Si	391.0514	-0.7	-0.3	24	48.3	6.5	even	ok
579.0715	C 16 H 7 F 4 N 16 O 5	579.0716	0.2	0.1	1	2.1	19.5	even	ok
	C 18 H 12 F 4 N 10 Na O 7	579.0719	0.7	0.4	2	2.8	15.5	even	ok
	C 15 H 4 F 4 N 20 Na O	579.0705	-1.7	-1.0	3	7.8	21.5	even	ok
	C 17 H 16 F 4 N 6 Na O 11	579.0705	-1.6	-1.0	4	10.4	10.5	even	ok
	C 21 H 18 F 3 N 2 O 14	579.0705	-1.8	-1.0	5	12.3	12.5	even	ok
	C 18 H 19 F 4 N 2 O 15	579.0716	0.2	0.1	6	13.5	8.5	even	ok
	C 24 H 17 F 6 O 10	579.0720	1.0	0.6	7	19.8	13.5	even	ok
	C 22 H 14 F 3 N 6 O 10	579.0718	0.5	0.3	8	20.1	17.5	even	ok
	C 21 H 9 F 6 N 10 O 4	579.0707	-1.4	-0.8	9	20.7	19.5	even	ok
	C 19 H 6 F 3 N 16 O 4	579.0705	-1.8	-1.0	10	20.9	23.5	even	ok
	C 23 H 14 F 6 N 4 Na O 6	579.0710	-0.9	-0.5	11	20.9	15.5	even	ok
	C 21 H 11 F 3 N 10 Na O 6	579.0707	-1.3	-0.8	12	21.2	19.5	even	ok
	C 24 H 19 F 3 Na O 12	579.0721	1.0	0.6	13	21.3	13.5	even	ok
	C 27 H 16 F 5 O 9	579.0709	-1.0	-0.6	14	34.2	17.5	even	ok
	C 24 H 10 F 6 N 8 Na O 2	579.0723	1.4	0.8	15	35.2	20.5	even	ok
	C 22 H 5 F 6 N 14	579.0720	0.9	0.5	16	35.3	24.5	even	ok
	C 22 H 7 F 3 N 14 Na O 2	579.0721	1.0	0.6	17	35.5	24.5	even	ok
	C 20 H 2 F 3 N 20	579.0718	0.5	0.3	18	35.5	28.5	even	ok
	C 28 H 12 F 5 N 4 O 5	579.0722	1.3	0.7	19	46.2	22.5	even	ok
	C 27 H 9 F 5 N 8 Na O	579.0712	-0.6	-0.3	20	47.0	24.5	even	ok
	C 31 H 11 F 4 N 4 O 4	579.0711	-0.7	-0.4	21	62.9	26.5	even	ok
	C 32 H 7 F 4 N 8	579.0724	1.6	0.9	22	75.4	31.5	even	ok
	C 37 H 11 F 3 N 2 Na O	579.0716	0.1	0.1	23	92.4	31.5	even	ok

A2. 4 HRMS in MeCN for receptor **75**.

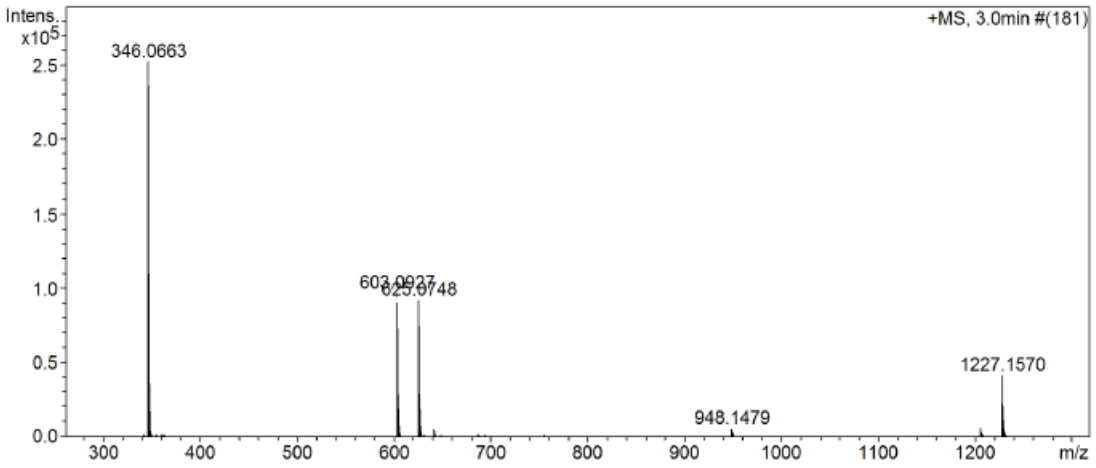

Meas. m/z	Formula	m/z	err [ppm]	err [mDa]	# Sigma	mSigma	rdb	e⁻ Conf	N-Rule
603.0927	C 20 H 13 F 6 N 10 O 6	603.0918	-1.5	-0.9	1	3.7	16.5	even	ok
	C 22 H 16 F 9 N 4 O 6	603.0921	-1.1	-0.7	2	4.0	12.5	even	ok
	C 22 H 18 F 6 N 4 Na O 8	603.0921	-1.1	-0.6	3	5.4	12.5	even	ok
	C 23 H 21 F 6 O 12	603.0932	0.7	0.4	4	9.5	10.5	even	ok
	C 25 H 15 F 12 N 2 O 2	603.0936	1.5	0.9	5	12.8	13.5	even	ok
	C 23 H 12 F 9 N 8 O 2	603.0934	1.1	0.7	6	13.0	17.5	even	ok
	C 21 H 9 F 6 N 14 O 2	603.0932	0.7	0.4	7	13.3	21.5	even	ok
	C 25 H 17 F 9 N 2 Na O 4	603.0937	1.6	0.9	8	13.4	13.5	even	ok
	C 23 H 14 F 6 N 8 Na O 4	603.0934	1.2	0.7	9	13.7	17.5	even	ok
	C 19 H 19 F 7 N 4 Na O 9	603.0932	0.8	0.5	10	18.1	8.5	even	ok
	C 18 H 14 F 10 N 8 Na O 3	603.0921	-1.0	-0.6	11	18.9	10.5	even	ok
	C 17 H 14 F 7 N 10 O 7	603.0930	0.4	0.2	12	20.4	12.5	even	ok
	C 19 H 17 F 10 N 4 O 7	603.0932	0.8	0.5	13	20.7	8.5	even	ok
	C 28 H 14 F 11 N 2 O	603.0925	-0.4	-0.2	14	27.5	17.5	even	ok
	C 28 H 16 F 8 N 2 Na O 3	603.0925	-0.3	-0.2	15	28.2	17.5	even	ok
	C 18 H 23 F 7 Na O 13	603.0919	-1.4	-0.8	16	28.6	3.5	even	ok
	C 18 H 21 F 10 O 11	603.0919	-1.4	-0.9	17	28.7	3.5	even	ok
	C 26 H 11 F 8 N 8 O	603.0923	-0.8	-0.5	18	32.0	21.5	even	ok
	C 33 H 14 F 7 N 2 O 2	603.0938	1.8	1.1	19	56.4	24.5	even	ok
	C 36 H 13 F 6 N 2 O	603.0927	-0.1	-0.1	20	73.1	28.5	even	ok
625.0748	C 22 H 15 F 9 N 4 Na O 6	625.0740	-1.3	-0.8	1	3.7	12.5	even	ok
	C 20 H 12 F 6 N 10 Na O 6	625.0738	-1.7	-1.1	2	4.0	16.5	even	ok
	C 22 H 13 F 12 N 4 O 4	625.0740	-1.4	-0.9	3	4.5	12.5	even	ok
	C 20 H 10 F 9 N 10 O 4	625.0737	-1.7	-1.1	4	4.9	16.5	even	ok
	C 23 H 18 F 9 O 10	625.0751	0.4	0.3	5	5.0	10.5	even	ok
	C 21 H 15 F 6 N 6 O 10	625.0748	0.0	0.0	6	5.2	14.5	even	ok
	C 23 H 20 F 6 Na O 12	625.0751	0.5	0.3	7	7.0	10.5	even	ok
	C 16 H 4 F 7 N 20 O	625.0760	1.8	1.1	8	9.5	21.5	even	ok
	C 18 H 16 F 7 N 6 O 11	625.0760	1.9	1.2	9	12.7	10.5	even	ok
	C 17 H 13 F 7 N 10 Na O 7	625.0749	0.1	0.1	10	15.2	12.5	even	ok
	C 19 H 16 F 10 N 4 Na O 7	625.0752	0.5	0.3	11	15.5	8.5	even	ok
	C 17 H 11 F 10 N 10 O 5	625.0749	0.1	0.1	12	15.9	12.5	even	ok
	C 16 H 8 F 10 N 14 Na O	625.0738	-1.6	-1.0	13	17.1	14.5	even	ok
	C 25 H 14 F 12 N 2 Na O 2	625.0756	1.2	0.8	14	18.2	13.5	even	ok
	C 23 H 11 F 9 N 8 Na O 2	625.0753	0.8	0.5	15	18.5	17.5	even	ok
	C 26 H 17 F 8 O 9	625.0739	-1.4	-0.9	16	18.6	14.5	even	ok
	C 23 H 9 F 12 N 8	625.0753	0.8	0.5	17	18.8	17.5	even	ok
	C 21 H 8 F 6 N 14 Na O 2	625.0751	0.5	0.3	18	18.8	21.5	even	ok
	C 21 H 6 F 9 N 14	625.0751	0.4	0.2	19	19.2	21.5	even	ok
	C 19 H 3 F 6 N 20	625.0748	0.0	0.0	20	19.6	25.5	even	ok
	C 16 H 17 F 7 N 6 Na O 11	625.0736	-2.0	-1.2	21	23.5	7.5	even	ok
	C 18 H 20 F 10 Na O 11	625.0738	-1.6	-1.0	22	23.8	3.5	even	ok
	C 17 H 20 F 7 N 2 O 15	625.0746	-0.3	-0.2	23	24.9	5.5	even	ok
	C 27 H 13 F 8 N 4 O 5	625.0753	0.7	0.5	24	30.9	19.5	even	ok
	C 28 H 13 F 11 N 2 Na O	625.0744	-0.6	-0.4	25	32.0	17.5	even	ok
	C 26 H 10 F 8 N 8 Na O	625.0742	-1.0	-0.6	26	37.2	21.5	even	ok
	C 30 H 12 F 7 N 4 O 4	625.0741	-1.1	-0.7	27	47.6	23.5	even	ok
	C 33 H 11 F 10 N 2	625.0757	1.4	0.9	28	59.9	24.5	even	ok
	C 31 H 8 F 7 N 8	625.0755	1.0	0.6	29	60.2	28.5	even	ok
	C 33 H 13 F 7 N 2 Na O 2	625.0757	1.5	0.9	30	60.3	24.5	even	ok
	C 36 H 12 F 6 N 2 Na O	625.0746	-0.3	-0.2	31	77.0	28.5	even	ok

A2. 5 HRMS in MeCN for receptor **76**.

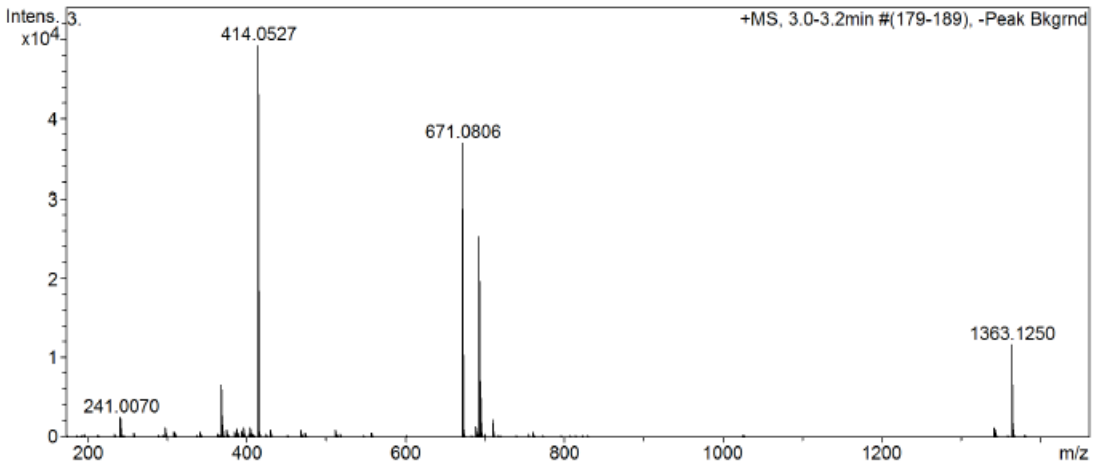

Meas. m/z	Formula	m/z	err [ppm]	err [mDa]	# Sigma	mSigma	rdb	e⁻ Conf	N-Rule
671.0806	C 19 H 9 F 10 N 14 O 3	671.0817	1.7	1.1	1	4.0	17.5	even	ok
	C 23 H 15 F 12 N 4 O 6	671.0794	-1.7	-1.1	2	10.2	12.5	even	ok
	C 17 H 10 F 10 N 14 Na O 3	671.0793	-1.9	-1.3	3	11.3	14.5	even	ok
	C 17 H 8 F 13 N 14 O	671.0792	-2.0	-1.3	4	11.6	14.5	even	ok
	C 19 H 13 F 13 N 8 Na O 3	671.0795	-1.6	-1.0	5	11.7	10.5	even	ok
	C 20 H 18 F 10 N 4 Na O 9	671.0806	0.1	0.1	6	13.9	8.5	even	ok
	C 18 H 13 F 10 N 10 O 7	671.0804	-0.3	-0.2	7	14.6	12.5	even	ok
	C 20 H 16 F 13 N 4 O 7	671.0806	0.0	0.0	8	15.0	8.5	even	ok
	C 21 H 21 F 10 O 13	671.0817	1.7	1.1	9	16.1	6.5	even	ok
	C 26 H 14 F 15 N 2 O 2	671.0810	0.7	0.5	10	21.0	13.5	even	ok
	C 24 H 11 F 12 N 8 O 2	671.0808	0.3	0.2	11	21.2	17.5	even	ok
	C 26 H 16 F 12 N 2 Na O 4	671.0811	0.7	0.5	12	22.0	13.5	even	ok
	C 19 H 20 F 13 O 11	671.0793	-2.0	-1.3	13	23.7	3.5	even	ok
	C 19 H 22 F 10 Na O 13	671.0793	-1.9	-1.3	14	24.0	3.5	even	ok
	C 17 H 19 F 11 N 4 Na O 10	671.0818	1.8	1.2	15	26.8	4.5	even	ok
	C 17 H 17 F 14 N 4 O 8	671.0817	1.7	1.2	16	32.7	4.5	even	ok
	C 29 H 13 F 14 N 2 O	671.0799	-1.0	-0.7	17	34.4	17.5	even	ok
	C 27 H 10 F 11 N 8 O	671.0796	-1.4	-0.9	18	34.6	21.5	even	ok
	C 29 H 15 F 11 N 2 Na O 3	671.0799	-1.0	-0.6	19	35.4	17.5	even	ok
	C 34 H 13 F 10 N 2 O 2	671.0812	0.9	0.6	20	63.7	24.5	even	ok
693.0615	C 17 H 7 F 13 N 14 Na O	693.0612	-0.4	-0.3	1	7.3	14.5	even	ok
	C 16 H 7 F 10 N 16 O 5	693.0620	0.8	0.6	2	8.8	16.5	even	ok
	C 18 H 10 F 13 N 10 O 5	693.0623	1.2	0.8	3	9.2	12.5	even	ok
	C 18 H 12 F 10 N 10 Na O 7	693.0623	1.2	0.8	4	10.1	12.5	even	ok
	C 20 H 15 F 13 N 4 Na O 7	693.0625	1.6	1.1	5	10.5	8.5	even	ok
	C 23 H 12 F 15 N 4 O 4	693.0614	-0.1	-0.1	6	11.3	12.5	even	ok
	C 21 H 9 F 12 N 10 O 4	693.0611	-0.5	-0.3	7	11.5	16.5	even	ok
	C 22 H 9 F 15 N 8 Na	693.0603	-1.7	-1.2	8	12.0	14.5	even	ok
	C 23 H 14 F 12 N 4 Na O 6	693.0614	-0.1	-0.1	9	12.7	12.5	even	ok
	C 24 H 17 F 12 O 10	693.0625	1.5	1.0	10	14.3	10.5	even	ok
	C 17 H 16 F 10 N 6 Na O 11	693.0610	-0.7	-0.5	11	19.6	7.5	even	ok
	C 19 H 19 F 13 Na O 11	693.0612	-0.4	-0.3	12	19.8	3.5	even	ok
	C 18 H 19 F 10 N 2 O 15	693.0620	0.8	0.6	13	22.3	5.5	even	ok
	C 17 H 14 F 13 N 6 O 9	693.0609	-0.8	-0.5	14	24.0	7.5	even	ok
	C 24 H 8 F 15 N 8	693.0627	1.8	1.2	15	24.9	17.5	even	ok
	C 22 H 5 F 12 N 14	693.0625	1.4	1.0	16	25.1	21.5	even	ok
	C 24 H 10 F 12 N 8 Na O 2	693.0627	1.8	1.3	17	25.5	17.5	even	ok
	C 27 H 16 F 11 O 9	693.0613	-0.2	-0.1	18	27.1	14.5	even	ok
	C 26 H 11 F 14 N 4 O 3	693.0602	-1.8	-1.2	19	30.0	16.5	even	ok
	C 26 H 13 F 11 N 4 Na O 5	693.0603	-1.7	-1.2	20	30.9	16.5	even	ok
	C 16 H 20 F 14 Na O 12	693.0623	1.3	0.9	21	35.0	-0.5	even	ok
	C 28 H 12 F 11 N 4 O 5	693.0627	1.7	1.2	22	38.2	19.5	even	ok
	C 29 H 12 F 14 N 2 Na O	693.0618	0.5	0.4	23	38.3	17.5	even	ok
	C 27 H 9 F 11 N 8 Na O	693.0616	0.2	0.1	24	38.5	21.5	even	ok
	C 30 H 15 F 10 O 8	693.0602	-1.8	-1.3	25	43.1	18.5	even	ok
	C 31 H 11 F 10 N 4 O 4	693.0615	0.1	0.1	26	54.9	23.5	even	ok
	C 32 H 11 F 13 N 2 Na	693.0607	-1.1	-0.8	27	55.4	21.5	even	ok
	C 30 H 8 F 10 N 8 Na	693.0604	-1.5	-1.0	28	55.6	25.5	even	ok

A2. 6 HRMS in MeCN for receptor **77**.

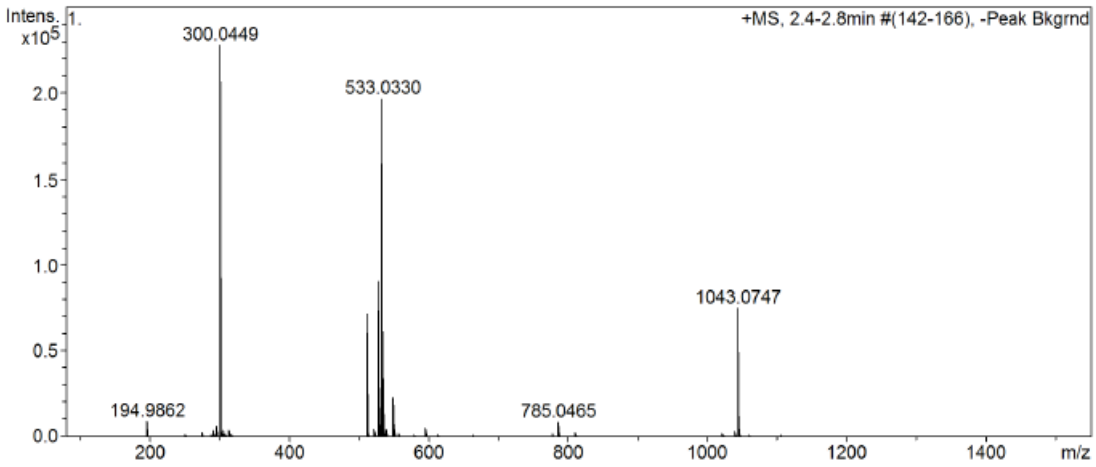

Meas. m/z	Formula	m/z	err [ppm]	err [mDa]	# Sigma	mSigma	rdb	e⁻ Conf	N-Rule
511.0511	C 14 H 4 F 5 N 14 O 3	511.0505	-1.2	-0.6	1	2.8	17.5	even	ok
	C 16 H 7 F 8 N 8 O 3	511.0508	-0.7	-0.4	2	3.1	13.5	even	ok
	C 16 H 9 F 5 N 8 Na O 5	511.0508	-0.6	-0.3	3	3.9	13.5	even	ok
	C 18 H 12 F 8 N 2 Na O 5	511.0511	-0.1	-0.1	4	4.2	9.5	even	ok
	C 17 H 12 F 5 N 4 O 9	511.0519	1.5	0.8	5	8.7	11.5	even	ok
	C 19 H 8 F 8 N 6 Na O	511.0524	2.5	1.3	6	11.4	14.5	even	ok
	C 17 H 5 F 5 N 12 Na O	511.0522	2.0	1.0	7	11.7	18.5	even	ok
	C 21 H 9 F 10 N 2 O 2	511.0499	-2.5	-1.3	8	15.6	13.5	even	ok
	C 19 H 6 F 7 N 8 O 2	511.0496	-2.9	-1.5	9	15.9	17.5	even	ok
	C 21 H 11 F 7 N 2 Na O 4	511.0499	-2.4	-1.2	10	16.2	13.5	even	ok
	C 16 H 16 F 5 O 13	511.0506	-1.1	-0.6	11	17.2	6.5	even	ok
	C 13 H 10 F 6 N 8 Na O 6	511.0520	1.6	0.8	12	21.8	9.5	even	ok
	C 13 H 8 F 9 N 8 O 4	511.0519	1.6	0.8	13	21.9	9.5	even	ok
	C 15 H 13 F 9 N 2 Na O 6	511.0522	2.1	1.1	14	22.1	5.5	even	ok
	C 23 H 10 F 7 N 2 O 4	511.0523	2.3	1.2	15	29.0	16.5	even	ok
	C 24 H 10 F 10 Na	511.0515	0.7	0.4	16	30.1	14.5	even	ok
	C 22 H 7 F 7 N 6 Na	511.0513	0.2	0.1	17	30.4	18.5	even	ok
	C 13 H 17 F 6 O 14	511.0517	1.1	0.6	18	31.8	2.5	even	ok
	C 26 H 9 F 6 N 2 O 3	511.0512	0.1	0.0	19	48.1	20.5	even	ok
	C 29 H 8 F 5 N 2 O 2	511.0500	-2.1	-1.1	20	58.4	24.5	even	ok
	C 32 H 9 F 5 Na	511.0517	1.0	0.5	21	71.1	25.5	even	ok
533.0330	C 14 H 3 F 5 N 14 Na O 3	533.0325	-0.9	-0.5	1	4.1	17.5	even	ok
	C 16 H 6 F 8 N 8 Na O 3	533.0327	-0.5	-0.3	2	4.4	13.5	even	ok
	C 14 H F 8 N 14 O	533.0325	-1.0	-0.5	3	4.9	17.5	even	ok
	C 15 H 6 F 5 N 10 O 7	533.0336	1.1	0.6	4	8.3	15.5	even	ok
	C 17 H 9 F 8 N 4 O 7	533.0338	1.5	0.8	5	8.6	11.5	even	ok
	C 17 H 11 F 5 N 4 Na O 9	533.0338	1.6	0.9	6	10.3	11.5	even	ok
	C 19 H 3 F 10 N 8	533.0316	-2.7	-1.4	7	14.5	17.5	even	ok
	C 21 H 8 F 10 N 2 Na O 2	533.0318	-2.2	-1.2	8	14.7	13.5	even	ok
	C 20 H 8 F 7 N 4 O 6	533.0327	-0.6	-0.3	9	14.7	15.5	even	ok
	C 19 H 5 F 7 N 8 Na O 2	533.0316	-2.6	-1.4	10	15.0	17.5	even	ok
	C 16 H 13 F 8 O 11	533.0325	-1.0	-0.5	11	17.9	6.5	even	ok
	C 16 H 15 F 5 Na O 13	533.0325	-0.9	-0.5	12	18.5	6.5	even	ok
	C 15 H 10 F 8 N 4 Na O 7	533.0314	-3.0	-1.6	13	19.4	8.5	even	ok
	C 14 H 10 F 5 N 6 O 11	533.0322	-1.4	-0.8	14	20.3	10.5	even	ok
	C 13 H 7 F 9 N 8 Na O 4	533.0339	1.7	0.9	15	23.1	9.5	even	ok
	C 23 H 7 F 10 N 2 O 2	533.0342	2.3	1.3	16	27.5	16.5	even	ok
	C 21 H 4 F 7 N 8 O 2	533.0340	1.9	1.0	17	27.8	20.5	even	ok
	C 23 H 9 F 7 N 2 Na O 4	533.0343	2.4	1.3	18	28.2	16.5	even	ok
	C 13 H 16 F 6 Na O 14	533.0336	1.2	0.7	19	33.0	2.5	even	ok
	C 23 H 7 F 6 N 4 O 5	533.0315	-2.8	-1.5	20	33.0	19.5	even	ok
	C 13 H 14 F 9 O 12	533.0336	1.2	0.6	21	38.0	2.5	even	ok
	C 26 H 6 F 9 N 2 O	533.0331	0.2	0.1	22	46.4	20.5	even	ok
	C 24 H 3 F 6 N 8 O	533.0329	-0.2	-0.1	23	46.6	24.5	even	ok
	C 26 H 8 F 6 N 2 Na O 3	533.0331	0.3	0.1	24	47.2	20.5	even	ok
	C 29 H 5 F 8 N 2	533.0320	-1.9	-1.0	25	57.1	24.5	even	ok
	C 27 H 2 F 5 N 8	533.0317	-2.4	-1.3	26	57.3	28.5	even	ok
	C 29 H 7 F 5 N 2 Na O 2	533.0320	-1.9	-1.0	27	57.6	24.5	even	ok
	C 31 H 6 F 5 N 2 O 2	533.0344	2.6	1.4	28	69.0	27.5	even	ok

A2. 7 HRMS in MeCN for receptor **78**.

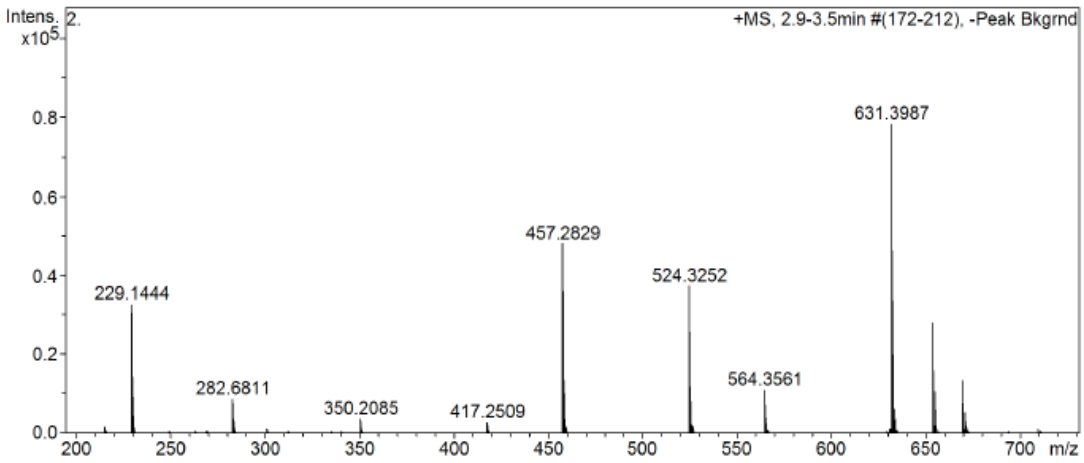

Meas. m/z	Formula	m/z	err [ppm]	err [mDa]	# Sigma	mSigma	rdb	e⁻ Conf	N-Rule
457.2829	C 28 H 38 N 2 Na O 2	457.2825	-0.8	-0.4	1	22.0	10.5	even	ok
	C 26 H 33 N 8	457.2823	-1.4	-0.7	2	24.2	14.5	even	ok
524.3252	C 30 H 38 N 9	524.3245	-1.3	-0.7	1	26.5	16.5	even	ok
	C 32 H 43 N 3 Na O 2	524.3247	-0.8	-0.4	2	27.4	12.5	even	ok
564.3561	C 33 H 42 N 9	564.3558	-0.6	-0.3	1	26.1	17.5	even	ok
	C 35 H 47 N 3 Na O 2	564.3560	-0.1	-0.0	2	26.9	13.5	even	ok
631.3987	C 37 H 47 N 10	631.3980	-1.2	-0.7	1	10.7	19.5	even	ok
	C 39 H 52 N 4 Na O 2	631.3982	-0.7	-0.5	2	12.9	15.5	even	ok
	C 40 H 55 O 6	631.3993	0.9	0.6	3	15.7	13.5	even	ok
653.3807	C 37 H 53 N 2 O 8	653.3796	-1.6	-1.0	1	24.5	12.5	even	ok
	C 37 H 46 N 10 Na	653.3799	-1.2	-0.8	2	35.0	19.5	even	ok
	C 38 H 49 N 6 O 4	653.3810	0.4	0.3	3	35.1	17.5	even	ok
	C 40 H 54 Na O 6	653.3813	0.9	0.6	4	36.4	13.5	even	ok

A2. 8 HRMS in MeCN for receptor **79**.

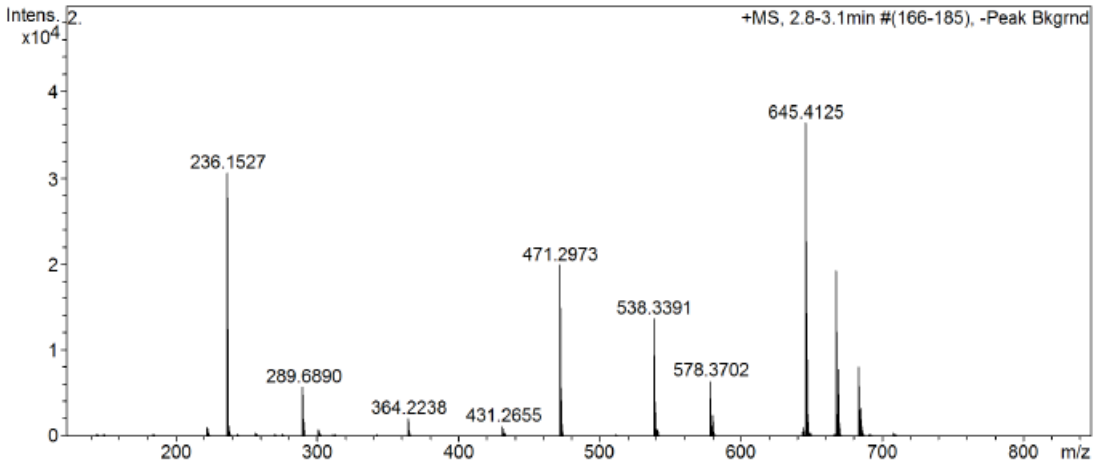

Meas. m/z	Formula	m/z	err [ppm]	err [mDa]	# Sigma	mSigma	rdb	e¯ Conf	N-Rule
471.2973	C 26 H 39 N 4 O 4	471.2966	-1.4	-0.7	1	14.7	9.5	even	ok
	C 27 H 35 N 8	471.2979	1.4	0.7	2	23.9	14.5	even	ok
	C 29 H 40 N 2 Na O 2	471.2982	2.0	0.9	3	24.8	10.5	even	ok
538.3391	C 30 H 44 N 5 O 4	538.3388	-0.6	-0.3	1	28.9	11.5	even	ok
	C 29 H 41 N 9 Na	538.3377	-2.6	-1.4	2	29.4	13.5	even	ok
	C 31 H 40 N 9	538.3401	1.9	1.0	3	40.7	16.5	even	ok
	C 33 H 45 N 3 Na O 2	538.3404	2.4	1.3	4	41.5	12.5	even	ok
578.3702	C 32 H 45 N 9 Na	578.3690	-2.1	-1.2	1	11.0	14.5	even	ok
	C 32 H 52 N O 8	578.3687	-2.5	-1.5	2	11.7	7.5	even	ok
	C 33 H 48 N 5 O 4	578.3701	-0.2	-0.1	3	12.4	12.5	even	ok
	C 34 H 44 N 9	578.3714	2.1	1.2	4	22.2	17.5	even	ok
	C 36 H 49 N 3 Na O 2	578.3717	2.6	1.5	5	23.4	13.5	even	ok
645.4125	C 37 H 53 N 6 O 4	645.4123	-0.4	-0.2	1	21.6	14.5	even	ok
	C 39 H 58 Na O 6	645.4126	0.1	0.1	2	23.2	10.5	even	ok
	C 38 H 49 N 10	645.4136	1.7	1.1	3	32.6	19.5	even	ok
667.3941	C 34 H 51 N 8 O 6	667.3926	-2.2	-1.4	1	9.4	13.5	even	ok
	C 36 H 56 N 2 Na O 8	667.3929	-1.7	-1.2	2	11.8	9.5	even	ok
	C 35 H 47 N 12 O 2	667.3939	-0.2	-0.1	3	17.7	18.5	even	ok
	C 37 H 52 N 6 Na O 4	667.3942	0.3	0.2	4	19.2	14.5	even	ok
	C 38 H 55 N 2 O 8	667.3953	1.9	1.2	5	20.6	12.5	even	ok
	C 38 H 48 N 10 Na	667.3956	2.3	1.5	6	30.4	19.5	even	ok
	C 50 H 51 O	667.3934	-0.9	-0.6	7	82.8	25.5	even	ok

A2. 9 HRMS in MeCN for receptor **80**.

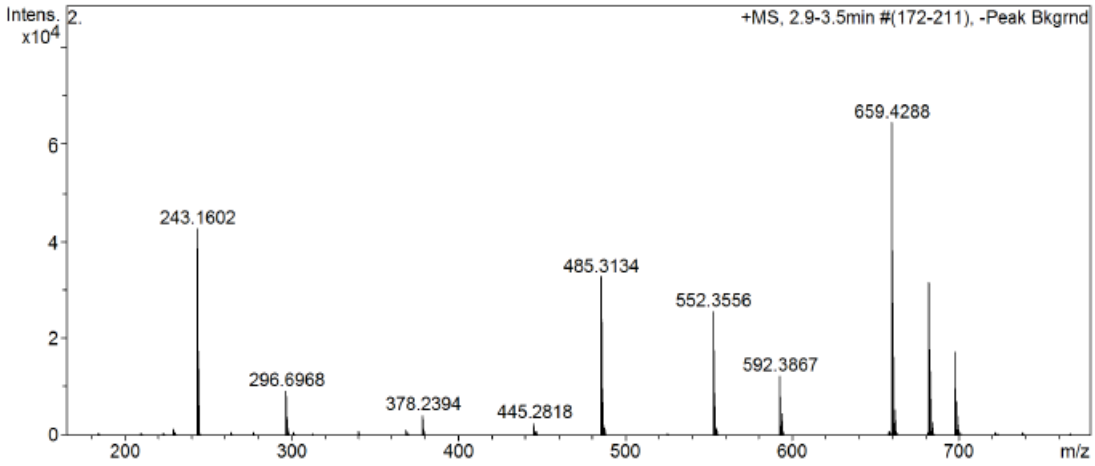

Meas. m/z	Formula	m/z	err [ppm]	err [mDa]	# Sigma	mSigma	rdb	e⁻ Conf	N-Rule
243.1602	C 14 H 19 N 4	243.1604	1.0	0.3	1	66.7	7.5	even	ok
485.3134	C 28 H 37 N 8	485.3136	0.4	0.2	1	22.7	14.5	even	ok
	C 30 H 42 N 2 Na O 2	485.3138	1.0	0.5	2	23.4	10.5	even	ok
552.3556	C 32 H 42 N 9	552.3558	0.2	0.1	1	26.5	16.5	even	ok
	C 34 H 47 N 3 Na O 2	552.3560	0.7	0.4	2	27.6	12.5	even	ok
592.3867	C 34 H 50 N 5 O 4	592.3857	-1.6	-1.0	1	15.2	12.5	even	ok
	C 35 H 46 N 9	592.3871	0.6	0.4	2	24.6	17.5	even	ok
	C 37 H 51 N 3 Na O 2	592.3873	1.1	0.7	3	26.0	13.5	even	ok
659.4288	C 38 H 55 N 6 O 4	659.4279	-1.4	-0.9	1	13.7	14.5	even	ok
	C 40 H 60 Na O 6	659.4282	-0.9	-0.6	2	15.8	10.5	even	ok
	C 39 H 51 N 10	659.4293	0.7	0.4	3	23.2	19.5	even	ok
	C 41 H 56 N 4 Na O 2	659.4295	1.1	0.7	4	24.7	15.5	even	ok
681.4103	C 36 H 49 N 12 O 2	681.4096	-1.0	-0.7	1	14.4	18.5	even	ok
	C 38 H 54 N 6 Na O 4	681.4099	-0.6	-0.4	2	16.0	14.5	even	ok
	C 39 H 57 N 2 O 8	681.4109	0.9	0.6	3	17.5	12.5	even	ok
	C 39 H 50 N 10 Na	681.4112	1.3	0.9	4	27.2	19.5	even	ok
	C 51 H 53 O	681.4091	-1.8	-1.2	5	79.8	25.5	even	ok

A2. 10 HRMS in MeCN for receptor **81**.

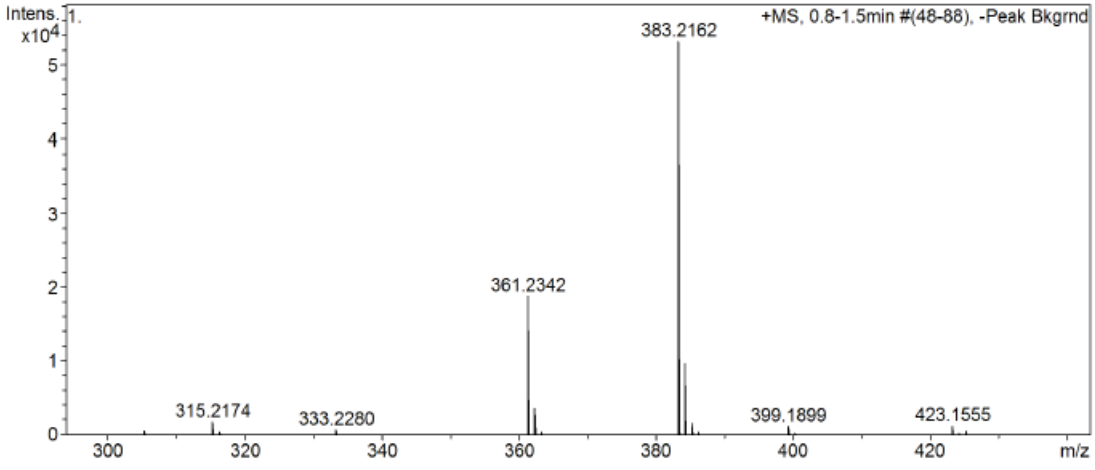

Meas. m/z	Formula	m/z	err [ppm]	err [mDa]	# Sigma	mSigma	rdb	e⁻ Conf	N-Rule
361.2342	C 18 H 29 N 6 O 2	361.2347	1.3	0.5	1	16.0	7.5	even	ok
383.2162	C 16 H 23 N 12	383.2163	0.3	0.1	1	24.9	11.5	even	ok
	C 18 H 28 N 6 Na O 2	383.2166	1.0	0.4	2	26.1	7.5	even	ok

A2. 11 HRMS in MeCN for compound **82a**.

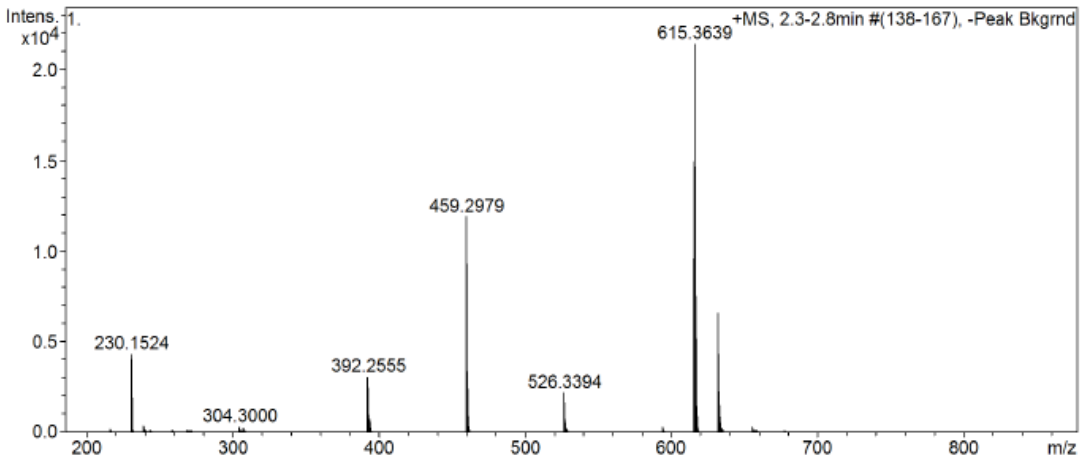

Meas. m/z	Formula	m/z	err [ppm]	err [mDa]	# Sigma	mSigma	rdb	e⁻ Conf	N-Rule
392.2555	C 22 H 30 N 7	392.2557	0.5	0.2	1	28.0	11.5	even	ok
	C 24 H 35 N Na O 2	392.2560	1.2	0.5	2	31.5	7.5	even	ok
459.2979	C 28 H 40 N 2 Na O 2	459.2982	0.6	0.3	1	28.8	9.5	even	ok
	C 26 H 35 N 8	459.2979	0.0	0.0	2	32.2	13.5	even	ok
615.3639	C 31 H 43 N 12 O 2	615.3626	-2.0	-1.2	1	19.5	16.5	even	ok
	C 33 H 48 N 6 Na O 4	615.3629	-1.5	-0.9	2	20.8	12.5	even	ok
	C 34 H 51 N 2 O 8	615.3640	0.2	0.1	3	21.8	10.5	even	ok
	C 34 H 44 N 10 Na	615.3643	0.6	0.4	4	32.2	17.5	even	ok

A2. 12 HRMS in MeCN for compound **82b**.

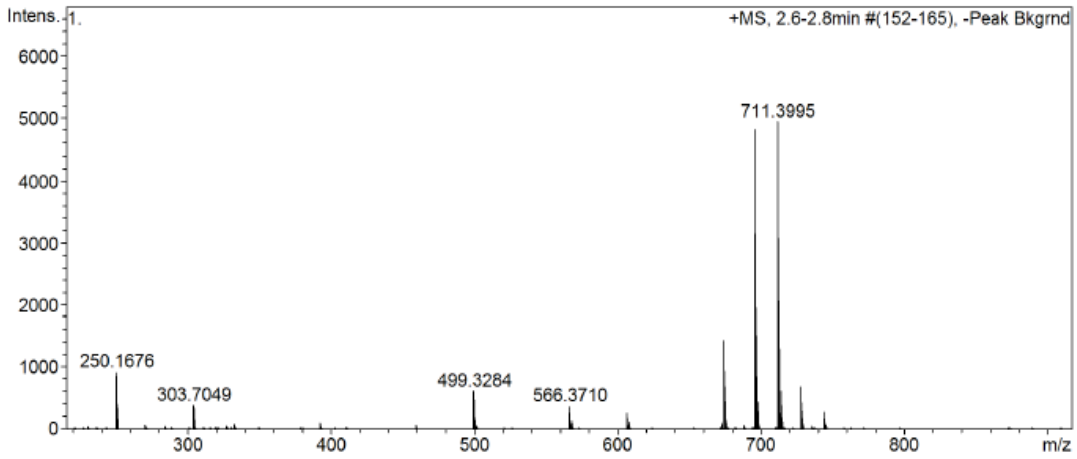

Meas. m/z	Formula	m/z	err [ppm]	err [mDa]	# Sigma	mSigma	rdb	e⁻ Conf	N-Rule
673.4436	C 40 H 53 N 10	673.4449	2.0	1.3	1	10.6	19.5	even	ok
	C 38 H 54 N 10 Na	673.4425	-1.6	-1.1	2	11.8	16.5	even	ok
	C 39 H 57 N 6 O 4	673.4436	-0.0	-0.0	3	15.0	14.5	even	ok
	C 41 H 62 Na O 6	673.4439	0.4	0.3	4	16.4	10.5	even	ok
695.4257	C 37 H 51 N 12 O 2	695.4252	-0.6	-0.4	1	23.6	18.5	even	ok
	C 39 H 56 N 6 Na O 4	695.4255	-0.2	-0.1	2	24.8	14.5	even	ok
	C 40 H 59 N 2 O 8	695.4266	1.4	0.9	3	25.4	12.5	even	ok
	C 40 H 52 N 10 Na	695.4269	1.7	1.2	4	36.4	19.5	even	ok
	C 52 H 55 O	695.4247	-1.3	-0.9	5	79.5	25.5	even	ok
711.3995	C 38 H 60 K N 2 O 8	711.3981	-2.0	-1.4	1	24.9	9.5	even	ok
	C 39 H 56 K N 6 O 4	711.3995	-0.1	-0.1	2	29.7	14.5	even	ok
	C 43 H 55 N 2 O 7	711.4004	1.2	0.9	3	31.5	17.5	even	ok
	C 40 H 47 N 12 O	711.3990	-0.7	-0.5	4	34.5	23.5	even	ok
	C 40 H 52 K N 10	711.4008	1.8	1.3	5	37.5	19.5	even	ok
	C 30 H 63 O 18	711.4009	1.9	1.4	6	43.7	-0.5	even	ok
	C 55 H 51	711.3985	-1.4	-1.0	7	85.4	30.5	even	ok

A2. 13 HRMS in MeCN for receptor **82**.

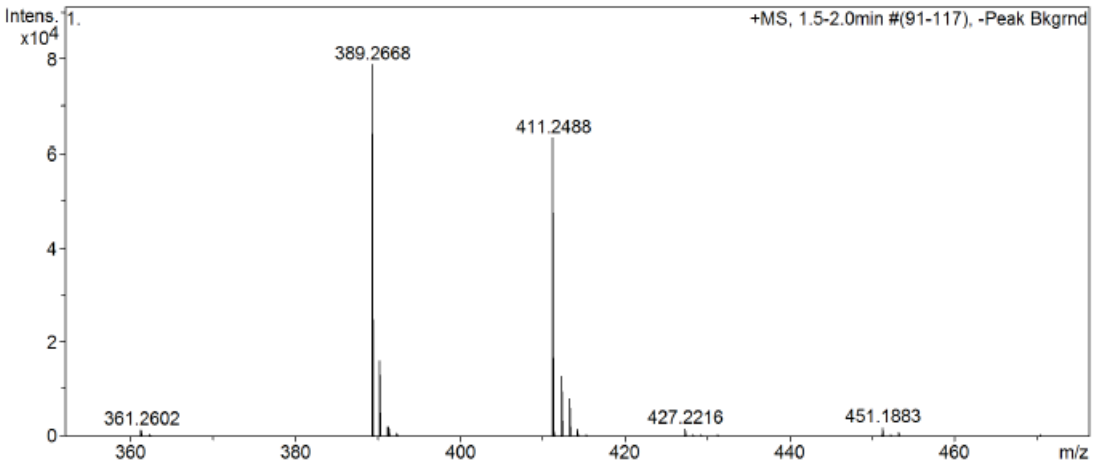

Meas. m/z	Formula	m/z	err [ppm]	err [mDa]	# Sigma	mSigma	rdb	e¯ Conf	N-Rule
389.2668	C 20 H 33 N 6 O 2	389.2660	-2.2	-0.8	1	25.8	7.5	even	ok
	C 22 H 38 Na O 4	389.2662	-1.4	-0.6	2	27.1	3.5	even	ok
	C 22 H 35 N 3 O 3	389.2673	1.3	0.5	3	32.6	7.0	odd	ok
	C 23 H 34 N 4 Na	389.2676	2.0	0.8	4	39.5	8.5	even	ok
411.2488	C 19 H 33 N 5 O 5	411.2476	-2.9	-1.2	1	24.9	6.0	odd	ok
	C 18 H 27 N 12	411.2476	-2.9	-1.2	2	26.1	11.5	even	ok
	C 20 H 32 N 6 Na O 2	411.2479	-2.2	-0.9	3	29.4	7.5	even	ok
	C 21 H 35 N 2 O 6	411.2490	0.4	0.2	4	30.9	5.5	even	ok
	C 20 H 29 N 9 O	411.2490	0.4	0.2	5	32.1	11.0	odd	ok
	C 22 H 34 N 3 Na O 3	411.2492	1.0	0.4	6	36.1	7.0	odd	ok

A2. 14 HRMS in MeCN for compound **83a**.

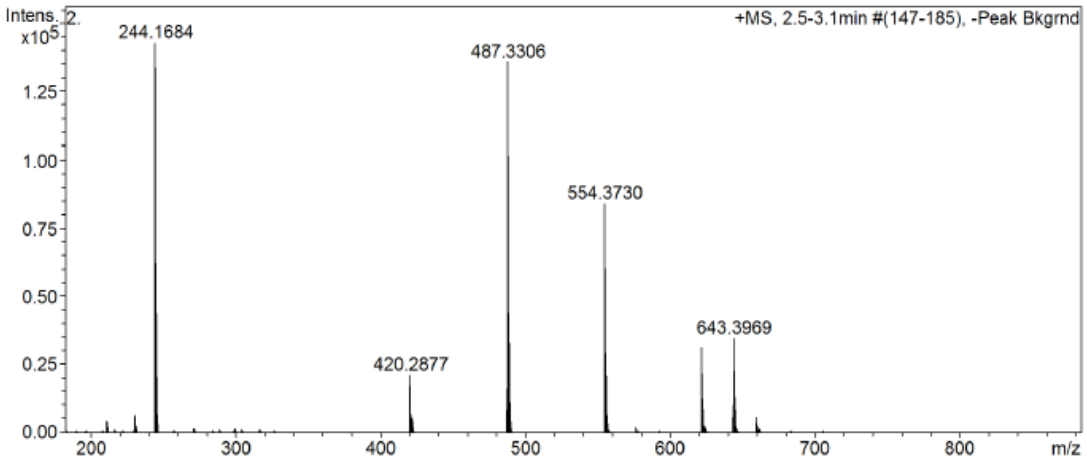

Meas. m/z	Formula	m/z	err [ppm]	err [mDa]	# Sigma	mSigma	rdb	e¯ Conf	N-Rule
244.1684	C 14 H 20 N 4	244.1682	-0.7	-0.2	1	68.3	7.0	odd	ok
420.2877	C 25 H 40 O 5	420.2870	-1.7	-0.7	1	18.9	6.0	odd	ok
	C 24 H 34 N 7	420.2870	-1.7	-0.7	2	25.3	11.5	even	ok
	C 26 H 39 N Na O 2	420.2873	-1.1	-0.4	3	26.0	7.5	even	ok
	C 26 H 36 N 4 O	420.2884	1.5	0.6	4	31.8	11.0	odd	ok
487.3306	C 28 H 39 N 8	487.3292	-2.9	-1.4	1	9.7	13.5	even	ok
	C 29 H 45 N O 5	487.3292	-2.9	-1.4	2	10.5	8.0	odd	ok
	C 30 H 44 N 2 Na O 2	487.3295	-2.3	-1.1	3	11.5	9.5	even	ok
	C 30 H 41 N 5 O	487.3306	-0.1	-0.1	4	15.0	13.0	odd	ok
	C 32 H 43 N 2 O 2	487.3319	2.6	1.3	5	21.7	12.5	even	ok
554.3730	C 33 H 50 N 2 O 5	554.3714	-2.8	-1.5	1	17.0	10.0	odd	ok
	C 32 H 44 N 9	554.3714	-2.8	-1.5	2	21.5	15.5	even	ok
	C 34 H 49 N 3 Na O 2	554.3717	-2.3	-1.3	3	22.6	11.5	even	ok
	C 34 H 46 N 6 O	554.3728	-0.3	-0.2	4	27.4	15.0	odd	ok
	C 36 H 51 Na O 3	554.3730	0.2	0.1	5	28.9	11.0	odd	ok
	C 36 H 48 N 3 O 2	554.3741	2.1	1.1	6	34.1	14.5	even	ok
621.4151	C 37 H 55 N 3 O 5	621.4136	-2.4	-1.5	1	15.6	12.0	odd	ok
	C 36 H 49 N 10	621.4136	-2.4	-1.5	2	18.0	17.5	even	ok
	C 38 H 54 N 4 Na O 2	621.4139	-2.0	-1.2	3	19.6	13.5	even	ok
	C 39 H 57 O 6	621.4150	-0.3	-0.2	4	21.2	11.5	even	ok
	C 38 H 51 N 7 O	621.4150	-0.3	-0.2	5	23.8	17.0	odd	ok
	C 40 H 56 N Na O 3	621.4152	0.2	0.1	6	26.0	13.0	odd	ok
	C 40 H 53 N 4 O 2	621.4163	1.9	1.2	7	30.9	16.5	even	ok
643.3969	C 26 H 54 N 9 Na O 8	643.3988	2.9	1.9	1	23.2	4.0	odd	ok
	C 36 H 55 N 2 O 8	643.3953	-2.5	-1.6	2	23.4	10.5	even	ok
	C 35 H 49 N 9 O 3	643.3953	-2.5	-1.6	3	28.0	16.0	odd	ok
	C 37 H 54 N 3 Na O 5	643.3956	-2.0	-1.3	4	29.2	12.0	odd	ok
	C 37 H 51 N 6 O 4	643.3966	-0.4	-0.3	5	34.4	15.5	even	ok
	C 36 H 48 N 10 Na	643.3956	-2.1	-1.3	6	34.6	17.5	even	ok
	C 39 H 56 Na O 6	643.3969	0.0	0.0	7	35.6	11.5	even	ok
	C 38 H 50 N 7 Na O	643.3969	0.0	0.0	8	40.5	17.0	odd	ok
	C 39 H 53 N 3 O 5	643.3980	1.7	1.1	9	40.9	15.0	odd	ok
	C 38 H 47 N 10	643.3980	1.7	1.1	10	46.3	20.5	even	ok
	C 40 H 52 N 4 Na O 2	643.3982	2.1	1.4	11	47.3	16.5	even	ok

A2. 15 HRMS in MeCN for compound **83b**.

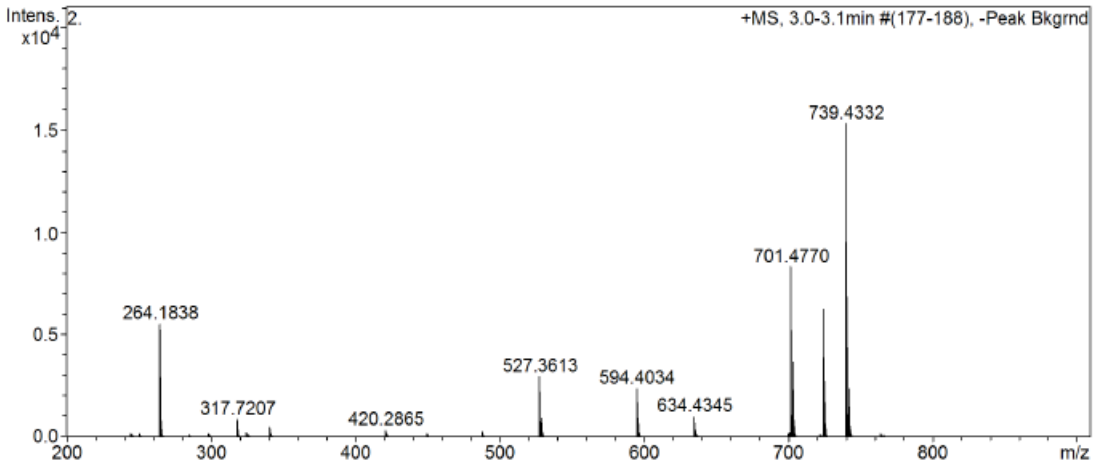

Meas. m/z	Formula	m/z	err [ppm]	err [mDa]	# Sigma	mSigma	rdb	e¯ Conf	N-Rule
527.3613	C 32 H 49 N O 5	527.3605	-1.4	-0.8	1	25.6	9.0	odd	ok
	C 31 H 43 N 8	527.3605	-1.4	-0.8	2	31.4	14.5	even	ok
	C 33 H 45 N 5 O	527.3619	1.1	0.6	3	37.1	14.0	odd	ok
594.4034	C 36 H 54 N 2 O 5	594.4027	-1.1	-0.7	1	14.9	11.0	odd	ok
	C 35 H 48 N 9	594.4027	-1.1	-0.7	2	19.0	16.5	even	ok
	C 37 H 50 N 6 O	594.4041	1.1	0.7	3	24.8	16.0	odd	ok
701.4770	C 43 H 63 N 3 O 5	701.4762	-1.2	-0.8	1	27.4	14.0	odd	ok
	C 32 H 66 N 6 Na O 9	701.4783	1.9	1.3	2	32.2	2.5	even	ok
	C 42 H 57 N 10	701.4762	-1.2	-0.8	3	32.3	19.5	even	ok
	C 44 H 62 N 4 Na O 2	701.4765	-0.8	-0.5	4	33.5	15.5	even	ok
	C 45 H 65 O 6	701.4776	0.8	0.5	5	34.0	13.5	even	ok
	C 44 H 59 N 7 O	701.4776	0.8	0.5	6	38.4	19.0	odd	ok
	C 46 H 64 N Na O 3	701.4778	1.2	0.8	7	40.1	15.0	odd	ok
723.4587	C 42 H 63 N 2 O 8	723.4579	-1.1	-0.8	1	24.9	12.5	even	ok
	C 41 H 57 N 9 O 3	723.4579	-1.1	-0.8	2	29.3	18.0	odd	ok
	C 43 H 62 N 3 Na O 5	723.4582	-0.7	-0.5	3	30.5	14.0	odd	ok
	C 31 H 66 N 5 Na O 12	723.4600	1.9	1.3	4	34.4	1.0	odd	ok
	C 42 H 56 N 10 Na	723.4582	-0.7	-0.5	5	35.7	19.5	even	ok
	C 43 H 59 N 6 O 4	723.4592	0.8	0.6	6	35.8	17.5	even	ok
	C 45 H 64 Na O 6	723.4595	1.2	0.8	7	37.0	13.5	even	ok
	C 44 H 58 N 7 Na O	723.4595	1.1	0.8	8	41.7	19.0	odd	ok
739.4332	C 43 H 62 K N 3 O 5	739.4321	-1.5	-1.1	1	27.9	14.0	odd	ok
	C 42 H 56 K N 10	739.4321	-1.5	-1.1	2	30.7	19.5	even	ok
	C 45 H 64 K O 6	739.4334	0.4	0.3	3	33.7	13.5	even	ok
	C 44 H 58 K N 7 O	739.4334	0.3	0.3	4	36.1	19.0	odd	ok
	C 46 H 55 N 6 O 3	739.4330	-0.2	-0.2	5	40.3	22.5	even	ok
	C 33 H 63 N 4 O 14	739.4335	0.5	0.3	6	41.0	4.5	even	ok
	C 48 H 57 N 3 O 4	739.4344	1.6	1.2	7	45.2	22.0	odd	ok

A2. 16 HRMS in MeCN for receptor **83**.

A.3 X-ray Crystallography

Slow evaporation of a solution of **73** in acetonitrile afforded single crystals (A3. 1). CCDC- 1053071; $C_{21}H_{16}N_4O_6$; Orthorhombic; space group: *Pnma*; *a*= 16.5475 (11) Å, *b*=22.8442 (16) Å, *c*= 4.9997 (4) Å; α= 90°, β= 90°, γ= 90°; *V*= 1890 (2) Å^3; μ= 0.111 mm^{-1}; T=100 (2) K; Z= 4; ρ_c=1.477 gcm^{-3}. Total reflections: 10813; reflections used: 2216; Θ_{max}=27.466; Θ_{min}= 3.040; 145 parameters; *R* indices (all data): R_1 = 0.0463, wR_2 = 0.0982, final *R* indices [I > 2σI]: R_1 = 0.0365, wR_2 = 0.0926.

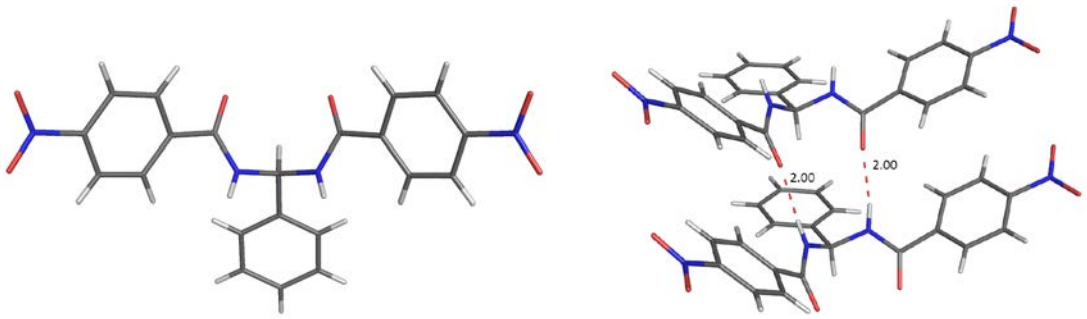

A3. 1 **Left-** Single crystal X-ray structure of **73**. **Right-**dimer with intermolecular hydrogen bonds. Red dashed lines show O···H distances.

Slow evaporation of a solution of **77** in DMSO afforded single crystals (A3. 2). CCDC- 1053070; $C_{26}H_{13}F_{15}N_2O_2$; Orthorhombic; space group: *Pnma*; *a*= 9.7085(2) Å, *b*=26.9582 (10) Å, *c*= 10.0203 (2) Å; α= 90°, β= 90°, γ= 90°; *V*= 2622 (12) Å^3; μ= 0.181 mm^{-1}; T=100 (2) K; Z= 4; ρ_c=1.698 gcm^{-3}. Total reflections: 16362; reflections used: 4347; Θ_{max}=63.986; Θ_{min}= 4.336; 215 parameters; *R* indices (all data): R_1 = 0.0581, wR_2 = 0.1431, final *R* indices [I > 2σI]: R_1 = 0.0483, wR_2 = 0.1294.

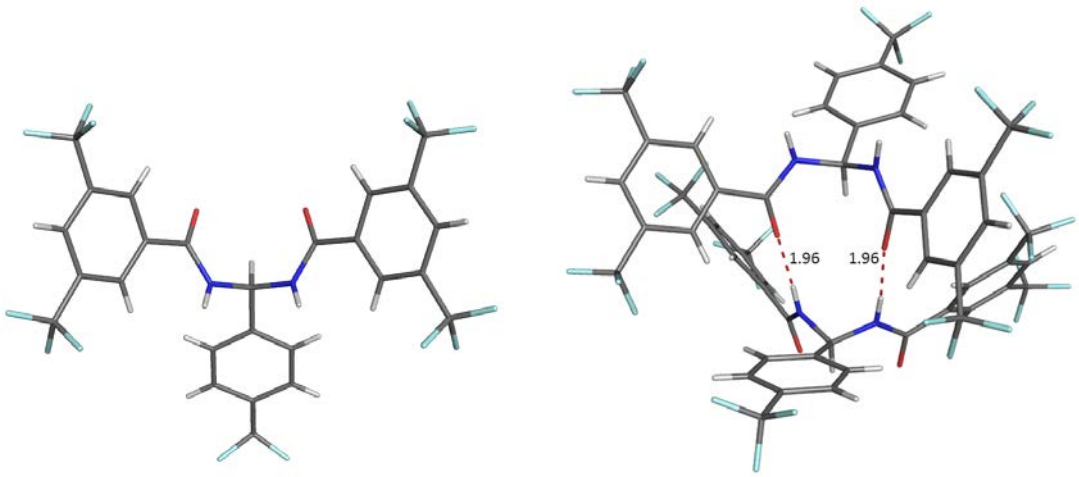

A3. 2 **Left-** Single crystal X-ray structure of **77**. **Right-** dimer with intermolecular hydrogen bonds red dashed lines show O···H distances.

Slow evaporation of a solution of **79** in methanol afforded single crystals (A3. 3). CCDC- 1497159; $C_{37}H_{46}N_{10}$; orthorhombic; space group: $Pca2_1$; a= 17.7644 (4) Å, b=11.6635 (2) Å, c= 32.0041 (7) Å; α= 90°, β= 90°, γ= 90°; V= 6631 (2) Å^3; μ= 0.08 mm^{-1}; T=120 (2)K; Z= 8; ρ_c=1.264 gcm^{-3}. Total reflections: 43299; reflections used: 14672; Θ_{max}=27.480; Θ_{min}= 2.952; 859 parameters; R indices (all data): R_1 = 0.0731, wR_2 = 0.112, final R indices [I > 2σI]: R_1 = 0.051, wR_2 = 0.123.

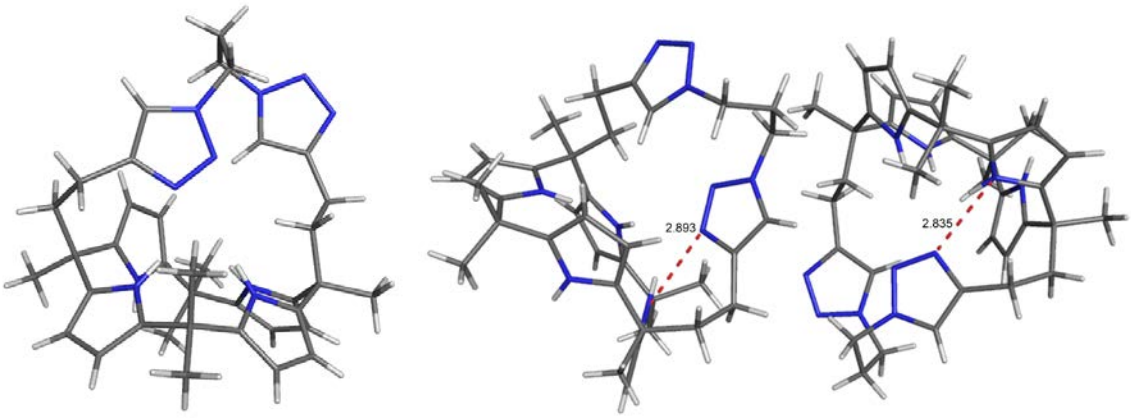

A3. 3 **Left-**Single crystal X-ray structure of **79**. **Right-** Packing diagram of two molecules, red dashed lines show N···N distances.

Slow evaporation of a solution of **79** and TBACl in methanol afforded single crystals (A3. 4). CCDC-1497435; $C_{53}H_{82}N_{11}Cl$; monoclinic; space group: $P2_1/n$; a= 13.5356 (2) Å, b=22.6654 (4) Å, c= 18.3173

(3) Å; α= 90°, β= 109.617 (1)°, γ= 90°; *V*= 5264 (15) Å^3; μ= 0.12 mm^{-1}; T=120 (2)K; Z= 4; ρ_c=1.147 gcm^{-3}. Total reflections: 64453; reflections used: 12053; Θ_{max}=27.480; Θ_{min}= 2.95; 612 parameters; *R* indices (all data): R_1 = 0.0908, wR_2 = 0.1473, final *R* indices [I > 2σI]: R_1 = 0.0584, wR_2 = 0.1653.

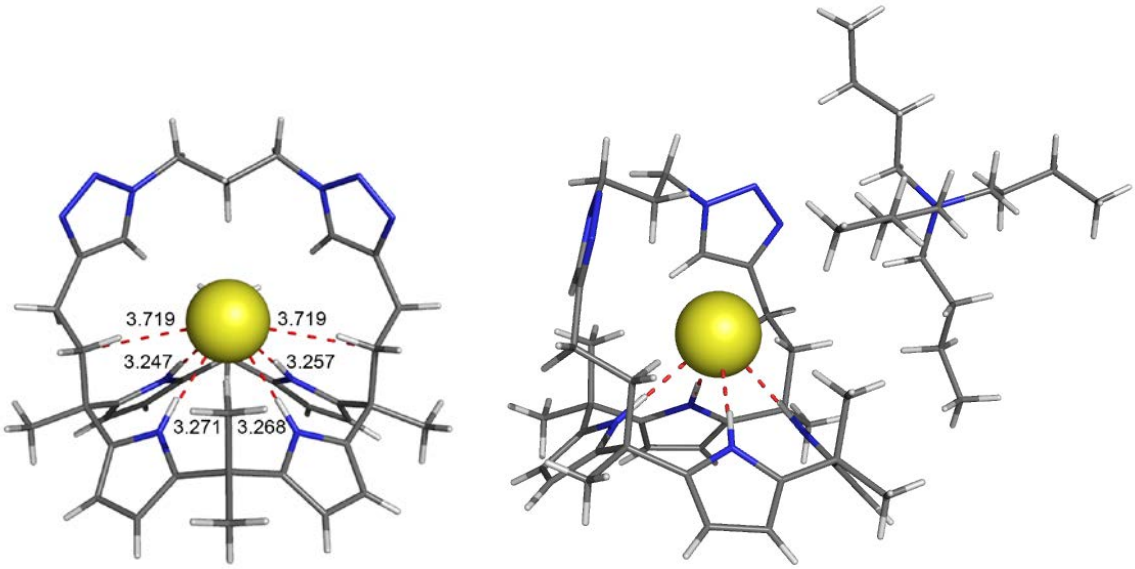

A3. 4 **Left-** Single crystal X-ray structure of **79- TBACl** with TBA omitted for clarity. Red dashed lines show N···Cl and C···Cl distance. **Right-**The full structure with TBACl present.

Slow diffusion of a solution of **79** and TBAF in chloroform into petroleum spirits afforded single crystals of a **79-TBAF** complex (A3. 5). CCDC- 1497159; F·$C_{37}H_{46}N_{10}$·$C_{16}H_{36}N$; monoclinic; space group: $P2_1/n$; *a*= 13.5283 (7) Å, *b*=22.8407 (8) Å, *c*= 18.0121 (8) Å; α= 90°, β= 109.545 (5)°, γ= 90°; *V*= 5245 (4) Å^3; μ= 0.07 mm^{-1}; T=100 (2)K; Z= 4; ρ_c=1.130 gcm^{-3}. Total reflections: 55028; reflections used: 13538; Θ_{max}=28.699; Θ_{min}= 2.932; 636 parameters; *R* indices (all data): R_1 = 0.170, wR_2 = 0.198, final *R* indices [I > 2σI]: R_1 = 0.087, wR_2 = 0.238.

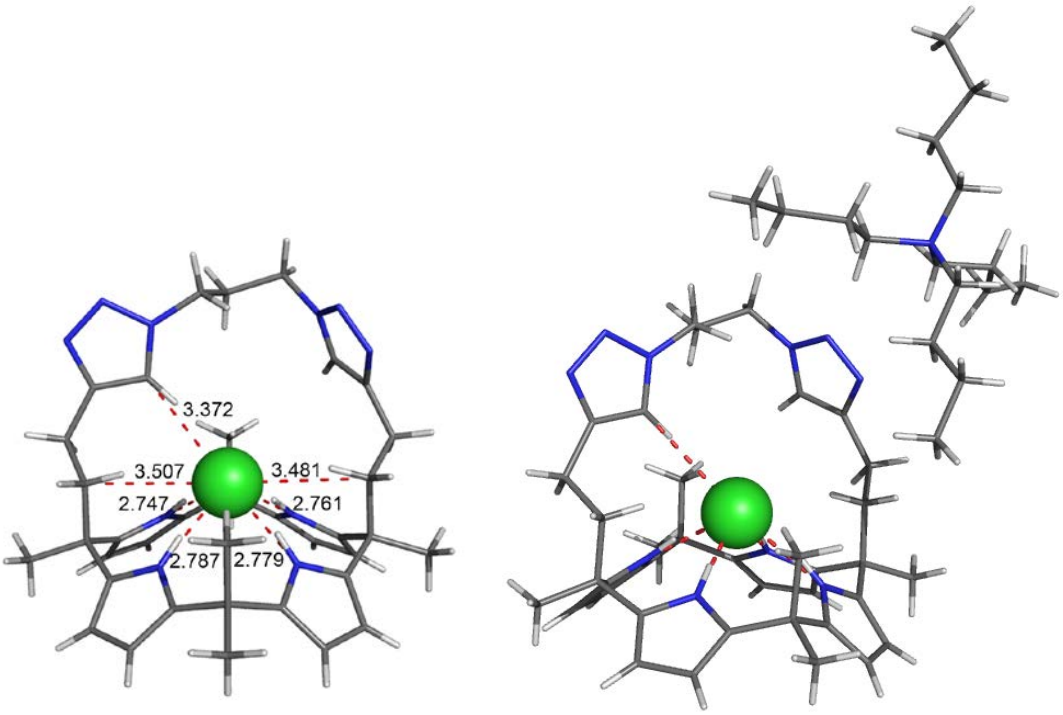

A3. 5 **Left-**Single crystal X-ray structure of **79-TBAF** with the TBA omitted for clarity, red dashed lines show N···F and C···F distances. **Right-**The full structure with TBAF present.

Slow diffusion of a solution of **80** in DCM into a solution of CsF in ethanol afforded single crystals of a **80-CsF** complex (A3. 6). CCDC- 1497158; $F{\cdot}C_{38}H_{48}N_{10}{\cdot}Cs{\cdot}2(C_2H_6O)$; Triclinic; space group: $P\bar{1}$; a= 11.5405 (3) Å, b=20.3342 (4) Å, c=20.4173 (5) Å; α= 117.361 (2)°, β= 97.175 (2)°, γ= 90.5504 (18)°; V= 4209.68 (19) Å^3; μ= 0.93 mm^{-1}; T=100 (2)K; Z= 4; ρ_c=1.403 gcm^{-3}. Total reflections: 55544; reflections used: 21736; Θ_{max}=28.699; Θ_{min}= 2.966; 1068 parameters; R indices (all data): R_1 = 0.0697, wR_2 = 0.123, final R indices [$I > 2\sigma I$]: R_1 = 0.0532, wR_2 = 0.131.

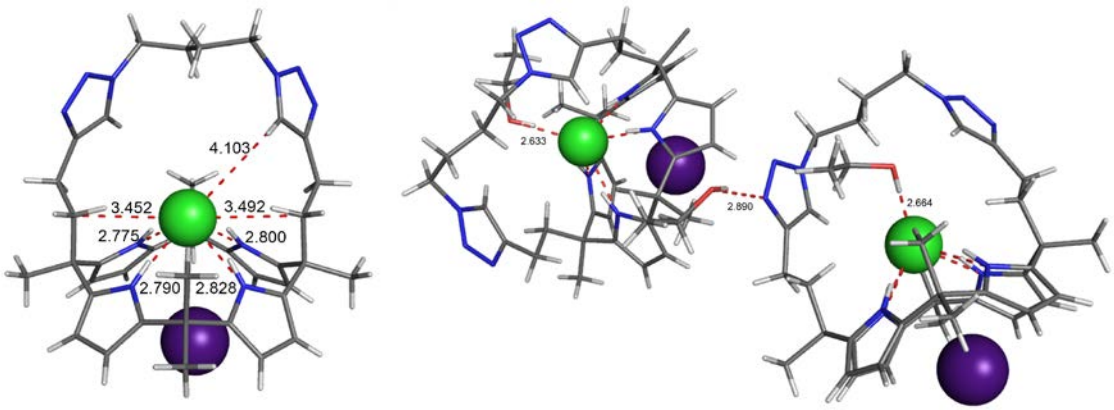

A3. 6 **Left-** Single crystal X-ray structure of **80-CsF** with solvent molecules omitted for clarity. **Right-** Full packing structure of two molecules with stabilising ethanol molecules. Red dashed lines show N···F, C···F, O···F and O···N distances.

Slow diffusion of a solution of **82** and TBACl in DCM into petroleum spirits afforded single crystals of a **82-TBACl** complex (A3. 7); $Cl{\cdot}C_{40}H_{52}N_{10}{\cdot}C_{16}H_{36}N{\cdot}H_2O$; Triclinic; space group: *P-1*; *a*= 10.9231 (3) Å, *b*=15.5131 (4) Å, *c*=16.1302 (4) Å; α= 96.100 (2)°, β= 94.136 (2)°, γ= 90.806(2)°; *V*= 2710.08(12) $Å^3$; μ= 0.120 mm^{-1}; T=100 (2)K; Z= 2; ρ_c=1.187 gcm^{-3}. Total reflections: 9532; reflections used: 8531; Θ_{max}=25.000 Θ_{min}= 1.733; 636 parameters; *R* indices (all data): R_1 = 0.0873, wR_2 = 0.2277, final *R* indices [$I > 2\sigma I$]: R_1 = 0.0819, wR_2 = 0.2260.

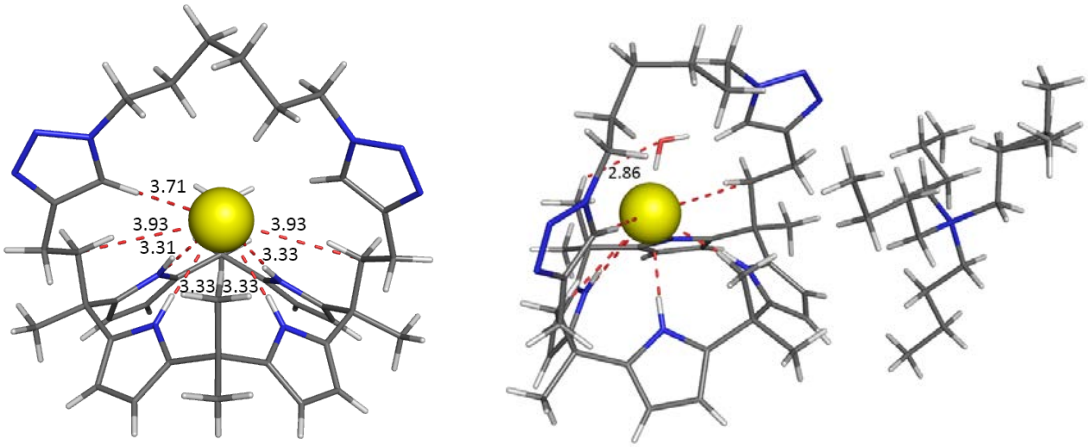

A3. 7 **Left-** Single crystal X-ray structure of **82-TBACl.** Solvent molecules, TBA^+ and disorder have been omitted for clarity. **Right-** The full structure with TBA (modelled disorder) and water present. Red dashed lines show N···Cl, C···Cl and O···H distances.

Slow evaporation of a solution of **83** and TBACl in DMSO afforded single crystals of a **83-TBACl** complex (A3. 8); $Cl{\cdot}C_{42}H_{56}N_{10}{\cdot}C_{16}H_{36}N{\cdot}C_2H_6OS$; Triclinic; space group: *P-1*; *a*= 13.2720 (4) Å, *b*=13.5498 (3) Å, *c*=17.9982 (5) Å; α= 104.085 (2)°, β= 93.540 (2)°, γ= 91.535(2)°; *V*= 3130.45(15) $Å^3$; μ= 0.141 mm^{-1}; T=100 (2)K; Z= 2; ρ_c=1.121 gcm^{-3}. Total reflections: 15603; reflections used: 10988; Θ_{max}=28.500 Θ_{min}= 1.698; 728 parameters; *R* indices (all data): R_1 = 0.0784, wR_2 = 0.1307, final *R* indices [$I > 2\sigma I$]: R_1 = 0.0483, wR_2 = 0.1179.

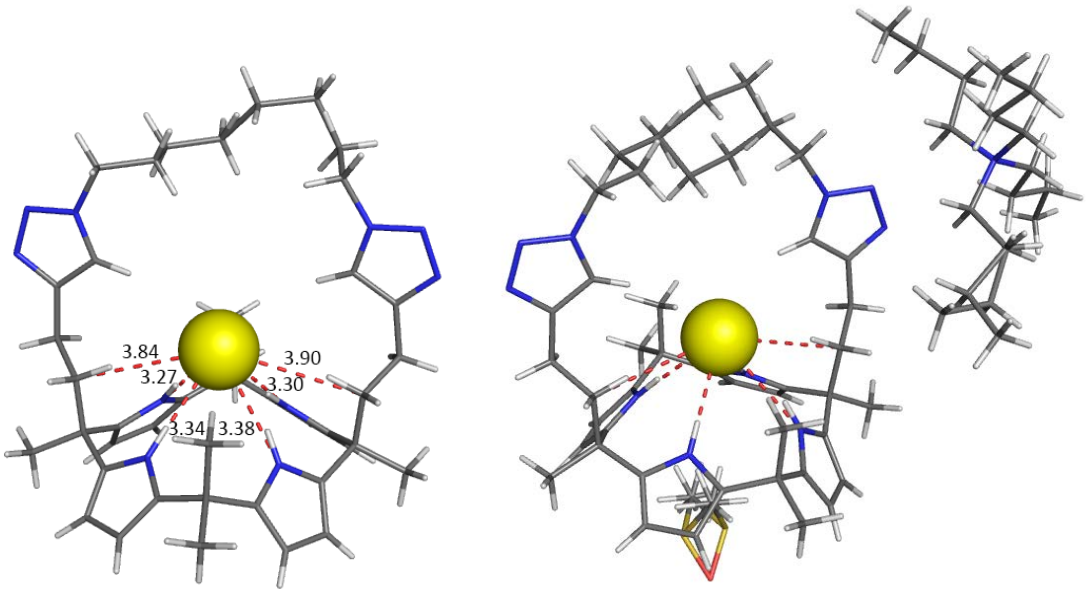

A3. 8 **Left-**Single crystal X-ray structure of **83-TBACl.** Solvent molecules, TBA^+ and disorder have been omitted for clarity. **Right-**The full structure with TBA (modelled disorder) and DMSO present. Red dashed lines show N···Cl and C···Cl distances.

Appendix B Binding data

B.1 NMR Titration Spectra

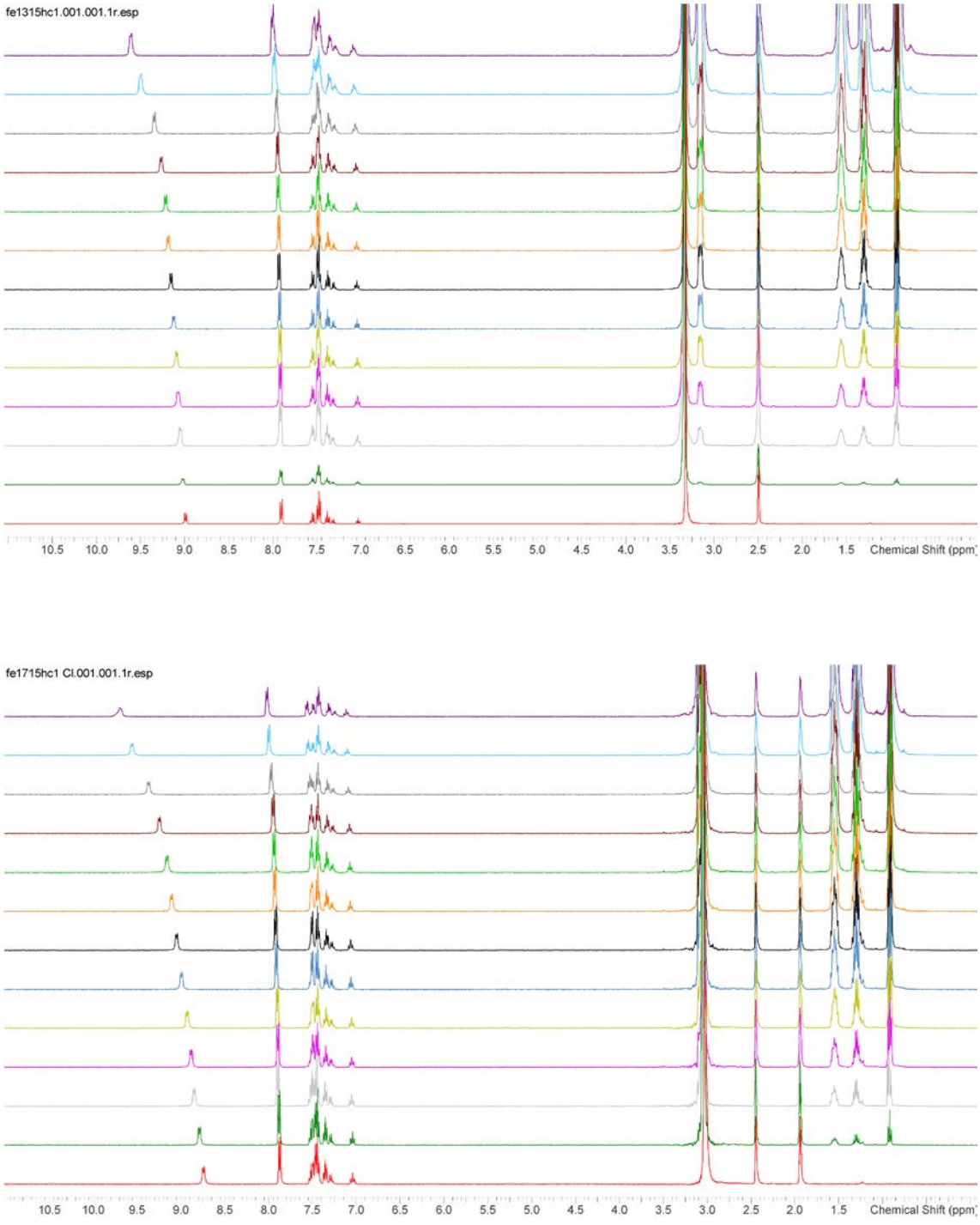

B1. 1 NMR titration spectra stack plot for receptor **72** with TBACl in DMSO-d_6 (top) and MeCN-d_3 (bottom).

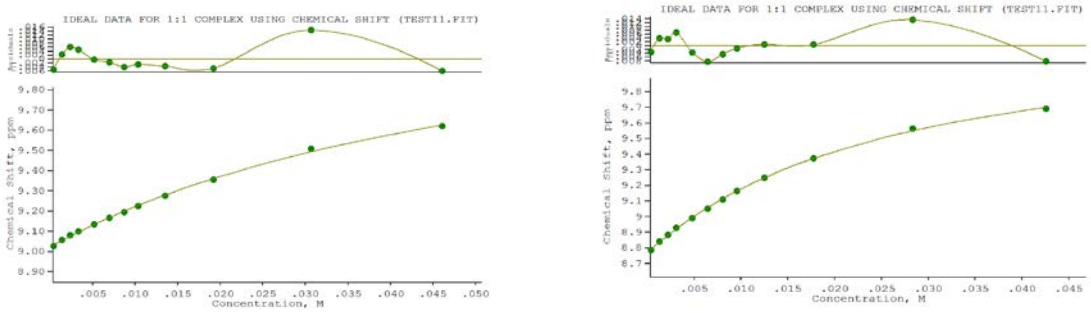

B1. 2 NMR binding curve for receptor **72** with TBACl in DMSO-d_6 (left) K_a = 19 ± 2 M^{-1} MeCN-d_3 and (right) K_a = 46 ± 2 M^{-1}.

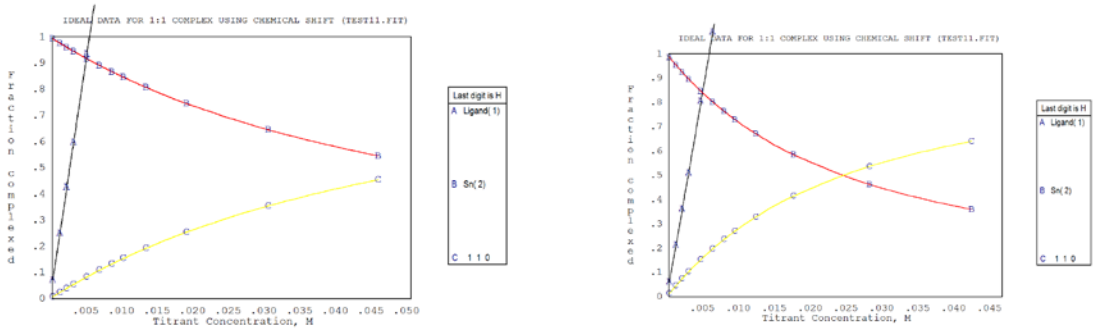

B1. 3 NMR species ratio for receptor **72** with TBACl in DMSO-d_6 (left) and MeCN-d_3 (right), A = guest concentration, B = free host concentration and C = complex concentration.

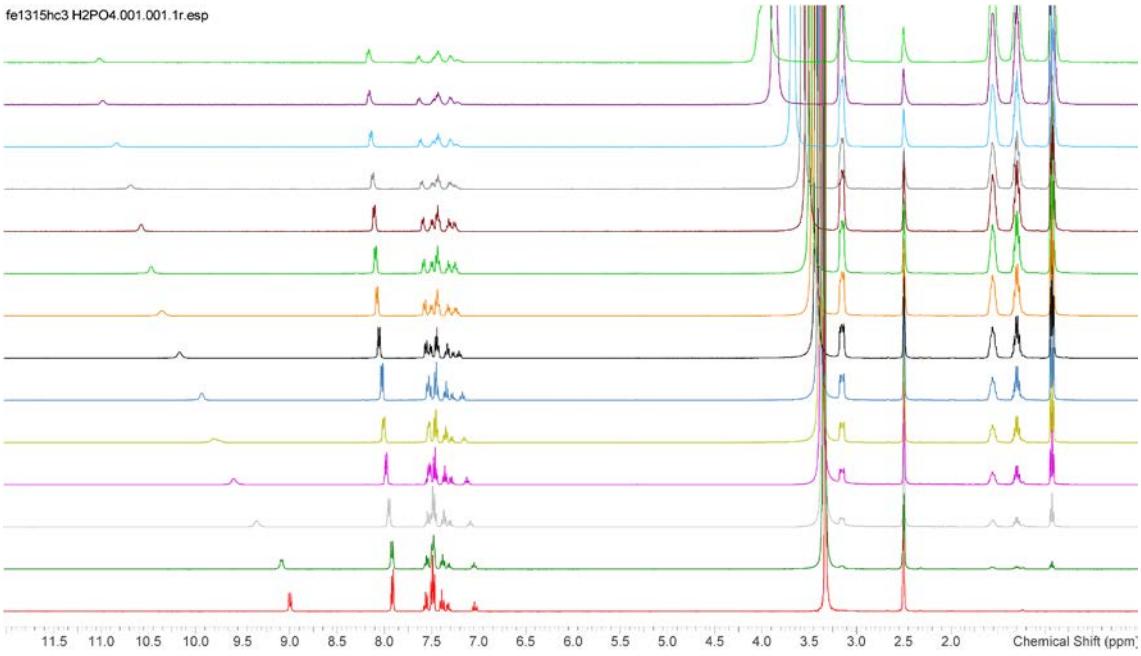

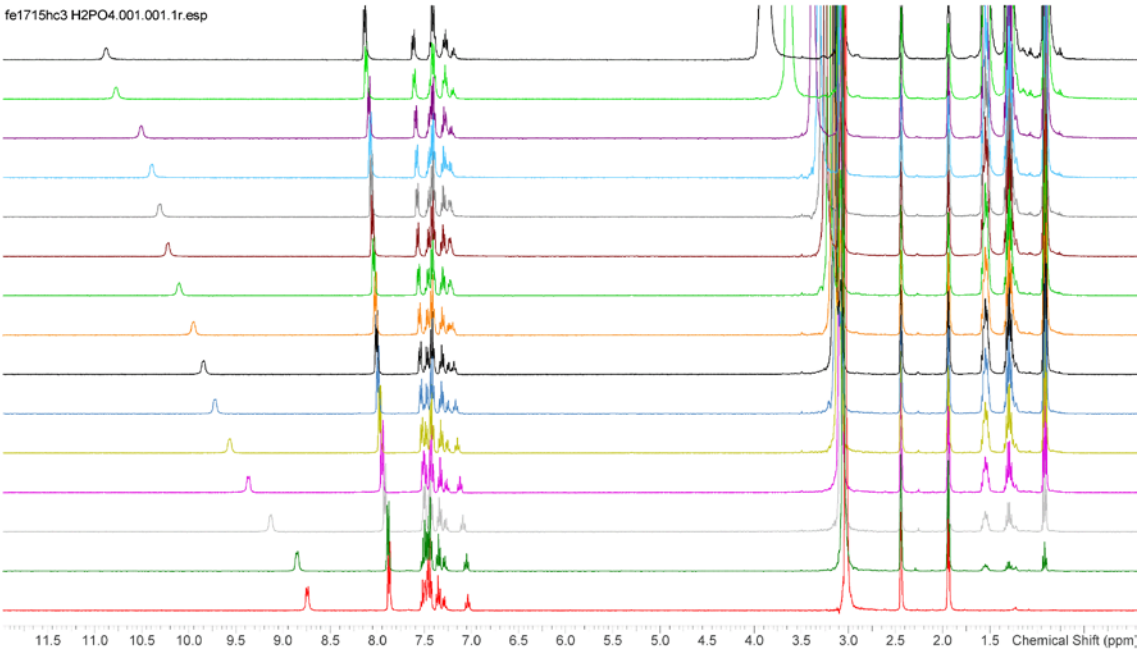

B1. 4 NMR titration spectra stack plot for receptor **72** with $TBAH_2PO_4$ in DMSO-d_6 (top) and MeCN-d_3 (bottom).

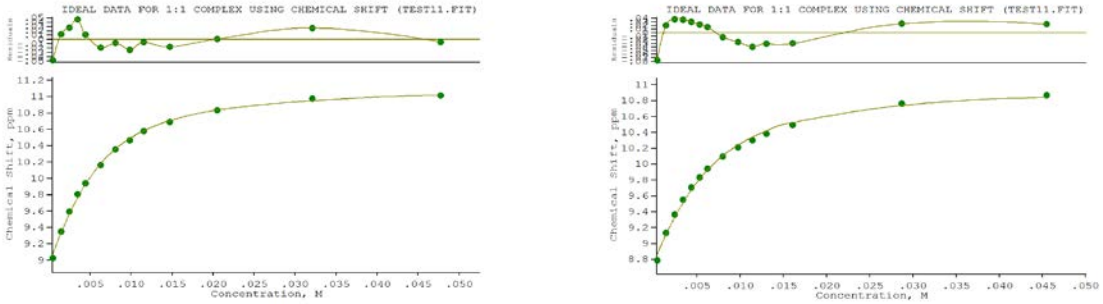

B1. 5 NMR binding curve for receptor **72** with $TBAH_2PO_4$ in DMSO-d_6 (left) K_a = 370 ± 26 M^{-1} and MeCN-d_3 (right) K_a = 296 ± 27 M^{-1}.

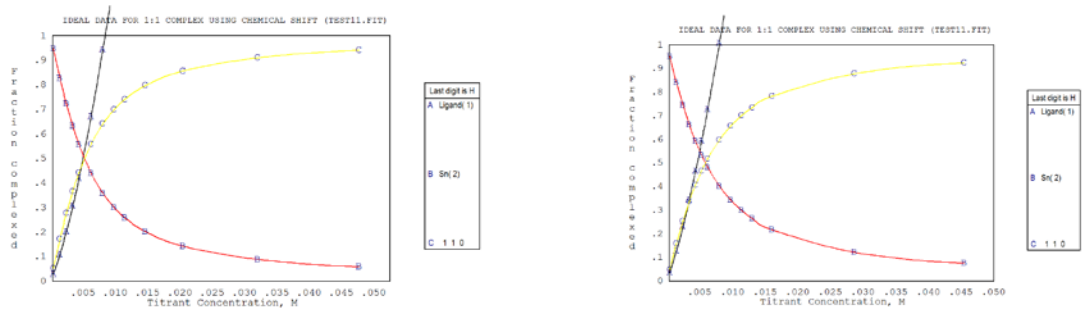

B1. 6 NMR species ratio for receptor **72** with $TBAH_2PO_4$ in DMSO-d_6 (left) and MeCN-d_3 (right), A = guest concentration, B = free host concentration and C = complex concentration.

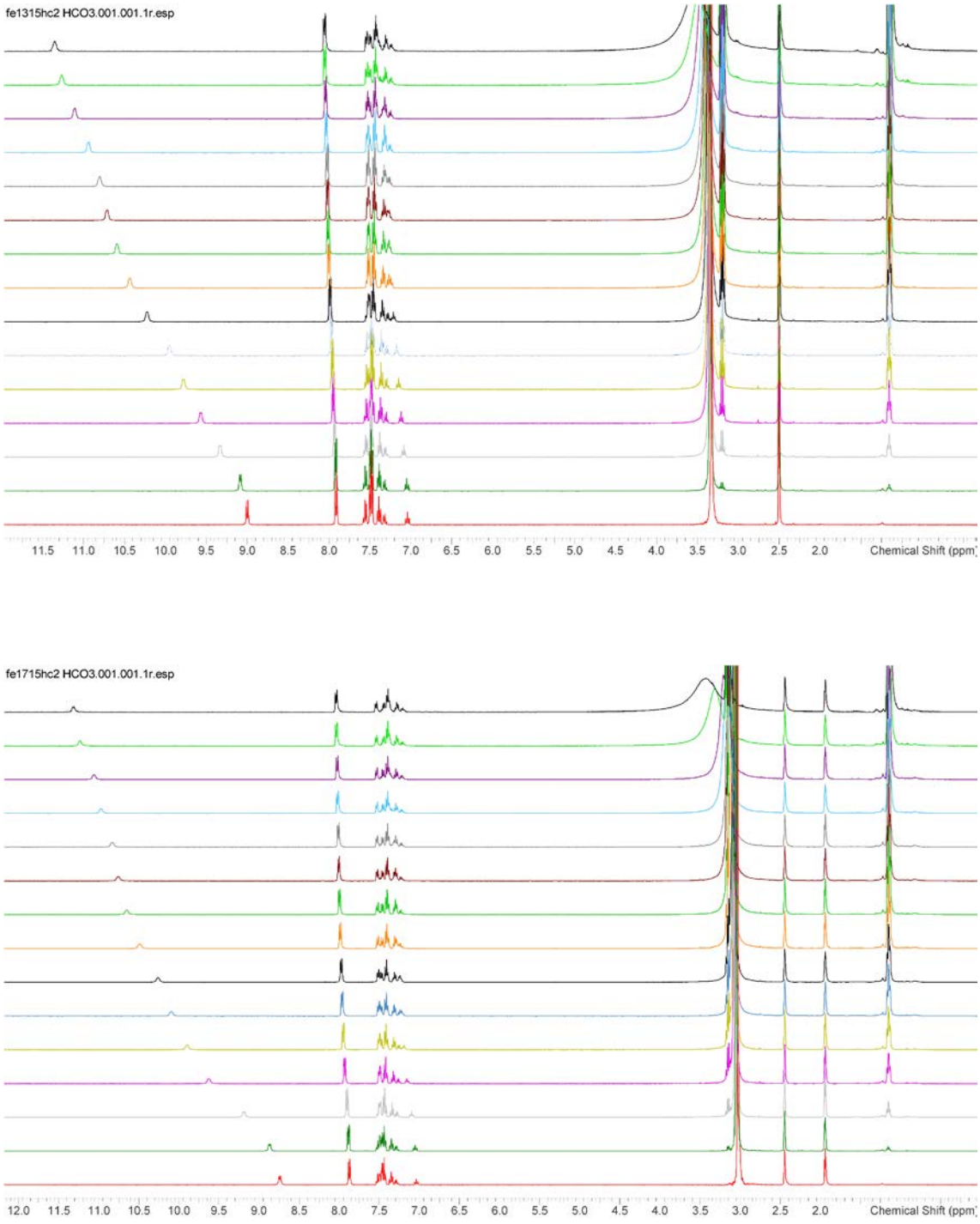

B1. 7 NMR titration spectra stack plot for receptor **72** with $TEAHCO_3$ in DMSO-d_6 (top) and MeCN-d_3 (bottom).

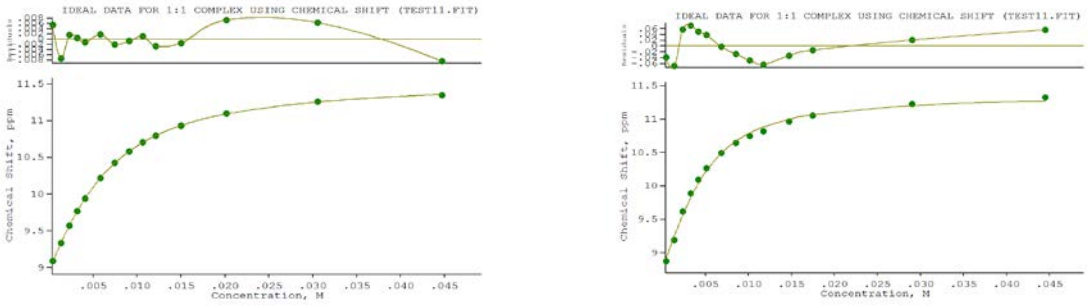

B1. 8 NMR binding curve for receptor **72** with $TEAHCO_3$ in DMSO-d_6 (left) K_a = 275 ± 3 M^{-1} and MeCN-d_3 (right) K_a = 550 ± 63 M^{-1}.

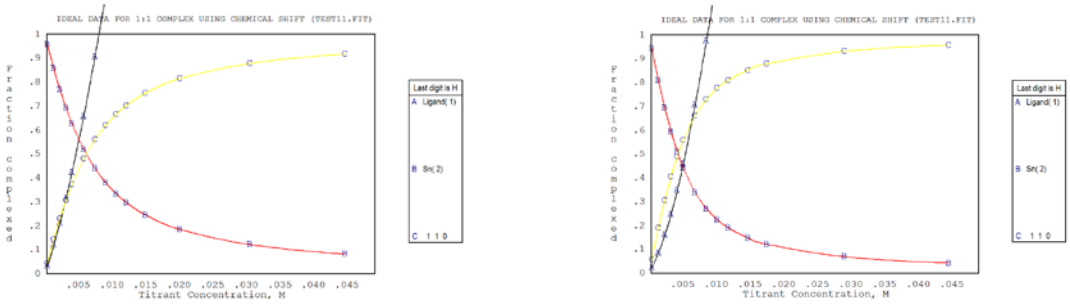

B1. 9 NMR species ratio for receptor **72** with $TEAHCO_3$ in DMSO-d_6 (left) and MeCN-d_3 (right), A = guest concentration, B = free host concentration and C = complex concentration.

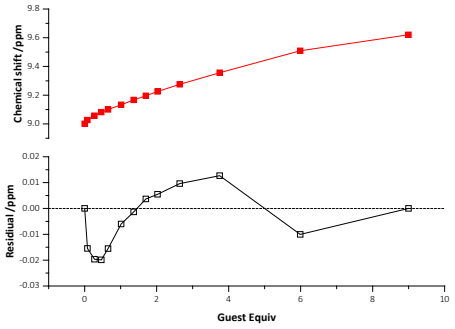

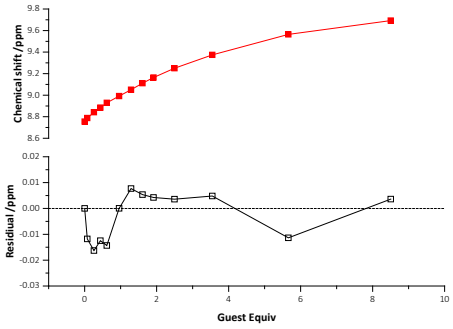

B1. 10 Bindfit NMR binding curve for receptor **72** with TBACl in DMSO-d_6 (left) $K_a = 27 \pm 5\ M^{-1}$ and MeCN-d_3 (right) $K_a = 51 \pm 2\ M^{-1}$.

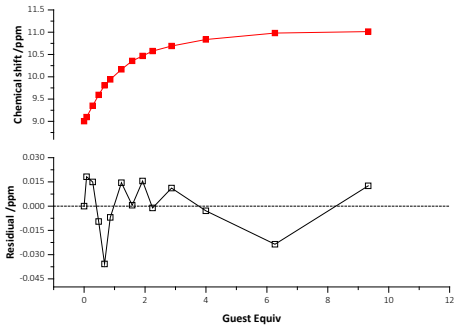

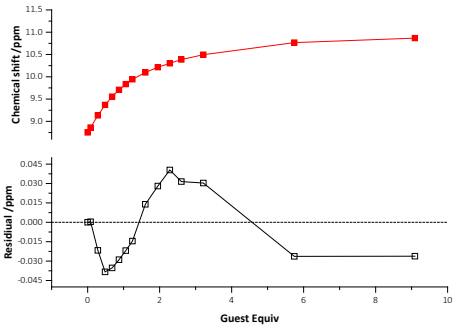

B1. 11 Bindfit NMR binding curve for receptor **72** with $TBAH_2PO_4$ in DMSO-d_6 (left) $K_a = 344 \pm 4\ M^{-1}$ and MeCN-d_3 (right) $K_a = 300 \pm 5\ M^{-1}$.

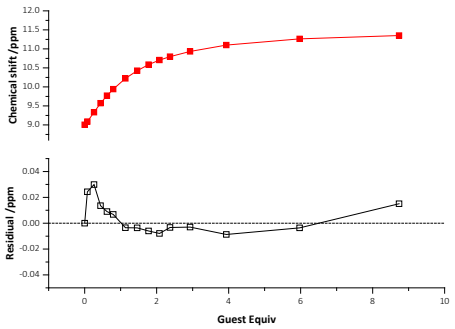

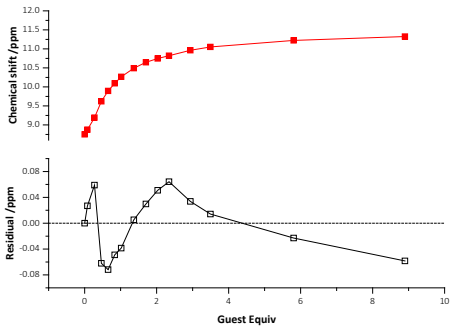

B1. 12 Bindfit NMR binding curve for receptor **72** with $TEAHCO_3$ in DMSO-d_6 (left) $K_a = 261 \pm 2\ M^{-1}$ and MeCN-d_3 (right) $K_a = 564 \pm 9\ M^{-1}$.

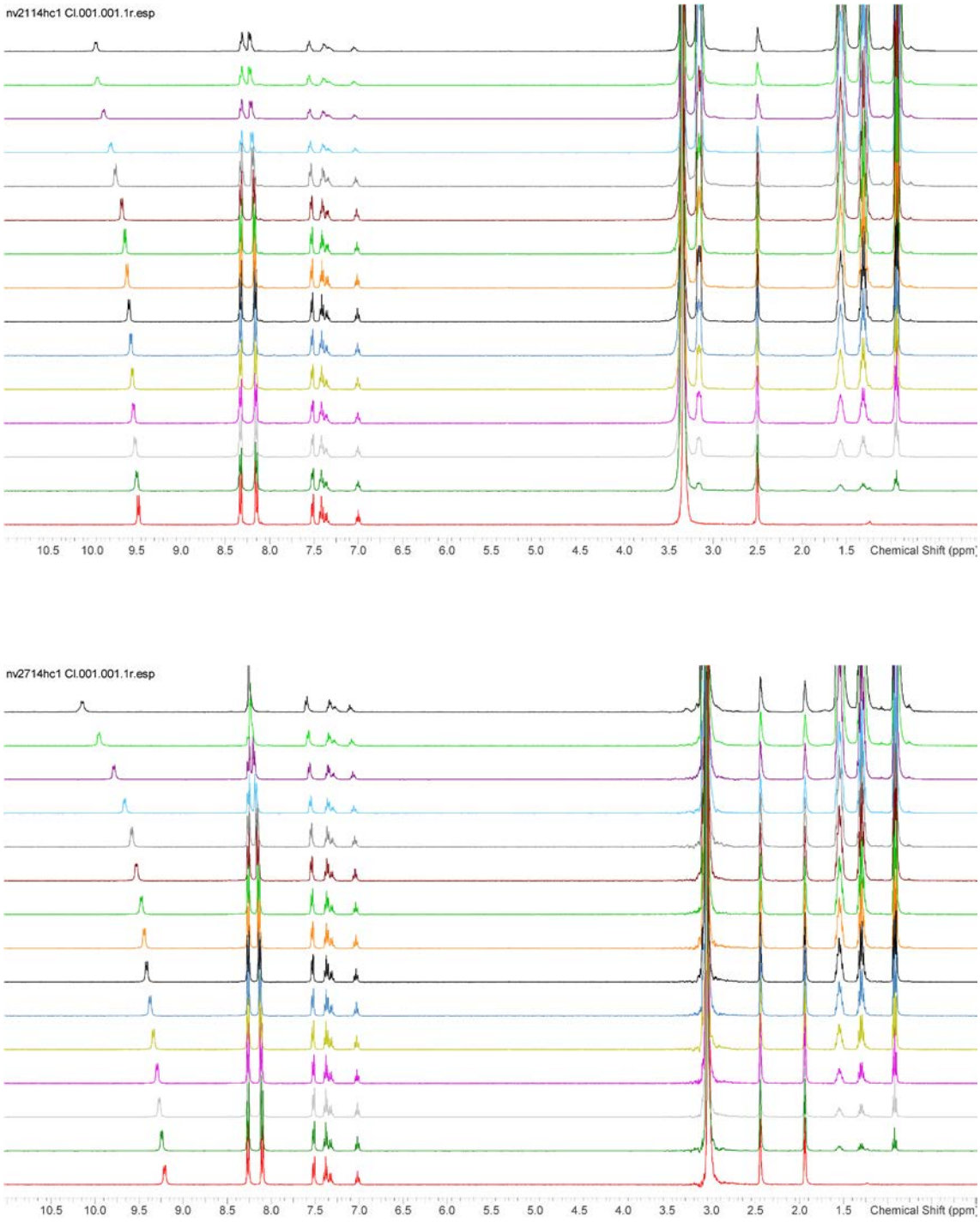

B1. 13 NMR titration spectra stack plot for receptor **73** with TBACl in DMSO-d_6 (top) and MeCN-d_3 (bottom).

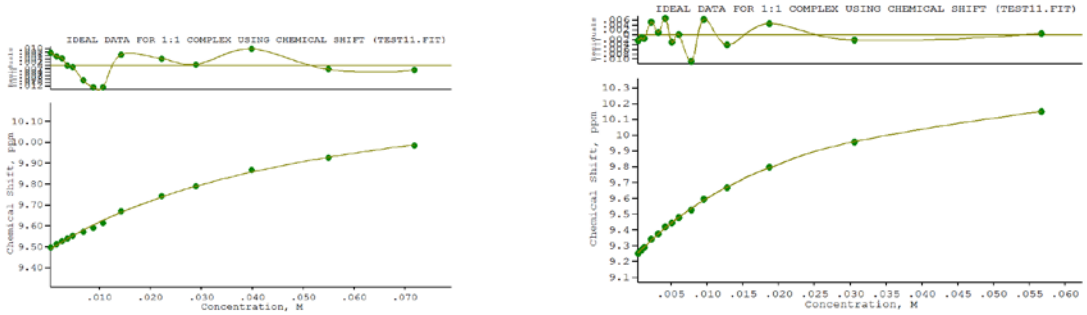

B1. 14 NMR binding curve for receptor **73** with TBACl in DMSO-d_6 (left) K_a = 19 ± 2 M^{-1} and MeCN-d_3 (right) K_a = 47 ± 1 M^{-1}.

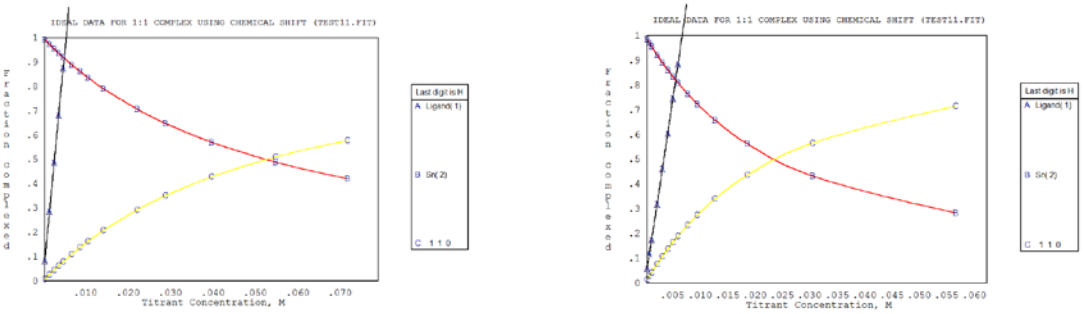

B1. 15 NMR species ratio for receptor **73** with TBACl in DMSO-d_6 (left) and MeCN-d_3 (right), A = guest concentration, B = free host concentration and C = complex concentration.

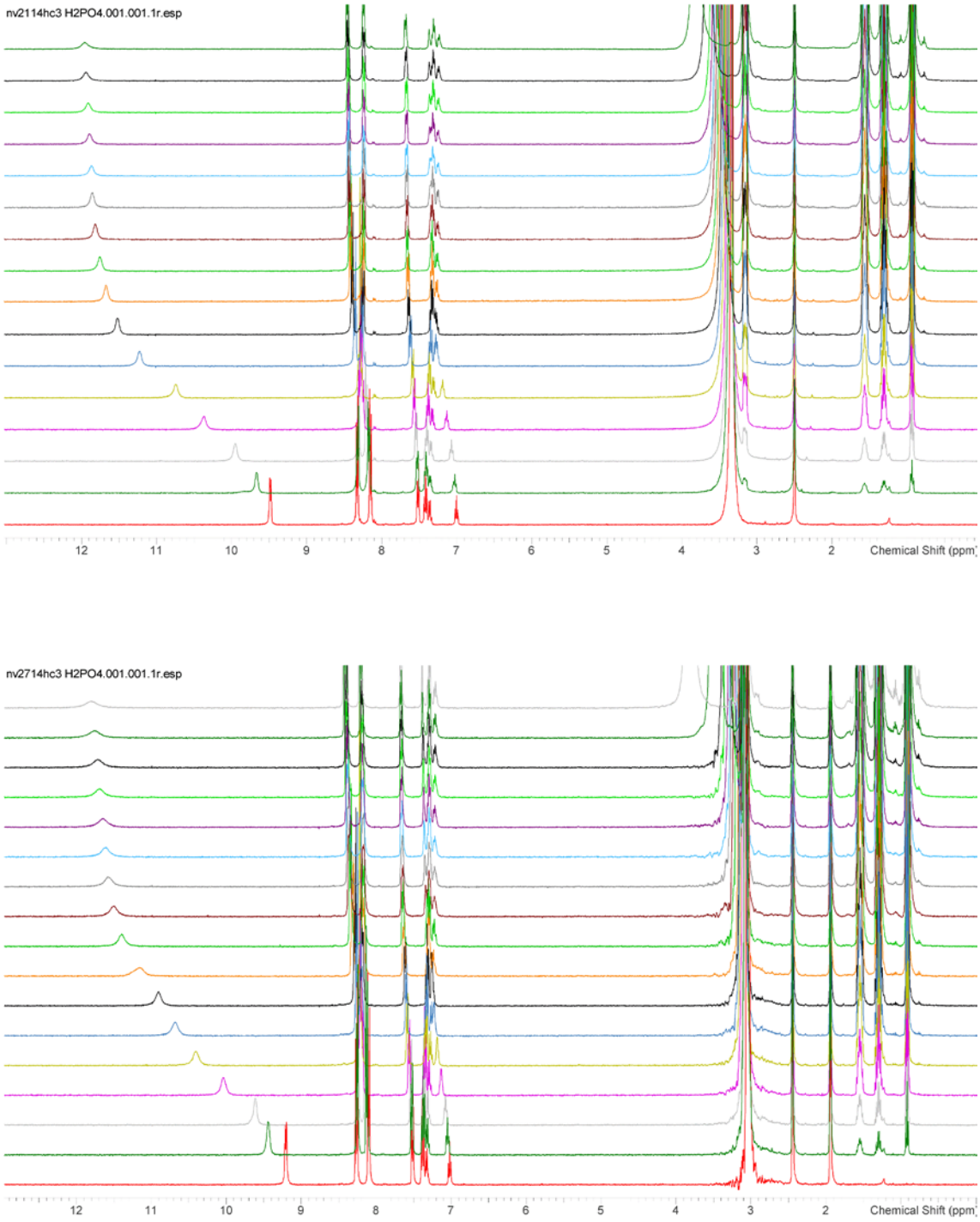

B1. 16 NMR titration spectra stack plot for receptor **73** with $TBAH_2PO_4$ in DMSO-d_6 (top) and MeCN-d_3 (bottom).

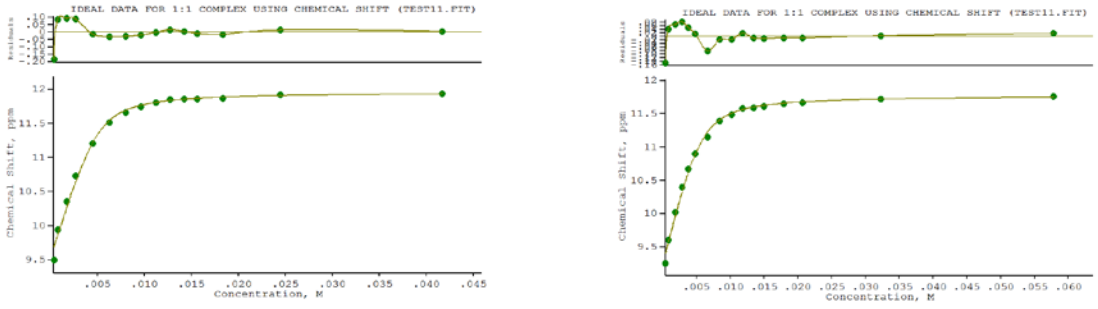

B1. 17 NMR binding curve for receptor **73** with $TBAH_2PO_4$ in DMSO-d_6 (left) K_a = 2270 ± 577 M^{-1} and MeCN-d_3 (right) K_a = 1630 ± 300 M^{-1}.

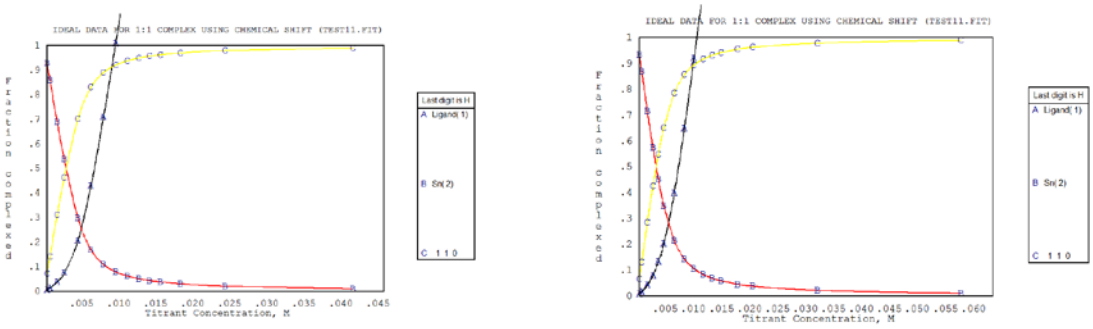

B1. 18 NMR species ratio for receptor **73** with $TBAH_2PO_4$ in DMSO-d_6 (left) and MeCN-d_3 (right), A = guest concentration, B = free host concentration and C = complex concentration.

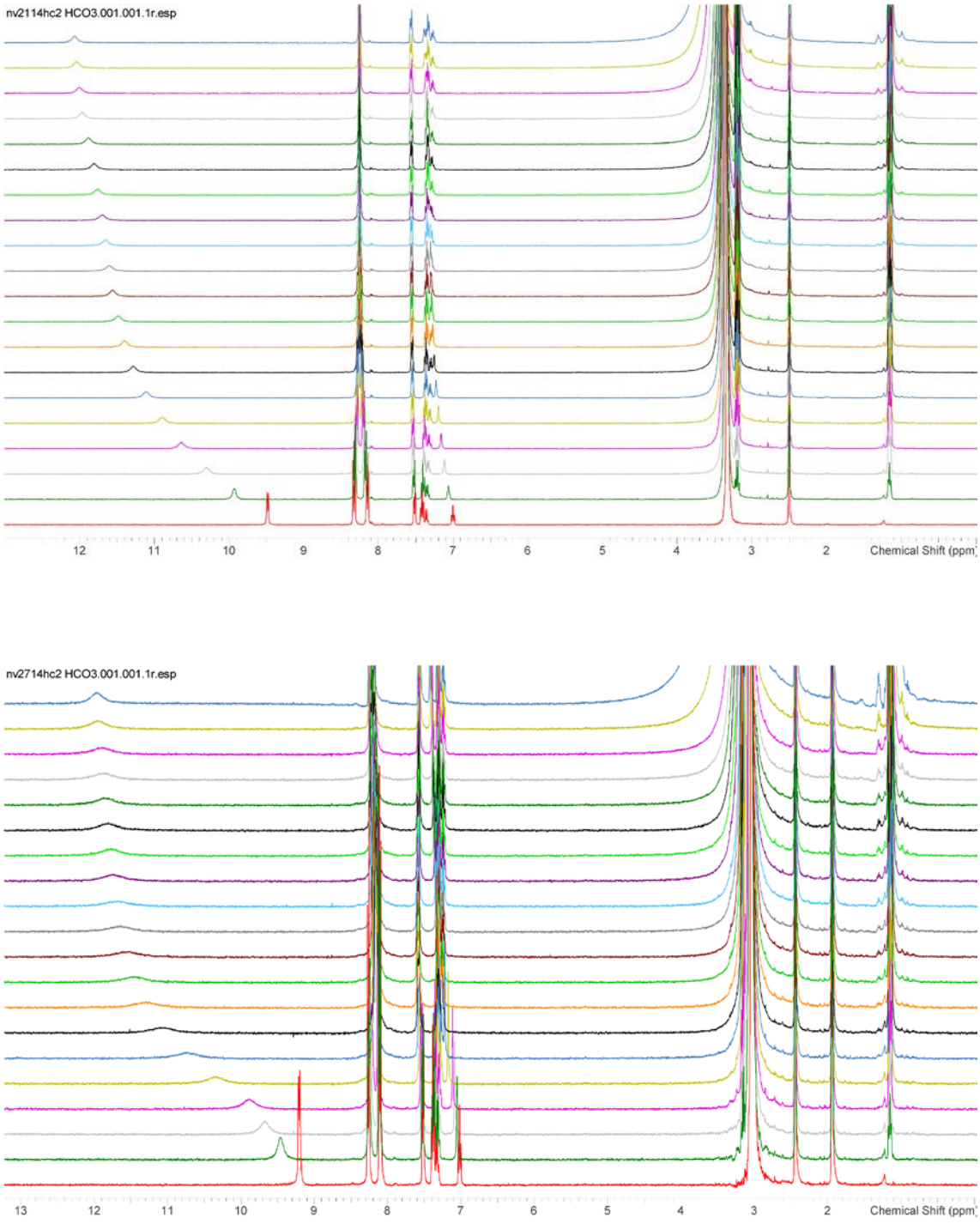

B1. 19 NMR titration spectra stack plot for receptor **73** with $TEAHCO_3$ in DMSO-d_6 (top) and MeCN-d_3 (bottom).

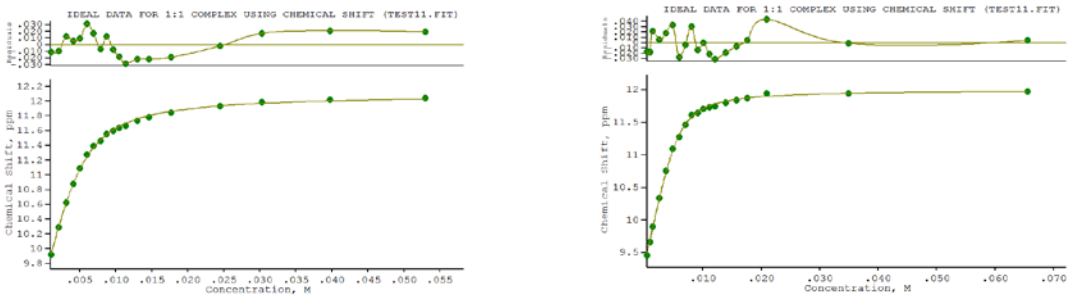

B1. 20 NMR binding curve for receptor **73** with $TEAHCO_3$ in DMSO-d_6 (left) K_a = 771 ± 29 M^{-1} and MeCN-d_3 (right) K_a = 1680 ± 93 M^{-1}.

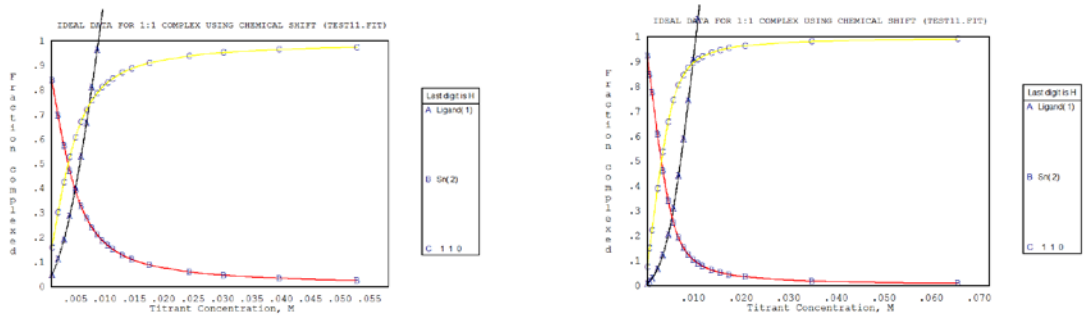

B1. 21 NMR species ratio for receptor **73** with $TEAHCO_3$ in DMSO-d_6 (left) and MeCN-d_3 (right), A = guest concentration, B = free host concentration and C = complex concentration.

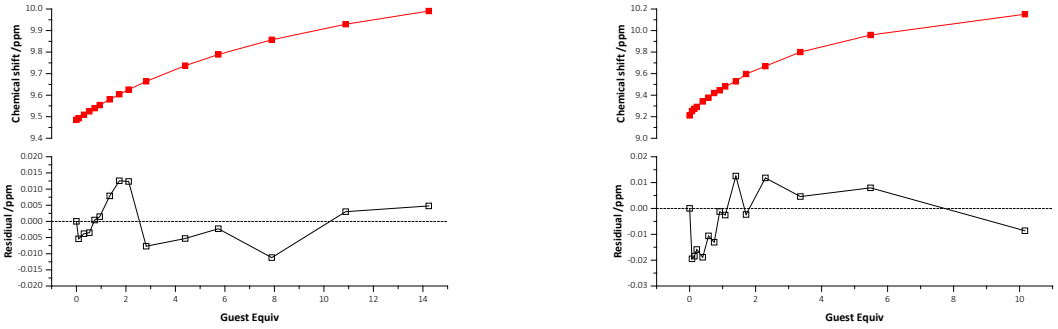

B1. 22 Bindfit NMR binding curve for receptor **73** with TBACl in DMSO-d_6 (left) K_a = 19 ± 3 M^{-1} and MeCN-d_3 (right) K_a = 57 ± 4 M^{-1}.

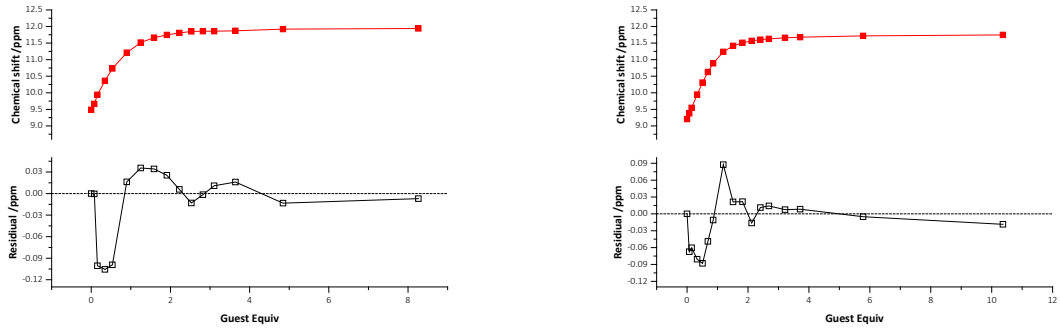

B1. 23 Bindfit NMR binding curve for receptor **73** with $TBAH_2PO_4$ in DMSO-d_6 (left) K_a = 2414 ± 21 M^{-1} and MeCN-d_3 (right) K_a = 1694 ± 16 M^{-1}.

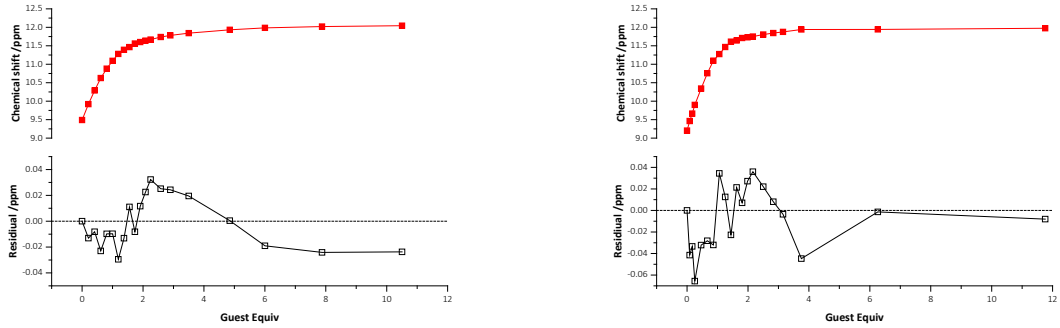

B1. 24 Bindfit NMR binding curve for receptor **73** with $TEAHCO_3$ in DMSO-d_6 (left) K_a = 815 ± 3 M^{-1} and MeCN-d_3 (right) K_a = 1808 ± 8 M^{-1}.

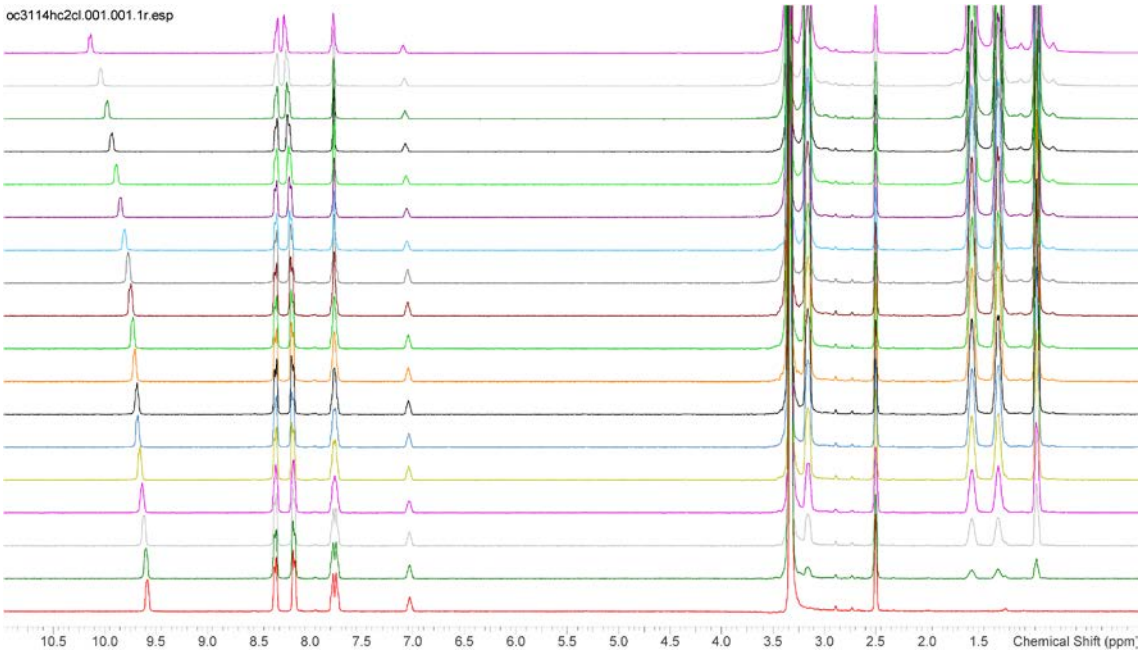

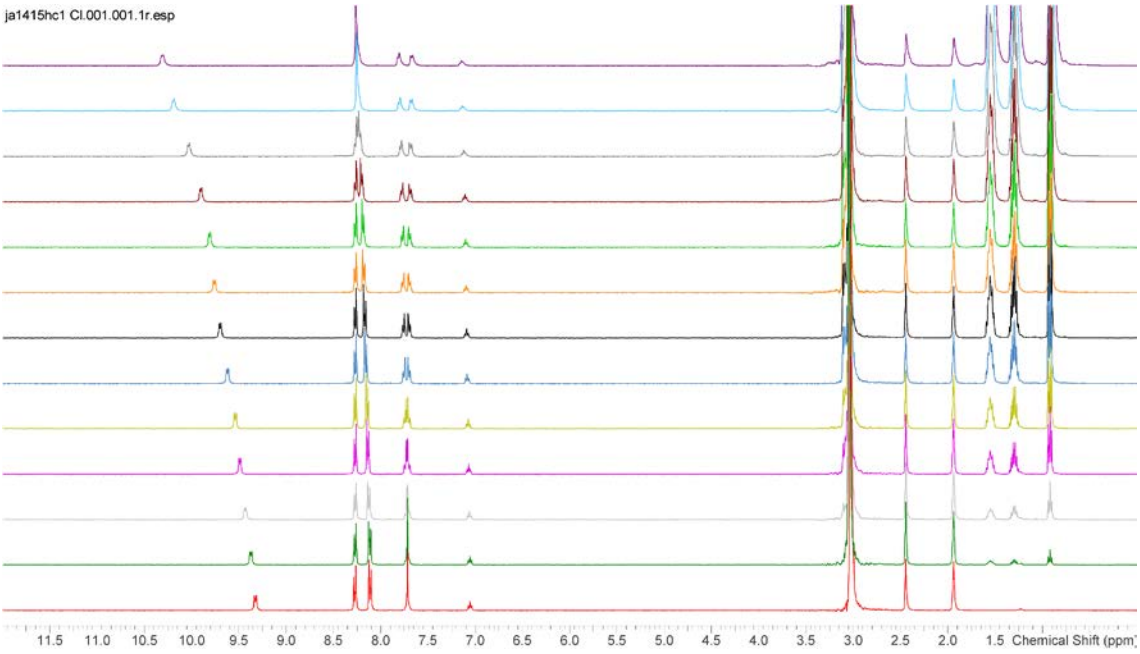

B1. 25 NMR titration spectra stack plot for receptor **74** with TBACl in DMSO-d_6 (top) and MeCN-d_3 (bottom).

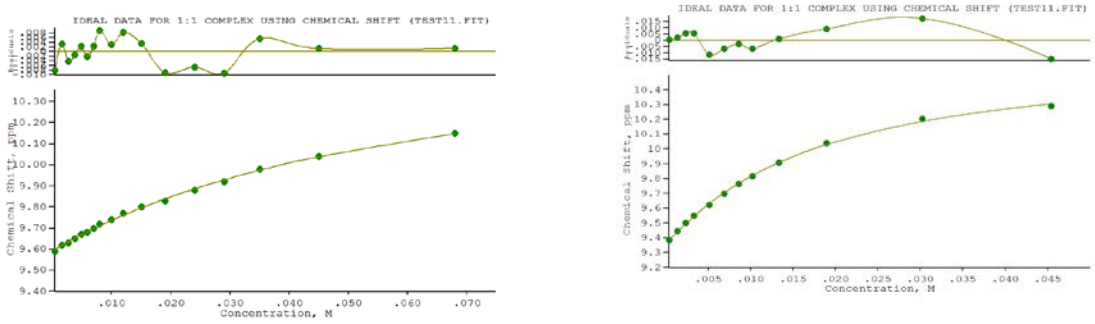

B1. 26 NMR binding curve for receptor **74** with TBACl in DMSO-d_6 (left) K_a = 17 ± 1 M^{-1} and MeCN-d_3 (right) K_a = 67 ± 4 M^{-1}.

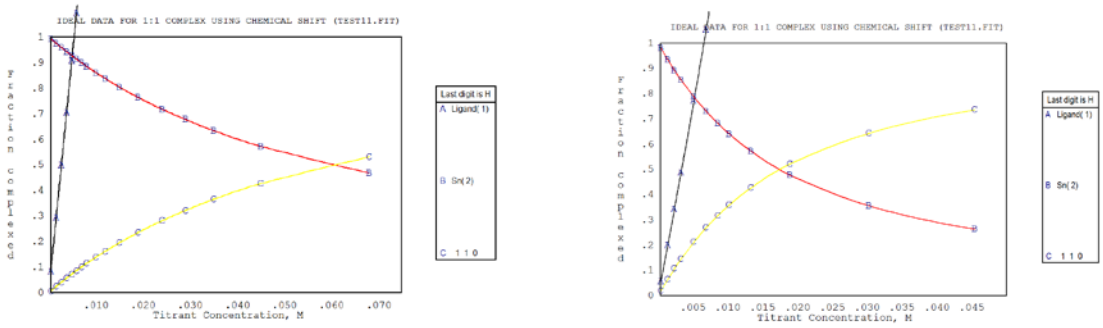

B1. 27 NMR species ratio for receptor **74** with TBACl in DMSO-d_6 (left) and MeCN-d_3 (right), A = guest concentration, B = free host concentration and C = complex concentration.

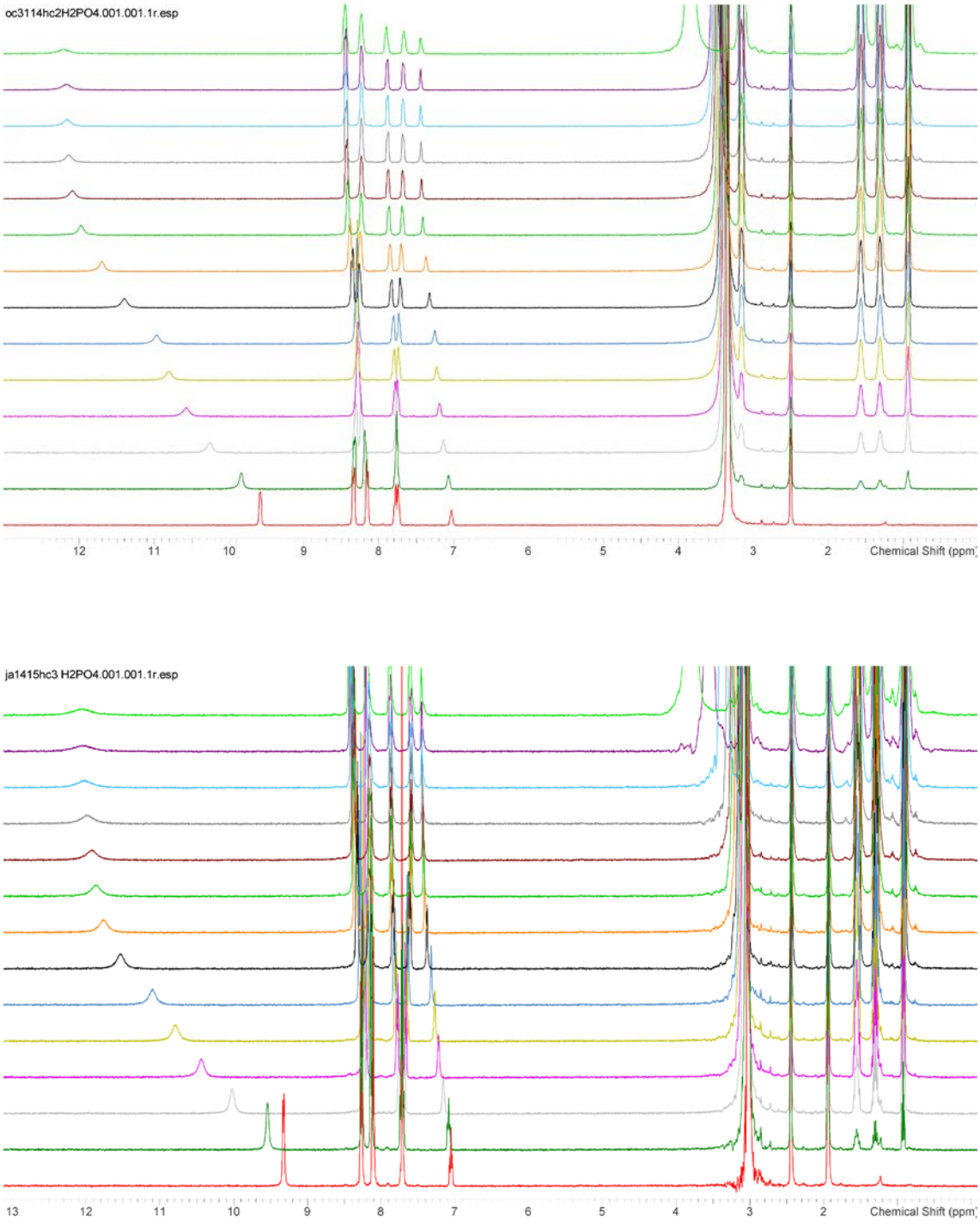

B1. 28 NMR titration spectra stack plot for receptor **74** with $TBAH_2PO_4$ in DMSO-d_6 (top) and MeCN-d_3 (bottom).

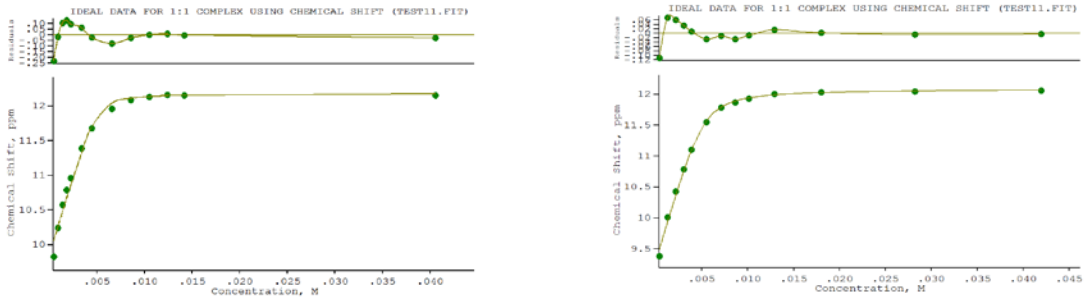

B1. 29 NMR binding curve for receptor **74** with $TBAH_2PO_4$ in DMSO-d_6 (left) K_a = 8290 ± 4000 M^{-1} and MeCN-d_3 (right) K_a = 3410 ± 622 M^{-1}.

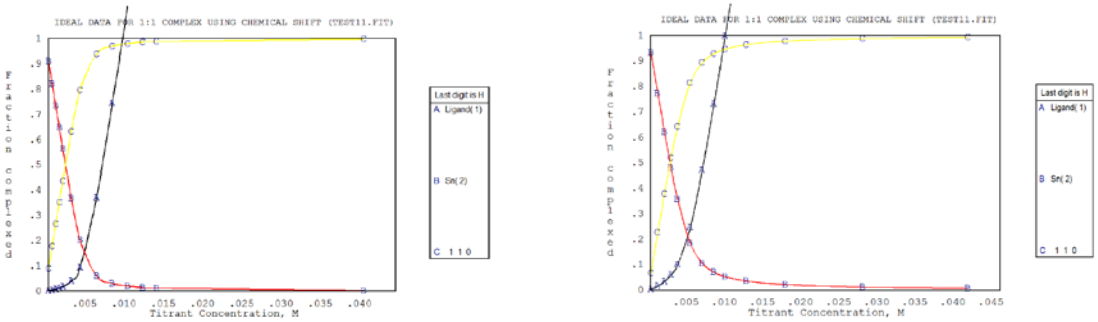

B1. 30 NMR species ratio for receptor **74** with $TBAH_2PO_4$ in DMSO-d_6 (left) and MeCN-d_3 (right), A = guest concentration, B = free host concentration and C = complex concentration.

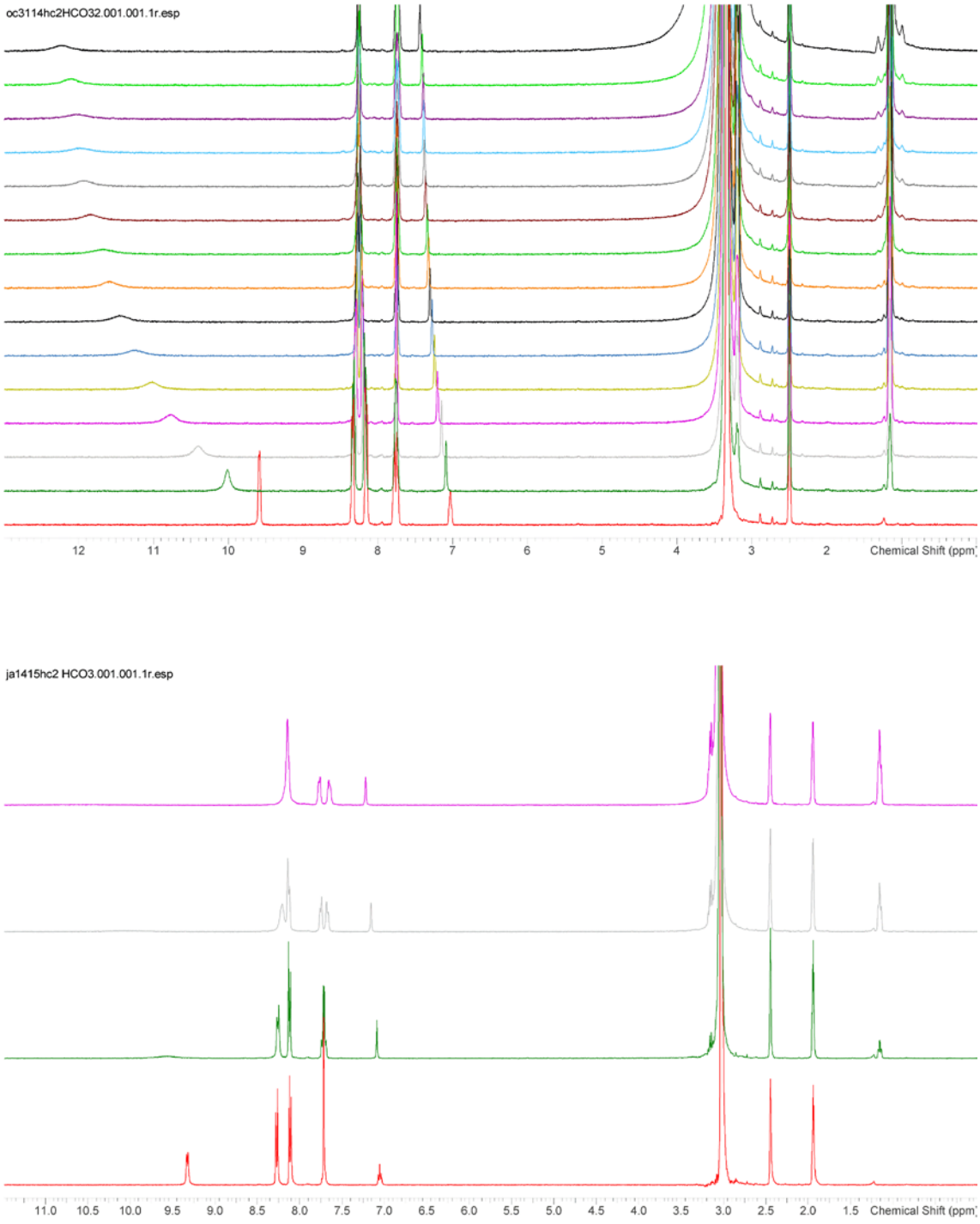

B1. 31 NMR titration spectra stack plot for receptor **74** with $TEAHCO_3$ in DMSO-d_6 (top) and MeCN-d_3 (bottom).

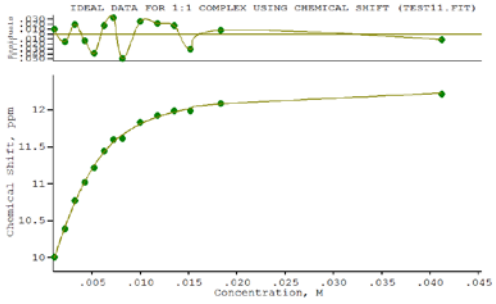

B1. 32 NMR binding curve for receptor **74** with $TEAHCO_3$ in DMSO-d_6 (left) K_a = 745 ± 52 M^{-1}.

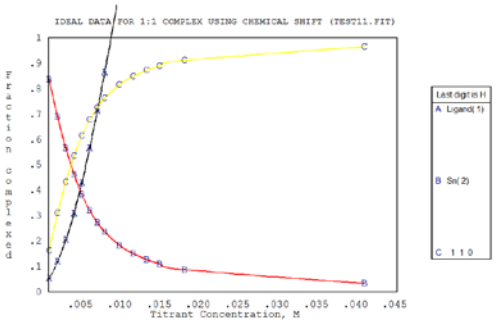

B1. 33 NMR species ratio for receptor **74** with $TEAHCO_3$ in DMSO-d_6; A = guest concentration, B = free host concentration and C = complex concentration.

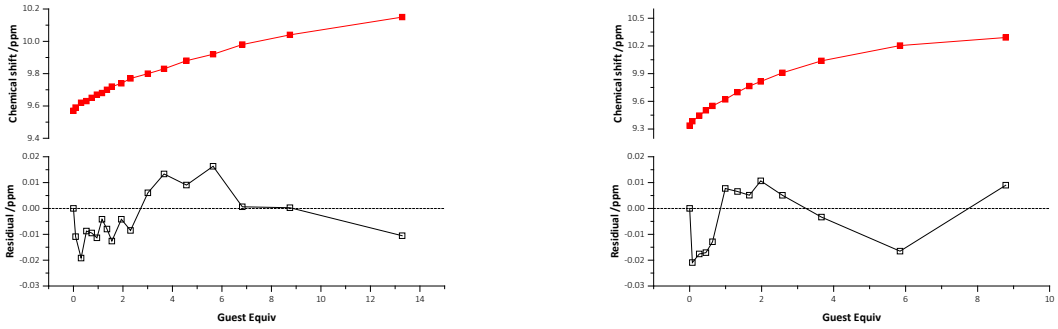

B1. 34 Bindfit NMR binding curve for receptor **74** with TBACl in DMSO-d_6 (left) K_a = 24 ± 4 M^{-1} and MeCN-d_3 (right) K_a = 76 ± 4 M^{-1}.

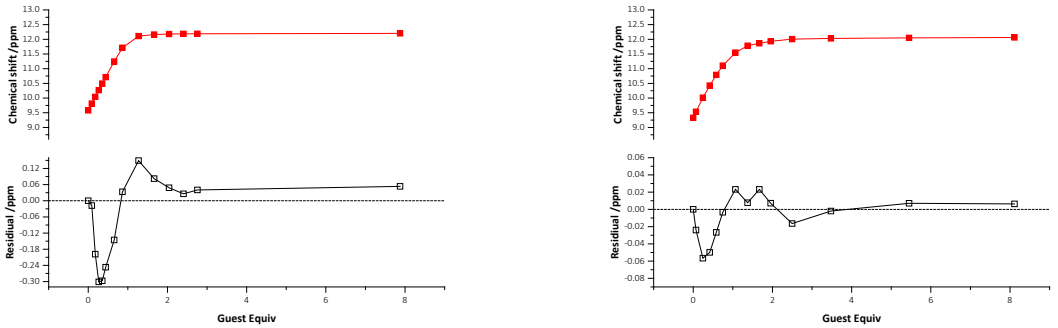

B1. 35 Bindfit NMR binding curve for receptor **74** with $TBAH_2PO_4$ in DMSO-d_6 (left) K_a = 16090 ± 243 M^{-1} and MeCN-d_3 (right) K_a = 3241 ± 12 M^{-1}.

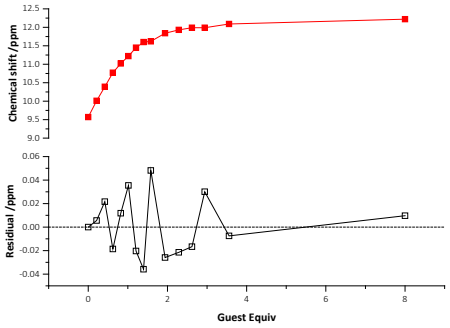

B1. 36 Bindfit NMR binding curve for receptor **74** with $TEAHCO_3$ in DMSO-d_6 (left) K_a = 755 ± 5M^{-1}

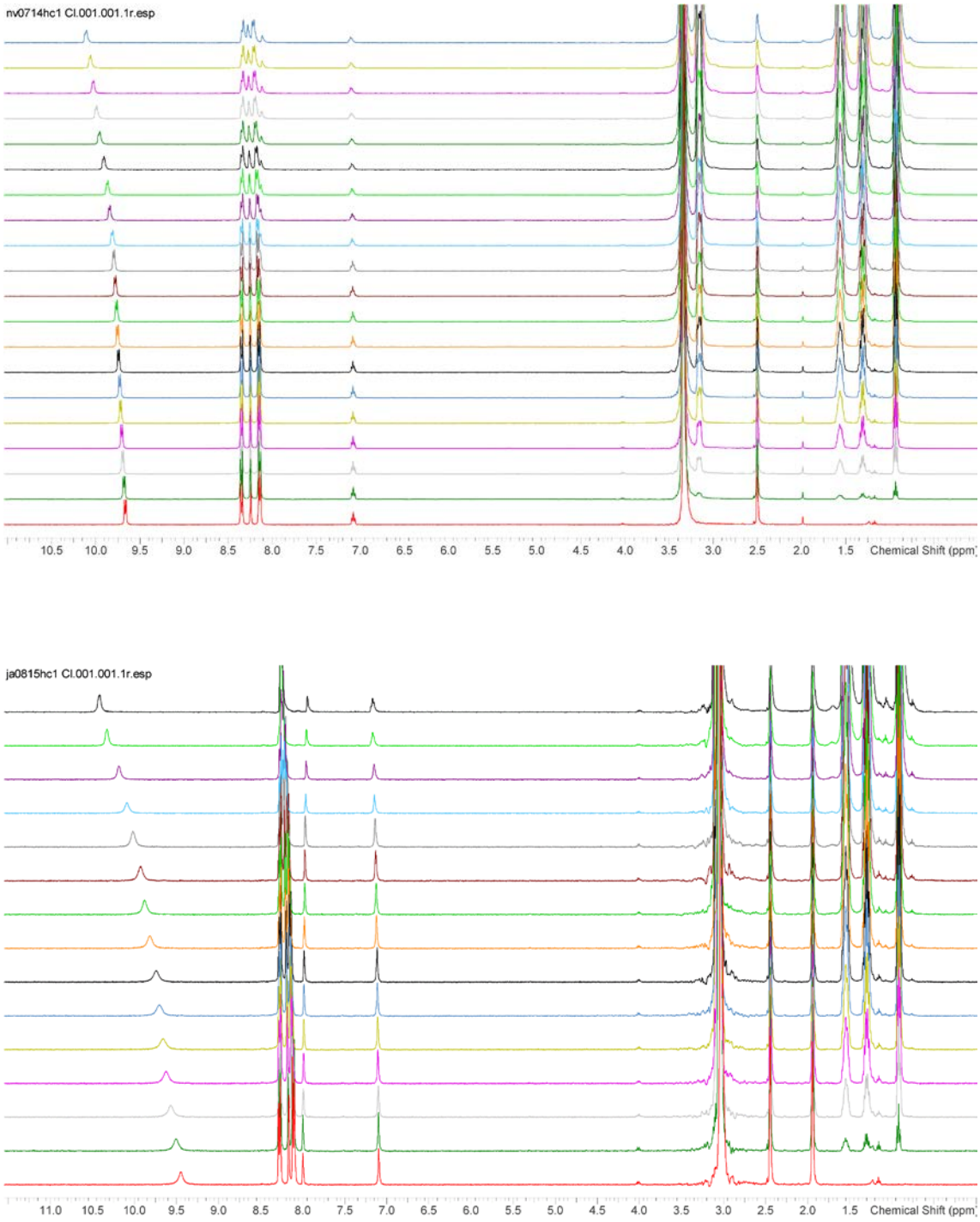

B1. 37 NMR titration spectra stack plot for receptor **75** with TBACl in DMSO-d_6 (top) and MeCN-d_3 (bottom).

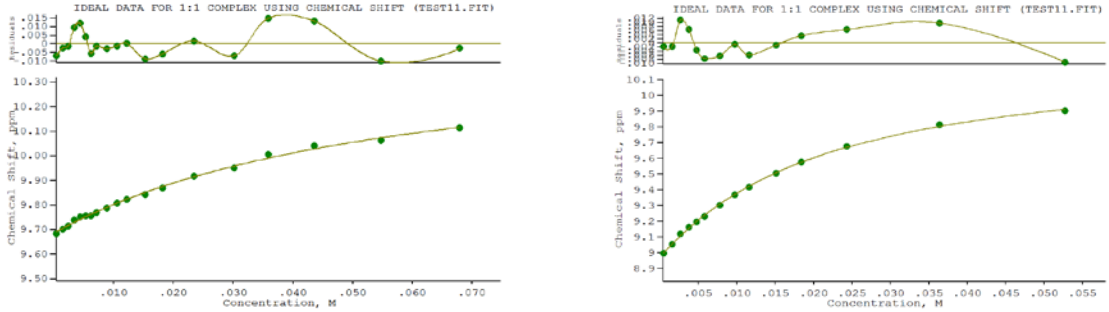

B1. 38 NMR binding curve for receptor **75** with TBACl in DMSO-d_6 (left) K_a = 18 ± 2 M^{-1} and MeCN-d_3 (right) K_a = 54 ± 2 M^{-1}.

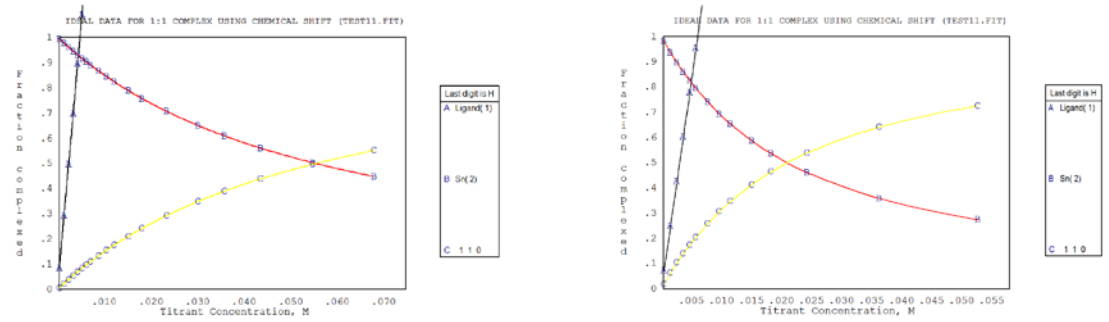

B1. 39 NMR species ratio for receptor **75** with TBACl in DMSO-d_6 (left) and MeCN-d_3 (right), A = guest concentration, B = free host concentration and C = complex concentration.

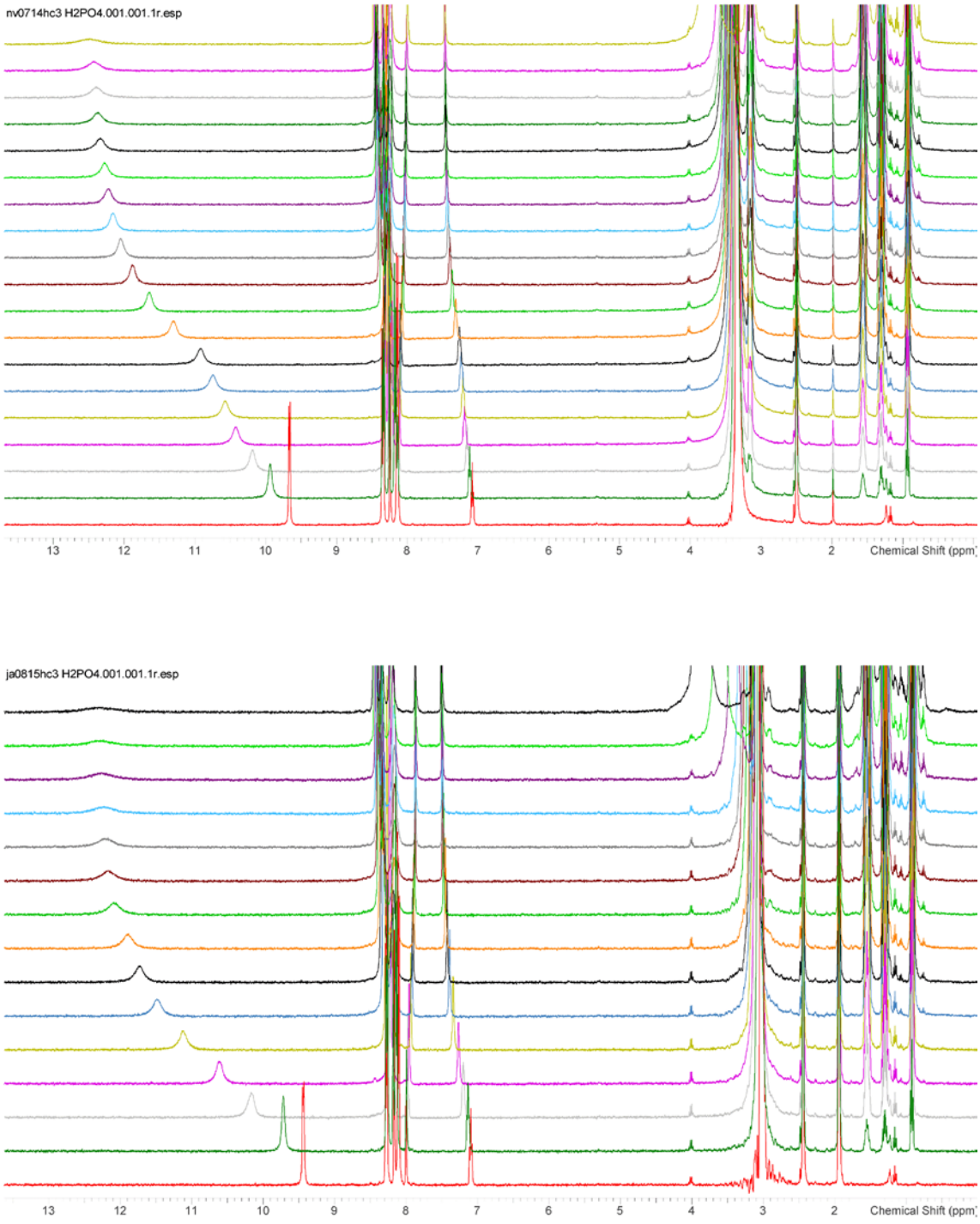

B1. 40 NMR titration spectra stack plot for receptor **75** with $TBAH_2PO_4$ in DMSO-d_6 (top) and MeCN-d_3 (bottom).

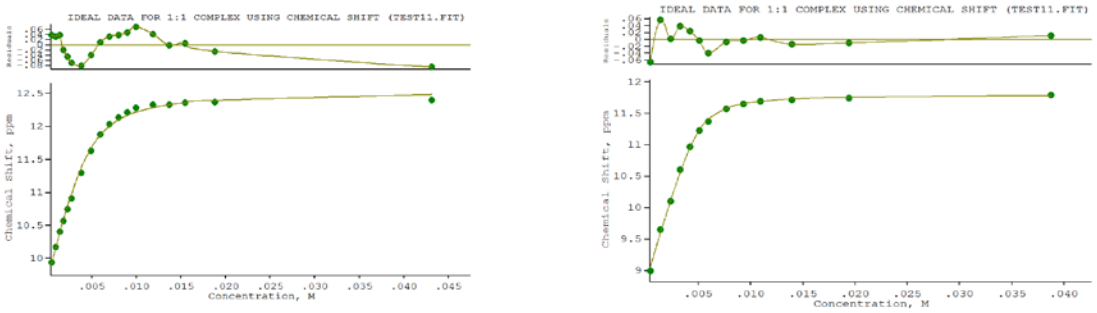

B1. 41 NMR binding curve for receptor **75** with $TBAH_2PO_4$ in DMSO-d_6 (left) K_a = 1350 ± 155 M^{-1} and MeCN-d_3 (right) K_a = 4030 ± 488 M^{-1}.

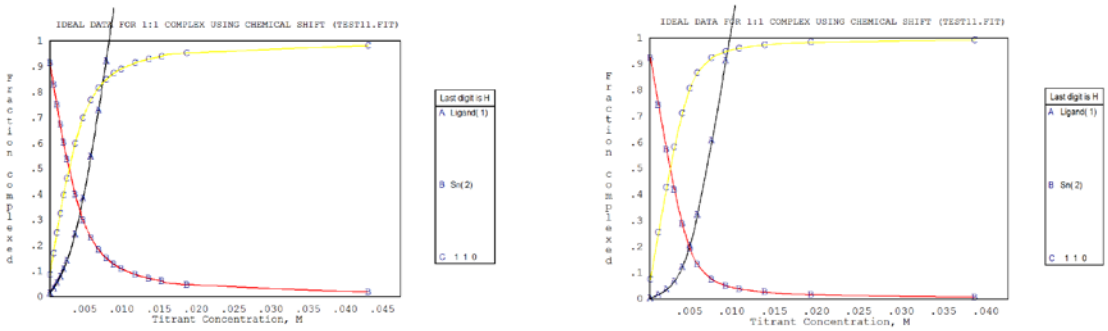

B1. 42 NMR species ratio for receptor **75** with $TBAH_2PO_4$ in DMSO-d_6 (left) and MeCN-d_3 (right), A = guest concentration, B = free host concentration and C = complex concentration.

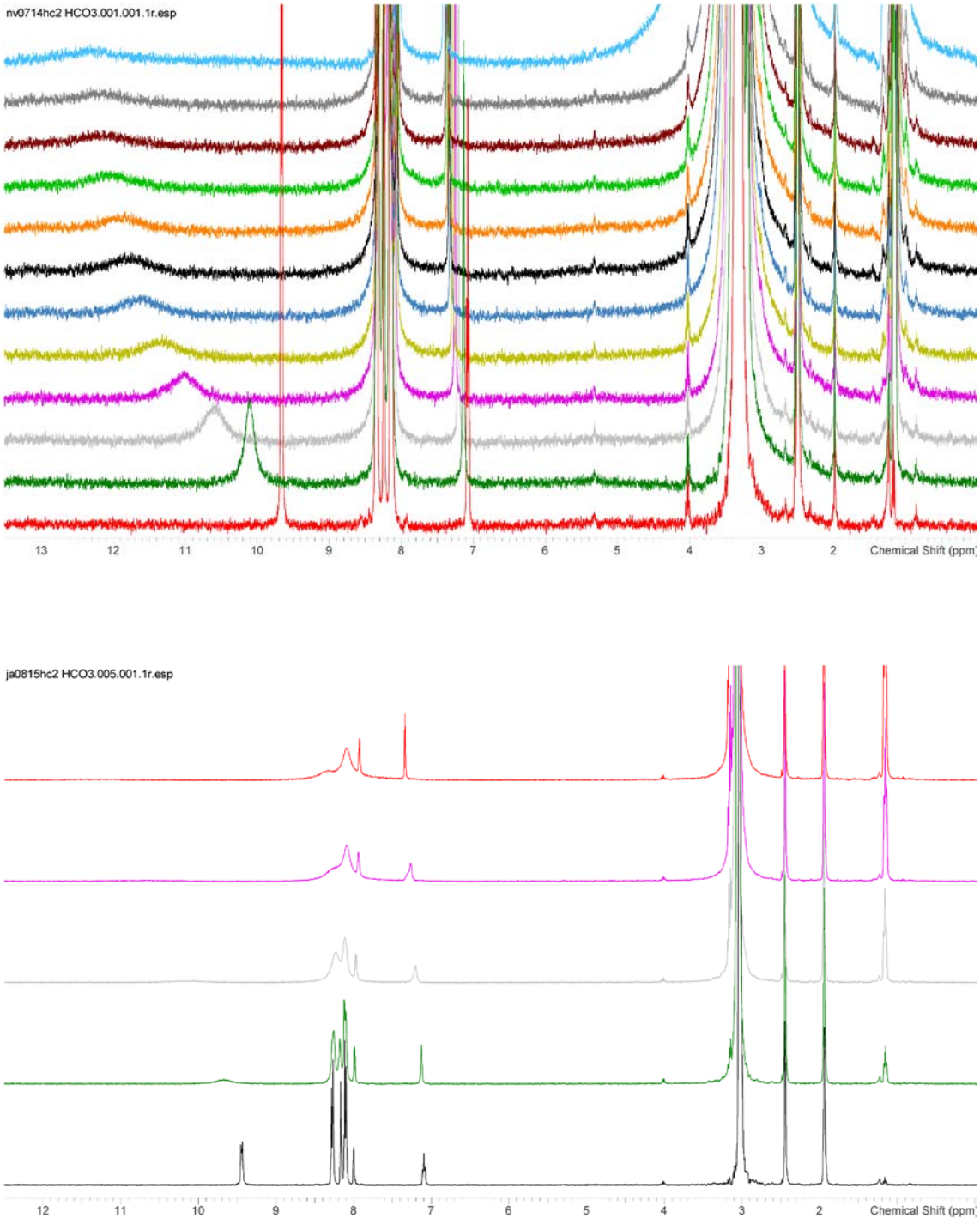

B1. 43 NMR titration spectra stack plot for receptor **75** with $TEAHCO_3$ in DMSO-d_6 (top) and MeCN-d_3 (bottom).

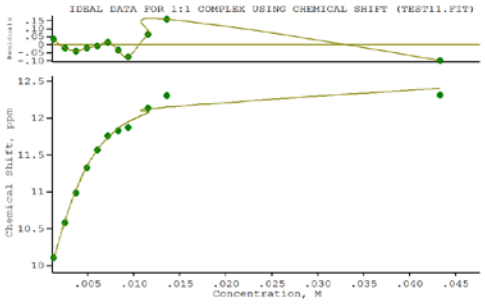

B1. 44 NMR binding curve for receptor **75** with $TEAHCO_3$ in DMSO-d_6 (left) K_a = 796 ± 500 M^{-1}.

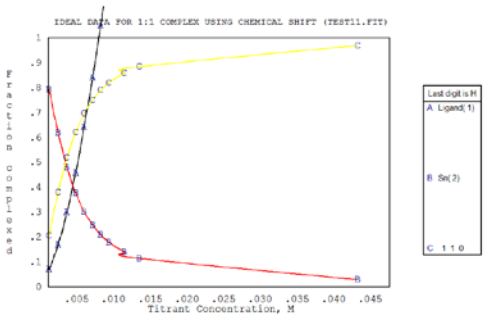

B1. 45 NMR species ratio for receptor **75** with $TEAHCO_3$ in DMSO-d_6; A = guest concentration, B = free host concentration and C = complex concentration.

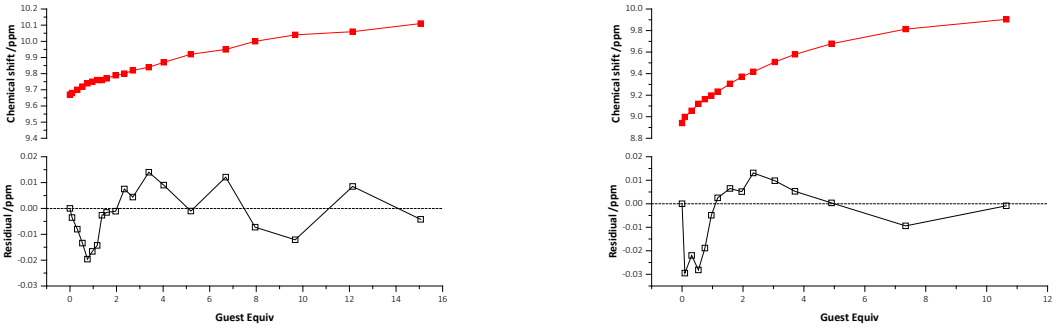

B1. 46 Bindfit NMR binding curve for receptor **75** with TBACl in DMSO-d_6 (left) K_a = 25 ± 4 M^{-1} and MeCN-d_3 (right) K_a = 66 ± 4 M^{-1}.

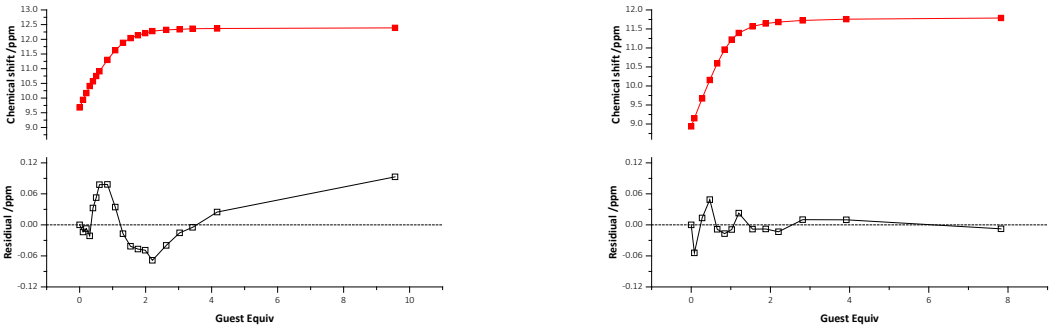

B1. 47 Bindfit NMR binding curve for receptor **75** with $TBAH_2PO_4$ in DMSO-d_6 (left) K_a = 1302 ± 10 M^{-1} and MeCN-d_3 (right) K_a = 3402 ± 9 M^{-1}.

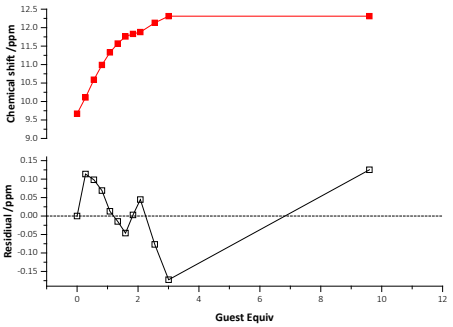

B1. 48 Bindfit NMR binding curve for receptor **75** with $TEAHCO_3$ in DMSO-d_6 (left) K_a = 616 ± 17 M^{-1}.

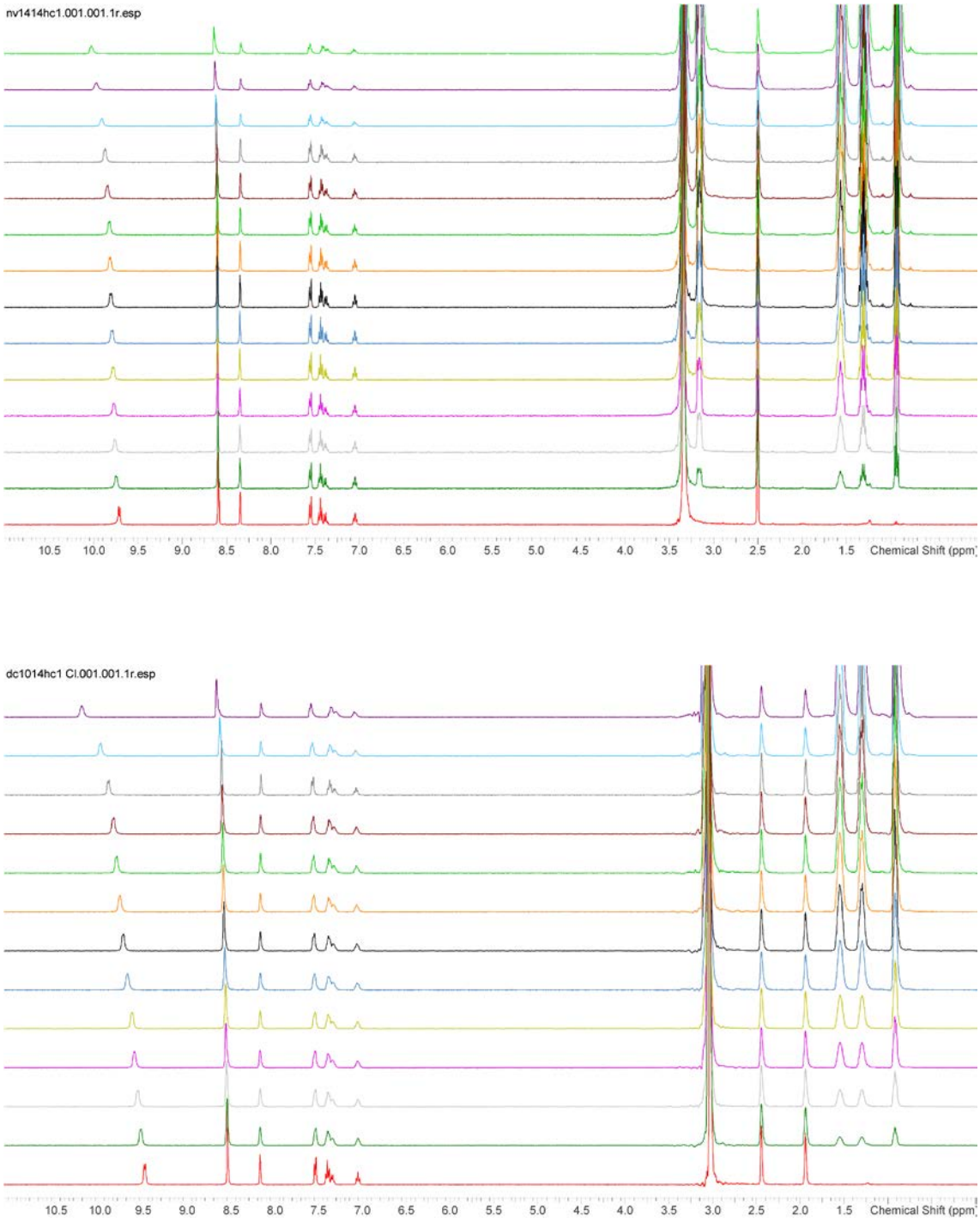

B1. 49 NMR titration spectra stack plot for receptor **76** with TBACl in DMSO-d_6 (left) and MeCN-d_3 (right).

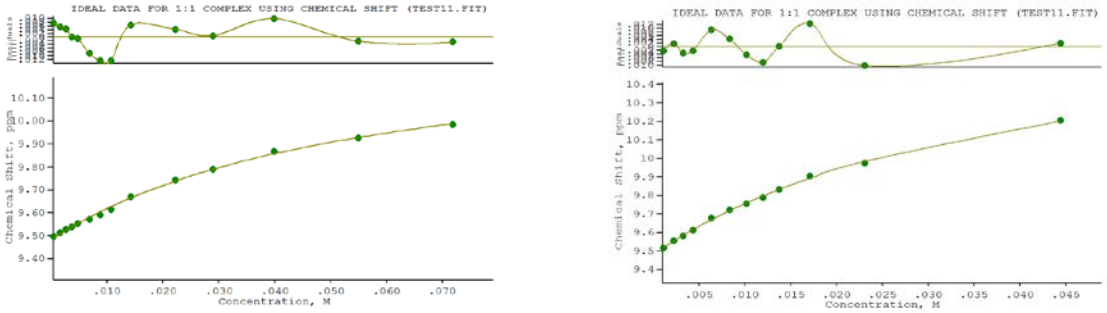

B1. 50 NMR binding curve for receptor **76** with TBACl in DMSO-d_6 (left) K_a = 11 ± 3 M^{-1} and MeCN-d_3 (right) K_a = 27 ± 2 M^{-1}.

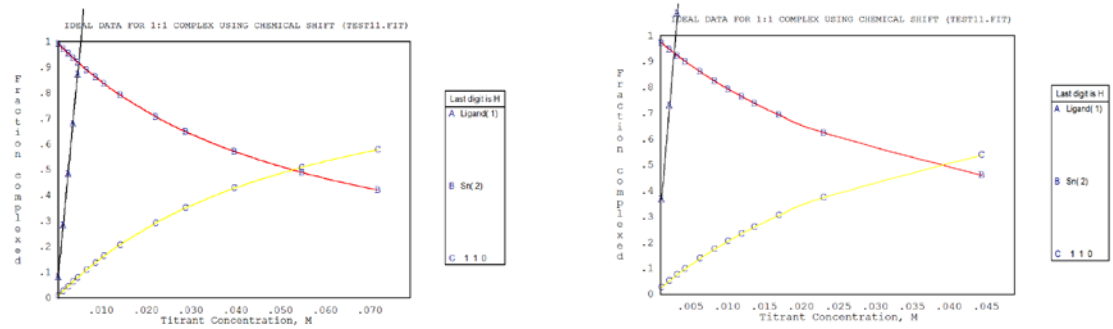

B1. 51 NMR species ratio for receptor **76** with TBACl in DMSO-d_6 (left) and MeCN-d_3 (right), A = guest concentration, B = free host concentration and C = complex concentration.

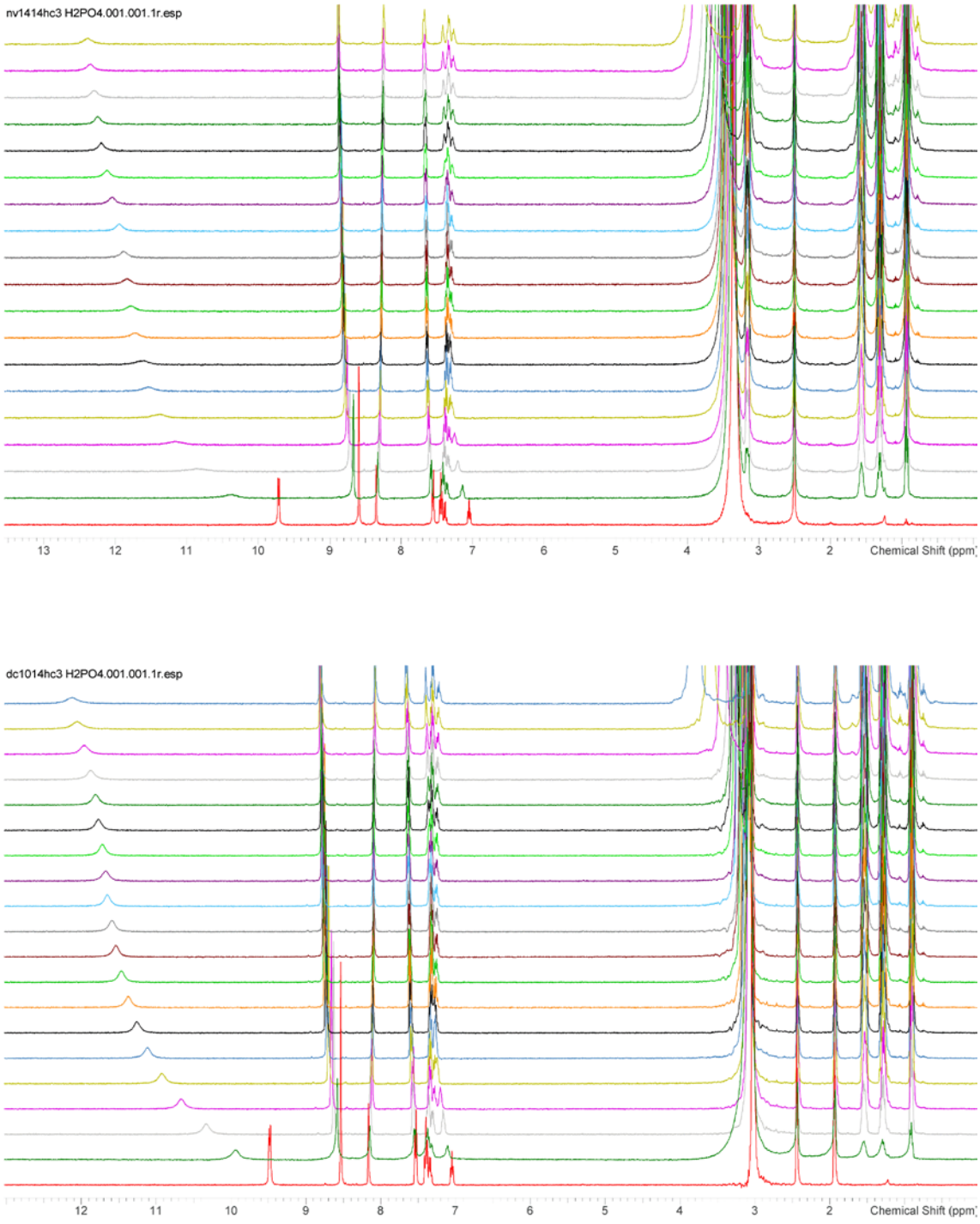

B1. 52 NMR titration spectra stack plot for receptor **76** with $TBAH_2PO_4$ in DMSO-d_6 (top) and MeCN-d_3 (bottom).

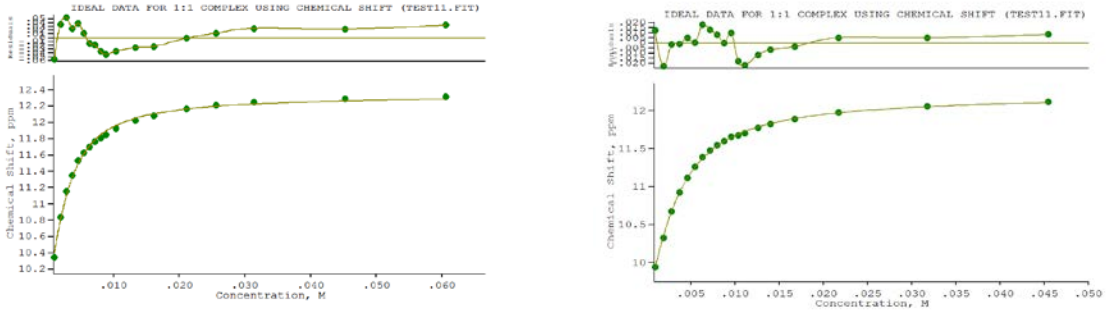

B1. 53 NMR binding curve for receptor **76** with $TBAH_2PO_4$ in DMSO-d_6 (left) K_a = 673 ± 48 M^{-1} and MeCN-d_3 (right) K_a = 530 ± 12 M^{-1}.

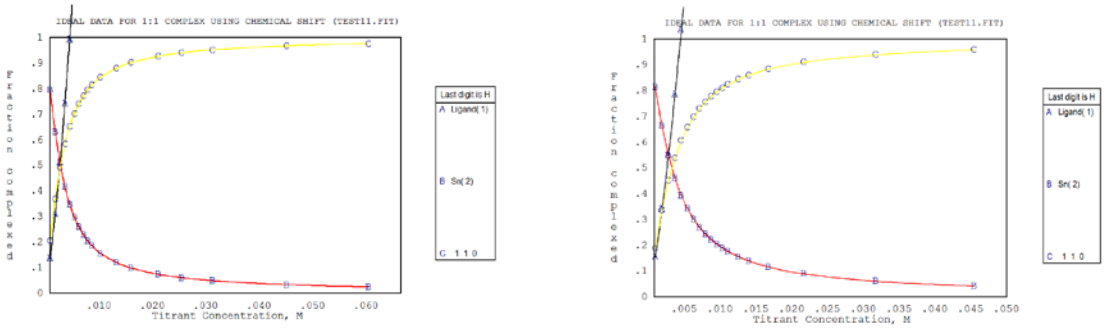

B1. 54 NMR species ratio for receptor **76** with $TBAH_2PO_4$ in DMSO-d_6 (left) and MeCN-d_3 (right), A = guest concentration, B = free host concentration and C = complex concentration.

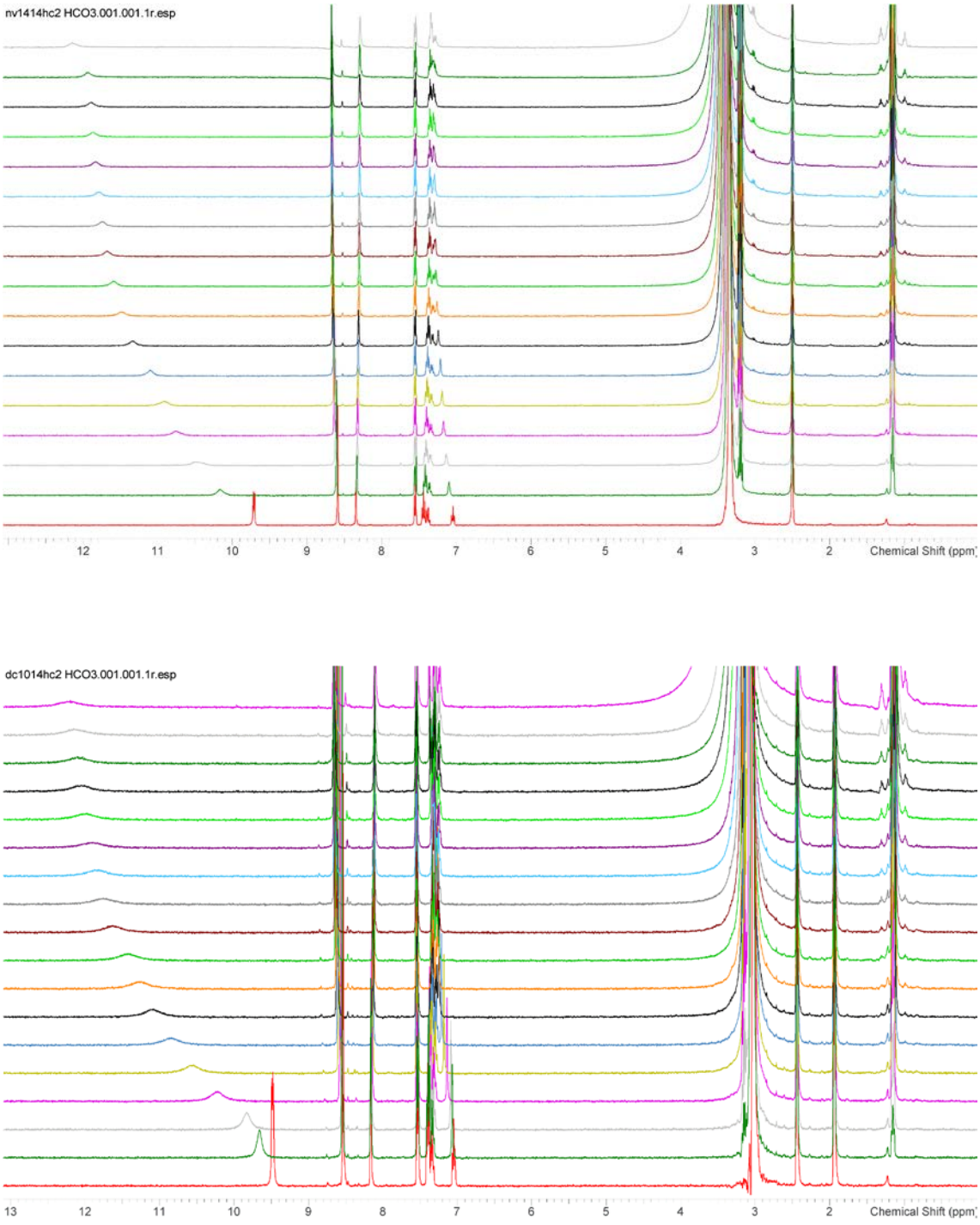

B1. 55 NMR titration spectra stack plot for receptor **76** with $TEAHCO_3$ in DMSO-d_6 (top) and MeCN-d_3 (bottom).

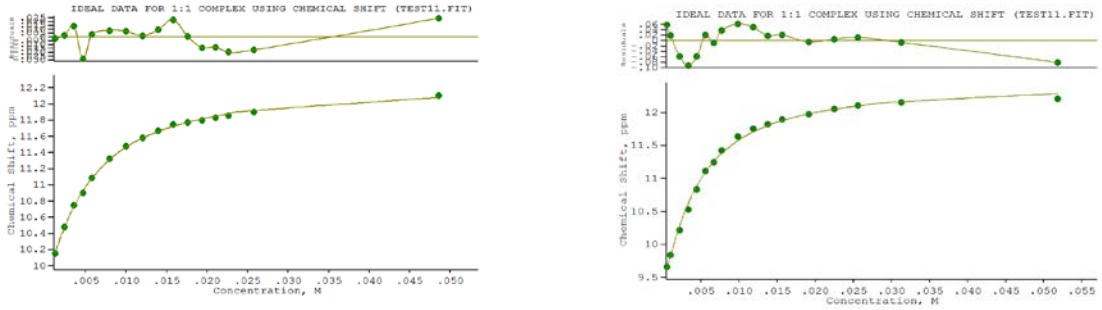

B1. 56 NMR binding curve for receptor **76** with $TEAHCO_3$ in DMSO-d_6 (left) K_a = 266 ± 10 M^{-1} and MeCN-d_3 (right) K_a = 314 ± 21 M^{-1}.

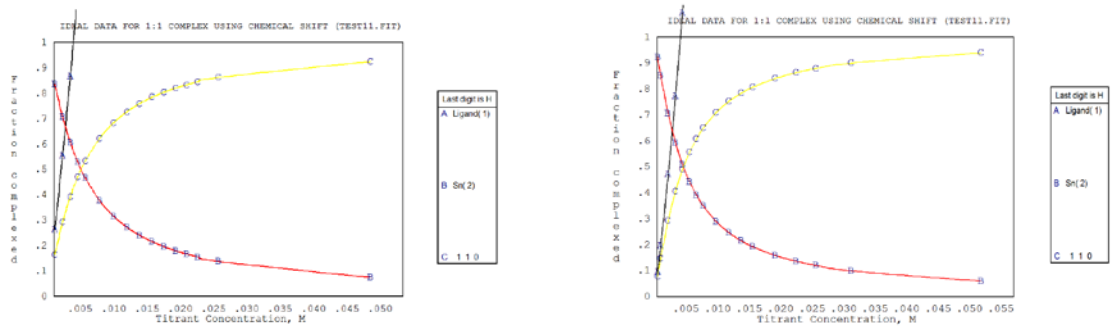

B1. 57 NMR species ratio for receptor **76** with $TEAHCO_3$ in DMSO-d_6 (left) MeCN-d_3 (right), A = guest concentration, B = free host concentration and C = complex concentration.

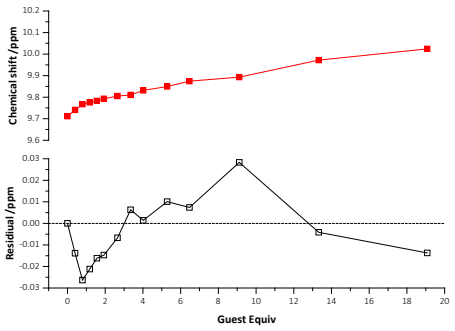

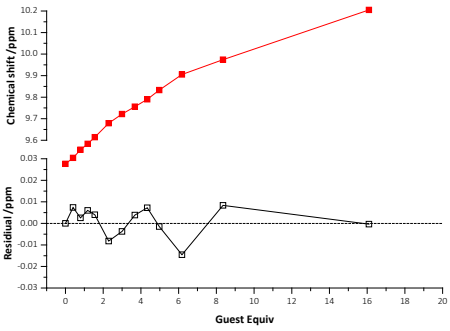

B1. 58 Bindfit NMR binding curve for receptor **76** with TBACl in DMSO-d_6 (left) K_a = 33 ± 12 M^{-1} and MeCN-d_3 (right) K_a = 26 ± 2 M^{-1}.

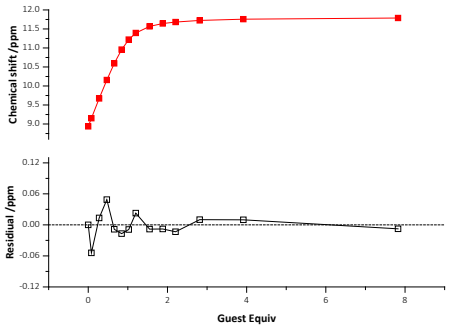

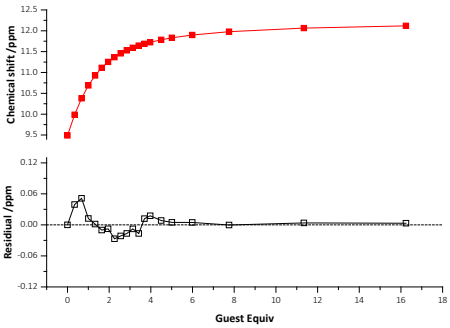

B1. 59 Bindfit NMR binding curve for receptor **76** with $TBAH_2PO_4$ in DMSO-d_6 (left) K_a = 3402 ± 9 M^{-1} and MeCN-d_3 (right) K_a = 484 ± 2 M^{-1}.

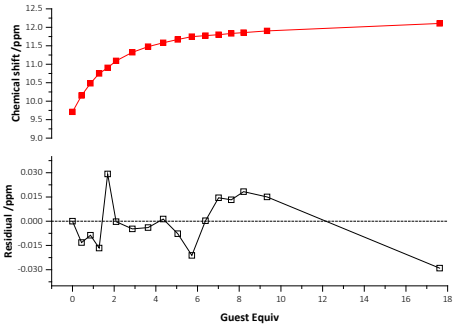

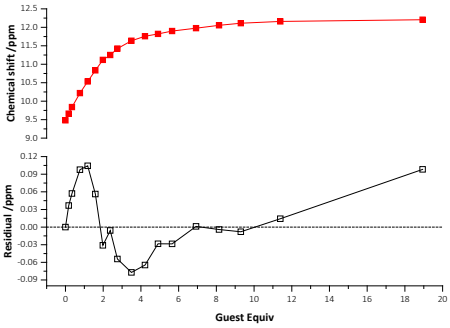

B1. 60 Bindfit NMR binding curve for receptor **76** with $TEAHCO_3$ in DMSO-d_6 (left) K_a = 276 ± 2 M^{-1} and MeCN-d_3 (right) K_a = 277 ± 6 M^{-1}.

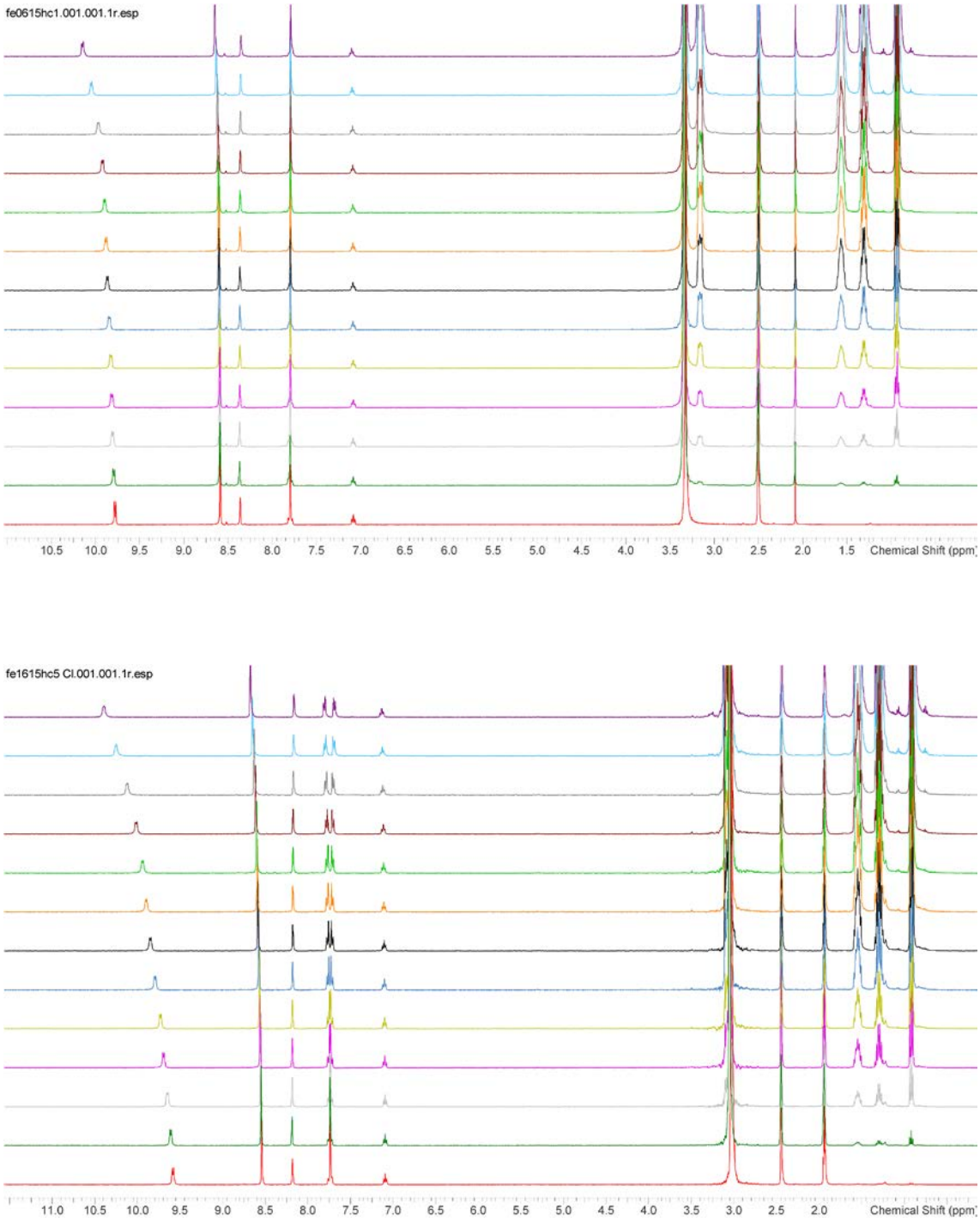

B1. 61 NMR titration spectra stack plot for receptor **77** with TBACl in DMSO-d_6 (top) and MeCN-d_3 (bottom).

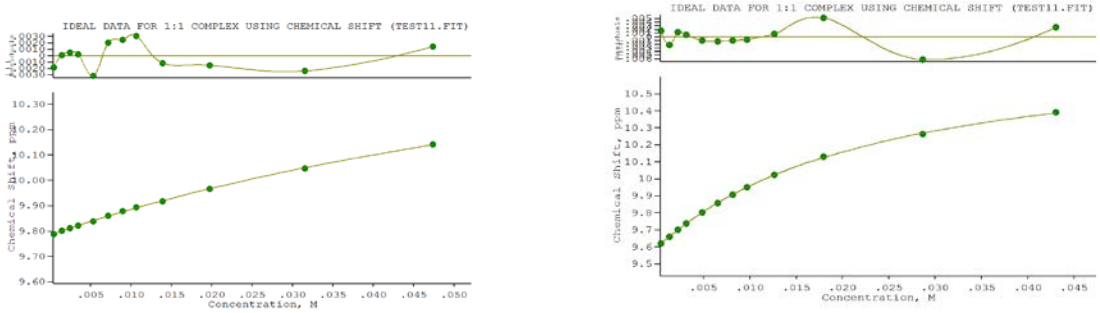

B1. 62 NMR binding curve for receptor **77** with TBACl in DMSO-d_6 (left) K_a = 10 ± 7 M^{-1} and MeCN-d_3 (right) K_a = 49 ± 11 M^{-1}.

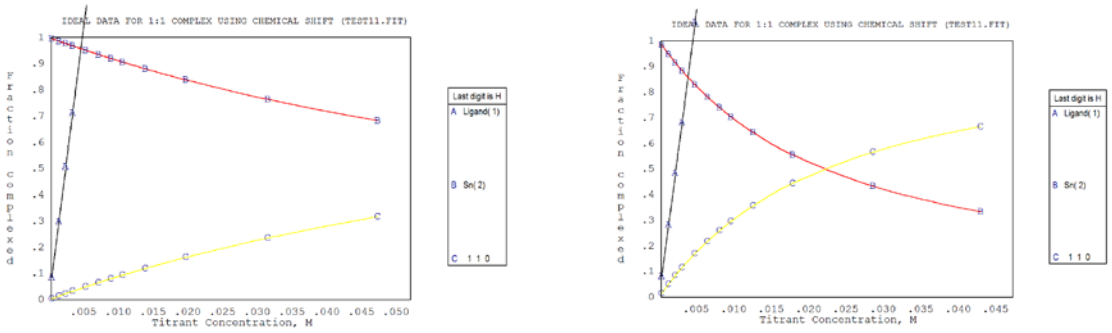

B1. 63 NMR species ratio for receptor **77** with TBACl in DMSO-d_6 (left) and MeCN-d_3 (right), A = guest concentration, B = free host concentration and C = complex concentration.

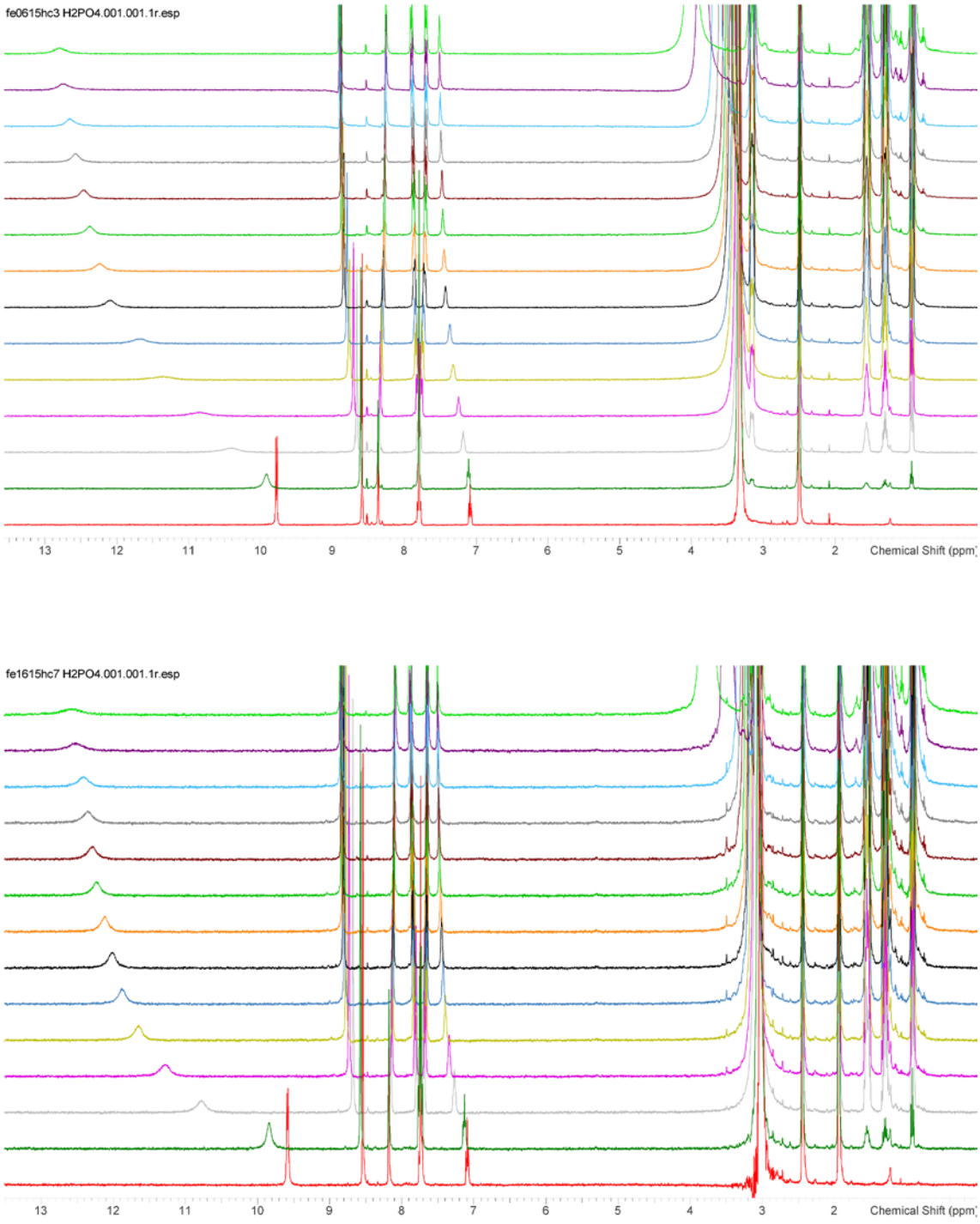

B1. 64 NMR titration spectra stack plot for receptor **77** with $TBAH_2PO_4$ in DMSO-d_6 (top) and MeCN-d_3 (bottom).

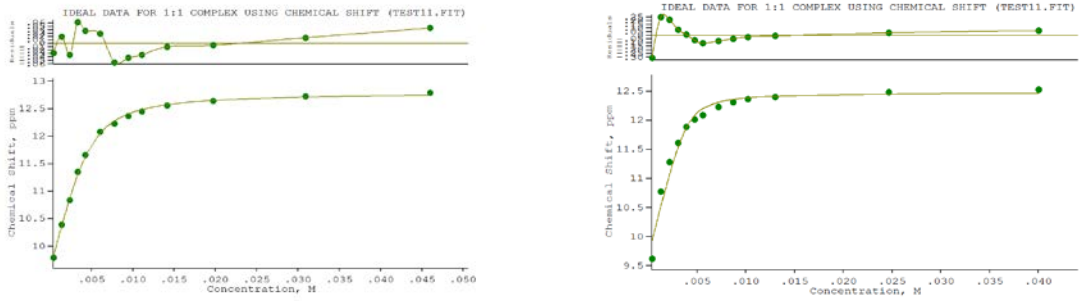

B1. 65 NMR binding curve for receptor **77** with $TBAH_2PO_4$ in DMSO-d_6 (left) K_a = 1320 ± 114 M^{-1} and MeCN-d_3 (right) K_a = 4370 ± 200 M^{-1}.

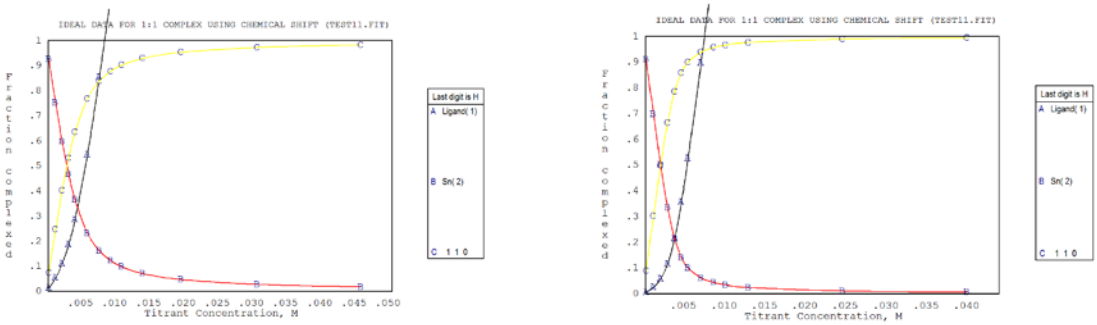

B1. 66 NMR species ratio for receptor **77** with $TBAH_2PO_4$ in DMSO-d_6 (left) and MeCN-d_3 (right), A = guest concentration, B = free host concentration and C = complex concentration.

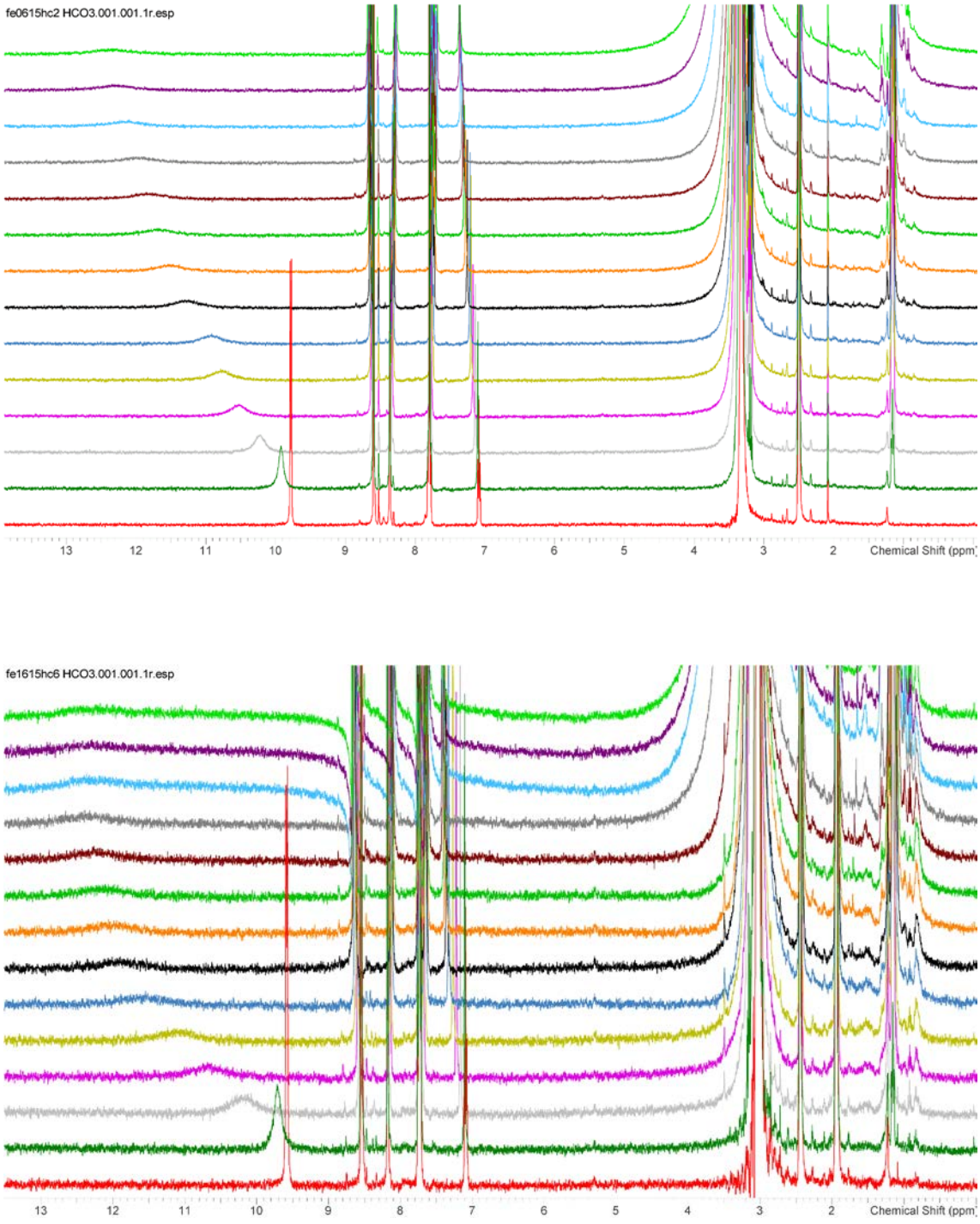

B1. 67 NMR titration spectra stack plot for receptor **77** with $TEAHCO_3$ in DMSO-d_6 (top) and MeCN-d_3 (bottom).

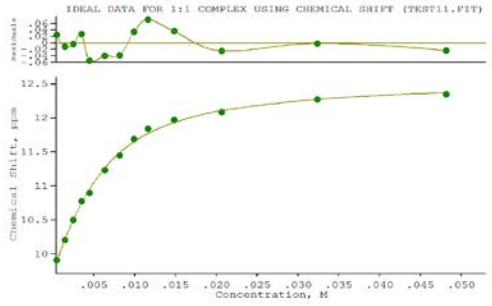

B1. 68 NMR binding curve for receptor **77** with $TEAHCO_3$ in DMSO-d_6 (left) K_a = 307 ± 24 M^{-1}.

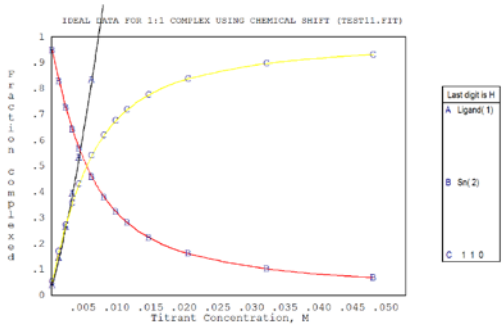

B1. 69 NMR species ratio for receptor **77** with $TEAHCO_3$ in DMSO-d_6; A = guest concentration, B = free host concentration and C = complex concentration.

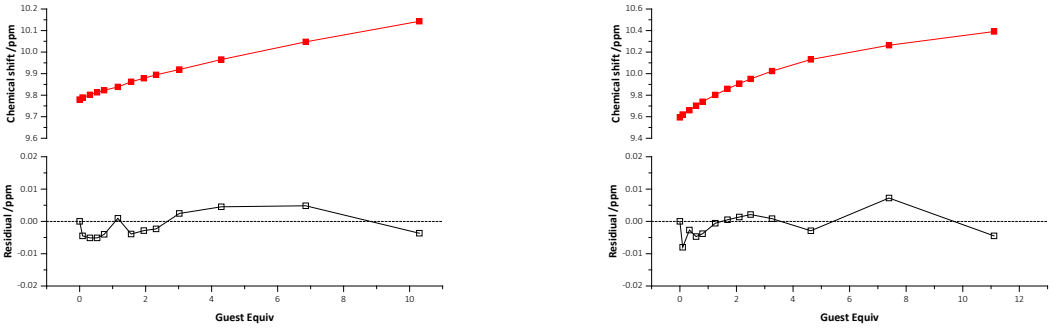

B1. 70 Bindfit NMR binding curve for receptor **77** with TBACl in DMSO-d_6 (left) K_a = 13 ± 2 M^{-1} and MeCN-d_3 (right) K_a = 52 ± 1 M^{-1}.

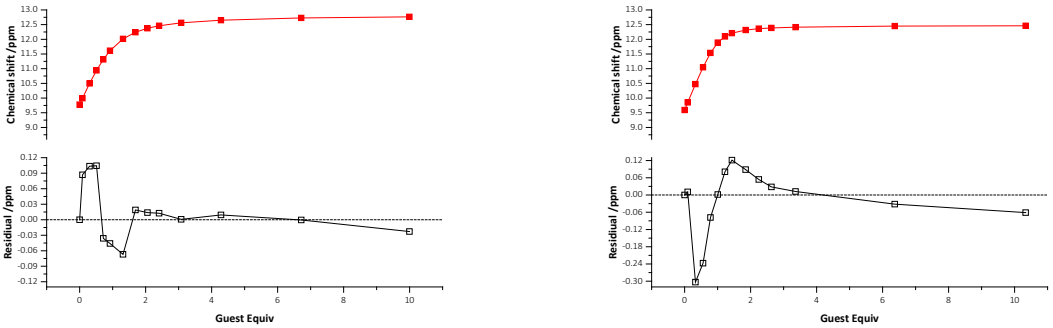

B1. 71 Bindfit NMR binding curve for receptor **77** with $TBAH_2PO_4$ in DMSO-d_6 (left) K_a = 1017 ± 12 M^{-1} and MeCN-d_3 (right) K_a = 4778 ± 54 M^{-1}.

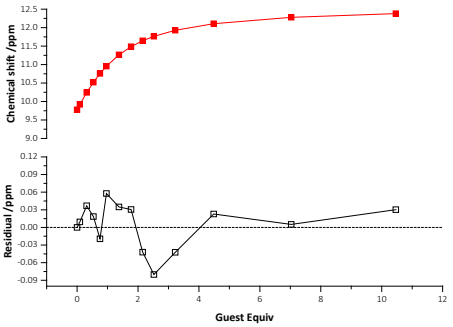

B1. 72 Bindfit NMR binding curve for receptor **77** with $TEAHCO_3$ in DMSO-d_6 (left) K_a = 290 ± 6 M^{-1}.

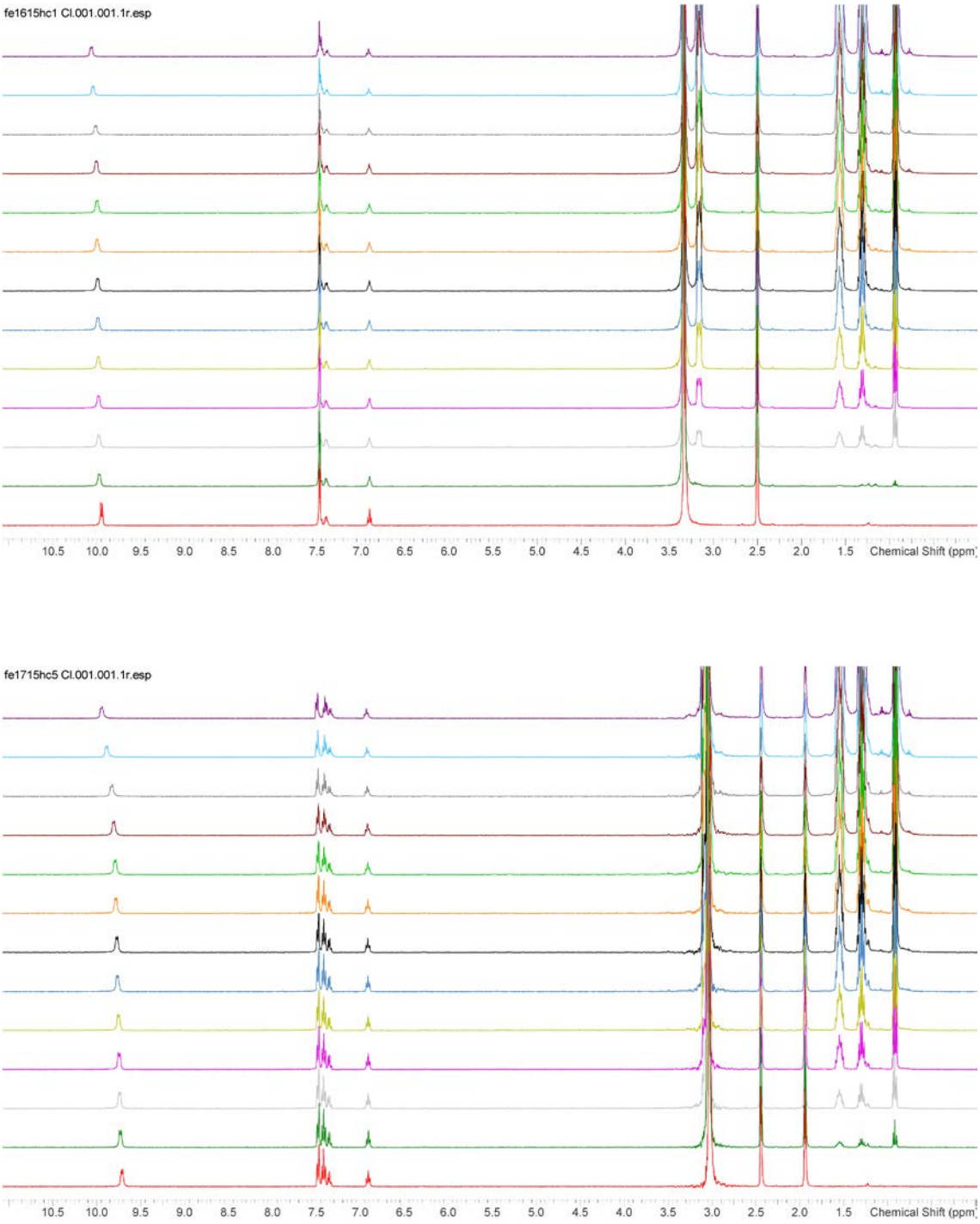

B1. 73 NMR titration spectra stack plot for receptor **78** with TBACl in DMSO-d_6 (top) and MeCN-d_3 (bottom).

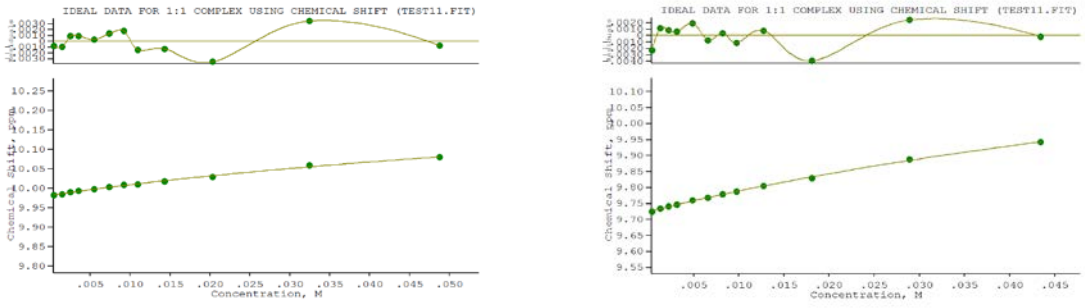

B1. 74 NMR binding curve for receptor **78** with TBACl in DMSO-d_6 (left) and MeCN-d_3 (right).

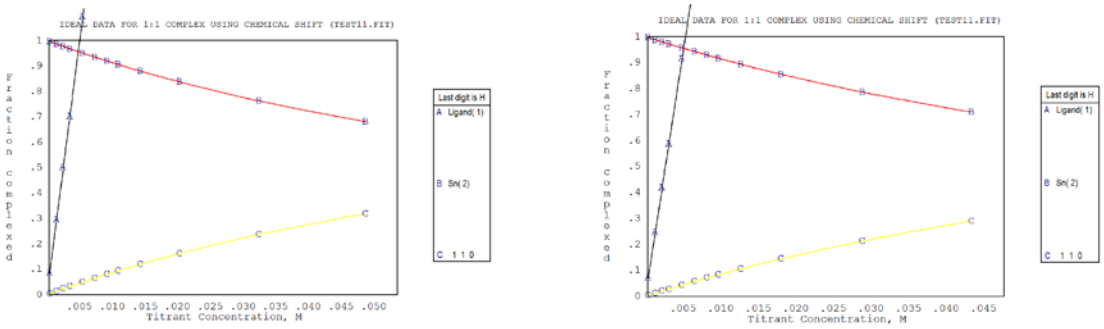

B1. 75 NMR species ratio for receptor **78** with TBACl in DMSO-d_6 (left) and MeCN-d_3 (right), A = guest concentration, B = free host concentration and C = complex concentration.

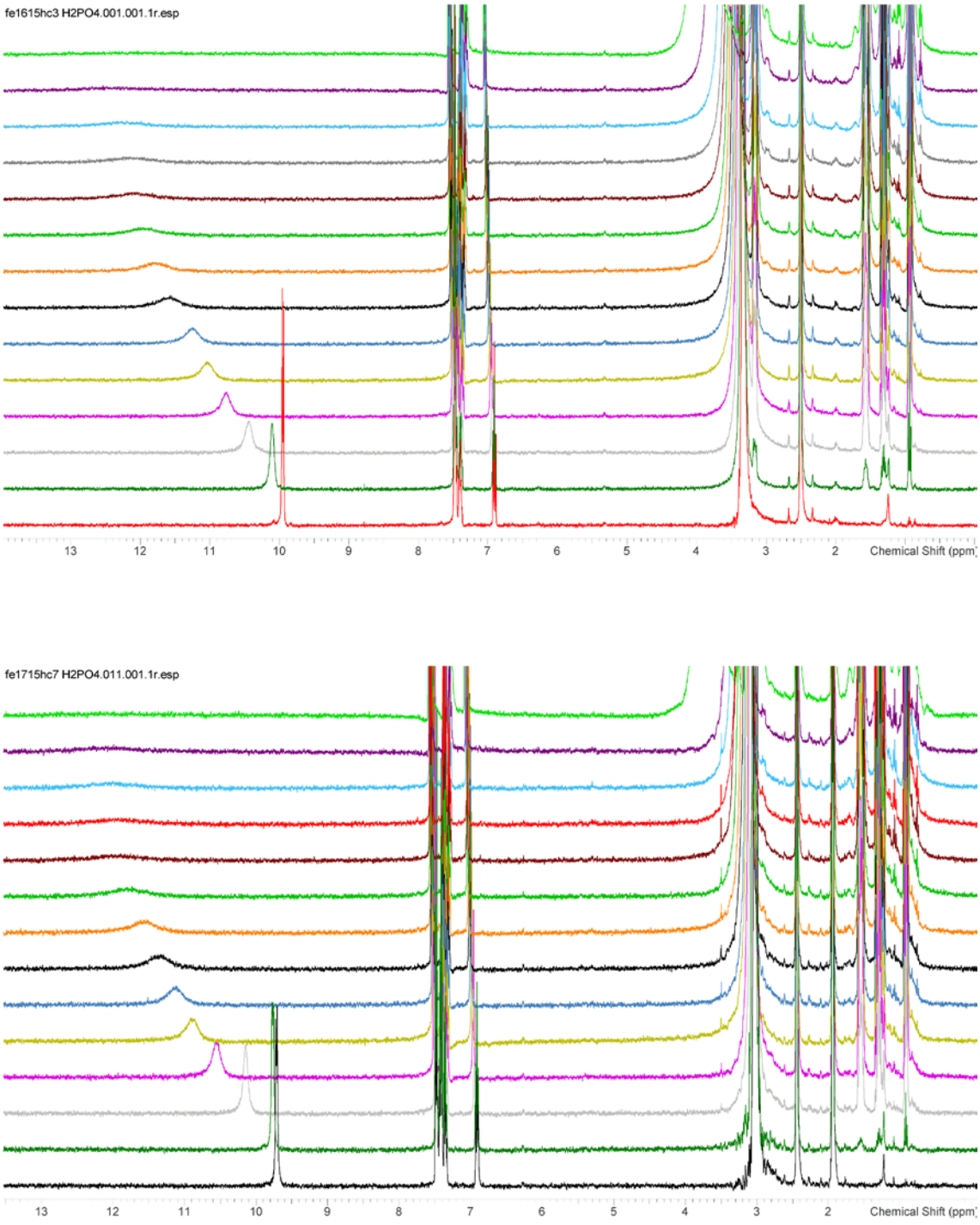

B1. 76 NMR titration spectra stack plot for receptor **78** with $TBAH_2PO_4$ in DMSO-d_6 (top) and MeCN-d_3 (bottom).

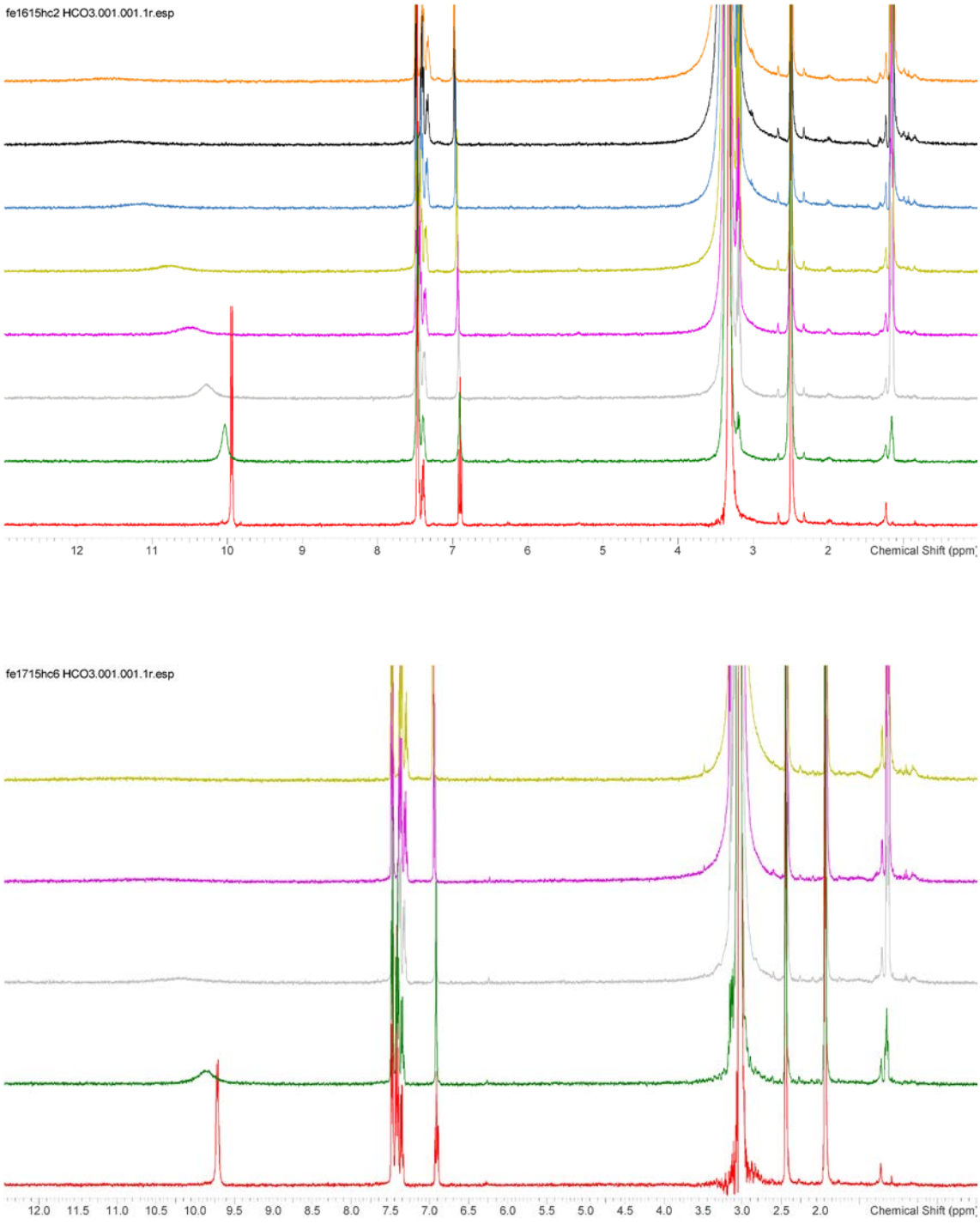

B1. 77 NMR titration spectra stack plot for receptor **78** with $TEAHCO_3$ in DMSO-d_6 (top) and MeCN-d_3 (bottom).

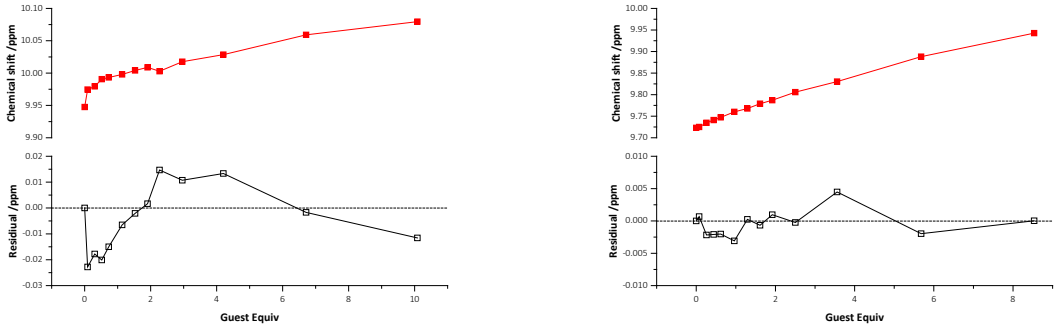

B1. 78 Bindfit NMR binding curve for receptor **78** with TBACl in DMSO-d_6 (left) K_a = 107 ± 38 M^{-1} and MeCN-d_3 (right) K_a = 11 ± 2 M^{-1}.

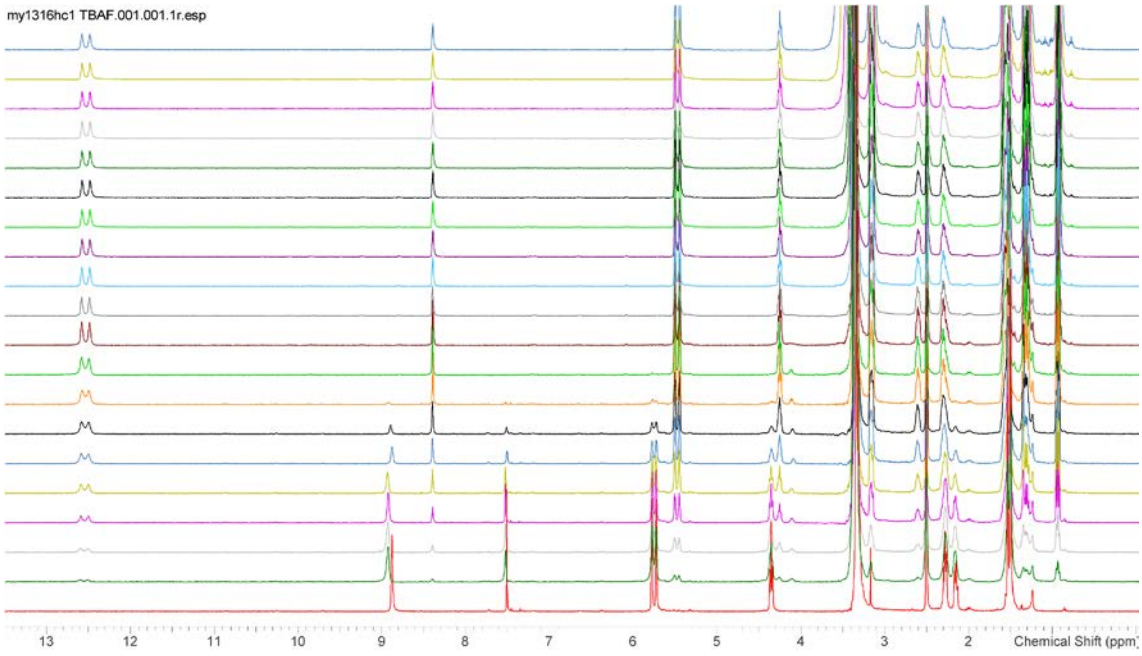

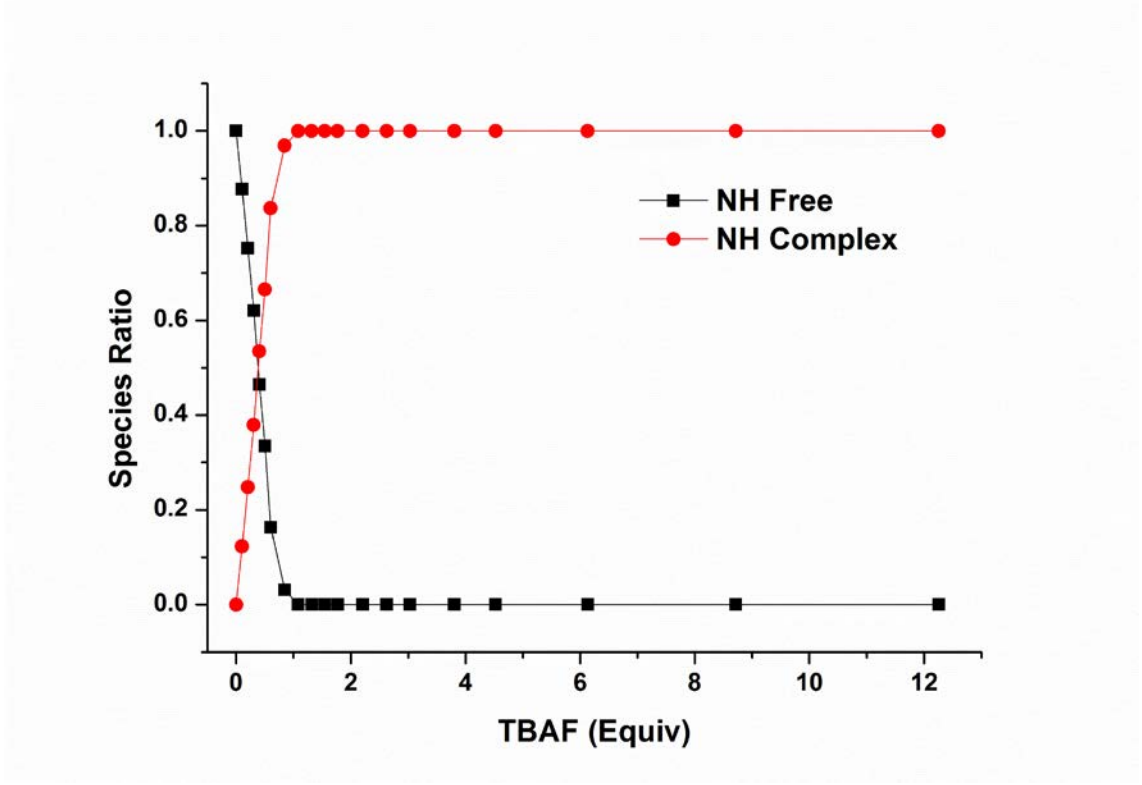

B1. 79 NMR titration spectra stack plot for receptor **16** with TBAF (top) and species ratio plot (bottom) in DMSO-d_6.

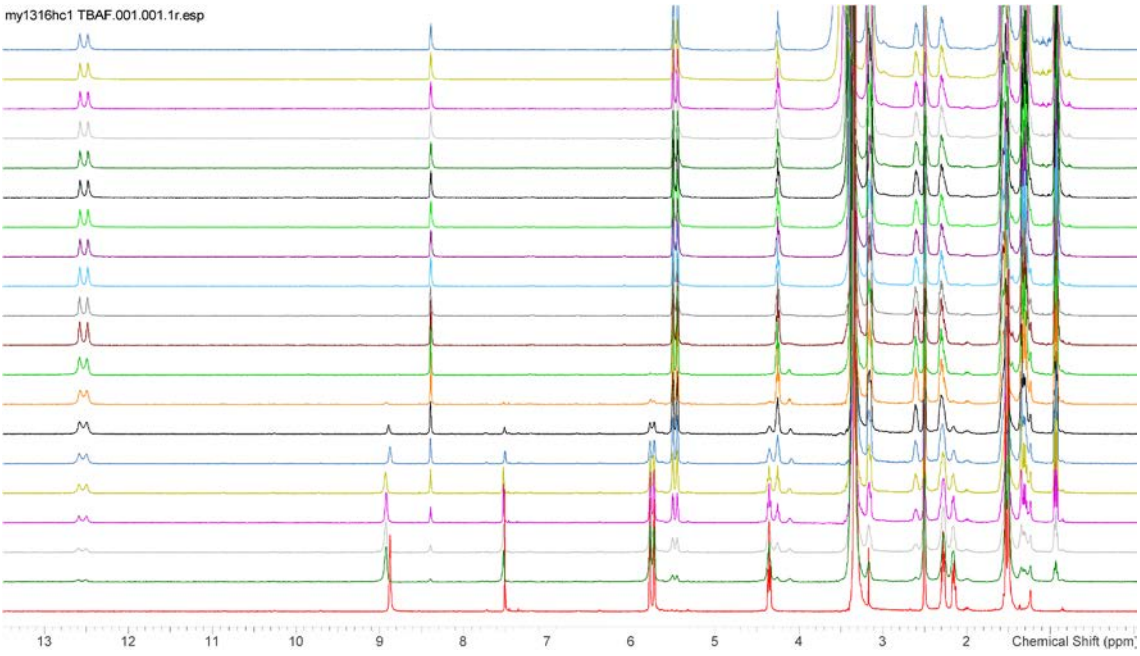

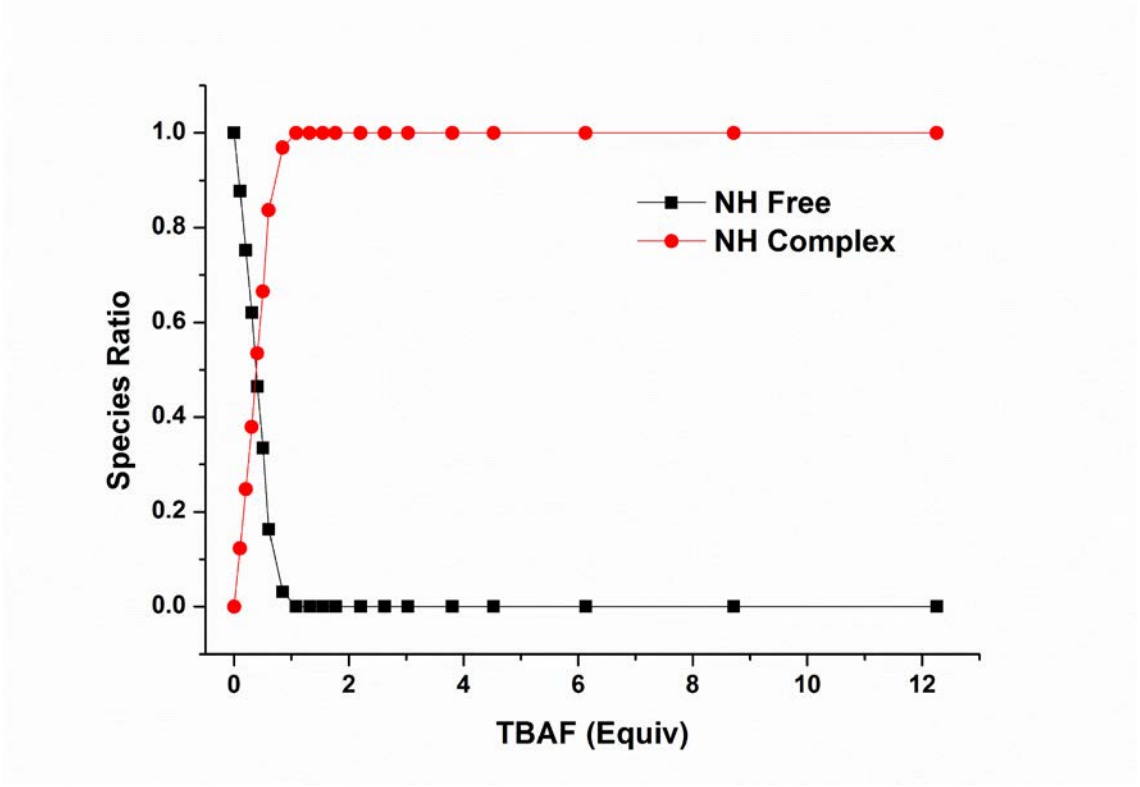

B1. 80 NMR titration spectra stack plot for receptor **79** with TBAF (top) and species ratio plot (bottom) in DMSO-d_6.

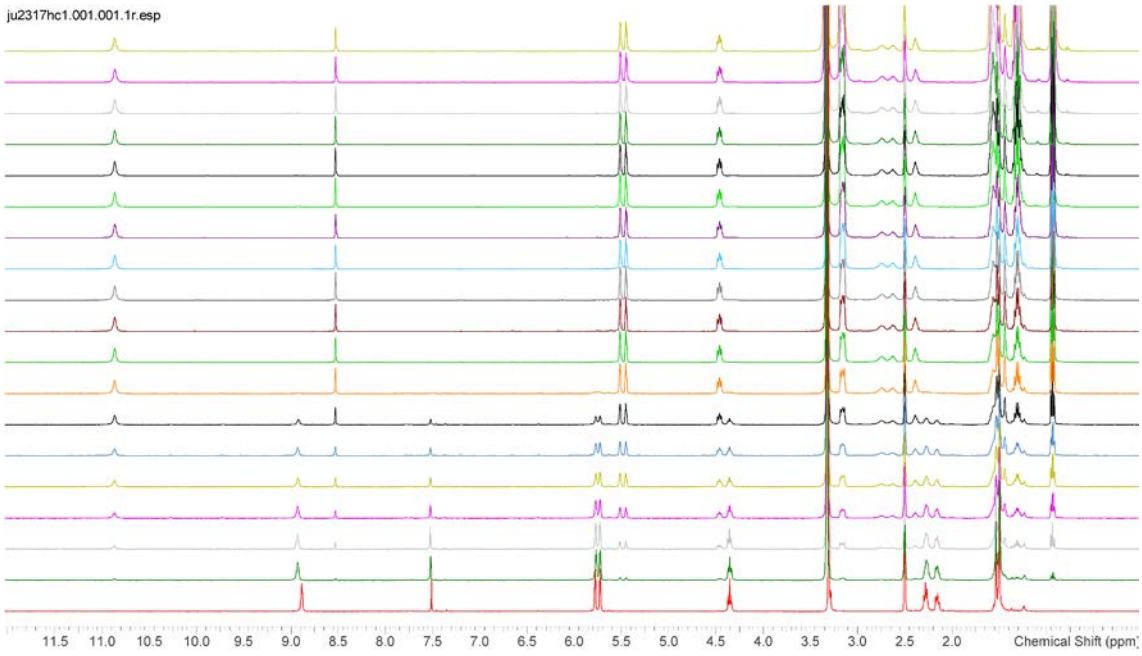

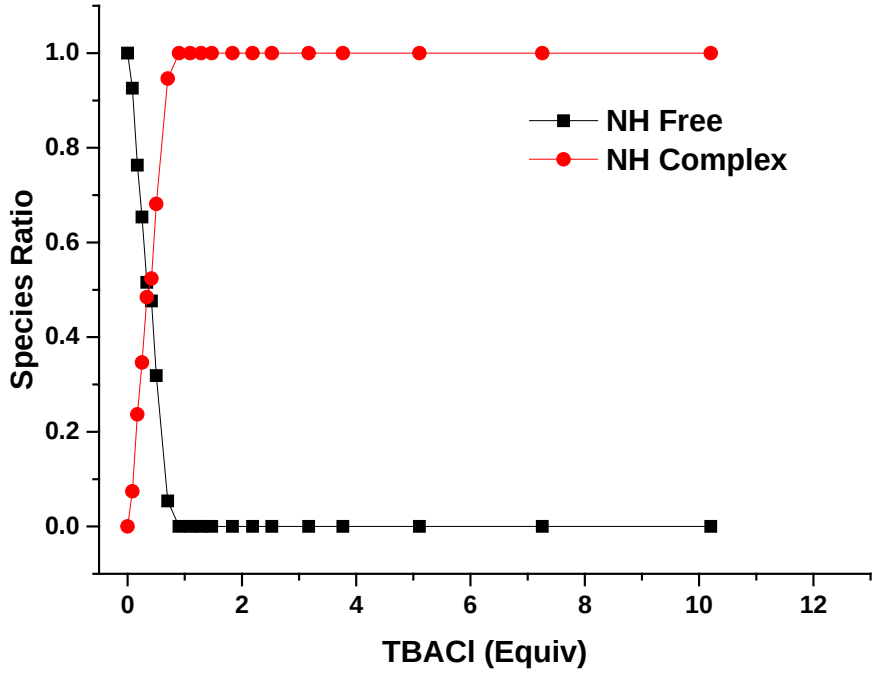

B1. 81 NMR titration spectra stack plot for receptor **79** with TBACl (top) and species ratio plot (bottom) in DMSO-d_6.

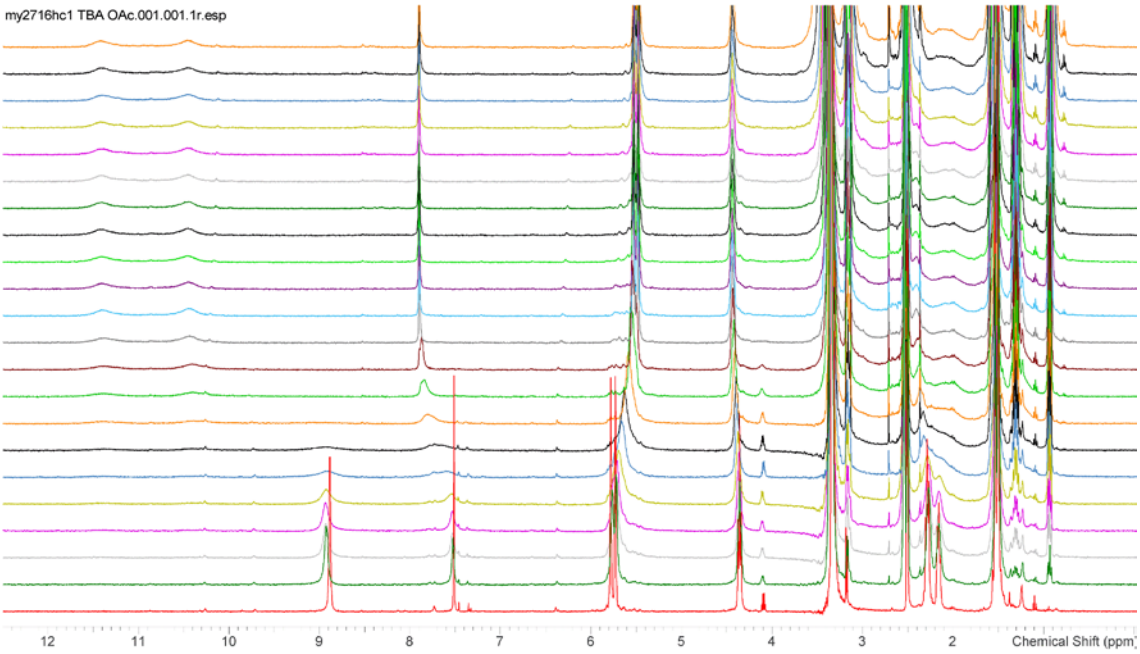

B1. 82 NMR titration spectra stack plot for receptor **79** with TBAOAc, no species ratio due to unusual splitting of NH peaks and broadening.

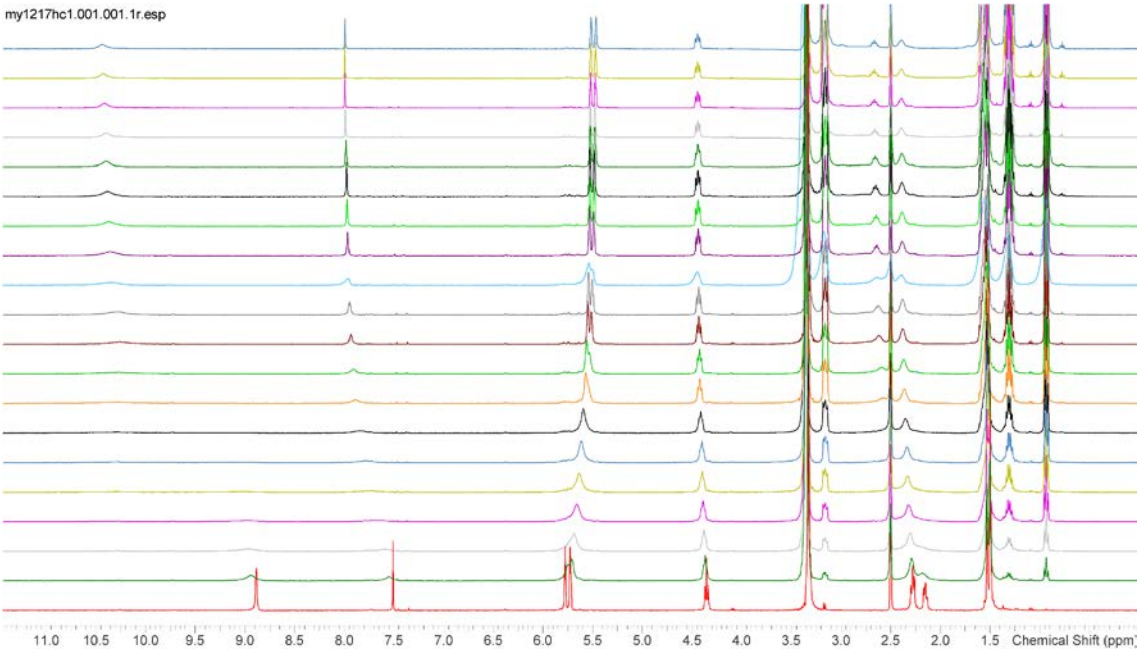

B1. 83 NMR titration spectra stack plot for receptor **79** with TBABr, no species ratio plot due to broadening of peak, only partial slow exchange character.

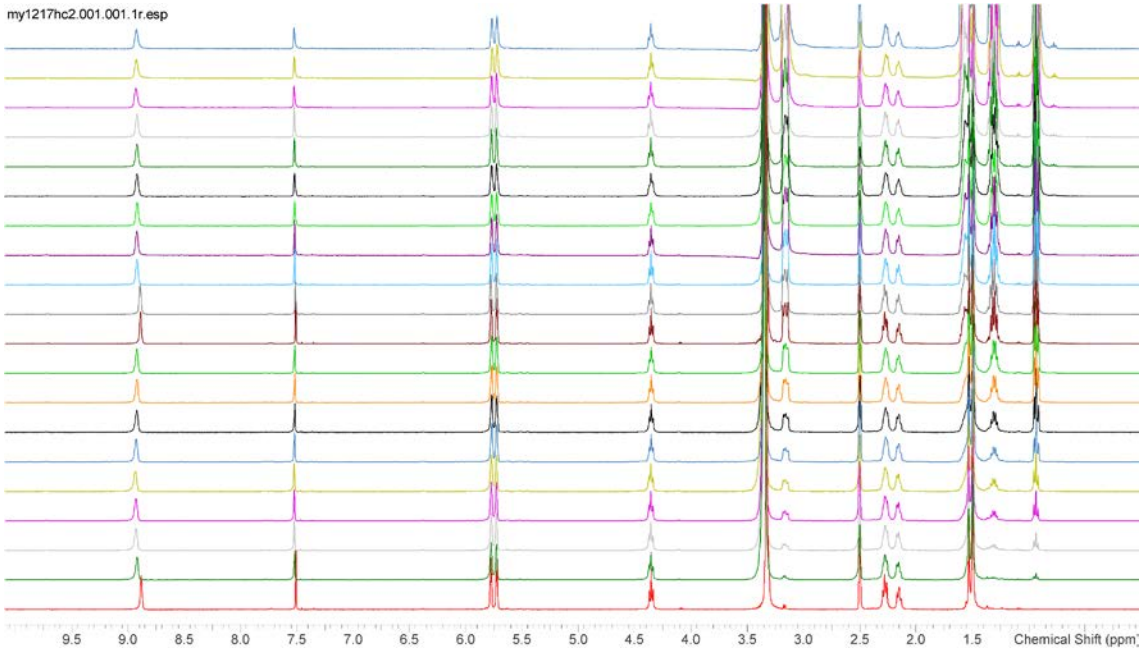

B1. 84 NMR titration spectra stack plot for receptor **79** with TBAI.

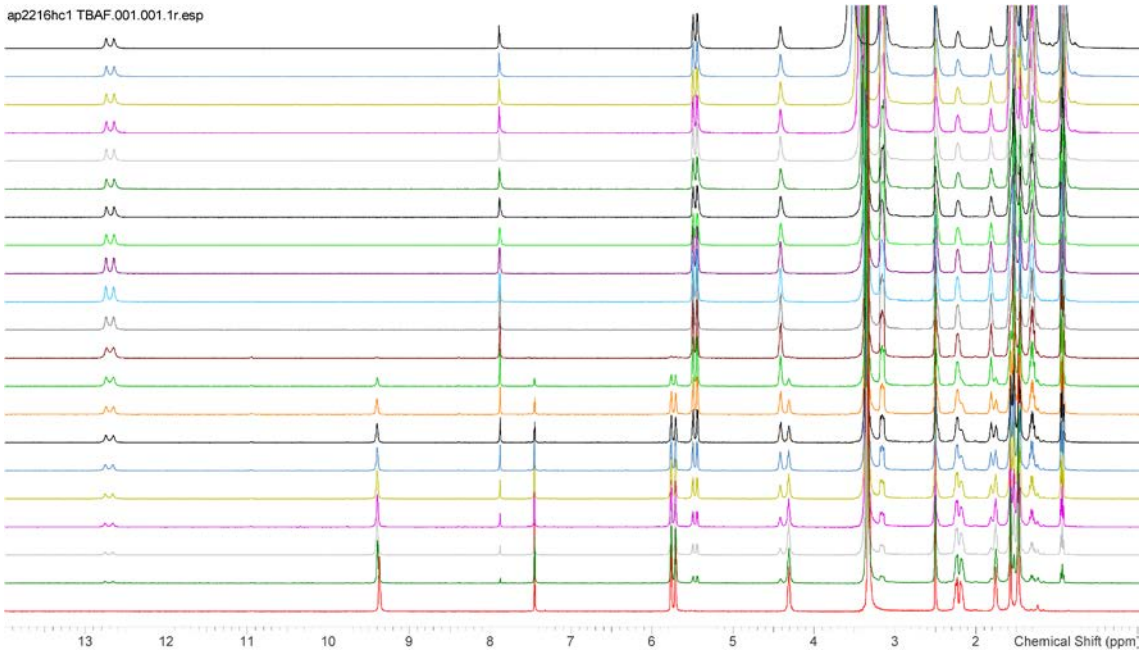

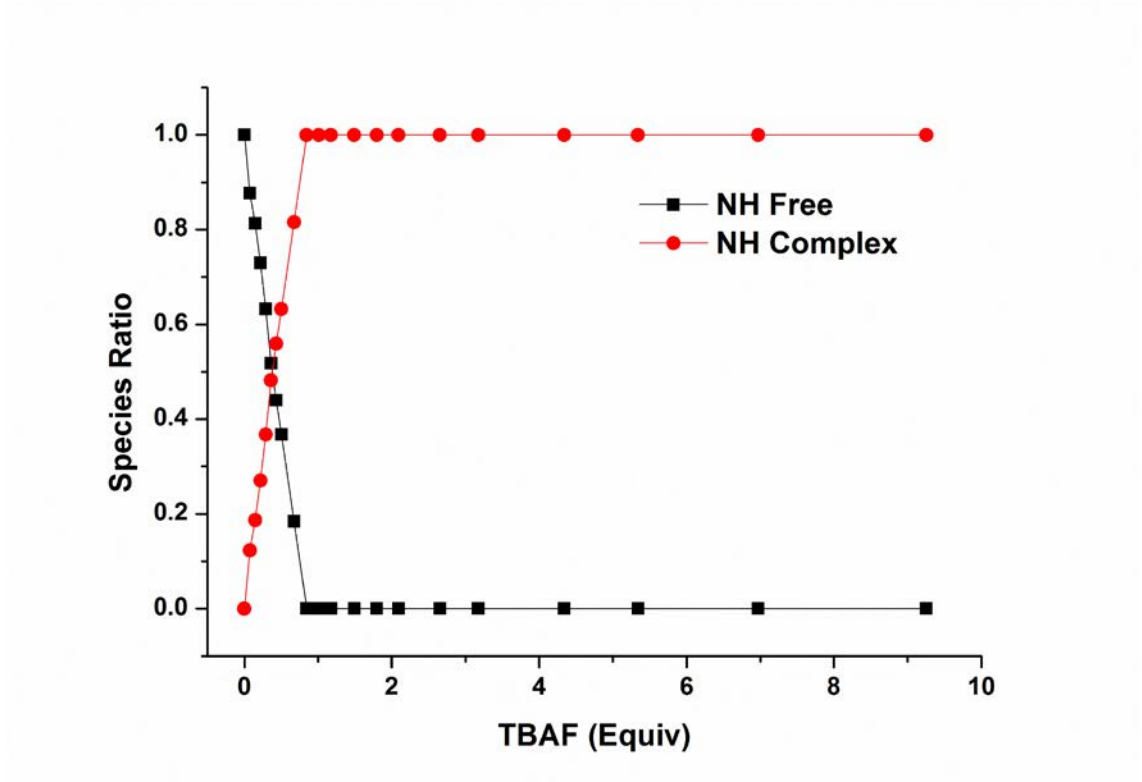

B1. 85 NMR titration spectra stack plot for receptor **80** with TBAF (top) and species ratio plot (bottom) in DMSO-d_6.

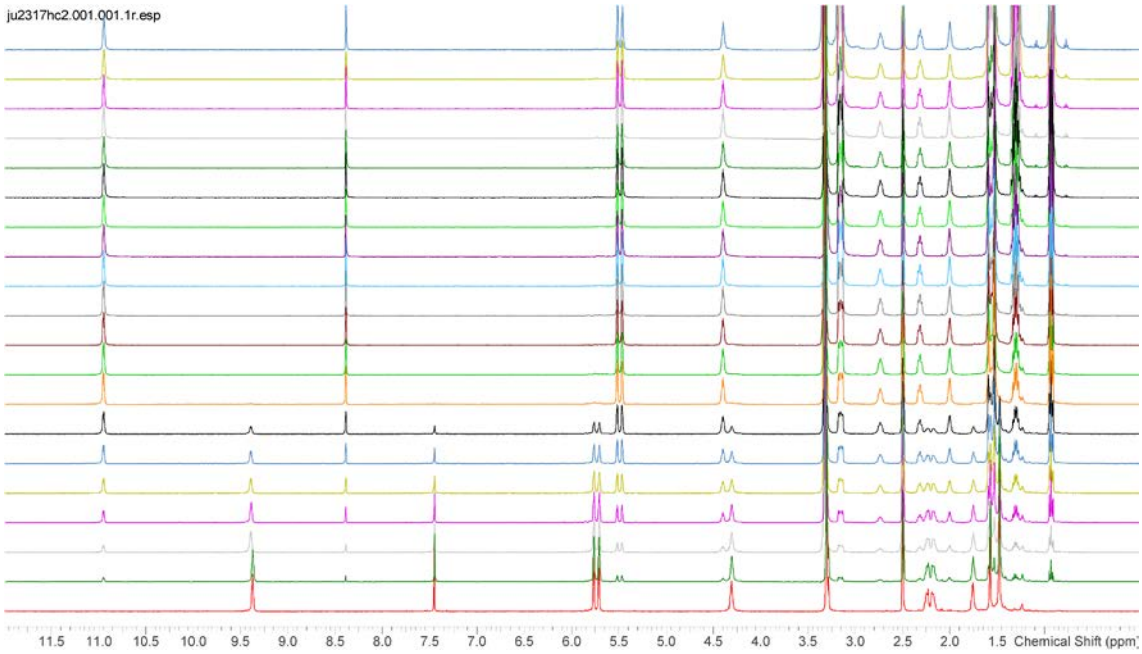

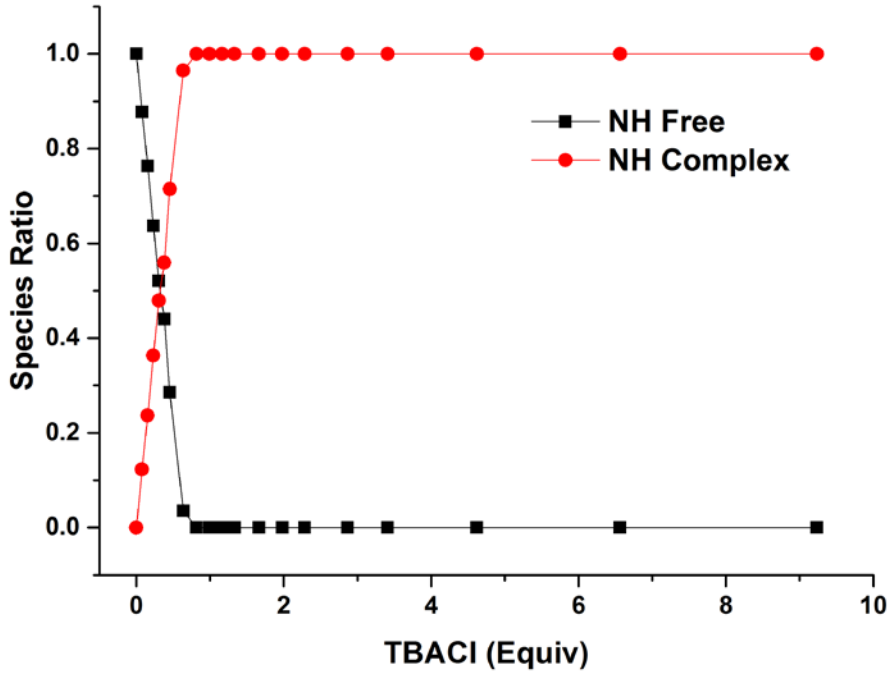

B1. 86 NMR titration spectra stack plot for receptor **80** with TBACl (top) and species ratio plot (bottom) in DMSO-d_6.

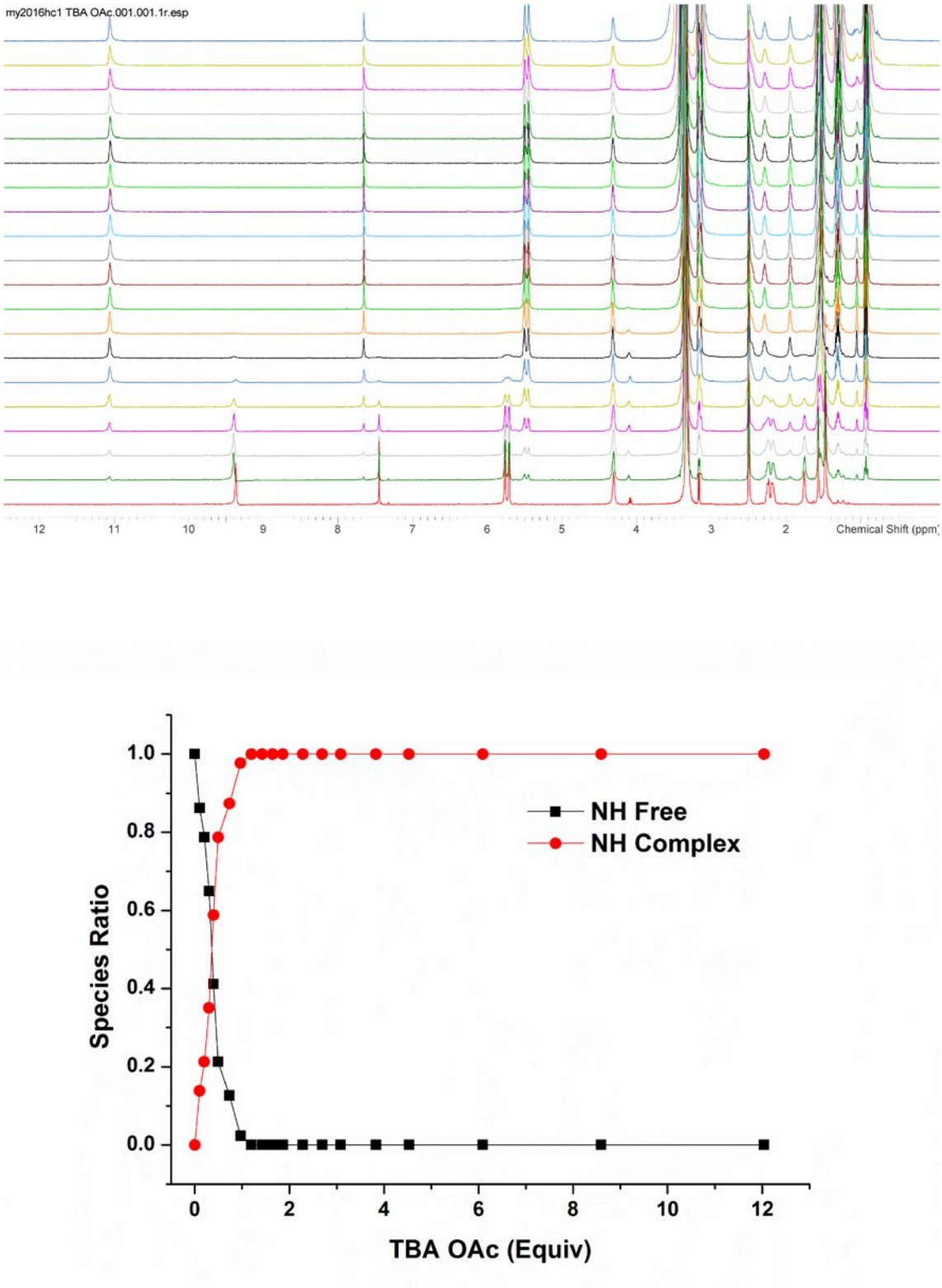

B1. 87 NMR titration spectra stack plot for receptor **80** with TBAOAc (top) and species ratio plot (bottom) in DMSO-d_6.

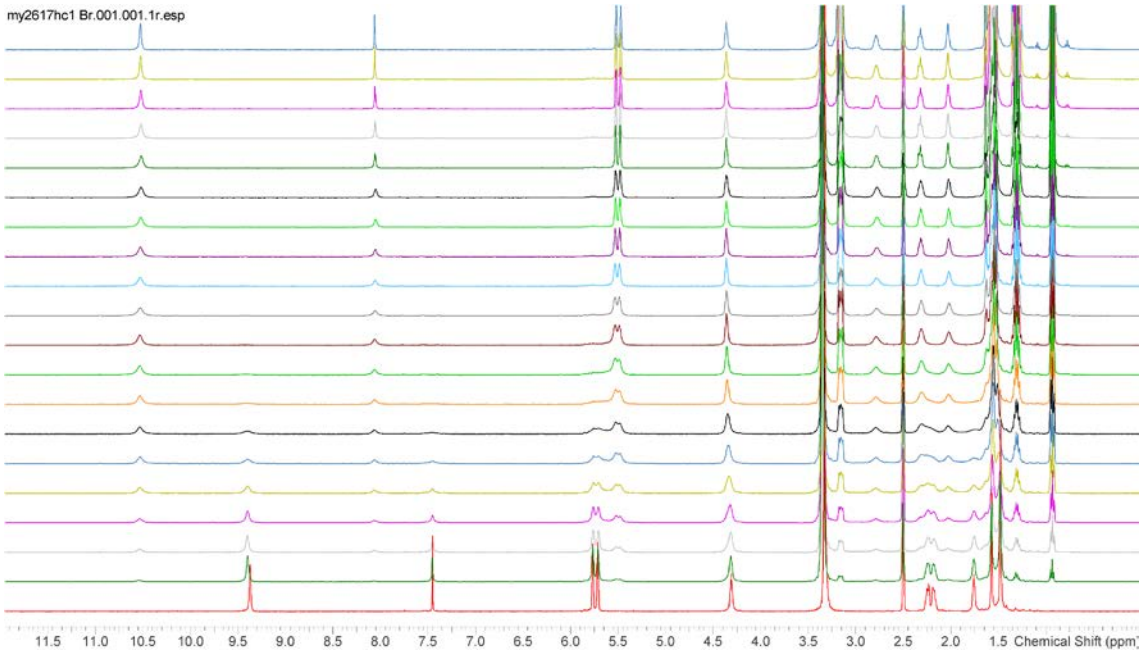

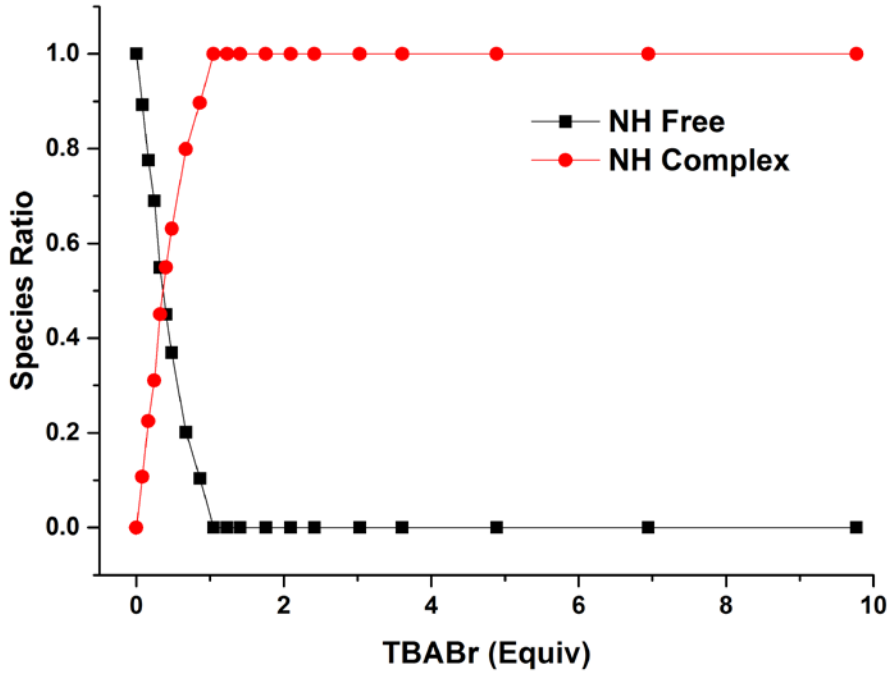

B1. 88 NMR titration spectra stack plot for receptor **80** with TBABr (top) and species ratio plot (bottom) in DMSO-d_6.

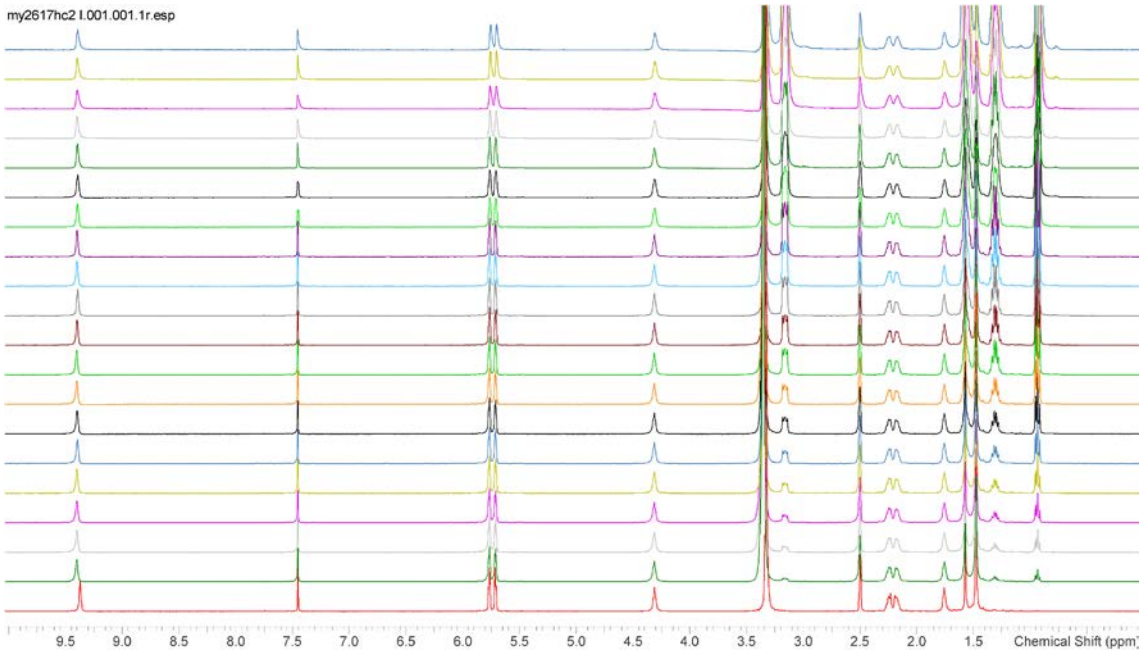

B1. 89 NMR titration spectra stack plot for receptor **80** with TBAI.

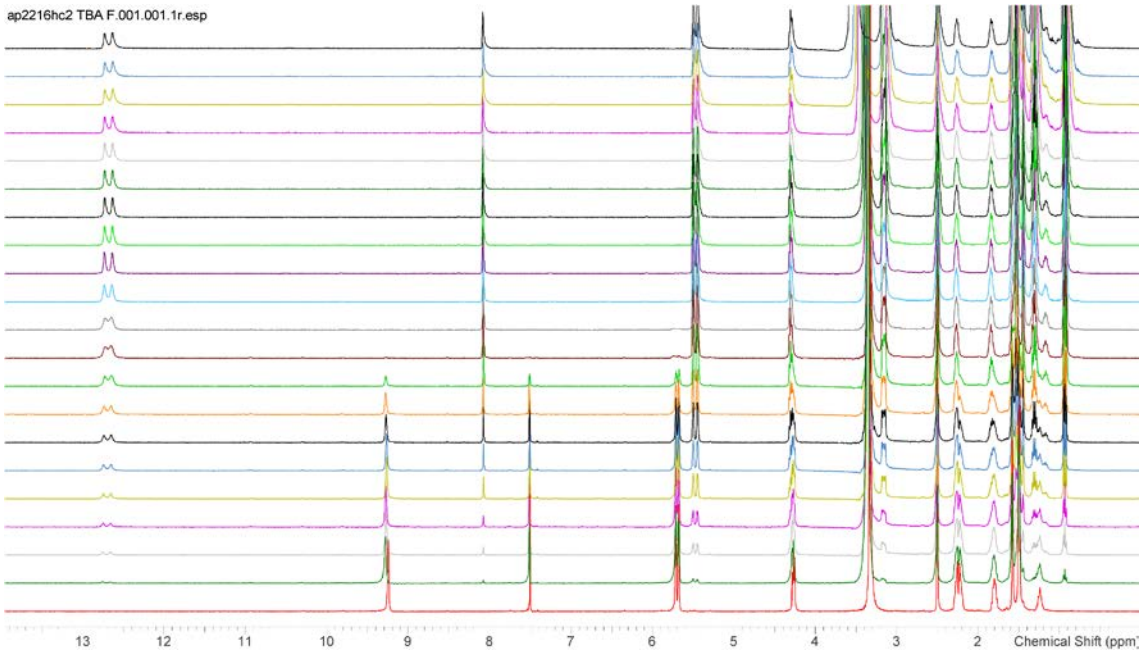

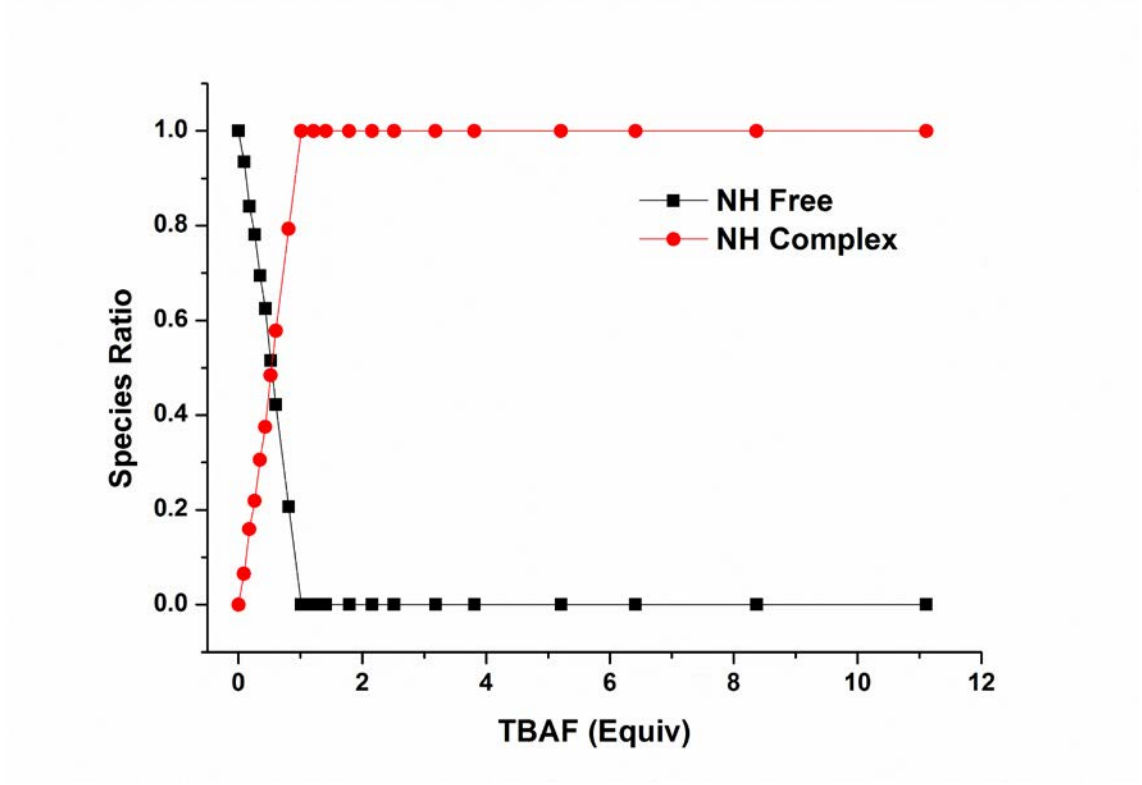

B1. 90 NMR titration spectra stack plot for receptor **81** with TBAF (top) and species ratio plot (bottom) in DMSO-d_6.

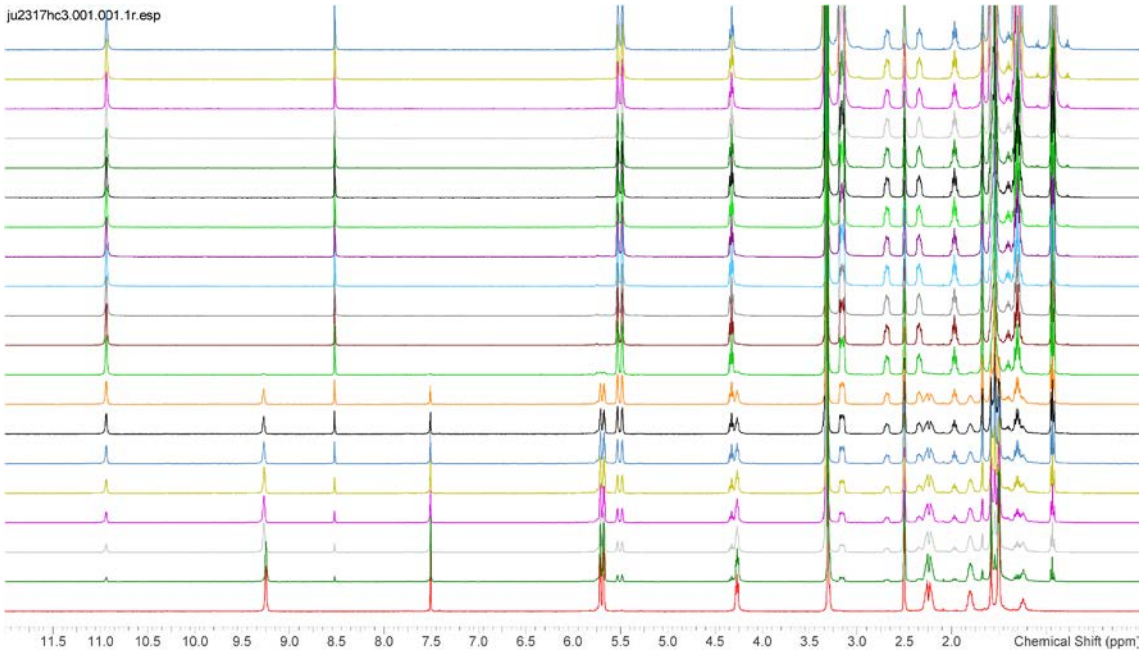

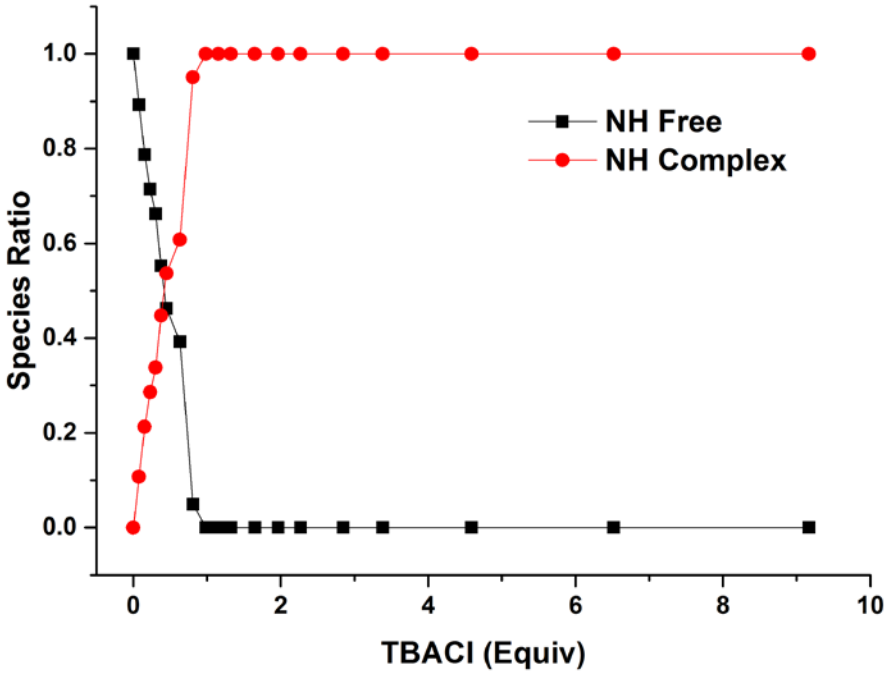

B1. 91 NMR titration spectra stack plot for receptor **81** with TBACl (top) and species ratio plot (bottom) in DMSO-d_6.

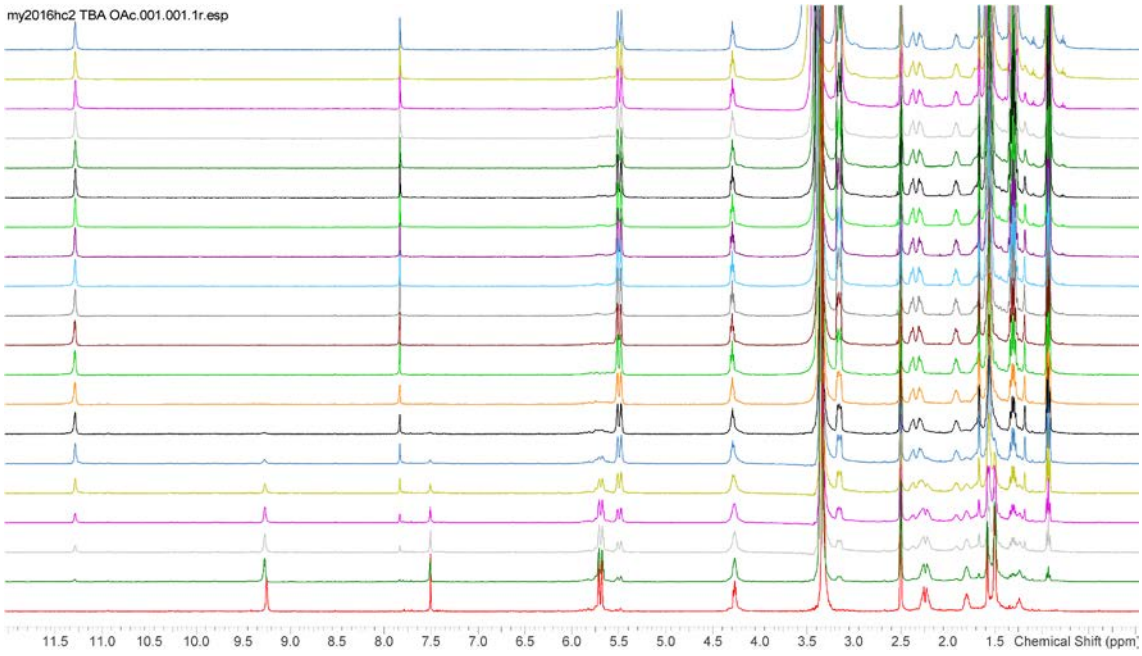

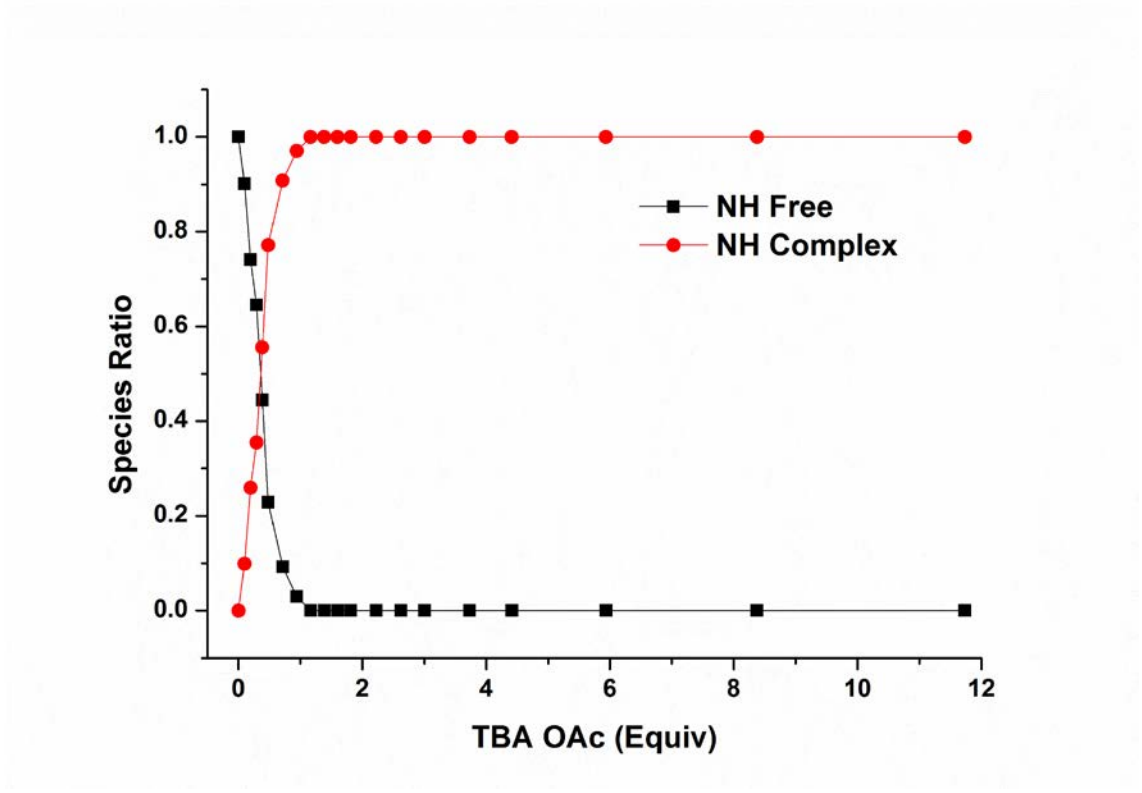

B1. 92 NMR titration spectra stack plot for receptor **81** with TBAOAc (top) and species ratio plot (bottom) in DMSO-d_6.

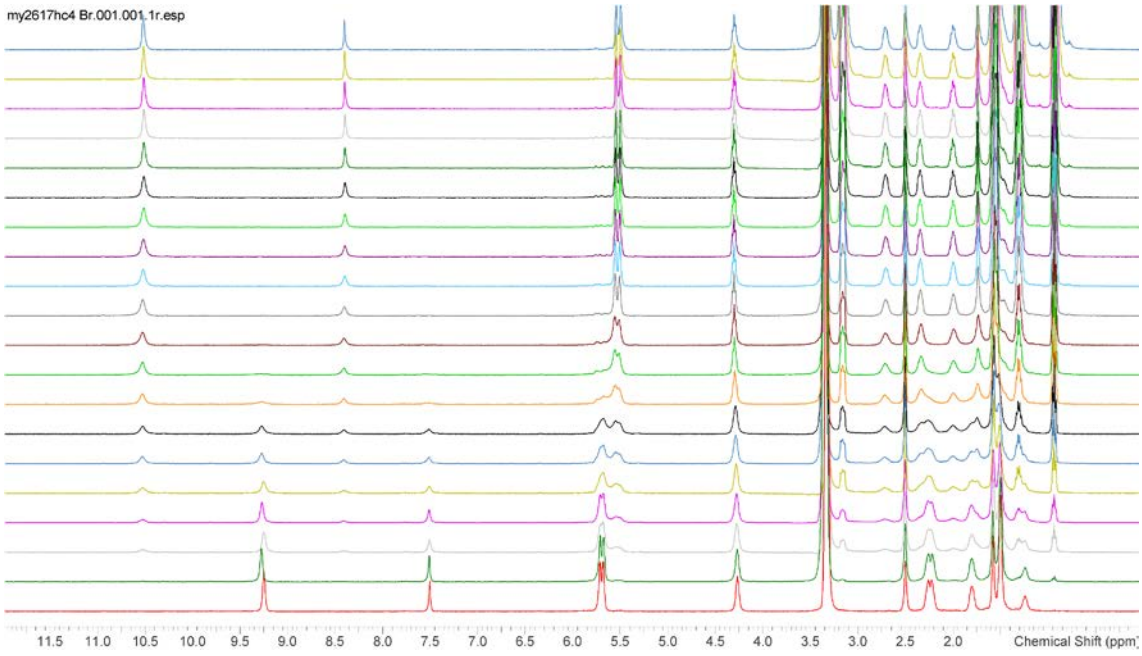

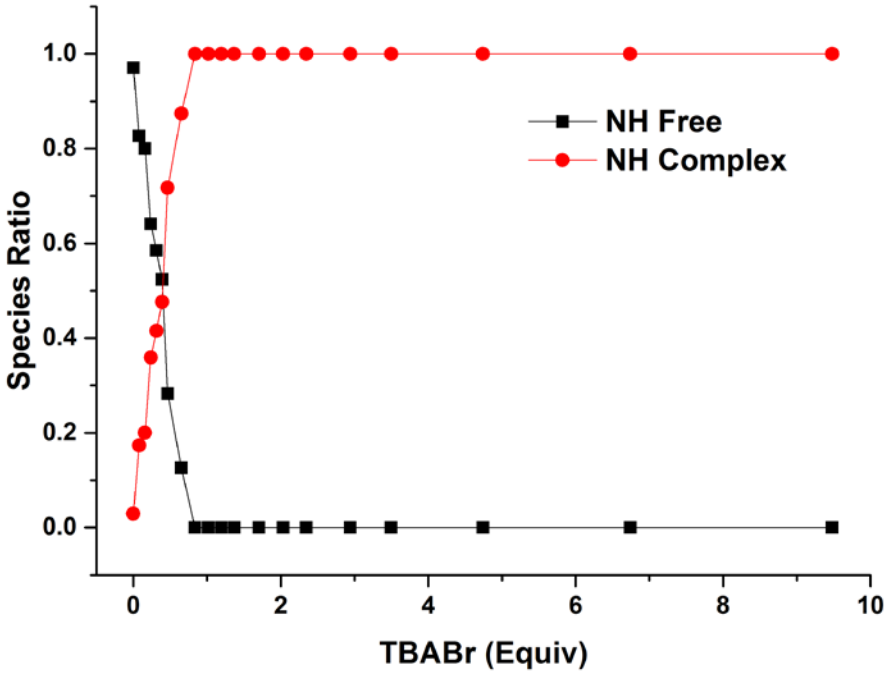

B1. 93 NMR titration spectra stack plot for receptor **81** with TBABr (top) and species ratio plot (bottom) in DMSO-d_6.

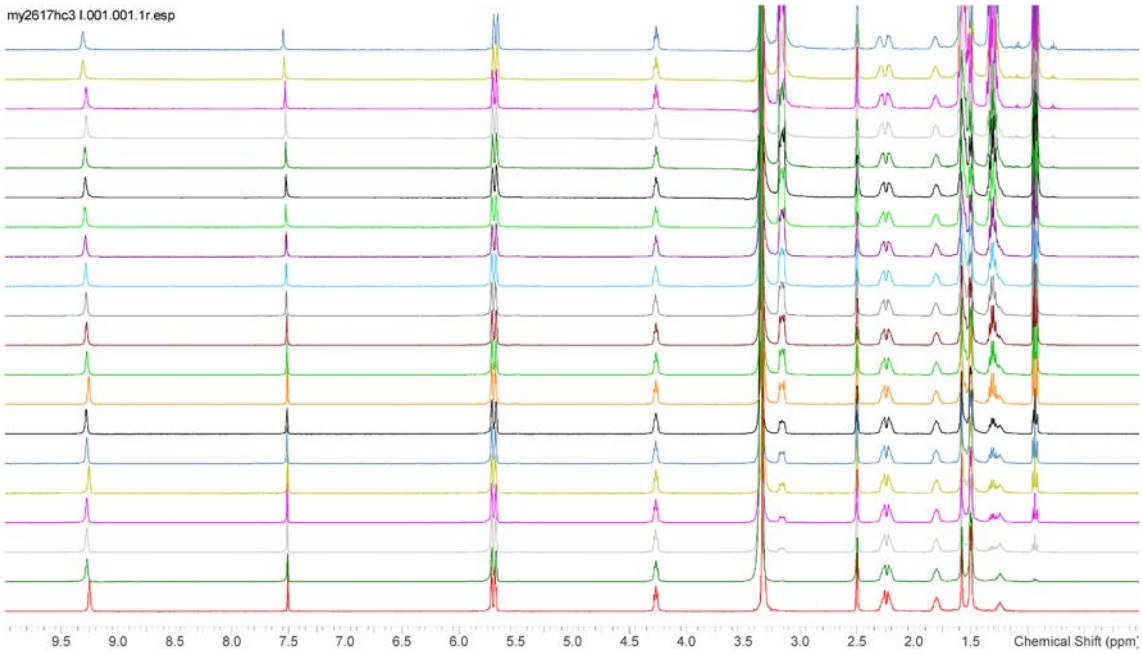

B1. 94 NMR titration spectra stack plot for receptor **81** with TBAI.

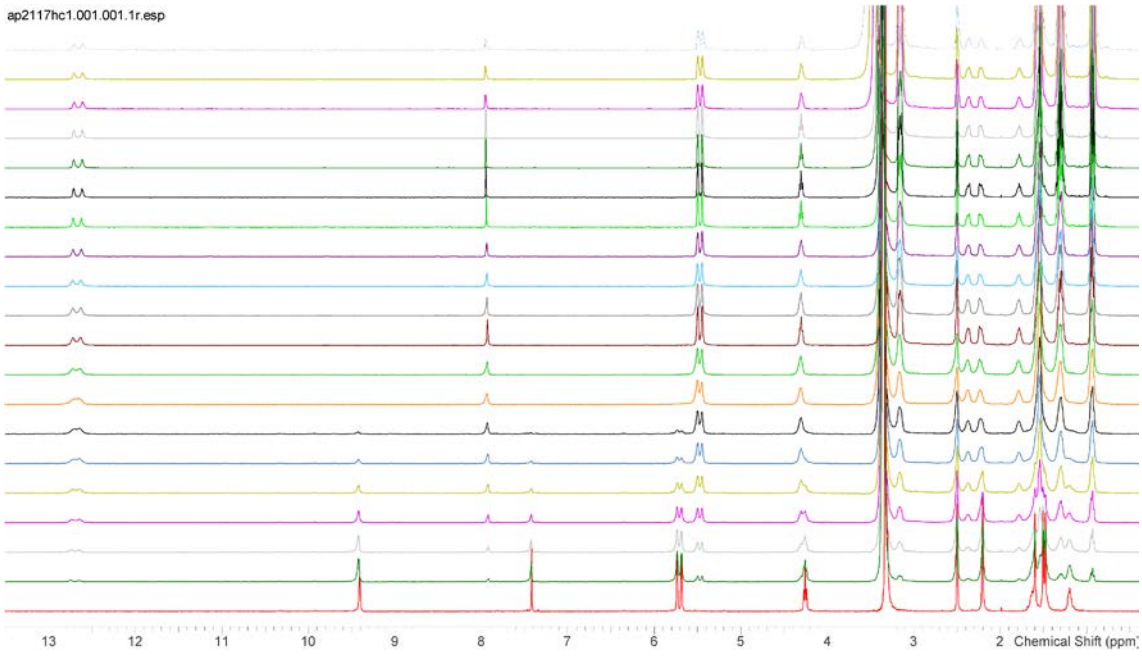

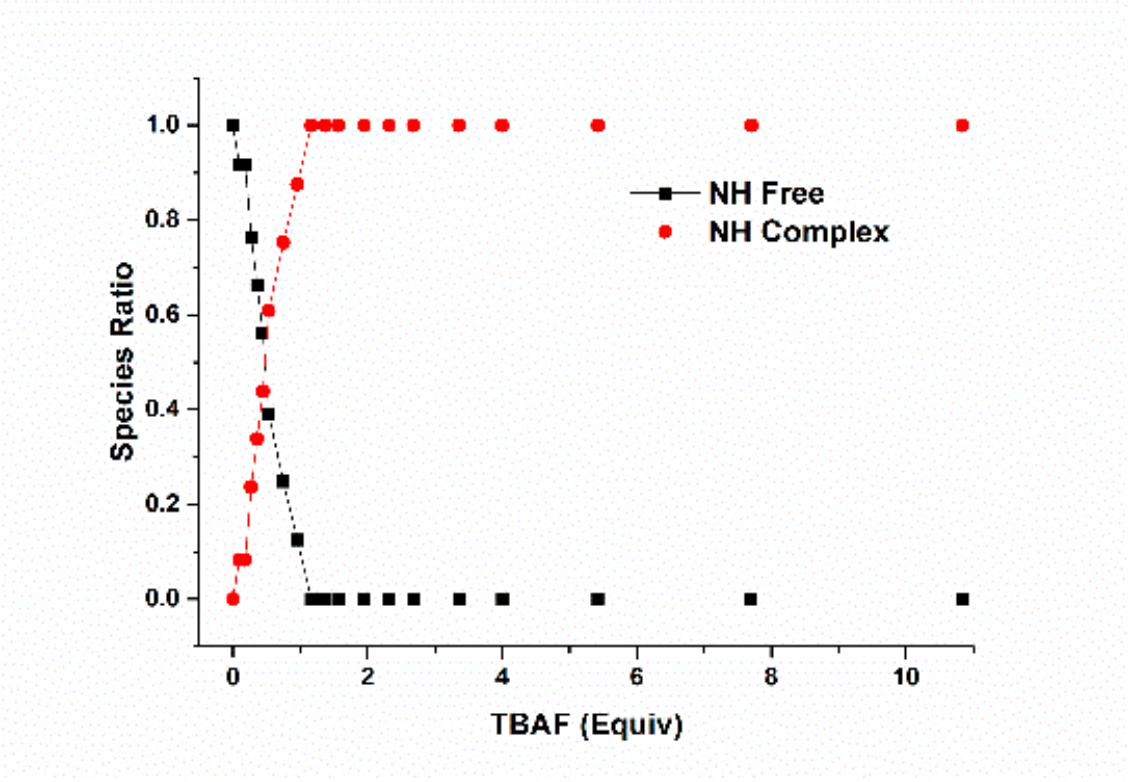

B1. 95 NMR titration spectra stack plot for receptor **82** with TBAF (top) and species ratio plot (bottom) in DMSO-d_6.

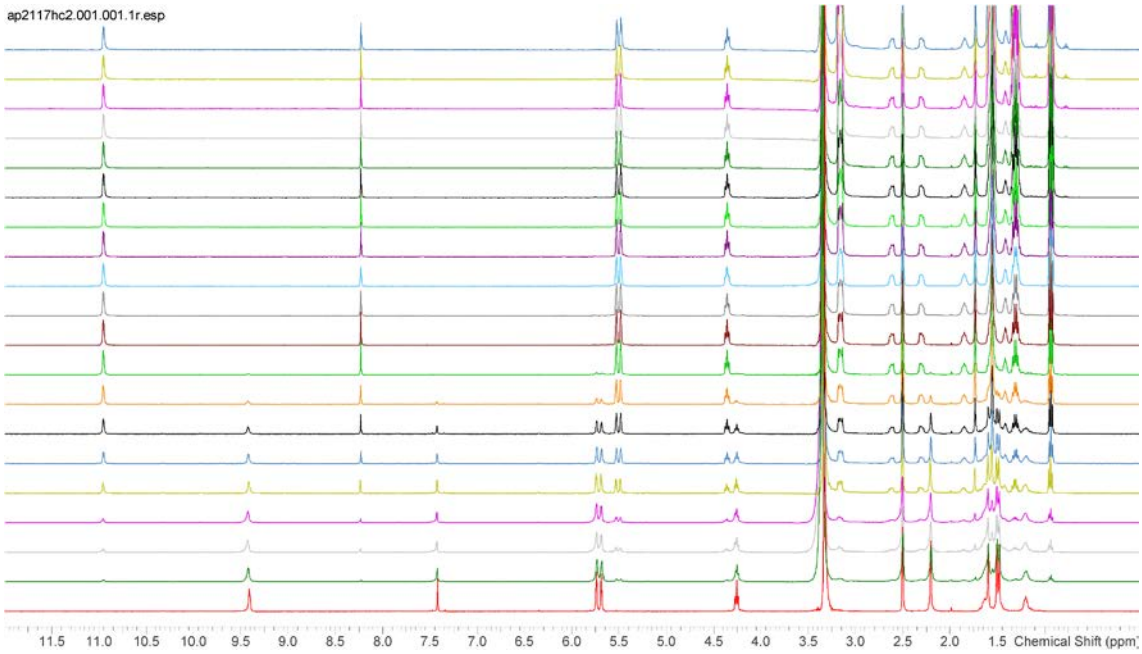

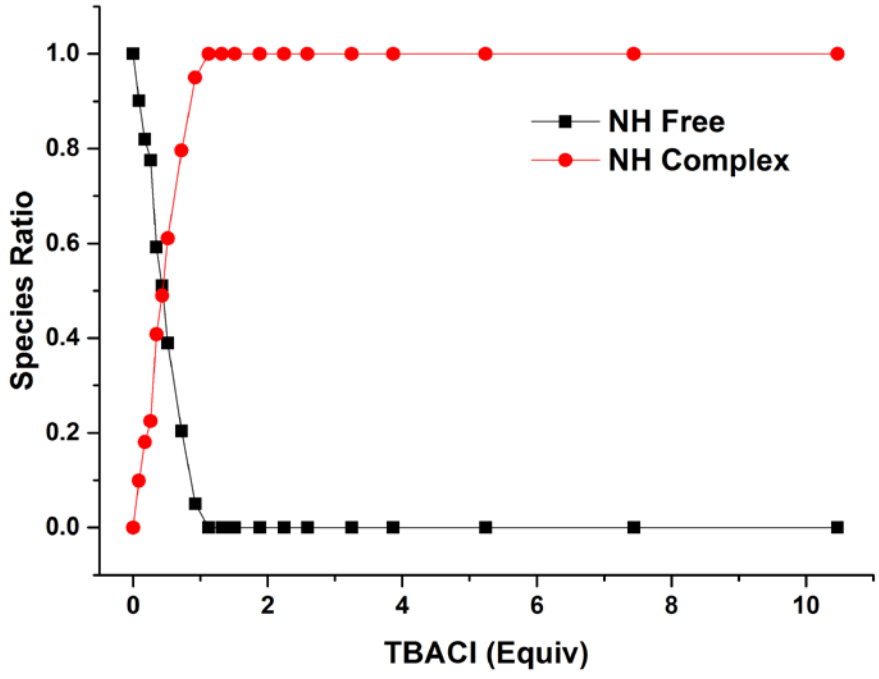

B1. 96 NMR titration spectra stack plot for receptor **82** with TBACl (top) and species ratio plot (bottom) in DMSO-d_6.

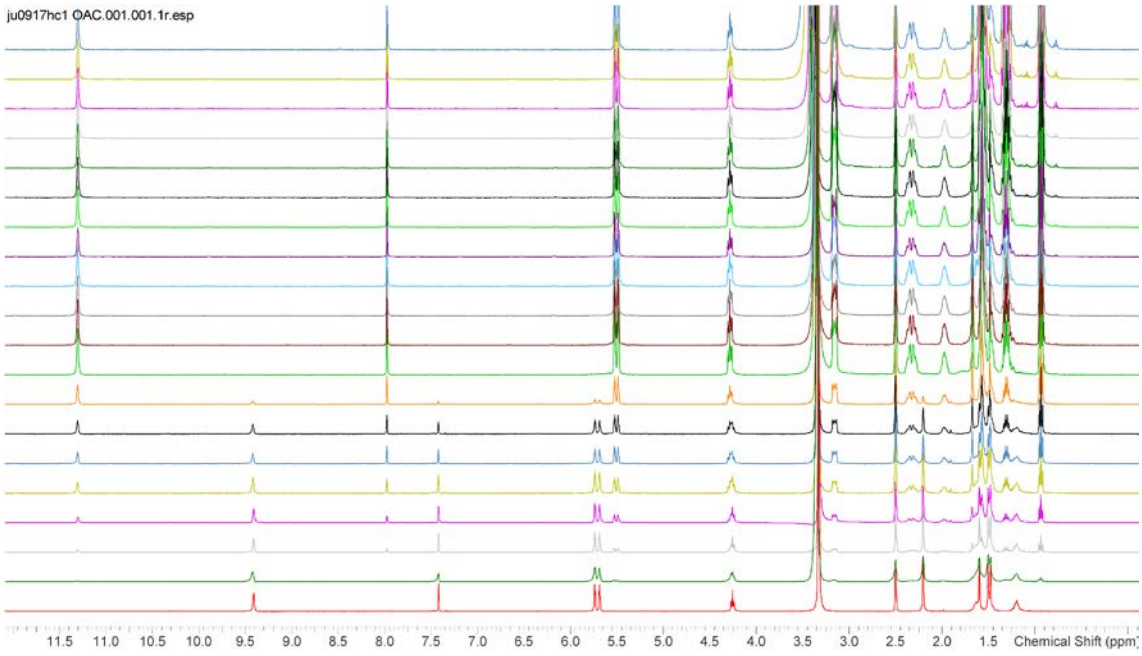

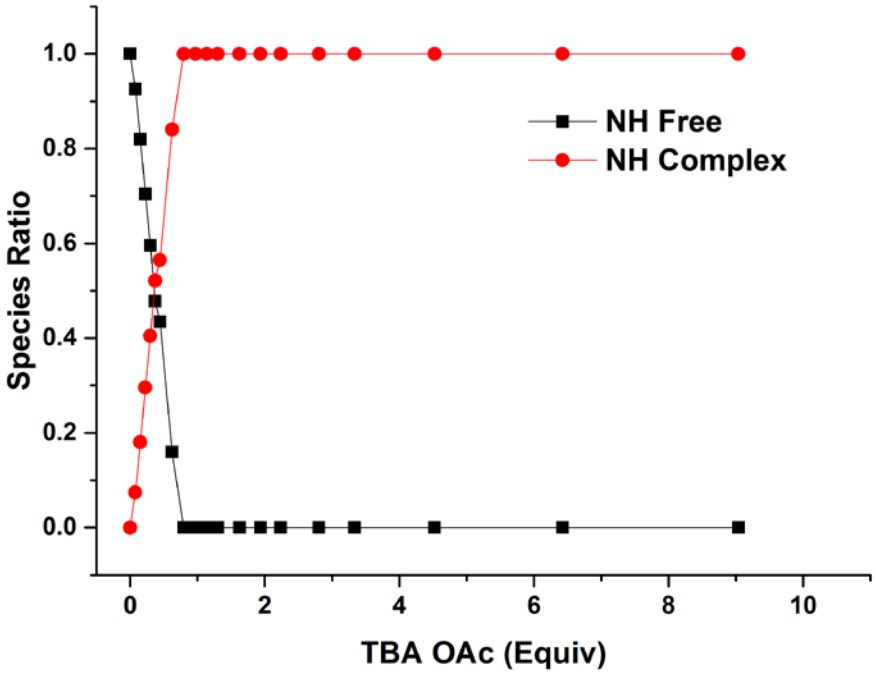

B1. 97 NMR titration spectra stack plot for receptor **82** with TBAOAc (top) and species ratio plot (bottom) in DMSO-d_6.

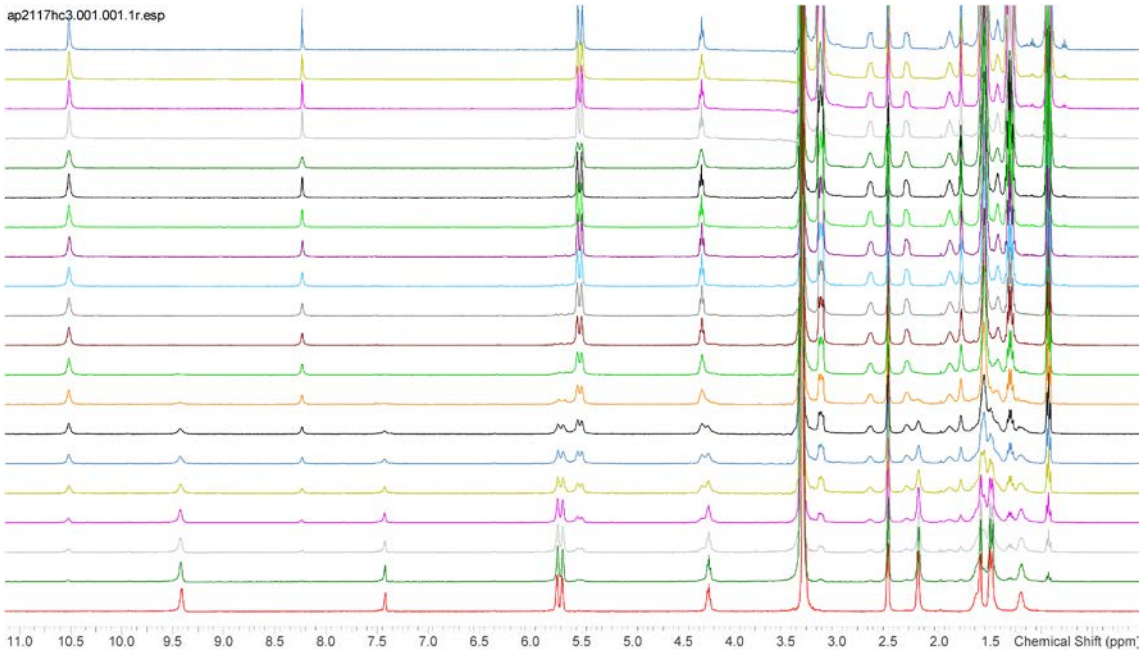

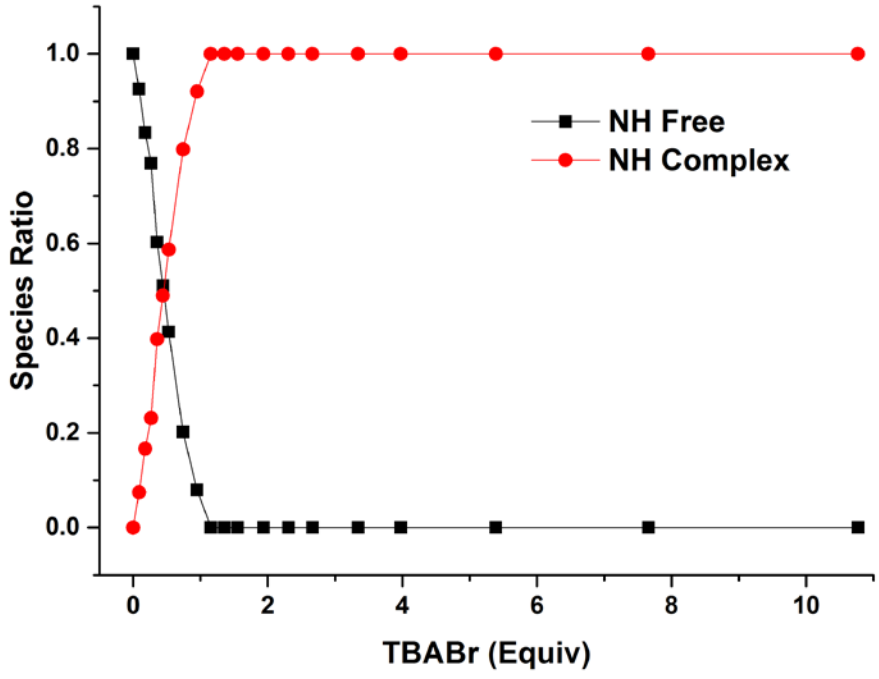

B1. 98 NMR titration spectra stack plot for receptor **82** with TBABr (top) and species ratio plot (bottom) in DMSO-d_6.

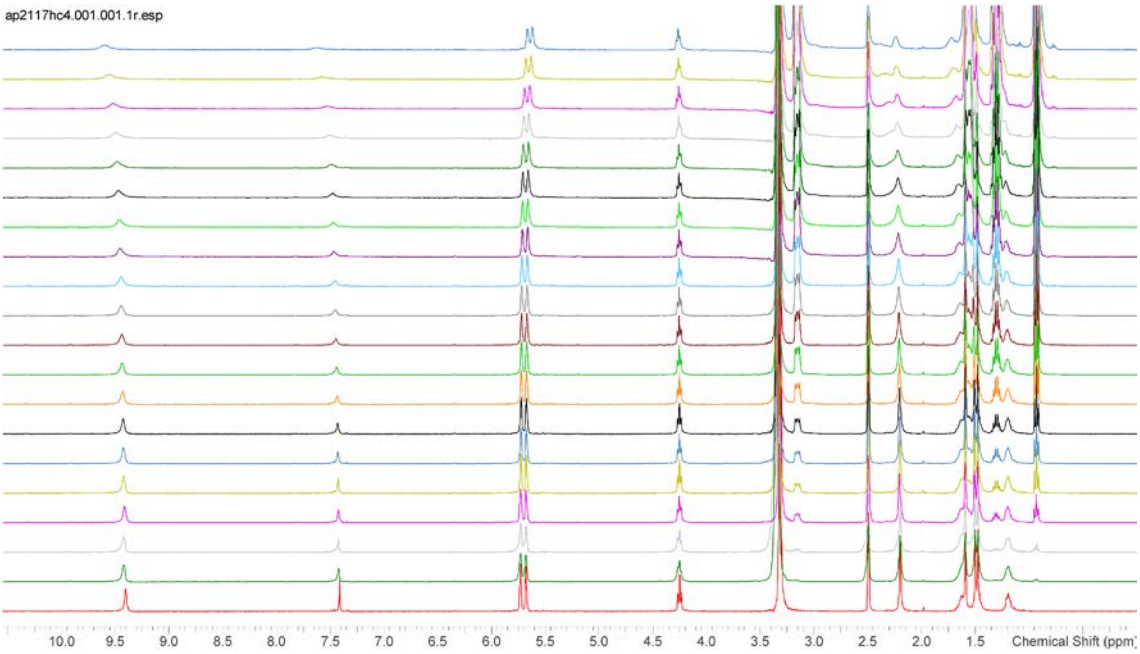

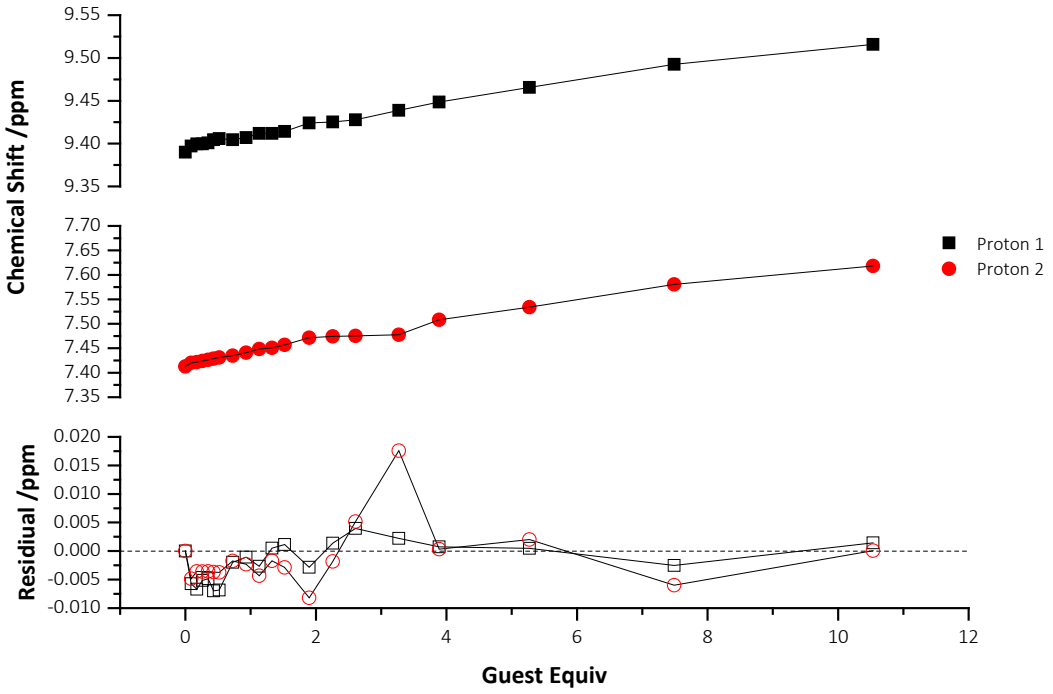

B1. 99 NMR titration spectra stack plot for receptor **82** with TBAI (top). Bindfit NMR binding curve for NH and triazole CH protons K_a= 11 ± 3 M^{-1} (bottom).

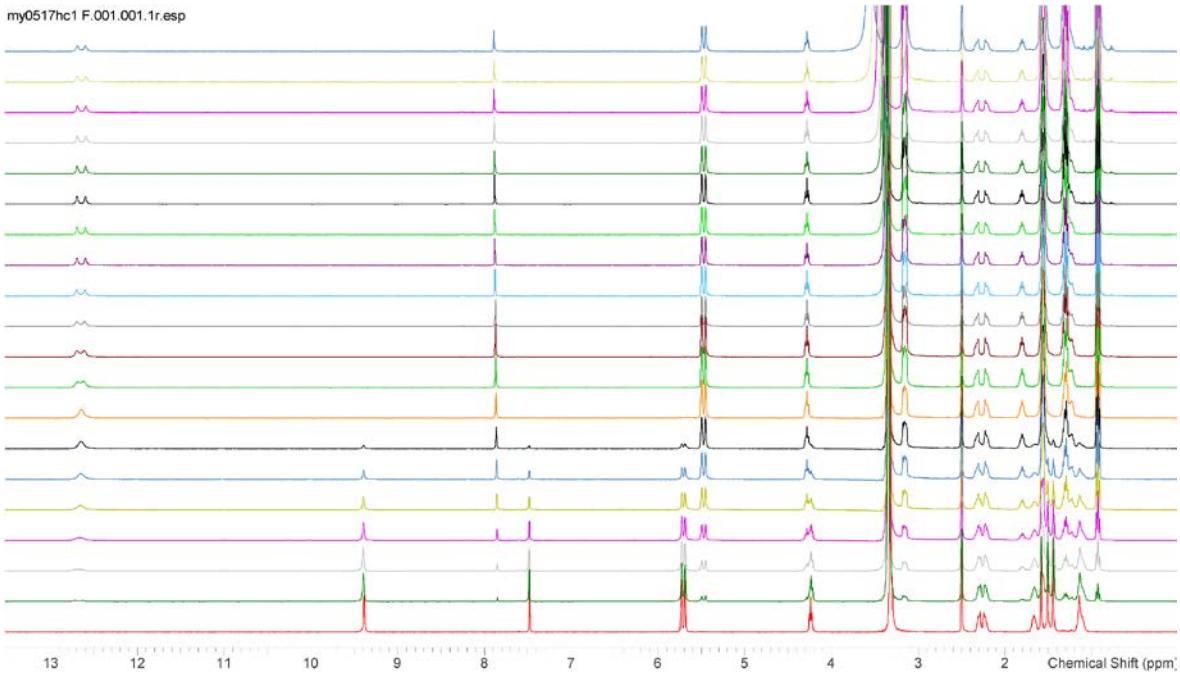

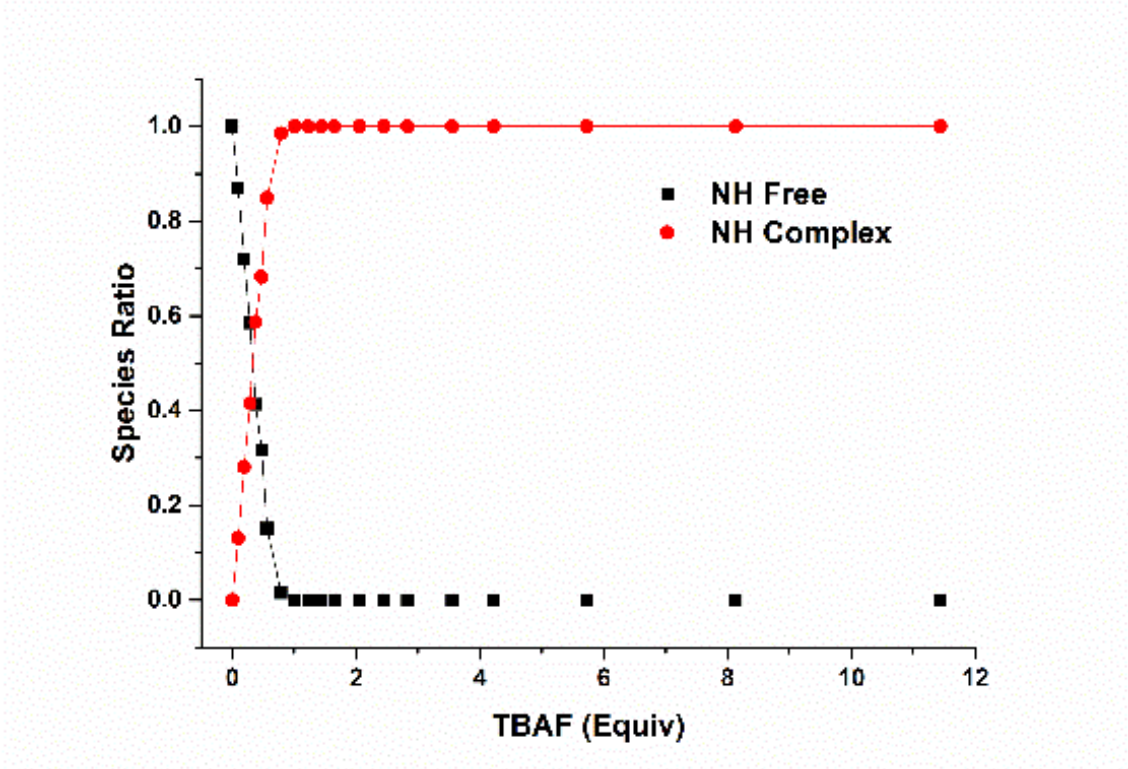

B1. 100 NMR titration spectra stack plot for receptor **83** with TBAF (top) and species ratio plot (bottom) in DMSO-d_6.

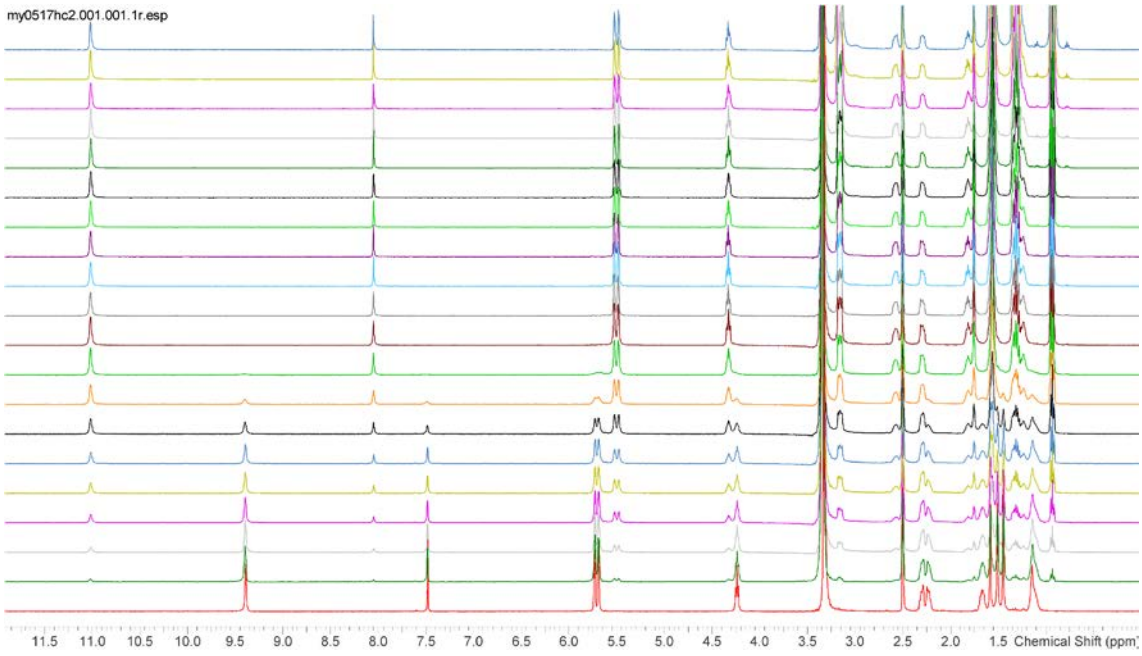

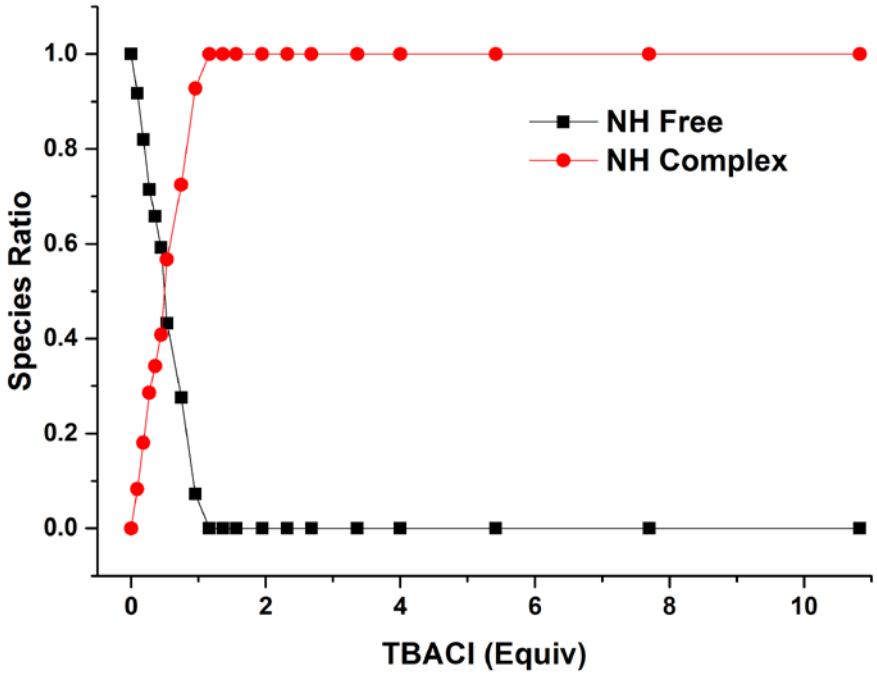

B1. 101 NMR titration spectra stack plot for receptor **83** with TBACl (top) and species ratio plot (bottom) in DMSO-d_6.

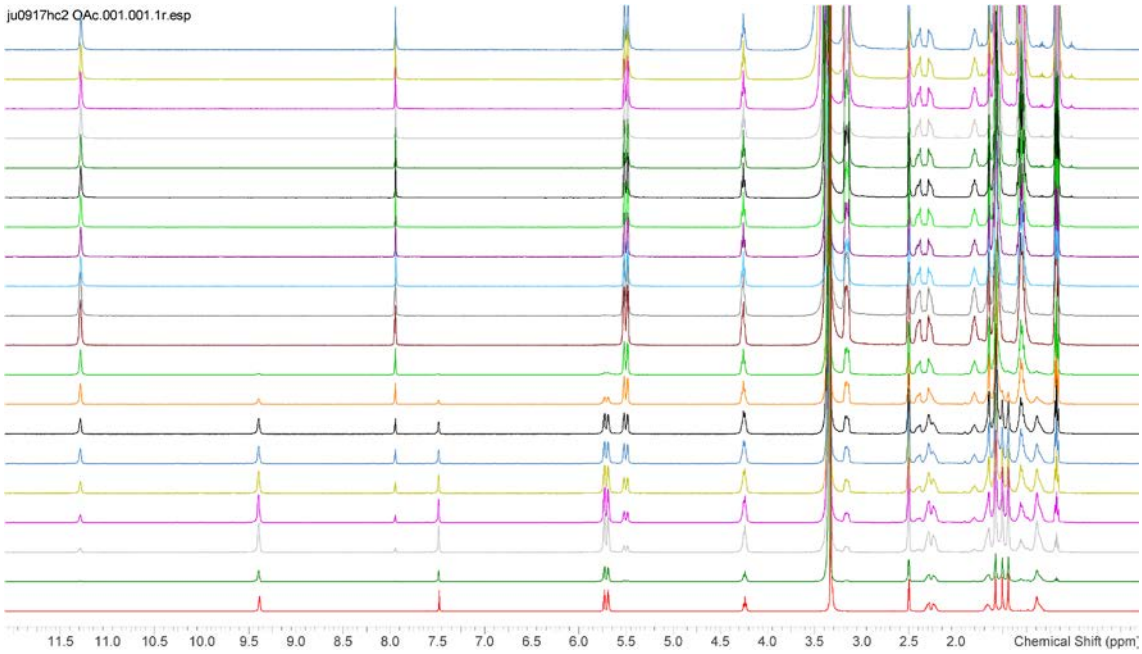

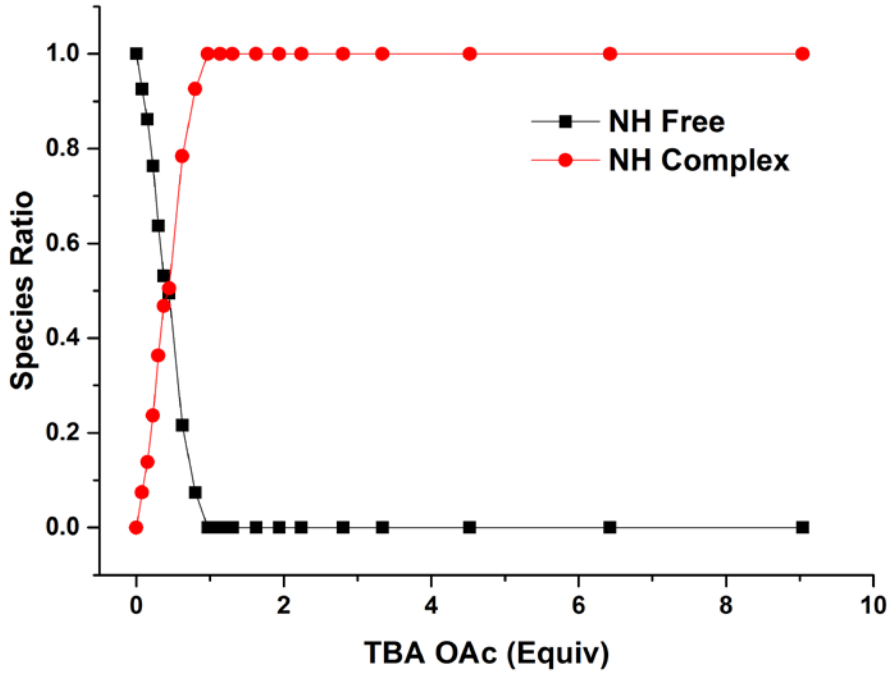

B1. 102 NMR titration spectra stack plot for receptor **83** with TBAOAc (top) and species ratio plot (bottom) in DMSO-d_6.

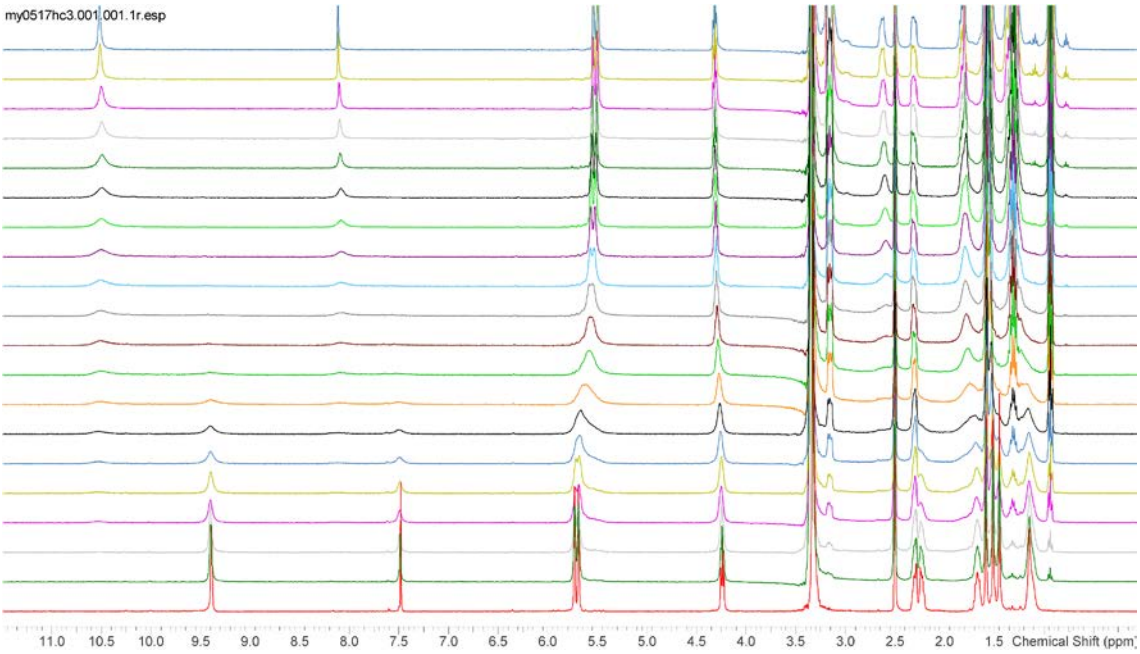

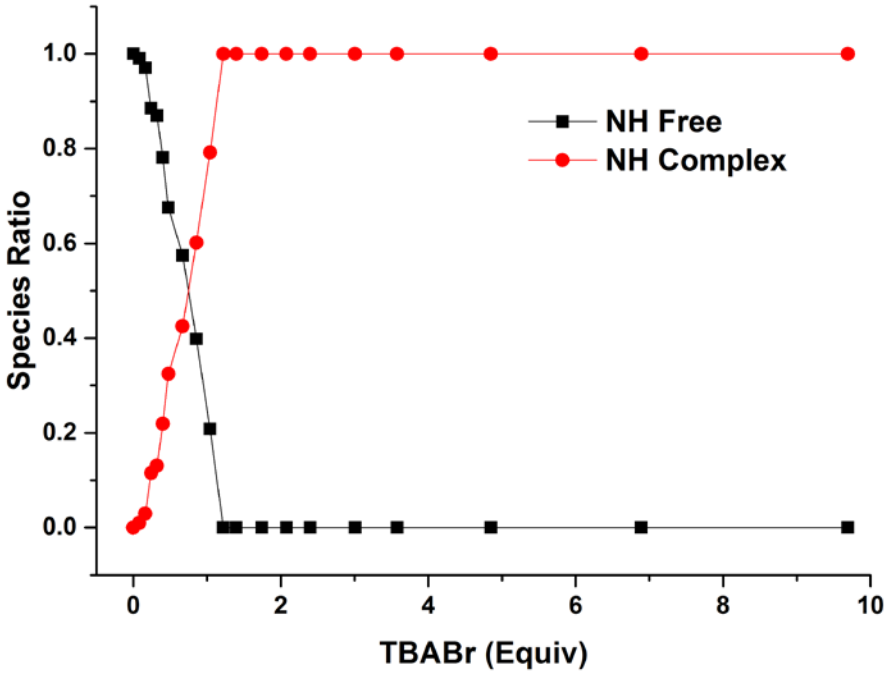

B1. 103 NMR titration spectra stack plot for receptor **83** with TBABr (top) and species ratio plot (bottom) in DMSO-d_6.

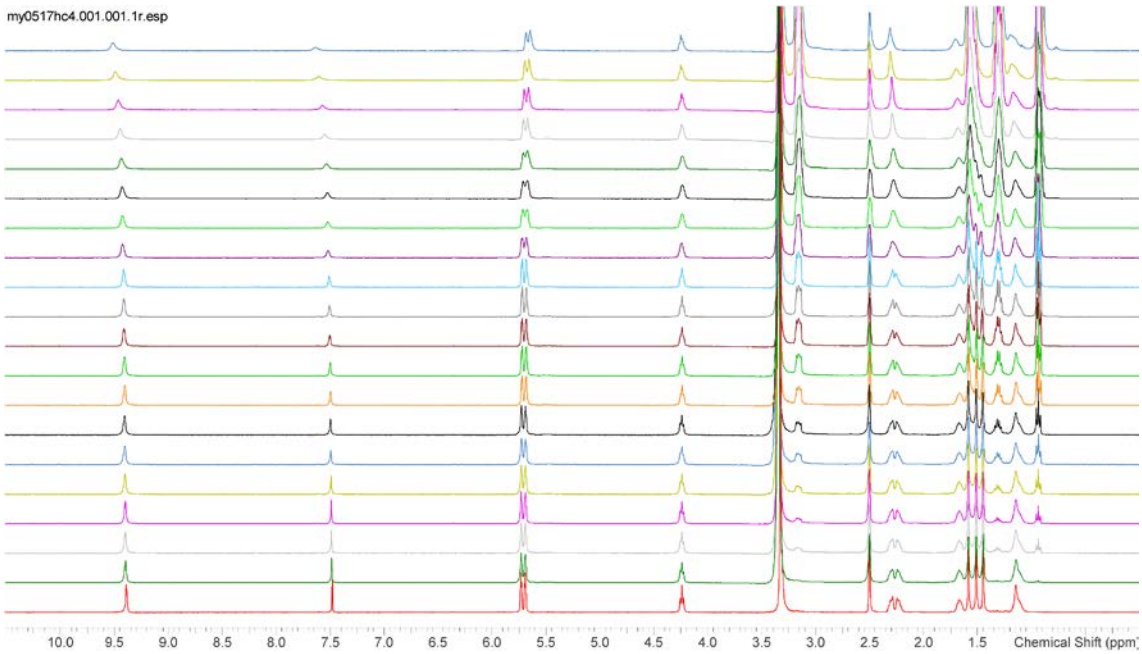

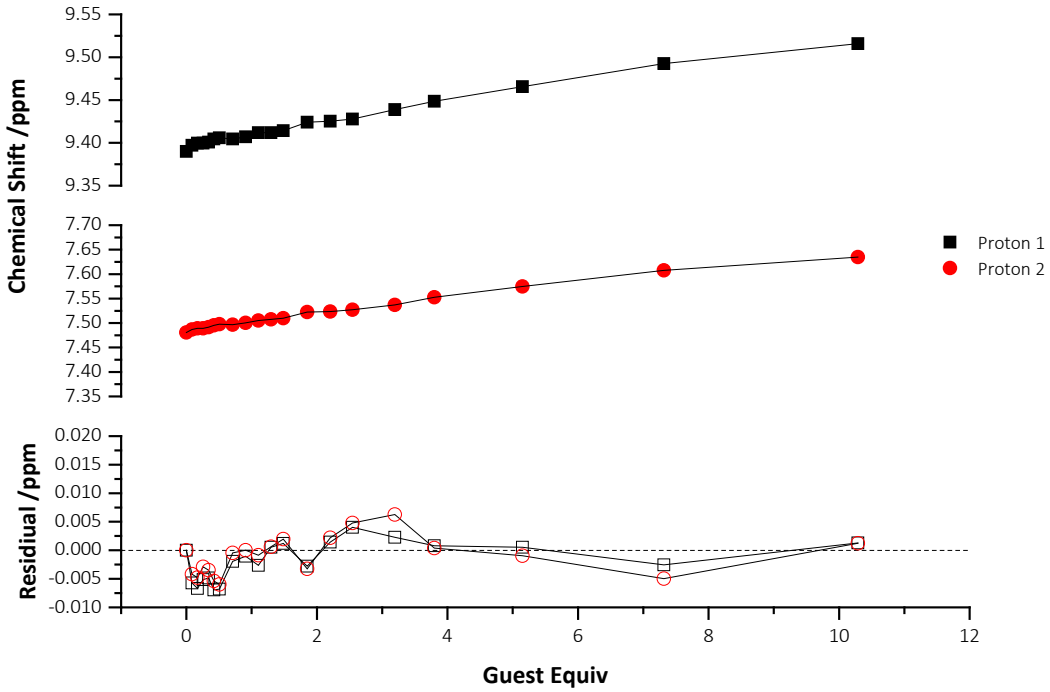

B1. 104 NMR titration spectra stack plot for receptor **83** with TBAI (top). Bindfit NMR binding curve for NH and triazole CH protons K_a= 11 ± 3 M^{-1} (bottom).

B.2 Isothermal titration calorimetry

Performed by F. Sommer under the supervision of Prof. S. Kubik.

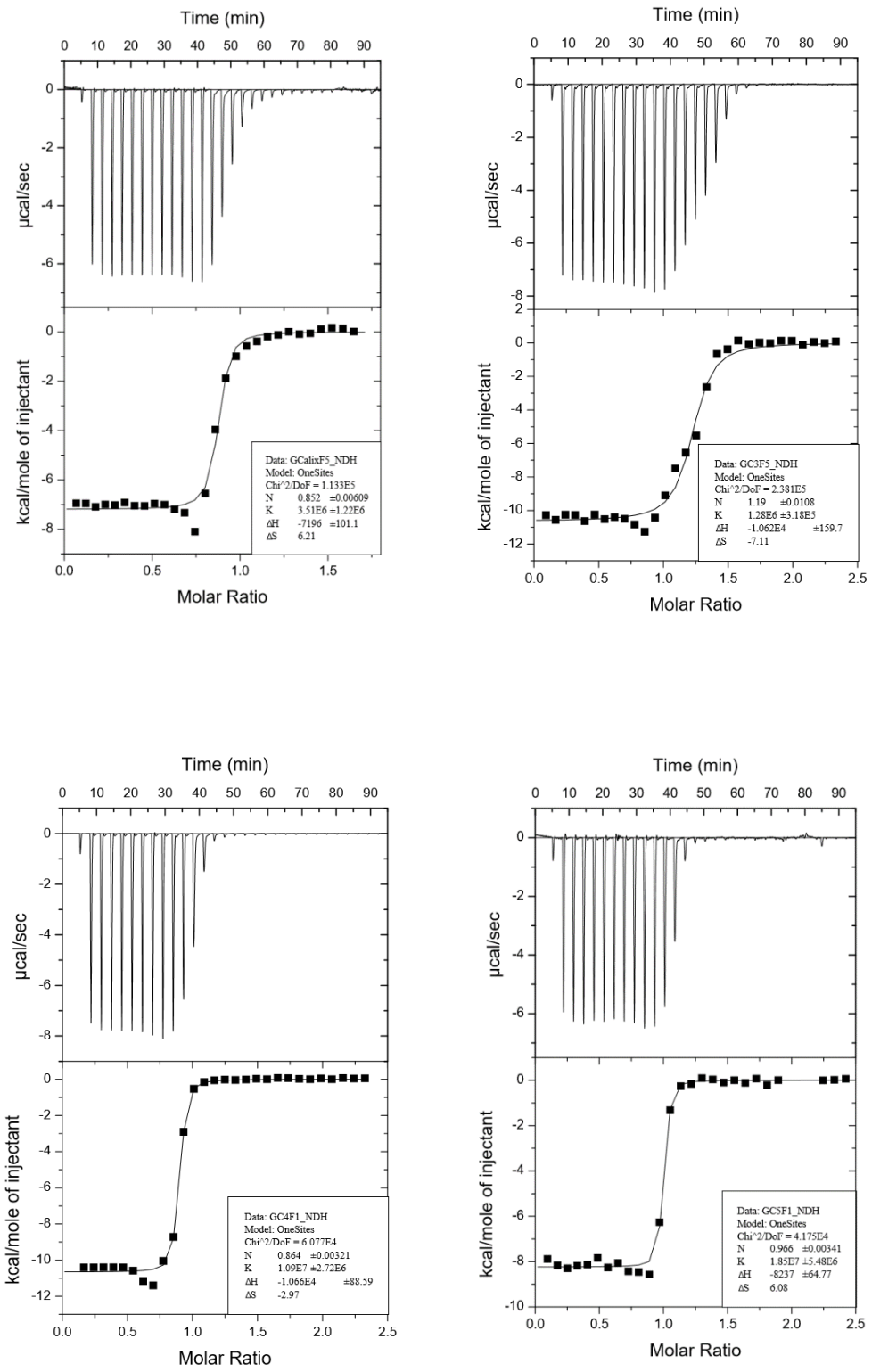

B2. 1 ITC curves from titration with TEAF in acetonitrile: receptor **16** (top left), receptor **79** (top right), receptor **80** (bottom left) and receptor **81** (bottom right).

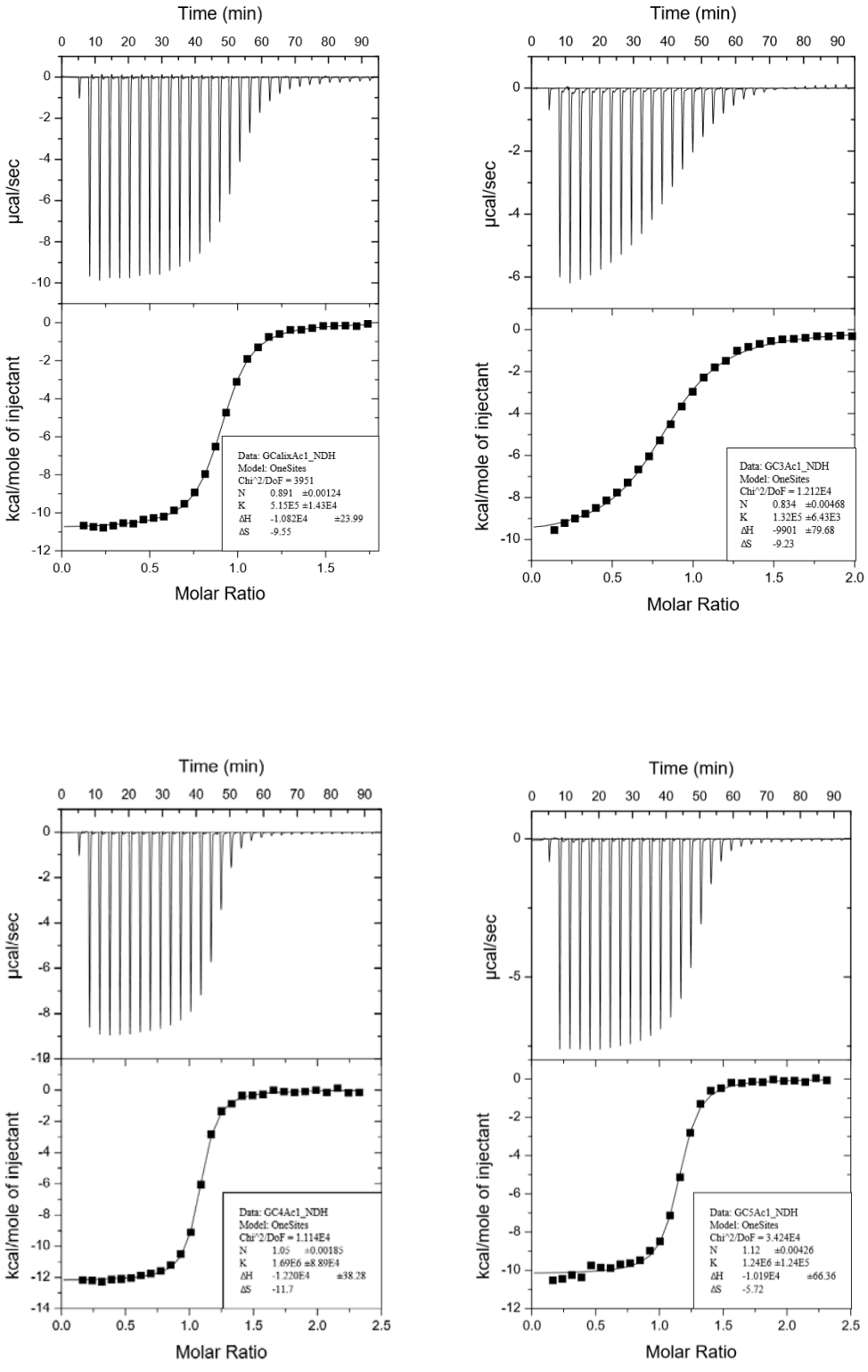

B2. 2 ITC curves from titration with TEAOAc in acetonitrile: receptor **16** (top left), receptor **79** (top right), receptor **80** (bottom left) and receptor **81** (bottom right).

Appendix C Transport and additional studies

C.1 N,N-(phenylmethylene)dibenzamide based receptors

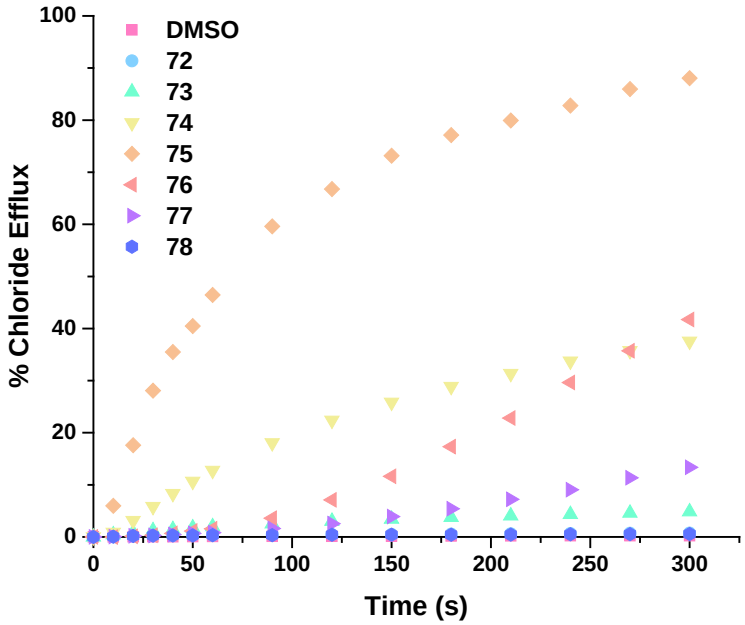

C1. 1 Chloride efflux promoted by receptors **72–78** at 2mol% (w.r.t. lipid) over 300 s. Vesicle conditions: Internal- NaCl, 489 mM; External- Na_2NO_3, 489 mM; all solutions were buffered to pH 7.2 with 5 mM sodium phosphate salts. At the end of the experiment the vesicles were lysed with detergent to calibrate to 100 % chloride efflux.

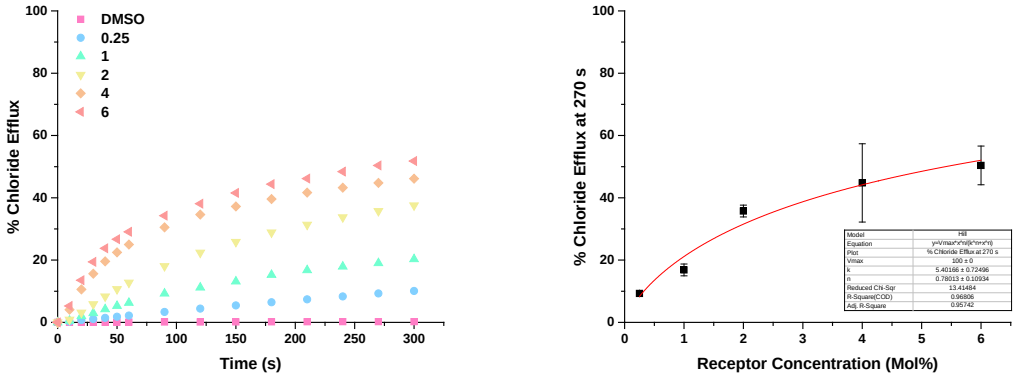

C1. 2 **Left-** Receptor **74** kinetic profile. **Right-** Hill plot; concentrations in mol% with respect to lipid. EC_{50}= 5.4 mol% n=0.8.

Appendix-C

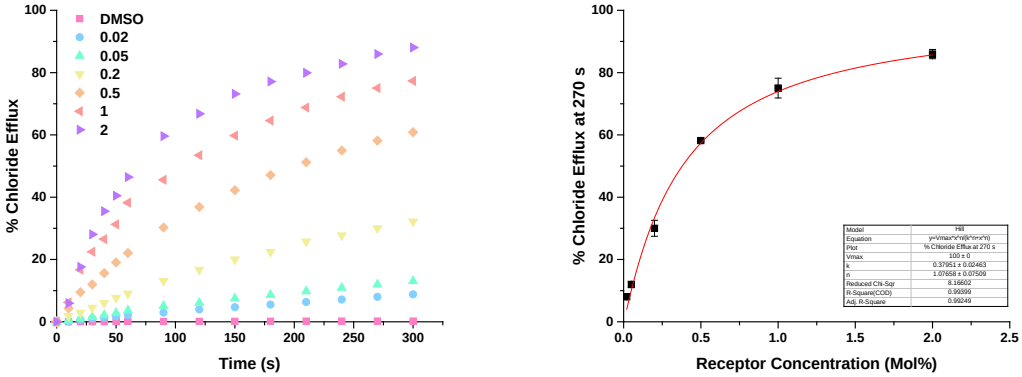

C1. 3 **Left-** Receptor **75** kinetic profile. **Right-** Hill plot; concentrations in mol% with respect to lipid.

EC_{50}=0.38 mol% n=1.07.

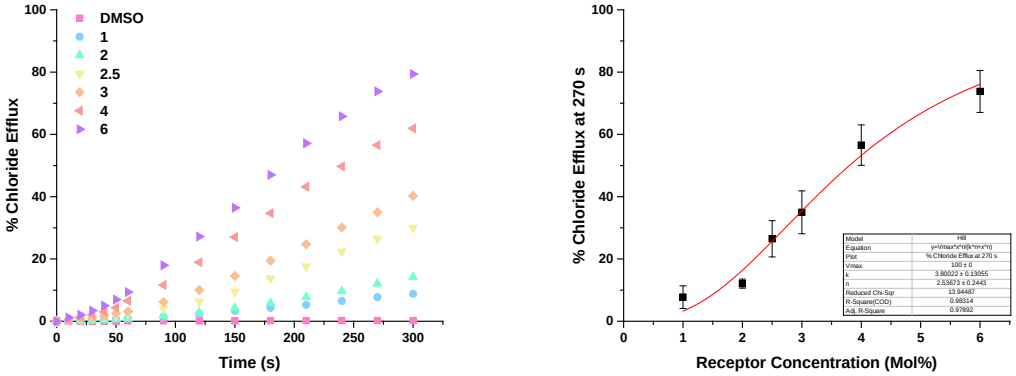

C1. 4 **Left-** Receptor **77** kinetic profile. **Right-** Hill plot; concentration in mol% with respect to lipid.

EC_{50}=3.8 mol% n=2.5.

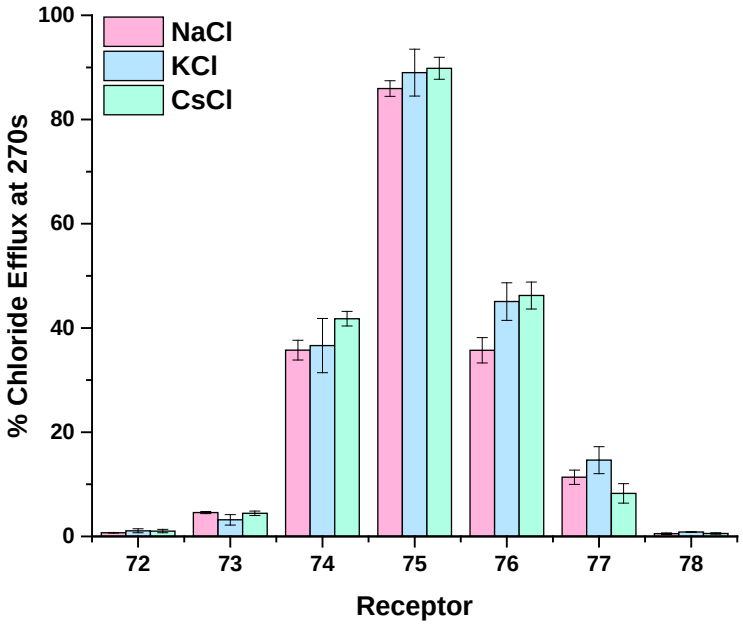

C1. 5 Chloride efflux promoted by receptors **72–78** at 2 mol% (w.r.t. lipid) after 270 s. Vesicle conditions: Internal- MCl, 489 mM (M= Na, K or Cs); External- $NaNO_3$, 489 mM; all solutions buffered to pH 7.2 with 5 mM sodium phosphate salts. At the end of the experiment the vesicles were lysed with detergent to calibrate to 100 % chloride efflux. Error bars represent the standard deviation of 3 repeats.

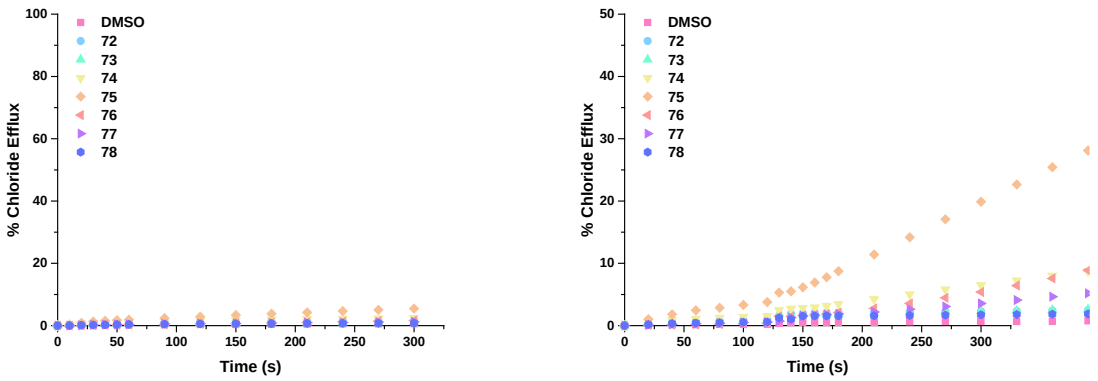

C1. 6 **Left**-Chloride efflux promoted by receptors **72–78** at 2 mol% (w.r.t. lipid) over 300 s. Conditions: Internal- NaCl, 450 mM; External- Na_2SO_4, 162 mM; all solutions were buffered to pH 7.2 with 20 mM sodium phosphate salts. At the end of the experiment the vesicles were lysed with detergent to calibrate to 100 % chloride efflux. **Right**- Chloride efflux promoted by receptors **72–78** at 2 mol% (w.r.t. lipid) over 420 s. Conditions: Internal- NaCl, 450 mM; External- Na_2SO_4, 162 mM; all solutions were buffered to pH 7.2 with 20 mM sodium phosphate salts. At 120 s a $NaHCO_3$ solution was added to give a 40 mM external concentration. At the end of the experiment the vesicles were lysed with detergent to calibrate to 100 % chloride efflux.

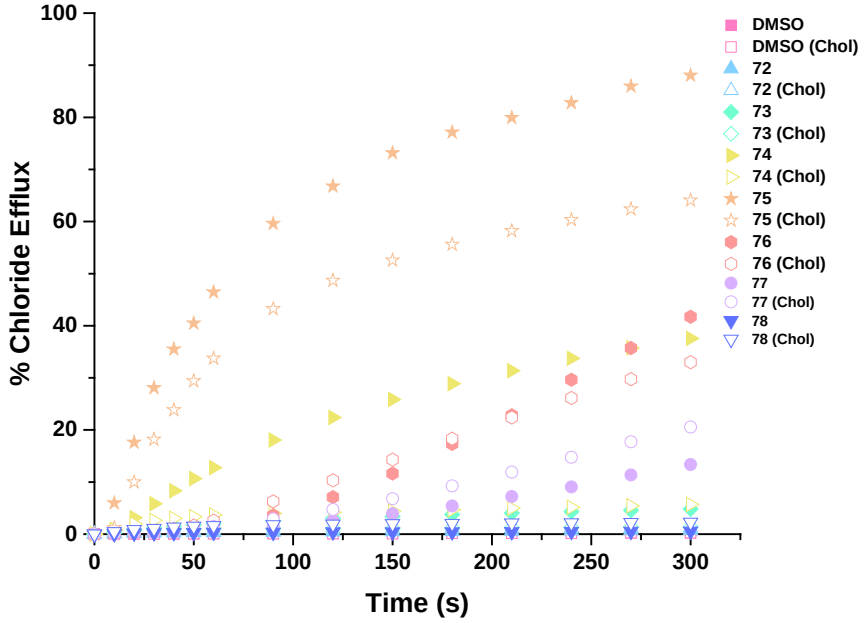

C1. 7 Chloride efflux promoted by receptors **72–78** at 2 mol% (w.r.t. lipid) over 300 s. Conditions: POPC or POPC: Cholesterol 7:3; Internal- NaCl, 489 mM; External- $NaNO_3$, 489 mM ; all solutions buffered to pH 7.2 with 5 mM sodium phosphate salts. At the end of the experiment the vesicles were lysed with detergent to calibrate to 100 % chloride efflux.

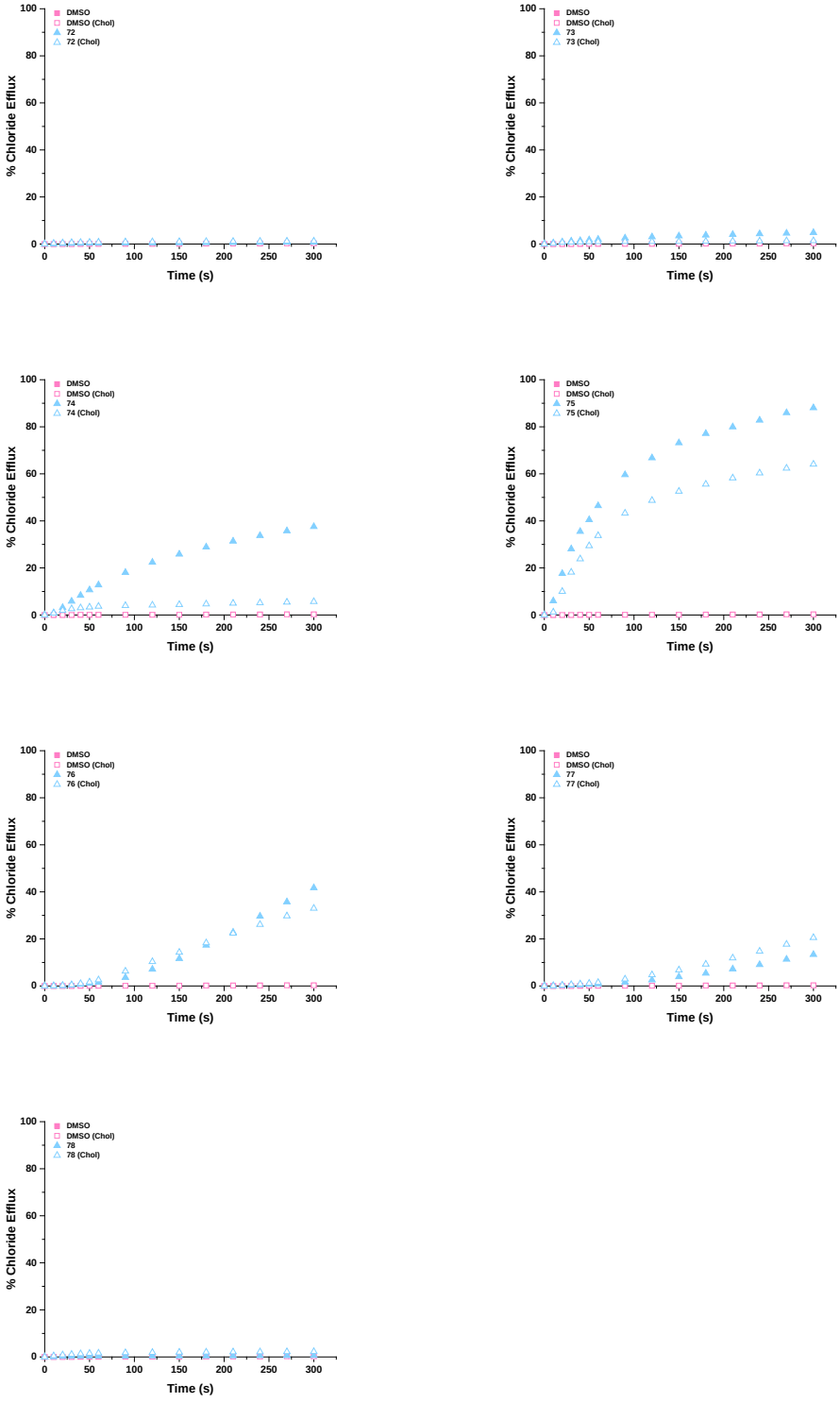

C1. 8 Chloride efflux promoted by receptors **72–78** at 2 mol% (w. r. t. lipid) over 300 s. plotted separately for clarity. Conditions: POPC or POPC: Cholesterol 7:3; Internal- NaCl, 489 mM; External- $NaNO_3$, 489 mM ; all solutions buffered to pH 7.2 with 5 mM sodium phosphate salts. At the end of the experiment the vesicles were lysed with detergent to calibrate to 100 % chloride efflux.

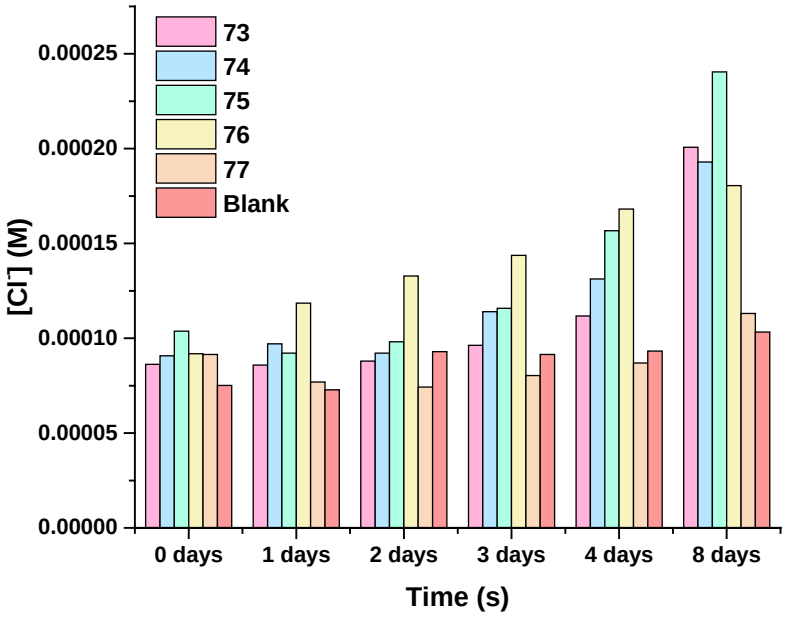

C1. 9 Chloride concentration change (M) in the receiver phase of the U-tubes facilitated by receptors **73–77**. Receptor **74** showed some signs of precipitation over the eight days studied.

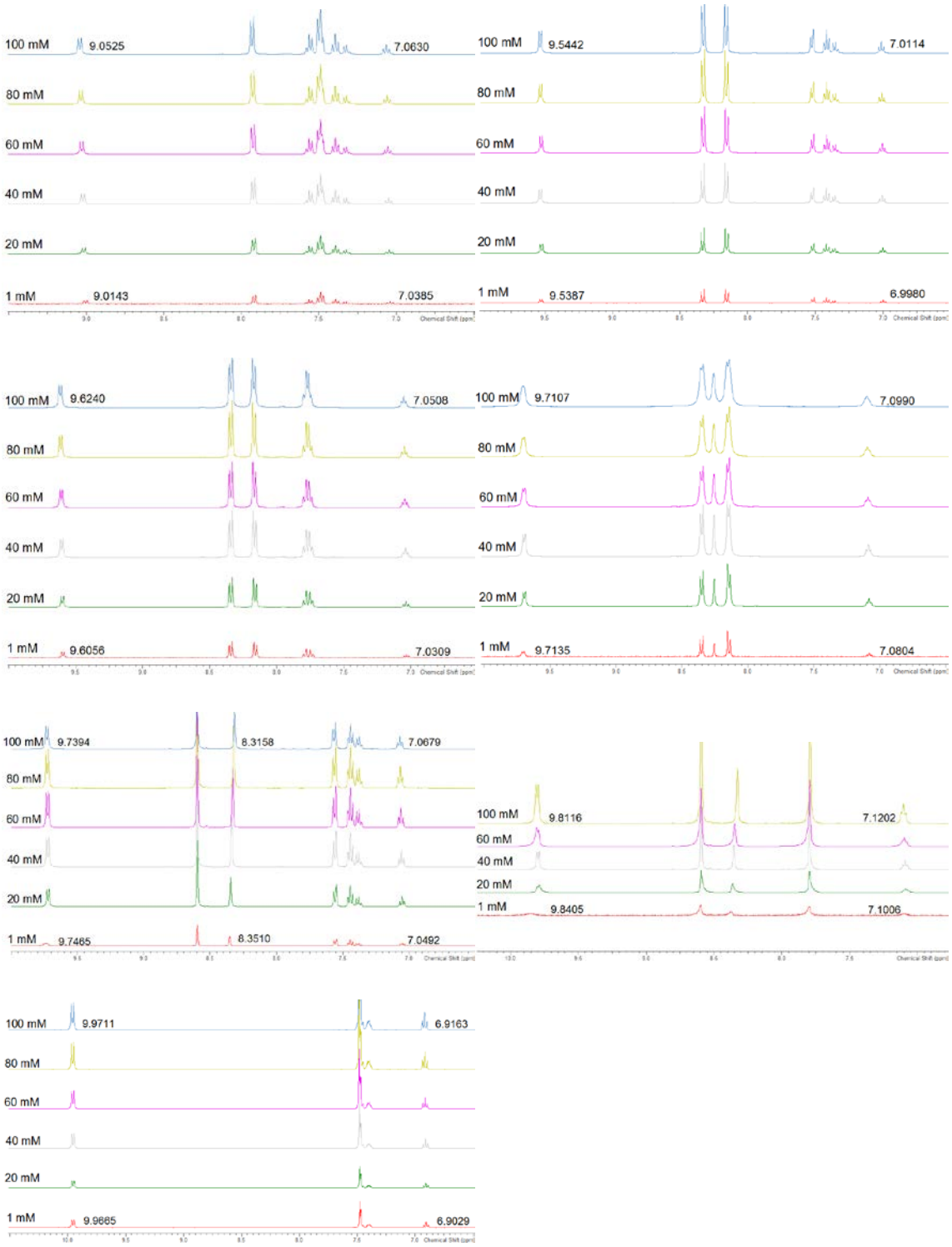

C1. 10 NMR dilution stack plots for receptors **72–78** (From left to right and top to bottom).

C.2 Fluoride transport of strapped calix[4]pyrroles

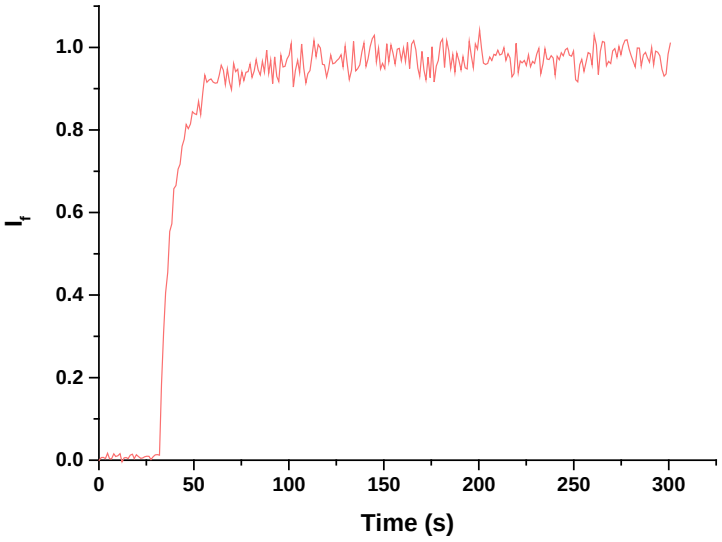

C2. 1 Base pulse HPTS test run. Conditions- Internal: NaF 300 mM and HPTS 1 mM, buffered to pH 7 with HEPES buffer 10 mM. External: NaF 300 mM buffered to pH 7 with HEPES buffer 10 mM.

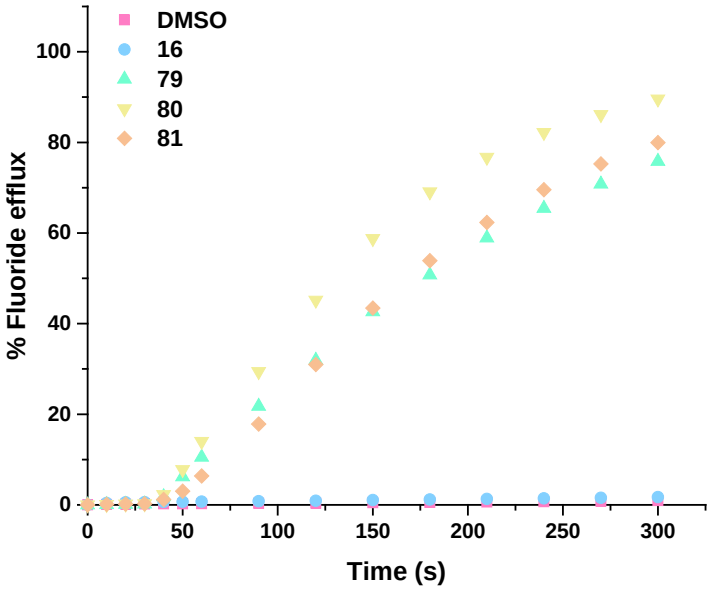

C2. 2 Fluoride efflux facilitated by **16, 79–81** at 2 mol% loading (w.r.t. lipid) from POPC vesicles. Conditions- Internal: KF 300 mM buffered to pH 7.2 with HEPES buffer 10 mM. External: KGlc 300 mM buffered to pH 7.2 with HEPES buffer. The transport was initiated by the addition of a DMSO solution of Vln (0.1 mol%) at t= 0 s and then the receptor at t= 30 s. The vesicles were lysed at 300 s. Each point is an average of 3 repeats.

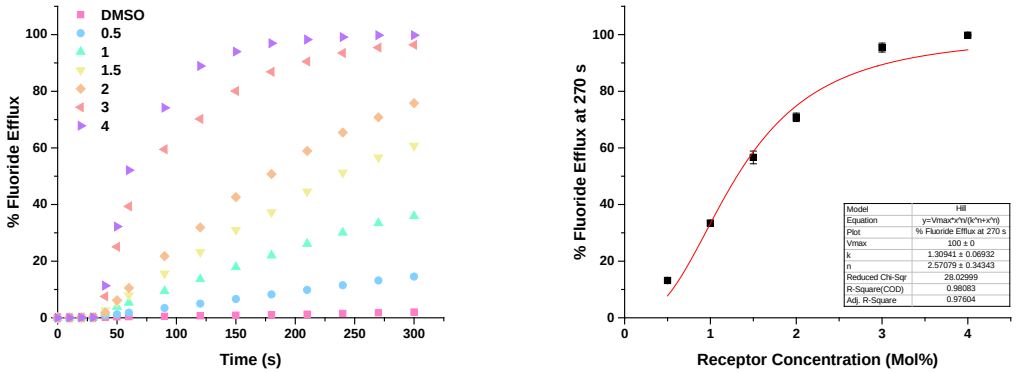

C2. 3 Fluoride dose response-**Left-** Receptor **79** kinetic profile. **Right-** Hill plot; concentrations in mol% with respect to lipid. EC_{50}= 1.3 mol% n=2.5.

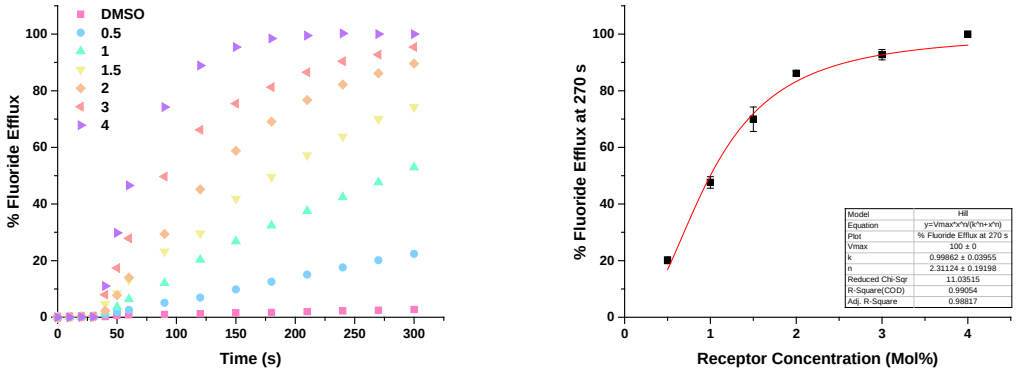

C2. 4 Fluoride dose response-**Left-** Receptor **80** kinetic profile. **Right-** Hill plot; concentrations in mol% with respect to lipid. EC_{50}= 0.9 mol% n=2.3.

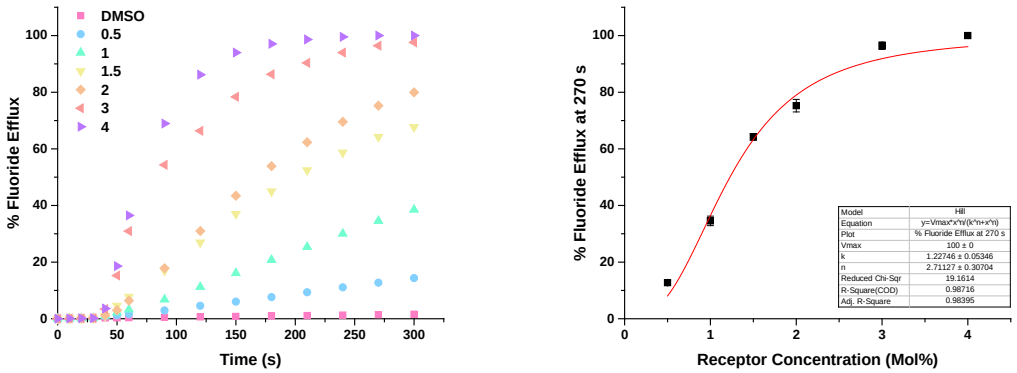

C2. 5 Fluoride dose response-**Left-** Receptor **81** kinetic profile. **Right-** Hill plot; concentrations in mol% with respect to lipid. EC_{50}= 1.2 mol% n=2.7.

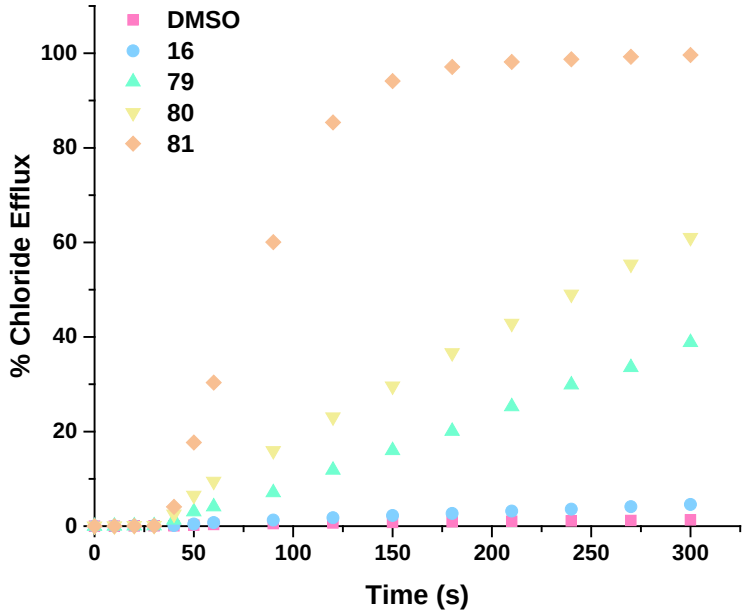

C2. 6 Chloride efflux facilitated by **16, 79–81** at 2 mol% loading (w.r.t. lipid) from POPC vesicles. Conditions- Internal: KCl 300 mM buffered to pH 7.2 with HEPES buffer 10 mM. External: KGlc 300 mM buffered to pH 7.2 with HEPES buffer. The transport was initiated by the addition of a DMSO solution of Vln (0.1 mol%) at t= 0 s and then the receptor at t= 30 s. The vesicles were lysed at 300 s. Each point is an average of 3 repeats.

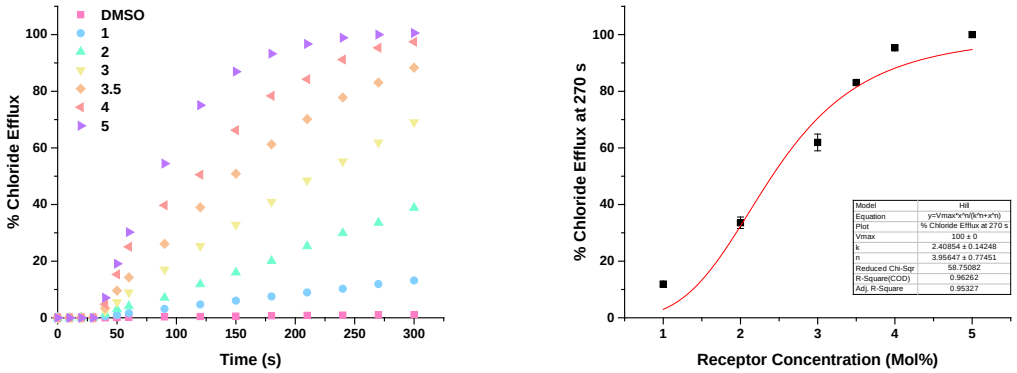

C2. 7 Chloride dose response-**Left-** Receptor **79** kinetic profile. **Right-** Hill plot; concentrations in mol% with respect to lipid. EC_{50}= 2.4 mol% n=3.9.

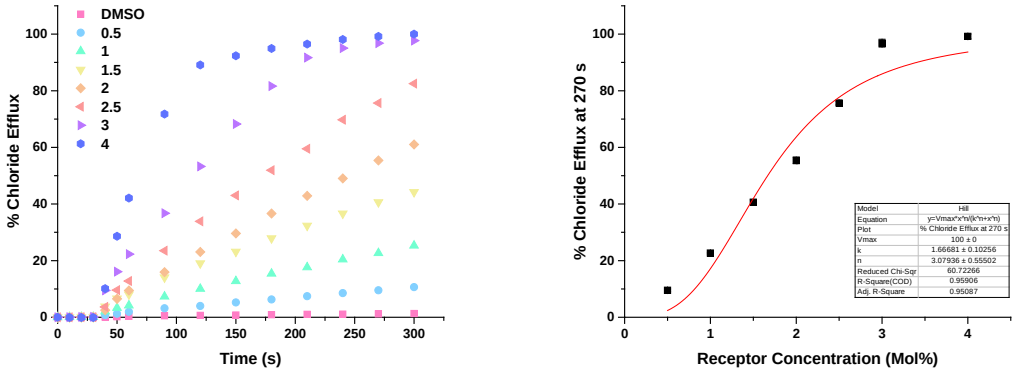

C2. 8 Chloride dose response-**Left-** Receptor **80** kinetic profile. **Right-** Hill plot; concentrations in mol% with respect to lipid. EC_{50}= 1.6 mol% n=3.0

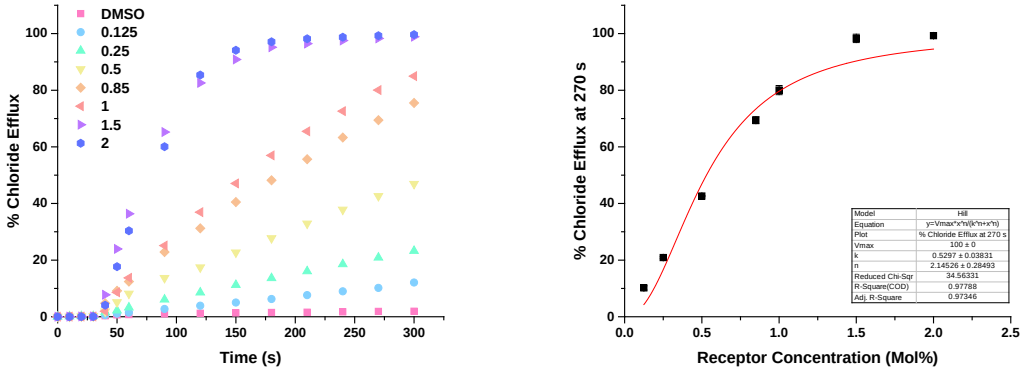

C2. 9 Chloride dose response-**Left-** Receptor **81** kinetic profile. **Right-** Hill plot; concentrations in mol% with respect to lipid. EC_{50}= 0.5 mol% n=2.1.

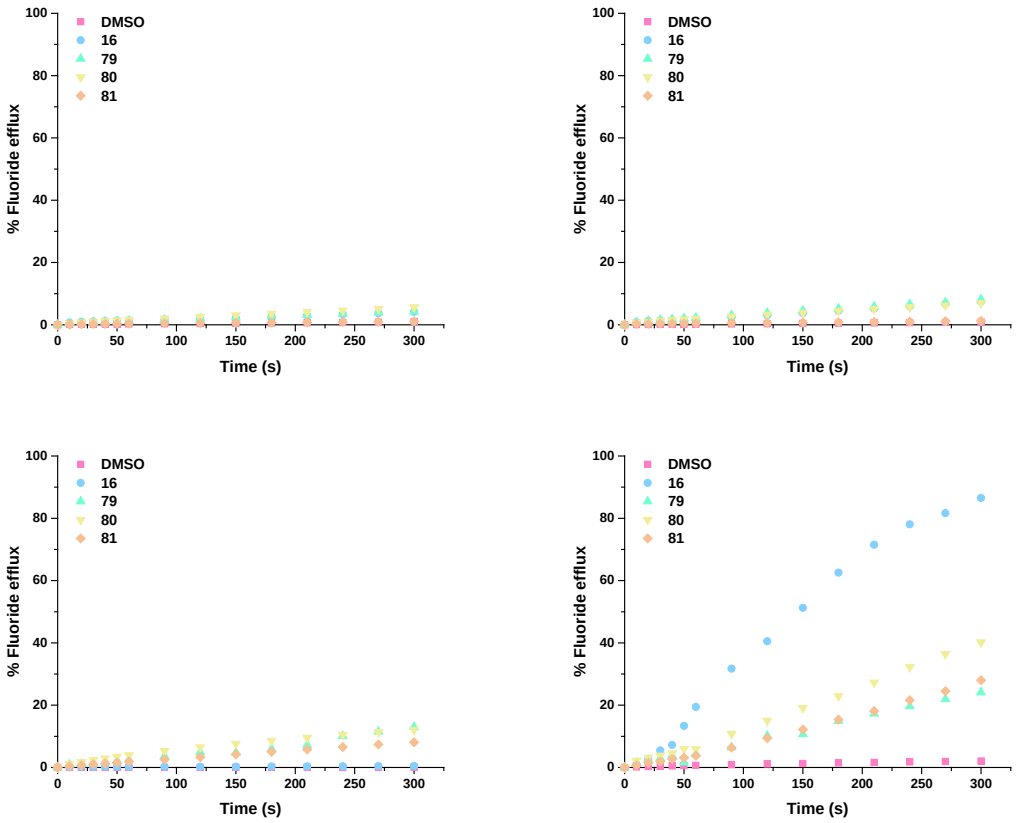

C2. 10 MF assay. Conditions- Internal: MF 300 mM buffered to pH 7.2 with HEPES buffer 10 mM (M= Na (top left), K (top right), Rb (bottom left), Cs (bottom right). External: KGlc 300 mM buffered to pH 7.2 with HEPES buffer. The transport was initiated by the addition of a DMSO solution of the receptor at t= 30 s. The vesicles were lysed at 300 s. Each point is an average of 3 repeats.

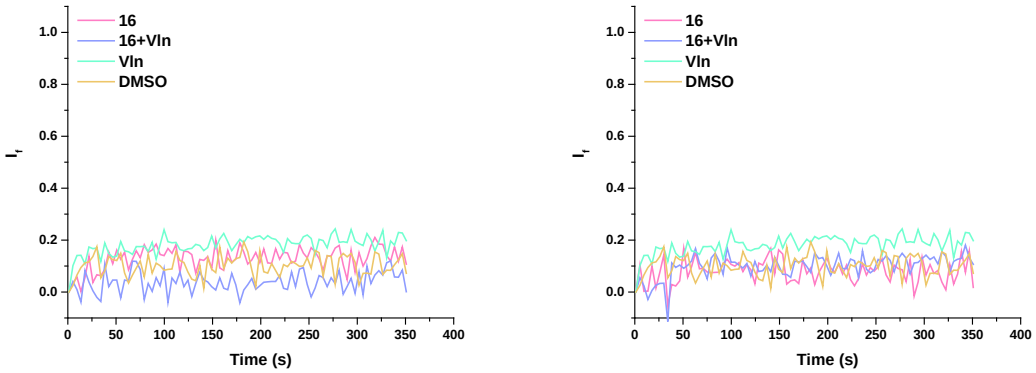

C2. 11 Osmotic assay results for receptor **16**. Conditions- Internal: KX (X=F or OAc) 300 mM buffered to pH 7.2 with HEPES buffer 10 mM. External: KGlc 300 mM buffered to pH 7.2 with HEPES buffer. The transport was initiated by the addition of a DMSO solution of Vln (0.1 mol%) and the receptor; at t= 500 s CCCP (5 mol%) was added to give maximum vesicle dehydration after t=600 s. Each plot is an average of 3 repeats. **Left-**light scattering caused by the efflux of fluoride and consequent dehydration of the vesicles via osmosis. **Right-** light scattering caused by the efflux of acetate (or acetic acid) and consequent dehydration of the vesicles via osmosis.

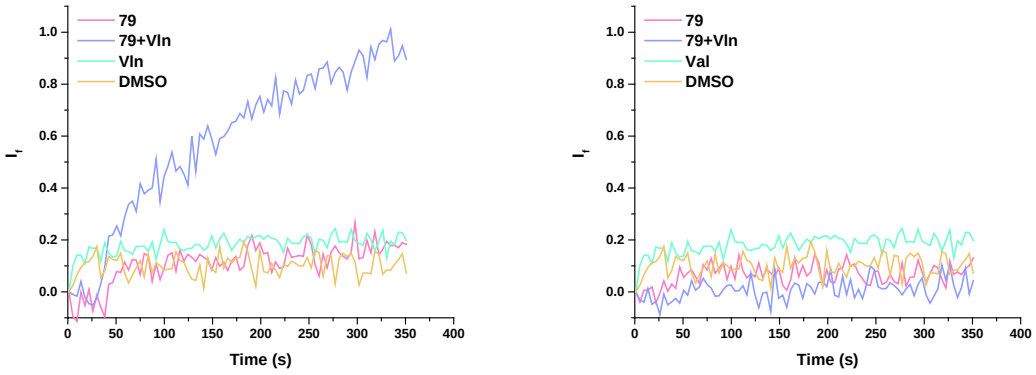

C2. 12 Osmotic assay results for receptor **79**. Conditions- Internal: KX (X=F or OAc) 300 mM buffered to pH 7.2 with HEPES buffer 10 mM. External: KGlc 300 mM buffered to pH 7.2 with HEPES buffer. The transport was initiated by the addition of a DMSO solution of Vln (0.1 mol%) and the receptor; at t= 500 s CCCP (5 mol%) was added to give maximum vesicle dehydration after t=600 s. Each plot is an average of 3 repeats. **Left-**light scattering caused by the efflux of fluoride and consequent dehydration of the vesicles via osmosis. **Right-** light scattering caused by the efflux of acetate (or acetic acid) and consequent dehydration of the vesicles via osmosis.

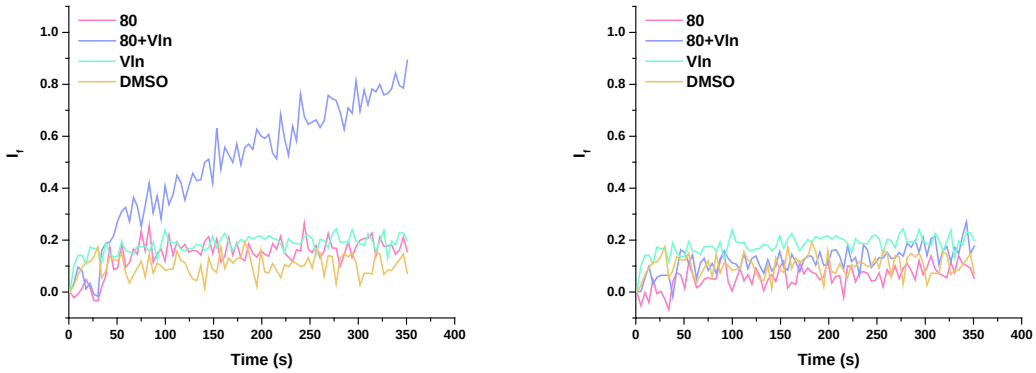

C2. 13 Osmotic assay results for receptor **80**. Conditions- Internal: KX (X=F or OAc) 300 mM buffered to pH 7.2 with HEPES buffer 10 mM. External: KGlc 300 mM buffered to pH 7.2 with HEPES buffer. The transport was initiated by the addition of a DMSO solution of Vln (0.1 mol%) and the receptor; at t= 500 s CCCP (5 mol%) was added to give maximum vesicle dehydration after t=600 s. Each plot is an average of 3 repeats. **Left-**light scattering caused by the efflux of fluoride and consequent dehydration of the vesicles via osmosis. **Right-** light scattering caused by the efflux of acetate (or acetic acid) and consequent dehydration of the vesicles via osmosis.

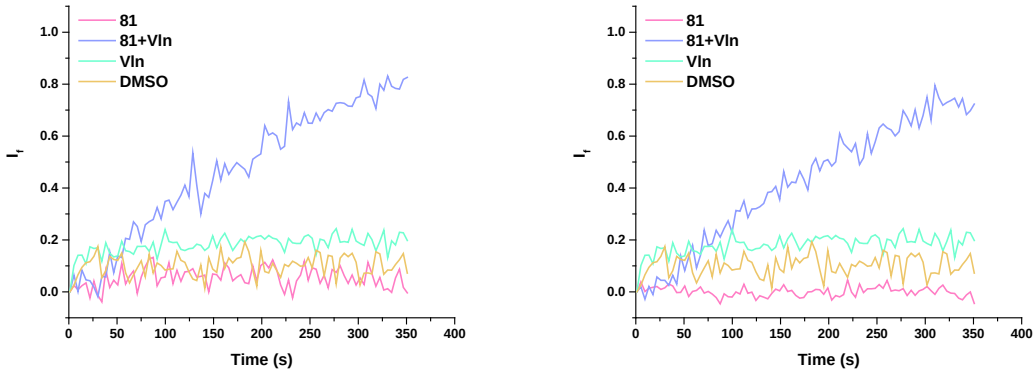

C2. 14 Osmotic assay results for receptor **81**. Conditions- Internal: KX (X=F or OAc) 300 mM buffered to pH 7.2 with HEPES buffer 10 mM. External: KGlc 300 mM buffered to pH 7.2 with HEPES buffer. The transport was initiated by the addition of a DMSO solution of Vln (0.1 mol%) and the receptor; at t= 500 s CCCP (5 mol%) was added to give maximum vesicle dehydration after t=600 s. Each plot is an average of 3 repeats. **Left-**light scattering caused by the efflux of fluoride and consequent dehydration of the vesicles via osmosis. **Right-** light scattering caused by the efflux of acetate (or acetic acid) and consequent dehydration of the vesicles via osmosis.

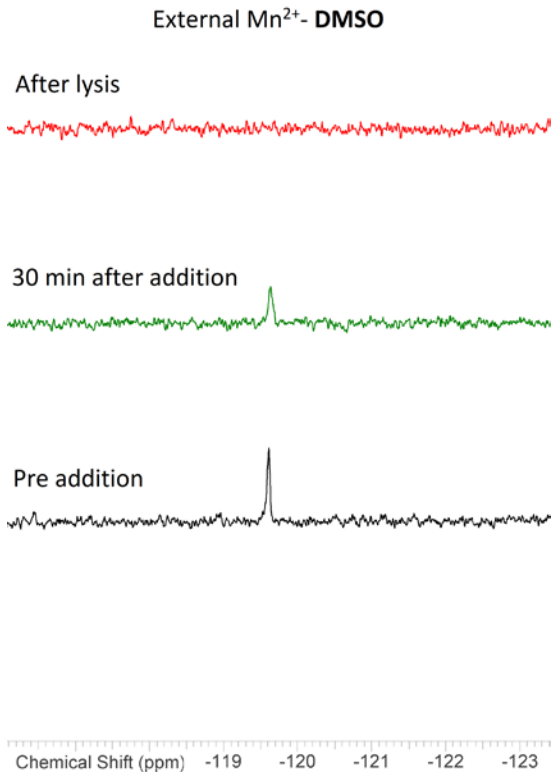

C2. 15 ^{19}F NMR experiments to detect fluoride transport with external Mn^{2+} a 'switch off' method. DMSO added as a control.

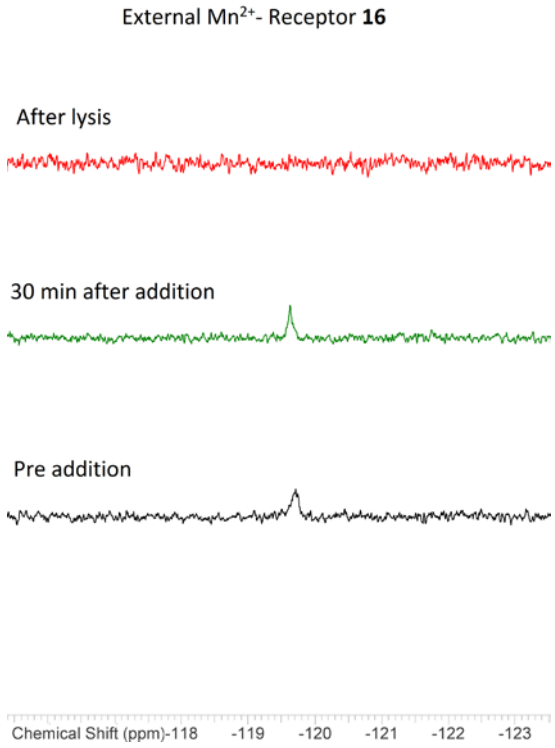

C2. 16 ^{19}F NMR experiments to detect fluoride transport with external Mn^{2+} a 'switch off' method. Receptor **16** and Vln added as a 2 mol% and 0.1 mol% DMSO solution respectively.

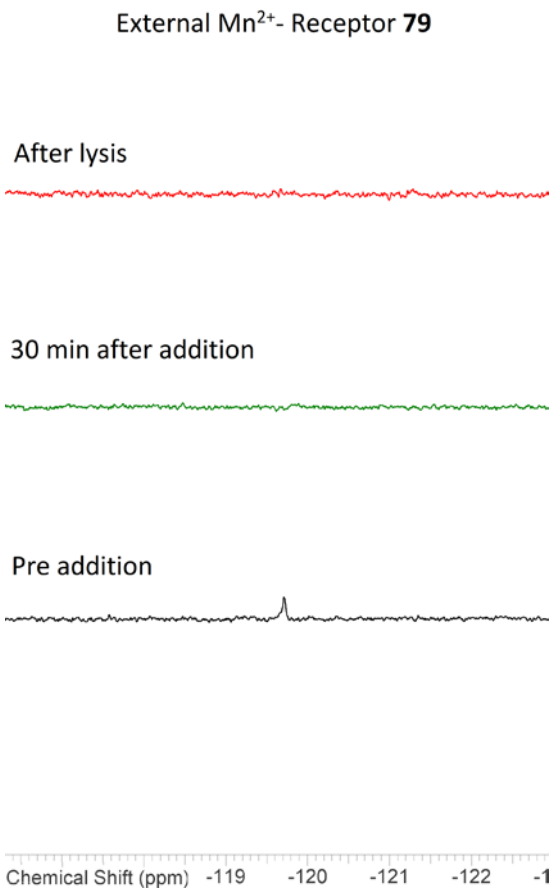

C2. 17 ^{19}F NMR experiments to detect fluoride transport with external Mn^{2+} a 'switch off' method. Receptor **79** and Vln added as a 2 mol% and 0.1 mol% DMSO solution respectively.

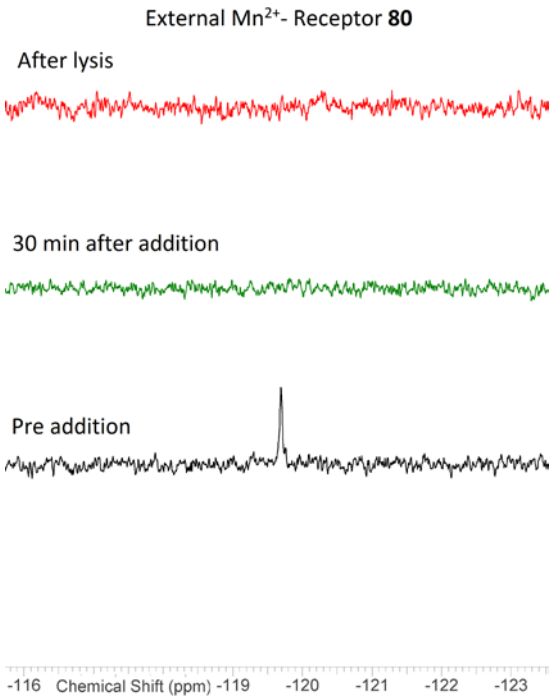

C2. 18 ^{19}F NMR experiments to detect fluoride transport with external Mn^{2+} a 'switch off' method. Receptor **80** and Vln added as a 2 mol% and 0.1 mol% DMSO solution respectively.

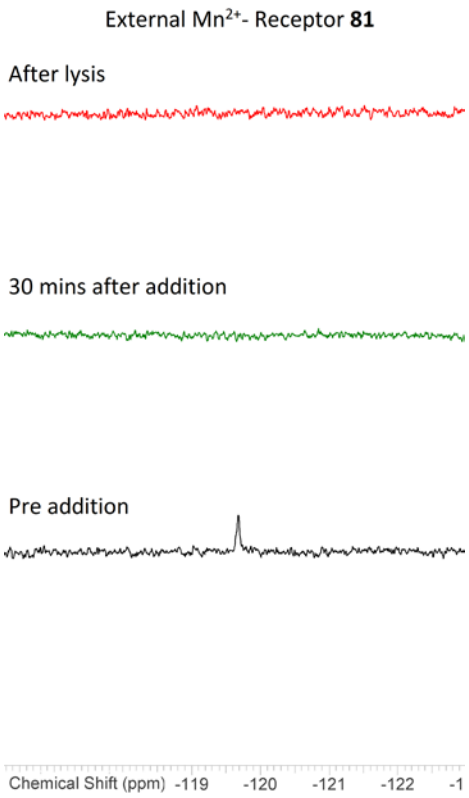

C2. 19 ^{19}F NMR experiments to detect fluoride transport with external Mn^{2+} a 'switch off' method. Receptor **81** and Vln added as a 2 mol% and 0.1 mol% DMSO solution respectively.

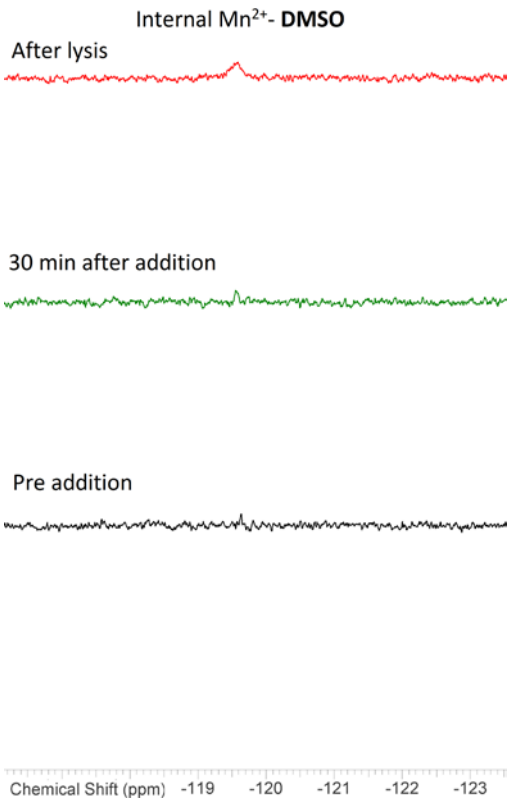

C2. 20 ^{19}F NMR experiments to detect fluoride transport with internal Mn^{2+} a 'switch on' method. DMSO added as a control.

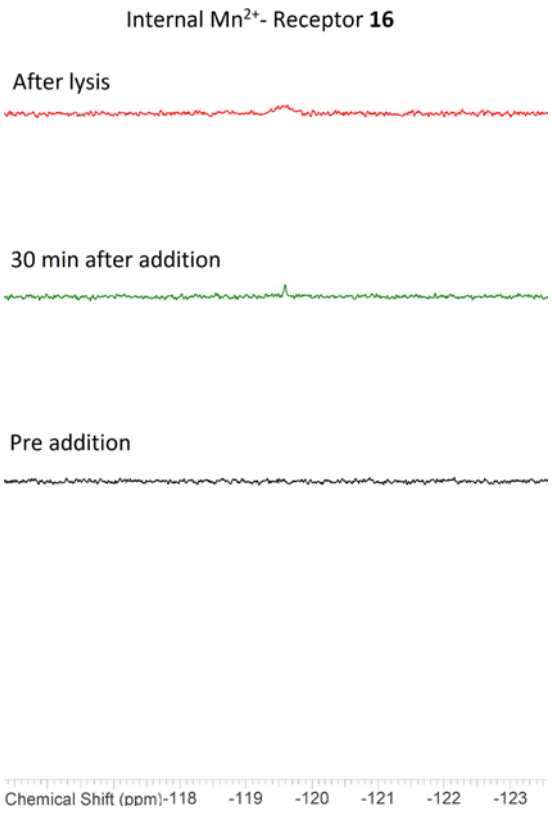

C2. 21 ^{19}F NMR experiments to detect fluoride transport with internal Mn^{2+} a 'switch on' method. Receptor **16** and Vln added as a 2 mol% and 0.1 mol% DMSO solution respectively.

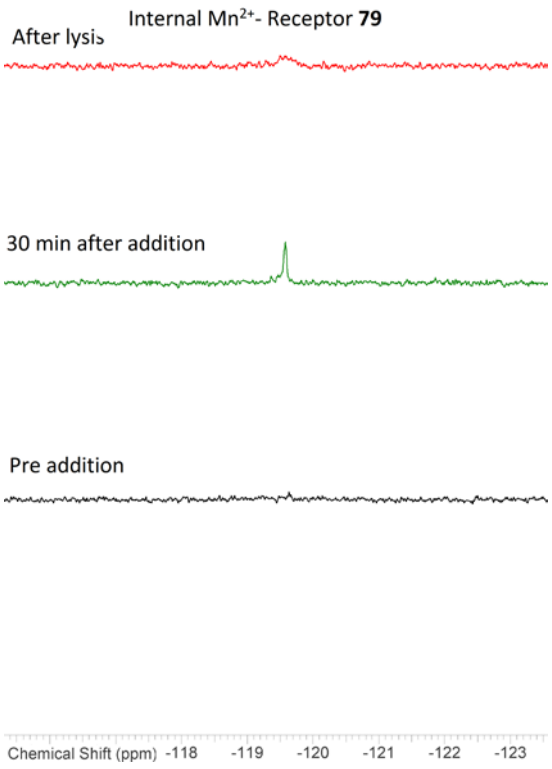

C2. 22 ^{19}F NMR experiments to detect fluoride transport with internal Mn^{2+} a 'switch on' method. Receptor **79** and Vln added as a 2 mol% and 0.1 mol% DMSO solution respectively.

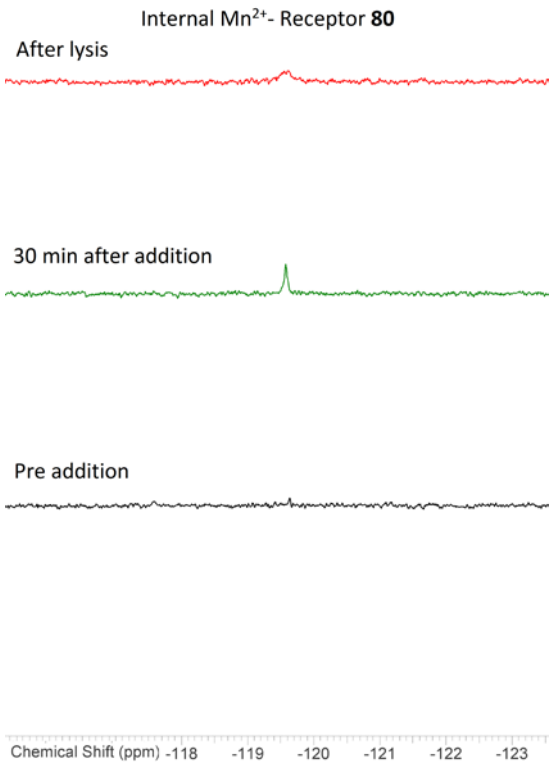

C2. 23 ^{19}F NMR experiments to detect fluoride transport with internal Mn^{2+} a 'switch on' method. Receptor **80** and Vln added as a 2 mol% and 0.1 mol% DMSO solution respectively.

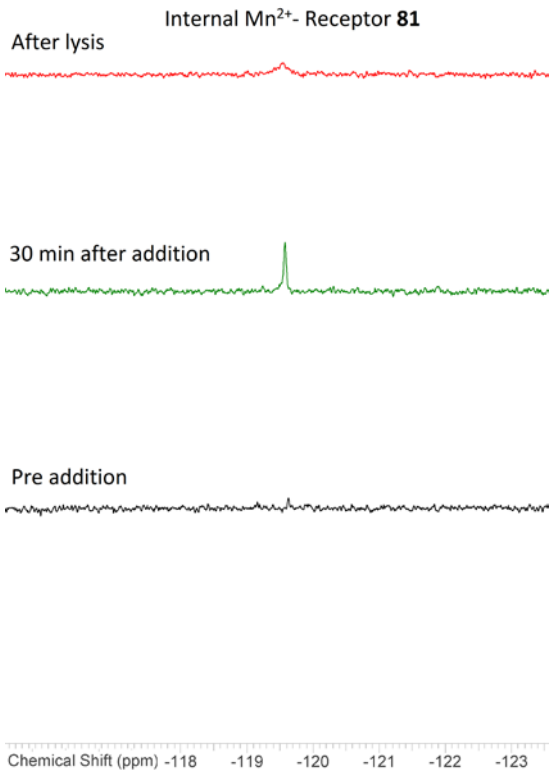

C2. 24 ^{19}F NMR experiments to detect fluoride transport with internal Mn^{2+} a 'switch on' method. Receptor **81** and Vln added as a 2 mol% and 0.1 mol% DMSO solution respectively.

C.3 Chloride over H^+/OH^- selectivity and halide selectivity of the extended series of strapped calix[4]pyrroles.

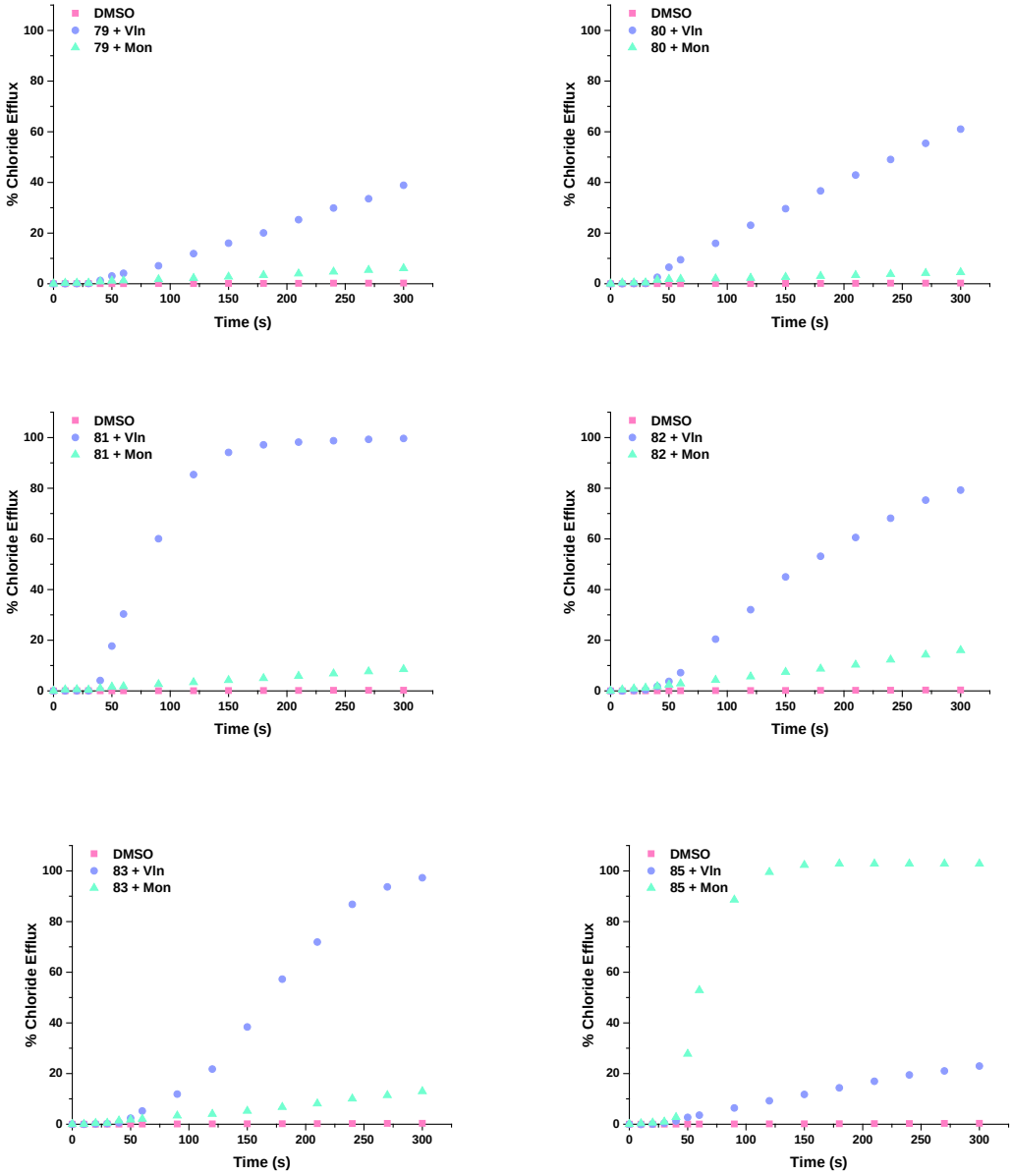

C3. 1 Coupling to valinomycin and monensin for **79–85**. Chloride efflux facilitated at 2 mol% loading (w.r.t. lipid) from POPC vesicles. The transport was initiated by the addition of a DMSO solution of Vln (0.1 mol%) or Mon (0.1 mol%) at t= 0 s and then the receptor at t= 30 s. The vesicles were lysed at 300 s. Each point is an average of 3 repeats.

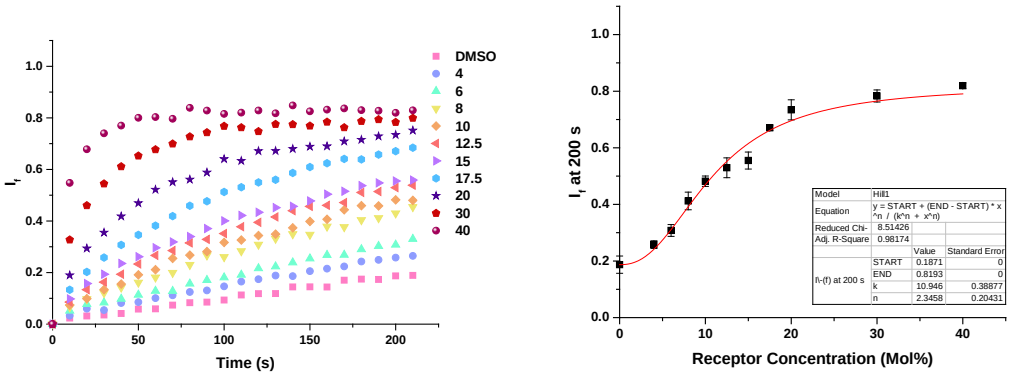

C3. 2 NMDG-Cl dose response-**Left-** Receptor **79** kinetic profile. **Right-** Hill plot; concentrations in mol% with respect to lipid. EC_{50}= 10.9 mol% n=2.3.

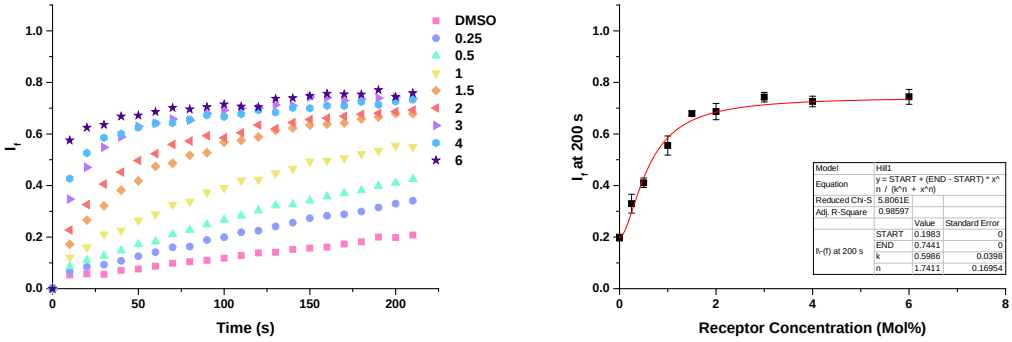

C3. 3 NMDG-Cl with Gra (0.1 mol%) dose response-**Left-** Receptor **79** kinetic profile. **Right-** Hill plot; concentrations in mol% with respect to lipid. EC_{50}= 0.6 mol% n=1.7.

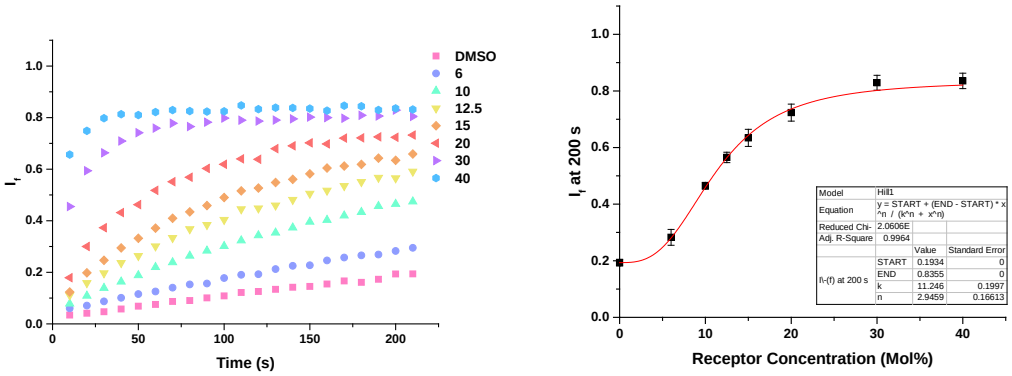

C3. 4 NMDG-Cl with OA (2 mol%) dose response-**Left-** Receptor **79** kinetic profile. **Right-** Hill plot; concentrations in mol% with respect to lipid. EC_{50}= 11.2 mol% n=2.9.

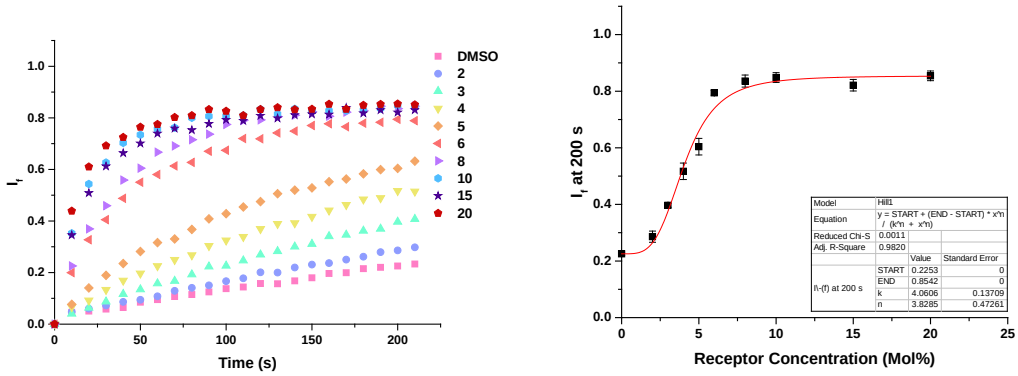

C3. 5 NMDG-Cl dose response-**Left-** Receptor **80** kinetic profile. **Right-** Hill plot; concentrations in mol% with respect to lipid. EC_{50}= 4.1 mol% n=3.8.

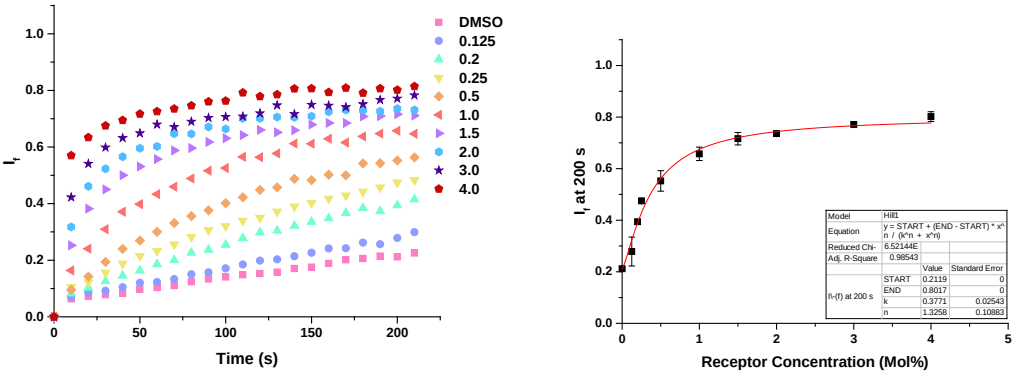

C3. 6 NMDG-Cl with Gra (0.1 mol%) dose response-**Left-** Receptor **80** kinetic profile. **Right-** Hill plot; concentrations in mol% with respect to lipid. EC_{50}= 0.4 mol% n=1.3.

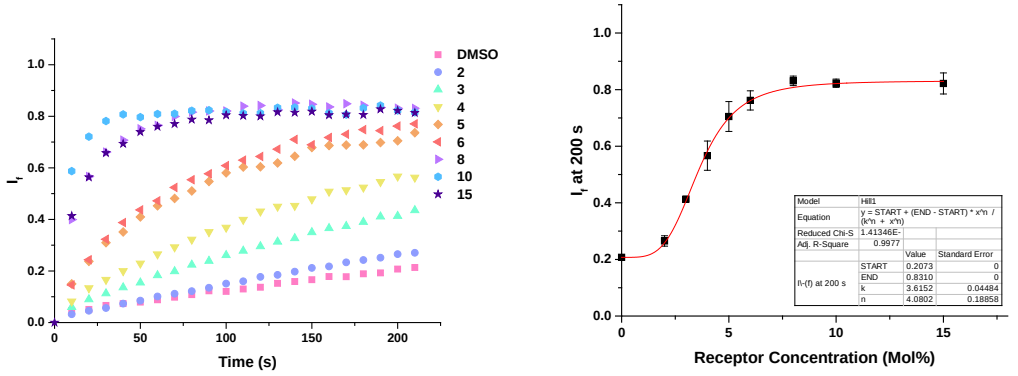

C3. 7 NMDG-Cl with OA (2 mol%)dose response-**Left-** Receptor **80** kinetic profile. **Right-** Hill plot; concentrations in mol% with respect to lipid. EC_{50}= 3.6 mol% n=4.0.

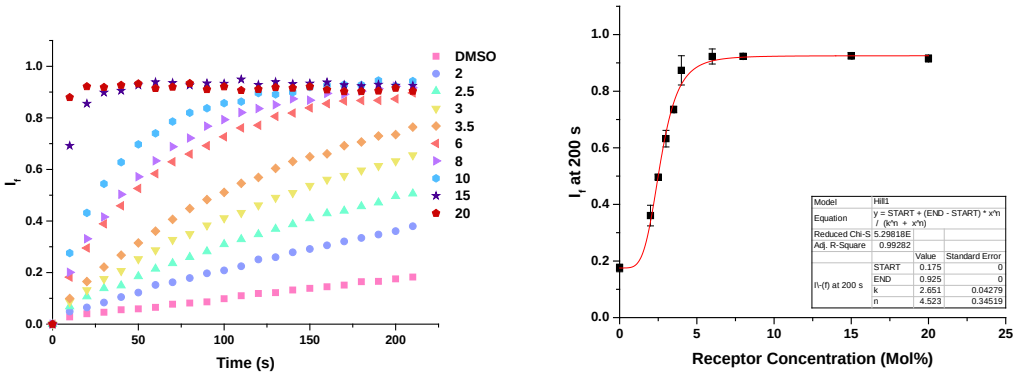

C3. 8 NMDG-Cl dose response-**Left-** Receptor **81** kinetic profile. **Right-** Hill plot; concentrations in mol% with respect to lipid. EC_{50}= 2.7 mol% n=4.5.

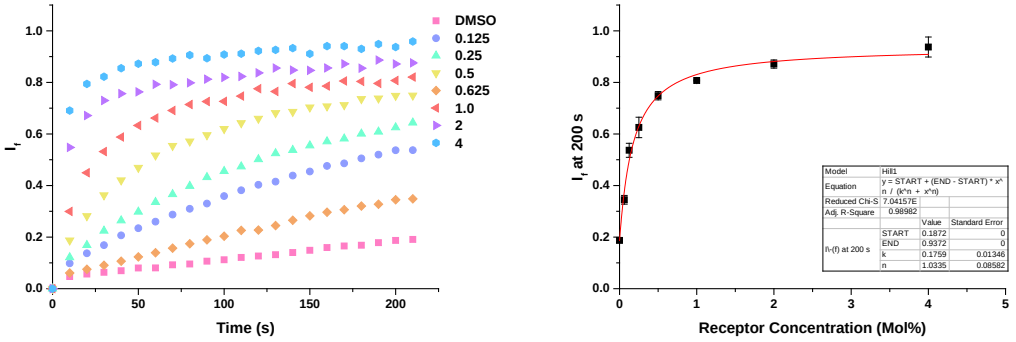

C3. 9 NMDG-Cl with Gra (0.1 mol%)dose response-**Left-** Receptor **81** kinetic profile. **Right-** Hill plot; concentrations in mol% with respect to lipid. EC_{50}= 0.2 mol% n=1.0.

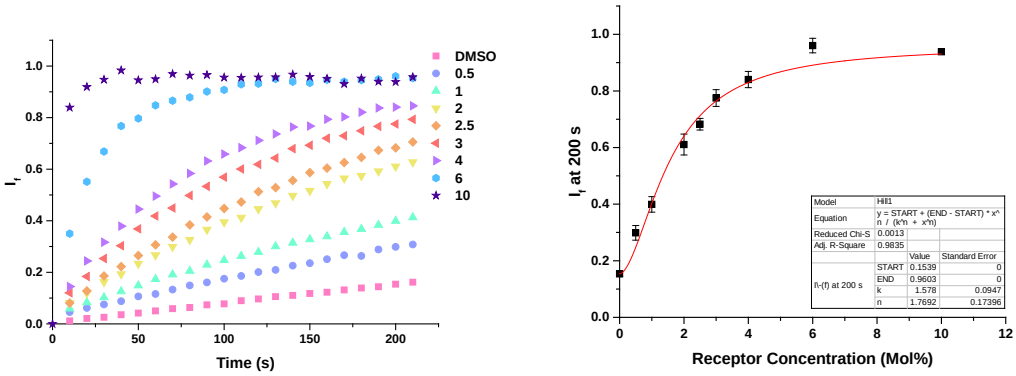

C3. 10 NMDG-Cl with OA (2 mol%) dose response-**Left-** Receptor **81** kinetic profile. **Right-** Hill plot; concentrations in mol% with respect to lipid. EC_{50}= 1.6 mol% n=1.8.

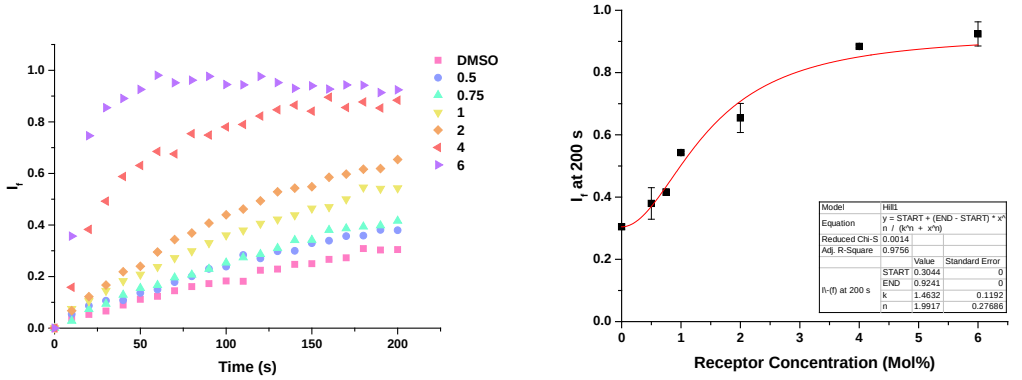

C3. 11 NMDG-Cl dose response-**Left-** Receptor **82** kinetic profile. **Right-** Hill plot; concentrations in mol% with respect to lipid. EC_{50}= 1.5 mol% n=2.0.

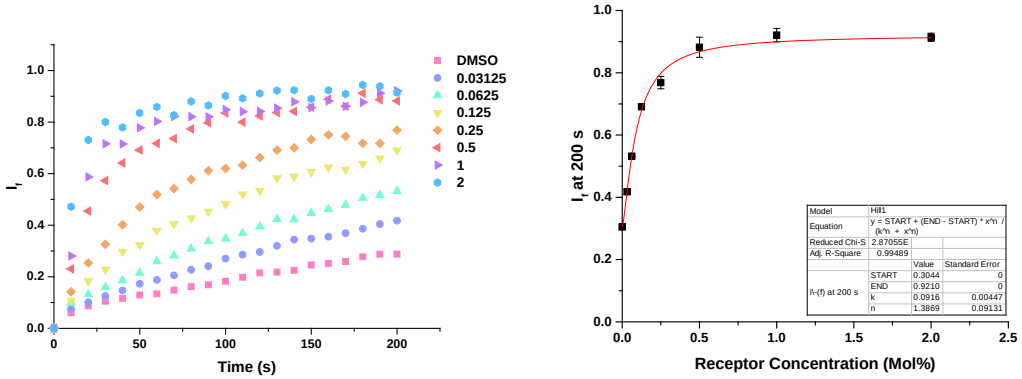

C3. 12 NMDG-Cl with Gra (0.1 mol%) dose response-**Left-** Receptor **82** kinetic profile. **Right-** Hill plot; concentrations in mol% with respect to lipid. EC_{50}= 0.1 mol% n=1.4.

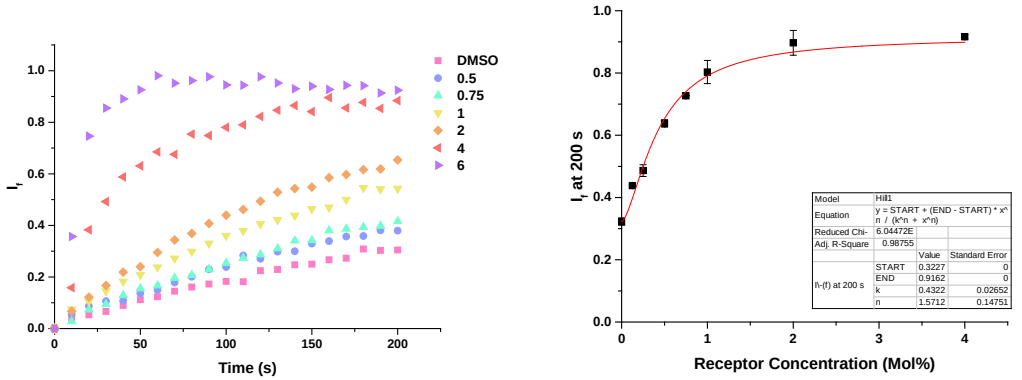

C3. 13 NMDG-Cl with OA (2 mol%) dose response-**Left-** Receptor **82** kinetic profile. **Right-** Hill plot; concentrations in mol% with respect to lipid. EC_{50}= 0.4 mol% n=1.6.

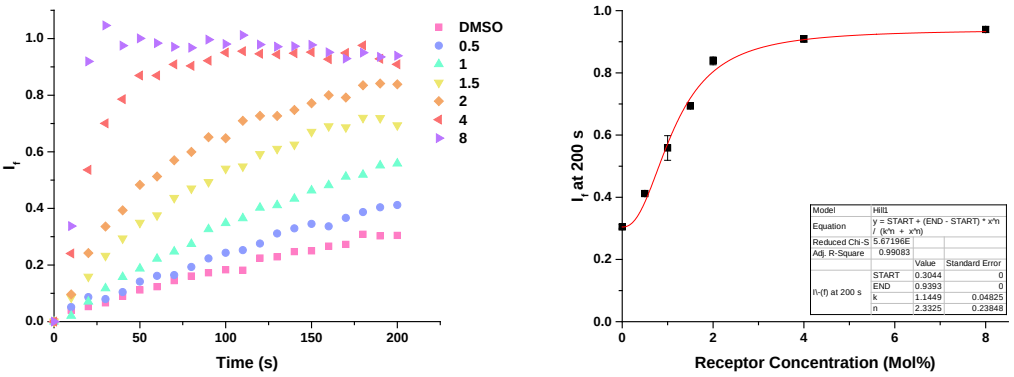

C3. 14 NMDG-Cl dose response-**Left-** Receptor **83** kinetic profile. **Right-** Hill plot; concentrations in mol% with respect to lipid. EC_{50}= 1.1 mol% n=2.3.

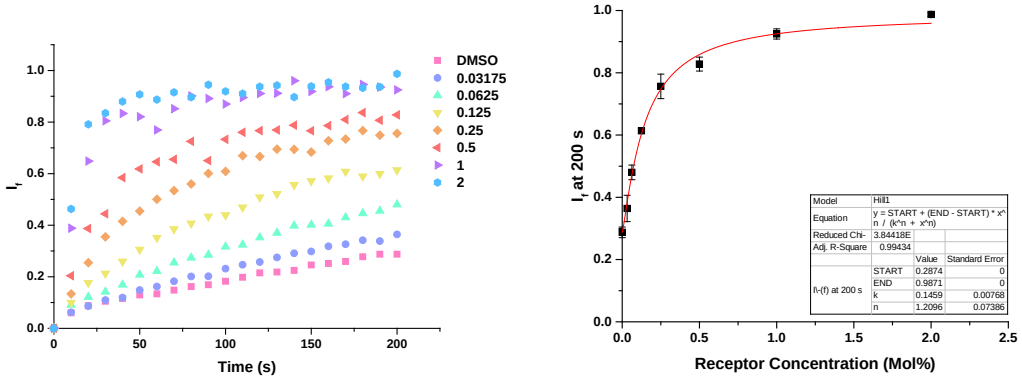

C3. 15 NMDG-Cl with Gra (0.1 mol%) dose response-**Left-** Receptor **83** kinetic profile. **Right-** Hill plot; concentrations in mol% with respect to lipid. EC_{50}= 0.1 mol% n=1.2.

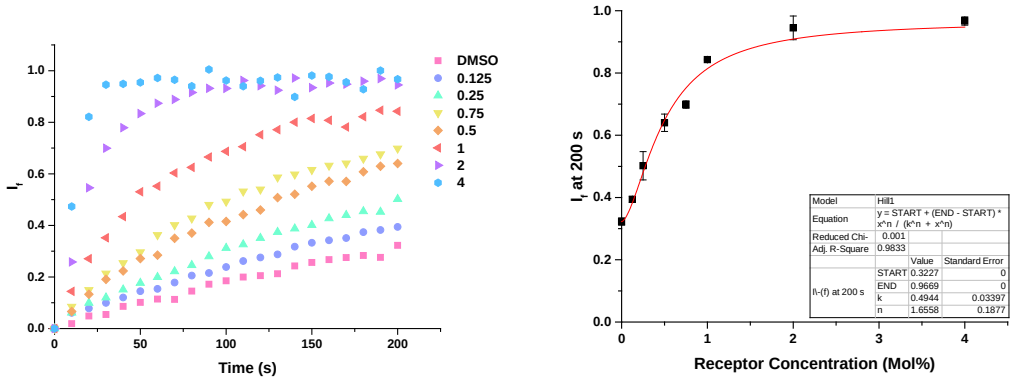

C3. 16 NMDG-Cl with OA (2 mol%) dose response-**Left-** Receptor **83** kinetic profile. **Right-** Hill plot; concentrations in mol% with respect to lipid. EC_{50}= 0.5 mol% n=1.6.

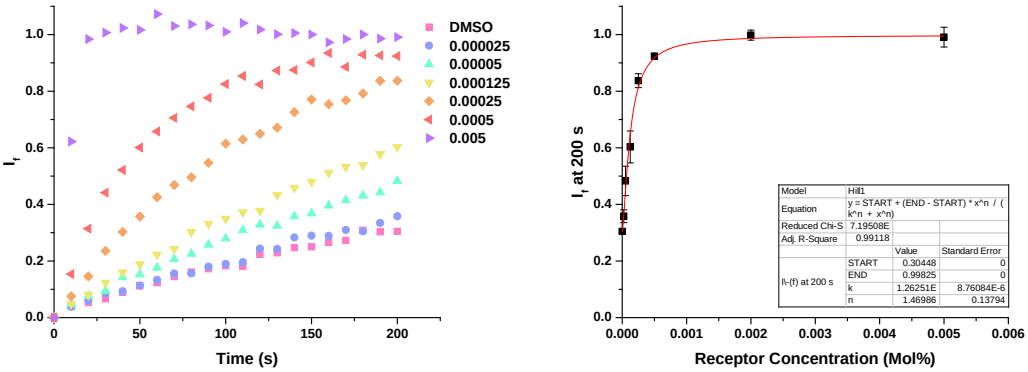

C3. 17 NMDG-Cl dose response-**Left-** Receptor **85** kinetic profile. **Right-** Hill plot; concentrations in mol% with respect to lipid. EC_{50}= 0.00013 mol% n=1.5.

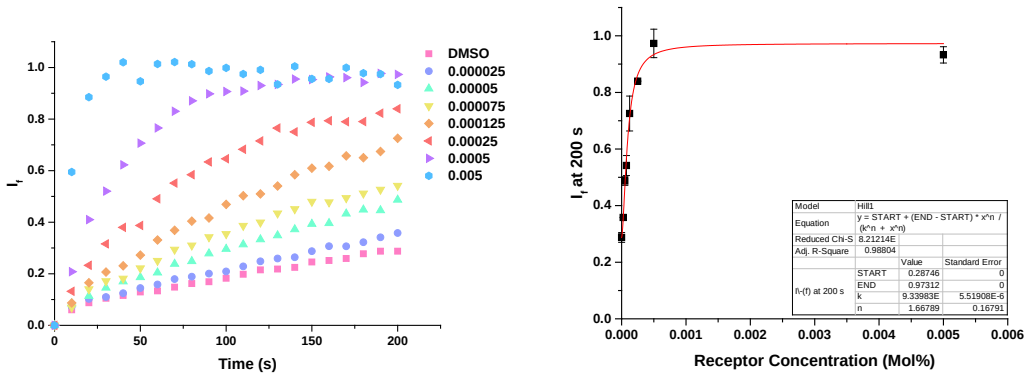

C3. 18 NMDG-Cl with Gra (0.1 mol%) dose response-**Left-** Receptor **85** kinetic profile. **Right-** Hill plot; concentrations in mol% with respect to lipid. EC_{50}= 0.000093 mol% n=1.7.

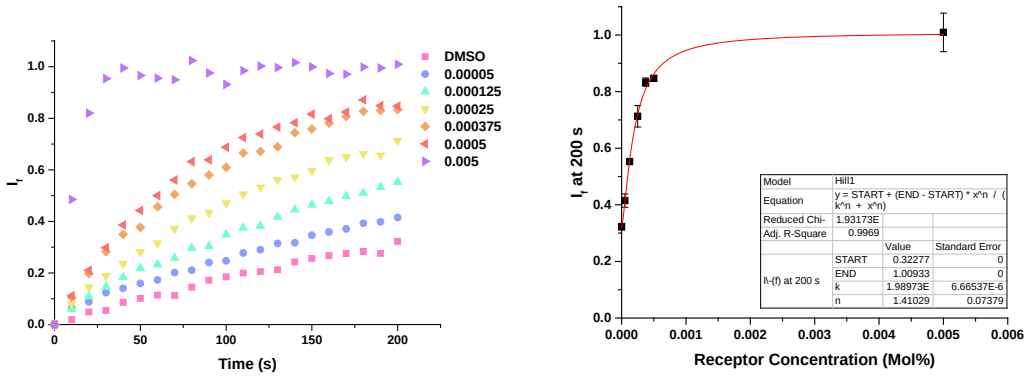

C3. 19 NMDG-Cl with OA (2 mol%) dose response-**Left-** Receptor **85** kinetic profile. **Right-** Hill plot; concentrations in mol% with respect to lipid. EC_{50}= 0.0002 mol% n=1.4.

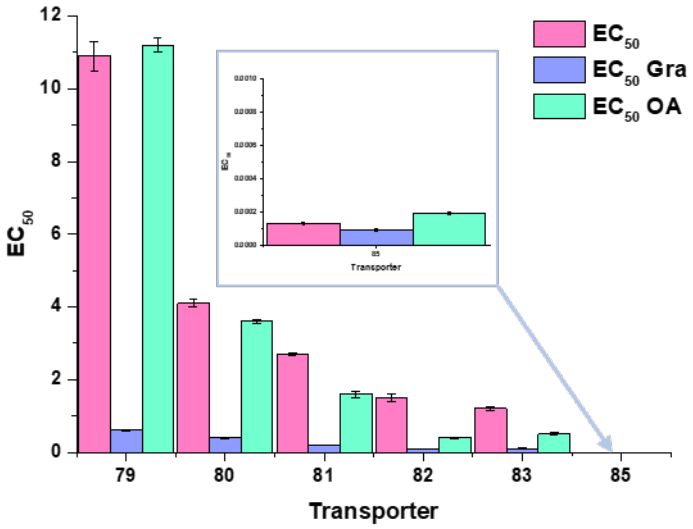

C3. 20 Bar chart of EC_{50} results for dose response studies with **79–83** and **85** from POPC vesicles. Conditions- Internal: NMDG-Cl 100 mM and HPTS 1 mM buffered to pH 7 with HEPES buffer 10 mM. External: NMDG-Cl 100 mM buffered to pH 7 with HEPES buffer 10 mM, pulse: NMDG to bring external pH to 8. The H^+/Cl^- symport was measured by monitoring the HPTS fluorescence ratio after the addition of a 5 mM NMDG pulse (with an additional pulse of Gra (0.1 mol%) or OA (2 mol%) as appropriate). The Hill equation was used to fit the dose-response curves for **79–83** and **85** alone, with Gra and with OA. Inset shows **85** is a very efficient transporter.

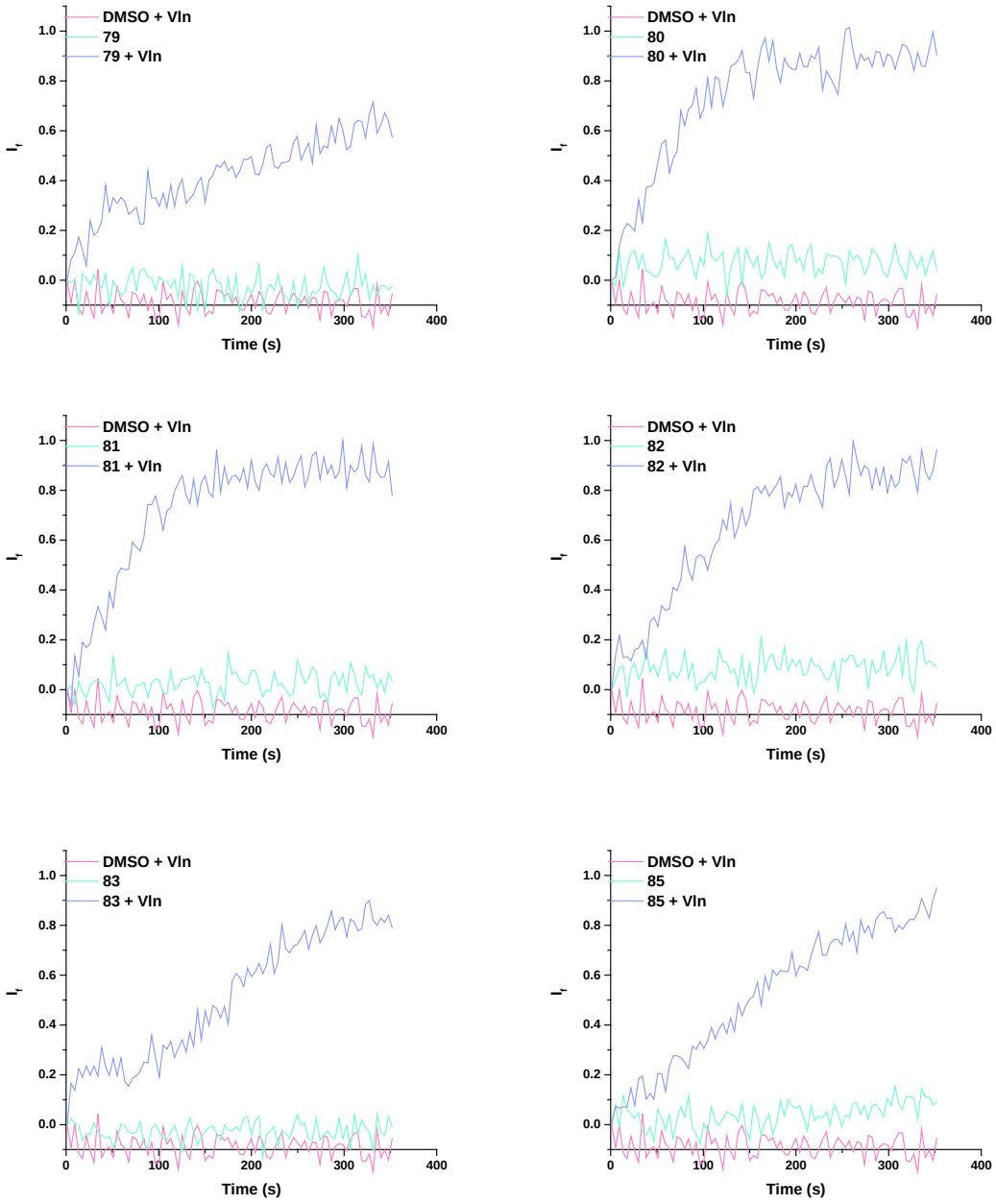

C3. 21 Osmotic assay results for **79**–**82** and **85** at 4 mol% loading (w.r.t. lipid) from POPC vesicles. Conditions-Internal: KCl 300 mM buffered to pH 7.2 with HEPES buffer 10 mM. External: KGlc 300 mM buffered to pH 7.2 with HEPES buffer. The transport was initiated by the addition of a DMSO solution of Vln (0.1 mol%) and the receptor, at t= 500 s tren-pentafluoropropylthiourea (8 mol%) was added to give maximum vesicle dehydration after t=600 s. Each plot is an average of 2 repeats. The plots show light scattering caused by the efflux of chloride and consequent dehydration of the vesicles via osmosis.

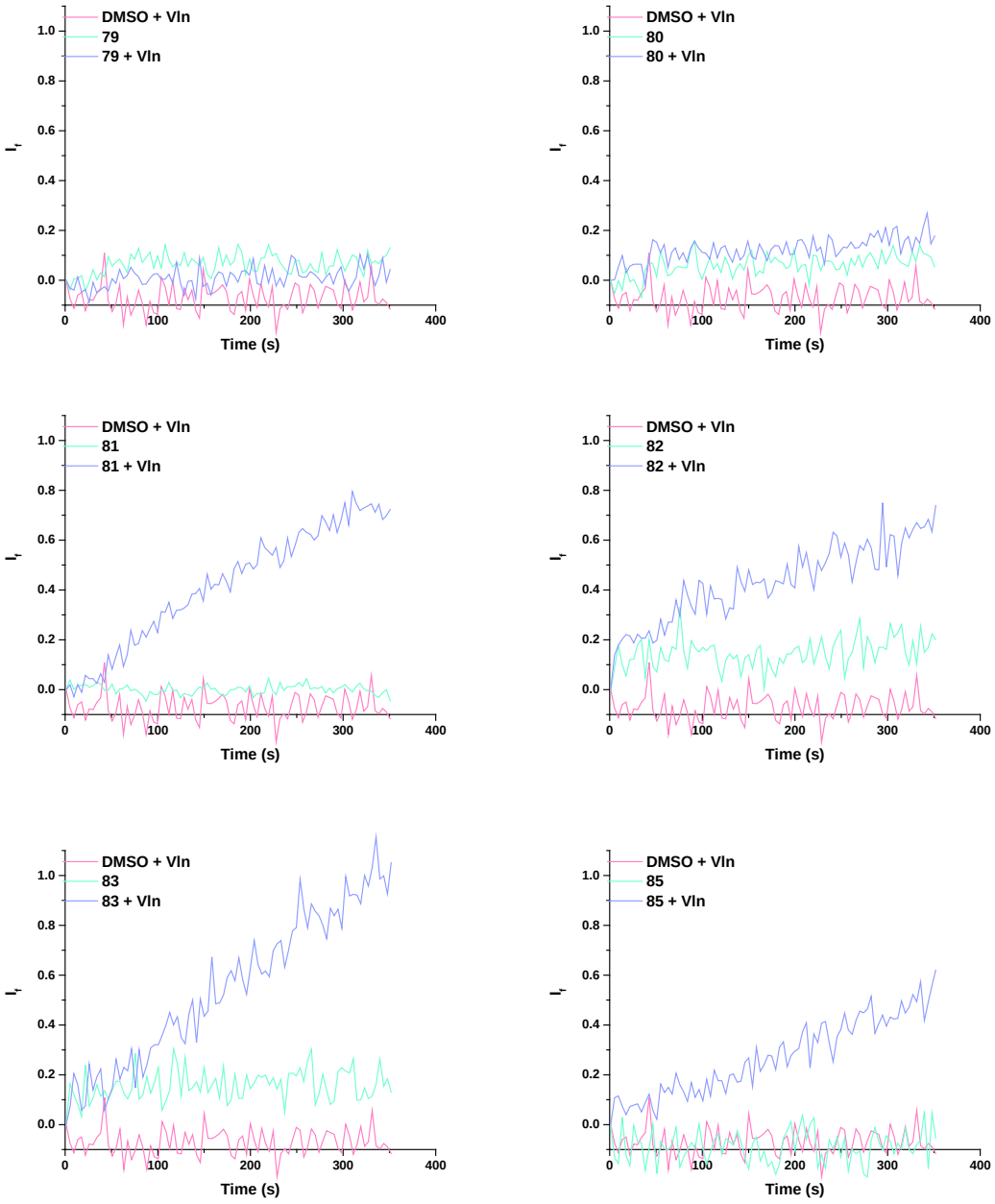

C3. 22 Osmotic assay results for **79**–**82** and **85** at 4 mol% loading (w.r.t. lipid) from POPC vesicles. Conditions-Internal: KOAc 300 mM buffered to pH 7.2 with HEPES buffer 10 mM. External: KGlc 300 mM buffered to pH 7.2 with HEPES buffer. The transport was initiated by the addition of a DMSO solution of Vln (0.1 mol%) and the receptor, at t= 500 s CCCP (5 mol%) was added to give maximum vesicle dehydration after t=600 s. Each plot is an average of 2 repeats. The plots show light scattering caused by the efflux of acetate and consequent dehydration of the vesicles via osmosis.

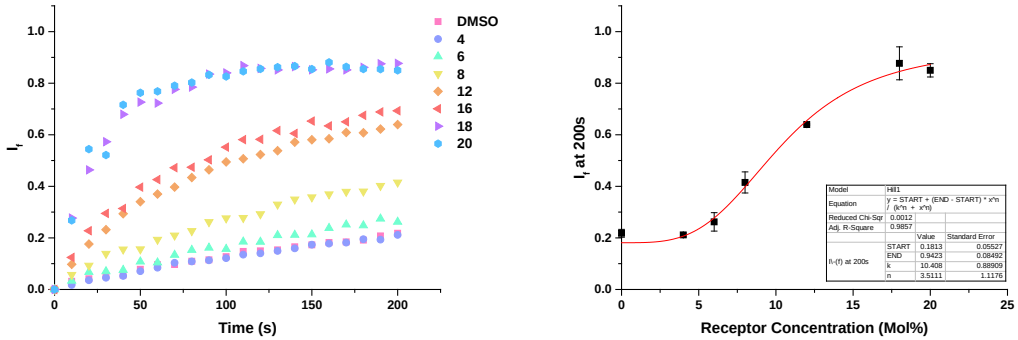

C3. 23 KCl dose response-**Left-** Receptor **79** kinetic profile. **Right-** Hill plot; concentrations in mol% with respect to lipid. EC_{50}= 10.4 mol% n=3.5.

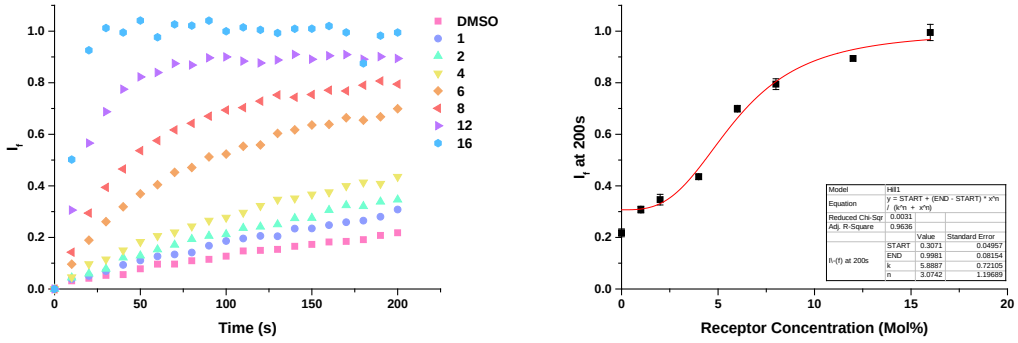

C3. 24 KCl dose response-**Left-** Receptor **80** kinetic profile. **Right-** Hill plot; concentrations in mol% with respect to lipid. EC_{50}= 5.9 mol% n=3.1.

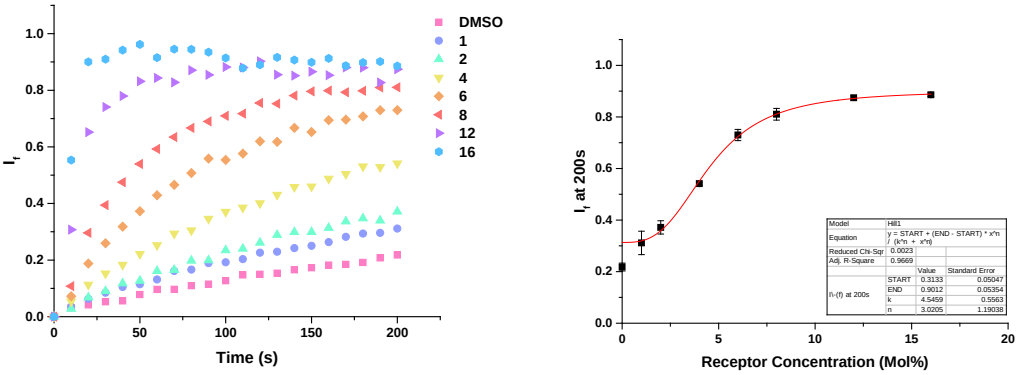

C3. 25 KCl dose response-**Left-** Receptor **81** kinetic profile. **Right-** Hill plot; concentrations in mol% with respect to lipid. EC_{50}= 4.5 mol% n=3.0.

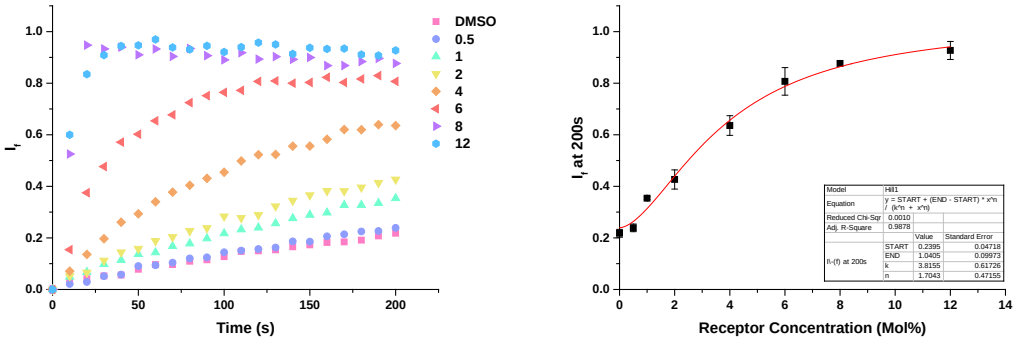

C3. 26 KCl dose response-**Left-** Receptor **82** kinetic profile. **Right-** Hill plot; concentrations in mol% with respect to lipid. EC_{50}= 3.8 mol% n=1.7.

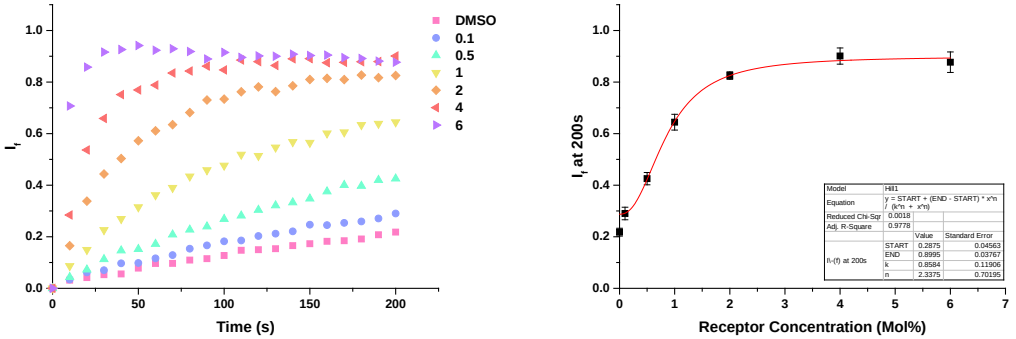

C3. 27 KCl dose response-**Left-** Receptor **83** kinetic profile. **Right-** Hill plot; concentrations in mol% with respect to lipid. EC_{50}= 0.9 mol% n=2.3.

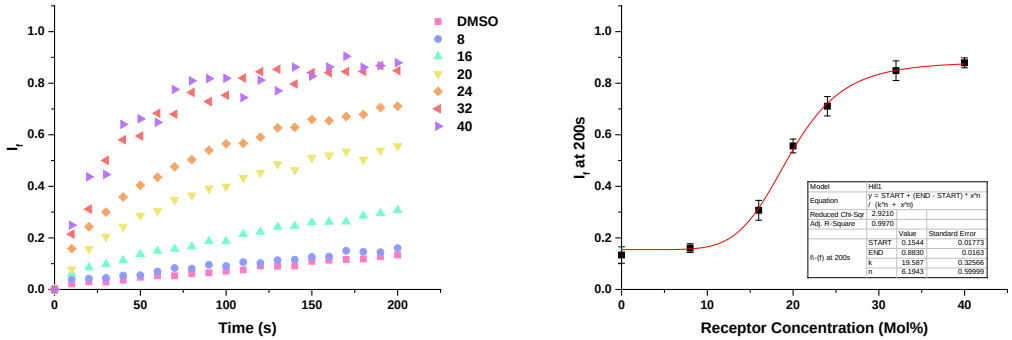

C3. 28 KBr dose response-**Left-** Receptor **79** kinetic profile. **Right-** Hill plot; concentrations in mol% with respect to lipid. EC_{50}= 19.6 mol% n=6.1.

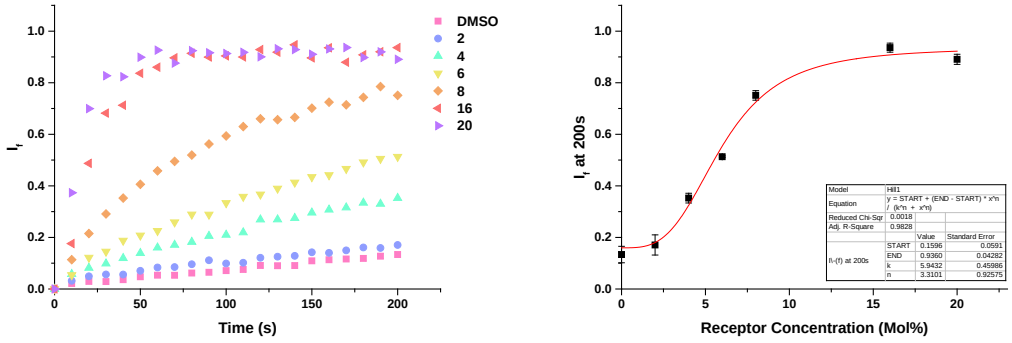

C3. 29 KBr dose response-**Left-** Receptor **80** kinetic profile. **Right-** Hill plot; concentrations in mol% with respect to lipid. EC_{50}= 5.9 mol% n=3.3.

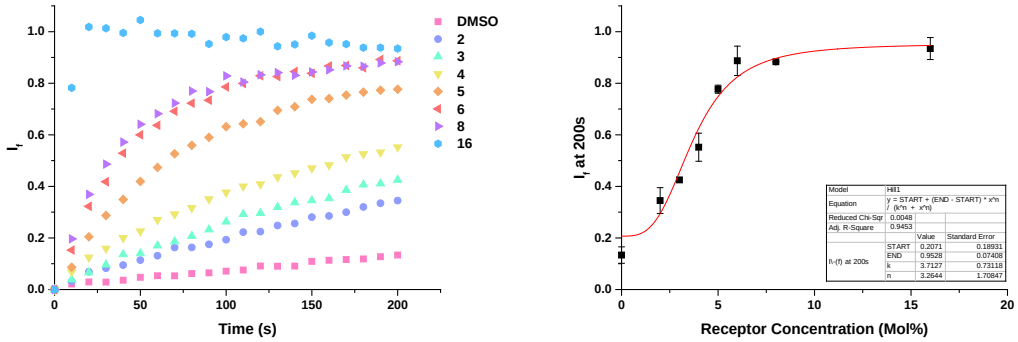

C3. 30 KBr dose response-**Left-** Receptor **81** kinetic profile. **Right-** Hill plot; concentrations in mol% with respect to lipid. EC_{50}= 3.7 mol% n=3.3.

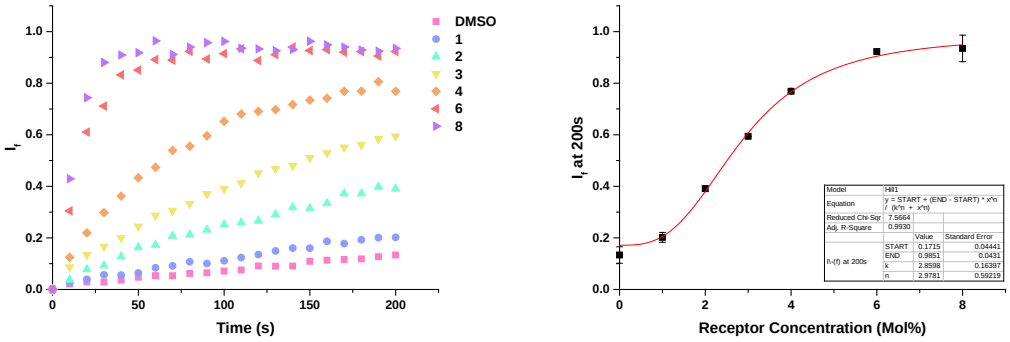

C3. 31 KBr dose response-**Left-** Receptor **82** kinetic profile. **Right-** Hill plot; concentrations in mol% with respect to lipid. EC_{50}= 2.9 mol% n=3.0.

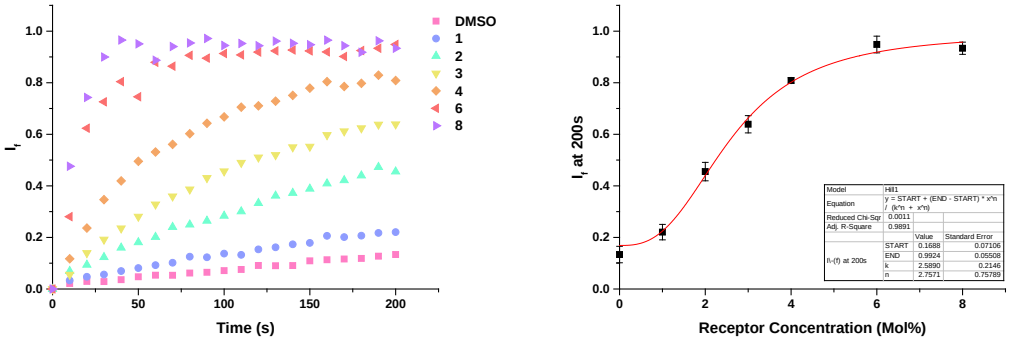

C3. 32 KBr dose response-**Left-** Receptor **83** kinetic profile. **Right-** Hill plot; concentrations in mol% with respect to lipid. EC_{50}= 2.6 mol% n=2.8.

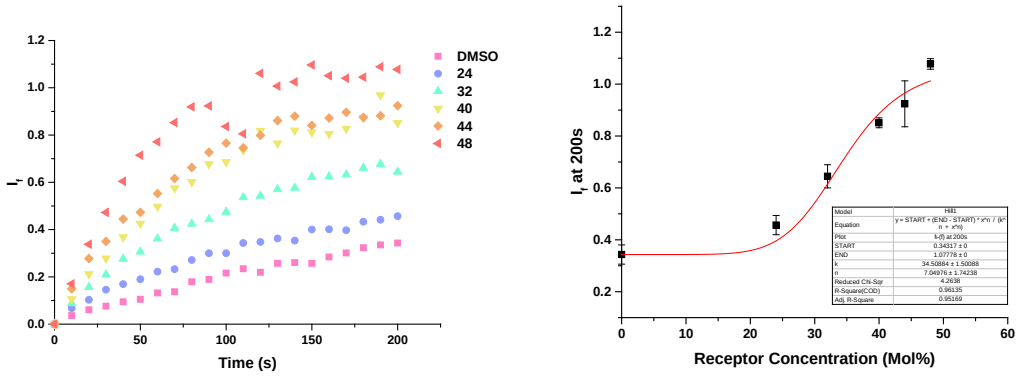

C3. 33 KI dose response-**Left-** Receptor **79** kinetic profile. **Right-** Hill plot; concentrations in mol% with respect to lipid. EC_{50}= 34.5 mol% n=7.0.

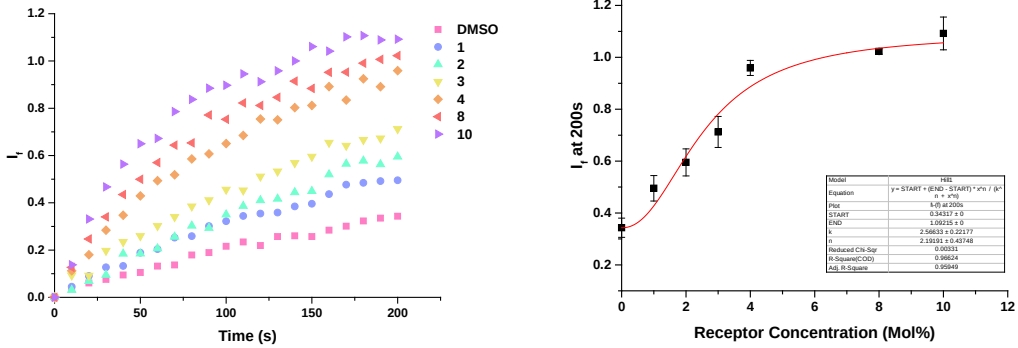

C3. 34 KI dose response-**Left-** Receptor **80** kinetic profile. **Right-** Hill plot; concentrations in mol% with respect to lipid. EC_{50}= 2.6 mol% n=2.2.

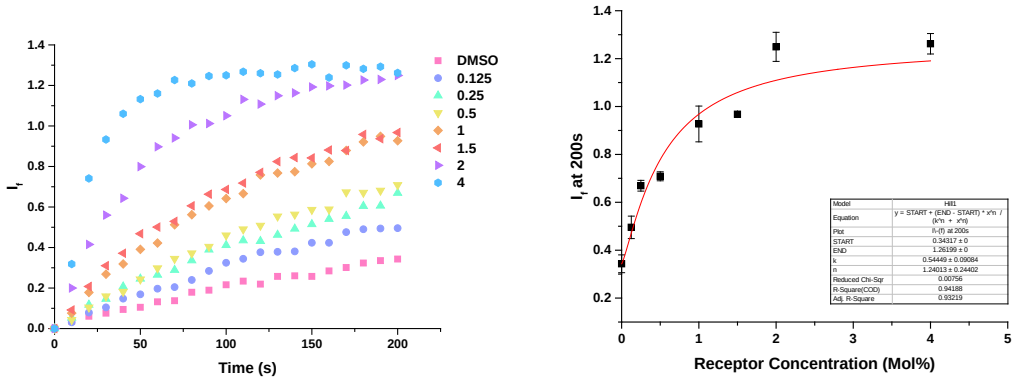

C3. 35 KI dose response-**Left-** Receptor **81** kinetic profile. **Right-** Hill plot; concentrations in mol% with respect to lipid. EC_{50}= 0.5 mol% n=1.2.

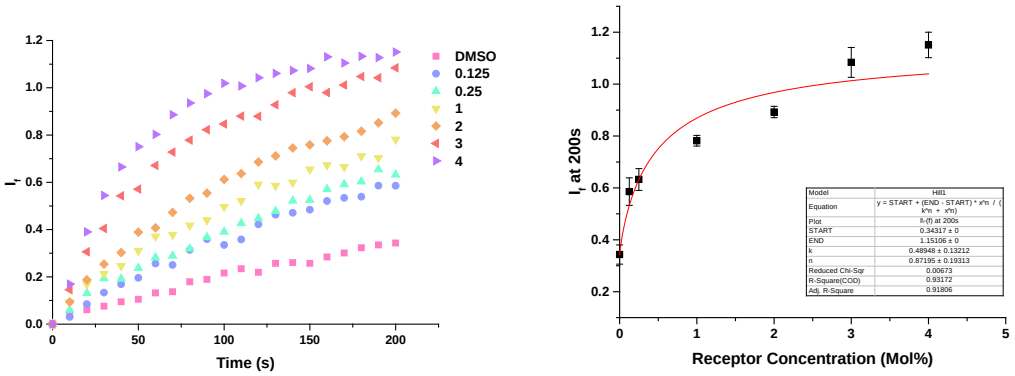

C3. 36 KI dose response-**Left-** Receptor **82** kinetic profile. **Right-** Hill plot; concentrations in mol% with respect to lipid. EC_{50}= 0.5 mol% n=0.9.

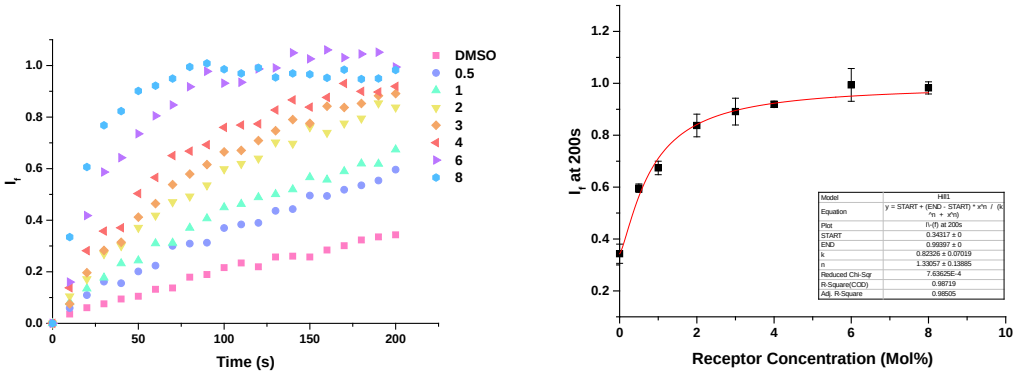

C3. 37 KI dose response-**Left-** Receptor **83** kinetic profile. **Right-** Hill plot; concentrations in mol% with respect to lipid. EC_{50}= 0.8 mol% n=1.3.

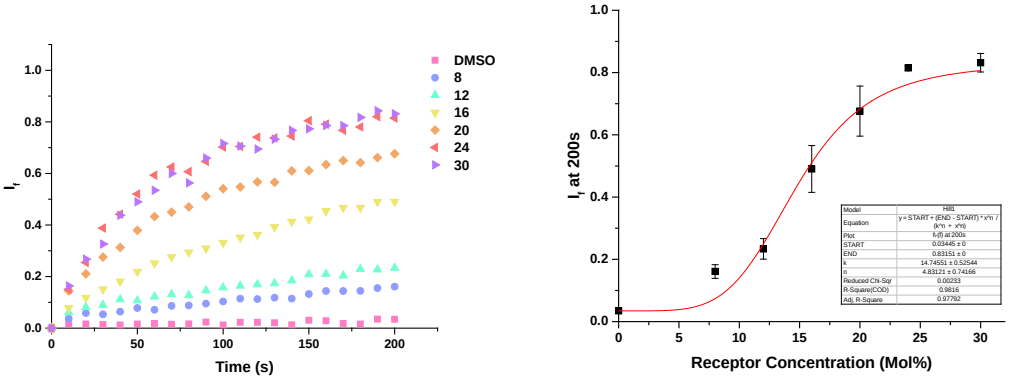

C3. 38 KNO_3 dose response-**Left-** Receptor **79** kinetic profile. **Right-** Hill plot; concentrations in mol% with respect to lipid. EC_{50}= 14.7 mol% n=4.8.

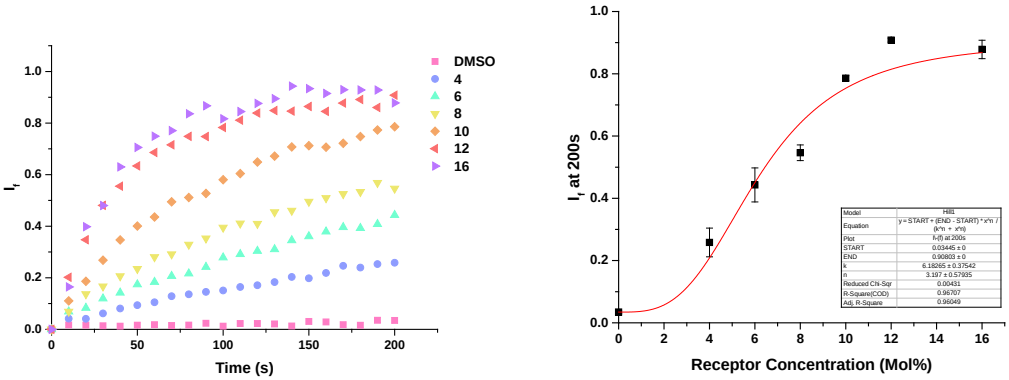

C3. 39 KNO_3 dose response-**Left-** Receptor **80** kinetic profile. **Right-** Hill plot; concentrations in mol% with respect to lipid. EC_{50}= 6.2 mol% n=3.1.

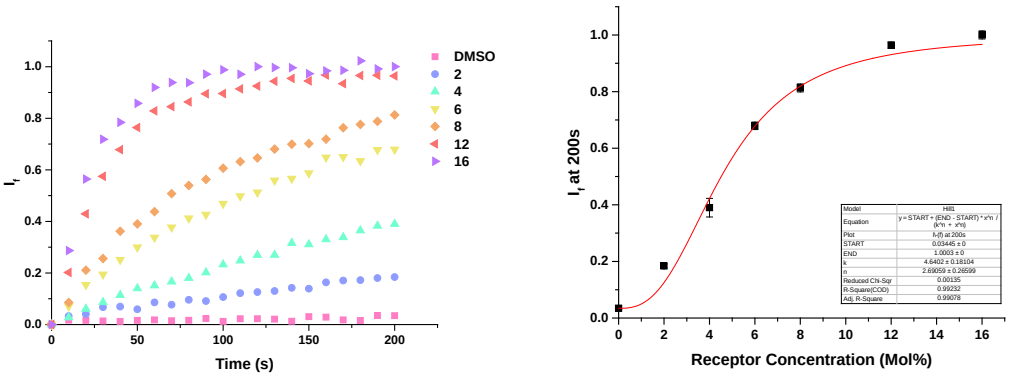

C3. 40 KNO_3 dose response-**Left-** Receptor **81** kinetic profile. **Right-** Hill plot; concentrations in mol% with respect to lipid. EC_{50}= 4.6 mol% n=2.7.

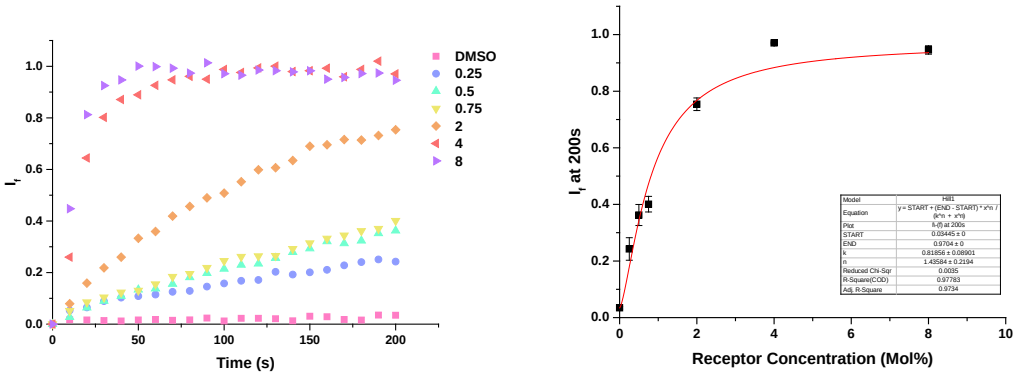

C3. 41 KNO_3 dose response-**Left-** Receptor **82** kinetic profile. **Right-** Hill plot; concentrations in mol% with respect to lipid. EC_{50}= 0.8 mol% n=1.4.

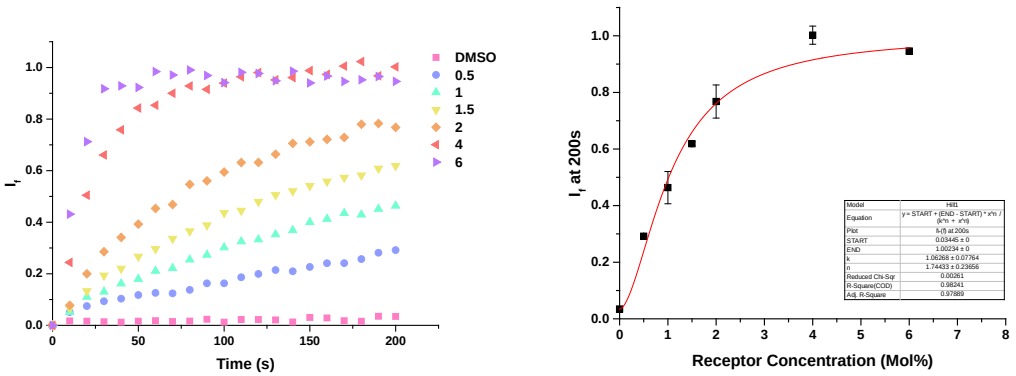

C3. 42 KNO_3 dose response-**Left-** Receptor **83** kinetic profile. **Right-** Hill plot; concentrations in mol% with respect to lipid. EC_{50}= 1.1 mol% n=1.7.

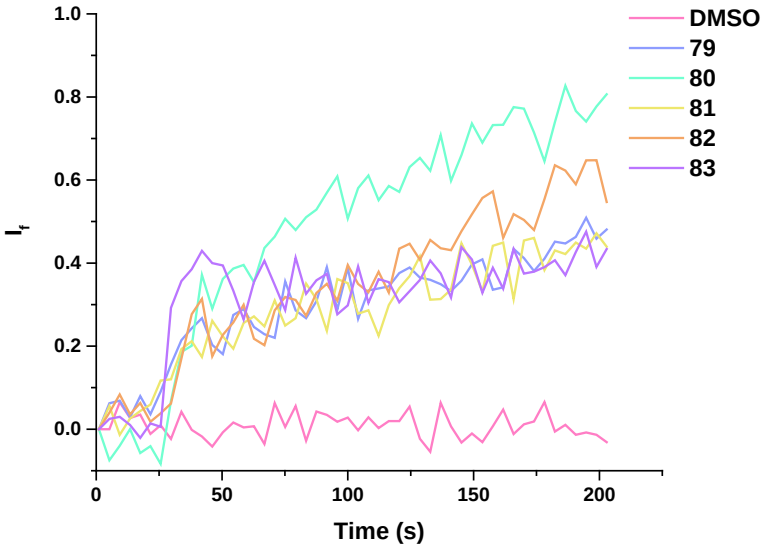

C3. 43 Kinetic profile from the caesium salt osmotic response assay, for CsF with receptors **79–83** at 4 mol% loading (w.r.t. lipid) from POPC vesicles. Conditions-Internal: CsF 300 mM buffered to pH 7.2 with HEPES buffer 10 mM. External: KGlc 300 mM buffered to pH 7.2 with HEPES buffer. The transport was initiated by the addition of a DMSO solution of the receptor at t= 30 s. Each plot is an average of 2 repeats.

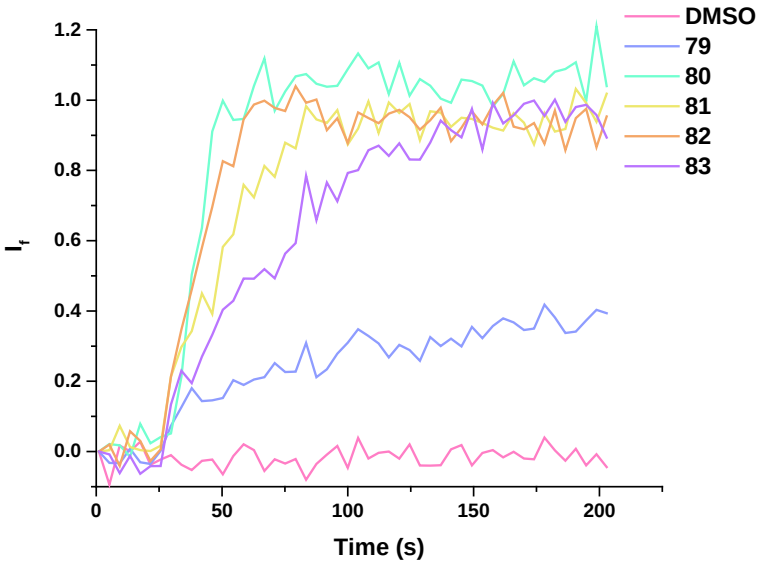

C3. 44 Kinetic profile from the caesium salt osmotic response assay, for CsCl with receptors **79–83** at 4 mol% loading (w.r.t. lipid) from POPC vesicles. Conditions-Internal: CsCl 300 mM buffered to pH 7.2 with HEPES buffer 10 mM. External: KGlc 300 mM buffered to pH 7.2 with HEPES buffer. The transport was initiated by the addition of a DMSO solution of the receptor at t= 30 s. Each plot is an average of 2 repeats.

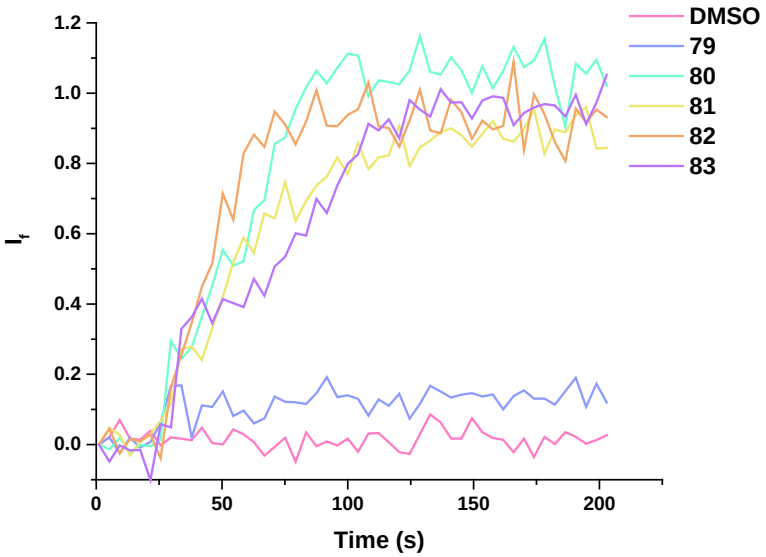

C3. 45 Kinetic profile from the caesium salt osmotic response assay, for CsBr with receptors **79–83** at 4 mol% loading (w.r.t. lipid) from POPC vesicles. Conditions-Internal: CsBr 300 mM buffered to pH 7.2 with HEPES buffer 10 mM. External: KGlc 300 mM buffered to pH 7.2 with HEPES buffer. The transport was initiated by the addition of a DMSO solution of the receptor at t= 30 s. Each plot is an average of 2 repeats.

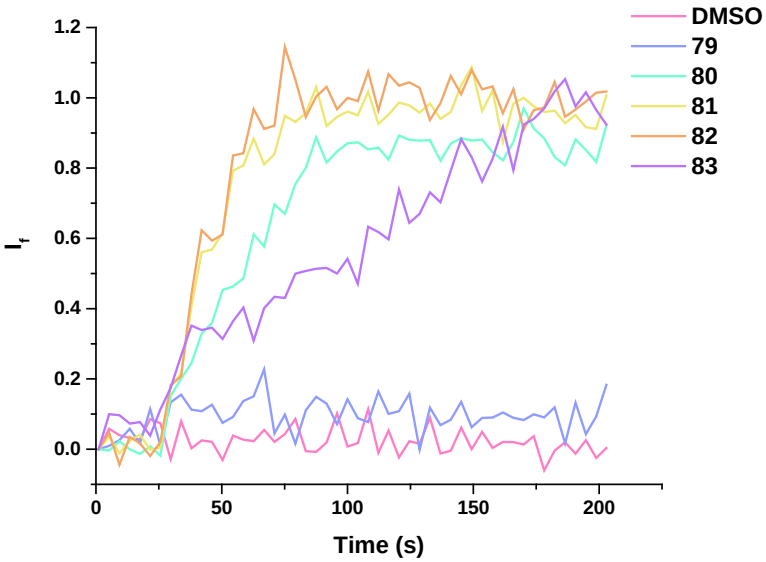

C3. 46 Kinetic profile from the caesium salt osmotic response assay, for CsI with receptors **79–83** at 4 mol% loading (w.r.t. lipid) from POPC vesicles. Conditions-Internal: CsI 300 mM buffered to pH 7.2 with HEPES buffer 10 mM. External: KGlc 300 mM buffered to pH 7.2 with HEPES buffer. The transport was initiated by the addition of a DMSO solution of the receptor at t= 30 s. Each plot is an average of 2 repeats.

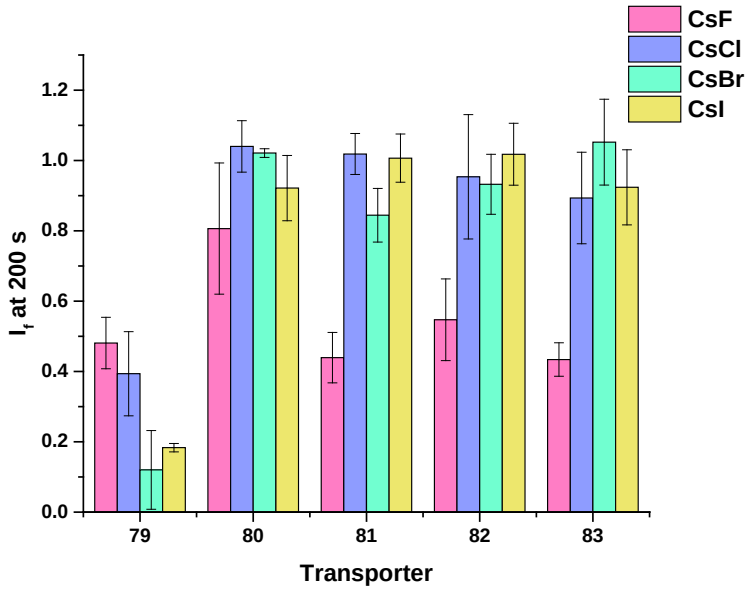

C3. 47 A bar chart showing the I_f at 200 s for **79–83** in the CsX osmotic assay. Internal: CsX 300 mM (X= F, Cl, Br or I) buffered to pH 7.2 with HEPES buffer 10 mM. External: KGlc 300 mM buffered to pH 7.2 with HEPES buffer.

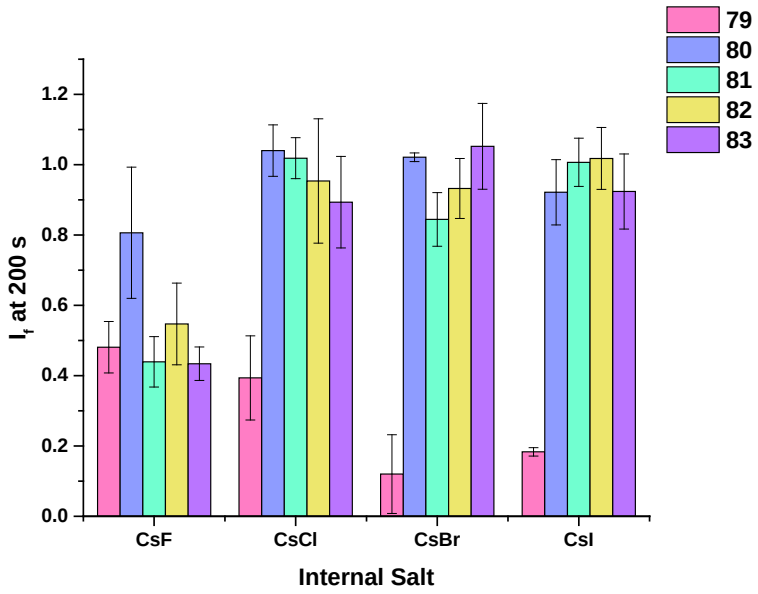

C3. 48 A bar chart showing the I_f at 200 s for **79–83** in the CsX osmotic assay. Internal: CsX 300 mM (X= F, Cl, Br or I) buffered to pH 7.2 with HEPES buffer 10 mM. External: KGlc 300 mM buffered to pH 7.2 with HEPES buffer. Alternative plot for clarity.